2013

Response of pteropod and related faunas to climate change and ocean acidification

Wall-Palmer, Deborah

Response of pteropod and related faunas to climate change and ocean acidification

Deborah Wall-Palmer

A thesis submitted to Plymouth University
in partial fulfilment for the degree of

PhD Geology

School of Geography, Earth and Environmental Sciences
Faculty of Science and Technology

January 2013

‘It is now that one reaps the benefit of all that counting
which at times had seemed almost hopeless’

Sir Alister Hardy, Great Waters.

Deborah Wall-Palmer, *Response of pteropod and related faunas to climate change and ocean acidification.*

Recent concern over the effects of ocean acidification upon calcifying organisms in the modern ocean has highlighted the aragonitic shelled thecosomatous pteropods as being at a high risk. Laboratory studies have shown that increased pCO_2, leading to decreased pH and low carbonate concentrations, has a negative impact on the ability of pteropods to calcify and maintain their shells. This study presents the micropalaeontological analysis of marine cores from the Caribbean Sea, Mediterranean Sea and Indian Ocean. Pteropods, heteropods and planktic foraminifera were picked from samples to provide palaeoenvironmental data for each core. Determination of pteropod calcification was made using the *Limacina* Dissolution Index (LDX) and the average shell size of *Limacina inflata* specimens. Pteropod calcification indices were compared to global ice volume and Vostok atmospheric CO_2 concentrations to determine any associations between climate and calcification.

Results show that changes in surface ocean carbonate concentrations throughout the Late Pleistocene did affect the calcification of thecosomatous pteropods. These effects can be detected in shells from marine sediments that are located well above the aragonite lysocline and have not undergone post-depositional dissolution. The results of this study confirm the findings of laboratory studies, showing a decrease in calcification during interglacial periods, when surface ocean carbonate concentrations were lower. During glacial periods, calcification was enhanced due to the increased availability of carbonate. This trend was found in all sediments studied, indicating that the response of pteropods to past climate change is of global significance. These results demonstrate that pteropods have been negatively affected by oceanic pH levels relatively higher and changing at a lesser rate than those predicted for the 21st Century.

Results also establish the use of pteropods and heteropods in reconstructing surface ocean conditions. The LDX is a fast and appropriate way of determining variations in surface water carbonate saturation. Abundances of key species were also found to constrain palaeotemperatures better than planktic foraminifera, a use which could be further developed.

CONTENTS

Wall-Palmer, D., Smart, C.W. and Hart, M.B. Global variations in pteropod calcification as an indicator of past ocean carbonate saturation. Submitted to

Quaternary Science Reviews October 2012, revised manuscript submitted December 2012.

Wall-Palmer, D., Smart, C.W., Hart, M.B., Leng, M.J., Conversi, A., Borghini, M., Manini, E. and Aliani, S. Quaternary planktonic foraminifera, pteropods and heteropods from the western Mediterranean Sea. Submitted to Marine Geology May 2012.

Wall-Palmer, D., Hart, M.B., Smart, C.W., Sparks, R.S.J., Le Friant, A., Boudon, G., Deplus, C. and Komorowski, J.C., 2012. Pteropods from the Caribbean Sea: variations in calcification as an indicator of past ocean carbonate saturation. *Biogeosciences,* **9,** 309-315

Wall-Palmer, D., Jones, M.T., Hart, M.B., Fisher, J.K., Smart, C.W., Hembury, D.J., Palmer, M.R. and Fones, G.R. 2011. Explosive volcanism as a cause for mass mortality of pteropods. Marine Geology, 282 (3-4), 231-239.

Hart, M., Pettit, L., Wall-Palmer, D., Smart, C., Hall-Spencer, J., Medina-Sanchez, A., Prol Ledesma, R.M., Rodolfo-Metalpa, R. and Collins, P. 2012. Investigation of the calcification response of foraminifera and pteropods to high CO_2 environments in the Pleistocene, Paleogene and Cretaceous. *EGU General Assembly Abstracts,* **14**, 9754.

Wall-Palmer. D., Smart, C.W., Hart, M.B. and Conversi, S. 2011. The dissolution of pteropods from the Caribbean and Mediterreanean Seas. *The Palaeontological Association 55th Annual Meeting Programme and Abstracts,* **55**, 42.

Wall-Palmer, D., Smart, C., Hart, M. and Conversi, A. 2011. The dissolution of pteropods from the Caribbean and Mediterreanean Seas. *Plankton 2011 Symposium Programme and Abstracts,* Poster 30.

Wall-Palmer, D., Smart, C.W. and Hart, M.B. 2010. The preservation of pteropods from the Caribbean Sea as an indicator of past ocean acidification. *Geological Society of America Abstracts with Programs,* **42**, 333.

Hart, M.B., Dias, B., Smart, C.W., Wall-Palmer, D., Hayden, J. and Hall-Spencer, J.M. 2010. Modern Seawater acidification: The response of foraminifera to high CO_2 conditions in the Mediterranean Sea and pteropods in the Caribbean Sea. *Geological Society of America Abstracts with Programs,* **42**, 333.

Hart. M., Wall-Palmer, D. and Smart, C. 2010. Response of pteropods and foraminifera to changing *p*CO2 and pH in the last 250,000 years. *EGU General Assembly Abstracts,* **12**, 4353.

LIST OF FIGURES, PLATES AND TABLES

ACKNOWLEDGEMENTS

My greatest thanks go to my primary and secondary supervisors, Dr Christopher Smart and Prof. Malcolm Hart, for their support throughout my research. Their patience, enthusiasm and knowledge have allowed me the freedom to work in my own way, whilst being kept on track with regular meetings and discussion. I am also grateful that they have often directed me towards exciting opportunities, such as taking part in international conferences and scientific cruises and publishing in peer reviewed journals. It is doubtless that without their guidance my research experience would not have been so enjoyable and fulfilling. I would also like to thank my third supervisor Dr Alessandra Conversi, whose enthusiasm and exciting ideas have allowed me to collaborate with other institutions and to expand my research.

As experts on holoplanktic gastropods, I am also extremely grateful to Dr Arie Janssen (Nationaal Natuurhistorisch Museum Naturalis, The Netherlands) and Prof. Roger Seapy (California State University, Fullerton, California, USA), who, although retired, swiftly responded to my questions about pteropods and heteropods. Their remarkable knowledge in this field has been invaluable to my research, especially in the identification of unusual specimens.

It is evident that, without the availability of suitable sediment cores, this research would not have been possible. Thanks are therefore due to the crew and scientists of all the cruises involved in this research. Cores were collected during the 2002 'Caraval' cruise of the R.V. *L'Atalante* (CAR-MON 2), in 2005 by the RRS *James Clark Ross* (JR123-35-V), in 2007 by the RRS *James Cook* (JC18-19), during the 2010 'BIOFUN'10' cruise of the R.V. *Urania* (B5-1) and by the Ocean Drilling Program in 1987 as part of Leg 115 on the *Joides Resolution* (716B). Thanks are also due to Mike Cassidy, Jess Trofimovs and BOSCORF at the National Oceanographic Centre, Southampton, for allowing me to visit and sample cores JC18-19 and JR123-35-V and for providing me with information and data on the cores. I would also like to thank Anne Le Friant for sending me samples from CAR-MON 2 and the curators at the IODP Kochi core centre in Japan for sending me samples from 716B.

My PhD research was funded by Plymouth University and I am extremely grateful to the staff of the Geology department for making it a great place to work and for their open door policies. In particular, I would like to thank Sally Greenwood for her immense organisational skills. She really is the glue holding us all together! I would like to thank Dr Helen Hughes for keeping the microscope lab tidy and well stocked and for presenting me with boxes of vials, filter paper and slides following panicked requests. Thanks are also due to technician Ian King for replacing and repairing an infinite number of broken microscope lights. I would also like to acknowledge a NERC grant which was awarded to carry out stable isotope analysis of B5-1. Melanie Leng, at the NERC Isotope Geosciences Laboratory, Keyworth, not only gave advice on preparing the proposal, but also kindly helped me to prepare my samples. I am also grateful to her colleague Hiliary Sloane who talked me through the analysis when I visited NIGL.

Finally I would like to give a huge thanks to my partner Matthew Fishwick who has supported me throughout my PhD, making me believe in myself and allowing me to take over the home office with my microscope, numerous vials of sediment and masses of papers.

AUTHOR'S DECLARATION

At no time during the registration for the degree of PhD Geology has the author been registered for any other University award without prior agreement of the Graduate Committee. This study was financed with the aid of a studentship from Plymouth University.

Relevant scientific seminars and conferences have been regularly attended during the course of this research and findings have been presented at conferences in the form of oral and poster presentations. Three manuscripts have been prepared for publication, two of which have been published in peer reviewed journals and one is currently under review. It is anticipated that two further manuscripts will be prepared from data collected during this study. During this research, a grant for oxygen isotope analysis was awarded from NERC and visits to their facilities in Keyworth were made for sample preparation. I have also taken part in two international cruises, one with the Integrated Ocean Drilling Program (IODP), which has allowed me to make contributions to the published Preliminary Report.

Peer reviewed publications:

Wall-Palmer, D., Smart, C.W. and Hart, M.B. Global variations in pteropod calcification as an indicator of past ocean carbonate saturation. **Submitted to Quaternary Science Reviews October 2012, revised manuscript submitted December 2012.**

Wall-Palmer, D., Smart, C.W., Hart, M.B., Leng, M.J., Conversi, A., Borghini, M., Manini, E. and Aliani, S. Quaternary planktonic foraminifera, pteropods and heteropods from the western Mediterranean Sea. **Submitted to Marine Geology May 2012.**

Manga, M., Hornbach, M.J. and Expedition 340 Scientists. 2012. Heat flow in the Lesser Antilles island arc and adjacent back arc Grenada basin. *Geochemistry Geophysics Geosystems,* **13**, Q08007. doi: 10.1029/2012GC004260

Stroncik, N., Le Friant, A., Ishizuka, O. and Expedition 340 Scientists. 2012. Expedition 340: Lesser Antilles Volcanism and Landslides. *IODP Preliminary Report,* **340**, doi: 10.2204/iodp.pr.340.2012

Wall-Palmer, D., Hart, M.B., Smart, C.W., Sparks, R.S.J., Le Friant, A., Boudon, G., Deplus, C., Komorowski, J.C., 2012. Pteropods from the Caribbean Sea: variations in calcification as an indicator of past ocean carbonate saturation. *Biogeosciences,* **9,** 309–315.

Wall-Palmer, D., Jones, M.T., Hart, M.B., Fisher, J.K., Smart, C.W., Hembury, D.J., Palmer, M.R. and Fones, G.R. 2011. Explosive volcanism as a cause for mass mortality of pteropods. *Marine Geology*, **282** (3-4), 231–239.

Conferences Attended:

- The Micropalaeontological Society AGM, London, UK. 18th November 2009.
- Geochemistry Group Research in Progress meeting, London, UK. 4th March 2010.
- Marine Institute Global Change conference, Plymouth, UK. 3rd June 2010.
- The 10th International Conference on Paleoceanography, La Jolla, San Diego, US. August 29th – September 3rd 2010.
- The Micropalaeontological Society AGM, London, UK. 17th November 2010.
- Centre for Research in Earth Sciences research conference, Plymouth, UK. 24th November 2010.
- Plankton 2011, Plymouth, UK. September 22nd – 23rd 2011.
- Centre for Research in Earth Sciences research conference, Plymouth, UK. 16th November 2011.
- The 55th annual meeting of the Palaeontological Association, Plymouth, UK. 17th – 20th December 2011.

Presentations given:

- *'Response of pteropod faunas to climate change and ocean acidification',* oral presentation within the Geology department. 22nd January 2010.
- *'BIOFUN 2010 cruise of the R/V Urania'*, oral presentation to the Italian science attaché and Plymouth University Italian community. 27th May 2010.
- *'Response of pteropod faunas to climate change and ocean acidification'*, poster presentation at the Marine Institute Global Change conference. 3rd

June 2010.

- *'The preservation of pteropods from the Caribbean Sea as an indicator of past ocean acidification',* poster presentation at the 10th International Conference on Paleoceanography. 31st August 2010.
- *'The preservation of pteropods from the Caribbean Sea as an indicator of past ocean acidification',* oral and poster presentation at the Centre for Research in Earth Sciences research conference. 24th November 2010.
- *'The preservation of pteropods from the Caribbean Sea as an indicator of past ocean acidification',* oral presentation at the Geological Society Young Geoscientist meeting. 8th December 2010.
- *'The dissolution of pteropods from the Caribbean and Mediterranean Seas',* poster presentation at Plankton 2011. 22nd September 2011 (*Plankton 2011 Symposium Programme and Abstracts).*
- *'The dissolution of pteropods from the Caribbean and Mediterranean Seas',* oral presentation at the 55th annual meeting of the Palaeontological Association. 18th December 2011 (*The Palaeontological Association 55th Annual Meeting Programme and Abstracts*).
- *'Butterflies, angels and elephants: uses in palaeoceanographic reconstruction',* oral seminar within the Geology department. 15th February 2012.

Word count of main body of thesis: **44,000 words**

Signed 

Date 24th January 2013

1 INTRODUCTION

1.1 RATIONALE

It is now widely accepted that ocean acidification is an imminent threat to our oceans and although we have a good understanding of the related changes in ocean chemistry, the biological response is still largely not understood (Orr *et al.,* 2005). It is generally considered that calcifying organisms will be greatly affected by ocean acidification due to under-saturation with respect to calcium carbonate. Experimental evidence demonstrates that a reduction in pH will generally lead to a decrease in calcification rates of a number of, but not all, organisms (Gattuso *et al.,* 1998; Orr *et al.,* 2005; Guinotte and Fabry, 2008; Fabry *et al.,* 2008; Ries *et al.,* 2009). Such studies have shown that the response will be complicated and species specific. However, to date, little information is available for important planktic producers of calcium carbonate. Some studies have looked at the effects on coccolithophores and planktic foraminifera, but only three species of the aragonite producing thecosome pteropods have been considered (Feely *et al.*, 2004; Fabry *et al.,* 2008; Comeau *et al.*, 2009, 2010a,b, 2012; Bednaršek *et al.,* 2012a, 2012b). Due to their highly soluble aragonite shells, thecosome pteropods are likely to be the most vulnerable of the major planktic producers of $CaCO_3$. They are also likely to be the first planktic fauna to experience persistent decreased $CaCO_3$ saturation states. As an important part of the food web, especially in the Arctic and Southern Oceans, their potential demise is of great significance.

By studying the effects of past changes in ocean chemistry on pteropod calcification over the most recent glacial and interglacial periods, a better understanding of the effects of ocean acidification upon these important

organisms can be attained. Since all of the species present during the studied time period are still extant, the findings may be applicable to the modern ocean.

1.2 AIMS AND OBJECTIVES

The key aim of this study is to investigate whether changes in surface ocean carbonate saturation during the Late Pleistocene can be detected by analysing the calcification of pteropod shells preserved in marine sediments. The primary microfossil analysis was carried out at high resolution (2 kyr) on a marine sediment core, CAR-MON 2, collected to the south west of the Island of Montserrat, in the Caribbean Sea. To check the reproducibility of data from CAR-MON 2, two further cores (JC18-19 and JR123-35-V) from this region were studied at varying lower resolution. To investigate whether trends found within CAR-MON 2 are due to local or global influences, cores from two further sites were studied at lower resolution (B5-1 2–4 kyr, 716B 5–50 kyr). Core B5-1 was collected to the south east of the Island of Mallorca, in the western Mediterranean Sea and ODP Hole 716B was collected on the Chagos-Laccadive Ridge in the Indian Ocean. All cores were analysed for microfossils, which provide palaeoenvironmental data and specimens of pteropods were used to create a calcification profile. The calcification profiles of the three study areas were compared to identify whether trends are local or global. Comparisons to previous studies which provide data on the abundances and preservation of fossil pteropods over this period and also comparisons to data collected in laboratory experiments on modern living pteropods are important in supporting any patterns found in pteropod calcification.

The secondary aim of this study will be to assess the use of pteropods and heteropods in the reconstruction of past surface water conditions. Pteropod and heteropod taxonomy will also be established for the sample sites.

To achieve these aims, the following objectives were accomplished:

- High resolution (every 5 cm, ~2 kyr) microfossil analysis of core CAR-MON 2, collected in the Caribbean Sea, has been carried out. Lower resolution (every 10 cm, ~2–4 kyr for B5-1 and variable, ~5–50 kyr for ODP Hole 716B) microfossil analysis of B5-1, collected in the Mediterranean Sea, and ODP Hole 716B, collected in the Indian Ocean, was also carried out.
- Two further cores, JC18-19 and JR123-35-V, collected in the Caribbean Sea, were analysed for microfossil content at lower resolution and varying sample intervals. The results from these cores were compared to CAR-MON 2 to check the reproducibility of data from one geographic location.
- Pteropods, heteropods and planktic foraminifera were picked from all samples using a standard foraminifera methodology. Grain size data have also been collected.
- Stable oxygen isotope analysis has been carried out for core B5-1, providing a stratigraphic framework for this core. All other cores have been previously analysed for stable oxygen isotopes for other studies.
- For every core, specimens of the pteropod *Limacina inflata* have been analysed using the *Limacina* Dissolution Index (LDX) to create a calcification profile throughout each core. This has been compared to oxygen isotope data to assess whether any relationship between

pteropod calcification and climatic change exists. Comparisons to the average shell size of *L. inflata* specimens have also been made.

- Abundance and diversity of pteropods, heteropods and planktic foraminifera, as well as percentage fragmentation of planktic foraminifera and proportions of the planktic foraminifera *Globorotalia menardii,* were used to assess further changes in the climate and surface water carbonate saturation levels. A palaeoceanographic reconstruction has been made for each site using this information.
- A detailed taxonomic study of pteropods and heteropods, including the use of SEM, has been made.

Please note: At the first mention, all species names are written in full, but the author of each species is not referenced. For species authors, please refer to Tables 4.1, 4.4 and 4.8 and to Chapter 4 for a detailed synonomy of pteropods and heteropods.

2 BACKGROUND

2.1 OCEAN ACIDIFICATION

At present, only half of the anthropogenic CO_2 produced since 1780 is present in the Earth's atmosphere (Royal Society, 2005). The remaining 50% has been taken up by the land biosphere (20%) and by the oceans (30%). Sabine *et al.* (2004) suggest that, without the ocean sink, the anthropogenic change in atmospheric CO_2 concentration would be 55% higher than the observed change. However, although this potentially useful ocean sink will reduce the extent of global warming, the resulting changes in ocean chemistry are expected to have damaging effects on marine biota.

The present oceans are saturated with respect to calcium carbonate, allowing organisms to produce calcium carbonate structures. However, when CO_2 enters the ocean from the atmosphere, it undergoes a number of reactions, ultimately resulting in the production of excess positively charged hydrogen ions, which lower the pH (Fig. 2.1). Hydrogen ions are extremely reactive and readily attach to carbonate ions (CO_3^{2-}) to form bicarbonate ions (HCO_3^-). By increasing the amount of dissolved CO_2, the amount of CO_3^{2-} is therefore decreased as the carbonate becomes bound as bicarbonate. This causes under-saturation with respect to $CaCO_3$; decreasing the amount of carbonate ions available for organisms to use in the manufacture of calcium carbonate. This not only makes it harder for organisms to maintain their shells, but also to build their shells in the first place.

The reaction can be summarised as: $\mathbf{CO_2 + CO_3^{2-} + H_2O \rightarrow 2HCO_3^-}$

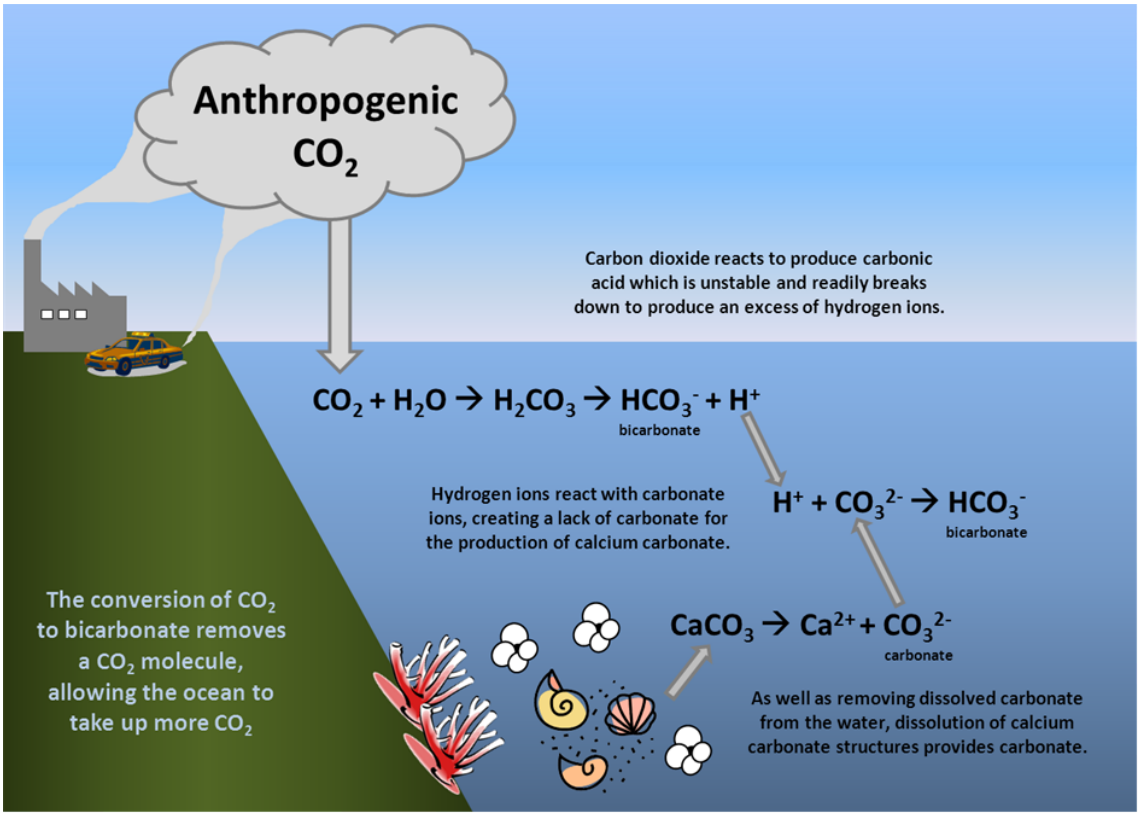

Figure 2.1 Illustrated effects of increased anthropogenic carbon dioxide upon ocean chemistry. Information from Royal Society (2005).

At present, the Earth's atmospheric CO_2 concentration is rising at a rate of ~0.5% year $^{-1}$ (Forster *et al.,* 2007). This is around 100 times faster than any changes during the past 650,000 years (Royal Society, 2005). The present atmospheric CO_2 level has increased from 280 ppmv to around 390 ppmv in a period of 200 years. The surface ocean pH is, therefore, already an average of 0.1 units lower than pre-industrial values (Orr *et al.,* 2005), relating to an approximate increase in hydrogen ion concentration of 30% (Guinotte and Fabry, 2008). Under the Intergovernmental Panel on Climate Change (IPCC) IS92a model scenario of 'business as usual', atmospheric CO_2 levels are expected to reach 780 ppmv by the year 2100 (http://www.ipcc-data.org). This relates to a reduction in surface ocean pH by a further 0.3–0.4 units (Orr *et al.,* 2005). A change in pH of such magnitude has not occurred for over 20 million

years (Feely *et al.,* 2004). Ridgwell and Schmidt (2010) regard the future rate of surface ocean acidification to be unprecedented in the past 65 million years. Such changes are soon thought to become irreversible for several centuries (Ridgwell and Schmidt, 2010; Gangstø *et al.,* 2011)

This alarming rapid decrease in ocean pH, termed 'ocean acidification' is of serious concern, particularly for calcifying marine organisms. Although it is likely that many areas of the oceans will remain saturated with respect to $CaCO_3$, most calcifying organisms require super-saturation to produce $CaCO_3$ structures (Gattuso *et al.,* 1998). Photosynthesising organisms are also at risk as some use bicarbonate as a source of carbon for photosynthesis (Sciandra *et al*., 2003). The extent to which organisms will be affected is determined by their distribution and the type of $CaCO_3$ that they produce.

Since the dissolution of carbon dioxide from the atmosphere occurs in the surface water of the oceans, this will be the greatest affected part of the water column. Shallow water organisms such as corals and planktic producers of calcium carbonate will therefore be greatly affected. Coccolithophores, foraminifera and thecosome pteropods are the key producers of planktic $CaCO_3$. These three groups alone account for nearly all the export flux of $CaCO_3$ from the upper ocean to the deep sea (Fabry *et al.,* 2008). Planktic foraminifera and coccolithophores produce calcite structures, which are more resistant to dissolution, however, thecosome pteropods produce shells made of aragonite, a polymorph of $CaCO_3$. Aragonite is 50% more soluble in seawater than calcite and hence puts pteropods at a greater risk of dissolution (Fabry *et al*., 2008).

The solubility of $CaCO_3$ increases with decreasing temperature and increasing pressure (Fabry *et al.,* 2008). Therefore, saturation states are

generally highest in tropical regions and lowest at high latitudes. Saturation states also vary around upwelling regions, where shoaling of the aragonite saturation horizons occur. These areas are present in the Pacific, north of ~40^{o}N, at the Equator and 10^{o}N (Fabry *et al.,* 2008). Calcium carbonate saturation also varies with depth in the ocean due to varying water masses. In general, the surface and shallow waters are saturated with respect to $CaCO_3$ and the deep waters are under-saturated. Ordinarily, the aragonite saturation depth shoals from ~1000m near 30^{o}S to 300m at the Equator. It then deepens to 550m near 30^{o}N and shoals again to ~100m north of 50^{o}N (Fabry *et al.,* 2008). At present, the increasing concentrations of CO_2 are causing a shallowing of the North Pacific aragonite saturation horizon at a rate of ~1–2 m per year (Feely *et al.,* 2008). The surface waters of the polar oceans will be the first to become under-saturated with respect to aragonite. Recent models have shown that this could occur in the Southern Ocean by 2050 (Orr *et al.,* 2005; McNeil and Matear, 2007) and as early as 2016 in the Arctic Ocean (Steinacher *et al.,* 2009).

It has been suggested by some scientists that the warming produced as an effect of global warming may counteract the absorption of some carbon dioxide into the ocean. Warm water has a lower capacity for dissolving CO_2 and seawater will release CO_2 as it warms. However, a study by Cao *et al.* (2007) suggests that ocean acidification will occur independent of climate change; that the increase in temperature will not be sufficient to alleviate the oceans of excessive CO_2. Gangstø *et al.* (2011) also propose that the reduced production and increased dissolution of calcium carbonate structures resulting from surface water acidification, will have a negligible effect on the pCO_2, offering no buffering to continued increases in acidification.

2.2 RECENT RESEARCH ON CALCIFYING ORGANISMS

Substantial experimental evidence has already been gathered which demonstrates that a reduction in pH will lead to a decrease in calcification rates of a number of, but not all, organisms (Doney *et al,* 2009; Ries *et al.,* 2009). There have been numerous recent studies on the effects of ocean acidification on calcifying marine organisms (for example Ries *et al.,* 2009), however, to date there are very few studies considering the effects upon planktonic calcifying species. Several studies have investigated the response of a limited number of coccolithophore (Riebesell *et al.,* 2000; Sciandra *et al.,* 2003; Langer *et al.,* 2006) and foraminifera species (Spero *et al.,* 1997; Bijma *et al.,* 2002), but the effects on only three species of the aragonite producing thecosome pteropods have been studied (Feely *et al.,* 2004; Comeau *et al.,* 2009, 2010a).

Reductions in marine calcification with relation to increased pCO_2 were first demonstrated by Alegian in 1985 by looking at the tropical red coralline algae *Porolithon gardineri*. This relationship has subsequently been identified in a number of photosynthetic and calcifying organisms and communities. Guttuso *et al.* (1998), Orr *et al.* (2005), Guinotte and Fabry (2008), Fabry *et al.* (2008), Doney *et al.* (2009) and Ries *et al.* (2009) have compiled studies on the effects on marine fauna and ecosystems.

The response of calcite forming reef-building corals has been well documented, although to date only studies with time periods of days to weeks and under laboratory conditions have been made. The results generally correspond to the predicted response. It has been found that at double pre-industrial CO_2 concentrations, the calcification rates of tropical reef-building corals will decrease by 20-60% (Gattuso *et al.,* 1998; Kleypas *et al*., 1999, 2006; Marubini and Thake, 1999; Langdon *et al.,* 2000; Marubini *et al.,* 2001;

Kleypas and Langdon, 2002; Langdon *et al.,* 2003; Langdon and Atkinson, 2005; Royal Society, 2005; Renegar and Riegl, 2005). Guinotte and Fabry (2008) suggest that a reduction in calcification of this magnitude may fundamentally alter the current structure and function of coral-reef ecosystems. Buddemeier *et al.* (2011) modelled the response of coral reefs in the Caribbean to global warming and ocean acidification. The results show that a reduction in coral cover to below 5% is likely to occur on most Caribbean reefs by the year 2035. Coralline algae, which are also an important component of coral reef systems, are at great risk. These algae produce another form of $CaCO_3$; high-magnesium calcite, which is even more susceptible to dissolution than aragonite. When exposed to seawater with chemistry relative to double the present CO_2 concentration, there was a 92% reduction in the total area covered by coralline algae (Kuffner *et al.,* 2008). Guinotte and Fabry (2008) also suggest that cold water corals are likely to be at a high risk from ocean acidification. Predictions of future aragonite saturation states indicate that 70% of present day scleractinian cold water corals could be in under-saturated water by the year 2100 (Turley *et al.,* 2007).

It is important, however, to note that whilst the majority of work in this area has shown the trend of reduced calcification with increased pCO_2, this is not the response of all calcifying species. Reynaud *et al.* (2003) found that the reef-building coral *Stylophora pistillata* decreased calcification by 50% when both temperature and pCO_2 were increased, however, when only pCO_2 was increased, the coral did not show signs of reduced calcification. Ries *et al.* (2009) demonstrate that several species of benthic invertebrate increase their net calcification rates with decreasing aragonite saturation. In a study by Pistevos *et al.* (2011), it was found that genetically identical individuals of the

colonial bryozoan *Celleporella hyalina* showed variation in their response to changes in pH and temperature, which may enable adaptation to future acidification.

Organisms that contribute less towards the global production of $CaCO_3$, such as echinoderms, benthic molluscs and bryozoans are also at risk from ocean acidification. A reduced calcification response to ocean acidification has been found in a range of benthic molluscs, including mussels, oysters and gastropods (Shirayama and Thorton, 2005; Gazeau *et al.,* 2007). Green *et al.* (2004) looked at the dissolution mortality of juvenile bivalves in sediments under-saturated with respect to pCO_2. It was found that bivalves showed significant mortality for each size class in under-saturation experiments. Portner *et al.* (2004) review other effects that may occur as a result of decreased ocean pH. These include effects on acid-base regulation, respiration, energy turnover and mode of metabolism. A reduced ability of juvenile benthic invertebrates to settle in an area with elevated pCO_2 and other adverse effects of increased pCO_2 such as reduced fertilisation success and poor development have also been seen in bivalves and echinoderms (Kurihara and Shirayama, 2004; Kurihara *et al.*, 2007; Cigliano *et al.,* 2010). The importance of assessing a variety of factors is highlighted in a study on the Arctic bivalve *Laternula elliptica* (Cummings *et al.,* 2011). Cummings *et al.* (2011) found that although the bivalve could function at increased pCO_2, it had to work much harder to calcify, a response that would be difficult to maintain in the long term.

Studies of benthic foraminifera show that the effects of increased pCO_2 levels are variable, but generally lead to reduced calcification. A study of large algal symbiont-bearing benthic foraminifera, with extremely soluble high-Mg calcite tests, found that forms with a hyaline structure reacted differently to

forms with a porcelaneous structure (Fujita *et al.,* 2011). Hyaline species *Baculogypsina sphaerulata* and *Calcarina gaudichaudii* showed increased calcification at intermediate levels of pCO_2 (580 and 770 ppmv) and decreased calcification at higher levels (970 ppmv). Whereas, porcelaneous species *Amphisorus hemprichii,* decreased calcification with all increases in pCO_2 (Fujita *et al.,* 2011). Dias *et al.* (2010) found that at natural CO_2 vents on the coast of Ischia, Italy, the assemblage of benthic foraminifera shifted to one of reduced calcifying forms and increased agglutinated forms in high pCO_2 (pH ~7.8) areas. Calcifying forms disappear completely at a pH of ~7.6. Interestingly, porcelaneous forms in this study also appear less well adapted than hyaline forms as they are not present at pH ~7.8, where hyaline forms still represent 25% of benthic foraminifera wall structures (Dias *et al.,* 2010).

As major planktic producers of $CaCO_3$, the effects of ocean acidification upon coccolithophores, planktic foraminifera and thecosome pteropods are extremely important. However, very few species have been studied for their calcification response to reduced pH. The majority of work has been carried out on the bloom forming coccolithophores *Emiliania huxleyi* and *Gephyrocapsa oceanica.* It was found that increasing the pCO_2 concentration from 560 to 840 ppmv caused a reduction in calcification of 25–66%. An increased number of malformations and incomplete coccospheres were also observed (Riebesell *et al.,* 2000; Sciandra *et al.,* 2003). However, Langer *et al.* (2006) found that reduced calcification is not always the response of coccolithophore species to increased pCO_2. It was found that *Coccolithus pelagicus* did not alter its calcification when subjected to increased pCO_2. Evidence for adaptation in the coccolithophore *Calcidiscus leptoporus* was also found by Langer *et al.* (2006). This species showed highest calcification rates at present pCO_2 levels with

malformed coccoliths and coccospheres at lower and higher pCO_2 concentrations. In sediments from the Last Glacial Maximum however, no malformed coccoliths were found in the same species, even though the pCO_2 was much lower (200ppmv) than the present day. The authors therefore concluded that *C. leptoporus* must have gradually adapted to present CO_2 levels, which means it may be able to adapt to future changes. Further to this, in a high resolution sediment core, Iglesias-Rodríguez *et al.* (2008) found an increase in the average coccolith mass (*C. leptoporus* and *Coccolithus pelagicus*) from the year 1960 to the year 2000, during the rise in anthropogenic atmospheric CO_2, suggesting that such species may be able to keep up with the high rate of CO_2 increase. Irie *et al.* (2010) predict that in coccolithophores, a more heavily calcified exoskeleton is favoured by natural selection as a response to ocean acidification. They suggest that this occurs due to the benefits of growing slower but being better defended compared to accelerating the cell cycle, but having a thinner exoskeleton. Complex assemblage-level responses to ocean acidification in coccolithophores are highlighted by Beaufort *et al.* (2011), who also show that differentially calcified species and morphotypes are distributed throughout the oceans according to carbonate chemistry.

Two species of planktic foraminifera have been directly investigated with respect to changing seawater CO_3^{2-} concentration. In these studies, it was found that shell mass decreased with decreasing CO_3^{2-} concentration (Spero *et al.,* 1997; Bijma *et al.,* 2002) in both *Orbulina universa* and *Globigerinoides sacculifer*. It was also found by Spero *et al.* (1997) that calcification rates in *O. universa* were 37% higher when grown in seawater with CO_3^{2-} concentration higher than the present day concentration, implying that planktic foraminifera

are already limited by the concentration of carbonate ions in the present ocean. Barker and Elderfield (2002) have suggested that changes in carbonate saturation are already detectable; that planktic foraminifera in the water column are lighter than those found in surface sediments of the same area. More recently, Moy *et al.* (2009) and de Moel *et al.* (2009) have gathered more evidence, showing that the effects of ocean acidification upon foraminifera are already detectable. Moy *et al.* (2009) found that since the end of the 18th Century, test weights of Antarctic foraminifera have declined by 30 to 35%. de Moel *et al.* (2009) found that the tests of modern *Globigerinoides ruber* in surface sediments of the Arabian Sea are lighter than those found slightly deeper in the sediments.

2.3 PTEROPODA

Due to their highly soluble aragonite shells, thecosome pteropods and heteropods are likely to be the most vulnerable of the major planktic producers of $CaCO_3$. They are also likely to be the first to experience persistent decreased $CaCO_3$ saturation states.

The group of holoplanktic molluscs known as the Pteropoda consists of two orders; the shell-less gymnosomes and the shell bearing thecosomes. These two orders are now considered to be less closely related than originally thought (Lalli and Gilmer, 1989) despite superficial similarities, however, the term pteropod is still widely used. This study focuses on the order Thecosomata, which is made up of the suborders Euthecosomata and Pseudothecosomata. It also takes account of a further form of holoplanktic mollusc, the Heteropoda (revised as the superfamily Pterotracheoidea by Bouchet *et al.*, 2005). Lalli and Gilmer (1989) and Bé and Gilmer (1977) provide

detailed studies of all aspects of the thecosome pteropods. Lalli and Gilmer (1989) and Seapy (2011) provide information on the heteropods.

Both the Thecosomata and the Heteropoda have evolved wing-like structures from the foot that characterises animals in the class Gastropoda. These 'wings' are uniquely adapted to enable the animals to live their entire lives as a planktic form (Bé and Gilmer, 1977). All thecosomes and some species of heteropod create calcareous shells from aragonite, a polymorph of calcium carbonate, which is particularly susceptible to dissolution (50% more susceptible than calcite). This makes them extremely vulnerable to dissolution caused by ocean acidification.

Thecosome pteropods are a common component of the water column throughout the world's oceans, whereas heteropods are found in moderate to low abundances primarily in tropical and sub-tropical regions. Shelled pteropods are the major planktic producers of aragonite (Orr *et al.,* 2005) and are the dominant calcifers in some areas such as the Southern Ocean, an area of particular concern (Royal Society, 2005; Hunt *et al.,* 2008). Pteropods have a global distribution, but are most abundant in polar and sub-polar waters where they can reach densities of 1,000 to 10,000 individuals per cubic metre, replacing krill as the dominant zooplankton group in some areas (Royal Society, 2005; Fabry *et al.,* 2008). In such areas, pteropods are an important food source for large cetaceans and often commercially important marine organisms, such as North Pacific salmon, mackerel, herring and cod (LeBrasseur, 1966; Takeuchi, 1972).

Shelled pteropods also play an important role in the cycling of $CaCO_3$ and transport of carbon to the deep oceans. Sediment traps show that aragonite constitutes a minimum of 12% of total $CaCO_3$ flux, a value which is likely under

estimated due to dissolution of aragonite when traps are deployed in under-saturated waters (Berner and Honjo, 1981). The exact contribution of pteropod shells to the $CaCO_3$ flux is poorly understood and varies substantially on temporal and regional scales. In some areas of the Southern Ocean, thecosome shells contribute over 50% of the carbonate flux (Hunt *et al.,* 2008). South of the Antarctic Polar Front, where ocean acidification is predicted to have a great effect, the pteropod *Limacina helicina* comprises nearly all of the $CaCO_3$ export to the ocean interior (Accornero *et al.,* 2003).

Studies directly relating to the response of pteropods to ocean acidification are limited to only three of the 34 known species: *Cavolinia inflexa, Clio pyramidata and L. helicina.* There are no studies of the effects upon shelled heteropods. Feely *et al.* (2004) first considered the effects of ocean acidification upon this highly sensitive, but very important group of organisms. It was found that when exposed to a level of aragonite under-saturation predicted under the IS92a emissions scenario to occur in the Southern Ocean surface waters by the year 2100, the shells of live and swimming *C. pyramidata* began to dissolve within 48 hours. In additional experiments, Fabry *et al.* (2008) describe that when *C. pyramidata* were placed in sealed jars and ^{24}Ca was added to measure calcification rates, the accumulation of metabolic CO_2 was sufficient to reduce the aragonite saturation state to below 1. The ^{24}Ca uptake experiments reveal a progressively reduced calcification rate as the CO_2 accumulated over time. After 36–48 hours, most of the ^{24}Ca that had been incorporated into shells had dissolved back into solution. This revealed that by 36 hours, the net dissolution had exceeded the net calcification, even though the animals were still actively swimming. Orr *et al.* (2005) provide further evidence in the use of SEM images to show that when *C. pyramidata* is subject to this level of under-saturation, a

marked dissolution occurs at the growing edge of the shell aperture within the 48 hours. It was found that although specimens remained alive and swimming, etch pits had formed at the apertural margin of the shell surface on each of the 14 individuals imaged. It is suggested by the authors that this initial damage peeled back the exterior layer of the shell exposing the underlying aragonitic rods to further dissolution. Control specimens incubated in open jars showed no signs of dissolution (Fabry *et al.,* 2008). Bednaršek *et al.* (2012) have more recently reinforced these studies by also showing reduced calcification and increased dissolution of *C. pyramidata* during prolonged periods in under-saturated waters.

Comeau *et al.* (2009, 2010a, 2010b, 2012), Lischka *et al.* (2011) and Bednaršek *et al.* (2012a, 2012b) have studied directly the impact of ocean acidification on the thecosome pteropod *L. helicina,* a key species in Arctic ecosystems and *C. inflexa,* a common Mediterranean species. Comeau *et al.* (2009) immersed live specimens of the pteropod *L. helicina* in calcein stain. They were then kept in culture under controlled conditions with either a pH of 8.09 or 7.8, corresponding to pCO_2 levels of 350 and 760 ppmv respectively. The live pteropods were sampled after 2, 4 and 6 hours in culture. Their calcification rate was then calculated by observing the linear extension of their shells since being immersed in stain. It was found that, at pCO_2 levels predicted for 2100, calcification was 28% lower than at pCO_2 of the present day.

Although this new technique is very useful in species which continuously produce linear extension, new techniques will have to be developed to observe changes in calcification of species which do not continually grow. Fabry (1990) notes that some pteropod species, for example those of the genus *Cavolinia,* do not continually increase shell length or width during development. As adults

these species only increase the thickness of the shell wall and therefore change in mass may be a better measure of calcification. Roger *et al.* (2011) use a novel approach by measuring the shell porosity. Comeau *et al.* (2009) also mention that linear extension is not always a good indicator of the rate of calcification because it does not necessarily correlate with shell thickness and density. In a further study of *L. helicina*, Comeau *et al.* (2010a) found no synergistic effects of elevated pCO_2 and temperature on calcification. This result is in contrast to the response of scleractinian corals (Reynaud *et al.,* 2003). Lischka *et al.* (2011) also found that shell diameter, shell increment and shell degradation of juvenile *L. helicina* were effected by pCO_2 but not by temperature. Temperature did, however, affect mortality of pteropods, which was 46% higher at 8ºC than at the in situ temperature of 3ºC (Lischka *et al.,* 2011). Comeau *et al.* (2010a) found that, unlike the previous study on *L. helicina* (Comeau *et al.,* 2009), a decreased incorporation of calcium carbonate was not seen after a few hours of incubation. It was found that incorporation was linear throughout the 8 hour incubation and that precipitation of calcium carbonate still occurred below aragonite saturation levels. It has been suggested that this differing result is due to a number of factors. Firstly, in the more recent study, the pteropods were pre-acclimated for 24 hours prior to the incubation which may have reduced stressors and aided in their continual growth. Secondly, in the previous study (Comeau *et al.,* 2009), larger individuals were used which are comparatively more difficult to maintain under laboratory conditions. It is also possible that smaller or juvenile specimens can adapt more readily to changing environments. The fundamental conclusions of the study however, supported the previous findings, that increased pCO_2 leads to decreased calcification. The results also suggest that *L. helicina* may be more

resilient to increases in pCO_2 than originally thought. However, effects upon wild populations are already becoming detectable. Roberts *et al.* (2008) demonstrate that changes in the shell weight of *L. helicina antarctica* forma *antarctica* are already occurring in the Southern Ocean. A study of mean shell weights of this sub-species from sediment traps deployed between 1997 and 2006 show a small but detectable decadal reduction in shell weight of -1.17±0.47 µg per year. When the shells of live *L. helicina* from the Southern Ocean were inspected immediately upon collection, Bednaršek *et al.* (2012b) found that in-life dissolution is already detectable in natural pteropod populations.

A study on the species *C. inflexa* takes into account the response of larval pteropods. Comeau *et al.* (2010b) maintained specimens in controlled pH-temperature experiments at pH of 8.1, 7.82 and 7.51. These values are equivalent to pCO_2 levels of 380, 857 and 1,713 ppmv respectively. The shells of larvae subjected to a pH of 7.82 showed malformations and lower shell growth when compared to the control specimens maintained at a pH of 8.1. At pH 7.51, the larvae failed to make shells. As in the studies upon *C. pyramidata,* the pteropods were able to survive without the presence of their shells, showing a normal development. Comeau *et al*. (2010b) however, point out that having a smaller shell or no shell will have ecological and biogeochemical consequences, making it unlikely that such shell-less pteropods could survive unless they could adapt very quickly to such a change. Comeau *et al.* (2011) note that shell-less individuals of the species *L. helicina* are not known to have ever existed and would not be expected to survive for long if they did.

It is interesting to note that although calcification was significantly reduced at high pCO_2 levels in all cases (Comeau *et al.,* 2009, 2010a,b, 2012; Lischka, *et al.,* 2011), juvenile forms of *L. helicina* were still able to calcify in

waters with a pH predicted for 2100. However, it is unlikely that pteropods could maintain a positive balance between shell calcification and dissolution after prolonged periods of immersion in such water. Comeau *et al.* (2012) found that, although linear extension of juvenile shells still occurred in under-saturated waters, dissolution marks were visible on the entire shells. This supports the results of Fabry *et al.* (2008), who showed that after 36 hours, net dissolution exceeds net calcification in the species *C. pyramidata.* These studies clearly show that the response of pteropods to elevated pCO_2 levels is species specific, reinforcing the need for more direct studies on the response of pteropods.

The overall effect of ocean acidification upon these holoplanktic molluscs is therefore little understood. Many factors must be considered, such as their resilience and ability to adapt to the changes in pH and their ability to flourish in a different climate if they were forced to migrate to lower latitudes. Should the habitat of pteropods approach aragonite under-saturation, their ability to produce shells will depend on whether the net rate of calcification exceeds the rate of dissolution. This in turn is dependent upon the degree of under-saturation and the duration that animals are exposed to such waters (Fabry *et al.,* 2008). Bijma *et al.* (1999) suggest that as the aragonite saturation state of the surface ocean decreases, pteropods may secrete under-calcified or thinner structures, which could lead to increased predation pressures and ultimately also the decline of pteropods. At present, our knowledge of pteropod distributions, migrations and life cycles are limited and thus our ability to predict their potential to evolve a tolerance to ocean acidification is poor. It is thought that high latitude pteropods (which will be affected first) have generation times of 0.6 to 1.5 years (Kobayashi, 1974; Dadon and de Cidre, 1992; Gannefors *et*

al., 2005). If the projected shoaling of saturation state occurs, this allows only 50 to 150 generations for the species to adapt to these changes (Fabry *et al.,* 2008) by the year 2100. This is unlikely, since although surface ocean pH has been reduced to a comparable level in the past, the rate of change has never before been so rapid and therefore, where once adaptation was possible, it now seems improbable. However, some species may already be experiencing such variations in ocean pH on a daily basis. As diel vertical migrators, shelled pteropods cover several hundred metres vertically through the surface ocean per day (Bé and Gilmer, 1977). It is also thought that high latitude overwintering pteropods are also subjected to extremely low water pH, since they tend to move to a lower position in the water column (Comeau *et al.,* 2012). The exact habits of pteropods are poorly known but it is expected that as the ACD shoals, pteropods will be exposed to increasingly corrosive waters during their migrations (Comeau *et al.* 2009). Comeau *et al.* (2011) modelled the effect of ocean acidification on pteropod calcification across the depth range of pteropod migration in a number of sites world-wide. It was found that high-latitude pteropods are at the highest risk of migrating through waters under-saturated with respect to aragonite. They also found that the aragonite saturation of surface waters across the Arctic would change at varying rates due to differing physical-chemical properties.

It is possible that the diel migration of pteropods may help them to adapt to ocean acidification. Fabry *et al.* (2008) note that in present day surface waters, the variability in pCO_2 values are greater than those expected for average surface waters in 2100. Comeau *et al.* (2011) suggest that although some vertical migratory pteropods may already be experiencing under-saturated waters, it is only for limited periods of time, which may not affect

calcification. Maas *et al.* (2011) studied the effects of elevated pCO_2 on oxygen consumption and ammonia excretion of five species of pteropod from tropical regions of the Pacific Ocean (1000 ppm). It was found that the species *Diacria quadridentata,* which does not migrate, responded to the increased pCO_2 by reducing oxygen consumption and ammonia excretion. However, the metabolism of species *Hyalocylis striata, C. pyramidata, Diacavolinia longirostris* and *Creseis virgula,* which regularly migrate into oxygen minimum zones were not affected by the increased pCO_2 levels. These results suggest that the natural environment of some species can influence their response and resistance to ocean acidification (Maas *et al.,* 2011).

If pteropods are unable to adapt they will have to alter their migration patterns. Gradually their habitat will be limited, first vertically in the water column and then latitudinally (Orr *et al.,* 2005; Comeau *et al.,* 2011). Fabry *et al.* (2008) express concerns of the ability of polar animals, adapted to living in low temperature regions, to move to warmer, more carbonate rich regions.

2.4 PREVIOUS STUDIES OF PTEROPODS IN THE FOSSIL RECORD

Although living pteropods and heteropods are found globally in modern oceans, their fossil shells, being fragile and sensitive to dissolution, are more difficult to find. Consequently, the stratigraphic range of pteropod shells only extends to the Paleogene (Lokho and Kumar, 2008). The first known occurrence of pteropods is in the latest Paleocene of Europe (Janssen and King, 1988) and North America (Janssen *et al.,* 2007). The stratigraphic range of heteropods is not known.

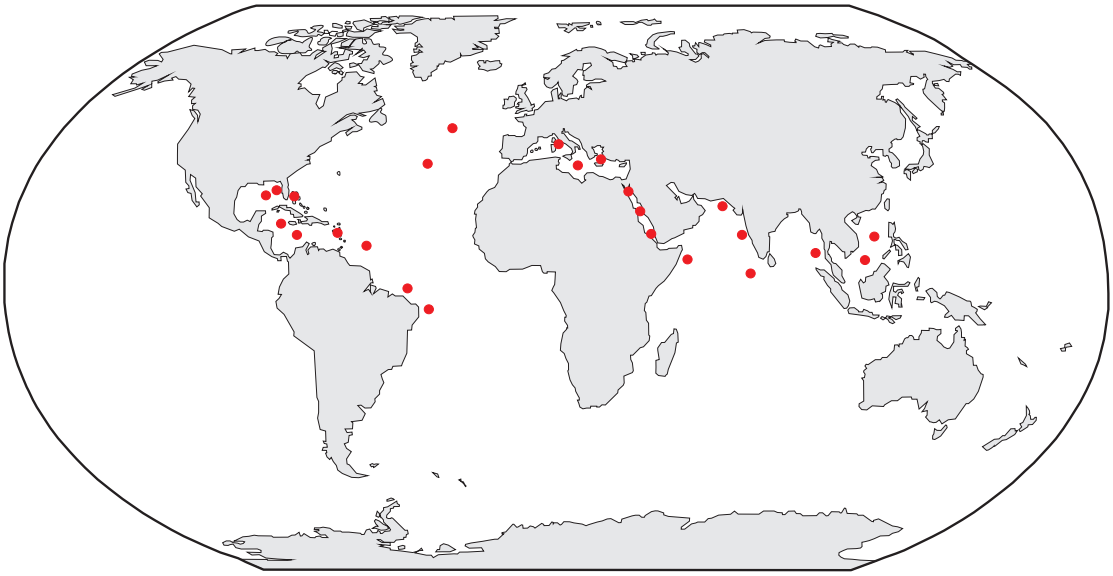

Figure 2.2 World map showing the position of previous studies of down-core assemblages, abundances and preservation of pteropods in the recent (Late Pleistocene to recent) fossil record.

There have been several previous studies investigating the down-core assemblages, abundances and preservation of pteropods in the fossil record at a number of locations (see Table 2.1, Fig. 2.2). Several of these authors have also extended their research to consider the condition of the pteropod shells. The details of such observations vary from merely mentioning periods of particularly good or bad preservation, to providing complete and detailed data that led to the creation of the LDX scale (Gerhardt *et al.,* 2000). This scale has subsequently been used by Klöcker and Henrich (2006) and Klöcker *et al*. (2006, 2007) to produce detailed records of the variations in preservation of pteropods from the Pakistan Shelf and Somalia respectively.

Author and Date	Location
Chen, 1968	Gulf of Mexico, Caribbean, Crete
Herman, 1971	Mediterranean
Damuth *et al.,* 1975	Western Equatorial Atlantic
Rottman, 1979	South China Sea
Almogi-Labin *et al.*, 1982	Red Sea
Ivanova, 1985	Gulf of Aden
Almogi-Labin *et al.*, 1986	Red Sea
Biekart, 1989	Tyrrhenian Sea
Cullen and Droxler, 1990	Indian Ocean
Gardulski *et al.,* 1990	Off shore Florida
Ganssen *et al.,* 1991	Eastern North Atlantic
Almogi-Labin, 1991	Central Red Sea
Haddad and Droxler, 1996	Caribbean, Western North Atlantic
Wang *et al.*, 1997	South China Sea
den Dulk *et al.,* 1998	Northern Arabian Sea
von Rad *et al.,* 1999	Pakistan
Gerhardt *et al.*, 2000	Brazil continental slope
Buccheri *et al.,* 2002	Tyrrhenian Sea
Klöcker and Henrich, 2006	Pakistan Shelf
Klöcker *et al.*, 2006	Arabian Sea
Klöcker *et al.*, 2007	Somalia
Singh, 2007	Eastern Arabian Sea
Messenger *et al.,* 2010	Caribbean (Montserrat)
Sijinkumar *et al.,* 2010	Andaman Sea

Table 2.1 Authors and locations of previous studies investigating down-core assemblages, abundances and preservation of pteropods in the recent (Late Pleistocene to recent) fossil record.

As far back as 1968, when looking at Pleistocene pelagic sediments, Chen (1968) realised that pteropod shells were more abundant during colder periods. It was found that the pteropod distribution throughout several cores (including two from the Caribbean Sea) correlated with the Ericson climatic curve (Chen, 1968, fig. 1) and with curves constructed on the basis of alternating cold and warm water species of pteropods. In several of the cores studied by Chen (1968), horizons of abundant pteropods were found which correspond to the most recent glacial period (MIS 2). This trend was found in cores from the Gulf of Mexico, the Venezuela Basin, the Caribbean Sea, the Mediterranean Sea and the Red Sea (Chen, 1968). Chen (1968) suggests that their occurrence was controlled by Late Pleistocene climate changes. This occurrence was also found by other authors in the Arabian Sea (Klöcker *et al.,* 2006; Singh, 2007), in the Andaman Sea (Sijinkumar *et al.,* 2010), in the Red Sea (Almogi-Labin *et al.*, 1991), off-shore Somalia (Klöcker and Henrich, 2006), in the Indian Ocean (Cullen and Droxler, 1990), in the South China Sea (Wang *et al.*, 1997), off-shore Florida (Gardulski, *et al.,* 1990), on the western flank of the Great Bahama Bank (Eberli *et al.,* 1997; Messenger *et al.,* 2010), in the Caribbean Sea (Messenger *et al.,* 2010) and in the Eastern North Atlantic (Ganssen *et al.,* 1991). It has also been suggested that this occurrence of well-preserved pteropod remains is the product of a deglaciation preservation spike (Berger, 1977). Berger (1977) describes this world-wide phenomenon as a pteropod-rich layer present at the end of the last glacial period, although, the exact timing and cause of this event are in some dispute. In cores from the South China Sea (Wang, *et al.,* 1997) and the Caribbean Sea (Haddad and Droxler, 1996), further concentrations of pteropod shells were found, corresponding to previous glacial periods MIS 4 and MIS 6.

Similarly, several authors have noted the absence or low abundance of pteropod remains during interglacial periods. Almogi-Labin *et al.* (2000) record the near absence of pteropods during interglacials (MIS 13, 11, 9, 7, 5 and 1) and Wang *et al.* (1997) found an increase in the occurrence of fragments of planktic foraminifera and a decrease in the abundance of pteropod shells during interglacial periods.

Such a number of occurrences of well preserved pteropods coinciding with glacial periods and the absence or low abundance of pteropods during interglacial periods clearly demonstrates that this trend is of global significance. This trend appears to be caused by variations in ocean carbonate saturation levels over time which can be created by several processes, reflecting either a post-depositional dissolution signal or an in-life dissolution/calcification signal. During cold glacial periods, atmospheric CO_2 levels are lower, creating lower dissolved CO_2 and higher carbonate saturation in the water column and particularly in the surface ocean water. This not only allows calcifying plankton to produce and maintain stronger shells, but also for these shells to reach the ocean floor and become buried in sediments without being dissolved. During interglacial periods, CO_2 levels are higher in both the atmosphere and the ocean, which leads to low carbonate saturation levels, poorly calcified shells which undergo in-life corrosion and an increased chance of dissolution of shells on the sea floor. The trend shown in a core can be due to either, or both of these processes and is largely dependant on the water depth and position of the Aragonite Lysocline (ALy), the depth where water begins to become undersaturated with respect to aragonite, at the site.

Studies in the western Equatorial Atlantic (Damuth *et al.,* 1975), on the Brazilian Slope (Gerhardt *et al.*, 2000) and in the Caribbean Sea (Haddad and

Droxler, 1996), present the reverse trend, with poor preservation of pteropod shells during glacial periods and enhanced preservation during interglacial periods. This trend is attributed to an increase in the volume of corrosive bottom waters during glacial periods, which dissolves pteropod shells and is generally found at deep-water Atlantic sites.

3 METHODOLOGY

3.1 SITES AND COLLECTION OF CORES

When choosing a site in which to study pteropods and other holoplanktic molluscs within the sedimentary record, several factors must be taken into account to reduce the impact of post-depositional dissolution: water temperature, depth and the depth of the aragonite lysocline (ALy). Thecosome pteropods and heteropods produce shells made of aragonite, a polymorph of calcium carbonate, which is 50% more susceptible to dissolution than calcite. Therefore, although such holoplanktic gastropods are found living in oceans worldwide (Bé and Gilmer, 1977), the occurrence of their shell remains is limited to sediments in relatively warm, shallow water, which is super-saturated with respect to aragonite. This makes it difficult to find regions where pteropods are preserved in the sediment. In more than 98% of oceanic regions, all of the aragonite shells produced by pteropods (and heteropods) are completely dissolved whilst sinking through the water column or upon reaching the ocean floor (Byrne *et al.,* 1984; Fabry, 1990).

For these reasons and with knowledge of pteropod remains having been previously found in these areas, three study sites have been chosen: one in the Caribbean Sea, one in the Mediterranean Sea and one in the Indian Ocean.

3.1.1 THE CARIBBEAN SEA: CAR-MON 2, JC18-19 AND JR123-35-V

Cores CAR-MON 2 (Caraval Cruise of the R.V. *L'Atlante*, CAR-MON), JC18-19 (Cruise 18 of the R.R.S. *James Cook*, JC) and JR123-35-V (Cruise 123 of the R.R.S. *James Clark Ross*, JR; vibrocore, V) were all collected close to the Island of Montserrat, in the Caribbean Sea (Table 3.1). This area of the Caribbean Sea is situated towards the northern end of the Lesser Antilles

volcanic island arc, which is being formed by the subduction of the North Atlantic Plate beneath the Caribbean Plate. The volcanic arc is 800 km long and splits into two groups of islands north of Martinique (Le Friant *et al.,* 2008) separated by the Anegada Passage. The sea around Montserrat, where CAR-MON 2, JC18-19 and JR123-35-V were collected, is relatively shallow and super-saturated with respect to aragonite. Water chemistry around the Lesser Antilles island arc is complicated by influences of several water masses flowing between the islands and through a number of deeper passages into the Caribbean Sea. Gerhardt and Henrich (2001) found that the influence of Antarctic Intermediate Water (AAIW), towards the south of the island arc, caused moderate to very poor preservation of pteropods (below 700 m water depth). However, towards the north of the island arc, where Montserrat is situated, the influence of AAIW is minor (maximum 10% of water composition) due to a large volume of Upper North Atlantic Deep Water (UNADW), which flows through the nearby Anegada Passage (Fig. 3.1). This area consequently records very good preservation of pteropods. Gerhardt and Henrich (2001) place the ALy at 2000 m and the Aragonite Compensation Depth (ACD) at 3800 m water depth in this area. CAR–MON 2, JC18-19 and JR123-35-V were collected in 1102 m, 1130 m and 765 m water depth respectively, which is well above the present day ALy and ACD thus discounting any effects that this may cause. It also explains why the sediments have retained such an excellent record of pteropods, heteropods and other marine molluscs.

During the period February to March 2002, the 'Caraval' cruise of the R.V. *L'Atalante* gathered marine survey data and collected a number of cores from submarine areas adjacent to the island of Montserrat (Le Friant *et al.,* 2004; Le Friant *et al.,* 2008). Of these, CAR-MON 2 (Fig. 3.2) was chosen to

undergo stratigraphical studies as it preserves the longest (575 cm) record for oxygen isotope stratigraphy. CAR-MON 2 was collected by piston corer from a location approximately 55 km to the south west of the island of Montserrat (16°27.699'N, 62°38.077'W) at a water depth of 1102 m. CAR-MON 2 is the primary core used in the study of this area. The two further cores, JC18-19 (megacore) and JR123-35-V (vibrocore), have also been analysed for microfossils to check the reproducibility of data from CAR-MON 2.

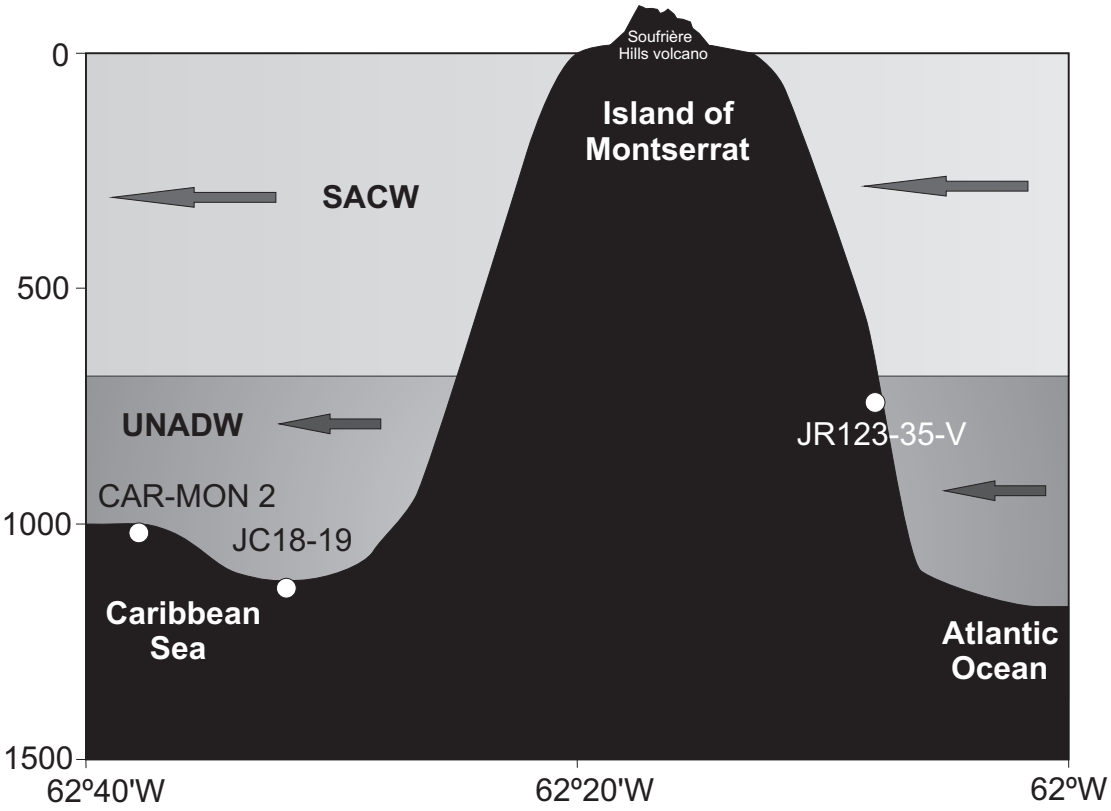

Figure 3.1 Modern water masses around the island of Montserrat, with the relative position of study sites. South Atlantic Central Water (SACW), Upper North Atlantic Deep Water (UNADW). UNADW contains a maximum of 10% Antarctic Intermediate Water. Information from Gerhardt and Henrich (2001).

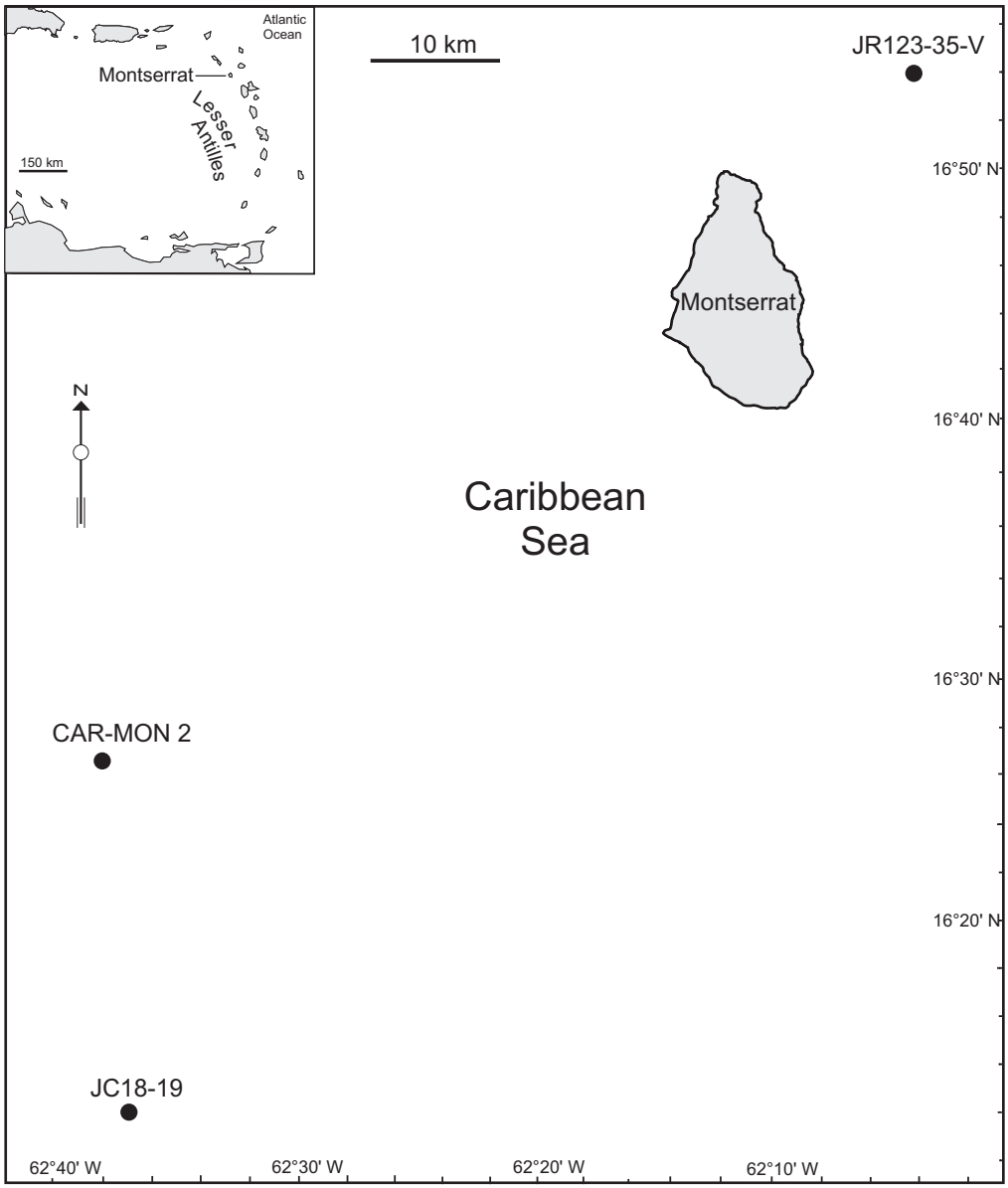

Figure 3.2 Location of core sites in the Caribbean Sea. CAR-MON 2 and JC18-19 are situated to the south-west of the Island of Montserrat, JR123-35-V is situated to the north-east.

Core JR123-35-V was collected in May 2005 during a research voyage of the RRS *James Clark Ross.* It was collected (16 km) to the north-east of Montserrat (16°53.50'N, 62°04.00'W) in 765 m water. JR123-35-V is 504 cm long and has been studied and dated previously by Trofimovs *et al.* (2010).

In December 2007, further sediment core samples were collected from 35 sites off-shore from Monserrat by the RRS *James Cook* (Cruise JC18).

Gravity core JC18-19 was collected 52 km to the south-west of the Island of Montserrat (16°22.70'N, 62°34.41'W) in 1130 m of water. Core JC18-19 is 365 cm long and has been studied previously by Cassidy (2012).

All three Caribbean cores (CAR-MON 2, JC18-19 and JR123-35-V) were collected by the crew and scientists of the respective cruises. Detailed descriptions of the techniques used in retrieving these cores are discussed in Le Friant *et al.* (2008), Trofimovs *et al.* (2010) and Cassidy (2012).

3.1.2 THE MEDITERRANEAN SEA: B5-1

The entire Western Mediterranean Sea is super-saturated with respect to calcium carbonate (Schneider *et al.,* 2007). Inflow of Atlantic Water (AW) at the straits of Gibraltar travels eastwards, gradually increasing in temperature and salinity and forming Modified Atlantic Water (MAW) in the eastern Mediterranean Sea. Winter winds then chill this water, causing it to sink, forming Levantine Intermediate Water (LIW), which travels westwards and leaves the Mediterranean Sea again through the straits of Gibraltar (Fig. 3.3). Eastern and Western Mediterranean Deep Waters (EMDW, WMDW) are also formed by strong evaporation and cooling of surface waters (Schneider *et al.,* 2007).

Climatic events within the Mediterranean Sea tend to be amplified due to the semi-enclosed nature of the basin (Pérez-Folgado *et al.,* 2003) and the relatively high sedimentation rate produces a high resolution sedimentary record. For these reasons, fossil remains of planktic foraminifera and holoplanktic gastropods are abundant in the sediments of the Mediterranean Sea, making this an ideal site for studying the effects of climate change upon calcareous micro-zooplankton.

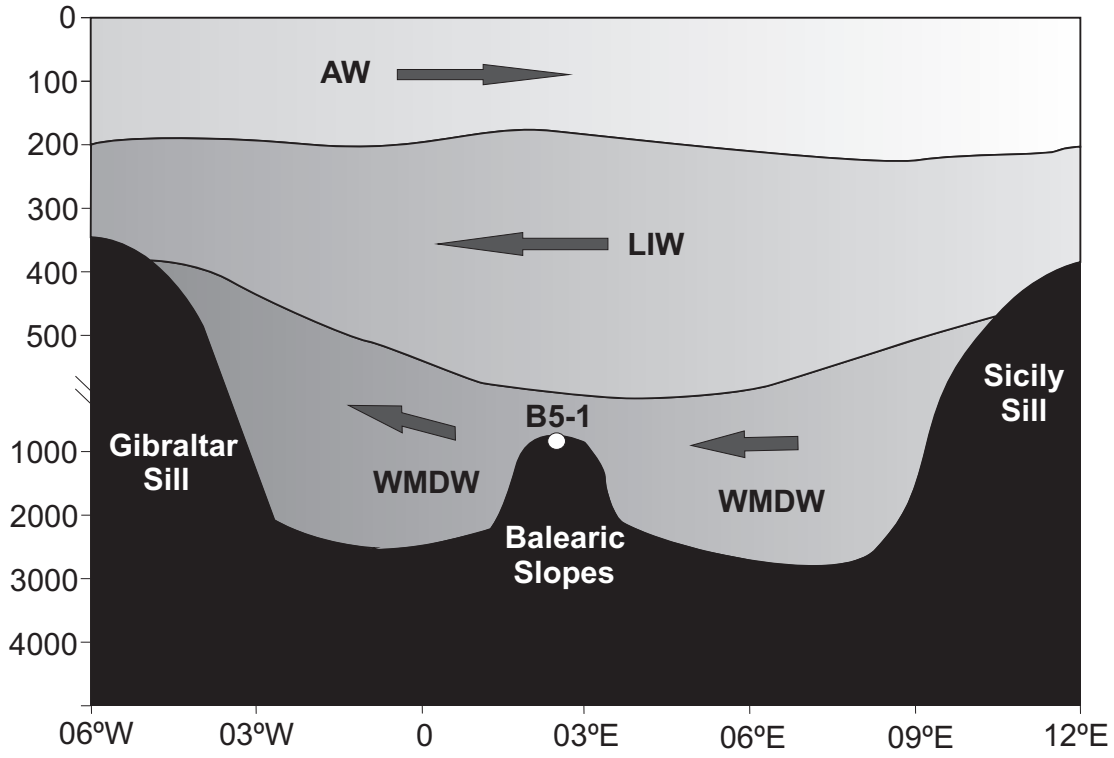

Figure 3.3 Modern water masses in the western Mediterranean Sea, with the relative position of study site B5-1. Atlantic Water (AW), Levantine Intermediate Water (LIW), Western Mediterranean Deep Water (WMDW). Information from Paul *et al.* (2001).

During May 2010, the BIOFUN'10 cruise of the R.V. *Urania* collected a variety of marine survey data (water and sediment) offshore from the Balearic Islands in the western Mediterranean Sea. Of the cores collected, gravity core B5-1 (Table 3.1) was chosen for analysis as it was collected in relatively shallow water (1519 m) and appears to be unaffected by turbidites, which are often recorded from the Balearic Abyssal Plain (for example, Hoogakker *et al.,* 2004). B5-1 was collected by gravity corer from a location approximately 23km (Fig. 3.4) to the south-east of Mallorca (39°14.942'N, 03°25.052'E). It has a length of 494 cm.

The BIOFUN'10 cruise formed the 'field work' element of my research project (Appendix 8.1.1.A). During the cruise, I helped in the collection of water

and sediment for analysis. For the purpose of this study, only one core, B5-1 has been analysed and the collection techniques are described below.

Gravity cores were collected using a 6 m long metal tube of 9 cm diameter, which was weighted at the top end. For each core, a plastic liner was inserted inside the metal tube and sealed at the base with a core catcher (to prevent sediment escaping once collected). Once retrieved, the working gravity cores were sampled onboard the ship to allow parallel samples to be collected from both halves of the cores for different studies. A replica archive core was also collected at each site: the archive core for B5-1 is recorded as B5-2.

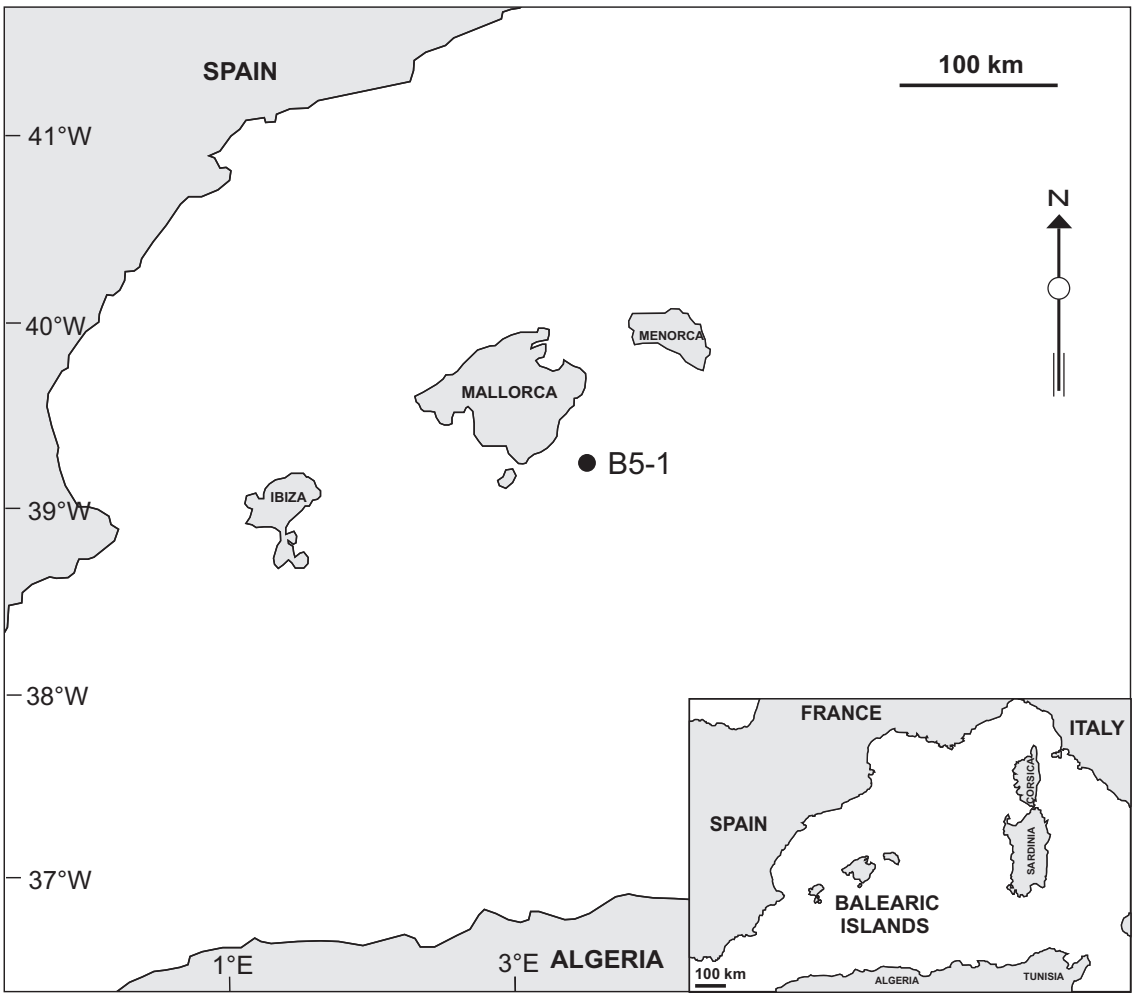

Figure 3.4 Location of core site B5-1 situated to the south-east of the Island of Mallorca.

Each core within its plastic liner was cut into approximately 1m lengths as it was removed from the gravity corer. These lengths were appropriately labelled and capped at each end. The working cores were then sliced length-ways in half. Using a scalpel and a small spatula, sub-samples of the core were then taken at 5 cm intervals throughout its length, producing half discs of 9 cm diameter. The outermost surface of each sample was removed to reduce the risk of contamination from smearing within the corer. The top 5 cm of sediment was sampled at higher resolution (at 1 cm intervals) and half of each of these was preserved in formalin for later analysis of the benthic foraminifera (separate study). All other samples were placed in foil boats and dried in an oven at 30°C for 4 hours. All samples were then placed in labelled plastic storage bottles or bags ready for transportation to the UK.

The sampled core halves were plugged to maintain the integrity of the core, wrapped in plastic film and frozen for transportation. The archive cores, in their 1m lengths, were placed in a refrigerator at 4°C, ready for transportation. The dried samples, samples in formalin and the frozen and refrigerated core sections, were transported to La Spezia, Italy. The dried samples and samples in formalin were shipped to the UK, arriving in June 2010. Cores from the BIOFUN'10 cruise are in cold storage at the Istituto di Scienze Marine, La Spezia, Italy.

3.1.3 THE INDIAN OCEAN: ODP HOLE 716B

Water circulation in the northern Indian Ocean is complicated by monsoonal influences (Fig. 3.5) and by the unique oceanographic setting. The floor of the equatorial Indian Ocean is comprised of a number of deep basins and several north-south trending topographic high ridges (Cullen and Droxler,

1990). ODP Site 716 is situated in a broad shallow basin on one of these ridges, the Chagos-Laccadive Ridge, and lies within the Maldives Islands. The water masses in this area (Fig. 3.5) are composed of the Indian Equatorial Water (IEW), which lies between 0–500 m, the Red Sea-Persian Gulf Intermediate Water (RSPGIW), which lies between 500–1500 m and the Circumpolar Deep Water (CDW), which lies between 1500 m and the sea floor (Emery, 2001). Climate and oceanography in the Indian Ocean is strongly influenced by the monsoonal wind system, which affects the cycling and upwelling of nutrients in the ocean. Strong monsoonal winds cause an increase of nutrients in surface waters, which ultimately lead to increased surface water productivity. This in turn creates a mid-water Oxygen Minimum Zone (OMZ, Fig. 3.5) by increasing the input and decay of organic matter in sub-surface waters. The increasing concentration of dissolved inorganic carbon then causes a lowering the pH, shoaling the ALy (Klöcker *et al.,* 2006).

In the Indian Ocean, the calcite saturation depth ranges from 2900 to 3900 m, with the deepest saturation situated in the central Indian Ocean (Sabine *et al.,* 2002). The ALy is extremely shallow in comparison to the Caribbean and Mediterranean Seas, between 200 and 1400 m, with the deepest saturation levels occurring to the south-west (Sabine *et al.,* 2002). At ODP Site 716, the ACD is positioned at 600 m, just 100 m below the coring site (Sabine *et al.,* 2002). However, pteropod remains have been found previously from this area (Gischler, 2006) and have also been noted for their abundance within ODP Hole 716B (Cullen and Droxler, 1990; Sarkar and Gupta, 2009). With such a shallow ACD, it is likely that this area will suffer greatly from the effects of modern ocean acidification and any shoaling of the ACD.

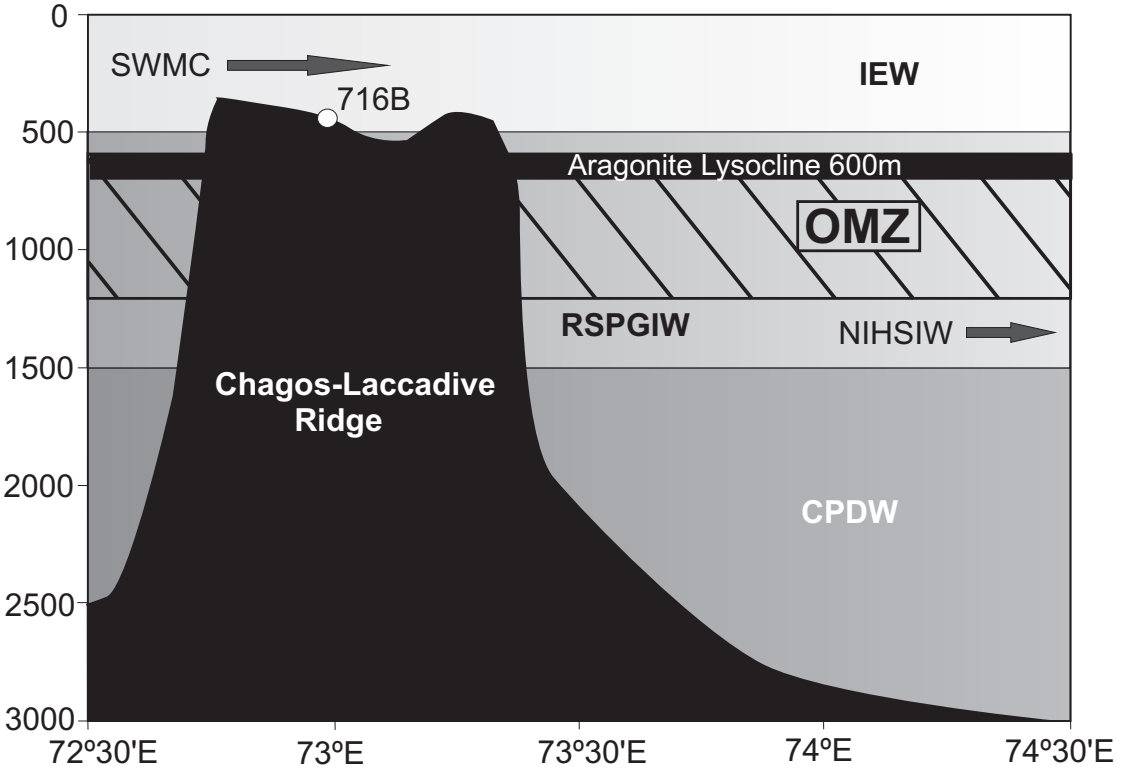

Figure 3.5 Modern water masses around the Chagos-Laccadive Ridge in the Indian Ocean, with the relative position of ODP Site 716, Hole B. Water masses include the Indian Equatorial Water (IEW), Red Sea-Persian Gulf Intermediate Water (RSPGIW) and the Circumpolar Deep Water (CDW). Currents include the summer South West Monsoon Current (SWMC) and the North Indian High Salinity Intermediate Water (NIHSIW). The Oxygen Minimum Zone (OMZ) for the Arabian Sea is applied to this area, producing an ALy at 600m. Information from Emery (2001) and Sabine *et al.* (2002). Partly modified from Sarkar and Gupta (2009).

ODP Hole 716B was collected by the Ocean Drilling Program in 1987 as part of Leg 115 (Table 3.1). Of all the cores collected during this leg, 716B has been chosen because of its shallow position, in the centre of the Maldives Ridge (04°56.0'N, 73°17.0'E) in 533.3 m water depth (Fig. 3.6). In this area of the Indian Ocean, calcium carbonate saturation is generally low, with the ALy at only 600 m water depth. However, pteropod remains have previously been recorded from this core (Backman *et al.,* 1988) and it is therefore suitable for

microfossil analysis in this study. Hole 716B was collected by hydraulic piston corer and has a length of 267.4 m. For the purpose of this study, only the uppermost 13 m of core was analysed for microfossil content.

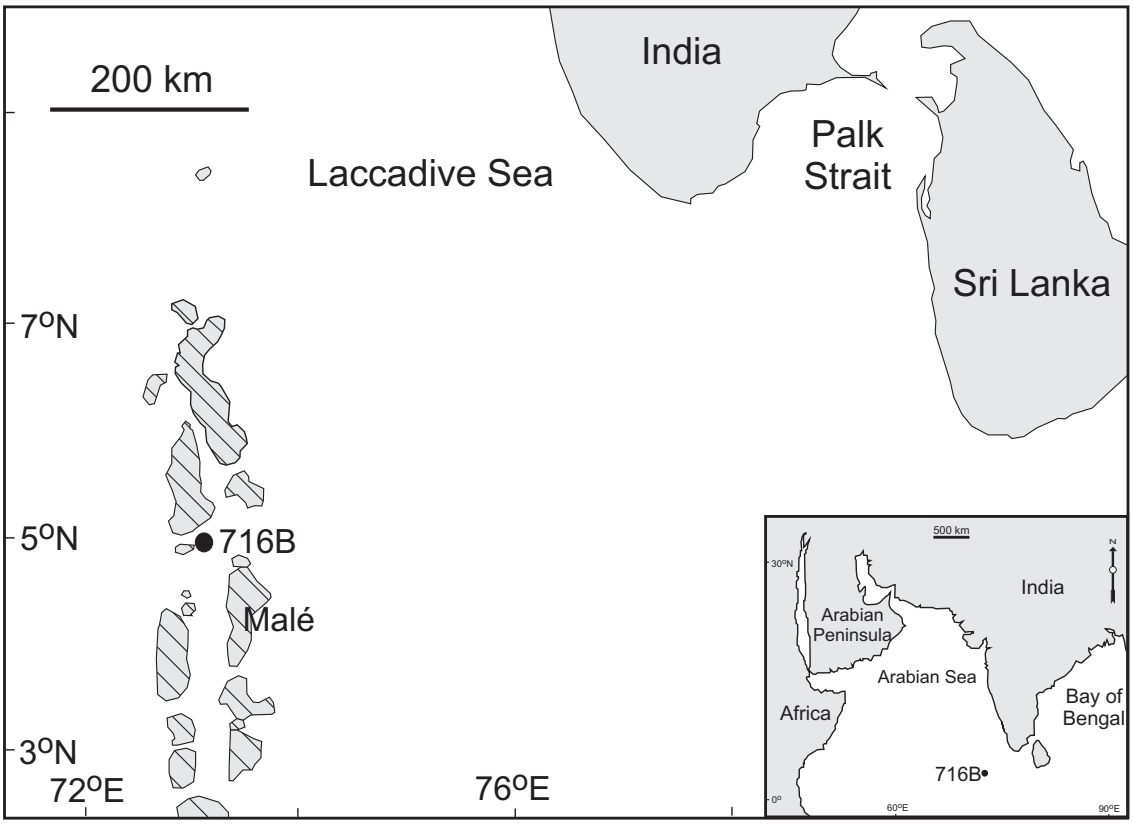

Figure 3.6 Location of ODP Site 716, Hole B situated on the Maldives Ridge, to the west of the Island of Kashidhoo. Hatched areas are lagoonal regions and groups of Maldives Islands.

Core	Location	Present Water Depth (m)
CAR-MON 2	16°27.69'N, 62°38.07'W	1102
JC18-19	16°22.70'N, 62°34.41'W	1130
JR123-35-V	16°53.50'N, 62°04.00'W	765
B5-1	39°14.94'N, 03°25.05'E	1519
716B	04°56.00'N, 73°17.00'E	533

Table 3.1 Summary of cores analysed in this study.

3.2 LABORATORY BASED SAMPLE COLLECTION AND PROCESSING

3.2.1 CAR-MON 2, JC18-19 AND JR123-35-V

All CAR-MON 2 samples analysed in this study from 90 cm to 575 cm were processed by M.B. Hart and E.J. Lock as reported by Le Friant *et al.* (2008). Samples from 0 cm to 90 cm were collected by A. Le Friant and processed by D. Wall-Palmer. Initial sub-sampling was carried out in Paris at the Institut de Physique du Globe de Paris (IPGP), with subsequent sample preparation at Plymouth University. Following the methodology of Le Friant *et al.* (2008) for the lower 90 cm to 575 cm section of the core, sediment for the upper 90 cm was sampled at 5 cm intervals. No chemicals were used to disaggregate the sediment, or at any stage in the processing. The samples were first dried and weighed, setting aside a small proportion as an archive. The samples were then soaked in de-ionised water, washed over a stainless steel 63 μm sieve and filtered. The >63 μm sediment was air dried. During the processing of the upper 90 cm, the <63μm fraction was not collected. This is because a <63μm fraction record of the upper 90 cm of CAR-MON 2 already exists, having been collected during previous processing of a replica set of samples, carried out by M.B. Hart and E.J. Lock.

Sampling of JC18-19 and JR123-35-V was carried out at the Southampton National Oceanographic Centre BOSCORF core store in December 2011 by D. Wall-Palmer. Both cores were sampled at varying intervals to coincide with key climatic events (identified by previous stable isotope analysis). Approximately 2 cm^3 of sediment was removed for each sample using a scalpel and spatula, avoiding the outer surface of the core to reduce the risk of contamination. All sample processing was carried out at Plymouth University following the same methodologies as those applied to the

samples of CAR-MON 2. For JC18-19 and JR123-35-V, neither the <63μm fraction nor an archive of each sample was retained.

3.2.2 B5-1

Sample collection was carried out by D. Wall-Palmer on board the R.V. *Urania.* All subsequent sample processing was carried out at Plymouth University by D. Wall-Palmer. Dried samples for gravity core B5-1 were gently disaggregated into large lumps and a small fraction of the sample was set aside as an archive. The remaining sediment was weighed and then re-hydrated using deionised water. Each sample was then sieved over a 63 μm sieve, retaining the <63 μm fraction. The thoroughly washed >63 μm fraction was then filtered, air dried and placed in vials for later microfossil analysis. The <63 μm fraction was filtered, air dried and then homogenised with a pestle and mortar. This has been stored at Plymouth University in case it is required for stable isotope analysis.

3.2.3 716B

Sampling of ODP Hole 716B was carried out at the Kochi Core Centre, Japan by an IODP curator. Wet sediment samples arrived at Plymouth University in September 2011 in sealed bags. These were kept refrigerated until processing. All sample processing was carried out at Plymouth University by D. Wall-Palmer. Samples for ODP Hole 716B were air dried and gently disaggregated into large lumps. A small fraction of the dried sample was set aside as an archive. The remaining sediment was weighed and then re-hydrated using deionised water. Each sample was then sieved over a 63 μm sieve, retaining the <63 μm fraction. The thoroughly washed >63 μm fraction

was then filtered, air dried and placed in vials for later microfossil analysis. The <63 μm fraction was filtered, air dried and then homogenised with a pestle and mortar. This has been stored at Plymouth University in case it is required for stable isotope analysis.

3.3 GRAIN SIZE ANALYSIS

The grain size of all samples was analysed to determine the mean grain size (for the production of logs) and the characteristics of any abnormal layers or volcanic ash previously recorded. Analysis was carried out using a stack of sieves ranging in size (500 μm, 250 μm, 125 μm and 63 μm). The mass of each fraction was measured to provide a proportion of each size fraction (Appendix 8.2.1.1, 8.2.2.1, 8.2.3.1). The proportion was then multiplied by the mid-grain size of each size fraction (1000 to 500 = 750 μm; 500 to 250 = 375 μm; 250 to 125 = 187.5 μm; 125 to 63 = 94 μm; 63 to 0 = 31.5 μm) to calculate the mean grain size. Samples rarely contained grains larger than 1000 μm, so the maximum grain size was set as 1000 μm. For CAR-MON 2, the <63 μm sediment had previously been removed from the sample. However, by calculating the average grain size >63 μm and knowing the percentage of sediment >63 μm (Le Friant *et al.,* 2008), it was possible to calculate the average grain size (Appendix 8.2.1.1.B). For all cores, the percentage of fine sediment <63 μm was also calculated (excluding CAR-MON 2, which was calculated by Le Friant *et al.,* 2008) by weighing dried, original sediment before and after processing.

3.4 MICROFOSSIL ANALYSIS

3.4.1 TESTING THE PTEROPOD PICKING METHODOLOGY

Due to differences in the methodologies employed by previous authors to collect pteropods, an initial study was carried out to determine the best method (Appendix 8.1.2.A). Many authors (Klöcker *et al.,* 2006; Klöcker and Henrich, 2006) use a minimum size fraction of 125 μm when collecting pteropods from sediments, while others (Almogi-Labin, 1982; Almogi-Labin *et al.,* 1986, 1991; Wang *et al.,* 1997) use a minimum size of 150 μm. To resolve this difference in methodology, just over 300 pteropod specimens were collected from two size fractions; 125–150 μm and >150 μm (sediment from CAR-MON 2 80–81 cm). It was found that the 125–150 μm sediment contained a large number of unidentifiable juvenile specimens of pteropods and the veliger shells of juvenile shell-less gymnosome pteropods. This fraction also contained an unrepresentative spread of species and those species well represented were equally or better represented in the larger size fraction (>150 μm). For microfossil analysis, sediment was therefore separated into two size fractions, 150–500 μm and >500 μm.

3.4.2 PTEROPOD AND HETEROPOD PICKING METHODOLOGY

For all cores, pteropods and heteropods were collected from both the 150–500 μm and >500 μm size fractions. Just over 300 (or until the sample was exhausted) pteropod specimens were collected from each size fraction. From collection curves produced during microfossil analysis, it was found that 300 specimens provided representatives of all species present for both size fractions (Fig. 3.7). Only whole specimens and fragments of pteropod and heteropod that have retained their protoconch were counted. Some authors choose to count fragments as specimens (Rottman, 1979; Klöcker and Henrich, 2006), however, Gerhardt *et al.* (2000) noted that pteropod tests are generally

very fragile and thus susceptible to mechanical damage, despite careful treatment during washing and sieving of the sediment. Therefore, counting fragments is likely to distort the actual pteropod abundance as one individual may become many fragments. Only counting those fragments which retain the protoconch will not distort the results since there is only one protoconch per specimen. This is also standard practice in the picking of foraminifera.

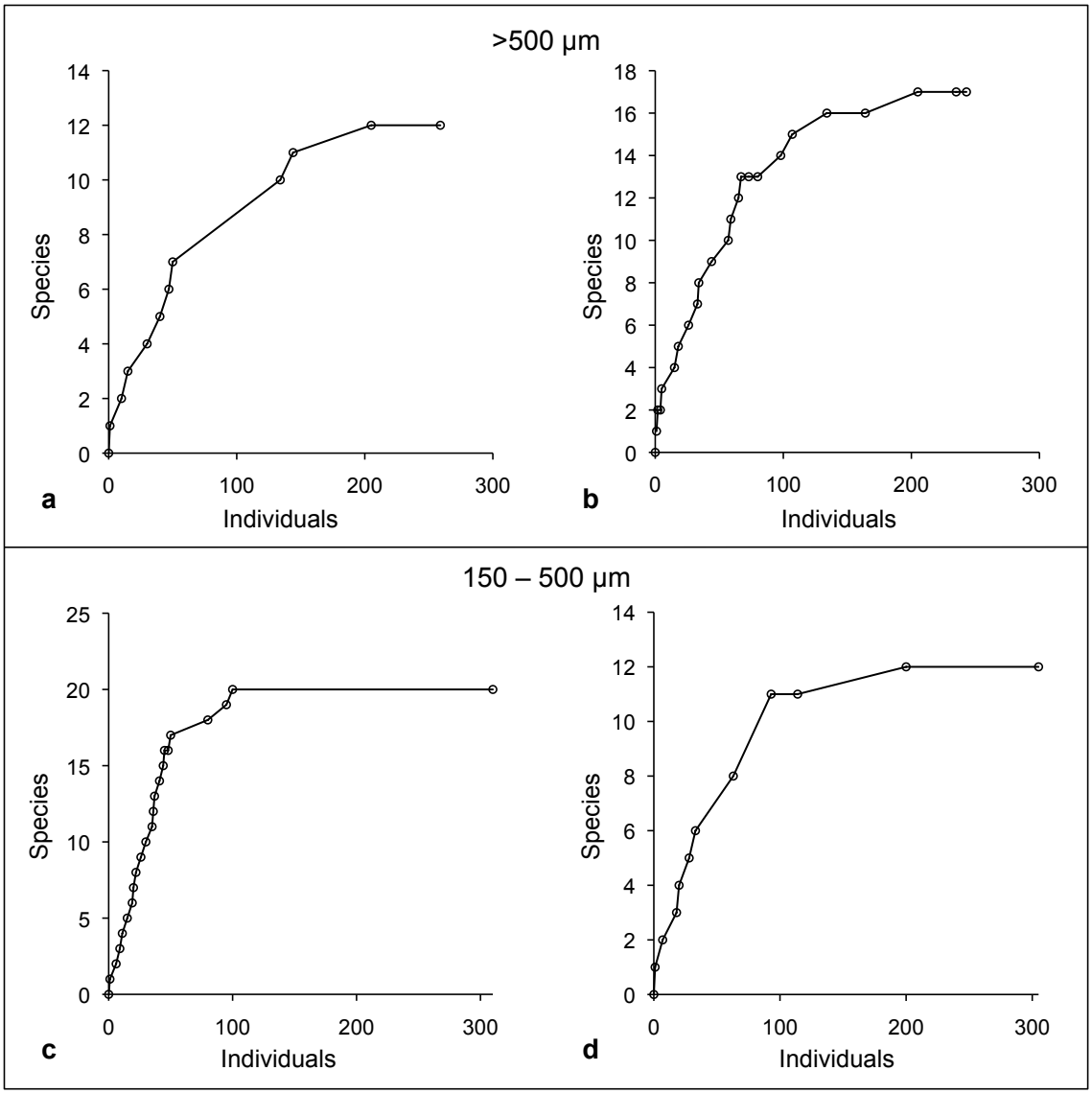

Figure 3.7 Examples of pteropod and heteropod collection curves, a) >500 µm CAR-MON 2 35–36 cm; b) >500 µm 716B 425–426 cm; c) 150–500 µm 716B 15–16 cm; d) 150–500 µm B5-1 10–11 cm.

Each size fraction was spread over a picking tray and observed using a binocular microscope (Olympus SZ11). Using a damp paintbrush, specimens were picked, sorted by species and mounted on slides for identification and photographing. Extant Euthecosome and Pseudothecosome pteropod species are well described. Consequently, identification of specimens without the soft body parts is possible by using the keys published by Bé and Gilmer (1977) and van der Spoel (1976), with addition of information from Tesch (1946, 1948). Identification of heteropods was more problematic, as species are not well defined and are often given different names by different authors. However, identification of most species was made using Tesch (1949), Thiriot-Quiévreux (1973), van der Spoel (1976) and the online guide by Seapy (2011). In this way, the abundance and diversity was found for each sample.

3.4.3 PLANKTIC FORAMINIFERA PICKING METHODOLOGY

Just over 300 (or until the sample was exhausted) planktic foraminifera and fragments of planktic foraminifera were collected from both the 150–500 μm and >500 μm size fractions of each sample. Collection curves produced at the time of fossil collection found that 300 specimens adequately represented all species present (Fig. 3.8). Planktic foraminifera identification was carried out using the guides by Saito *et al.* (1981) and Kennett and Srinivasan (1983).

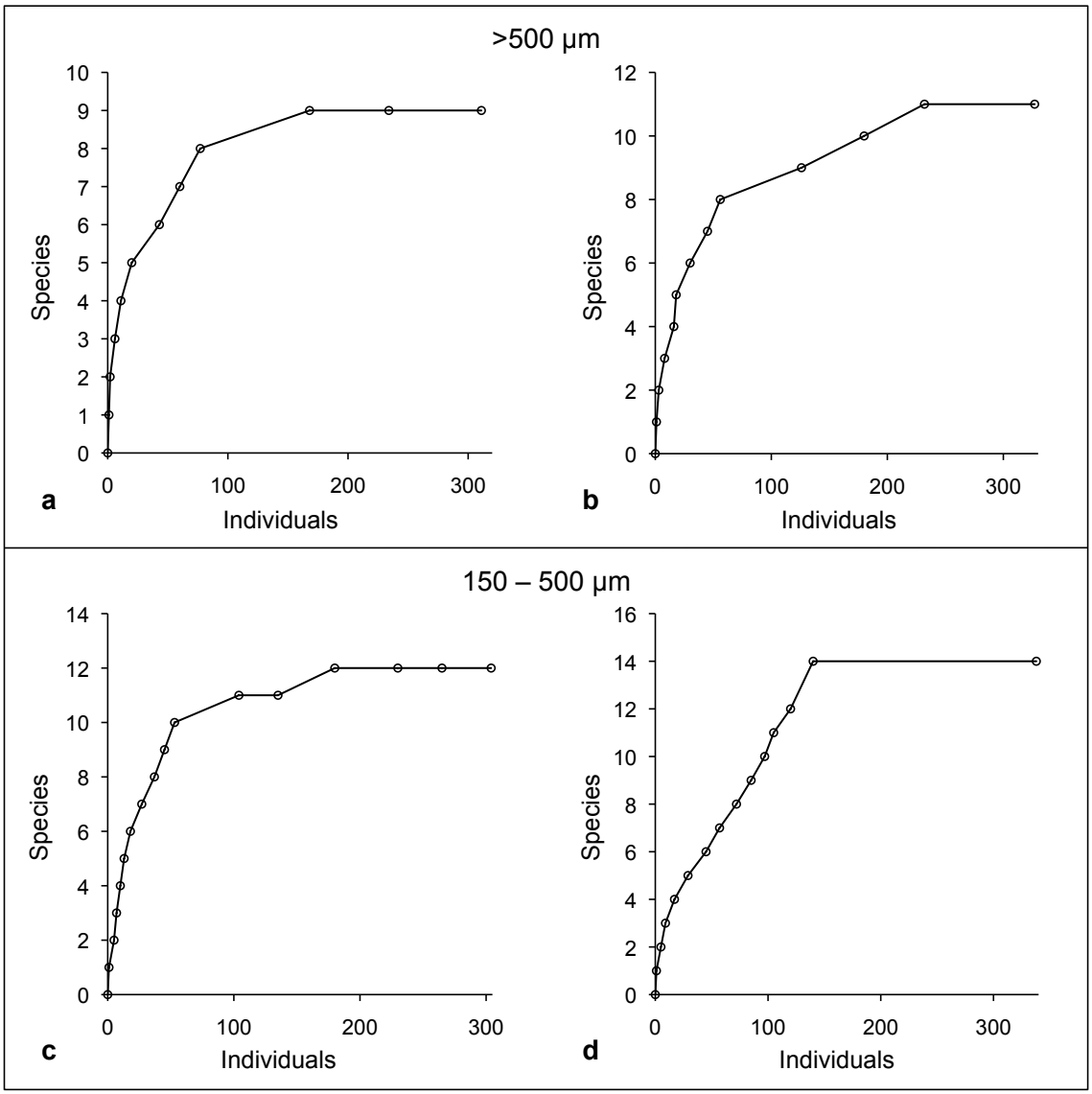

Figure 3.8 Examples of planktic foraminifera collection curves, a) >500 µm CAR-MON 2 170–171 cm; b) >500 µm 716B 1005–1006 cm; c) 150–500 µm B5-1 0–1 cm; d) 150–500 µm 716B 775776 cm.

Planktic foraminifera were collected from all samples to provide palaeoenvironmental data. Whole specimens were collected to provide abundance, diversity and environmental data. They were also collected to calculate the proportion of *Globorotalia menardii* present. *Globorotalia menardii* preferentially resides in warm (16–30 °C) sub-tropical waters (Bé and Tolderlund, 1971) and is, therefore, an excellent indicator of water temperature. Abundances of this species can be used to correlate with the known *G.*

menardii zonation (Ericson and Wollin, 1956; Reid *et al.,* 1996; Le Friant *et al.,* 2008), which can aid in the stratigraphy of a core. *Globorotalia menardii* is only present in the Caribbean Sea and Indian Ocean cores. For the Caribbean Sea, counts of *G. menardii* also include counts of the similar species *Globorotalia tumida.* The similarity in their morphology in the Caribbean Sea meant there was a lack of distinction between the two species, although, they were more defined in the Indian Ocean, allowing more accurate individual counts.

Fragments of planktic foraminifera were collected to provide a fragment-to-whole specimen ratio. During times of enhanced dissolution, fragments are more common as the tests of the planktic foraminifera are weakened and easily broken. Thus a high fragment to whole specimen ratio symbolises reduced calcification or increased dissolution (Gonzalez-Mora *et al.,* 2008).

3.4.4 LIMACINA DISSOLUTION INDEX

Determination of the calcification of pteropod shells was made using the *Limacina* Dissolution Index (LDX), which was devised by Gerhardt *et al.* (2000) and published as a scale by Gerhardt and Henrich in 2001 (Fig. 3.9). The LDX is a scale of pteropod shell dissolution, which was originally designed to determine the position of the ALy by studying surface sediments (Gerhardt *et al.,* 2000; Gerhardt and Henrich, 2001). However, the methodology is also of use as a scale of shell calcification. Low surface ocean carbonate concentrations result in the corrosion and poor maintenance of shells, producing dissolution damage of the outer aragonite layer whilst the pteropod is still alive (Bednaršek *et al.,* 2012b). This in-life corrosion can be used as a measure of pteropod calcification, since the inability to maintain the shell structure demonstrates the inability to calcify. The LDX methodology involves

the qualitative analysis of the surface of *Limacina inflata* shells on a scale of zero to five; zero being a shell that is transparent, lustrous and perfectly preserved and five being a shell that is opaque-white, totally lustreless and perforated. Using the original methodology as described by Gerhardt and Henrich (2001), at least ten shells (maximum of thirty shells) of adult *L. inflata* of a size of 300 µm or larger were allocated a value from this scale by the use of light microscopy for each sample. The mean for each sample was then calculated to provide the LDX value. This was carried out for all samples containing the relevant number of adult *L. inflata.*

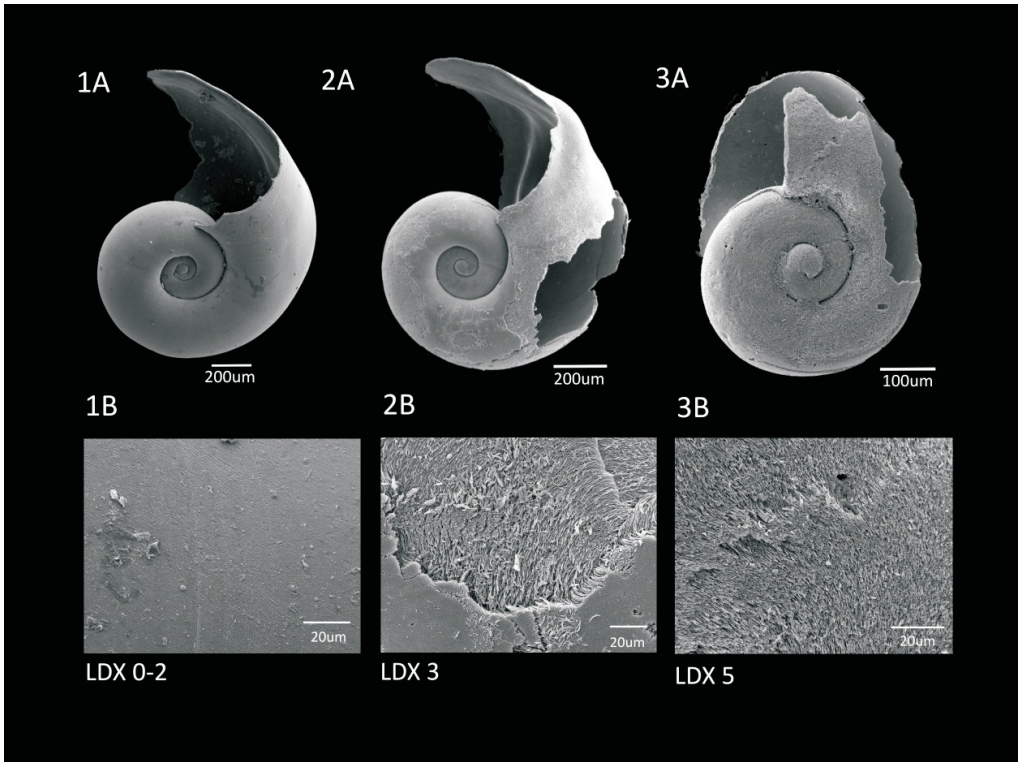

Figure 3.9 Examples of the pteropod *L. inflata* at different stages of the *Limacina* Dissolution Index. 1A–B LDX value 0–2, good calcification, intact surface layer; 2A–B LDX value 3, moderate to poor calcification; 3A–B LDX value 5, poor calcification.

The simple nature of the LDX scale means that the allocation of LDX values for individual shells must be a whole number to allow analysis using light

microscopy. However, since the condition of a shell can fall between two points on this scale, the mean is presented to two decimal places. Although theoretically wrong, since the original data are whole numbers, presenting the mean to two decimal places takes into account variability within a single sample and makes it easier to differentiate between two samples with very similar values. This produces a more detailed calcification profile. For the same reason, the mean LDX has been used rather than the median, as the median was found to present a simplified profile which did not always adequately represent shells within a sample. Median LDX values for CAR-MON 2, B5-1 and 716B are presented alongside mean LDX values in Figures 4.17, 4.30 and 4.45.

3.4.5 REPRODUCIBILITY OF LDX DATA

Despite its wide use as a measure of pteropod dissolution, the *Limacina* Dissolution Index has not been extensively used to demonstrate pteropod calcification. The reliability and reproducibility of LDX data was, therefore, tested in two ways. Firstly, by performing multiple analyses on different groups of *L. inflata* from a single sample to show whether analysis varied through a sample. Secondly, the LDX methodology was tested by checking the reproducibility between size fractions (specimens 300–500 µm and >500 µm), since some samples show a smaller average size of pteropod (Appendix 8.1.2.B).

It was found that the average LDX is reproducible using different specimens of the same sample. Standard deviations of the average LDX results (in all cases based on ten specimens) from within the same sample is between 0.08 and 0.17 for all samples tested. Although more variable, the LDX is reliable across different sized shells, with the smaller size fraction generally

showing slightly better calcification (lower LDX). This may indicate that pteropods find it easier to maintain smaller shells. The average LDX of *L. inflata* specimens from the >500 μm fraction of sample 35–36 cm ranged between 2 and 2.5 (based on ten repetitions), whereas the average value for specimens in the 150–500 μm fraction (graticule used to identify 300–500 μm shell size) was between 1.9 and 2.1 (based on four repetitions). Similarly, the average LDX for >500 μm shells from samples 305–306 cm was between 1.7 and 1.9 (based on four repetitions), whereas the average LDX in the 150–500 μm fraction was between 1.3 and 1.7 (based on four repetitions).

The LDX is not reproducible across different species of pteropod, even within the same genus. For core B5-1, the LDX was applied to both (Appendix 8.2.2.4.A) *L. inflata* and *Limacina retroversa*. It was found that *L. retroversa* showed a more variable result, with specimens within the same sample showing a range of LDX between 1–5. Gerhardt *et al.* (2000) applied the LDX to three species; *L. inflata, Limacina bulimoides* and *Limacina lesueuri.* It was found that the three species showed distinctly different degrees of susceptibility to dissolution. Despite having a smaller, but thicker shell, *L. inflata* showed higher sensitivity than the shells of other *Limacina* species. This is because *L. inflata* has a different shell structure to other *Limacina* species. The shells of euthecosome pteropods are composed of rods of aragonite, which are arranged in different ways (Bé and Gilmer, 1977). With the exception of *L. inflata,* the Limacinidae have a cross-lamellar aragonite microstructure, with an inner prismatic layer, whereas, the Cavolinidae and *L. inflata* have a helical aragonite microstructure (Bé and Gilmer, 1977). This means that *L. inflata* is more susceptible to dissolution than other species of *Limacina.*

3.4.6 PTEROPOD SIZE ANALYSIS

The average size of the pteropod *L. inflata* was calculated by using a photomicroscope (Nikon DS-Fi1 camera mounted on a Nikon eclipse LV100POL microscope) to measure the diameter of shells perpendicular to the line of the aperture on the spiral side (Fig. 3.10). The line of the aperture was often estimated using the position of the protoconch, due to damage to the growing edge of shells. Measurements were made for all appropriate shells >150 μm that had been picked for the species diversity study. The average size was then calculated. Average shell size can be used to indicate post-depositional dissolution, enhanced calcification and also increased productivity.

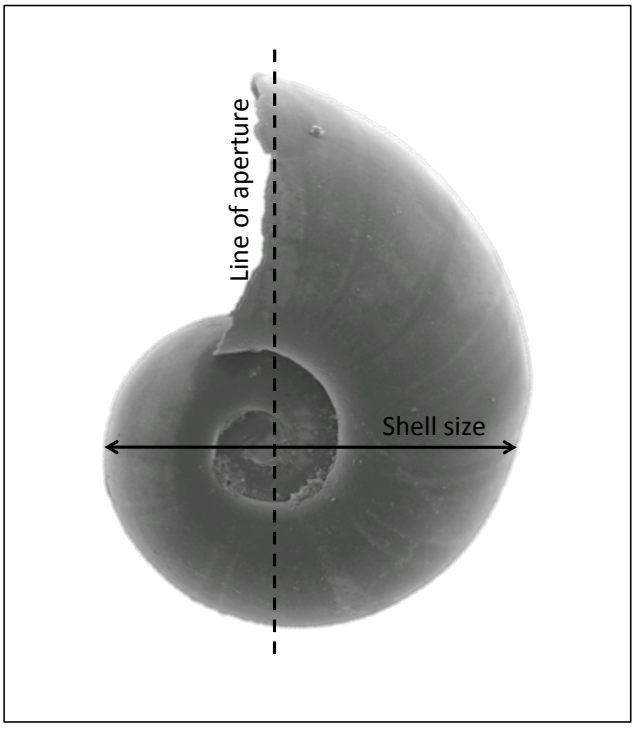

Figure 3.10 Measuring the diameter of pteropod *L. inflata* perpendicular to the line of the aperture. The line of the aperture is frequently an approximation since the position of the aperture is often not a definite line, however, the line of the aperture should pass through the centre (protoconch) of the shell.

3.4.7 SCANNING ELECTRON MICROSCOPY

All species of pteropod and heteropod were imaged at Plymouth University using a JEOL JSM-5600V scanning electron microscope. Specimens were mounted on metal stubs using carbon tabs and sputter coated in gold (thickness 10–12 Å) before imaging.

3.4.8 STABLE ISOTOPE ANALYSIS

Only core B5-1 was analysed for stable isotopes as it was the only core missing these data. Stable isotope analysis ($\delta^{18}O$, $\delta^{13}C$) was carried out at the NERC Isotope Geosciences Laboratory, British Geological Survey, Keyworth. Ten specimens of *G. ruber* of size 250–355 µm (example of this size fraction, Lawrence and Herbert, 2005) were analysed for each data point using a GV IsoPrime mass spectrometer plus Multiprep device. Isotope values ($\delta^{13}C$, $\delta^{18}O$) are reported as *per mille* (‰) deviations of the isotopic ratios ($^{13}C/^{12}C$, $^{18}O/^{16}O$) calculated to the VPDB scale using a within-run laboratory standard calibrated against NBS standards. Analytical reproducibility of the standard calcite (KCM) is <0.1‰ for $\delta^{13}C$ and $\delta^{18}O$. The isotope profiles produced are comparable to published data for sediments in the area (Weldeab *et al.,* 2003).

Throughout this study, the oxygen isotope record, or global ice volume, is used as an indicator of climate change and not an indicator of sea level change. The oxygen isotope record is closely linked to variations in atmospheric CO_2 and therefore also dissolved CO_2 and surface water carbonate concentrations. Throughout this study, calcification indices are statistically compared to the oxygen isotope record for each core, rather than the Vostok CO_2 record (Petit *et al.,* 1999). The oxygen isotope records allow direct comparison and correlation

to species and calcification data within a core and are also available in higher resolution than Vostok CO_2 data.

The oxygen isotope record is also used in this study to provide an age framework for core B5-1. This is achieved by comparing the oxygen isotope data from B5-1 to global oxygen isotope records, the LR04 stack (Lisiecki and Raymo, 2005) and SPECMAP record (Petit *et al.,* 1999), and to records collected in the same area. Identification of Marine Isotope Stage boundaries and minor isotope excursions then allows ages to be allocated to the core (see section 4.2.2) at a low resolution.

3.5 STATISTICAL METHODOLOGY

Details of statistical methodologies used can be found in Appendix 8.1.3 (p. 261). Correlation of calcification indices (LDX and shell size), abundance, diversity, percentage species composition and oxygen isotope data was carried out with a bivariate, two-tailed Pearson correlation using the Statistical Package for the Social Sciences, SPSS. Species diversity, heterogeneity and assemblage evenness was calculated using the Paleontological Statistics package, PAST (http://folk.uio.no/ohammer/past/). Diversity was measured using the Fisher Alpha diversity, assemblage heterogeneity was measured using the Shannon-Wiener index and the assemblage evenness was measured using Pielou's Evenness index. These are standard statistical methodologies used in the analysis of fossil foraminifera assemblages and are therefore appropriate for the analysis of fossil planktic gastropod assemblages. Using the same methodologies for planktic foraminifera and planktic gastropods will also allow direct comparisons of the two assemblages.

4 RESULTS

4.1 THE CARIBBEAN SEA: CAR-MON 2, JC18-19 and JR123-35-V

A summary of Caribbean Sea results can be found in Figure 4.17

4.1.1 SEDIMENTOLOGY

4.1.1.1 CORE DESCRIPTION AND LOGS

CAR-MON 2 was described by Le Friant *et al.* (2008), providing a detailed core description and log, which is partly modified in Fig. 4.1. The core is composed of relatively un-interrupted hemipelagic sediments with several thin deposits of volcanic ash and one large deposit of volcanic ash, between 330–270 cm (Fig. 4.1). The presence of intact, thin layers of volcanic ash suggest little bioturbation, however, Le Friant *et al.* (2008) noted some bioturbation between 370–390 cm. Planktic foraminifera, pteropods and heteropods were found to be abundant within the sediments throughout most of the core (see section 4.1.3.1). The average grain size of CAR-MON 2 (Fig. 4.1) shows that the core is composed of very fine to medium sand (Appendix 8.2.1.1.A, 8.2.1.1.B). The >63 μm grain size distribution produced by Le Friant *et al.* (2008) is in agreement with the average grain size, showing a larger average grain size when the percentage of >63 μm sediment is higher. Periods of larger grain size occur during, immediately before and after, extreme glacial periods MIS 6 and 2 (Fig. 4.1). The highest average grain size of 327 μm occurs at 75 cm, on the boundary of MIS 3 and 2.

JC18-19 was described by Cassidy (2012), providing a detailed core description and log, which is partly modified in Fig. 4.2. The core is composed of hemipelagic sediment and volcanic ash, which has been disturbed by turbidite deposits. The top 80 cm of the core is, however, relatively un-interrupted and was found to contain abundant planktic foraminifera, pteropods

and heteropods (see Appendix 8.2.1.2.E, 8.2.1.2.F). It was found that, below 95 cm, pteropod and heteropod remains were absent, whilst planktic foraminifera were still abundant. The average grain size of JC18-19 (Fig. 4.2) shows that the core is composed of very fine to fine sand (Appendix 8.2.1.1.C). The >63 μm grain size distribution is in agreement with the average grain size, showing a larger average grain size when the percentage of >63 μm sediment is higher. The highest average grain size of 182 μm occurs at 195 cm, where layers of volcanic ash is shown on the core log (Cassidy, 2012).

JR123-35-V was described by Trofimovs *et al.* (2010), providing a detailed core description and log, which is partly modified in Fig. 4.3. The core is composed of relatively un-interrupted hemipelagic sediments containing one large turbidite between 145 cm and 85 cm, which is composed of 55–90% bioclasts and 10–45% volcanic material (Fig. 4.3). The hemipelagic sediments were found to contain abundant planktic foraminifera, pteropods and heteropods (see Appendix 8.2.1.2.E, 8.2.1.2.F). The average grain size of JR123-35-V (Fig. 4.4) shows that the core is composed of silt to medium sand (Appendix 8.2.1.1.A, 8.2.1.1.B). The >63 μm grain size distribution is in agreement with the average grain size, showing a larger average grain size when the percentage of >63 μm sediment is higher. A large increase in grain size coincides with the turbidite described by Trofimovs *et al.* (2010), with the highest grain size of 198 μm occurring at 80 cm, towards the top of the turbidite.

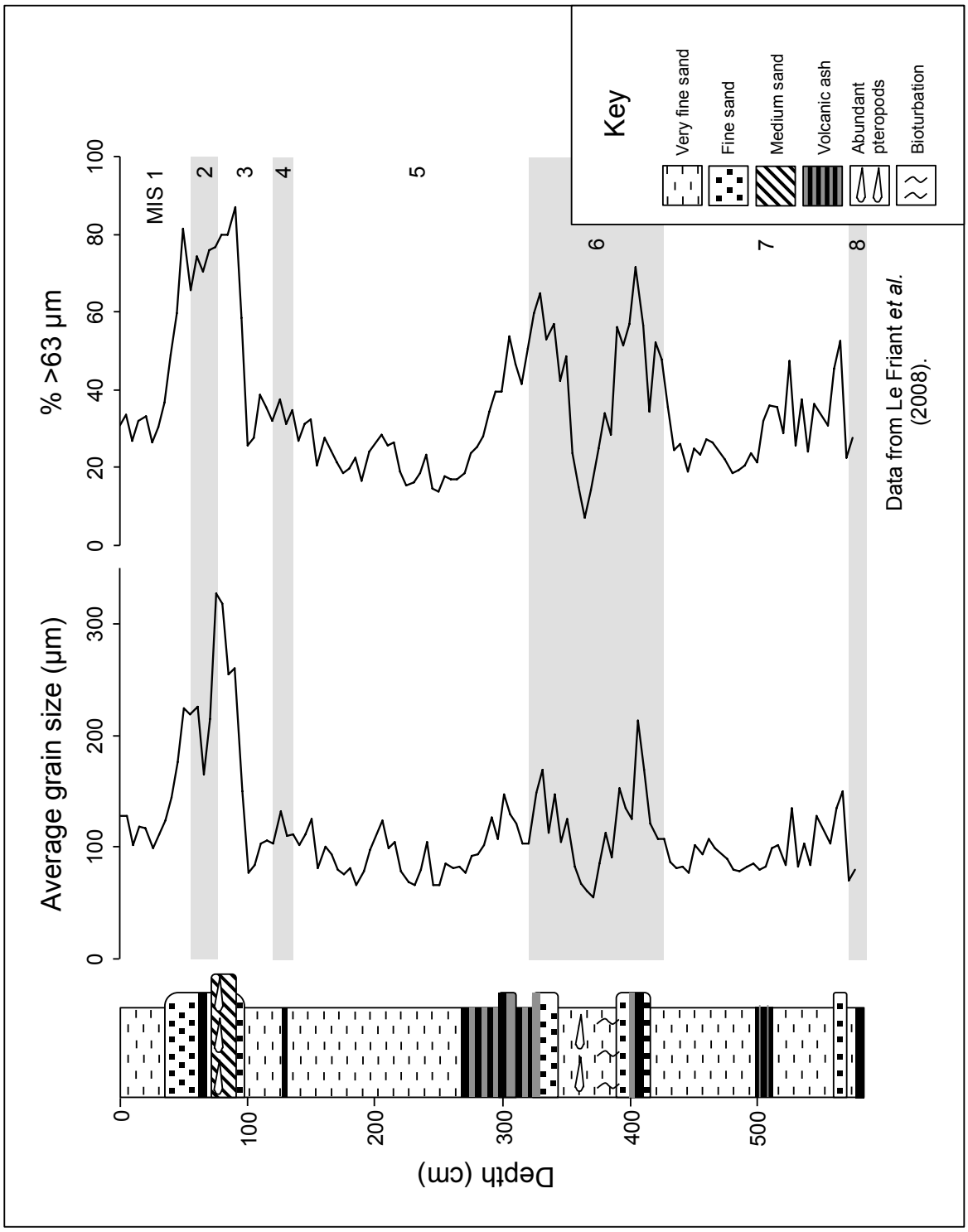

Figure 4.1 CAR-MON 2 lithology (core description from Le Friant *et al.,* 2008), average grain size and percentage of sediment >63 µm (data from Le Friant *et al.,* 2008).

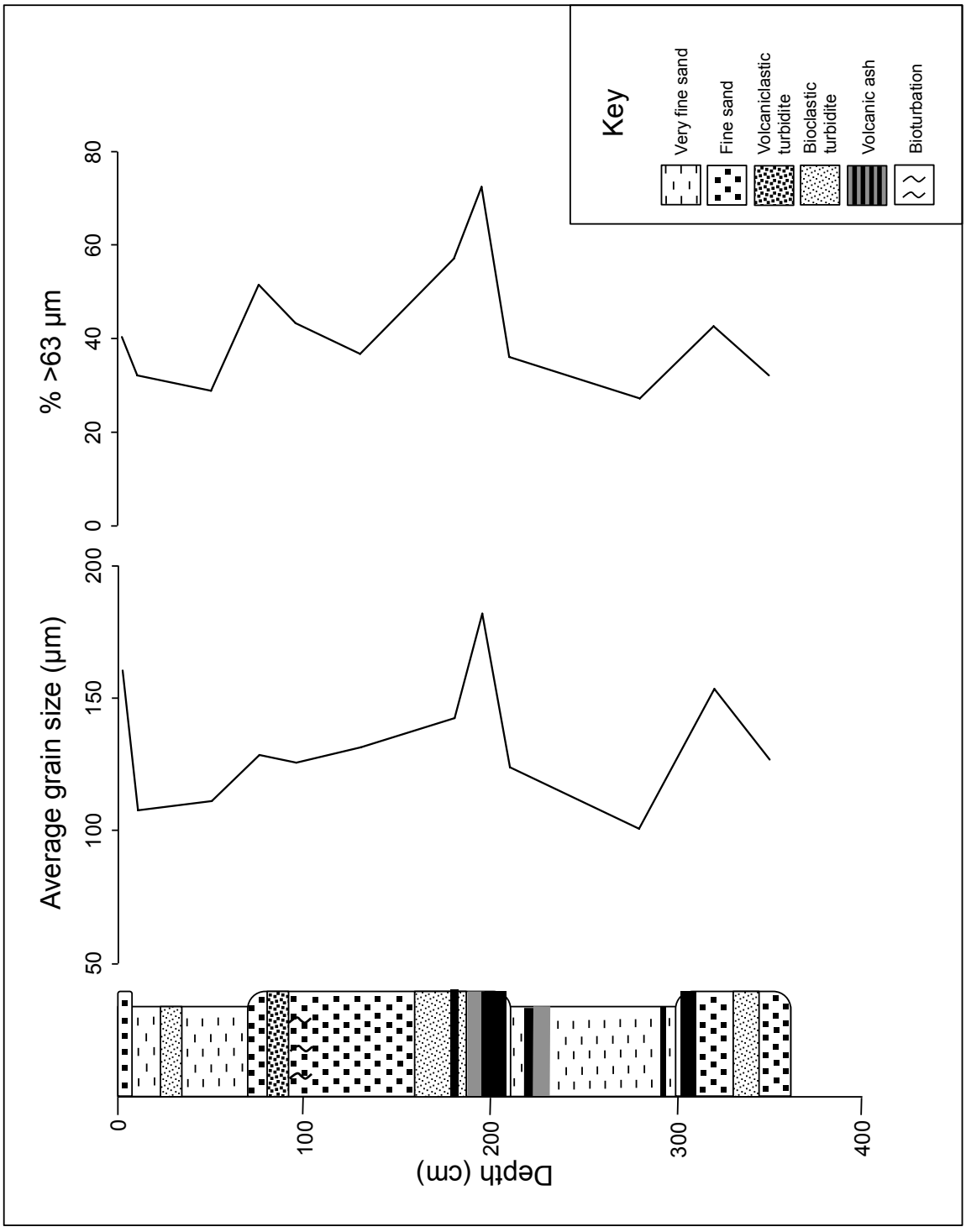

Figure 4.2 JC18-19 lithology (core description from Cassidy, 2012), average grain size and percentage of sediment >63 µm.

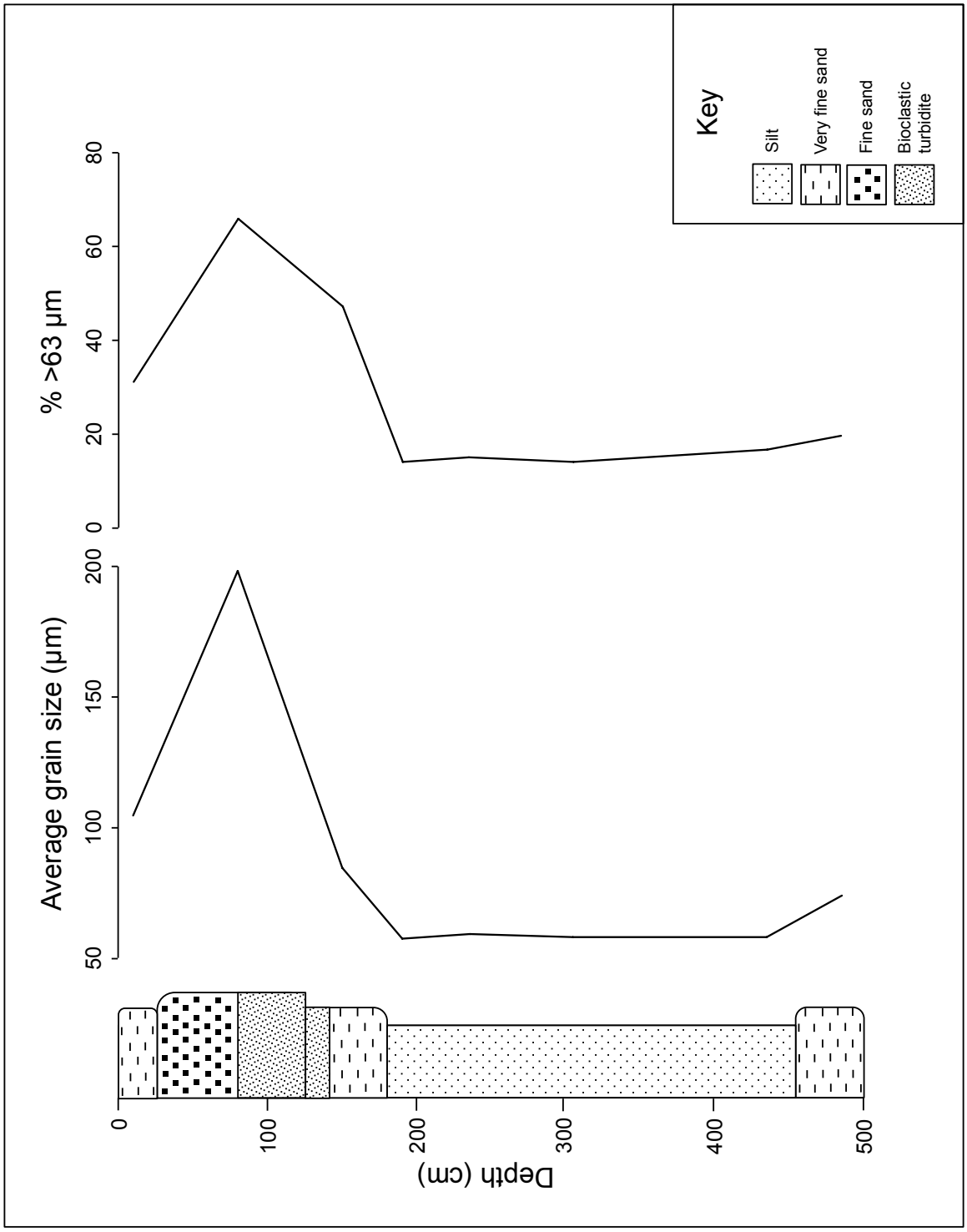

Figure 4.3 JR123-35-V lithology (core description from Trofimovs *et al.,* 2010), average grain size and percentage of sediment >63 µm.

4.1.1.2 SEDIMENTATION RATES

The rate of sedimentation in CAR-MON 2 has been calculated as varying between 1 and 3 cmkyr^{-1}, with an average rate of 2.3 cmkyr^{-1} (Le Friant *et al.,* 2008, fig. 6). Sedimentation at this site is higher due to the frequent deposition of air-borne ash. Between 270–300 cm, there is a concentration of ash layers which represent events spanning 23 kyr (Le Friant *et al.,* 2008). CAR-MON 2 provides a sediment record back 250 kyrs (Le Friant *et al.,* 2008).

The sedimentation rate of JC18-19 varies between 3.04 cmkyr^{-1} between 0–10 cm and 11.19 cmkyr^{-1} between 35–65 cm. Below 65 cm, the sedimentation rate has been influenced by the deposition of several bioclastic and volcaniclastic turbidites, which both add material and erode material from the sedimentary record. This has dramatically increased the sedimentation rate to around 74 cmkyr^{-1} between 65–180 cm. The average rate of normal hemipelagic (without turbidites) sedimentation (0–10 cm, 35–65 cm) is 7.12 cmkyr^{-1} (Cassidy, 2012). JC18-19 provides a sediment record back 109 kyrs (Cassidy, 2012).

The sedimentation rate of JR123-35-V varies throughout the core, with a higher rate of 6.88 cmkyr^{-1} at the base of the core (439–272 cm), 3.70 cmkyr^{-1} prior to the bioclastic deposit (222–149 cm) and 5.84 cmkyr^{-1} at the top of the core (60–0 cm). Sedimentation rates are higher at this site in comparison to CAR-MON 2. JR123-35-V provides a sediment record back 120 kyrs (Trofimovs *et al.,* 2010).

4.1.2 STABLE ISOTOPE STRATIGRAPHY AND DATING

4.1.2.1 OXYGEN ISOTOPE ANALYSIS

Oxygen isotope analysis of CAR-MON 2 (Fig. 4.4) was carried out and published by Le Friant *et al.* (2008). Analysis was carried out at the NERC Isotope Geosciences Laboratory (British Geological Survey, Keyworth) using homogenised <63 μm sediment containing a range of calcareous nannofossils, small foraminifera, pteropod fragments, calcified dinoflagellates and other calcareous material. Le Friant *et al.* (2008) provide a detailed methodology for the stable isotope analysis of CAR-MON 2.

Oxygen isotope analysis of JC18-19 (Fig. 4.4) was carried out by Cassidy (2012). Two separate analyses were made upon specimens of the benthic foraminifera genus *Cibicidoides* and upon homogenised <63 μm bulk carbonate material. Analysis was carried out at the National Oceanographic Centre, Southampton. Cassidy (2012) provides a detailed methodology for the stable isotope analysis of JC18-19.

Oxygen isotope analysis of JR123-35-V (Fig. 4.4) was carried out and published by Trofimovs *et al.* (2010). Analysis was carried out at the NERC Isotope Geosciences Laboratory (British Geological Survey, Keyworth) using specimens of the planktic foraminifera *G. ruber.* Trofimovs *et al.* (2010) provide a detailed methodology for the stable isotope analysis of JR123-35-V.

In addition, several samples in CAR-MON 2 and JC18-19 have been dated using Ar^{40}/Ar^{39} ratio analysis to provide specific dates for ash deposits (Le Friant *et al.,* 2008; Cassidy, 2012). AMS Radiocarbon dating was also carried out for several samples from core JR123-35-V (Trofimovs *et al.,* 2010).

4.1.2.2 CORRELATION TO KNOWN BIOZONES

The zonation of *Globorotalia menardii* provides a record of climatically induced migration events (Ericson and Wollin, 1956; Reid *et al.,* 1996; Le Friant *et al.,* 2008). Zonal boundaries are identified at points where levels of *G. menardii* drop below, or rise above 1% of the planktic foraminifera (Le Friant *et al.* 2008). The *G. menardii* record in CAR-MON 2 has been published by Le Friant *et al.* (2008). However, during planktic foraminifera analysis in the current study, composite percentages of *G. menardii* and *Globorotalia tumida* were also calculated (Appendix 8.2.1.2.A). The records are very comparable (Fig. 4.5), showing an identical trend ($r=0.619$, $p=<0.001$, $n=113$). Values calculated during the present study are slightly higher than those published by Le Friant *et al.* (2008). Since counts were made on aliquotes of exactly the same sample, this is most likely due to the subjective identification of *Globorotalia flexuosa.* Data for JC18-19 and JR123-35-V are also comparable (Fig. 4.6) to the records for CAR-MON 2. It is apparent that JC18-19 is missing *G. menardii* zone Y. This suggests that MIS 3 and 2 are missing from the sedimentary record of JC18-19, which is consistent with a gap in the argon-argon ($^{40}Ar/^{39}Ar$) dating found by Cassidy (2012) between 3.3 kyr and 38 kyr.

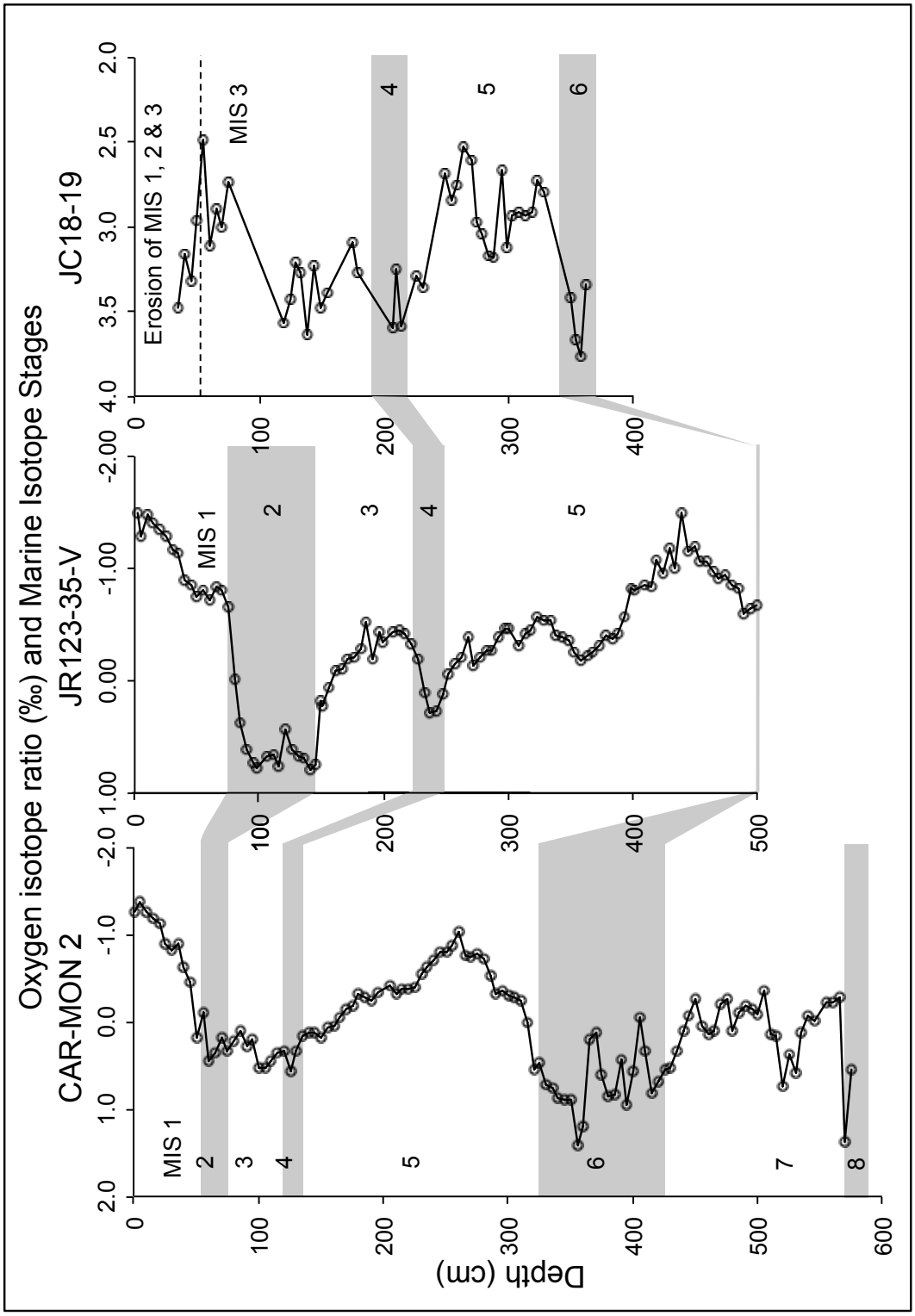

Figure 4.4 Oxygen isotope ratios and the position of Marine Isotope Stages (MIS) of CAR-MON 2, JR123-35-V and JC18-19. Data from Le Friant *et al.* (2008), Trofimovs *et al.* (2010) and Cassidy (2012) respectively.

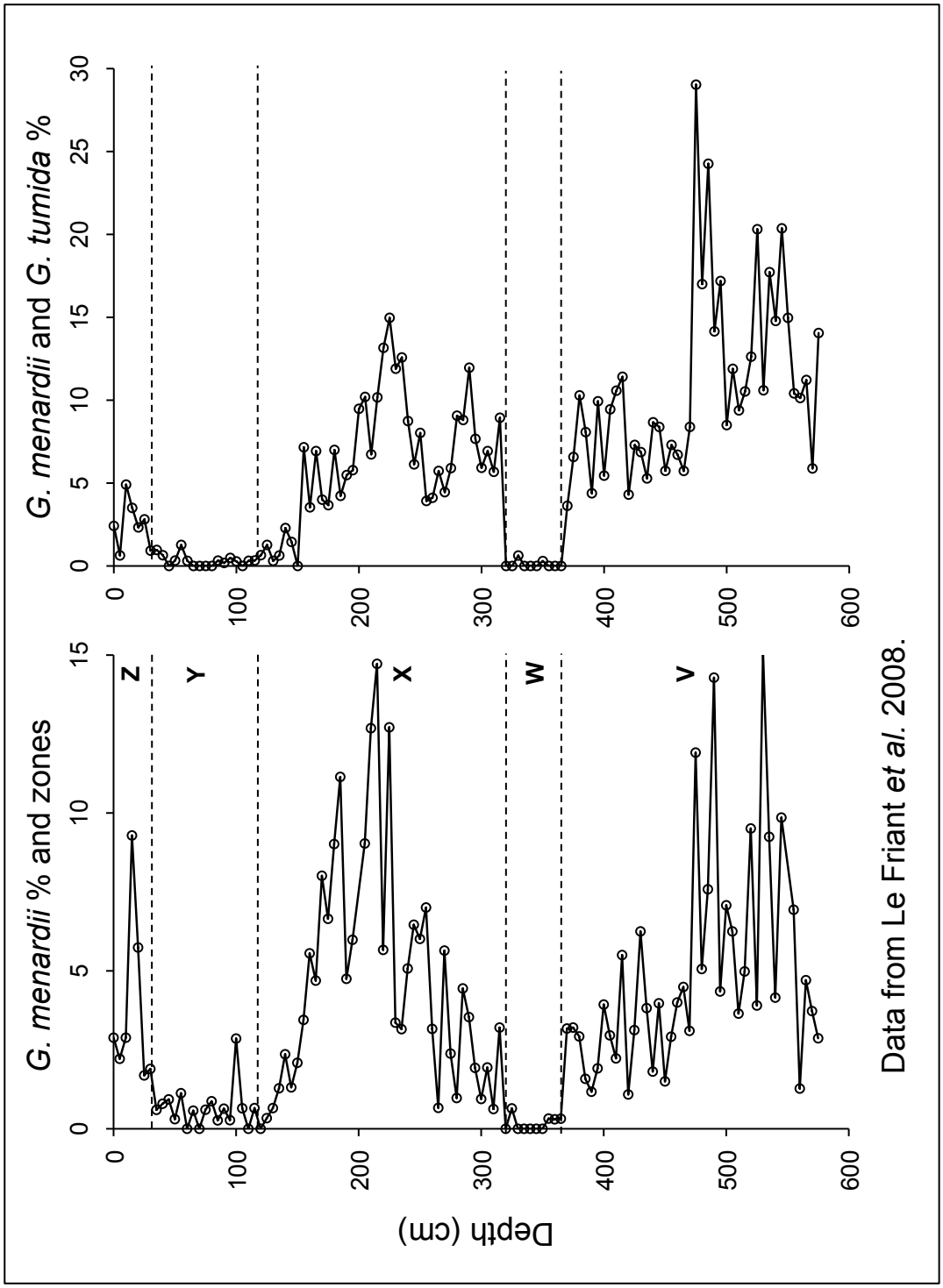

Figure 4.5 *Globorotalia menardii* zonation analysis for CAR-MON 2 carried out during this study (150–500 μm fraction, including *G. tumida*) compared to data published for the same core (Le Friant *et al.,* 2008).

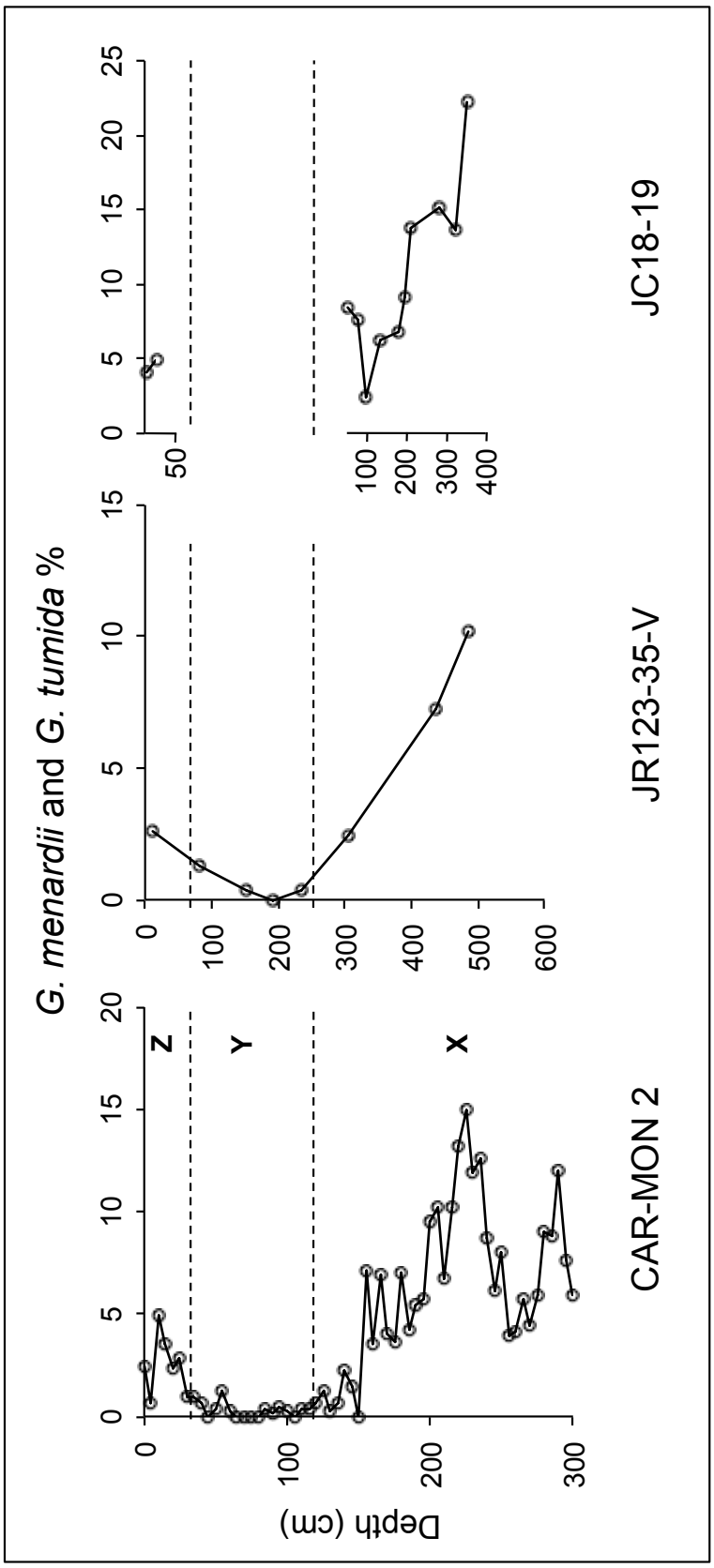

Figure 4.6 Low resolution composite *G. menardii and G. tumida* counts for JR123-35-V and JR18-19 with data from CAR-MON 2 (all data for 150–500 μm fraction). The depth scale changes for each core.

4.1.3 MICROPALAEONTOLOGY

Twenty five species of pteropod, sixteen species of heteropod and twenty five species of planktic foraminifera were identified from the 150–500 μm and > 500 μm size fractions in CAR-MON 2 (Table 4.1; Appendix 8.2.1.2.A–D). Some unidentifiable pteropod and heteropod species are labelled alphabetically within their genera. The composition of pteropod, heteropod and planktic foraminifera species in cores JC18-19 and JR123-35-V (Appendix 8.2.1.2.G, 8.2.1.2.H) is the same as that found in CAR-MON 2. Several samples in the >500 μm fraction of CAR-MON 2 contained very low numbers of pteropods and heteropods. For this reason, abundance and diversity analysis of pteropods and heteropods has been based on the 150–500 μm fraction only.

4.1.3.1 ABUNDANCE

Patterns of abundance differ between planktic foraminifera and pteropods and heteropods, however, changes in both groups appear to be related to changes in climate.

4.1.3.1.1 PLANKTIC FORAMINIFERA

Planktic foraminifera were found in both size fractions in all samples from cores CAR-MON 2, JC18-19 and JR123-35-V. The abundance of planktic foraminifera in the >500 μm fraction is much lower than that of the 150–500 μm fraction. Since the sediments are largely composed of the shells of planktic organisms, this is most likely due to the greater mass of tests in the >500 μm fraction (Appendix 8.2.1.2.G, 8.2.1.2.I). The trends in abundance are generally the same in both size fractions (Appendix 8.2.1.2.G, 8.2.1.2.I). High planktic foraminifera abundance generally coincides with warm periods (MIS 7, 5, 3 and

1) across all Caribbean cores. In CAR-MON 2, the highest peaks in abundance occur at 140 cm and 100 cm core depth for the >500 μm (9297 planktic foraminifera per gram of sediment, pfg^{-1}) and 150–500 μm (48400 pfg^{-1}) fractions respectively (Fig. 4.7). Periods of low planktic foraminifera abundance generally coincide with cool periods (MIS 8, 6, 4 and 2) across all Caribbean cores. In CAR-MON 2, the lowest abundances occur at 95 cm and 155 cm core depth for the >500 μm (546 pfg^{-1}) and 150–500 μm (435 pfg^{-1}) fractions respectively (Fig. 4.7). However despite visually appearing to show a trend, the relationship between planktic foraminifera abundance and oxygen isotope data does not produce a significant correlation (150–500 μm, r=-0.068, p=0.471, n=114; >500 μm, r=-0.230, p=0.014, n=114).

4.1.3.1.2 PTEROPODS AND HETEROPODS

Pteropods and heteropods are present in the majority of samples in both size fractions of cores CAR-MON 2, JC18-19 and JR123-35-V. Specimens are absent from several samples in the CAR-MON 2, >500 μm fraction of MIS 5. No pteropod or heteropod species were recorded in both the 150–500 μm and >500 μm fractions of JC18-19 below 96 cm (Appendix 8.2.1.2.F, 8.2.1.2.J). Trends in abundance are similar for all Caribbean cores (Appendix 8.2.1.2.F, 8.2.1.2.J). Periods of high pteropod and heteropod abundance generally coincide with (MIS 8, 6 and 2), or immediately follow (MIS 4), cool periods. A bivariate, two-tailed Pearson correlation of pteropod and heteropod abundance (150–500 μm) with oxygen isotope data shows that this relationship is significant (r=0.201, p=0.032, n=114). However, in CAR-MON 2, the highest peak in abundance occurs during MIS 3, at 100 cm core depth for the 150–500 μm (24320 pteropods and heteropods per gram of sediment, pg^{-1}) fraction (Figs

4.7, 4.17). This peak in abundance may be related to factors other than climate, such as increased productivity. Periods of low pteropod and heteropod abundance generally coincide with warm periods (MIS 7, 5 and 1) in all Caribbean cores. In CAR-MON 2, the lowest abundances occur at 405 cm (243 pg^{-1}) and at 155 cm (308 pg^{-1}) for the 150–500 µm fraction (Fig. 4.7).

4.1.3.2 DIVERSITY

Fisher Alpha diversity, heterogeneity and assemblage evenness of planktic foraminifera, pteropods and heteropods show very little association to changes in climate. However, diversity data for pteropods and heteropods are often lower during the transition between Marine Isotope Stages, in particular MIS 7 to 6 and MIS 6 to 5.

4.1.3.2.1 PLANKTIC FORAMINIFERA

In all Caribbean cores, the Fisher Alpha diversity, heterogeneity and evenness of planktic foraminifera in both the 150–500 µm and >500 µm size fractions remains fairly constant throughout the core. In CAR-MON 2, the Fisher Alpha diversity (Fig. 4.8) ranges between 2.76 (95 and 485 cm) and 4.81 (395 cm) in the 150–500 µm fraction, and between 1.50 (345 cm) and 5.78 (370 cm) in the >500 µm fraction. The Shannon-Wiener heterogeneity of planktic foraminifera (Fig. 4.9) is generally higher in the 150–500 µm fraction, with values ranging from 1.58 (90 cm) and 2.51 (295 cm). Values in the >500 µm fraction range between 1.20 (430 cm) and 2.08 (25 and 370 cm). Pielou's evenness of species assemblages (Fig. 4.10) shows higher variation, with values ranging between 0.33 (90 cm) and 0.76 (220 cm) in the 150–500 µm fraction and values ranging between 0.33 (475 cm) and 0.81 (320 cm) in the

>500 µm fraction. The Fisher Alpha diversity and Shannon-Wiener heterogeneity of planktic foraminifera in the 150–500 µm fraction, shows a weak, but significant negative correlation to the oxygen isotope data (FA, r=-0.205, p=0.028, n=114; S-W, r=-0.195, p=0.038, n=114). This indicates higher diversity and heterogeneity of smaller planktic foraminifera species and juveniles during warm periods. However, the diversity and abundance of planktic foraminifera in the >500 µm fraction shows no correlation to the oxygen isotope data (FA, r=-0.077, p=0.415, n=114; S-W, r=-0.167, p=0.076, n=114). Surprisingly, oxygen isotope data does not show a significant correlation to Pielou's evenness for planktic foraminifera in the 150–500 µm fraction (r=-0.123, p=0.191, n=114), but does for the >500 µm fraction (r=0.252, p=0.007, n=114). This indicates a more even assemblage of larger planktic foraminifera species during glacial periods.

4.1.3.2.2 PTEROPODS AND HETEROPODS

The pteropod and heteropod Fisher Alpha diversity, heterogeneity and assemblage evenness in the 150–500 µm fraction of all the Caribbean cores does not show much variation (Figs 4.8–4.10). Fisher Alpha diversity, Shannon-Wiener heterogeneity and Pielou's evenness do not show significant correlations to oxygen isotope data (FA, r=-0.034, p=0.717, n=114; S-W, r=-0.049, p=0.605, n=114; P, r=-0.052, p=0.581, n=114). However, in CAR-MON 2 there are several peaks in diversity, which occur both during glacial (MIS 6 and 4) and interglacial (MIS 7, 5, 3 and 1) periods. Periods of low diversity appear to coincide with a transitional climate, at the boundaries of Marine Isotope Stages (Figs 4.8, 4.17). The Fisher Alpha diversity in CAR-MON 2 ranges between 2.48 (295 cm), at the MIS 6/5 boundary, and 6.36 (200 cm) in MIS 5. The

Shannon-Wiener heterogeneity (Fig. 4.9) and Pielou's assemblage evenness (Fig. 4.10) of pteropods and heteropods in CAR-MON 2 shows a similar trend of lower values during transitional periods. Heterogeneity varies between 0.97 (430 cm) at the MIS 7/6 boundary and 2.49 (80 cm) in MIS 3 and the assemblage evenness varies between 0.20 (430 cm) at the MIS 7/6 boundary and 0.68 (470 cm) in MIS 7.

PTEROPODA	HETEROPODA
Cavolinia inflexa (Lesueur, 1813) *Clio convexa* (Boas, 1886) *Clio cuspidata* (Bosc, 1802) *Clio pyramidata* Linnaeus, 1767 *Creseis acicula* (Rang, 1828) *Creseis chierchiae* (Boas, 1886) *Creseis virgula* (Rang, 1828) *virgula* (Rang, 1828) *Creseis* spp. *Cuvierina columnella* (Rang, 1827) *Diacria quadridentata* (Lesueur, 1821) *Diacria trispinosa* (Lesueur, 1821) *Hyalostylus striata* (Rang, 1828) *Limacina bulimoides* (d'Orbigny, 1836) *Limacina inflata* (d'Orbigny, 1836) *Limacina lesueuri* (d'Orbigny, 1836) *Limacina trochiformis* (d'Orbigny, 1834) *Limacina* sp. C *Limacina* sp. D *Styliola subula* (Quoy and Gaimard, 1827) *Gleba cordata* Forskål, 1776 *Peracle diversa* (Monterosato, 1875) *Peracle moluccensis* (Tesch, 1903) *Peracle* spp. *Paedoclione doliiformis* Danforth, 1907 Gymnosome veligers	*Atlanta brunnea* Gray, 1850 *Atlanta californiensis* Seapy and Richter, 1993 *Atlanta gaudichaudi* Gray, 1850 *Atlanta helicinoidea* Gray, 1850 *Atlanta inclinata* Gray, 1850 *Atlanta peronii* Lesueur, 1817 *Atlanta rosea* Gray, 1850 *Atlanta selvagensis* de Vera and Seapy, 2006 *Atlanta turriculata* d'Orbigny, 1835 *Atlanta* sp. D *Atlanta* spp. *Carinaria pseudorugosa* Vayssière, 1904 *Carinaria lamarckii* de Blainville, 1817 *Carinaria* spp. *Firoloida desmarestia* Lesueur, 1817 *Oxygyrus keraudreni* (Lesueur, 1817)
GLOBIGERINIDA (PLANKTIC FORAMINIFERA)	
Candeina nitida d'Orbigny, 1839 *Globigerina bulloides* d'Orbigny, 1826 *Globigerina digitata* Brady, 1879 *Globigerina rubescens* Hofker, 1956 *Globigerinella aequilateralis* (Brady, 1879) *Globigerinella calida* (Parker, 1962) *Globigerinita glutinata* (Egger, 1893) *Globigerinoides conglobatus* (Brady, 1879) *Globigerinoides elongatus* (d'Orbigny, 1926) *Globigerinoides pyramidalis* Jones, 1994 *Globigerinoides ruber* (d'Orbigny, 1839) *Globigerinoides sacculifer* (Brady, 1877) *Globigerinoides trilobus* (Reuss)	*Globorotalia crassaformis* (Galloway and Wissler, 1927) *Globorotalia flexuosa* (Koch, 1923) *Globorotalia inflata* (d'Orbigny, 1839) *Globorotalia menardii* (Parker, Jones and Brady, 1865) *Globorotlia scitula* (Brady, 1882) *Globorotalia truncatulinoides* (d'Orbigny, 1839) *Globorotalia tumida* (Brady, 1877) *Neogloboquadrina dutertrei* (d'Orbigny, 1839) *Neogloboquadrina incompta* (Cifelli, 1961) *Orbulina universa* d'Orbigny, 1839 *Pulleniatina obliquiloculata* (Parker and Jones, 1865) *Sphaeroidinella dehiscens* (Parker and Jones, 1865)

Table 4.1 Species of pteropod, heteropod and planktic foraminifera identified from both size fractions of sediment for CAR-MON 2.

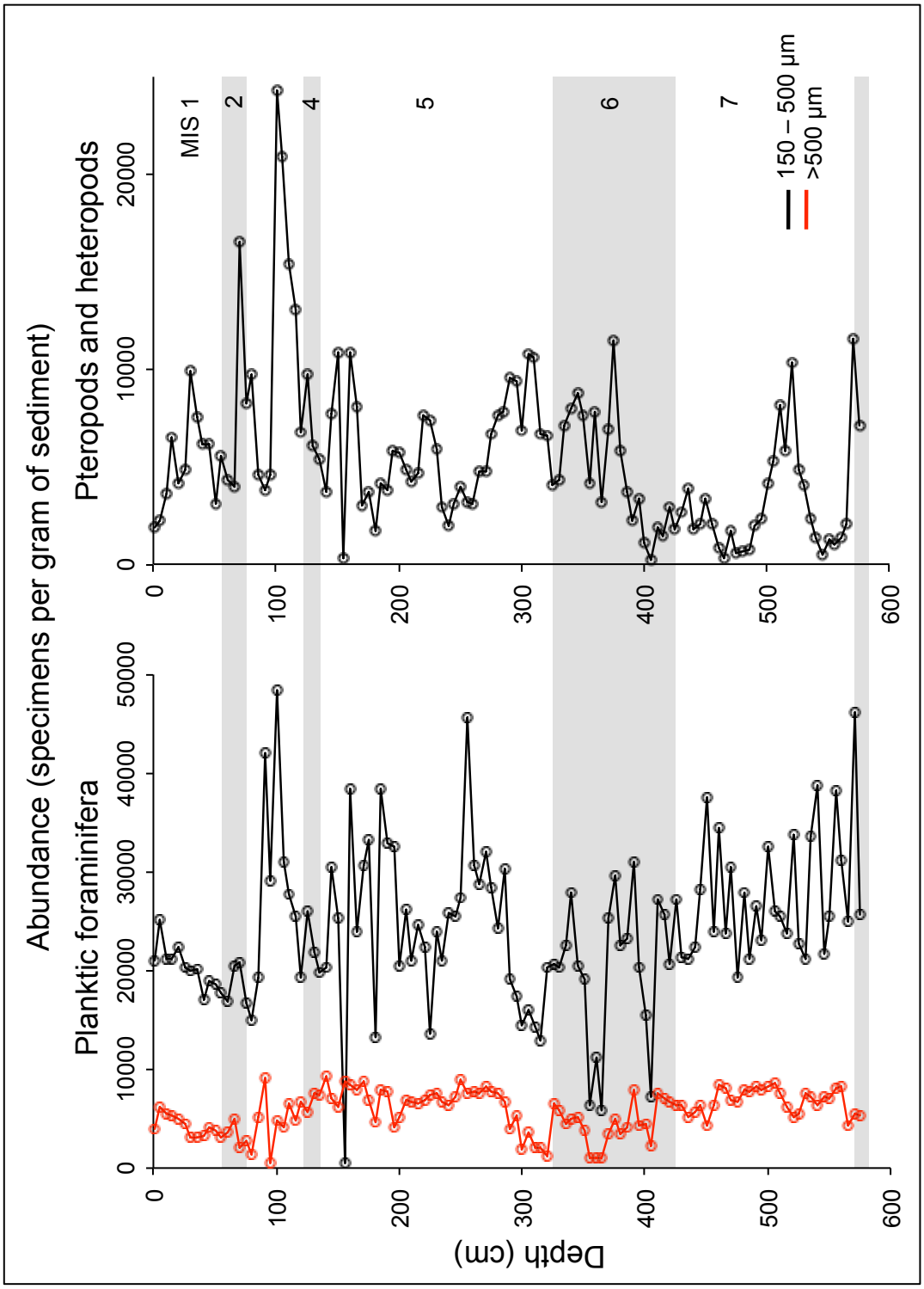

Figure 4.7 Abundance of planktic foraminifera (planktic foraminifera per gram of sediment, (pfg^{-1}) and pteropods and heteropods (pteropods and heteropods per gram of sediment, pg^{-1}) in CAR-MON 2. Grey boxes indicate glacial periods, as designated in Figure 4.4.

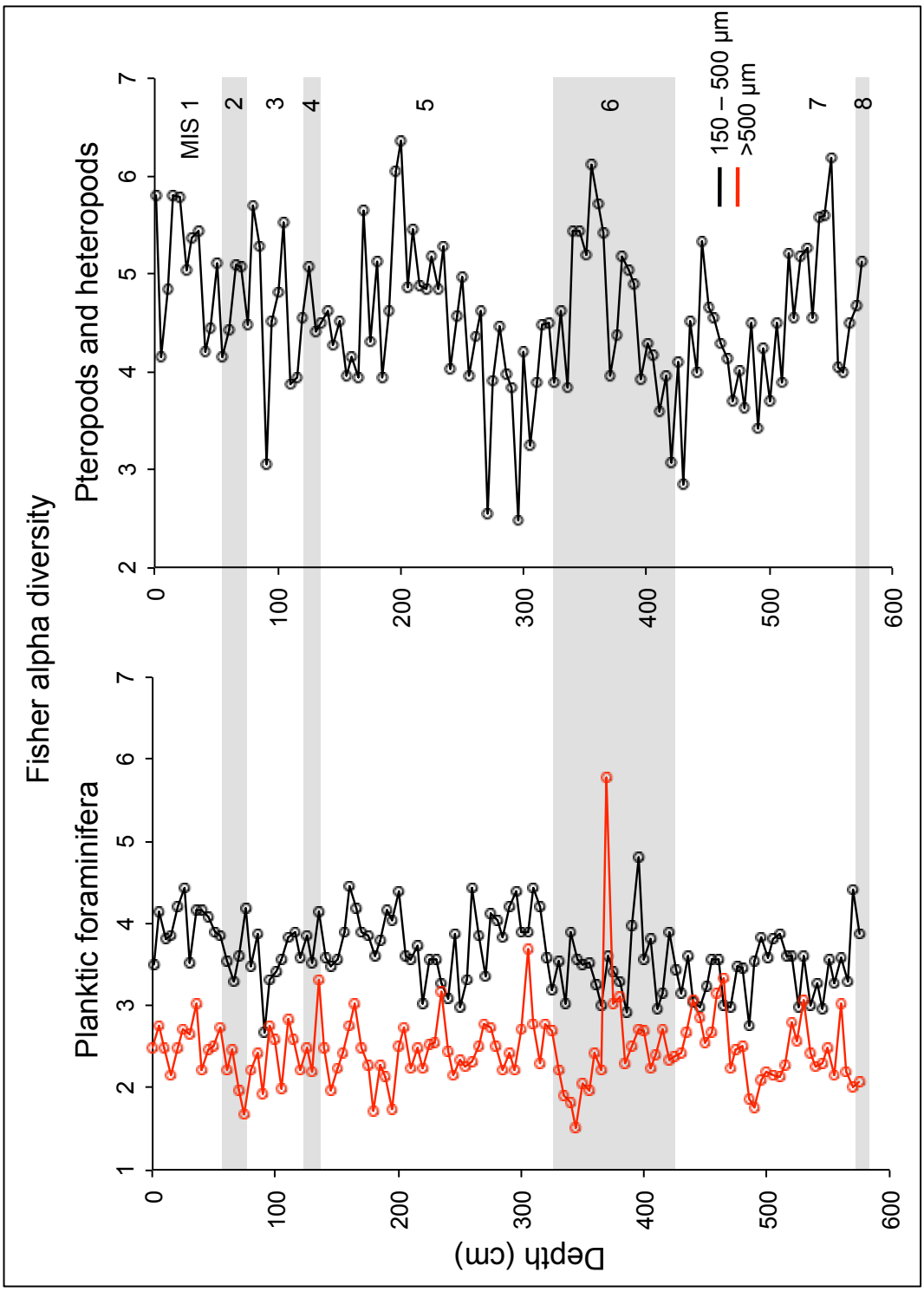

Figure 4.8 Fisher Alpha diversity of planktic foraminifera and pteropods and heteropods in CAR-MON 2. Grey boxes indicate glacial periods.

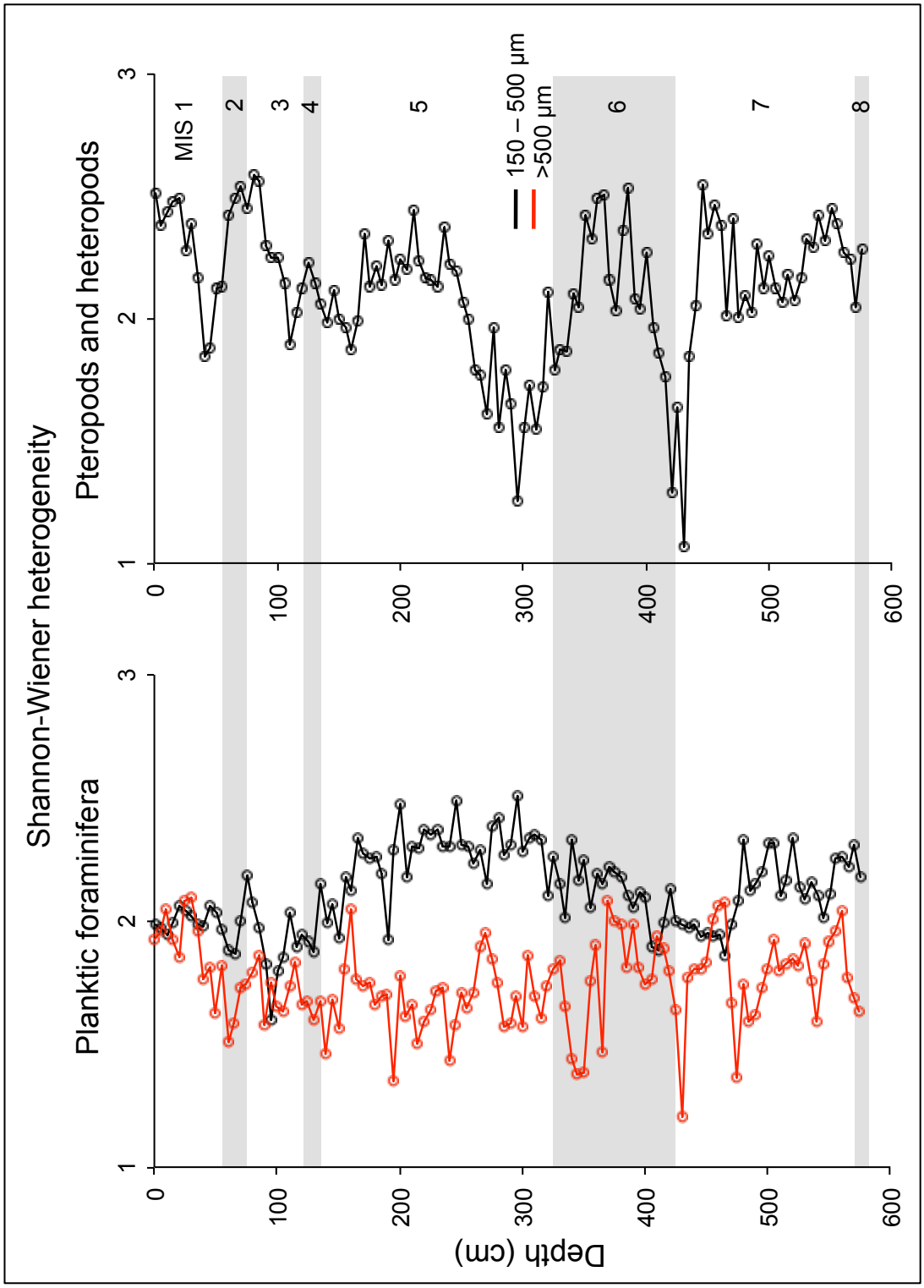

Figure 4.9 Shannon-Wiener heterogeneity of planktic foraminifera and pteropods and heteropods in core CAR-MON 2. Higher values indicate a more heterogeneous species assemblage. Grey boxes indicate glacial periods.

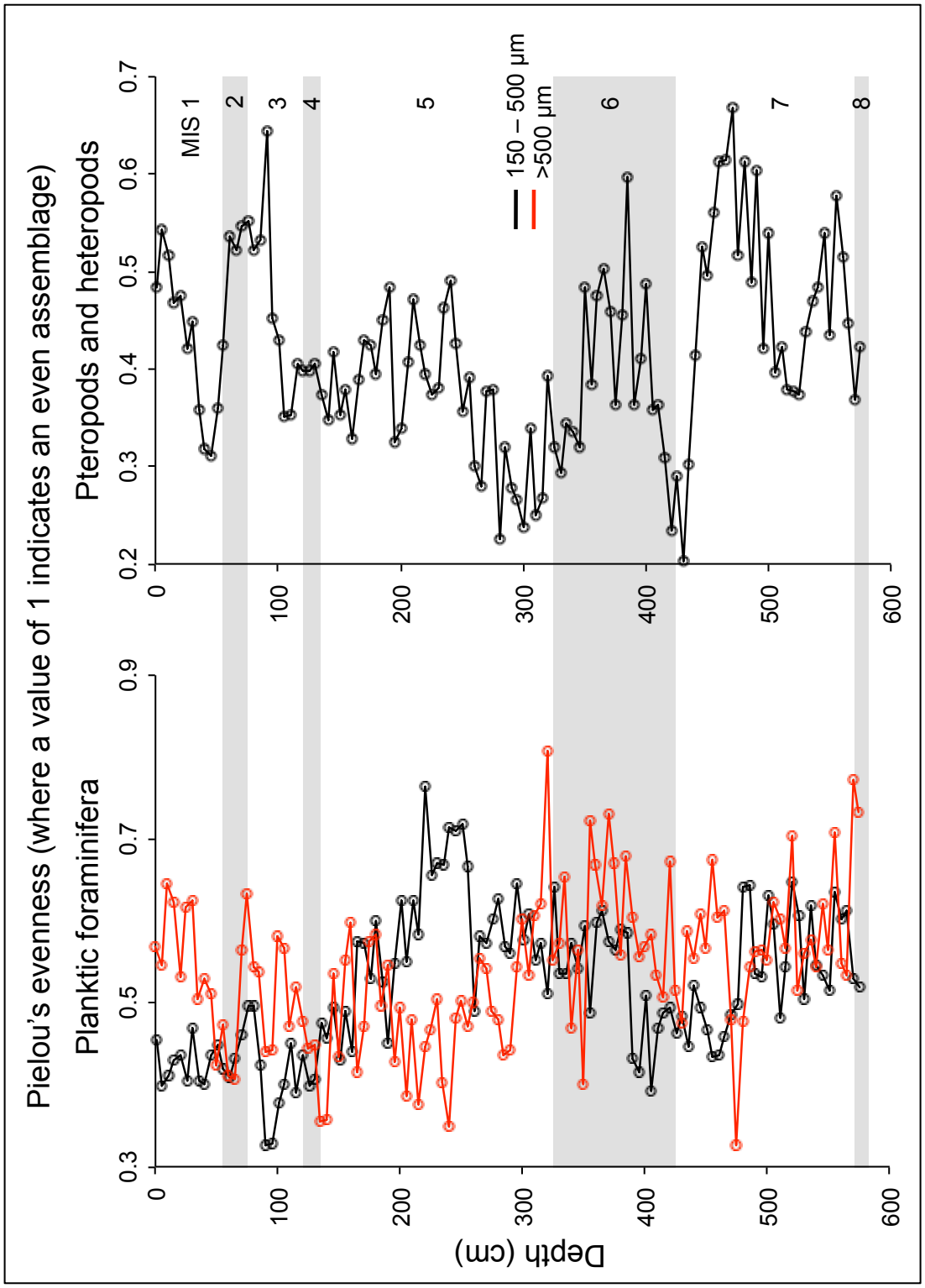

Figure 4.10 Pielou's evenness of planktic foraminifera and pteropods and heteropods in CAR-MON 2. Grey boxes indicate glacial periods.

4.1.3.3 SPECIES COMPOSITION AND CLIMATE

Due to the low latitude location of the Caribbean sites, and the consequent low variation in surface water temperature between glacial and interglacial periods, very little change in species composition occurs throughout the cores. Foster (2008) reconstructs the range in temperature from the last glacial maximum at MIS 2.2 to the last interglacial maximum at MIS 5.5 as being between 25.7 and 29.1°C. Schmidt *et al.* (2006) show a comparable reconstruction for Caribbean surface water, finding temperatures of 2.1–2.7°C colder than the present during the last three glacial maxima.

The species assemblage throughout cores CAR-MON 2, JC18-19 and JR123-35-V is composed of warm water sub-tropical species of planktic foraminifera, pteropods and heteropods. Dominant planktic foraminifera species include *G. ruber, G. sacculifer* (including *Globigerinoides trilobus*) and *Neogloboquadrina dutertrei.* Other common species include *Globigerinella aequilateralis*, *Globigerinoides conglobatus, Globigerinita glutinata* and *Globorotalia truncatulinoides.* The pteropod genus *Limacina* dominates the assemblage of holoplanktic gastropods. The most abundant species being *L. inflata* (up to 70% of the 150–500 μm pteropod and heteropod population of CAR-MON 2). Other common and often abundant species of pteropod include *Creseis acicula, C. virgula, L. bulimoides, Limacina trochiformis* and *Styliola subula.* The dominant heteropod genus is *Atlanta,* with the most abundant species being *Atlanta peronii* and *Atlanta selvagensis.* Other common and often abundant heteropod species include *Firoloida desmaresti* and *Carinaria lamarckii*.

Wells (1975) found that euthecosome pteropods deposited in the upper sediments close to Barbados accurately reflect the species composition and

relative abundances of the overlying waters. All species of pteropod found in the surface waters of the Western Caribbean (Table 4.2) are present in CAR-MON 2. The majority are represented within the surface 1 cm of sediment. The distribution of living shelled heteropods is not well documented and no published data from the Caribbean Sea were found. It is assumed that, like the shelled pteropods, the living assemblage of heteropods is well represented within the surface sediments of CAR-MON 2.

No extensive studies have been made of the modern living planktic foraminifera assemblage of the Caribbean Sea. More generally, Bé and Tolderlund (1971) have published the distribution of living planktic foraminifera in the surface waters of the Atlantic (Table 4.3). This study includes species distribution maps, which allow the living planktic foraminifera assemblage of the Lesser Antilles to be inferred. All species included in the maps of Bé and Tolderlund (1971) for the Lesser Antilles are present within the surface sediments of CAR-MON 2 with one exception, *Hastigerina pelagica,* which is absent from the entire core. However, Bé and Tolderlund (1971) only found *H. pelagica* to be present within the surface waters in low numbers (0.1–4.9 %) and it may, therefore not have been present in the waters overlying this site.

Although there appear to be several species present within the surface sediments of CAR-MON 2 that were not found by Bé and Tolderlund (1971), these are largely more recently described species. For example, *G. trilobus* would have been included within the counts of *G. sacculifer* by Bé and Tolderlund (1971), but has now been identified as a different species. It can be concluded that the surface sediments of CAR-MON 2 accurately represent the species and relative abundances of shelled pteropods, planktic foraminifera and most likely also shelled heteropods, living in the overlying waters.

Shelled pteropod species of the Caribbean Sea	Occurrence in CAR-MON 2 surface 1cm
Cavolinia inflexa	**Common**
Cavolinia uncinata	Absent
Clio pyramidata	**Present**
Creseis acicula	**Present**
Creseis virgula	**Common**
Cuvierina columnella	Absent
Diacavolinia longirostris	**Present**
Diacria quadridentata	Absent
Diacria trispinosa	**Common**
Hyalocylis striata	Absent
Limacina bulimoides	**Common**
Limacina helicina	Absent
Limacina helicoides	Absent
Limacina inflata	**Abundant**
Limacina lesueuri	**Present**
Limacina trochiformis	**Common**
Peraclis apicifulva	Absent
Peraclis reticulata	Absent
Styliola subula	**Common**

Table 4.2. Summary of shelled pteropod species of the modern Caribbean Sea, from Wells (1975, 1976) and Parra-Flores (2009), with those found in the surface (0–1 cm, >150 μm) sediments of CAR-MON 2 (Present <5%; Common 5–20%; Abundant >20%).

Planktic foraminifera species of the Caribbean Sea	Presence in surface 1cm sample of CAR-MON 2
Candeina nitida	**Present**
Globigerinella aequilateralis	**Present**
Globigerinita glutinata	**Present**
Globigerinoides conglobatus	**Common**
Globigerinoides ruber	**Common**
Globigerinoides sacculifer	**Abundant**
Globorotalia menardii	**Common**
Globorotalia truncatulinoides	**Present**
Hastigerina pelagica	Absent
Neogloboquadrina dutertrei	**Common**
Orbulina universa	**Common**
Pulleniatina obliquiloculata	**Present**

Table 4.3. Summary of planktic foraminifera species of the modern Caribbean Sea, from Bé and Tolderlund (1971), with those found in the surface (0–1 cm, >150 μm) sediments of CAR-MON 2 (Present <5%; Common 5–20%; Abundant >20%).

In general, variations in species composition (Appendix 8.2.1.2.A–D) are not synchronous with changes in the oxygen isotope record, with one exception, the planktic foraminifera *G. sacculifer* (including *G. trilobus*) (Fig. 4.11). However, the variation in percentage composition of some species do appear to change synchronously with the LDX calcification profile (Fig. 4.12). Three species of planktic foraminifera, one cool water species *Globigerina bulloides,* one cosmopolitan species *G. ruber* and one warm water species *G. menardii* (including *G. tumida*) show a similar trend to the LDX profile. In CAR-MON 2, *G. menardii* shows a positive relationship to the LDX, however, despite visually appearing to correlate, the relationship is not significant (r=0.154, p=0.128, n=99). *Globigerina bulloides* and *G. ruber* show a negative relationship to the LDX in CAR-MON 2, with significant, but weak correlations in the data (*G. bulloides* 120–575 cm r=-0.306, p=0.0012, n=66; *G. ruber* 0–575 cm r=-0.198, p=0.035, n=114). Two species of holoplanktic gastropod, one pteropod (*L. inflata*) and one heteropod (*A. peronii*), show a clear association to the LDX calcification profile (Fig. 4.13). In CAR-MON 2, *A. peronii* shows a significant negative correlation to the LDX profile (r=-0.611, p=<0.001, n=1.07), whereas *L. inflata* shows no correlation to the LDX profile (r=-0.058, p=0.539, n=114). However, if the LDX data is shifted down by 35 cm (see section 4.1.4.2 and Appendix), *L. inflata* shows a weak, but significant positive correlation to the LDX (r=0.287, p=0.003, n=107). Two further species (*S. subula* and *Atlanta* sp. D) show a partial association and significant correlation to the LDX. Between 320–0 cm in CAR-MON 2, percentages of *S. subula* show a positive correlation to the LDX data (r=0.481, p=<0.001, n=65). Between 575–125 cm in CAR-MON 2, *Atlanta* sp. D shows a negative correlation to the LDX data (r=-0.480, p=<0.001, n=86). In CAR-MON 2, several sub-tropical species of

holoplanktic gastropod show a peak in abundance between 230–190 cm (*A. peronii, Atlanta* sp. D, *F. desmaresti*), which coincides with the LDX excursion at this interval, suggesting a change in surface water conditions not detected by the oxygen isotope analysis.

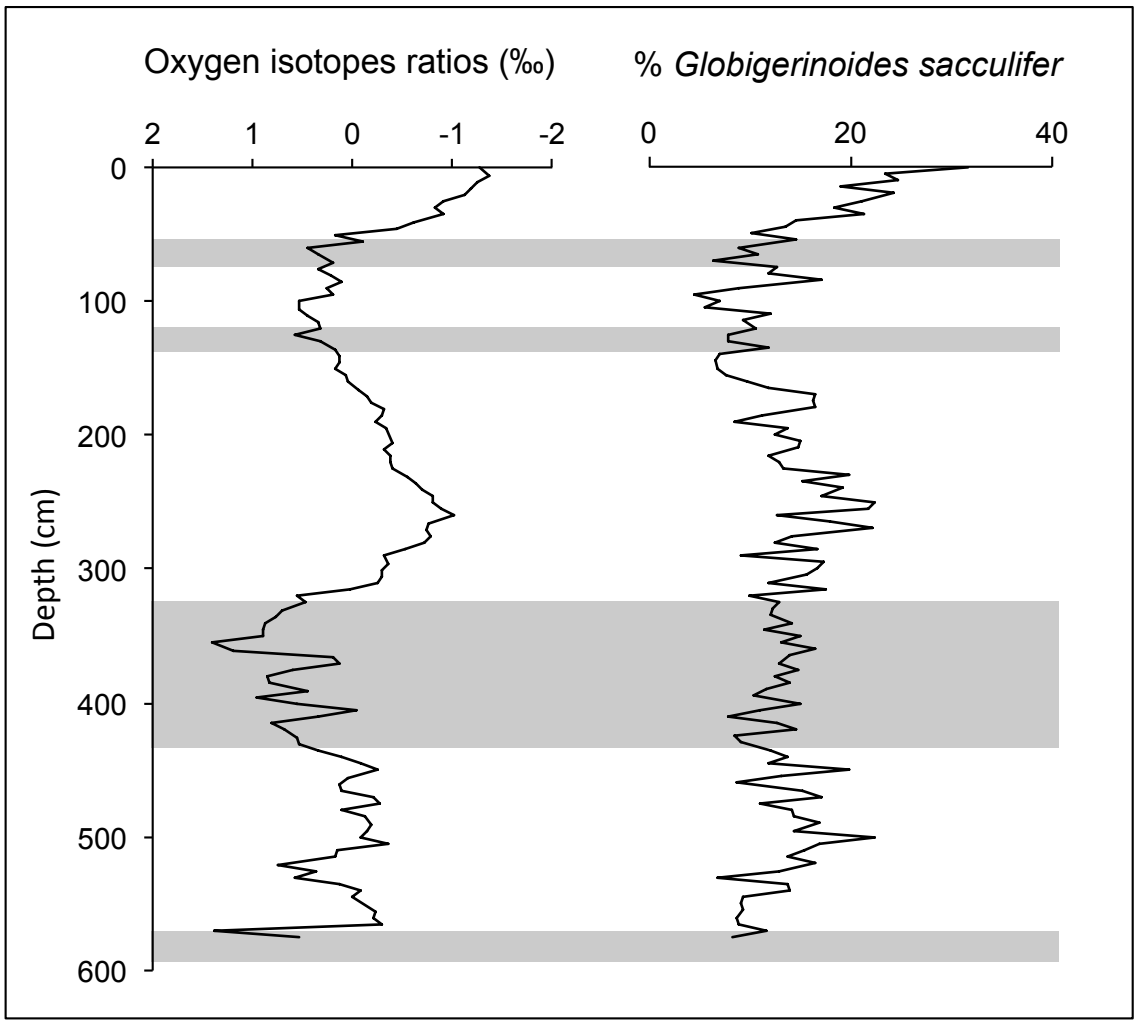

Figure 4.11 Changes in % of the planktic foraminifera species *Globigerinoides sacculifer* (150–500 µm fraction) compared to variations in oxygen isotope ratios in CAR-MON 2. Grey boxes indicate glacial periods.

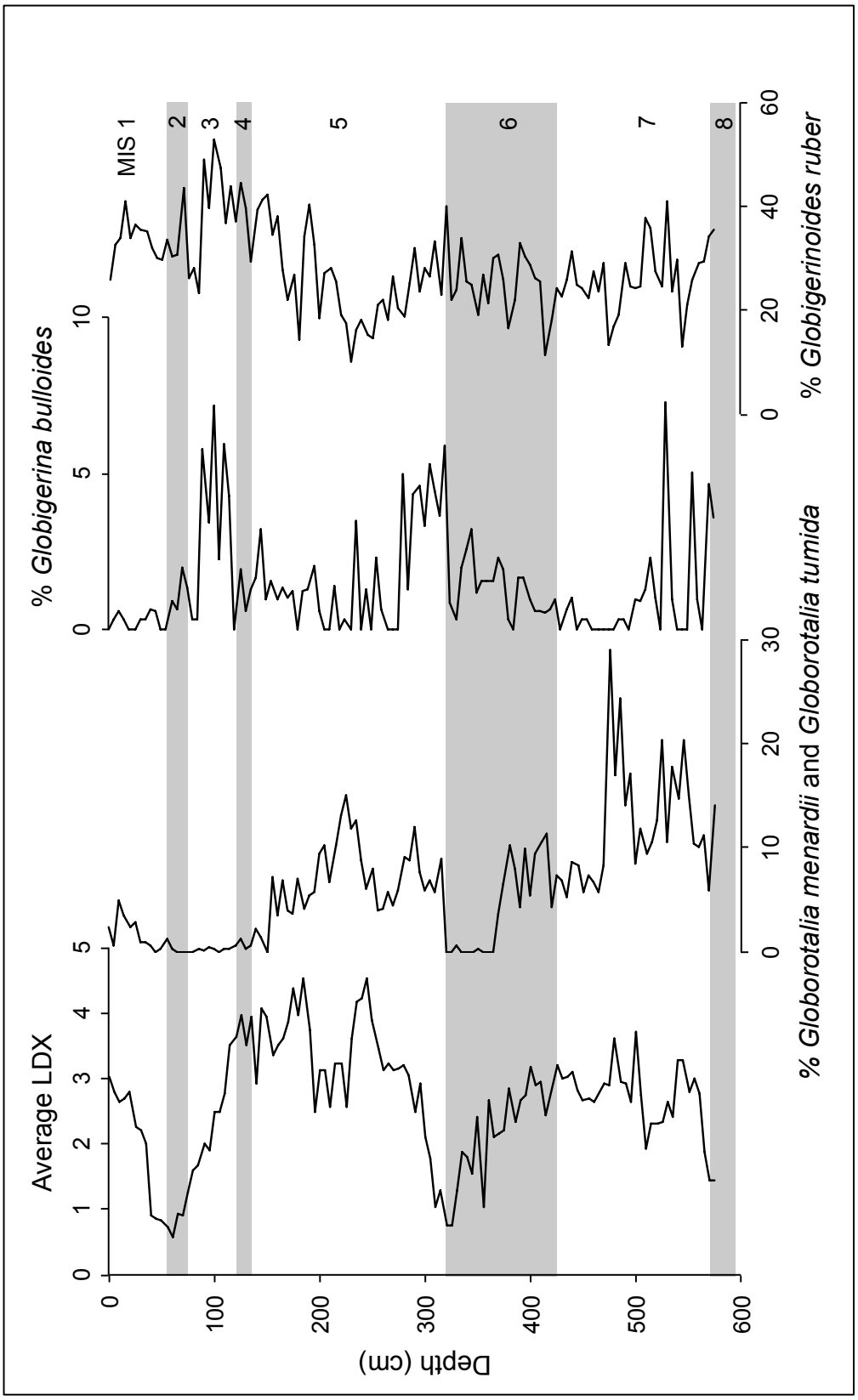

Figure 4.12 Changes in % of the planktic foraminifera species *Globorotalia menardii* (including *G. tumida*), *Globigerina bulloides* and *Globigerinoides ruber* (150–500 µm fraction) compared to variations in average LDX in CAR-MON. Grey boxes indicate glacial periods.

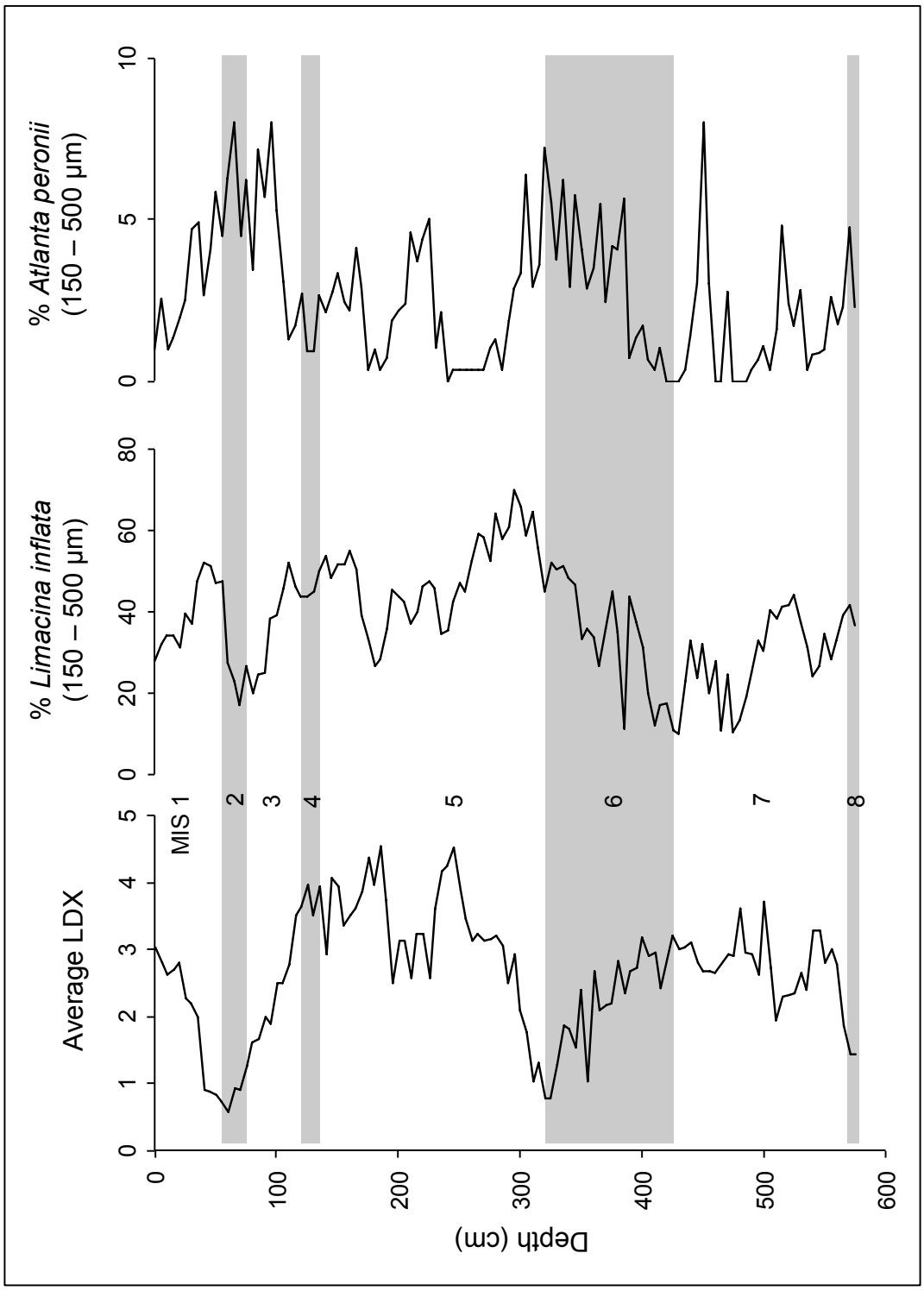

Figure 4.13 Changes in % of pteropod *Limacina inflata* (150–500 µm) and heteropod *Atlanta peronii* (150–500 µm) compared to variations in LDX for CAR-MON 2. Grey boxes indicate glacial periods.

4.1.4 CALCIFICATION INDICES

4.1.4.1 PLANKTIC FORAMINIFERA FRAGMENTATION

The percentage fragmentation of planktic foraminifera tests (Fig. 4.14) varies between the 150–500 μm and the >500 μm size fractions (Appendix 8.2.1.2.G, 8.2.1.2.I). In the >500 μm fraction of CAR-MON 2, there is no clear trend, with a generally constant fragmentation of between 5 and 17%. In the >500 μm fraction, the highest fragmentation of 24.2% occurs at MIS 6.5 (370 cm). There are 3 low excursions from the profile at 325 cm, 180 cm and 90 cm (3.8, 2.2 and 3.7% respectively). The low fragmentation at 180 cm and 90 cm coincide with MIS 5.1 and 3.1. In core JC18-19 and JR123-35-V, fragmentation in the >500 μm fraction is higher during interglacial periods and lower during glacial periods. In all the Caribbean cores, fragmentation of planktic foraminifera tests is slightly higher in the 150–500 μm fraction and appears to follow the climate more closely. Percentage fragmentation shows lower values during or immediately following cold periods. In CAR-MON 2, the lowest fragmentation (4.8%) occurs at 360 cm, coinciding with MIS 6.4 (Fig. 4.14). In CAR-MON 2, there are three particularly high peaks in fragmentation at 480 cm, 120 cm and 0 cm (20.9, 23.4 and 21.7% respectively) (Fig. 4.14). The peak in fragmentation at 480 cm coincides with MIS 7.3. High fragmentation in the surface sample may be an artefact of drilling disturbance at the water-sediment interface.

4.1.4.2 LDX CALCIFICATION

The LDX calcification profiles of cores CAR-MON 2, JC18-19 and JR123-35-V show a similar trend to global ice volume and Vostok (Petit *et al.,* 1999) atmospheric CO_2 concentration (Figs 4.15–4.17, Appendix 8.2.1.3.A, 8.2.1.3.B and 8.2.1.3.D), which is reproducible across the Montserrat sites. Since global

ice volume is closely related to changes in temperature and atmospheric CO_2 concentration (Mudelsee, 2001), it can be assumed that variations in pteropod calcification are related to variations in atmospheric CO_2 concentration (Figs 4.14, 4.17). For CAR-MON 2, Figure 4.15 shows that during periods of high oxygen isotope ratio (cool climate, low atmospheric CO_2 concentration), pteropod calcification is high with low LDX values (MIS 8.2, 570 cm, LDX 1.43; MIS 6.4, 355 cm, LDX 1.03; MIS 2.2, 60 cm, LDX 0.57). However, during periods of low oxygen isotope ratio (warm climate, high atmospheric CO_2 concentration), pteropod calcification is low with high LDX values (MIS 7.3, 480 cm, LDX 3.60; MIS 5, 245 cm, LDX 4.53; MIS 1, 0 cm, LDX 3.03). Cores JC18-19 and JR123-35-V also show this trend of high LDX values during interglacial periods and low LDX values during glacial periods (Fig. 4.15). The reproducibility of data across the studied area shows that trends in the LDX are not due to local surface water conditions. However, the relationship between oxygen isotope ratios and calcification (LDX) is not straightforward, as illustrated by CAR-MON 2 (Figs 4.14, 4.16). Figures 4.14–4.17 show that the LDX profile has several excursions from the general trend (for example, between 195–225 cm) and changes in calcification appear not to be proportional to changes in oxygen isotope ratio.

A bivariate, two-tailed Pearson correlation of LDX and global ice volume for CAR-MON 2 shows that the association is significant, but weak ($r=-0.318$, $p=0.001$, $n=112$). However, by shifting the LDX data down by 35 cm (Fig. 4.16, Appendix 8.2.1.3.C), correlation is greatly improved ($r=-0.572$, $p=<0.001$, $n=105$). This shift in data equates to around 15.2 kyr, assuming a constant sedimentation rate of 2.3 $cmkyr^{-1}$ in this area. However, the sedimentation rate of CAR-MON 2 varies and is complicated by regular inputs of volcanic ash. This

means that the lag in data may be shorter than 15.2 kyr if volcanic ash was removed from the sedimentation rate. This shift, or lag, in calcification data may indicate a number of processes which are discussed in section 6.3.1. However, reconstructed surface water carbonate concentrations for the Caribbean Sea (Foster, 2008) show a significant correlation to the global ice volume record of CAR-MON 2 ($r=0.886$, $p=<0.001$, $n=15$). This indicates that the lag in LDX calcification data does not reflect a delay in the response of surface water carbonate levels.

4.1.4.3 PTEROPOD SHELL SIZE

The average shell size of *L. inflata* specimens in CAR-MON 2 (Appendix 8.2.1.3.E) shows a similar trend to the oxygen isotope profile. However, average shell size shows a better association to the LDX calcification profile (Figs 4.14, 4.17), producing a significant negative correlation ($r=-0.577$, $p=0.019$, $n=16$). During periods of high calcification (low LDX values; MIS 8, 6 and 2), the average diameter of *L. inflata* shells is larger (265 μm, 459 μm and 580 μm for MIS 8, 6 and 2 respectively). Whereas, during periods of low calcification (high LDX values; MIS 7, 5 and 1), the average diameter of shells is smaller (223 μm, 227 μm and 266 μm for MIS 7, 5 and 1 respectively). Larger shells may also indicate increased productivity during glacial periods.

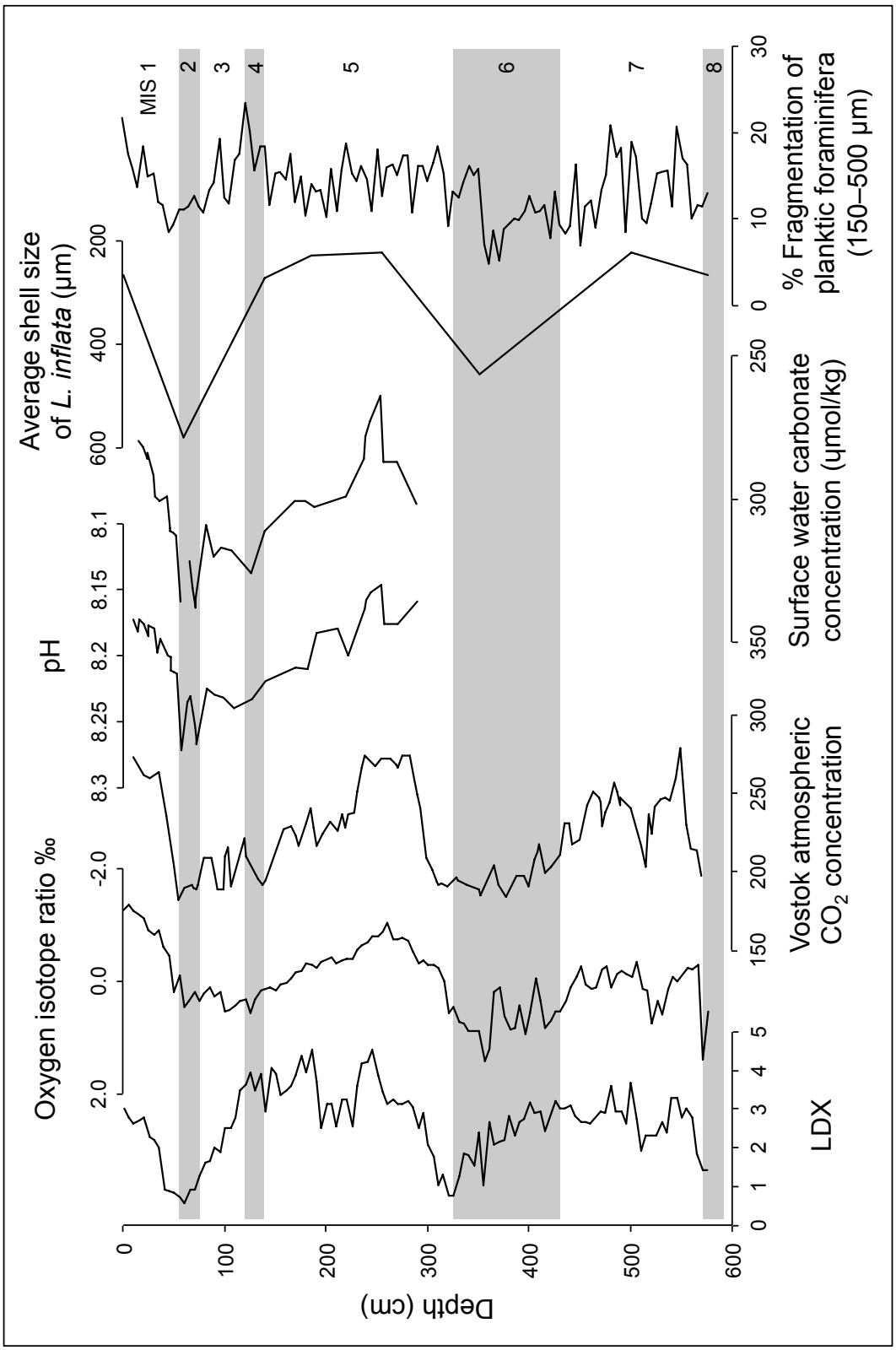

Figure 4.14 CAR-MON 2 LDX calcification profile, oxygen isotope profile, Vostok atmospheric CO_2 (Petit *et al.,* 1999), pH and surface water carbonate (Foster, 2008), average *L. inflata* shell size and planktic foraminifera fragmentation. Grey boxes indicate glacial periods.

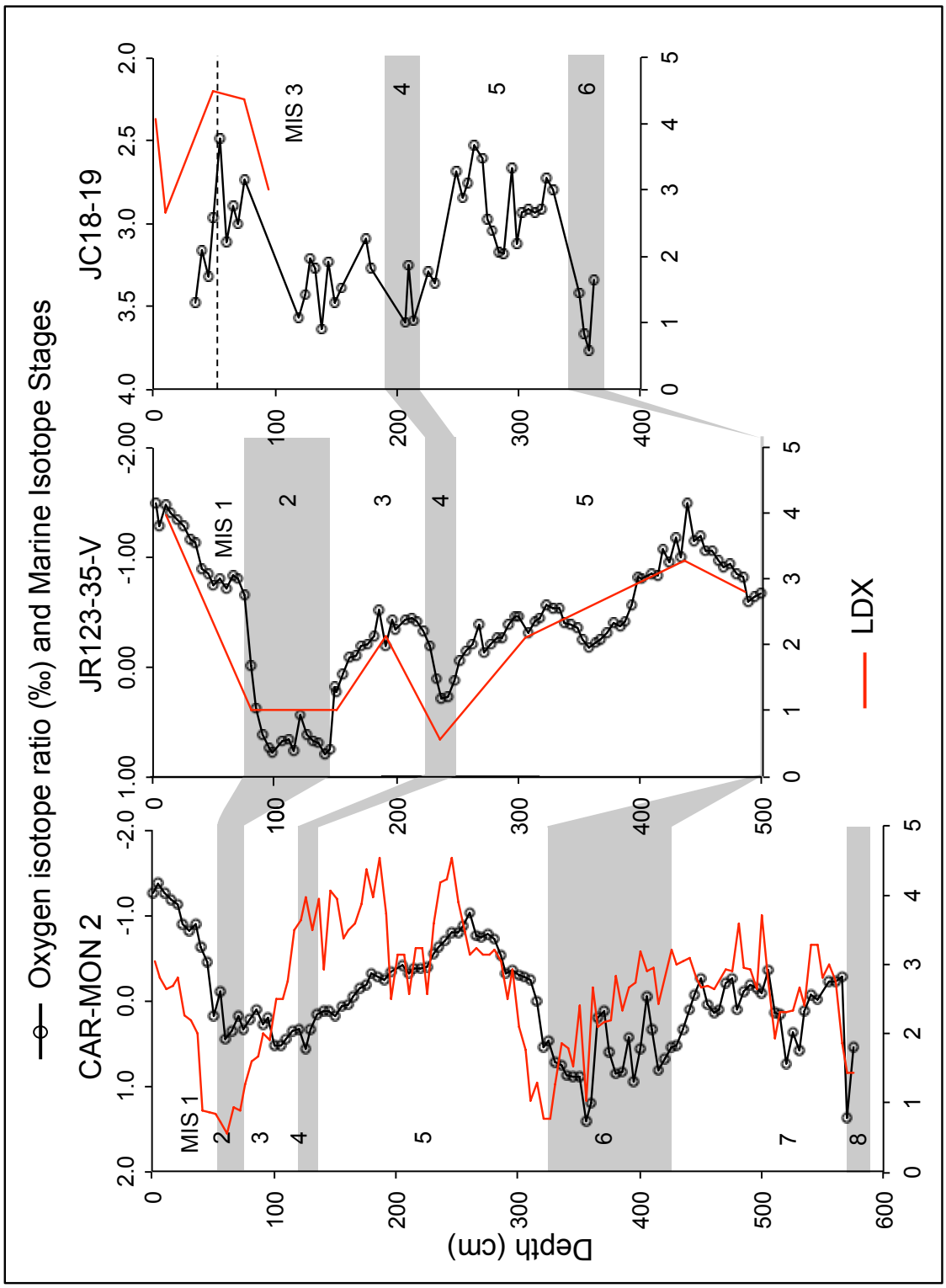

Figure 4.15 LDX calcification profiles (in red) and oxygen isotope profiles (in black) for JC18-19, JR123-35-V and CAR-MON 2.

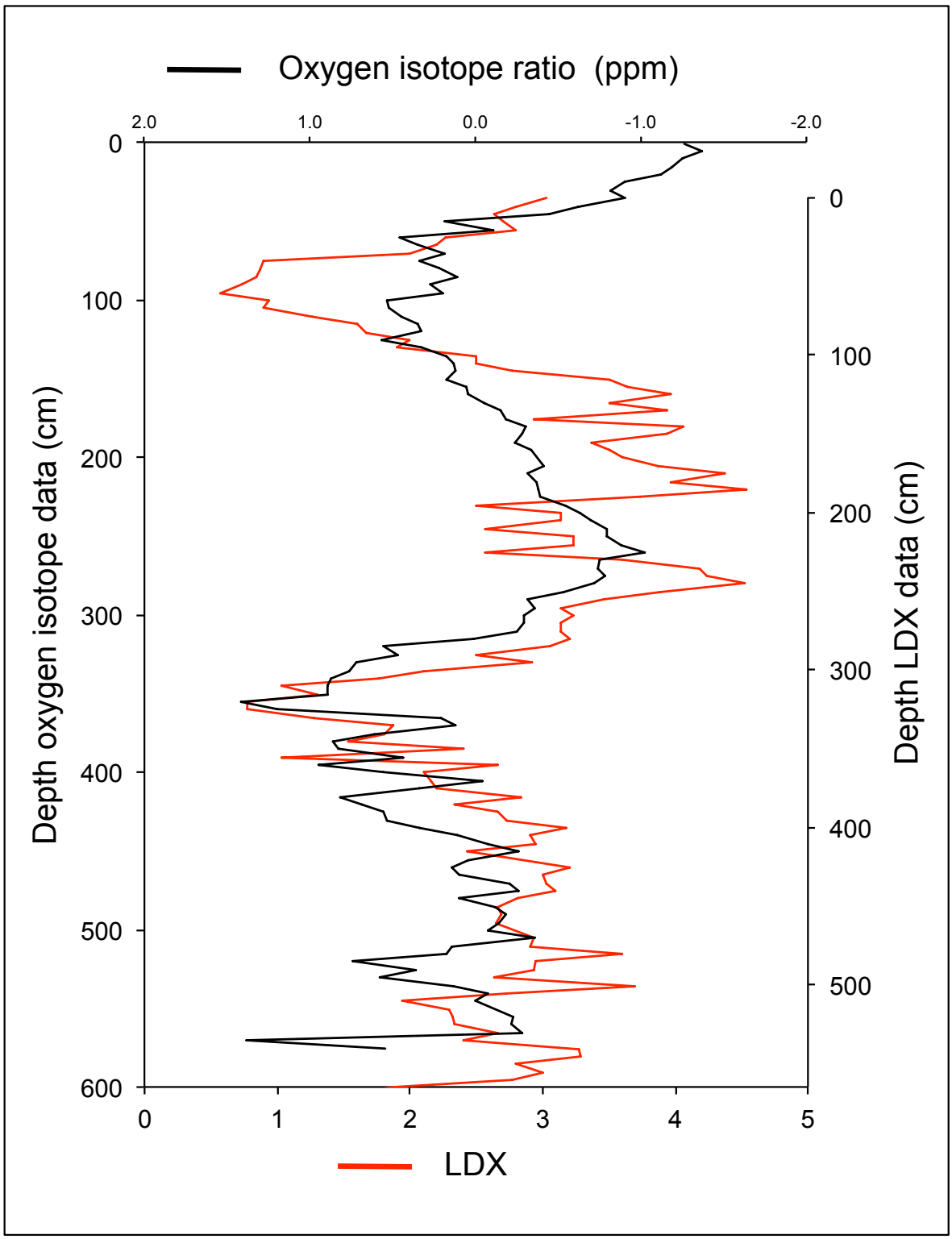

Figure 4.16 LDX calcification profile (in red) shifted down by 35 cm (Appendix 8.2.1.3.C) with the original oxygen isotope profile (in black) for CAR-MON 2.

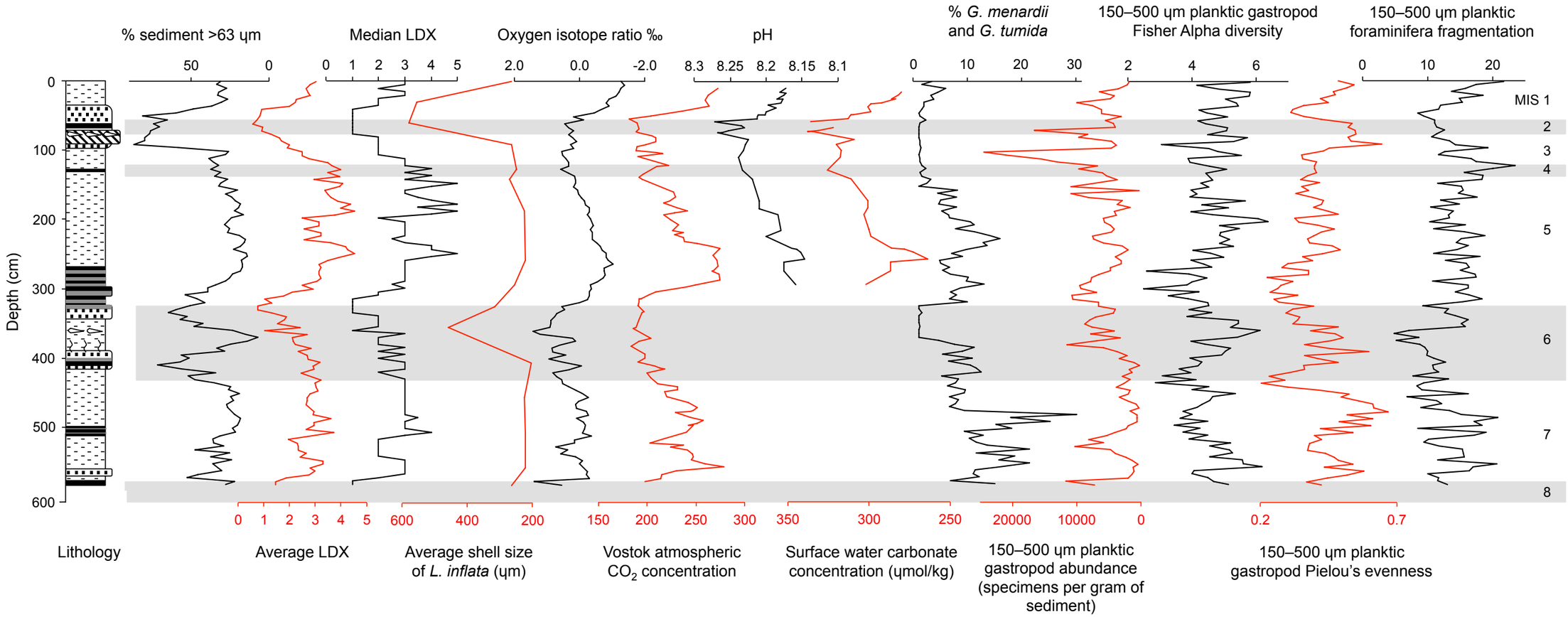

Figure 4.17 CAR-MON 2: % sediment >63 ɥm (Le Friant *et al.,* 2008), Average LDX, Median LDX, Average *L. inflata* shell size, Oxygen isotope profile (Le Friant *et al.,* 2008), Vostok atmospheric CO_2 concentration (Petit *et al.,* 1999), pH and surface water carbonate concentration (Foster, 2008), % *G. menardii* and *G. tumida,* Planktic gastropod abundance, Fisher Alpha diversity and Pielou's evenness and Planktic foraminifera fragmentation. Scales for % sediment >63 ɥm, Average *L. inflata* shell size, Oxygen isotope profile, pH and surface water carbonate concentration and Planktic gastropod abundance are reversed.

4.2 THE MEDITERRANEAN SEA: B5-1

A summary of Mediterranean Sea results can be found in Figure 4.30.

4.2.1 SEDIMENTOLOGY

4.2.1.1 CORE DESCRIPTION AND GRAIN SIZE

Core B5-1 is 494 cm long and composed of green-grey, hemipelagic, foraminifera and pteropod bearing sediments (Fig. 4.18, Appendix 8.2.2.1.A, 8.2.2.1.B), with a grain size of silt to very fine sand (Fig. 4.18). The core is relatively un-interrupted and shows little evidence of bioturbation. It contains abundant remains of planktic foraminifera, pteropods and heteropods.

4.2.1.2 SEDIMENTATION RATES

Sedimentation in core B5-1 has occurred at a fairly continuous rate of 2.5 $cmkyr^{-1}$, with a higher rate of 5 $cmkyr^{-1}$ in the top of the core (Fig. 4.19). This is in line with other published data (Weldeab *et al.,* 2003). Sections of the core have been dated using oxygen isotope stratigraphy (see section 4.2.2) and biozonation of planktic foraminifera (see section 4.2.2.3).

4.2.2 STABLE ISOTOPE STRATIGRAPHY AND DATING

4.2.2.1 OXYGEN ISOTOPE ANALYSIS

The oxygen isotope data (Appendix 8.2.2.2.A) suggest that B5-1 contains a relatively un-interrupted marine isotope record extending back to Marine Isotope Stage (MIS) 6 based on visual 'wiggle matching'. The length of the core and estimated age are in agreement with the oxygen isotope record published by Weldeab *et al.* (2003) for site SL87, approximately 60 km south east of B5-1 (Fig. 4.20). A bivariate, two-tailed Pearson correlation of $\delta^{18}O$ data at minor MIS stages, identified within cores B5-1 and SL87, show a significant

relationship between the two records (r=0.892, p=0.001, n=10). The record also compares well to the LR04 stack (Lisiecki and Raymo, 2005) and SPECMAP (Petit *et al.,* 1999) records of Marine Isotope Stages (Fig. 4.20).

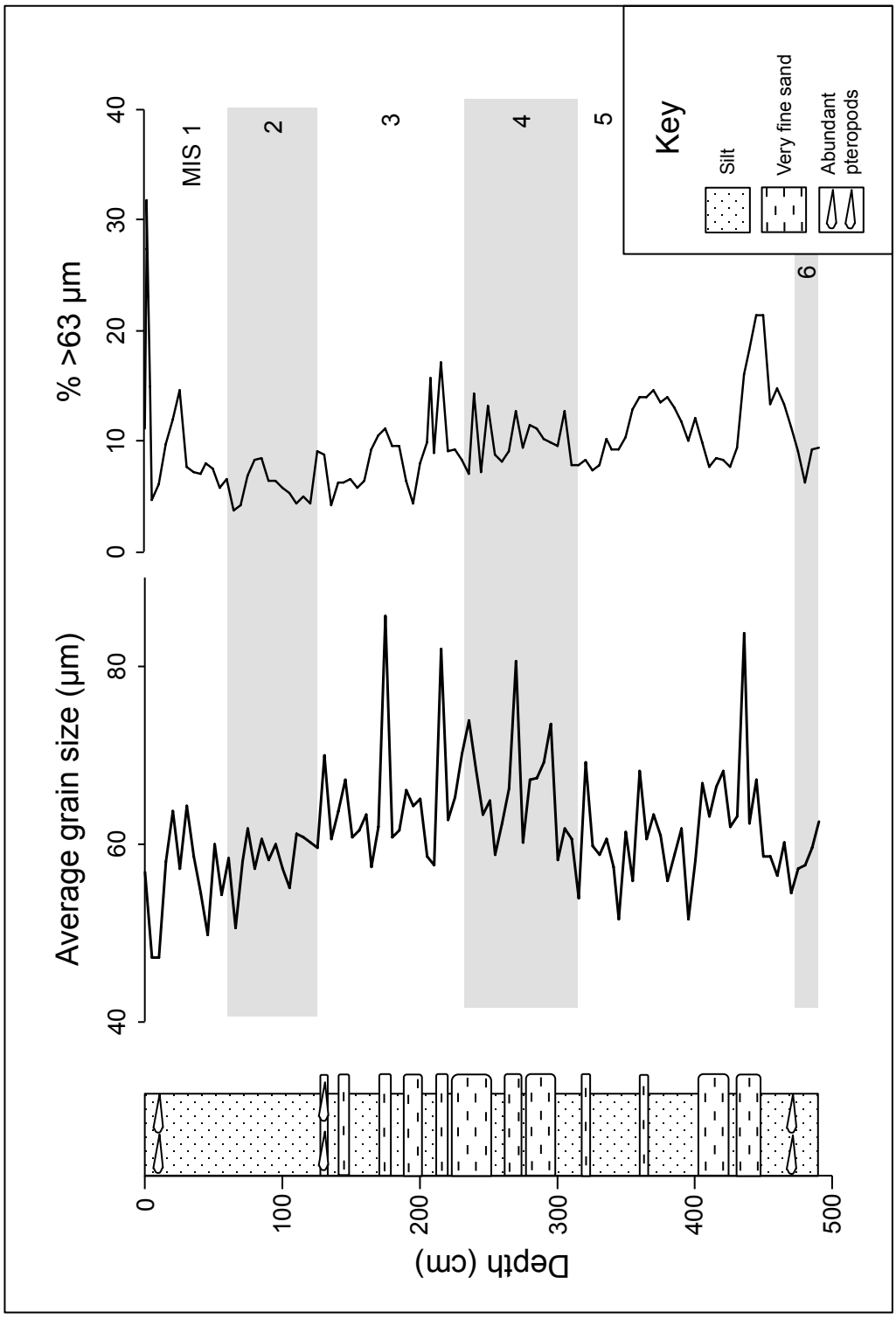

Figure 4.18 B5-1 lithology, average grain size and percentage of sediment >63 µm.

4.2.2.2 CARBON ISOTOPE ANALYSIS

Changes in the carbon isotope record (Fig. 4.21), although more variable, generally coincide with changes in the oxygen isotope record. Periods of higher $\delta^{13}C$ are generally associated with glacial phases (MIS 6, 4 and 2) and periods of lower $\delta^{13}C$ are associated with interglacial phases (MIS 5, 3 and 1). Since in general increased $\delta^{13}C$ values are associated with increases in productivity, these data suggest higher productivity during glacial periods. This trend has been found in the western Mediterranean by Pierre *et al.* (1999) and Weldeab *et al.* (2003).

4.2.2.3 CORRELATION TO KNOWN BIOZONES

The down hole distribution of several key species of planktic foraminifera (Appendix 8.2.2.3.A) within core B5-1 correlate well with distributions and bioevents published by Pujol and Vergnaud-Grazzini (1989) and Pérez-Folgado *et al.* (2003) for the Mediterranean Sea. These co-occurring events highlight several minor climatic episodes, providing additional dating points through the core (Fig. 4.22). Events P1, P2, P3 and P4 can be identified within the distribution of *N. dutertrei*; events B1, B2, B3, B4 and B5 can be identified within the distribution of *G. bulloides*; events 12, 13 and 14 can be identified within the distribution of *Globorotalia inflata*; events Ra, Ra2 and Ra3 can be identified within the distribution of *G. ruber* and event Sc2 can be identified in the distribution of *Globorotalia scitula.* Many of these changes in species abundance coincide with stadials (slight cooling during interglacial periods), interstadials (slight warming during glacial periods) and Heinrich Events (inputs of cold, fresh water during glacial periods) (Pérez-Folgado *et al.,* 2003).

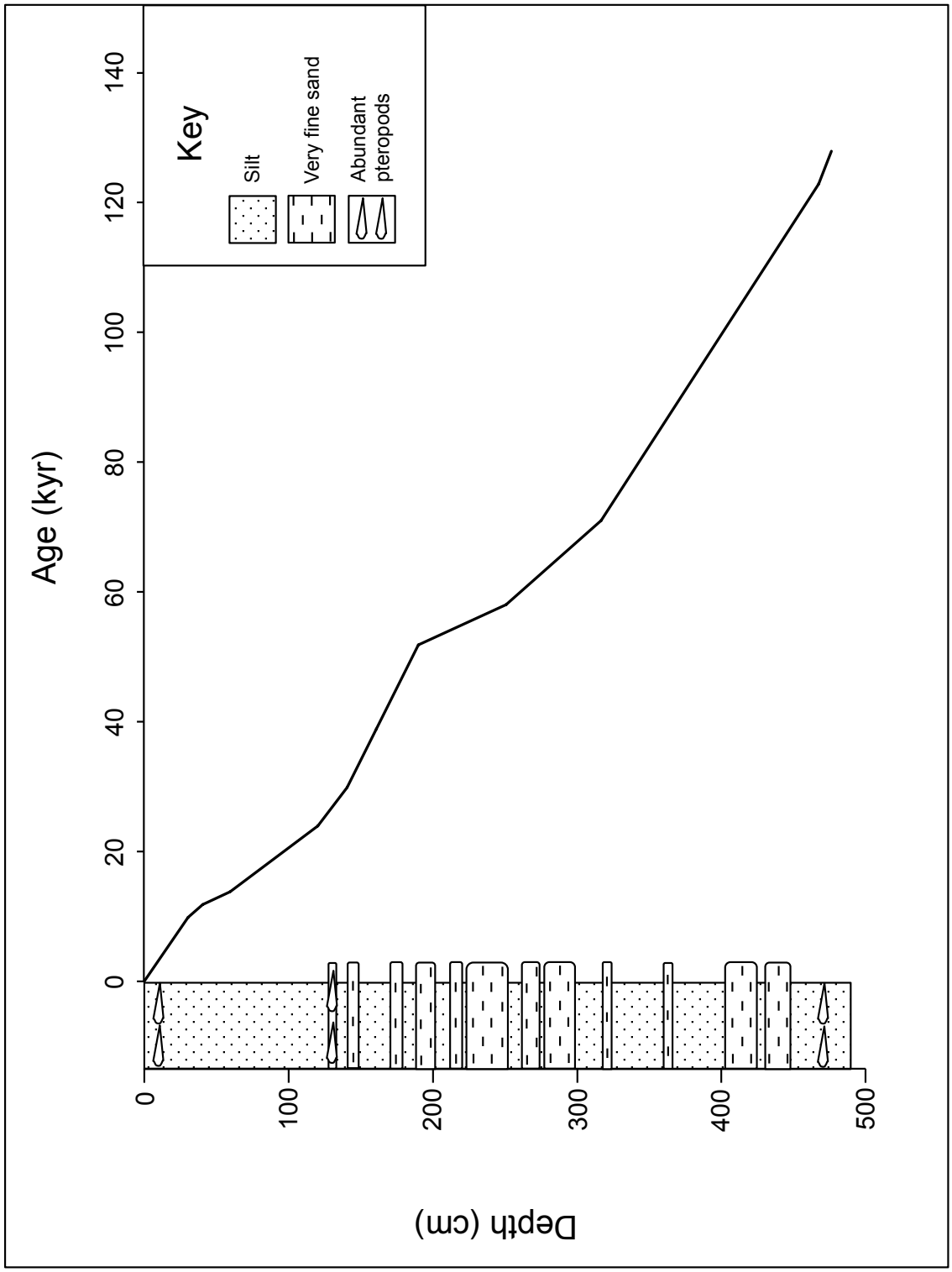

Figure 4.19 Lithology and age depth plot for B5-1 showing a fairly continuous rate of sedimentation. Sections of the core have been dated using oxygen isotope stratigraphy (see section 4.2.2) and biozonation of planktic foraminifera (see section 4.2.2.3).

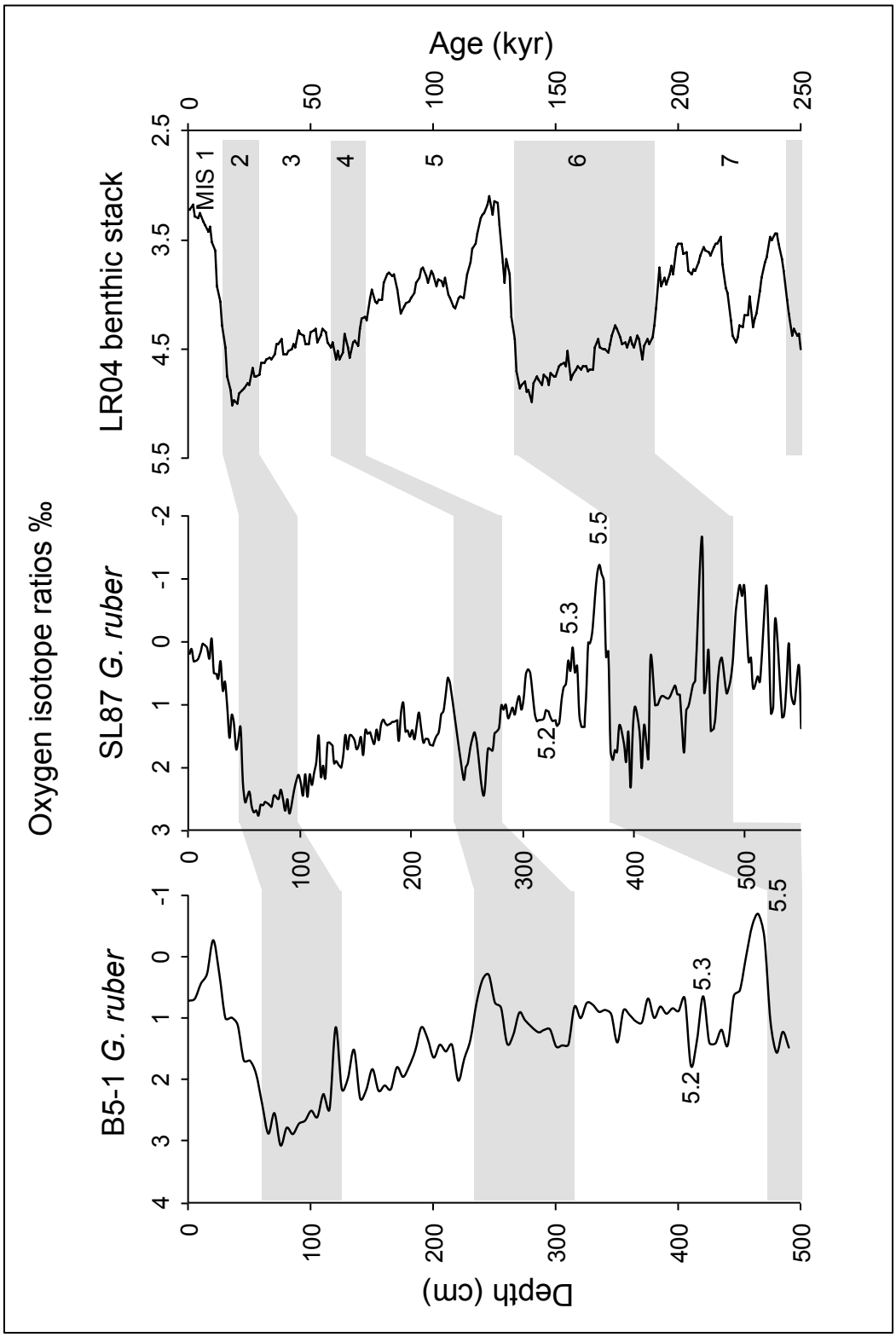

Figure 4.20 Comparison of the marine isotope records for B5-1, SL87 (Weldeab *et al.,* 2003), approximately 60 km south east of B5-1, and the LR04 benthic stack (Lisiecki and Raymo, 2005) with Marine Isotope Stages.

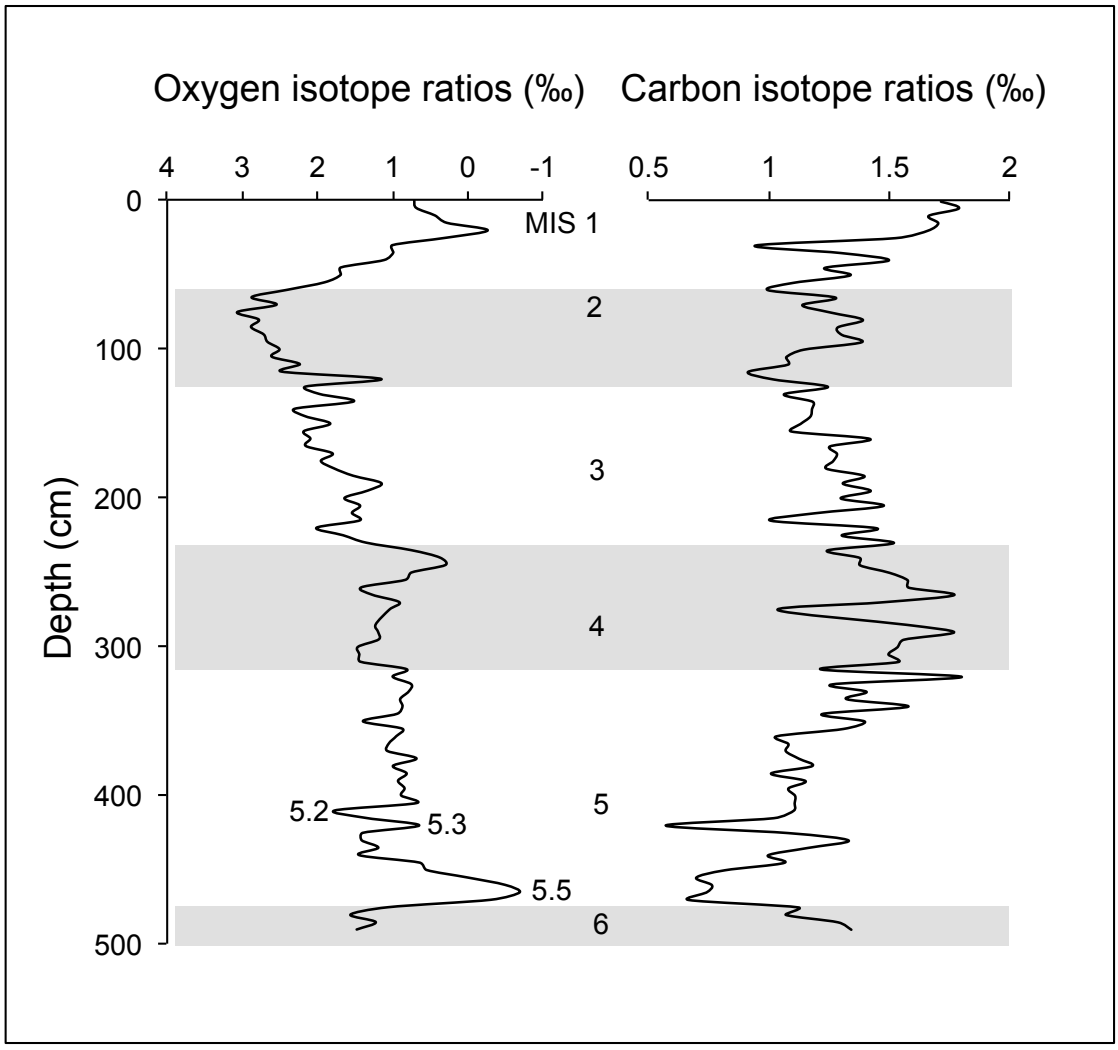

Figure 4.21 Oxygen and carbon isotope analysis for B5-1 with MIS. Grey boxes indicate glacial periods as designated in Figure 4.20.

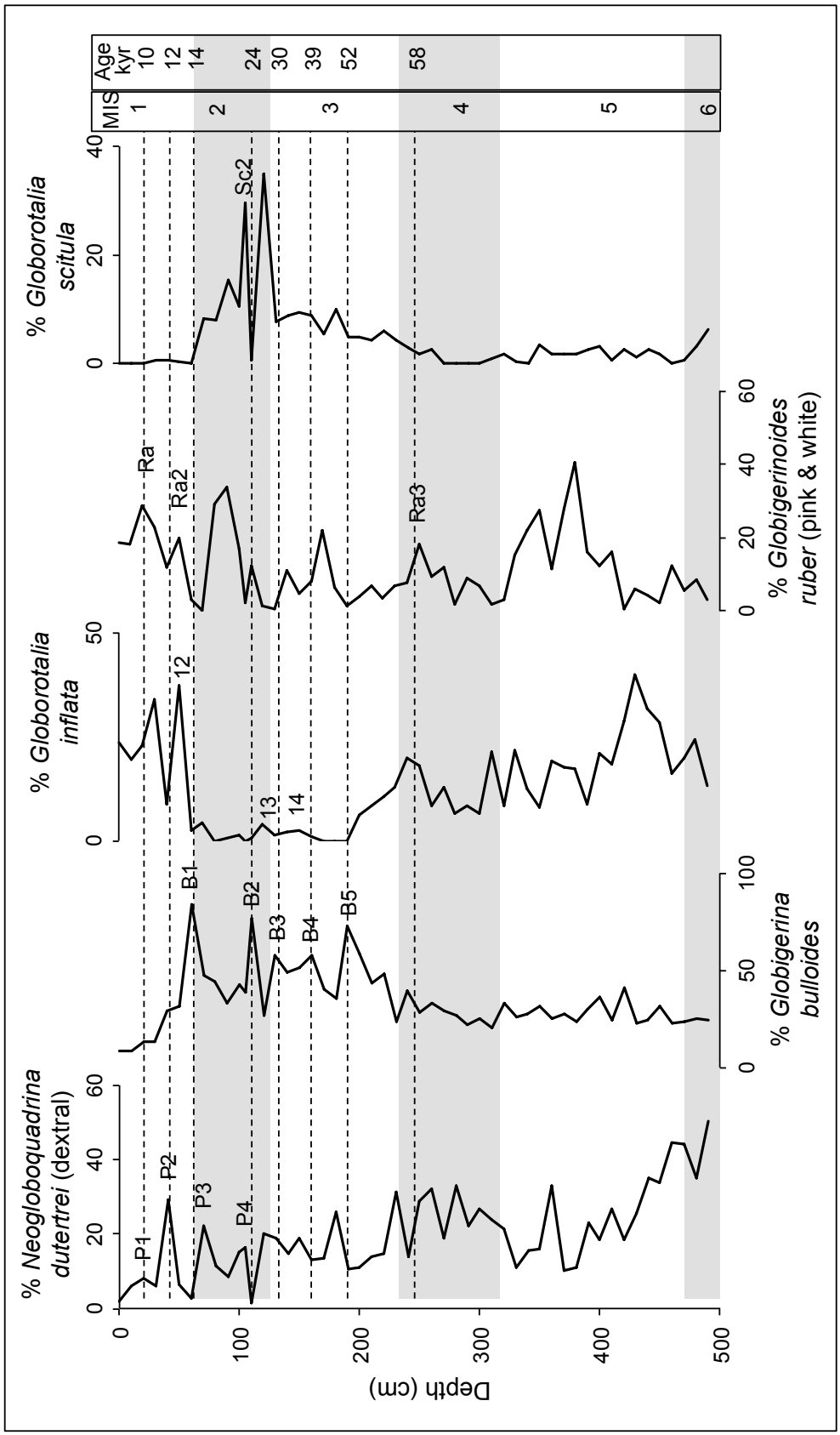

Figure 4.22 Bioevents of Pujol and Vergnaud-Grazzini (1989) and Pérez-Folgado *et al.* (2003) identified within B5-1 planktic foraminifera data.

4.2.3 MICROPALAEONTOLOGY

Nineteen species of pteropod, nine species of heteropod and twenty one species of planktic foraminifera were identified from the 150–500 μm and >500 μm size fractions of B5-1 (Table 4.4, Appendix 8.2.2.3.A–C). Some unidentifiable pteropod and heteropod species are labelled alphabetically within their genera. The >500 μm size fraction of several B5-1 samples were found to contain too few specimens of both planktic foraminifera and pteropods to be used in statistical analysis. Therefore, for the analysis of abundance and diversity, only the 150–500 μm size fraction was used.

4.2.3.1 ABUNDANCE

The trend in abundance of calcareous micro-zooplankton does not appear to change closely with isotope stages (Fig. 4.23) but with extremes of climate (from major interglacial MIS 5, to major glacial MIS 2). Abundance is variable, but generally lower during warm periods (MIS 5–4 and 1) and higher during cool periods (MIS 6 and 3–2) (Appendix 8.2.2.3.D, 8.2.2.3.E).

4.2.3.1.1 PLANKTIC FORAMINIFERA

The abundance of planktic foraminifera is relatively high at the base of the core, with a peak of 39,747 pfg^{-1}at the MIS 6/5 boundary. Abundance is then variable but generally low throughout MIS 5 and 4 (between 14,679–32,959 fg^{-1}), increasing again through MIS 3 with a peak at 230 cm (41,052 pfg^{-1}). Abundance of planktic foraminifera remains high through MIS 3 and 2, with the highest value occurring at 40 cm (40,789 pfg^{-1}). There are also two periods of low abundance during MIS 3 and 2, at 170 cm and 110 cm (15,048 pfg^{-1} and 15,148 pfg^{-1} respectively). The abundance of planktic foraminifera in

the 150–500 μm fraction shows no correlation to oxygen isotope data (r=0.184, p=0.201, n=50). This indicates no re;ationship between abundance and climate.

PTEROPODA	HETEROPODA
Cavolinia inflexa (Lesueur, 1813) *Clio pyramidata* Linnaeus, 1767 *Clio cuspidata* (Bosc, 1802) *Creseis acicula* (Rang, 1828) *Creseis virgula* (Rang, 1828) *virgula* (Rang, 1828) *Creseis virgula* (Rang, 1828) *constricta* (Chen and Bé, 1964) *Cuvierina columnella* (Rang, 1827) *Diacria trispinosa* (Lesueur, 1821) *Limacina bulimoides* (d'Orbigny, 1836) *Limacina inflata* (d'Orbigny, 1836) *Limacina retroversa* (Fleming, 1823) *Limacina trochiformis* (d'Orbigny, 1834) *Limacina* sp. B *Limacina* sp. D *Styliola subula* (Quoy and Gaimard, 1827) *Gleba cordata* Forskål, 1776 *Peracle* spp. *Paedoclione doliiformis* Danforth, 1907 Gymnosome veligers	*Atlanta helicinoidea* Gray, 1850 *Atlanta peronii* Lesueur, 1817 *Atlanta rosea* Gray, 1850 *Atlanta selvagensis* de Vera and Seapy, 2006 *Atlanta* spp. *Carinaria lamarckii* de Blainville, 1817 *Carinaria* spp. *Firoloida desmarestia* Lesueur, 1817 *Oxygyrus keraudreni* (Lesueur, 1817)
GLOBIGERINIDA (PLANKTIC FORAMINIFERA)	
Beella digitata (Brady, 1879) *Candeina nitida* d'Orbigny, 1839 *Globigerina bulloides* d'Orbigny, 1826 *Globigerina cariacoensis* Rögl and Bolli, 1973 *Globigerinella aequilateralis* (Brady, 1879) *Globigerinella calida* (Parker, 1962) *Globigerinita glutinata* (Egger, 1893) *Globigerinoides elongatus* (d'Orbigny, 1839) *Globigerinoides pyramidalis* Jones, 1994 *Globigerinoides ruber* (d'Orbigny, 1839) *Globigerinoides sacculifer* (Brady, 1877)	*Globigerinoides trilobus* (Reuss) *Globorotalia crassaformis* (Galloway and Wissler, 1927) *Globorotalia inflata* (d'Orbigny, 1839) *Globorotalia scitula* (Brady, 1882) *Globorotalia truncatulinoides* (d'Orbigny, 1839) *Globorotaloides hexagona* (Natland, 1938) *Hastigerina pelagica* (d'Orbigny, 1839) *Neogloboquadrina dutertrei* (d'Orbigny, 1839) *Orbulina universa* d'Orbigny, 1839 *Turborotalia humilis* (Brady, 1884)

Table 4.4 Species of pteropod, heteropod and planktic foraminifera identified from both size fractions of sediment for B5-1.

4.2.3.1.2 PTEROPODS AND HETEROPODS

The abundance of pteropods is generally much lower than the abundance of planktic foraminifera. At the base of the core, abundance is fairly high at the MIS 6/5 boundary and then decreases and remains low throughout MIS 5 and 4, with a low of 39 pteropods per gram (pg^{-1}) between 340–330 cm. Throughout MIS 3 to 1, abundance is much higher, ranging between 1410 pg^{-1} and the peak in abundance of 10,132 pg^{-1}at 130 cm. There are three excursions to low abundances at 170 cm (2584 pg^{-1}), 110 cm (3314 pg^{-1}) and 60 cm (1410 pg^{-1}), which coincide with similar reductions in planktic foraminifera abundance. These points coincide with climatic events. The two excursions to low abundance at 170 cm and 110 cm coincide with Heinrich Events at 39 kyr and 24 kyr respectively. These are brief cool periods in the climate during the interglacial period MIS 3. The reduced abundance at 60 cm coincides with interstadial 1, a slight warming of the climate at 14 kyr following the last glacial period. However, pteropod and heteropod abundance in the 150–500 μm fraction does not produce a significant correlation to oxygen isotope data ($r=0.160$, $p=0.270$, $n=50$).

4.2.3.2 DIVERSITY

The Fisher Alpha diversity (Fig. 4.24), Shannon-Wiener heterogeneity (Fig. 4.25) and Pielou's assemblage evenness (Fig. 4.26) of planktic foraminifera, pteropods and heteropods in B5-1 do not change closely with all MIS, but with extreme MIS (glacial and interglacial maxima). Values are generally higher during warm periods (MIS 5–4 and 1) and lower during cool periods (MIS 6 and 3–2).

4.2.3.2.1 PLANKTIC FORAMINIFERA

The Fisher Alpha diversity, Shannon-Wiener heterogeneity and Pielou's assemblage evenness of planktic foraminifera show low variability, but are generally higher during warm periods and low during cool periods. Fisher Alpha diversity and Shannon-Wiener heterogeneity show a significant negative relationship to oxygen isotope data for B5-1 (FA, r=-0.488, p=0.001, n=50; S-W, r=-0.436, p=0.002, n=50), indicating a higher diversity during warm periods. However, Pielou's evenness does not show a significant correlation to oxygen isotope data (r=-0.202, p=0.160, n=50). The highest diversity occurs at 410 cm (MIS 5) and 0 cm (MIS 1) with values of 3.02 and 3.03 respectively. The highest heterogeneity and evenness also occur within warm periods, with the highest heterogeneity of 2.33 at 10 cm (MIS 1) and the most even assemblage at 270 cm (MIS 4) with a value of 0.78. The lowest diversity, heterogeneity and evenness all occur during cool periods. The lowest diversity occurs at 140 cm (MIS 3) with a value of 1.27 and the lowest assemblage evenness occurs at 110 cm (MIS 3) with a value of 0.22. There are three low excursions in planktic foraminifera heterogeneity at 190, 110 and 60 cm with values of 1.00, 0.90 and 0.70 respectively. These data points coincide with climatic events previously identified in the abundances of planktic foraminifera, pteropods and heteropods. The two excursions to low evenness at 190 cm and 60 cm coincide with interstadials 14 and 1 respectively and the reduction at 110 cm coincides with a Heinrich Event at 24 kyr. In general these data show a more diverse, heterogeneous and even assemblage of planktic foraminifera during warm periods.

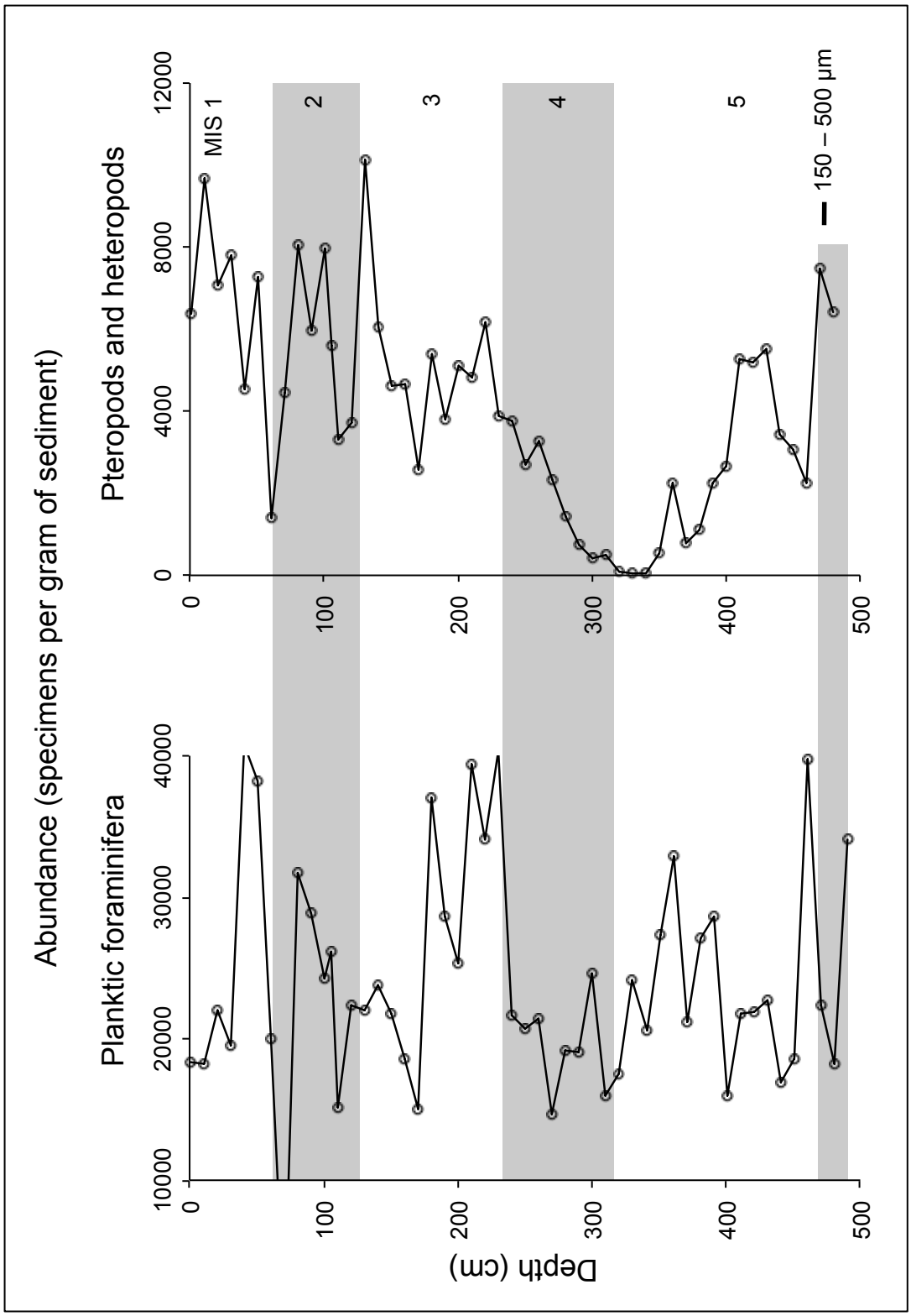

Figure 4.23 Abundance of planktic foraminifera and pteropods and heteropods for the size fraction 150–500 µm of B5-1. Grey boxes indicate glacial periods.

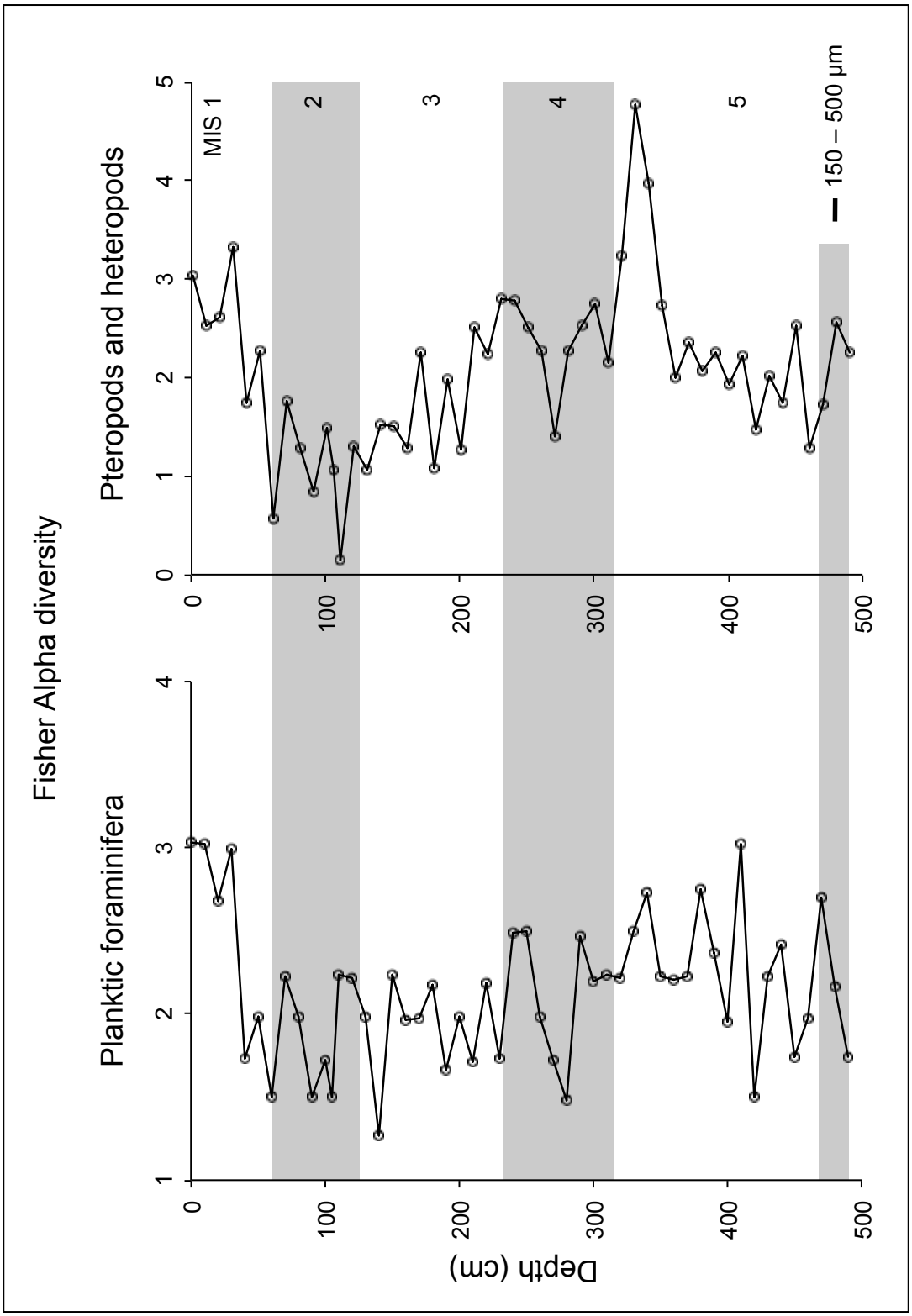

Figure 4.24 Fisher Alpha diversity of planktic foraminifera and pteropods and heteropods size fraction 150–500 µm in B5-1. Grey boxes indicate glacial periods.

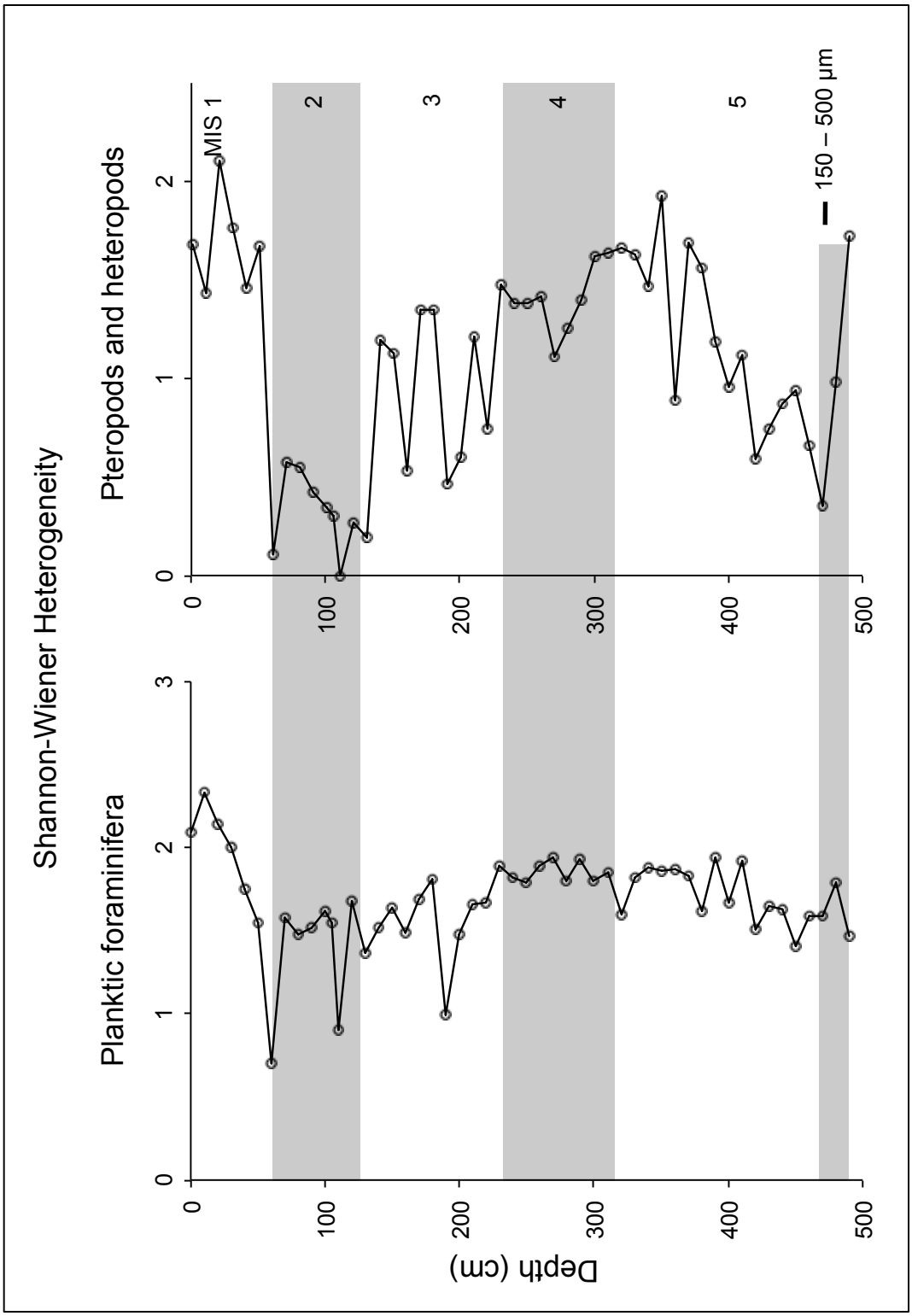

Figure 4.25 Shannon-Wiener heterogeneity of planktic foraminifera and pteropods and heteropods for the size fraction 150–500 µm in core B5-1. Higher values indicate a more heterogeneous species assemblage. Grey boxes indicate glacial periods.

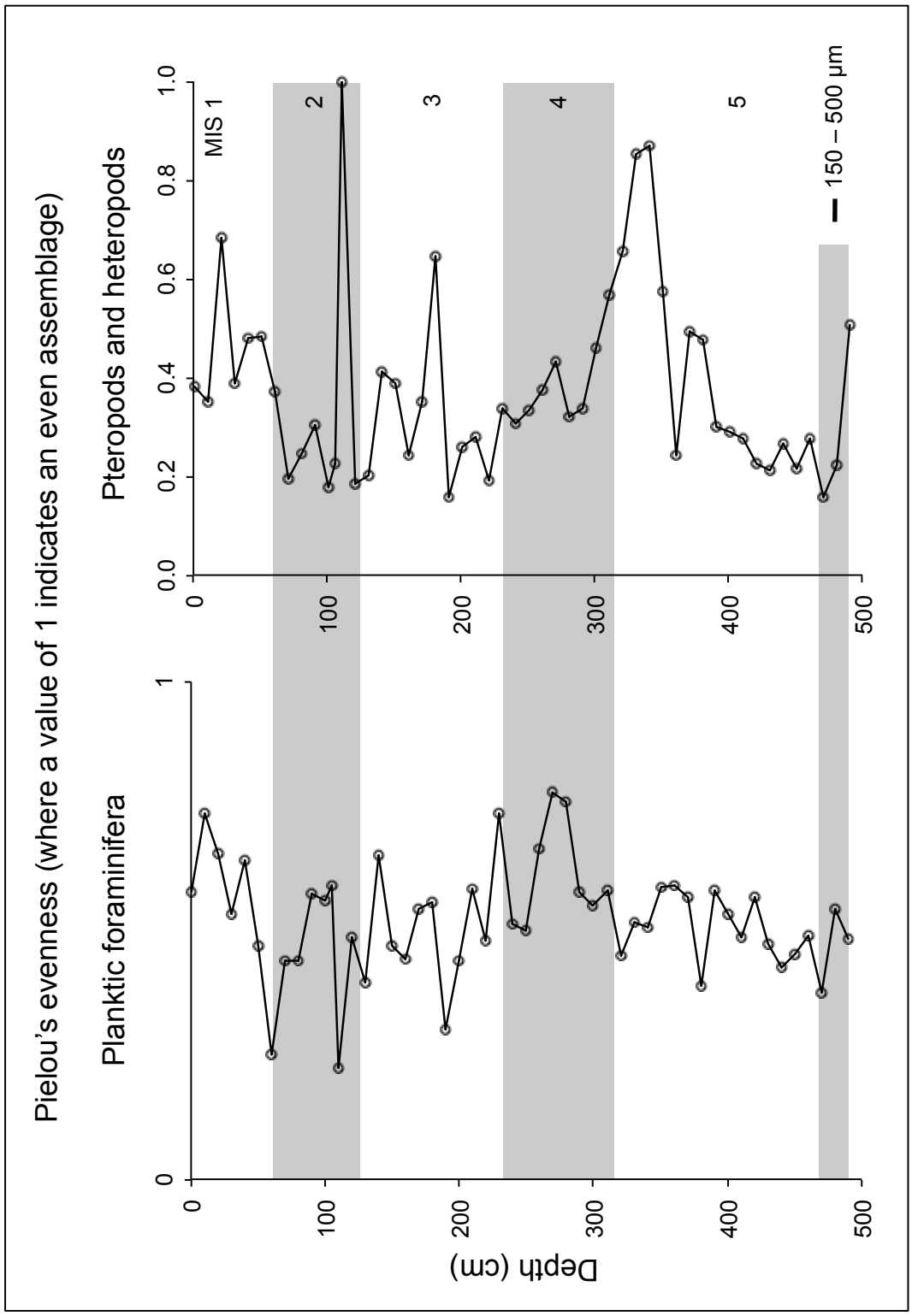

Figure 4.26 Pielou's evenness of planktic foraminifera and pteropods and heteropods for the size fraction 150–500 µm in core B5-1. Grey boxes indicate glacial periods.

4.2.3.2.2 PTEROPODS AND HETEROPODS

The Fisher Alpha diversity of pteropods and heteropods is more variable but shows a similar trend to planktic foraminifera (Figs 4.24, 4.25, 4.26), with higher values during warm periods (MIS 5–4 and 1) and lower values during cool periods (MIS 6 and 3–2). Fisher Alpha diversity and Shannon-Wiener heterogeneity show a significant negative correlation to oxygen isotope data (FA, r=-0.436, p=0.002, n=50; S-W, r=-0.412, p=0.003, n=50), indicating higher diversity and heterogeneity during warm periods. Pielou's evenness however, does not show a significant relationship to climate (r=-0.092, p=0.527, n=50). Diversity, heterogeneity and evenness all show their highest values during warm periods. The highest diversity occurs at 330 cm (MIS 5) with a value of 4.78 and the highest heterogeneity occurs at 20 cm (MIS 1) with a value of 2.11. The highest assemblage evenness at 110 cm is an anomalous point since it is based on just one species (*L. inflata*) and therefore shows perfect evenness with a value of 1.00. The second most even assemblage occurs at 340 cm (MIS 5) with a value of 0.87. The lowest diversity, heterogeneity and evenness of pteropod and heteropod assemblages all occur during cool periods. The lowest diversity of 0.15 occurs at 110 cm (MIS 3), where the assemblage is made up of only one species and the least even assemblage occurs at 470 cm (MIS 6) and 190 cm (MIS 3), both with a value of 0.16. The lowest heterogeneity matches that of the planktic foraminifera, with three low excursions at 190, 110 and 60 cm (0.46, 0.00 and 0.11 respectively).

4.2.3.3 SPECIES COMPOSITION AND CLIMATE

The pteropod distributions of the modern oceans are described by Bé and Gilmer (1977). The western Mediterranean Sea pteropod assemblage consists of only a few common and abundant species and a number of species that are considered present, which are summarised in Table 4.5. Due to the patchy, swarming nature of pteropod distributions, it is unlikely that representatives of all the species found in the western Mediterranean will be found within the sediments of one particular area. It is therefore not surprising that not all of the common and abundant species detailed by Bé and Gilmer (1977) are present in the surface sediments of B5-1. The species of the surface sediments and overlying waters are therefore reasonably comparable and there are no species of pteropod in the surface sediments that are not recognised as living in the over-lying waters (Table 4.4).

Shelled pteropod species of the Mediterranean Sea	Occurrence in B5-1 surface 1 cm
Cavolinia gibbosa	Absent
Cavolinia inflexa	Absent
Cavolinia longirostris	Absent
Cavolinia tridentata	Absent
Clio cuspidata	Absent
Clio pyramidata	**Present**
Creseis acicula	**Present**
Creseis virgula	**Present**
Cuvierina columnella	Absent
Diacria quadridentata	Absent
Diacria trispinosa	Absent
Hyalocylis striata	Absent
Limacina bulimoides	**Present**
Limacina inflata	**Abundant**
Limacina lesueuri	Absent
Limacina trochiformis	**Common**
Styliola subula	**Present**

Table 4.5 Summary of pteropod species of the modern Mediterranean Sea, from Bé and Gilmer (1977) and those found in the surface (0–1 cm, >150 μm) sediments of B5-1 (Present <5%; Common 5–20%; Abundant >20%).

Shelled heteropod species of the Mediterranean Sea	Occurrence in B5-1 surface 1 cm
Atlanta fusca	Absent
Atlanta lesueuri	Absent
Atlanta peronii	**Present**
Carinaria lamarcki	Absent
Firoloida desmaresti	**Common**
Oxygyrus keraudreni	**Present**
Pterotrachea spp.	Absent

Table 4.6 Summary of calcareous heteropod species of the modern Mediterranean Sea, from Thiriot-Quiévreux (1973) and those found in the surface (0–1 cm, >150 μm) sediments of B5-1 (Present <5%; Common 5–20%; Abundant >20%).

Planktic Foraminifera species of the Mediterranean Sea	Occurrence in B5-1 surface 1 cm
Globigerina bulloides	**Present**
Globigerina falconensis	Absent
Globigerina rubescens	Absent
Globigerinella aequilateralis	**Present**
Globigerinita glutinata	Absent
Globigerinoides conglobatus	Absent
Globigerinoides ruber	**Present**
Globigerinoides sacculifer	**Present**
Globorotalia crassaformis	**Present**
Globorotalia hirsuta	Absent
Globorotalia inflata	**Common**
Globorotalia truncatulinoides	**Abundant**
Hastigerina pelagica	Absent
Neogloboquadrina dutertrei	**Present**
Neogloboquadrina pachyderma	Absent
Orbulina universa	**Abundant**
Pulleniatina obliquiloculata	Absent

Table 4.7 Summary of planktic foraminifera species of the modern Mediterranean Sea, from Bé (1977) and those found in the surface (0–1 cm, >150 μm) sediments of B5-1 (Present <5%; Common 5–20%; Abundant >20%).

Data on the modern Mediterranean heteropod species have been summarised by Thiriot-Quiévreux (1973). All but two of the seven species (or genera) are present throughout B5-1, although, only three species are present in the surface (0–1 cm) sediments (Table 4.6). There are also some species that were found within the surface sediments of B5-1 that are not recognised from the Mediterranean Sea (Table 4.3). These include *Atlanta rosea* and *A. selvagensis*, which are found in tropical and sub-tropical waters of the Atlantic and Indian Oceans. This is partly due to the improved recognition of species, since *A. selvagensis* was not described until 2006 (de Vera and Seapy, 2006).

Relatively few substantial studies have been made of the modern living planktic foraminifera assemblage in the Mediterranean Sea. An extensive study detailing seasonal distribution patterns of live planktic foraminifera throughout the Mediterranean has been published by Pujol and Verhaud-Grazzini (1995). As well as this, the modern sub-tropical species of planktic foraminifera have been described by Bé (1977) and Arnold and Parker (2002). The list of sub-tropical species published by Bé (1977) incorporates the Mediterranean Sea and lists any species, which have a particular distribution (such as Indo-Pacific only). Several of the species: *Globorotalia hirsuta, Globigerina falconensis, H. pelagica* and *G. glutinata*, which Bé (1977) found to be dominant, are not found in the surface sediments of B5-1 (Table 4.7). All but one species, *Globigerinella calida*, found within the surface sediments of B5-1 are recorded from the Mediterranean Sea.

Core B5-1 contains two distinct planktic assemblages, which divide the core up into 4 major zones (*Zone C* is further subdivided into 5 subzones), two of which have been previously recognised (*Zones B and A*). These zones are not coincident with the isotope stages, but are characterised by a homogenous

set of species preferring either sub-polar water or tropical warm water (Fig. 4.27).

Zone D *(490–471 cm)*

This is a cool period, with a high global ice volume, which occurs during MIS 6. The duration of this zone is unknown as it may extend past the collected record. The species present during this period are representative of a sub-polar assemblage similar to that of the modern North Atlantic (Bé and Gilmer, 1977; Bé, 1977). It is very similar in composition to *Zone B*, with increased numbers of the sub-polar pteropod species *L. retroversa* (25–72% of planktic gastropods) and low numbers of *L. inflata* (17–38%). Some warm water transitional species are also found in *Zone D,* suggesting that this is the late transition from a colder period, which was not recovered in the core. Based on the dominant species of planktic foraminifera and pteropod present, the temperature during this period was between 12–16°C (Fig. 4.28).

Zone C *(470–221 cm)*

This is a zone mainly composed of warm sub-tropical to tropical planktic species. It spans MIS 5 and 4, ending at the MIS 4/3 boundary, and contains alternating warm periods with short term cooler periods. It signifies a gradual warming from the boundary of MIS 6 throughout MIS 5 and then a gradual cooling throughout MIS 4. The overall species composition of *Zone C* is similar to that of the modern western Mediterranean Sea.

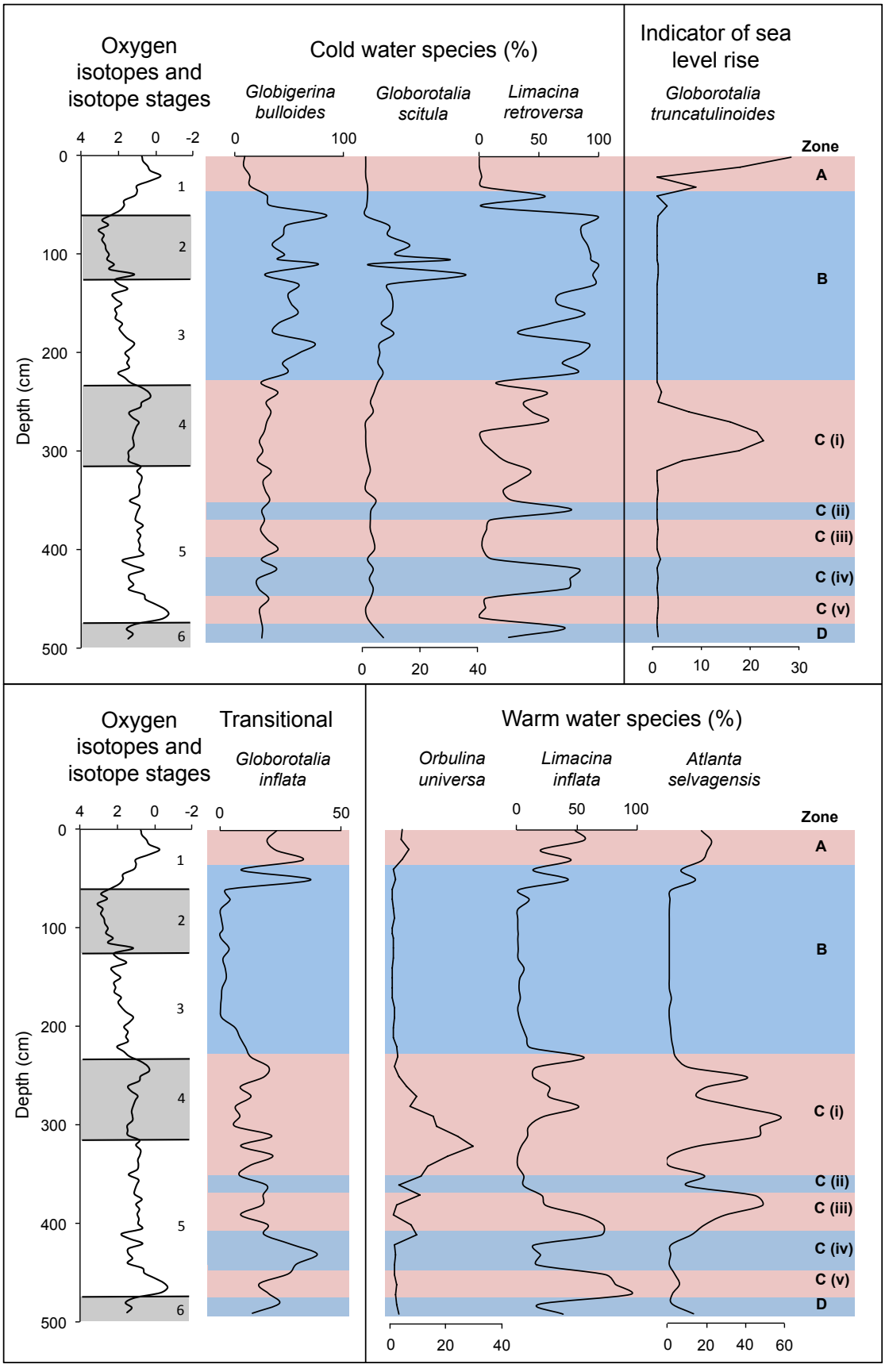

Figure 4.27 Percentages (150–500 μm) of indicative warm and cold water species throughout B5-1 compared to the oxygen isotope record and Marine Isotope Stages.

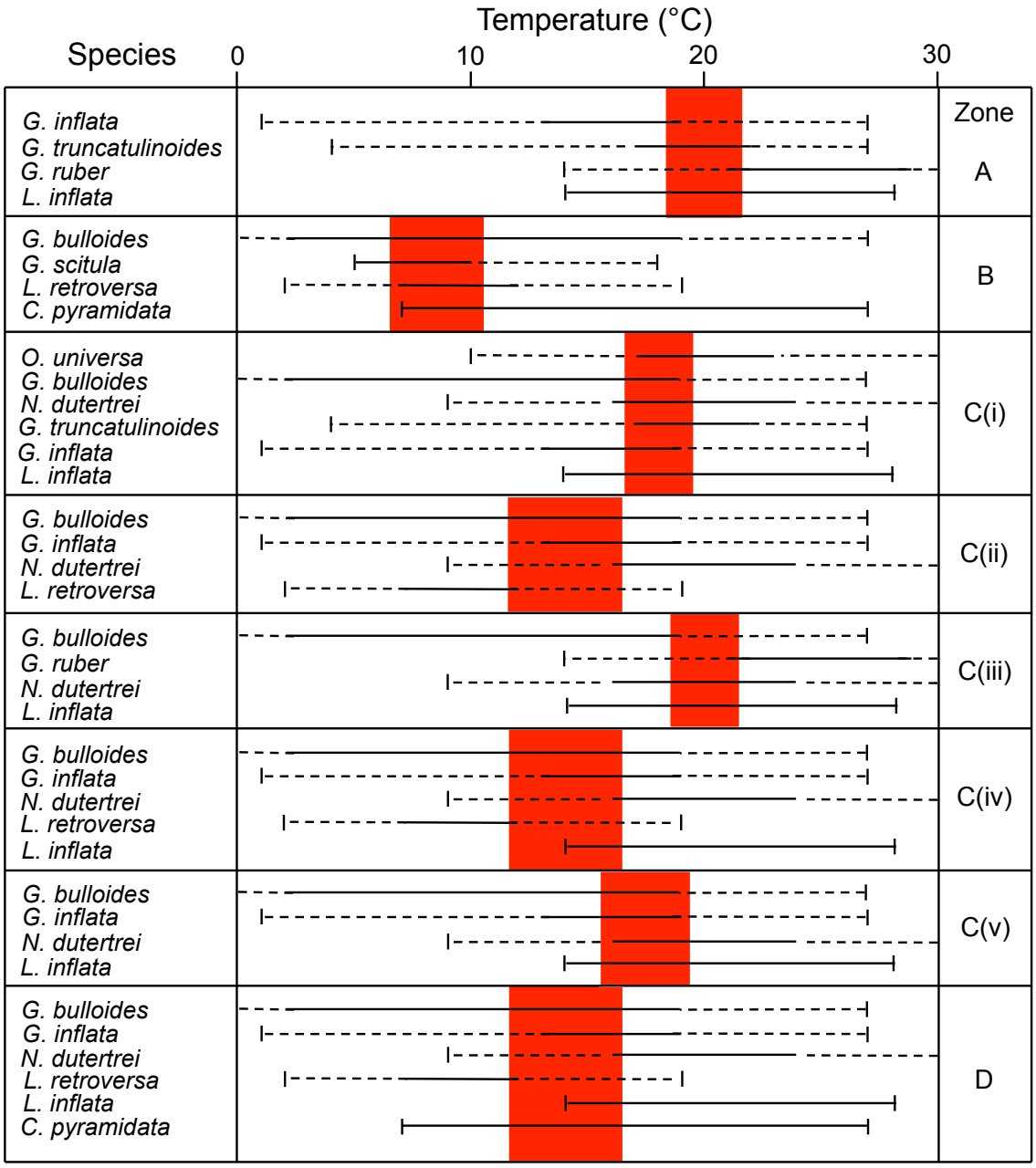

Figure 4.28 Temperature reconstruction for the zones described in Figure 4.27 based on dominant indicative species for each zone. Solid lines represent optimal temperatures, dashed line represent total temperature ranges and red boxes represent reconstructed sea surface temperature ranges. Species temperature data from Bé and Gilmer (1977) and Bé and Tolderlund (1971).

Sub-Zone C (v) *(470–441 cm)*

This is a short warm period, occurring during MIS 5.5, characterised by an increase in the abundance of *L. inflata* (73–93%) and a coinciding decrease in the abundance of *L. retroversa* (1–6%). It is similar in species composition to *Zone C(i)* and *C(iii)*. Cold water species do not disappear, but remain in lower numbers. The temperature during this time had risen to between 16–19°C (Fig. 4.28).

Sub-zone C (iv) *(440–411 cm)*

This is a short cooler period, occurring during MIS 5.4 to 5.2 and is characterised by a sharp peak in *L. retroversa* (from 6% at 450 cm to 83% at 420 cm) and a coinciding reduction in the abundance of *L. inflata* (from 73% at 450 cm to 13% at 420 cm). The warm water species such as *L. bulimoides* and *A. selvagensis* do not disappear, but remain at a lower abundance, suggesting that this period is cooler but not sub-polar. Cold water planktic foraminifera *G. bulloides* is also present, but in low numbers. The temperature during this period was between 12–16°C (Fig. 4.28)

Sub-zones C (iii) *410–371 cm; ii) 370–351 cm; i) 350–221 cm*

This section is characterised by a relatively high abundance of the sub-tropical planktic foraminifera *O. universa* (up to 29% of planktic foraminifera). In common with *Zone A*, it contains a higher abundance of the pteropod *L. inflata* (average 25%), the heteropod *A. selvagensis* (average 30%) and the planktic foraminifera *G. inflata* (6–22%) and a low abundance of the sub-polar pteropod *L. retroversa* (variable between 2–57%). The temperature during *Sub-Zone C (iii)* was between 19–21°C (Fig. 4.28). With exception to this, there is a very

short cooler period between 370 and 351 cm with a higher abundance of *L. retroversa* (*Sub-Zone C(ii)*). During *Sub-Zone C (ii)* the temperature decreases to between 12–16°C. The surface water then warms again during *Sub-Zone C (i)* to between 17–19°C (Fig. 4.28). In general, pteropod species *L. bulimoides* and *C. virgula r*eturn to *Zone C* with an increase in the abundance of *Diacria trispinosa* (Lesueur, 1821), a warm water cosmopolitan species of pteropod. During MIS 4 (320–250 cm), *Zone C* also sees a rise in sea level, indicated by a peak in the abundance of *G. truncatulinoides* (Fig. 4.27), a species infrequently found within the Mediterranean Sea as it resides in deeper water and is often unable to cross the shallow sill at the Straits of Gibraltar. Other than a high abundance of specimens in the surface sediments (Zone *A*), only occasional specimens are present elsewhere in the core. Although this rise in sea level suggests an increase in temperature, a slight cooling is detected by the complete disappearance of several warm water species including *G. aequilateralis* and *G. sacculifer.* This may indicate an episode similar to a Henrich event (Bard *et al.,* 2000). The climate switches to reflect a sub-polar assemblage (*Zone B*) at the MIS 4/3 boundary (60 kyr, 220 cm).

Zone B *(220–31 cm)*

This cool period appears to have been a major turning point in the climate, with steady cooling towards the Last Glacial Maximum (MIS 2.2). This is a zone of sub-polar species similar to that of the modern North Atlantic (Bé and Gilmer, 1977; Bé, 1977), which spans MIS 3, 2 (the last glacial maximum) and part of MIS 1. It is characterised by a very high abundance of the sub-polar pteropod *L. retroversa* (up to 100% but generally 85% of planktic gastropods) and the sub-polar planktic foraminifera *G. bulloides* (average 50% of planktic foraminifera).

There are also higher abundances of the planktic foraminifera *G. scitula* (10%) and *G. glutinata* (10%), which have a range of habitats from sub-polar to equatorial. The abundance of the heteropod *A. rosea* which, surprisingly, is only known from warm waters, fluctuates throughout this zone. It is interesting to note that peaks in *A. rosea* occur when the abundance of *L. retroversa* reduces and may therefore signify temperature fluctuations in this sub-polar zone. There are no planktic species exclusively found in *Zone B*. The surface water temperature during this period, as indicated by dominant species of planktic foraminifera and pteropod, was between 7–10°C (Fig. 4.28). This is in agreement with temperature reconstruction data published by Sbaffi *et al.* (2001) and Hayes *et al.* (2005).

Zone B has been described by several authors. It is comparable to *Zone 3* described by Biekart (1989) in a deep sea core from the Tyrrhenian Sea. Biekart (1989) found similar abundances of *L. retroversa*, but much higher abundances of *D. trispinosa,* which are only present in this section of B5-1 in low numbers (Maximum 13%). Chen (1968) also recorded this period of abundant *L. retroversa* in a core collected south of the Island of Crete and Herman (1971) detected it in cores throughout the eastern Mediterranean Sea and in the Balearic Sea. Carboni and Esu (1987), Buccheri *et al.* (2002) and Jorissen *et al.* (1993) all detected this zone in the Tyrrhenian Sea. Jorissen *et al.* (1993) also found it in the Adriatic Sea, being characterised by the common occurrence of *G. scitula.* Capotondi *et al.* (1999) and Sbaffi *et al.* (2001) have expanded on the work of Jorissen *et al.* (1993), splitting the previous '*Zone 3*' into more detailed zones. At either end of *Zone B* (220 cm to 140 cm and 50 cm to 31 cm) an increased abundance of the transitional species *C. pyramidata* and *G. inflata* signifies the transition between warm and cold periods. Many authors

consider the upper transitional period (50 cm to 31 cm) as a distinct zone (Carboni and Esu, 1989; Jorissen *et al.,* 1992; Buccheri *et al.,* 2002) characterised by an increase in transitional and warmer water species. Capotondi *et al.* (1999) and Sbaffi *et al.* (2001) also subdivide this period into smaller bio-zones.

Zone A *(30–0 cm depth)*

This is a zone of sub-tropical species, which occurs during MIS 1 and is characterised by a high abundance of the tropical pteropod *L. inflata* (generally 50% of planktic gastropods) and a very low abundance of the sub-polar pteropod *L. retroversa* (under 2%). The transitional planktic foraminifera *G. inflata* (19–34% of planktic foraminifera) and the sub-tropical heteropod *A. selvagensis* (16–22%) are also abundant. *Zone A* contains the warm water pteropods *L. bulimoides and C. virgula* and the tropical planktic foraminifera *G. aequilateralis* and *G. sacculifer* which are not found at all in *Zone B*. This zone also contains high abundances of *G. truncatulinoides*, which suggests the sea level has risen since MIS 2 and is possibly comparable to that found in *Zone C(i).* This assemblage is similar to that found in Holocene sediments described from the Tyrrhenian Sea (Carboni and Esu, 1987; Jorissen *et al.,* 1993; Capotondi *et al.,* 1999; Sbaffi *et al.,* 2001; Buccheri *et al.,* 2002), the Adriatic Sea (Jorissen *et al.,* 1993; Capotondi *et al.,* 1999), south of Sicily (Capotondi *et al.,* 1999), in the western Mediterranean Sea (Pérez-Folgado *et al.,* 2003) and south of the Island of Crete (Chen, 1968). Species present within *Zone A* indicate a sub-tropical to tropical climate similar to that of the modern day western Mediterranean Sea (Bé and Gilmer, 1977; Bé, 1977). The sea surface temperature at this time, averaged over the entire Mediterranean Sea, ranged

from 14–25 °C (Sbaffi *et al.,* 2001). At the site of B5-1, the dominant species present indicate a temperature of between 19–21°C (Fig. 4.28).

4.2.4 CALCIFICATION INDICES

4.2.4.1 PLANKTIC FORAMINIFERA FRAGMENTATION

Figure 4.29 shows four main shifts in planktic foraminifera fragmentation in the 150–500 µm fraction (Appendix 8.2.2.3.D). At the base of the core (MIS 6), fragmentation is relatively low with a decrease towards the MIS 6/5 boundary. The fragmentation continues to decrease, with the lowest value of the entire core (1.2%) occurring at MIS 5.5. This is surprising since it is expected that the highest fragmentation would occur at this point in the core. This suggests a lag in the response of surface waters to climate change. From MIS 5.5, the fragmentation increases steadily to the MIS 4/3 boundary (320 cm), where the maximum fragmentation (60%) occurs. The fragmentation then reduces through MIS 4 until the boundary with MIS 3. Low fragmentation values (down to 2%) persist throughout MIS 3 and 2 and only begin to increase again towards the MIS 2/1 boundary. The fragmentation increases between 30 cm and the surface of the core (up to 37%). Fragmentation of planktic foraminifera shows a significant positive correlation to LDX values ($r=0.52$, $p=0.004$, $n=29$).

4.2.4.2 LDX CALCIFICATION

The *Limacina* Dissolution Index for B5-1 is interrupted (Figs 4.29, 4.30) because several sections of core either contain too few specimens of *L. inflata* for analysis, or, are devoid of the species all together (Appendix 8.2.2.4.A and 8.2.2.4.B). This is largely due to the dominant presence of the pteropod *L. retroversa* during cool climatic periods, which appears to replace *L. inflata.*

However, the overall trend in LDX shows reduced calcification (high LDX values) during extreme interglacial periods (MIS 5) and increased calcification (low LDX values) during glacial periods (MIS 2) (Fig. 4.29). Between 490 cm and 460 cm (MIS 6 and MIS 6/5 boundary), the LDX values are fairly low, between 2.14 and 2.60. However, following this, the LDX values increase, with high values (2.82 to 4.11) throughout MIS 5. This high LDX signifies reduced calcification and enhanced in-life corrosion. The maximum LDX value (4.11) occurs at 370 cm within MIS 5. Through MIS 4, the LDX values begin to reduce, with a transition to a lower LDX between 250 cm and 220 cm (LDX 3.07 to 1.56), at the MIS 4/3 boundary. No LDX data is available for the section 220 cm to 50 cm. However, when *L. inflata* return to the core at 50 cm, the LDX values are very low, remaining low throughout MIS 2 and 1 (LDX 0.81 to 1.78). These low values indicate enhanced calcification spanning MIS 2 and 1.

The LDX does not produce a significant correlation when compared to the oxygen isotope data ($r=0.14$, $p=0.49$, $n=28$) or the Vostok atmospheric CO_2 record ($r=-0.46$, $p=0.073$, $n=16$). This may be a factor of the poor representation of *L. inflata.* However, when the LDX profile is shifted down by 35 cm (Appendix 8.2.1.3.C), a significant correlation to the oxygen isotope data is produced ($r=-0.505$, $p=0.010$, $n=25$). This equates to a lag in the LDX calcification profile by 7–14 kyrs, assuming a sedimentation rate of between 2.5–5 cm kyr^{-1}.

4.2.4.3 PTEROPOD SHELL SIZE

The average shell size of *L. inflata* specimens in B5-1 (Appendix 8.2.2.4.C) shows a similar trend to the LDX calcification profile (Fig. 4.29). During periods of high calcification (low LDX values), the average diameter of *L. inflata* shells is larger. Whereas, during periods of low calcification (high LDX

values), the average diameter of shells is smaller. Despite only having 6 corresponding data points, the shell size shows a significant negative (increased LDX shows reduced calcification) correlation with the LDX (r=-0.871, p=0.024, n=6).

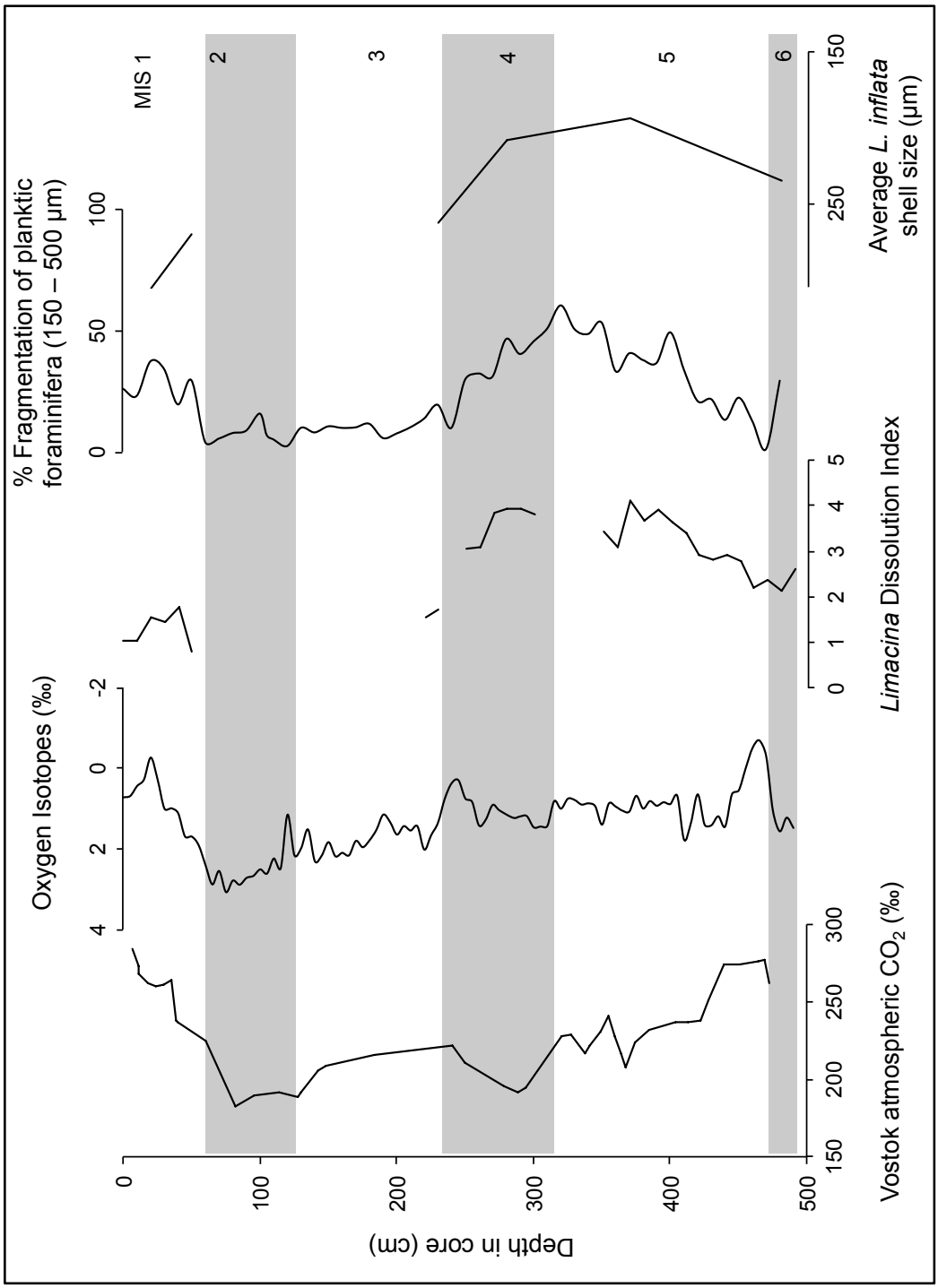

Figure 4.29 Vostok atmospheric CO_2, oxygen isotope profile, *Limacina* Dissolution Index profile, percentage fragmentation of planktic foraminifera (150–500 µm fraction) and average *L. inflata* shell size for B5-1.

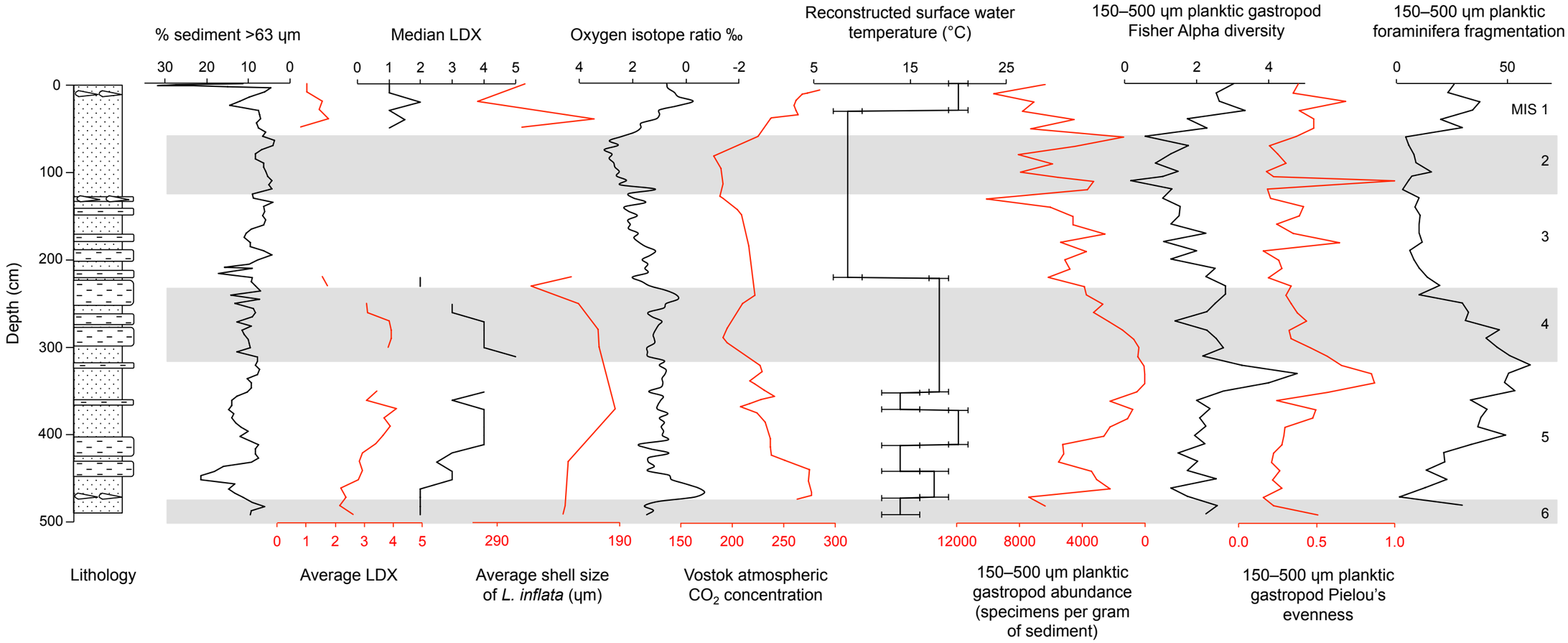

Figure 4.30 B5-1: % sediment >63 µm, Average LDX, Median LDX, Average *L. inflata* shell size, Oxygen isotope profile, Vostok atmospheric CO_2 concentration (Petit *et al.,* 1999), Reconstructed surface water temperature, Planktic gastropod abundance, Fisher Alpha diversity and Pielou's evenness and Planktic foraminifera fragmentation. Scales for % sediment >63 µm, Average *L. inflata* shell size, Oxygen isotope profile and Planktic gastropod abundance are reversed.

4.3 THE INDIAN OCEAN: ODP HOLE 716B

A summary of Indian Ocean results can be found in Figure 4.43.

4.3.1 SEDIMENTOLOGY

4.3.1.1 CORE DESCRIPTION AND LOG

ODP Hole 716B was described by Backman *et al.* (1988), providing a detailed core description and log, which is partly modified in Fig. 4.31. The top 13 metres of ODP Hole 716B used in this study (Fig. 4.31) is composed of uniform, relatively uninterrupted pteropod and foraminifera bearing nannofossil ooze (Backman *et al.* 1988) with a grain size of very fine to fine sand (Appendix 8.2.3.1.A). The >63 μm grain size distribution is in agreement with the average grain size (Fig. 4.31), showing a larger average grain size when the percentage of >63 μm sediment is higher. In general, grain size is larger during glacial periods and smaller during interglacial periods

4.3.1.2 SEDIMENTATION RATES

The rate of sedimentation for the first 13 metres of ODP Hole 716B has been calculated as 3.8 $cmkyr^{-1}$ (Backman *et al.,* 1988). Calculations were made using nannofossil datums.

4.3.2 STABLE ISOTOPE STRATIGRAPHY AND DATING

4.3.2.1 OXYGEN ISOTOPE ANALYSIS

Low resolution oxygen isotope analysis (Fig. 4.32) has been carried out on 716B by Droxler *et al.* (1990). Isotope analysis was carried out at Rice University, using specimens of *G. sacculifer* at 20 cm intervals. Droxler *et al.* (1990) provide a detailed methodology for oxygen isotope analysis of 716B. The

early stages of MIS 5 are missing from the record due to the loss of sediment between cores during drilling (between points 290 and 410 cm).

4.3.2.2 CORRELATION TO KNOWN BIOZONES

Although *G. menardii* is present throughout Hole 716B (Appendix 8.2.3.2.A), the low resolution of data does not allow the identification of *G. menardii* zones. The data show no percentage abundance drop to zero and thus, boundaries cannot be defined (Fig. 4.32). The low resolution 'relative % of *G. menardii*' produced for 716B by Cullen and Droxler (1990) also does not show any clear zonation.

4.3.3 MICROPALAEONTOLOGY

Twenty four species of pteropod, fifteen species of heteropod and twenty seven species of planktic foraminfera were identified from both the 150–500 μm and >500 μm size fractions in Hole 716B (Table 4.8, Appendix 8.2.3.2.A–D). Some pteropod and heteropod specimens unidentifiable to species level are labelled alphabetically within their genera. Several samples in the >500 μm fraction of Hole 716B contained very low numbers of pteropods and heteropods, with specimens missing from two samples. For this reason, abundance and diversity analysis of pteropods and heteropods has been based on the 150–500 μm fraction only.

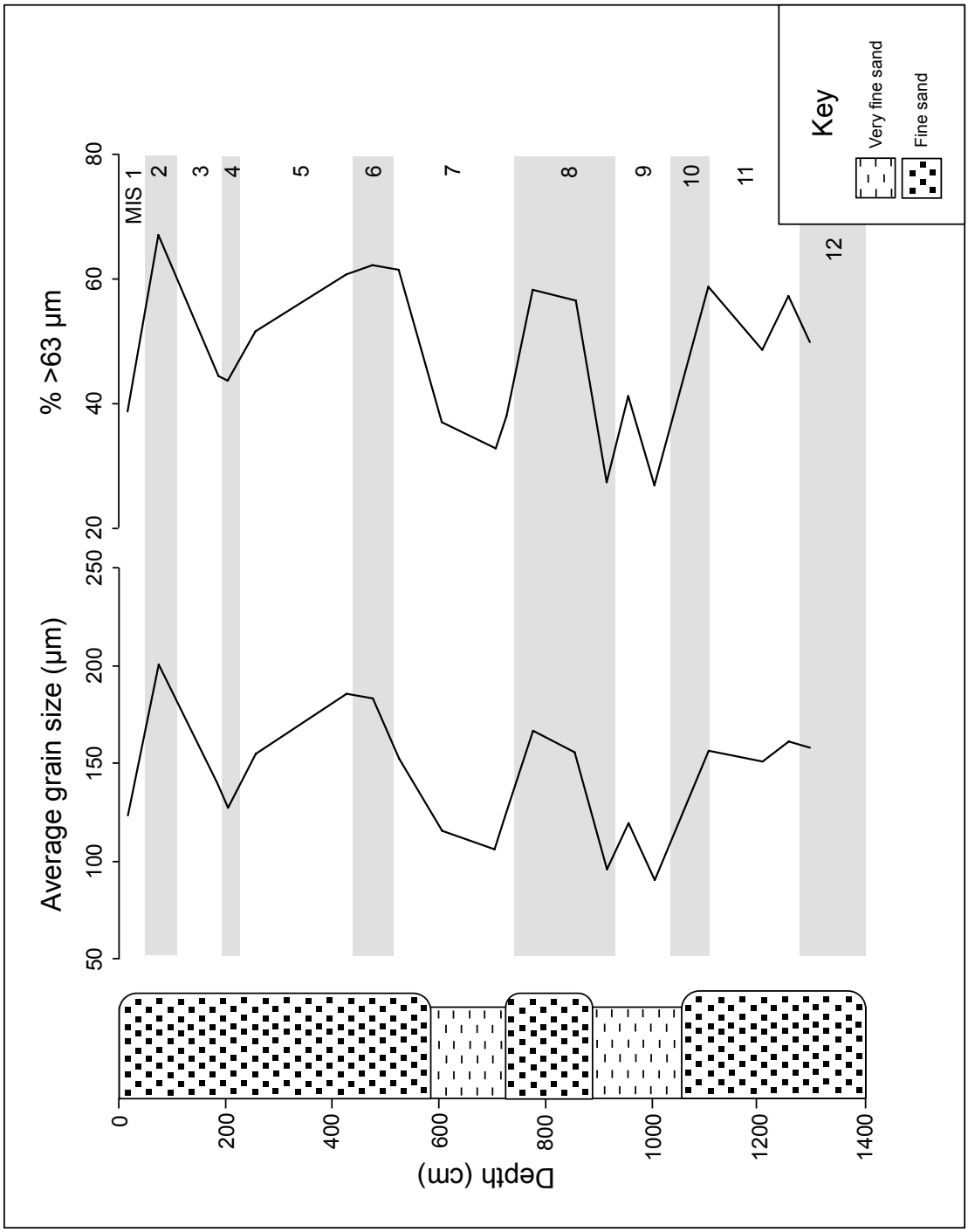

Figure 4.31 ODP Hole 716B lithology (core description from Droxler *et al.,* 1990), average grain size and percentage of sediment >63 µm.

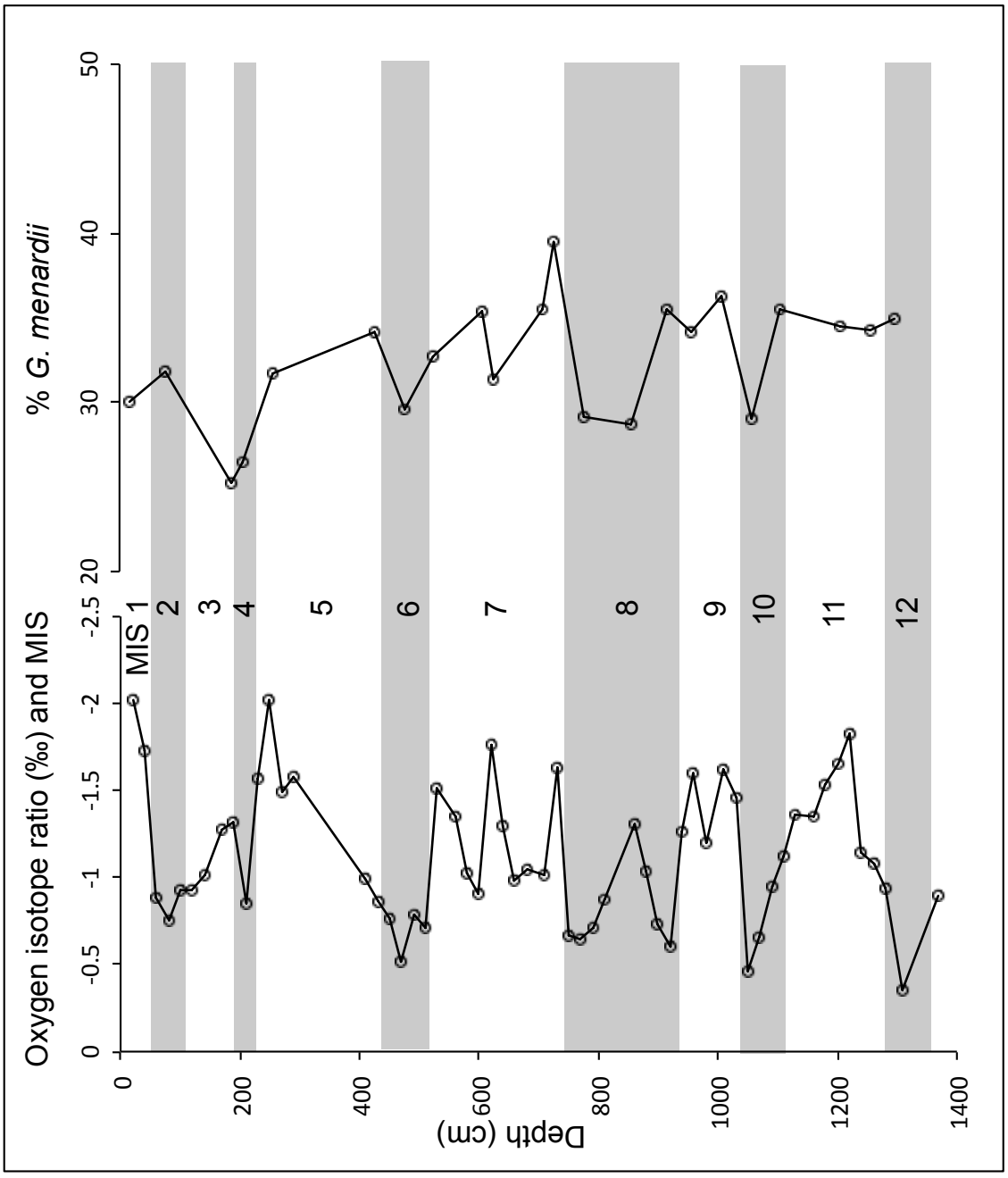

Figure 4.32 ODP Hole 716B oxygen isotope ratios with Marine Isotope Stages (Droxler *et al.,* 1990) and *Globorotalia menardii* zonation analysis using species assemblages of both the150–500 µm and >500 µm fractions.

PTEROPODA	HETEROPODA
Cavolinia inflexa (Lesueur, 1813) *Clio convexa* (Boas, 1886) *Clio cuspidata* (Bosc, 1802) *Clio pyramidata* Linnaeus, 1767 *Creseis acicula* (Rang, 1828) *Creseis chierchiae* (Boas, 1886) *Creseis virgula* (Rang, 1828) *virgula* (Rang, 1828) *Creseis virgula* (Rang, 1828) *constricta* (Chen and Bé, 1964) *Diacavolinia longirostris* (de Blainville, 1821) *Diacria quadridentata* (Lesueur, 1821) *Diacria trispinosa* (Lesueur, 1821) *Hyalocylus striata* (Rang, 1828) *Limacina bulimoides* (d'Orbigny, 1836) *Limacina inflata* (d'Orbigny, 1836) *Limacina lesueuri* (d'Orbigny, 1836) *Limacina trochiformis* (d'Orbigny, 1834) *Limacina* sp. C *Limacina* spp. *Styliola subula* (Quoy and Gaimard, 1827) *Gleba cordata* Forskål, 1776 *Peracle diversa* (Monterosato, 1875) *Peracle moluccensis* (Tesch, 1903) *Paedoclione doliiformis* Danforth, 1907 Gymnosome veligers	*Atlanta brunnea* Gray, 1850 *Atlanta californiensis* Seapy and Richter, 1993 *Atlanta frontieri* Richter, 1993 *Atlanta gaudichaudi* Gray, 1850 *Atlanta helicinoidea* Gray, 1850 *Atlanta inclinata* Gray, 1850 *Atlanta peronii* Lesueur, 1817 *Atlanta rosea* Gray, 1850 *Atlanta selvagensis* de Vera and Seapy, 2006 *Atlanta turriculata* d'Orbigny, 1835 *Carinaria pseudorugosa* Vayssière, 1904 *Carinaria lamarckii* de Blainville, 1817 *Carinaria* spp. *Firoloida desmarestia* Lesueuer, 1817 *Oxygyrus keraudreni* (Lesueur, 1817)
GLOBIGERINIDA (PLANKTIC FORAMINIFERA)	
Candeina nitida d'Orbigny, 1839 *Globigerina bulloides* d'Orbigny, 1826 *Globigerina digitata* Brady, 1879 *Globigerina rubescens* Hofker, 1956 *Globigerinella aequilateralis* (Brady, 1879) *Globigerinella calida* (Parker, 1962) *Globigerinita glutinata* (Egger, 1893) *Globigerinoides conglobatus* (Brady, 1879) *Globigerinoides elongatus* (d'Orbigny, 1926) *Globigerinoides ruber* (d'Orbigny, 1839) *Globigerinoides sacculifer* (Brady, 1877) *Globigerinoides trilobus* (Reuss) *Globoquadrina conglomerata* (Schwager, 1866) *Globorotalia crassaformis* (Galloway and Wissler, 1927)	*Globorotalia flexuosa* (Koch, 1923) *Globorotalia menardii* (Parker, Jones and Brady, 1865) *Globorotlia scitula* (Brady, 1882) *Globorotalia theyeri* Fleisher, 1974 *Globorotalia truncatulinoides* (d'Orbigny, 1839) *Globorotalia tumida* (Brady, 1877) *Hastigerina pelagica* (d'Orbigny, 1839) *Neogloboquadrina dutertrei* (d'Orbigny, 1839) *Neogloboquadrina incompta* (Cifelli, 1961) *Neogloboquadrina pachyderma* (Ehrenberg, 1861) *Orbulina universa* d'Orbigny, 1839 *Pulleniatina obliquiloculata* (Parker and Jones, 1865) *Sphaeroidinella dehiscens* (Parker and Jones, 1865)

Table 4.8 Species of pteropod, heteropod and planktic foraminifera identified from the 150–500 µm and >500 µm size fractions of sediment for 716B.

4.3.3.1 ABUNDANCE

The abundance of planktic foraminifera, pteropods and heteropods does not change dramatically with variations in climate (Fig. 4.33), although there is a general trend of higher values during glacial periods (Appendix 8.2.3.2.E, 8.2.3.2.F).

4.3.3.1.1 PLANKTIC FORAMINIFERA

Planktic foraminifera were found in all samples, in both the 150–500 µm and >500 µm size fractions of Hole 716B. The abundance in the >500 µm fraction is much lower than that of the 150–500 µm fraction, due to the greater weight of tests in the >500 µm fraction. The abundance in the 150–500 µm fraction generally shows an increase during glacial periods, however this trend is not significant in either size fraction (150–500 µm, r=0.246, p=0.271, n=22; >500 µm, r=0.076, p=0.735, n=22). Three peaks in abundance occur at 705, 475 and 75 cm (39082, 34945 and 32421 pfg^{-1} respectively). The lowest abundance of 7306 pfg^{-1} occurs at 1105 cm, at the transition between MIS 11 and 10. Abundance in the >500 µm fraction shows very little variability, ranging from 3659 pfg^{-1} (75 cm) to 7834 pfg^{-1} (705 cm).

4.3.3.1.2 PTEROPODS AND HETEROPODS

Pteropods and heteropods are present in the majority of samples in both the 150–500 µm and >500 µm size fractions of Hole 716B. Specimens were generally found in low numbers in the >500 µm fraction and no specimens were found in samples at 1005 cm and 1205 cm. In the 150–500 µm fraction, abundance shows a similar trend to planktic foraminifera abundance, with generally higher values during glacial periods (MIS 10, 8 and 6). However the abundance of pteropods and heteropods in the 150–500 µm faction does not

show a significant relationship to oxygen isotope data (r=0.255, p=0.253, n=22). There are three increasingly large peaks in abundance at 1055, 705 and 475 cm (8483 pg^{-1}, 11547 pg^{-1} and 13421 pg^{-1} respectively). The lowest abundance of 474 pg^{-1} occurs at 1205 cm, within MIS 11.

4.3.3.2 DIVERSITY

The diversity, heterogeneity and evenness of planktic foraminifera, pteropods and heteropods appear to change closely with climate. Planktic foraminifera show higher diversity during glacial periods, whereas, pteropods and heteropods show lower diversity during glacial periods.

4.3.3.2.1 PLANKTIC FORAMINIFERA

The Fisher Alpha diversity of both the 150–500 µm and >500 µm size fractions of Hole 716B show a trend of generally higher values during glacial periods (Fig. 4.34). However, this trend is not significant (150–500 µm , r=0.280, p=0.207, n=22; >500 µm, r=0.118, p=0.600, n=22). The diversity of >500 µm planktic foraminifera is generally lower than that of the 150–500 µm assemblage. In the >500 µm fraction, Fisher Alpha diversity varies between 2.2 (705 cm) and 3.0 (915 cm). In the 150–500 µm fraction there are three peaks in diversity at 1005, 625 and 205 cm (Fisher Alpha 4.4, 4.4 and 4.9 respectively). The lowest diversity occurs at 605 cm, with a Fisher Alpha of 2.7.

The Shannon-Wiener heterogeneity of planktic foraminifera is fairly constant throughout Hole 716B for both the 150–500 µm and >500 µm size fractions (Fig. 4.35). More heterogeneous assemblages (larger values) generally occur during glacial periods (>500 µm MIS 10, 8 and 4; 150–500 µm MIS 10, 6 and 4), but do not produce a significant correlation when compared to

oxygen isotope data (150–500 µm, r=0.246, p=0.270, n=22; >500 µm, r=0.019, p=0.934, n=22). Values range between 1.5 (705 cm) and 2.0 (205 cm) for the >500 µm assemblage and between 2.1 (1205 cm) and 2.5 (1105 cm) for the 150–500 µm assemblage. Pielou's evenness of planktic foraminifera assemblages agrees with this trend, generally showing a more even, heterogeneous assemblage during glacial periods (Fig. 4.36), but also not producing a significant correlation with oxygen isotope data (150–500 µm, r=-0.083, p=0.715, n=22; >500 µm, r=-0.041, p=0.855, n=22). This trend is more defined in the >500 µm size fraction, where peaks in evenness occur within MIS 10, 8 and 4. The largest peak occurs in MIS 8 at 855 cm with a value of 0.63. The lowest value also occurs in MIS 8 at 915 cm with a value of 0.35. The Pielou's evenness of the 150–500 µm fraction is more variable through the core, but also shows peaks during glacial periods MIS 10 and 4. Values in the 150–500 µm fraction vary between 0.50 (725 cm) and 0.68 (15 cm).

4.3.3.2.2 PTEROPODS AND HETEROPODS

The Fisher Alpha diversity of pteropods and heteropods in the 150–500 µm size fraction of Hole 716B is very variable throughout the core, but generally shows a trend of lower diversity during glacial periods (Fig. 4.34). However, a correlation between pteropod and heteropod diversity in the 150–500 µm fraction and oxygen isotope data does not produce a significant correlation (r=-0.345, p=0.116, n=22). Lower values occur during MIS 12, 10, 8, 6 and 4, with a large peak in diversity during MIS 2. Fisher Alpha diversity ranges from 4.18 (475 cm) to 7.10 (855 cm).

The Shannon-Wiener heterogeneity (Fig. 4.35) and the Pielou's evenness (Fig. 4.36) of pteropods and heteropods in the 150–500 µm size

fraction of Hole 716B agree with the diversity, showing less heterogeneous assemblages during glacial periods. More even and heterogeneous pteropod and heteropod assemblages occur during interglacial periods, during MIS 11, 9, 7, 5 and 1. There are no data points within MIS 3. Correlation of heterogeneity and evenness with oxygen isotope data shows that this trend is significant (S-W, r=-0.781, p=<0.001, n=22; P, r=-0.640, p=0.001, n=22). Shannon-Wiener heterogeneity varies between 1.63 (915 cm) in MIS 8 and 2.25 (625 cm) in MIS 7. The Pielou's evenness of pteropods and heteropods varies between 0.24 (915 cm) in MIS 8 and 0.45 (15 cm) in MIS 1. These evenness values are generally much lower than those for the planktic foraminifera in the 150–500 µm size fraction.

4.3.3.3 SPECIES COMPOSITION AND CLIMATE

Due to the low latitude (04°56.0'N) location of Hole 716B and the consequent low variation in surface water temperature changes across glacial and interglacial periods, very little variation in species composition occurs throughout the cores. Barrows and Juggins (2005) reconstruct the sea-surface temperature at ODP Site 716 to range between 25–28°C at the Last Glacial Maximum (18 cm core depth, MIS 2.2, 18 kyr ago). The mean annual sea-surface temperature close to ODP Site 716 at this time was 27°C, just one degree lower than that of today (Barrows and Juggins, 2005). Cullen and Droxler (1990) reconstruct the sea surface temperature at ODP Site 716 to be below 26°C during MIS 6–8 and suggest that any variation in species abundances are more likely to be due to changes in other environmental parameters, such as salinity and nutrient availability.

The species assemblage throughout Hole 716B is composed of warm water sub-tropical species of planktic foraminifera, pteropods and heteropods, with some transitional species. The dominant planktic foraminifera species is *G. menardii,* making up to 55% of planktic foraminifera in the >500 μm assemblage. Other abundant species include *G. sacculifer* (including *G. trilobus*), *N. dutertrei* and *Globoquadrina conglomerata. Globigerinella aequilateralis* and *O. universa* are also common throughout the core. The pteropod genus *Limacina* dominates the assemblage of holoplanktic gastropods, the most abundant species being *L. inflata* (up to 62% of the 150–500 μm pteropod and heteropod population of 716B). Other common and often abundant species of pteropod include *L. trochiformis* and *Clio convexa* (Boas, 1886). The dominant heteropod genus is *Atlanta*, with common and often abundant heteropod species including *Atlanta frontieri* and *C. lamarckii.*

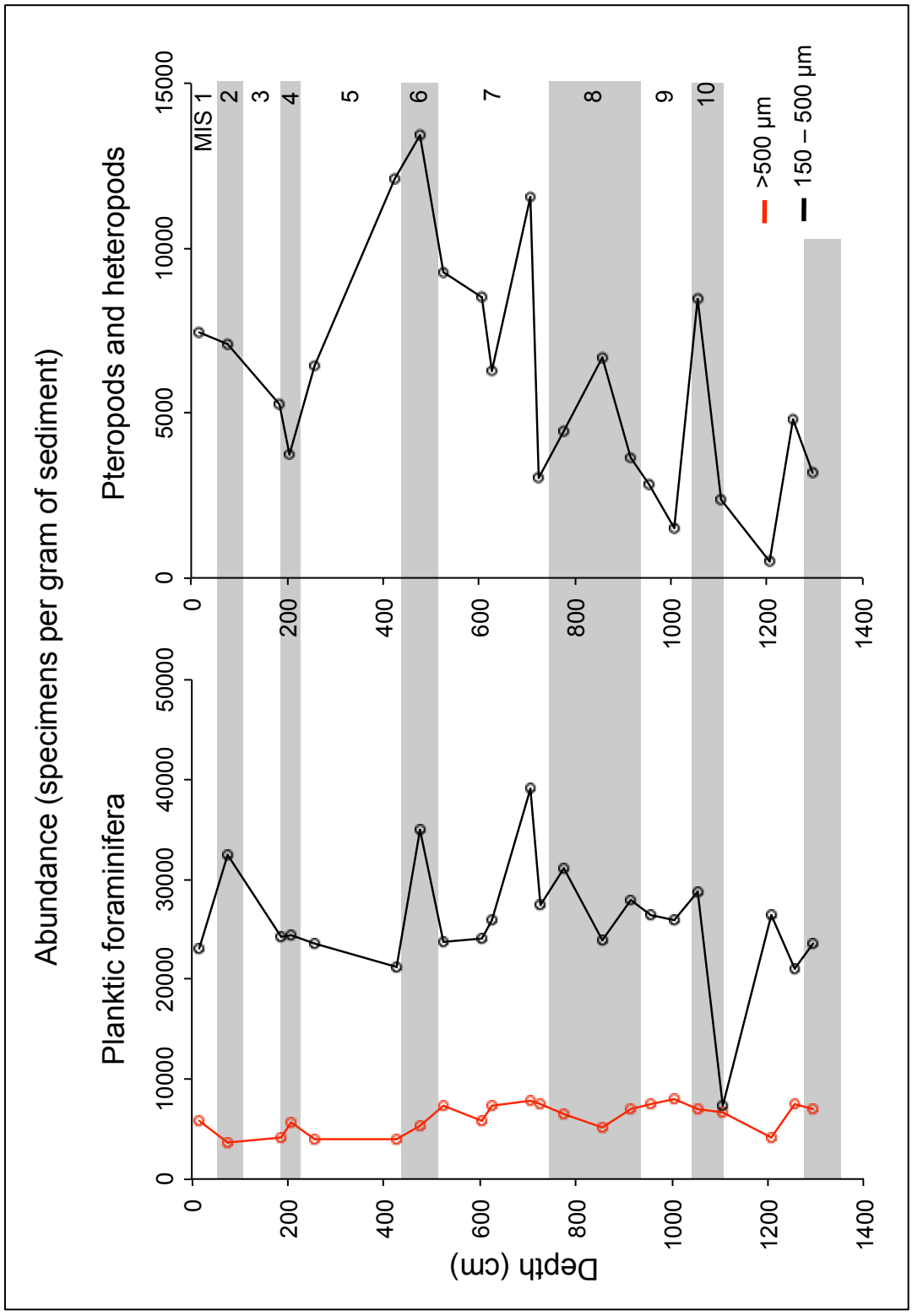

Figure 4.33 Abundance of planktic foraminifera (planktic foraminifera per gram of sediment, pfg^{-1}) and pteropods and heteropods (pteropods and heteropods per gram of sediment, pg^{-1}) in 716B. Grey boxes indicate glacial periods as designated in Figure 4.32.

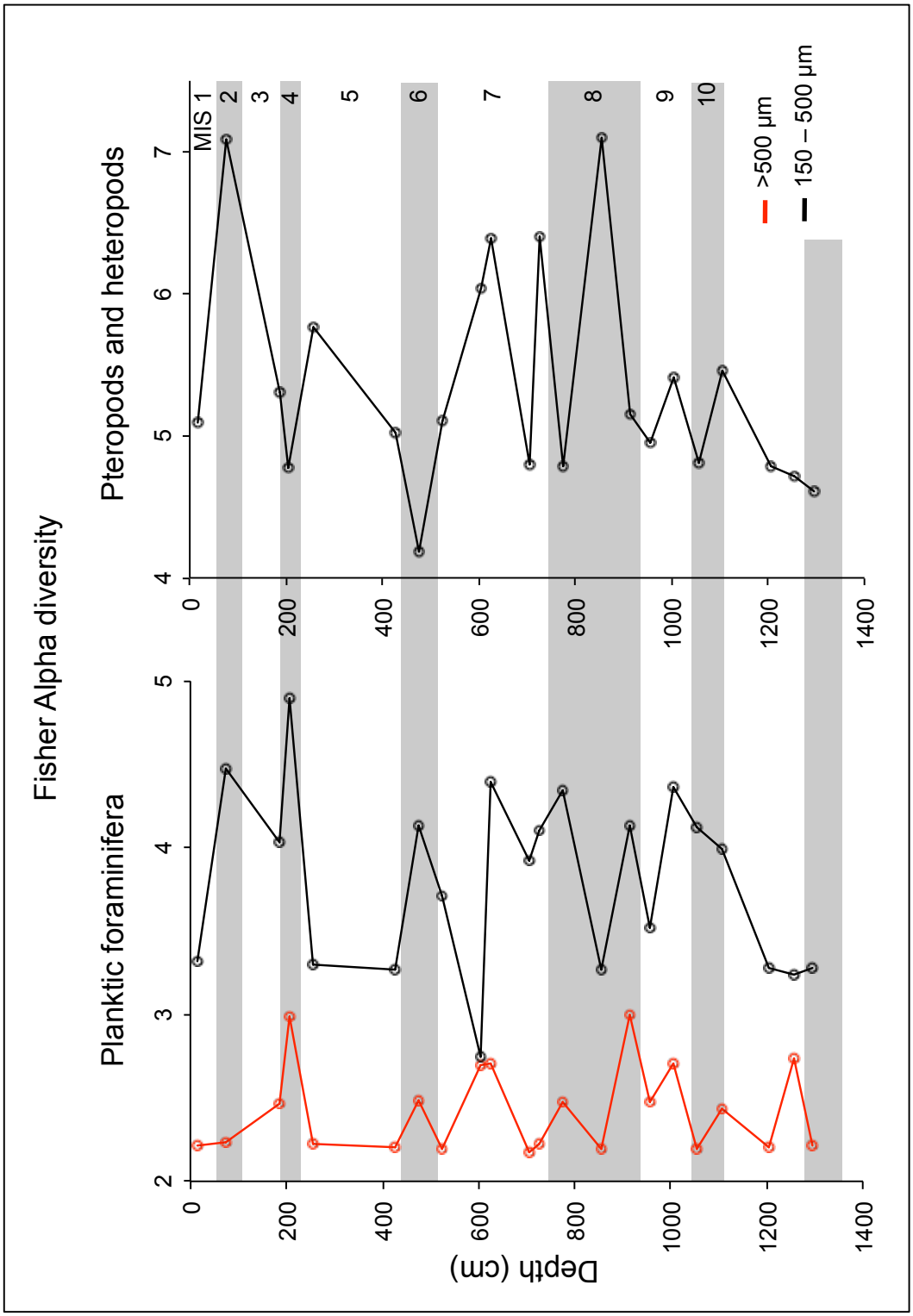

Figure 4.34 Fisher Alpha diversity of planktic foraminifera and pteropods and heteropods in 716B. Grey boxes indicate glacial periods.

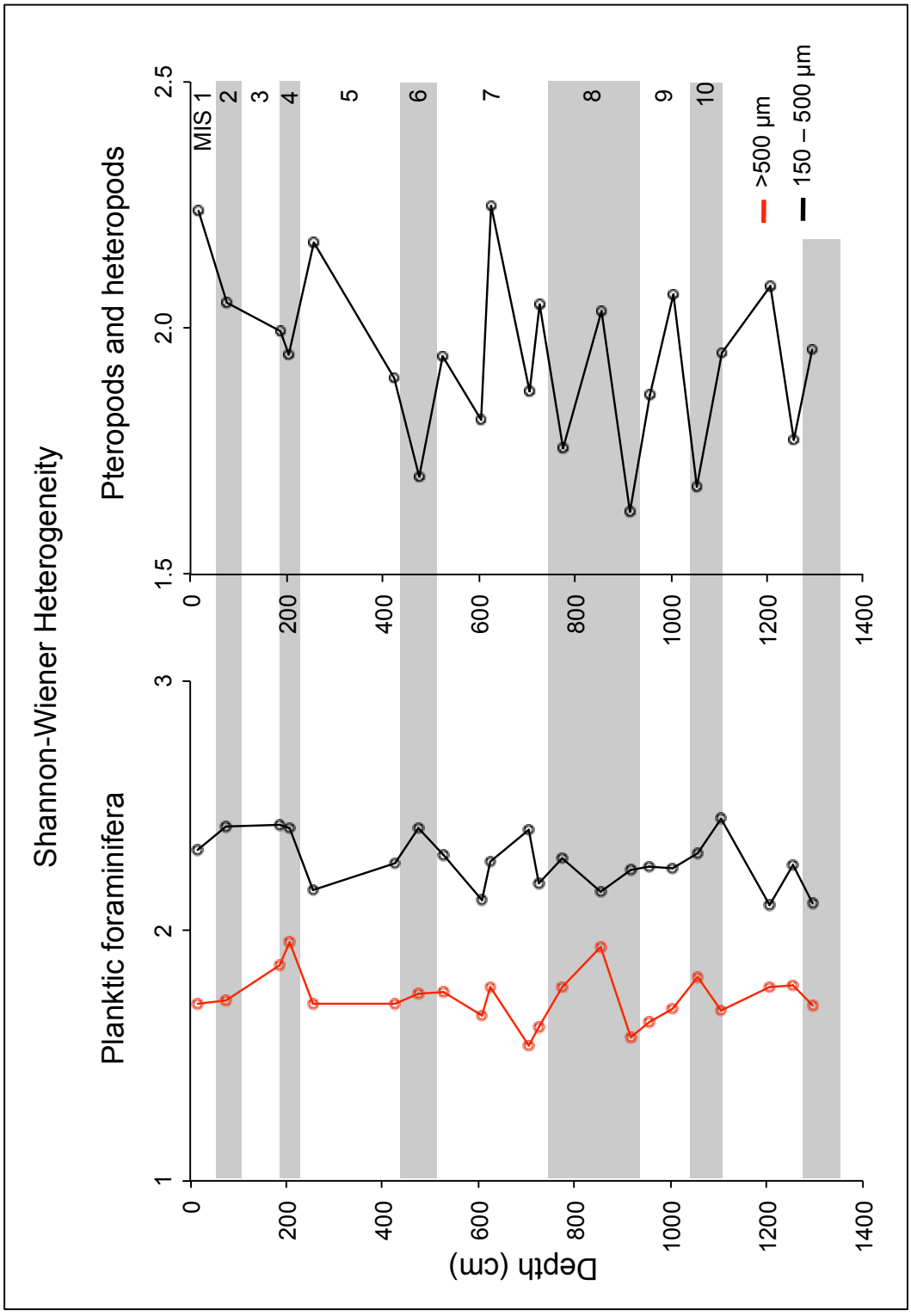

Figure 4.35 Shannon-Wiener heterogeneity of planktic foraminifera and pteropods and heteropods in 716B. Higher values indicate a more heterogeneous species assemblage. Grey boxes indicate glacial periods.

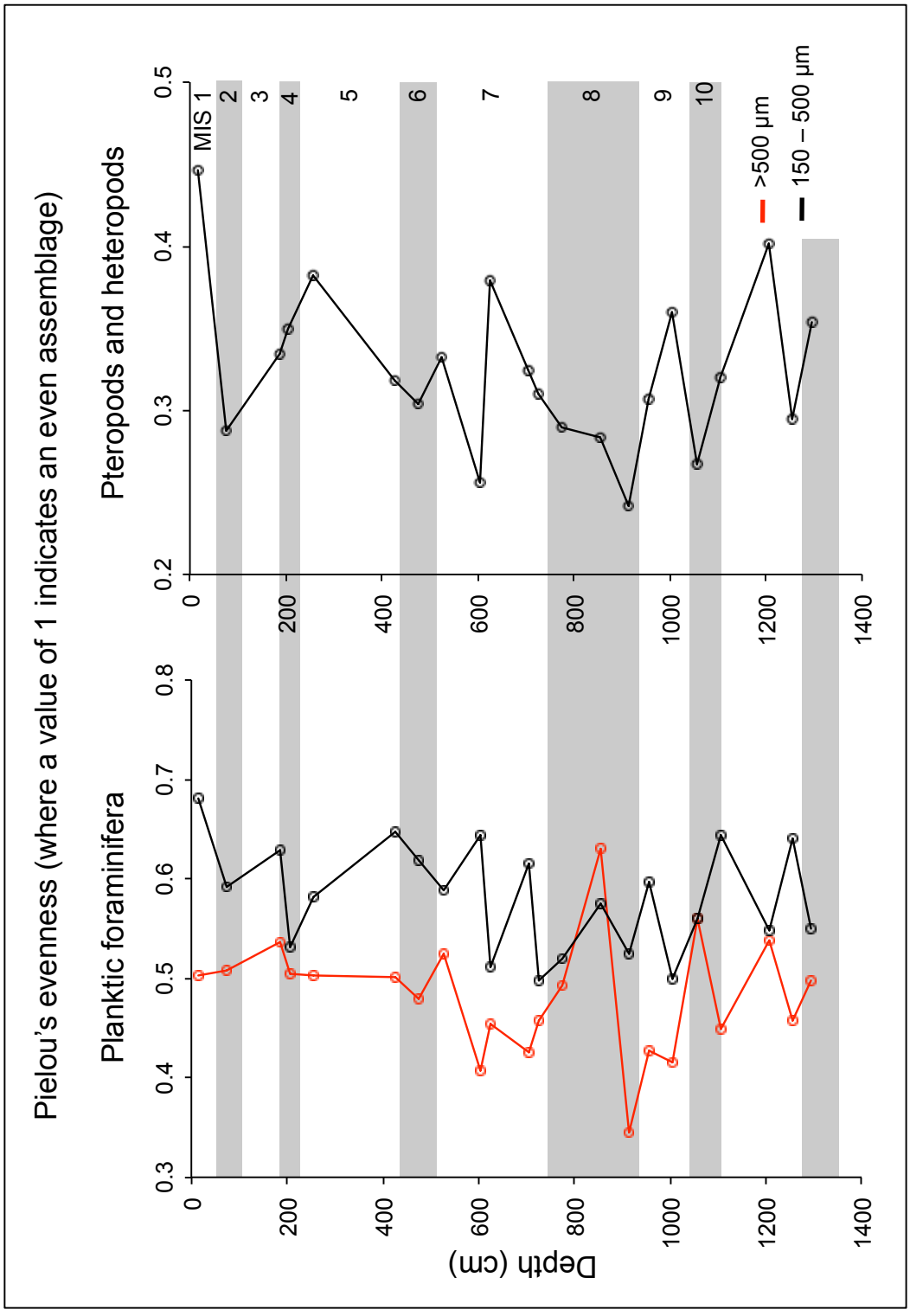

Figure 4.36 Pielou's evenness of planktic foraminifera and pteropods and heteropods in 716B. Grey boxes indicate glacial periods.

Due to drilling disturbance at the top of ODP Hole 716B, the uppermost sample at this site was collected at 15–16 cm in the core. Assuming the average sedimentation rate of 3.8 cmkyr^{-1} (Backman *et al.,* 1988), this sample actually represents 4 kyr and not the present day. Planktic species present in the overlying waters at ODP Site 716 will, therefore, not be accurately represented within this sample. However, many of the species of pteropod and heteropod found within the overlying waters are also found within the 15–16 cm sample (Tables 4.9, 4.10). Species missing from the sediments primarily appear to be the larger *Cavolinia* spp. and *Clio* spp. All pteropod species found within sample 15–16 cm are recorded by Bé and Gilmer (1977) as being present in the overlying waters at ODP Site 716B. However, several of the *Atlanta* species found within sample 15–16 cm are not recorded as living in the modern Indian Ocean by Tesch (1949), Thiriot-Quiévreux (1973) and Aravindakshan (1977). This is largely due to the improved recognition of species. *Atlanta californiensis* and *A. frontieri* were described in 1993 and *A. selvagensis* was not described until 2006.

The majority of planktic foraminifera species found in the overlying waters of the Indian Ocean (Bé and Tolderlund, 1971; Cullen and Prell, 1984) are present within the sample 15–16 cm (Table 4.11). Species missing from the sample are uncommon in the overlying waters, found only to be 'present' (<5%). These include *Candeina nitida* and *H. pelagica,* which are found elsewhere in the core, and *Globigerinoides tenellus,* which was not found in the sediments of ODP Hole 716B. Several species found in the sample 15–16 cm of 716B were not recorded from the overlying water. This is both a factor of the 4 kyr gap and also because some species are more recently described, and not recognised by Bé and Tolderlund (1971) or Cullen and Prell (1984). Species found in the

sample 15–16 cm, but not recorded in the overlying waters include *G. bulloides, G. trilobus, G. tumida*, *Globorotalia theyeri* and *Sphaeroidinella dehiscens.*

The percentage of several species of planktic foraminifera, pteropod and heteropod show trends that match the oxygen isotope data and/or the LDX profile throughout the core. Although appearing to correlate, many of the trends are not significant, or are only significant in some parts of the core. In particular, several species either show a more significant correlation in the very upper and lower sections of the core, or only in the central section of the core.

No species of planktic foraminifera shows a significant correlation to the oxygen isotope profile throughout the core (Appendix 8.2.3.2.B, 8.2.3.2.D), with the exception of *G. conglomerata* (Fig. 4.37), which shows a significant correlation when shifted down by 20cm (>500 µm r=-0.451, p=0.035, n=22; 150–500 µm µm r=-0.559, p=0.007, n=22). Three species of planktic foraminifera show a partial correlation to the oxygen isotope record. In both >500 µm and 150–500 µm assemblages of planktic foraminifera, *G. conglobatus* (Fig. 4.38) shows a significant correlation to the isotope profile in the top (0–725 cm) and the base (1055–1295 cm) of the core (>500 µm r=-0.502, p=0.048, n=16; 150–500 µm µm r=-0.529, p=0.017, n=20). In the >500 µm assemblage of planktic foraminifera *Pulleniatina obliquiloculata* shows a significant correlation (Fig. 4.38) in the central part (205–1005 cm) of the core (r=-0.694, p=0.006, n=14) and in the 150–500 µm assemblage, *G. menardii* shows a significant correlation in the lower half (425–1295 cm) of the core (r=-0.614, p=0.009, n=17). One species of planktic foraminifera in the 150–500 µm µm assemblage, *N. dutertrei,* shows a significant correlation to the LDX profile throughout the core (r=-0.507, p=0.016, n=22).

Two pteropod species and one heteropod species in the 150–500 μm assemblage show a significant correlation to the oxygen isotope profile in Hole 716B (Fig. 4.39). *Limacina inflata* shows a positive correlation, with higher numbers during interglacial periods and lower numbers during glacial periods (r=0.649, p=0.001, n=22). *Carinaria lamarcki* and *C. convexa* show a negative correlation to the isotope profile (*C. lamarcki* r=-0.547, p=0.008, n=22; *C. convexa* r=-0.652, p=0.001, n=22). The correlation is improved in both species by removing outlying points. *Carinaria lamarcki* shows a more significant correlation at the top (0–525 cm) and base (915–1295 cm) of the core (r=-0.691, p=0.003, n=16). By removing the value at 205 cm, the correlation between *C. convexa* and the oxygen isotope ratios in 716B is also improved (r=-0.666, p=0.001, n=21).

Shelled pteropod species of the Indian Ocean	**Occurrence in 716B surface sample (15–16 cm)**
Cavolinia gibbosa	Absent
Cavolinia globulosa	Absent
Cavolinia inflexa	**Present**
Cavolinia uncinata	Absent
Cavolinia tridentata	Absent
Clio balantium	Absent
Clio convexa	**Common**
Clio cuspidata	Absent
Clio pyramidata	Absent
Creseis acicula	**Present**
Creseis virgula	**Common**
Cuvierina columnella	Absent
Diacavolinia longirostris	Absent
Diacria quadridentata	**Present**
Diacria trispinosa	Absent
Hyalocylis striata	Absent
Limacina bulimoides	**Present**
Limacina inflata	**Abundant**
Limacina lesueuri	Absent
Limacina trochiformis	**Common**
Styliola subula	**Present**

Table 4.9 Summary of shelled pteropod species of the modern Indian Ocean (Bé and Gilmer, 1977) with those found in the surface (15-16 cm, >150 μm) sediments of Hole 716B (Present <5%; Common 5–20%; Abundant >20%).

Shelled heteropod species of the Indo-Pacific	Occurrence in 716B surface sample (15-16 cm)
Atlanta brunnea	Absent
Atlanta gaudichaudi	Absent
Atlanta helicinoidea	**Present**
Atlanta inclinata	**Present**
Atlanta inflata	Absent
Atlanta lesueuri	Absent
Atlanta peronii	**Present**
Atlanta rosea	**Present**
Atlanta turriculata	**Present**
Carinaria galea	Absent
Carinaria lamarckii	**Common**
Firoloida desmaresti	**Present**
Oxygyrus keraudreni	**Present**

Table 4.10 Summary of shelled heteropod species of the modern Indo-Pacific (Tesch, 1949;Thiriot-Quiévreux, 1973; Aravindakshan, 1977) with those found in the surface (15-16 cm, >150 μm) sediments of Hole 716B (Present <5%; Common 5–20%; Abundant >20%).

Planktic foraminifera species of the Indian Ocean	Abundance (Bé and Tolderlund, 1971; Cullen and Prell, 1984)	Occurrence in 716B surface sample (15-16 cm)
Candeina nitida	Present	Absent
Globoquadrina conglomerata	Present	**Common**
Globigerinella aequilateralis	Present – Common	**Common**
Globigerinella calida	Present – Common	**Present**
Globigerinita glutinata	Present	**Present**
Globigerinoides conglobatus	Present	**Common**
Globigerinoides ruber	Abundant	**Common**
Globigerinoides sacculifer	Abundant	**Abundant**
Globigerinoides tenellus	Present	Absent
Globorotalia menardii	Present – Common	**Abundant**
Hastigerina pelagica	Present	Absent
Neogloboquadrina dutertrei	Present	**Common**
Orbulina universa	Present – Common	**Common**
Pulleniatina obliquiloculata	Present	**Common**

Table 4.11 Summary of planktic foraminifera species of the modern Indian Ocean, close to the Maldives, and their abundances (Bé and Tolderlund, 1971; Cullen and Prell, 1984), with those found in the surface (15–16 cm, >150 μm) sediments of Hole 716B (Present <5%; Common 5–20%; Abundant >20%).

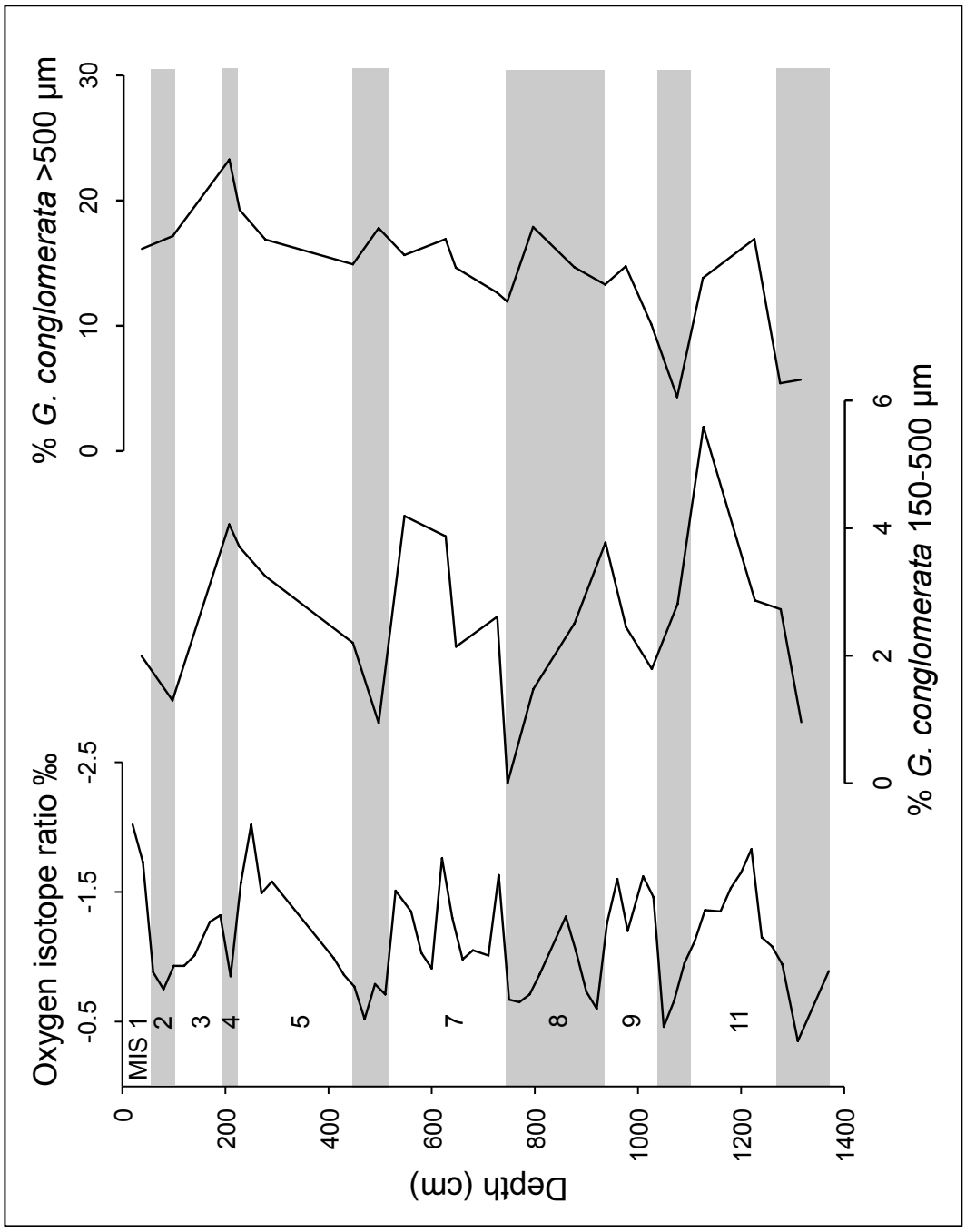

Figure 4.37 Percentage (percentage of planktic foraminifera) of *G. conglomerata* shifted down by 20 cm with oxygen isotope data for 716B.

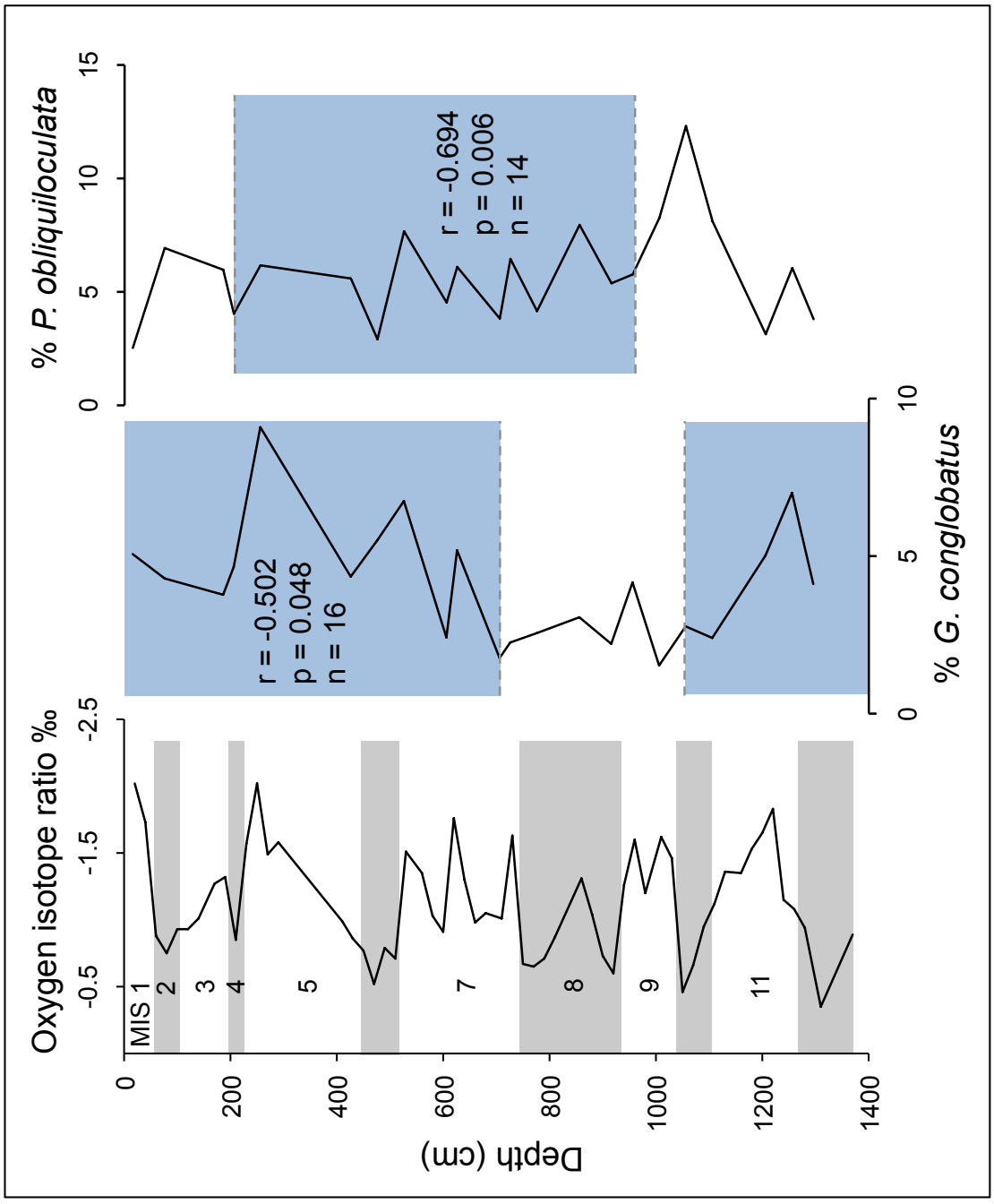

Figure 4.38 Percentage of >500 µm *G. conglobatus* and *P. obliquiloculata* with oxygen isotope ratios for 716B. Blue boxes indicate sections where % species show significant correlation to the oxygen isotope record.

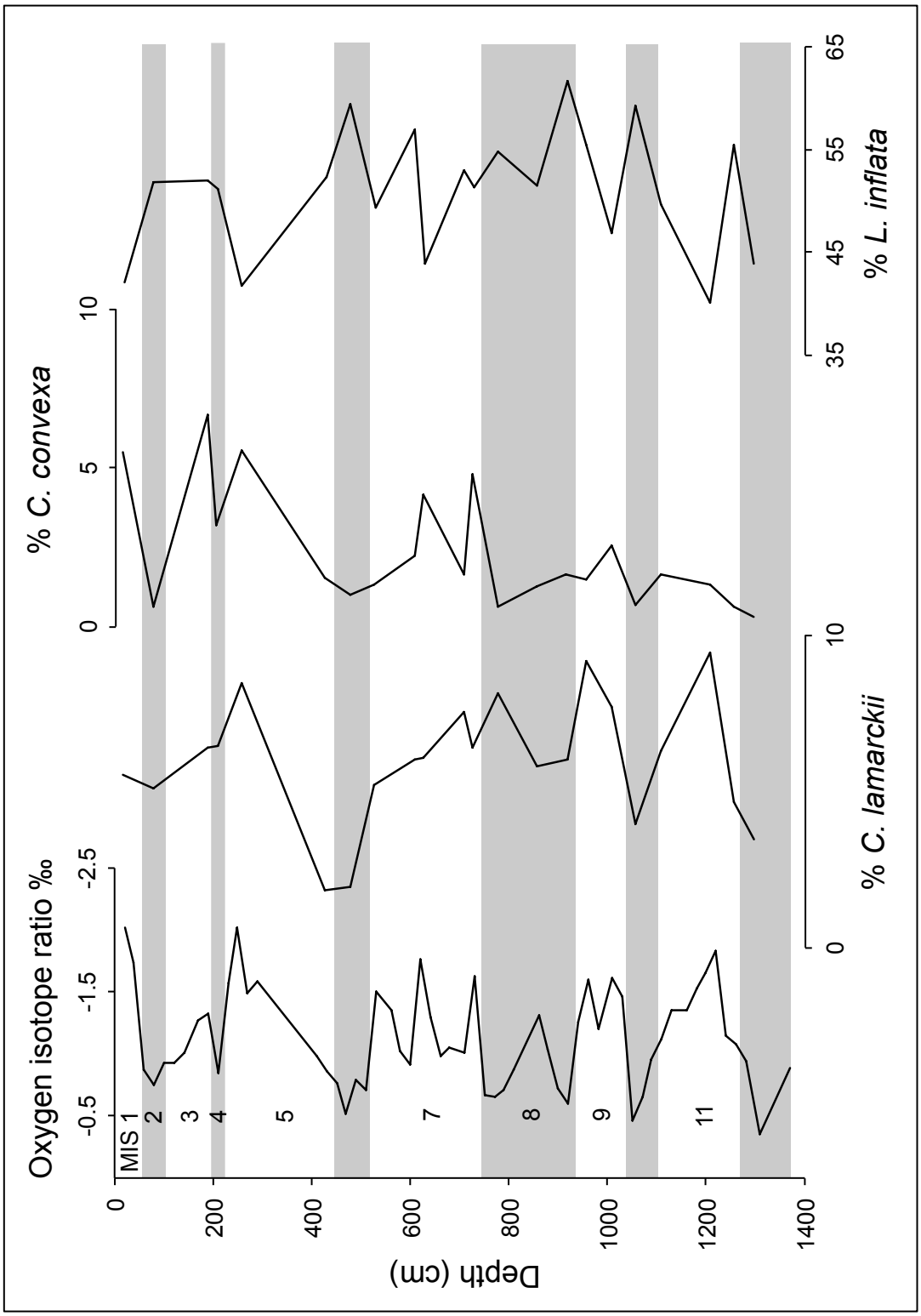

Figure 4.39 Species of pteropod and heteropod that show a significant correlation to the oxygen isotope profile throughout 716B.

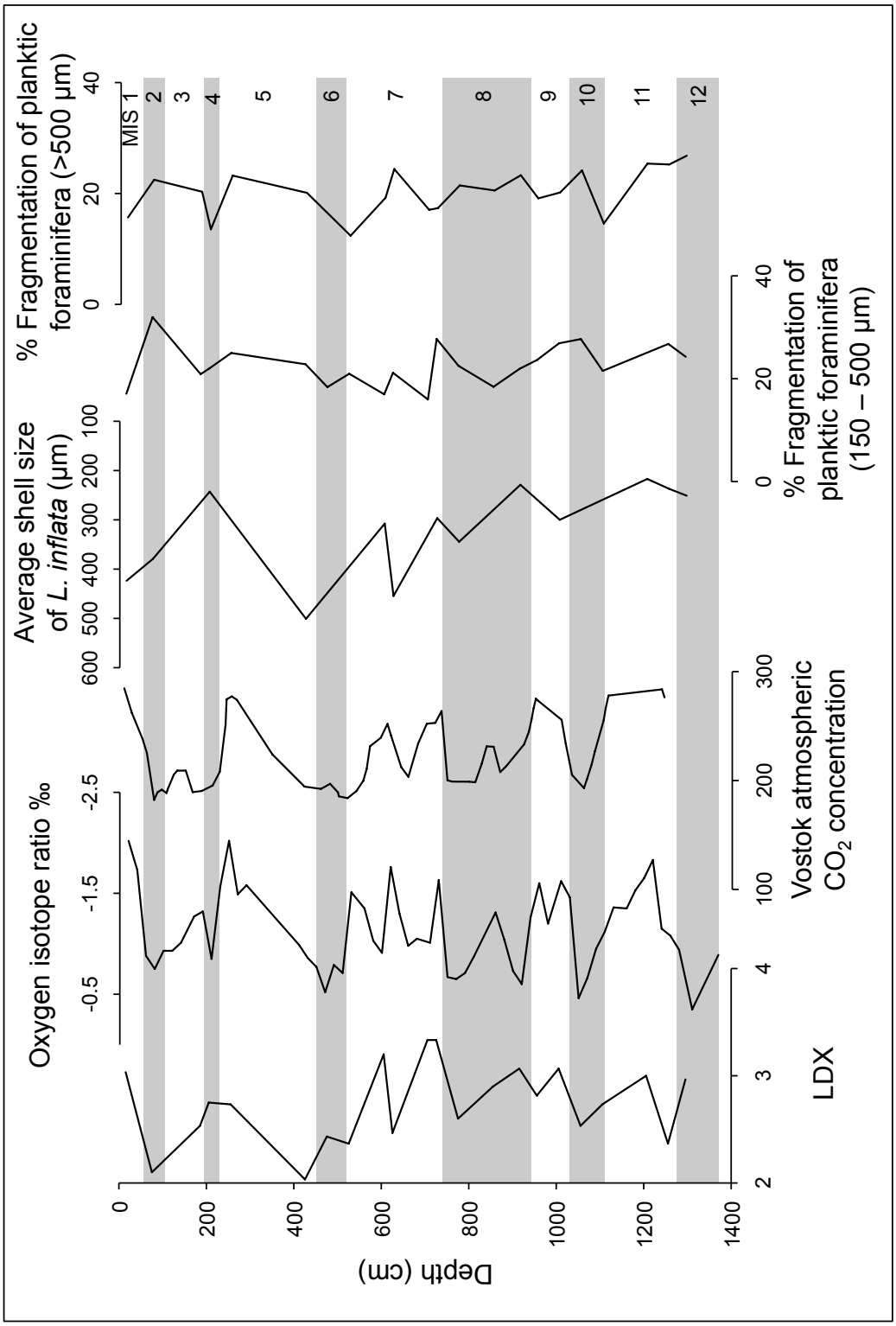

Figure 4.40 ODP Hole 716B LDX calcification profile, oxygen isotope profile, Vostok atmospheric CO_2 (Petit *et al.,* 1999), average *L. inflata* shell size and planktic foraminifera fragmentation.

4.3.4 CALCIFICATION INDICES

4.3.4.1 PLANKTIC FORAMINIFERA FRAGMENTATION

Fragmentation of planktic foraminifera in the 150–500 μm fraction of sediments shows little variation (Fig. 4.40, Appendix 8.2.3.2.F), with values ranging from 16.0% at 705 cm and 32.0% at 75 cm. In general, there is a trend of lower fragmentation during glacial periods, although fragmentation often increases towards the end of glacial periods (MIS 12, 10, 8 and 6). The >500 μm fraction produces similar results, with values ranging between 12.4% at 525 cm and 26.8% at 1295 cm. Fragmentation in the >500 μm fraction also increases towards the end of glacial periods (MIS 10, 6 and 4). Cullen and Droxler (1990) also found very little planktic foraminifera fragmentation in 716B.

4.3.4.2 LDX CALCIFICATION

Comparison of the oxygen isotope analysis and LDX calcification profile (Appendix 8.2.3.3.A and 8.2.3.3.B) for ODP Hole 716B shows that there is an association between pteropod calcification and global ice volume (Fig. 4.40). There is also an association between the LDX calcification profile and Vostok atmospheric CO_2 concentration (Fig. 4.40)

Figure 4.40 shows that during periods of high oxygen isotope ratio (cool climate, low atmospheric CO_2 concentration), pteropod calcification is generally high with low LDX values (MIS 10, 1055 cm, LDX 2.53; MIS 8, 775 cm, LDX 2.6; MIS 2, 75 cm, LDX 2.1). During periods of low oxygen isotope ratio (warm climate, high atmospheric CO_2 concentration), pteropod calcification is low with high LDX values (MIS 11, 1205 cm, LDX 3.00; MIS 9, 1005 cm, LDX 3.07; MIS 7, 705 cm, LDX 3.33; MIS 1, 15 cm, LDX 3.03). LDX values are higher overall than those in other cores studied (see sections 4.1.4.2, 4.2.4.2). This is almost

certainly due to the overall lower saturation of $CaCO_3$ in the surface waters of the Indian Ocean (Sabine *et al.,* 2002).

Despite visually appearing to correlate, the LDX and Vostok atmospheric CO_2 concentration (r=0.622, p=0.008, n=17) and the LDX and oxygen isotope profiles do not produce a significant relationship (r=-0.159, p=0.570, n=22). When the LDX profile is shifted down by 20 cm (Fig. 4.41, Appendix 8.2.1.3.C), the a significant correlation to the oxygen isotope profile is produced (r=-0.633, p=0.002, n=21). This equates to a lag in time of approximately 5.3 kyrs.

During LDX analysis of shells from 716B, it was noticed that most samples contained several shells (of different species) that appeared to be flecked with black spots (Fig. 4.42). Upon subsequent SEM imaging, it was found that these black flecks are tiny holes in the shell surface, approximately 2–3 μm in diameter. This arrangement of holes is most likely due to bioerosion, in the form of microboring and not the result of dissolution from undersaturated waters.

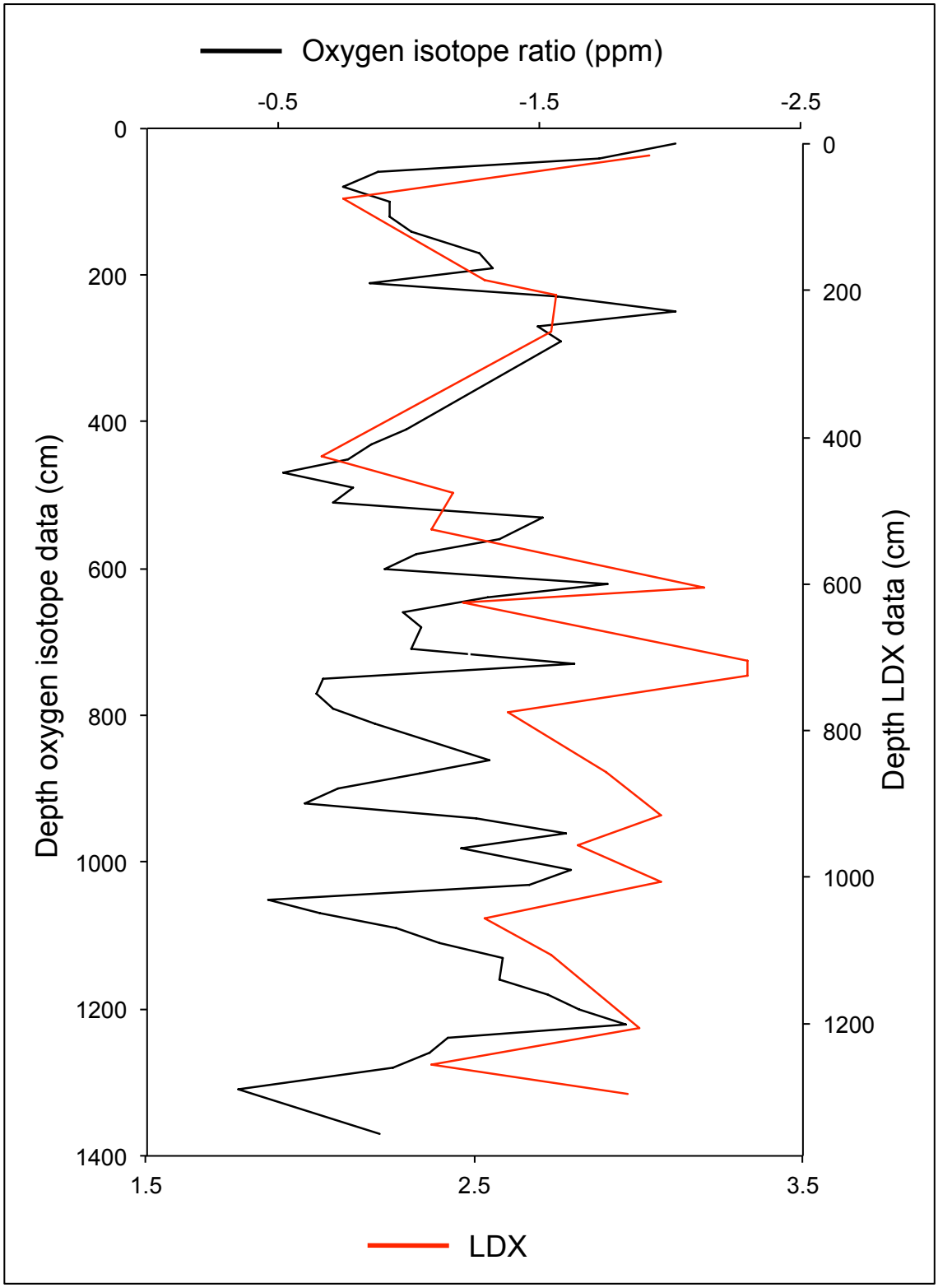

Figure 4.41 LDX calcification profile (in black) shifted down by 20 cm with the original oxygen isotope profile (in red) of 716B.

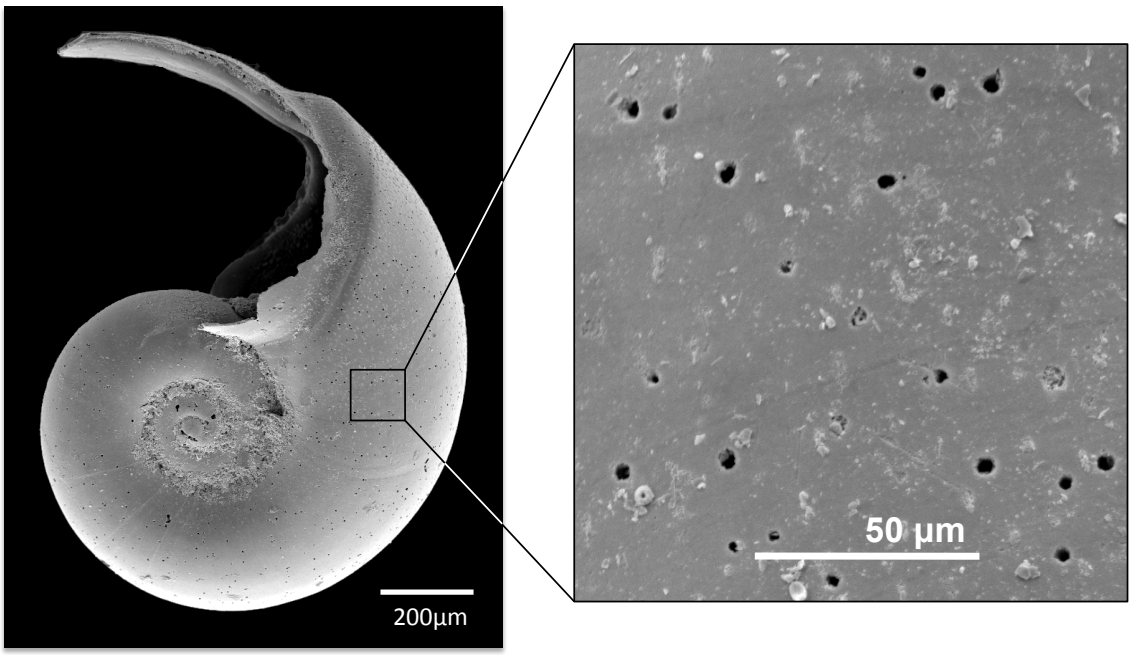

Figure 4.42 Specimen of *L. inflata* from 716B (>500 µm, 475–476 cm) showing the well calcified surface structure with micro-boring damage.

4.3.4.3 PTEROPOD SHELL SIZE

The average shell size of *L. inflata* (Appendix 8.2.3.3.C) is generally higher towards the end of, or directly following glacial periods (1005 cm, 299.9 µm; 775 cm, 344.5 µm; 425 cm, 500.9 µm; 75 cm, 379.4 µm). Average shell sizes are generally lower towards the end of interglacial periods, or at the base of glacial periods (1205 cm, 217.0 µm; 915 cm, 228.9 µm; 205 cm, 242.8 µm). The average shell size does not produce a significant correlation with the oxygen isotope profile ($r=-0.229$, $p=0.451$, $n=13$) or the Vostok atmospheric CO_2 profile ($r=-0.066$, $p=0.876$, $n=8$) for 716B. This suggests that the average shell size, like the LDX, shows a lag in response to the change in climate. The average shell size shows a significant negative correlation to the LDX profile ($r=-0.525$, $p=0.037$, $n=16$), with larger shells being produced when calcification is higher and smaller shells being produced when calcification is lower.

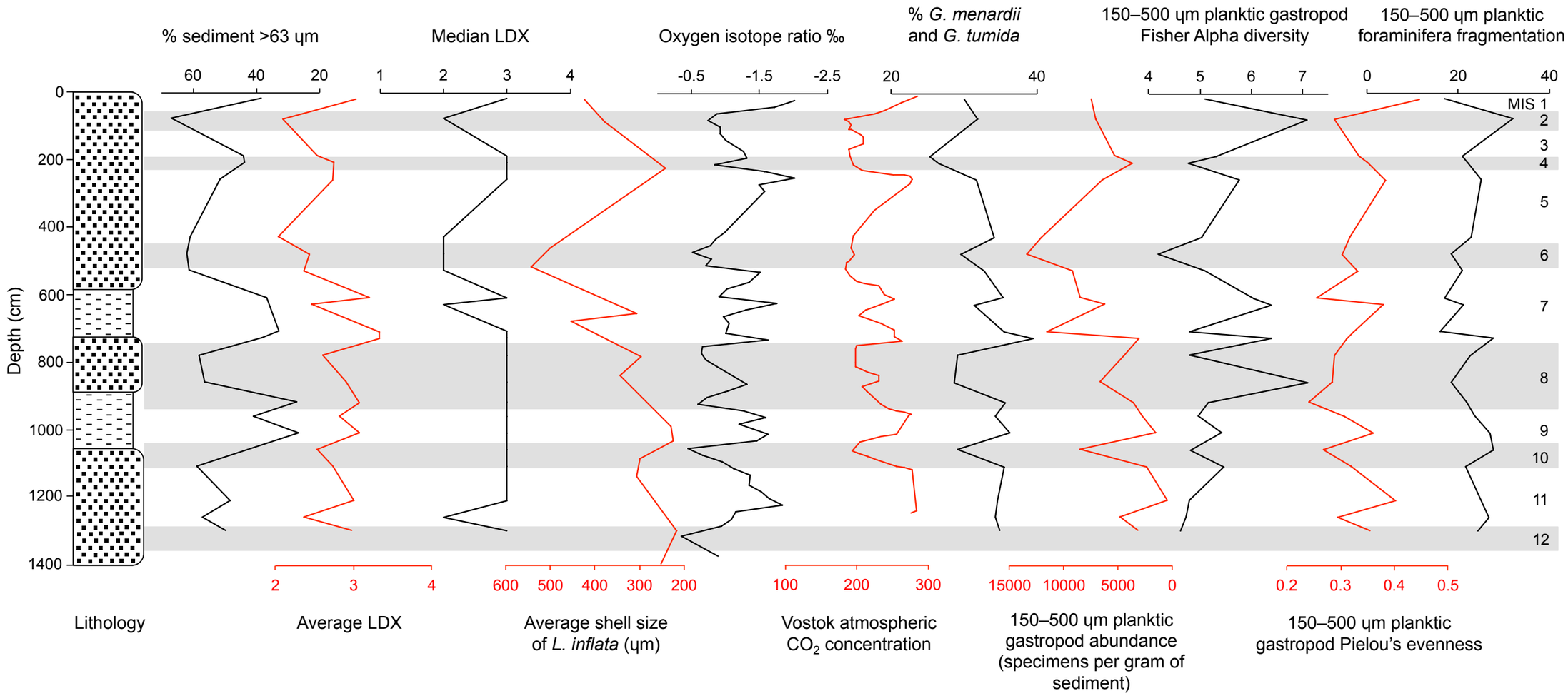

Figure 4.43 ODP Hole 716B: % sediment >63 µm, Average LDX, Median LDX, Average *L. inflata* shell size, Oxygen isotope profile (Droxler *et al.,* 1990), Vostok atmospheric CO_2 concentration (Petit *et al.,* 1999), % *G. menardii* and *G. tumida,* Planktic gastropod abundance, Fisher Alpha diversity and Pielou's evenness and Planktic foraminifera fragmentation. Scales for % sediment >63 µm, Average *L. inflata* shell size, Oxygen isotope profile and Planktic gastropod abundance are reversed.

5 TAXONOMY OF HOLOPLANKTIC GASTROPODS

The most recent reference within the synonymised taxa (at the base of each list) refers to the main figures used in the identification of specimens during this study.

5.1 PTEROPOD TAXONOMY

Information on synonymised taxa for pteropods was found in Rosenberg (2009), Janssen (2012) and CLEMAM (2012).

Pteropod species	Caribbean Sea	Mediterranean Sea	Indian Ocean
Cavolinia inflexa	**O**	**O**	**O**
Clio convexa	**O**	**-**	**O**
Clio cuspidata	**O**	**O**	**O**
Clio pyramidata	**O**	**O**	**O**
Creseis acicula	**O**	**O**	**O**
Creseis chierchiae	**O**	**-**	**O**
Creseis virgula virgula	**O**	**O**	**O**
Creseis virgula constricta	**-**	**O**	**O**
Cuvierina columnella	**O**	**O**	**-**
Diacavolinia longirostris	**-**	**-**	**O**
Diacria quadridentata	**O**	**-**	**O**
Diacria trispinosa	**O**	**O**	**O**
Hyalostylus striata	**O**	**-**	**O**
Limacina bulimoides	**O**	**O**	**O**
Limacina inflata	**O**	**O**	**O**
Limacina lesueuri	**O**	**-**	**O**
Limacina retroversa	**-**	**O**	**-**
Limacina trochiformis	**O**	**O**	**O**
Limacina sp. B	**O**	**O**	**-**
Limacina sp. C	**O**	**-**	**O**
Styliola subula	**O**	**O**	**O**
Gleba cordata	**O**	**O**	**O**
Peracle diversa	**O**	**-**	**O**
Peracle moluccensis	**O**	**O**	**O**
Paedoclione doliiformis	**O**	**O**	**O**
Gymnosome veligers	**O**	**-**	**O**

Table 5.1 Species of shelled pteropod present at each studied location. Present **O**; Absent **–.**

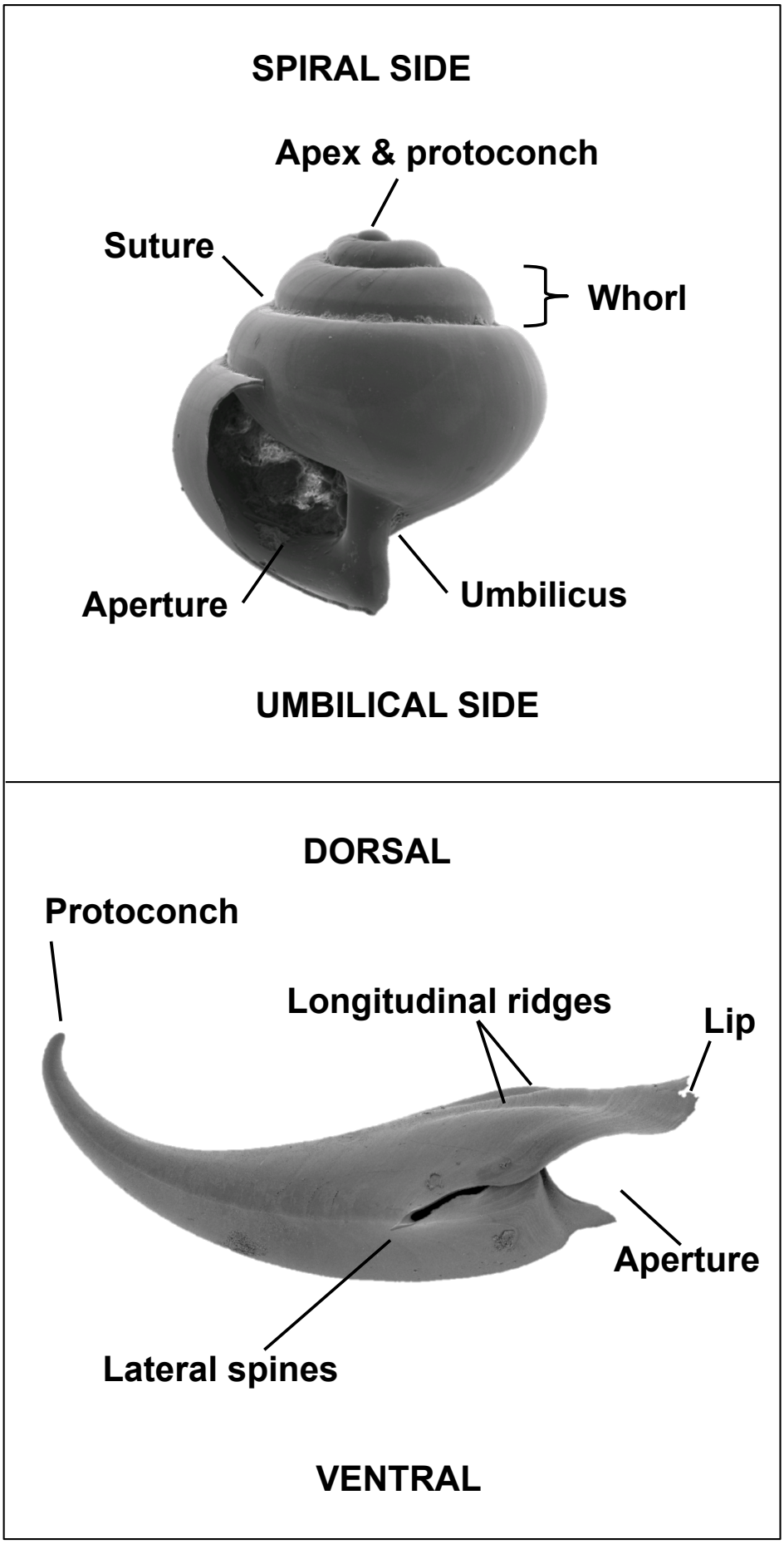

Figure 5.1 Morphological terms used in taxonomy.

PHYLUM **Mollusca**

CLASS **Gastropoda**

SUBCLASS **Opistobranchia**

ORDER **Thecosomata** de Blainville, 1824

SUBORDER **Euthecosomata** Meisenheimer, 1905

FAMILY **Limacinidae** Gray, 1847

GENUS ***Limacina*** Bosc, 1817

Type species: *Limacina helicina* (Phipps, 1774).

Diagnosis: The genus *Limacina* is characterised by sinistrally coiling trochospiral shells with variable spire height.

***Limacina bulimoides* (d'Orbigny, 1836)**

Plate 1, Figure 4a–d.

Atlanta bulimoides d'Orbigny, 1834: p. 179, pl. 12, figs 36–38.
Spiratella bulimoides (d'Orbigny, 1834) – Pastouret, 1970: p. 238, pl. 1, fig. 5.
Limacina bulimoides (d'Orbigny, 1836) – van Straaten, 1966: p. 431.
Spirialis bulimoides (Eydoux & Souleyet), 1840 – Vérany, 1853: p. 381.
Limacina bulimoides (d'Orbigny, 1836) – Bé & Gilmer, 1977: p. 800, pl. 3, fig. 4a–d.

Diagnosis: A large, highly spired shell with a shell height greater than the maximum shell diameter. There are five to six rapidly expanding whorls in the adult shell, with a closed umbilicus and shallow suture notches.

Remarks: The juvenile shell differs from *L. trochiformis* by the presence of discontinuous longitudinal striations, which are also found in adult specimens. Sutures are also more pronounced in juvenile *L. bulimoides. Limacina*

bulimoides was found in higher abundances during warm periods in all cores studied. This is particularly noticeable in core B5-1 (Fig. 4.27).

Distribution: The geographical range of *L. bulimoides* extends to the northern and southern subtropical provinces, roughly between 40°N and 40°S (Bé and Gilmer, 1977). The vertical range is 80–120 m in waters of temperature 13.8°C–27.8°C (van der Spoel, 1967).

Limacina inflata **(d'Orbigny, 1836)**

Plate 1, Figure 1a–c.

Atlanta inflata d'Orbigny, 1834: pl. 12, figs 16–19.
Spiratella inflata (d'Orbigny, 1834) – Blanc-Vernet *et al.,* 1969, p. 220.
Limacina inflata (d'Orbigny, 1836) – Steuer, 1911: p. 714, fig. 1.
Spirialis rostralis Eydoux & Souleyet, 1840: p. 236
Limacina scaphoidea Gould, 1852: pp. 485–486.
Embolus planorboides Seguenza, 1875: p. 148.
Limacina inflata (d'Orbigny, 1836) – Bé & Gilmer, 1977: p. 800, pl. 3, fig. 1a–d.

Diagnosis: *Limacina inflata* has a large adult shell, formed by three rapidly expanding whorls. The apex is depressed by subsequent, expanding whorls, producing an almost planispiral shell. A thickened rib or 'tooth' develops on the outer margin of adult shells.

Remarks: A very common species, easily distinguished from other *Limacina* species by the depressed apex. Juvenile specimens with a non-depressed apex, possibly a sub-species of *L. inflata,* were found from the Indian Ocean in Hole 716B.

Distribution: *Limacina inflata* is a warm water cosmopolitan species, widely distributed in the tropical and subtropical regions of all oceans, between roughly 50°N and 45°S. The vertical range is <100–300 m in waters of 14.0°C–28.0°C (Bé and Gilmer, 1977). *Limacina inflata* was found in higher abundances during warm periods in all cores studied. This is particularly noticeable in core B5-1 (Fig. 4.27).

Limacina lesueurii (d'Orbigny, 1836)

Plate 1, Figure 6a–b.

Atlanta lesueurii d'Orbigny, 1835: pl. 20, figs 12–15.
Limacina lesueurii (d'Orbigny, 1836) – van der Spoel, 1967, p. 52, fig. 20.
Spirialis ventricosa Eydoux & Souleyet, 1840: pp. 236–237.
Spiratella lesueuri (d'Orbigny, 1835) – Vatova, 1974: p. 107.
Limacina lesueurii (d'Orbigny, 1836) – Bé & Gilmer, 1977: p. 800, pl. 3, fig. 5a–d.

Diagnosis: *Limacina lesueurii* has a large, low spired shell with a shell height less than the maximum shell diameter. There are four to five rapidly expanding whorls in the adult shell, with a narrow umbilicus and large aperture.

Remarks: The juvenile form is very similar to juvenile *L. retroversa* but with a lower spire and less prominent sutures. Adult shells have a similar morphology to *Limacina helicina* and *Limacina helicinoides,* but can be distinguished by the reduced size of the umbilicus and the lack of transverse surface striations. The geographical ranges and temperature preferences of these species also differ.

Distribution: The geographical range of *L. lesueurii* extends to the northern and southern subtropical provinces, between roughly 40°N and 40°S, with lower numbers in equatorial regions (Bé and Gilmer, 1977). The vertical range of this species is between 100–600 m in waters of 13.0°C–27.0°C (van der Spoel, 1967).

Limacina retroversa (Fleming, 1823)

Plate 1, Figure 7a–b.

Trochus lunaris Gmelin, 1791: p. 3587.
Fusus retroversus Fleming, 1823: pp. 498–500, pl. 15, fig. 2.
Limacina retroversa (Fleming, 1823) – van Straaten, 1966: p. 431.
Spiratella retroversa (Fleming, 1823) – Froget, 1967: p. 2968.
Scaea stenogyra (Philippi, 1844): p. 164, pl. 25, fig. 20.
Spirialis jeffreysii Forbes & Hanley, 1849: p. 386, pl. 57, fig. 8.
Spirialis macandrei Forbes & Hanley, 1849: pp. 385–386, pl. 57, figs 6–7.
Spirialis gouldii Stimpson, 1851: p. 8, pl. 1, fig. 4.
Heterofusus alexandri Verrill, 1872: p. 281.
Limacina retroversa (Fleming, 1823) – Bé & Gilmer, 1977: p. 800, pl. 3, fig. 3a–d.

Diagnosis: A highly spired shell with a shell height greater than the maximum shell diameter, consisting of five to six gradually increasing whorls with a distinct open umbilicus. The whorls are rounded in profile and show distinct suture notches.

Remarks: The form present is the smaller subspecies, *L. retroversa retroversa,* as described by Bé and Gilmer (1977). This species was present in sections of core B5-1 relating to cold climatic periods only.

Distribution: This species resides in the upper 150 m of sub-polar and transitional waters of both hemispheres, between 40°N–55°N and 38°S–70°S (Bé and Gilmer, 1977). The water temperature range of this species is 2.0°C–19.0°C (Bigelow, 1926).

Limacina trochiformis **(d'Orbigny, 1834)**

Plate 1, Figure 5a–d.

Atlanta trochiformis d'Orbigny, 1834: pp. 177–178, pl. 12, figs 29–31.
Limacina trochiformis (d'Orbigny, 1834) – van der Spoel, 1967: p. 53.
Spirialis trochiformis (d'Orbigny, 1834) – Rang & Souleyet, 1852: p. 64.
Spiratella trochiformis (d'Orbigny, 1834) – Pastouret, 1970: p. 238, pl. 1, fig. 4.
Limacina naticoides Souleyet, 1852 – Rang & Souleyet, 1852: p. 64, pl. 10, figs 1–2.
Limacina contorta (Monterosato) – Sykes, 1905: p. 327, fig. 1.
Limacina trochiformis (d'Orbigny, 1834) – Bé & Gilmer, 1977: p. 800, pl. 3, fig. 2a–d.

Diagnosis: *Limacina trochiformis* has a medium sized, moderately spired shell, with a shell height equal to the maximum shell diameter. The adult shell is composed of four rapidly expanding whorls with a closed umbilicus.

Remarks: the juvenile shell differs from *L. bulimoides* by the lack of longitudinal striations and no visible sutures in the first two whorls.

Distribution: *Limacina trochiformis* is a warm water species, with high abundances in tropical regions. The geographical range of this species is between 45°N–45°S, at a water depth of less than 100 m and at a temperature of between 13.8°C–27.9°C (Bé and Gilmer, 1977).

***Limacina* sp. B**

Plate 1, Figure 3.

Diagnosis: A shell similar in form to *L. inflata,* however, the outer and umbilical apertural margin curls around rather than ending in a tooth. The shell is composed of two or three rapidly expanding whorls, with a depressed apex and umbilicus. The curled apertural margin is larger than the main shell and has obvious longitudinal striations, which terminate at the junction with the aperture.

Remarks: This may be a species of the gastropod genus *Sinum.* However, a lack of specimens does not allow a definite identification. Three specimens were found in total, two from the 150–500 µm fraction of B5-1 and one from the >500 µm fraction of B5-1. The oldest specimen was from MIS 6 (B5-1 490 cm).

Distribution: During this study, *Limacina* sp. B was found in Mediterranean Sea sediments only. All specimens were found in sediments relating to cool periods.

***Limacina* sp. C [*Heliconoides* sp.?]**

Plate 3, Figure 3 a–c.

Diagnosis: A shell similar to *L. inflata* but with whorls that inflate more gradually. The aperture is circular and the apertural margin ends in a thick lip. The apex is not depressed, but protrudes slightly, with no defined whorl sutures, giving a smooth domed apex.

Remarks: It is likely that this species is, or is derived from, a previously recorded extinct genus, *Heliconoides* (Cahuzac and Janssen, 2010), known from the Paleocene to the Pliocene. The specimens are all in good condition and are unlikely to be the result of sediment reworking. Fifteen specimens were collected in total from the >500 µm fraction throughout CAR-MON 2 and from the >500 µm and 150–500 µm of 716B. The youngest specimen was collected at 10 cm core depth in CAR-MON 2, which is approximately 4 kyr.

Distribution: During this study, *Limacina* sp. C was found in the Caribbean Sea and in the Indian Ocean and showed no temperature preference through the cores.

***Limacina* sp. D**

Plate 3, Figure 1a–b.

Diagnosis: *Limacina* sp. D has a small shell, similar in morphology to *L. inflata* and *Limacina* sp. C, consisting of two and a half whorls arranged as in *Limacina* sp. C, with a rounded, slightly protruding apex and no defined whorl sutures. The final whorl rapidly inflates to a large, eye-shaped aperture. The umbilical side of the apertural margin curls around the shell, covering the umbilical and attaching to the spiral side 180° from the spiral side of the apertural margin.

Remarks: Only two specimens of *Limacina* sp. D were found, one from the >500 µm fraction of CAR-MON 2 and one from the 150–500 µm fraction of B5-1.

Distribution: During this study, *Limacina* sp. D was found in the Caribbean Sea and in the Mediterranean Sea and showed no temperature preference.

FAMILY **Cavoliniidae** Fischer, 1883

Diagnosis: Species of the family Cavoliniidae are characterised by elongate, cone-shaped shells.

SUBFAMILY **Cuvierininae**

GENUS ***Cuvierina*** Boas, 1886

Type species: *Cuvierina columnella* (Rang, 1827).

Diagnosis: The genus *Cuvierina* is characterised by an elongate shell, conical in the juvenile form and bottle shaped in the adult form.

***Cuvierina columnella* (Rang, 1827)**

Plate 3, Figure 2.

Cuvierina columnella (Rang, 1827) – Bé and Gilmer, 1977: p. 802, Pl. 5, figs 8a–e.
Cuvierina columnella var. typica Boas, 1886: pp. 134, 215.
Cuvierina spoeli Rampal, 2002: pp. 214–215, fig. 1A–B.
Cuvierina columnella (Rang, 1827) – Bé & Gilmer, 1977: p. 802, pl. 5, fig. 8a–e.

Diagnosis: The adult shell of *C. columnella* is large and bottle shaped with a rounded base and kidney shaped aperture. The juvenile shell of *C. columnella* is conical and elongate and is usually discarded.

Remarks: This is a very distinct species and easily recognised by the kidney shaped aperture. Juvenile stages were not found during this study.

Distribution: This is a warm water cosmopolitan species with a patchy distribution in tropical and subtropical waters, between 50°N and 50°S. The vertical range of this species is between 100–250 m (Bonnevie, 1913) in waters of temperature 17.9°C–26.2°C (van der Spoel, 1967).

SUBFAMILY **Clioinae**

GENUS ***Hyalocylis*** Fol, 1875

Type species: *Hyalocylis striata* (Rang, 1828).

Diagnosis: The genus *Hyalocylis* is characterised by a conical, transverselly ridged shell.

***Hyalocylis striata* (Rang, 1828)**

Plate 2, Figure 5.

Creseis striata (Rang, 1828): p. 315, pl. 17, fig. 3.
Hyalocylis striata (Rang, 1828) – van der Spoel, 1967: p. 64, figs 46a–b, 47, 347.
Creseis compressa Eschscholtz, 1829: p. 18, pl. 15, fig. 7.
Creseis zonata delle Chiaje, 1830: pl. 82, pl. 9.
Creseis annulata Deshayes, 1853: p. 62, pl. 103, figs 11–12.
Hyalocylix striata Pelseneer, 1888 – Oberwimmer, 1898: p. 590.
Hyalocylis obtusa di Geronimo, 1974: p. 114, figs 1a –b, 2a–b, 3a–b.

Hyalocylis striata (Rang, 1828) – Bé & Gilmer, 1977: p. 802, pl. 5, fig. 9a–b.

Diagnosis: A squat conical shell, often with a slight dorsal curvature. The aperture is circular and there are very defined transverse ridges over the entire surface of the shell. The shell is thin and brittle, often with the protoconch missing.

Remarks: Specimens were often found to be broken and no protoconch were found during this study.

Distribution: The geographical distribution of this tropical species is between 45°N to 45°S, with increased abundances in equatorial waters. The vertical range of this species is between 100–500 m in waters of temperature ranging between 17.5°C and 27.8°C (van der Spoel, 1967; Bé and Gilmer, 1977).

GENUS ***Styliola*** Lesueur, 1825

Type species: *Styliola subula* (Quoy and Gaimard, 1827).

Diagnosis: The genus *Styliola* is characterised by an elongate shell with a longitudinal groove.

***Styliola subula* (Quoy and Gaimard, 1827)**

Plate 2, Figure 9a–b.

Cleodora subula Quoy & Gaimard, 1827: p. 233, pl. 8D. figs 1–3.
Styliola subula (Quoy & Gaimard, 1827) – Menzies, 1958: p. 387, fig. 4a–e.
Creseis subula (Quoy & Gaimard, 1827) – Rang, 1828: p. 314, pl. 18, fig. 1.
Cleodora spinifera Rang, 1828: p. 313, pl. 17, fig. 1.
Cleodora subulata Quoy & Gaimard, 1832: p. 382, pl. 27, figs 14–16.

Styliola subula (Quoy & Gaimard, 1827) – Bé & Gilmer, 1977: p. 802, pl. 5, fig. 10a–d.

Diagnosis: A large, elongate conical shell, oval in cross section with an oval aperture. The adult shell has fine transverse striations over the surface and a longitudinal groove, which runs obliquely along the dorsal length. The protoconch is small and pointed.

Remarks: This is a very common species and is easily recognised by the large longitudinal groove, which runs along the length of the shell.

Distribution: The geographical range of *S. subula* extends across the northern and southern subtropical regions, between 50°N and 45°S, with generally lower numbers in equatorial waters. The vertical range of this species is <400 m, in water ranging in temperature between 14.2°C – 27.7°C (Chen and Bé, 1964; Bé and Gilmer, 1977)

GENUS ***Creseis*** Rang, 1828

Type species: *Creseis virgula* (Rang, 1828).

Diagnosis: The genus *Creseis* is characterised by an elongate shell with a smooth surface.

***Creseis virgula* (Rang, 1828) *virgula* (Rang, 1828)**

Plate 2, Figure 3.

Creseis conica Eschscholtz, 1829: p. 17, pl. 15, fig. 3.
Creseis virgula (Rang, 1828): p. 316, pl. 17, fig. 2.
Creseis unguis Eschscholtz, 1829: p. 17, pl. 15, fig. 4.
Creseis cornucopiae Eschscholtz, 1829: p. 17, pl. 15, fig. 5.

Creseis caligula Eschscholtz, 1829: p. 18, pl. 15, fig. 6.
Hyalaea corniformis d'Orbigny, 1834: pp. 120–121, pl. 8, figs 20–22.
Cleodora placida Gould, 1852: p. 490.
Cleodora munda Gould, 1852: pp. 489–490.
Cleodora falcata Gould, 1852: pp. 490–491.
Styliola vitrea Verrill, 1872: p. 284, pl. 6, fig. 7.
Creseis rotunda Sowerby – Reeve & Sowerby, 1878: pl. 5, fig. 28a–b.
Cleodora flexa Pfeffer, 1879: pp. 241–242, figs 15–16.
Creseis virgulata Locard, 1886: p. 24.
Creseis virgula frontieri Rampal, 2002: pp. 234–236, fig. 10E–F.
Creseis virgula virgula (Rang, 1828) – Bé & Gilmer, 1977: p. 802, pl. 5, fig. 14a–c.

Diagnosis: An elongate, conical shell with a circular cross section and aperture. The diameter of the cross section increases more rapidly than *C. acicula.* The shell is curved dorsally to an angle of about 50°. There is no defined protoconch or surface ornamentation.

Remarks: This subspecies is clearly recognisable from the other *C. virgula* subspecies by the curvature of the shell.

Distribution: This is a warm water cosmopolitan species with tropical affinities, which lives in the upper 319 m. The geographical range is between 45°N and 40°S, with higher abundances in equatorial regions (Bé and Gilmer, 1977). The temperature range of *C. virgula virgula* is 15.0°C–27.9°C (Chen and Bé, 1964; van der Spoel, 1967).

***Creseis virgula* (Rang, 1828) *constricta* (Chen & Bé, 1964)**

Plate 2, Figure 2a–b.

Creseis virgula constricta Chen & Bé, 1964: p. 194, figs 3d, 4d.

Creseis virgula constricta (Chen & Bé, 1964) – Bé & Gilmer, 1977: p. 802, pl. 5, fig. 12a–b.

Diagnosis: An elongate, conical shell with a circular cross section and aperture. The diameter of the cross section increases more rapidly than *C. acicula.* The shell is straight but constricted at the protoconch, which is fairly long. There is no surface ornamentation.

Remarks: This subspecies is clearly recognisable from the other *C. virgula* subspecies by the pinched-in, or constricted, top of the protoconch. This subspecies is often regarded as *C. chierchiae* (for example, Janssen, 2012), but was found during this study to be noticeably different, with a longer and more slender protoconch than that of *C. chierchiae.*

Distribution: *Creseis virgula constricta* is a subtropical species, previously only recorded from the Sargasso Sea (Chen and Bé, 1964). It was found at all sites in this study, expanding the previous geographical range to the Caribbean Sea, Mediterranean Sea and Indian Ocean.

Creseis acicula **(Rang, 1828)**

Plate 2, Figure 4.

Creseis acicula (Rang, 1828): p. 318, pl. 17, fig. 6.
Creseis clava Rang, 1828: p. 317, pl. 17, fig. 5.
Creseis acus Eschscholtz, 1829: p. 17, pl. 15, fig. 2.

Hyalœa aciculate d'Orbigny, 1834: p. 123, pl. 8, figs 29–31.
Cleodora acicula Rang, 1828 – Vérany, 1853: p. 380.
Stiliola acus Dunker, 1875: p. 240.
Creseis rotunda Sowerby, 1877: pl. 5, fig. 28a–b.
Creseis aciculata Sowerby – Reeve & Sowerby, 1878: pl. 5, fig. 29a–b.
Dentalium ecostatum Kirk, 1880: p. 806.
Creseis acicula (Rang, 1828) – Bé & Gilmer, 1977: p. 802, pl. 5, fig. 11a–b.

Diagnosis: Shell extremely elongate, straight, thin and pencil-like. The shell is circular in cross section with a circular aperture. There is no shell ornamentation or defined protoconch.

Remarks: This species often has slight bends along its length and is not completely straight.

Distribution: *Creseis acicula* is a warm water cosmopolitan species with a geographical range between 45°N to 40°S. The vertical range of this species is <750 m (Bonnevie, 1913) in water ranging between 10.0°C–27.9°C (van der Spoel, 1967).

***Creseis chierchiae* (Boas, 1886)**

Plate 2, Figure 1a–b.

Creseis chierchiae (Boas, 1886) – Rampal, 1975: p. 12, fig. 2.
Cleodora chierchiae Boas, 1886: p. 62, 202, pl. 3, fig. 39.

Diagnosis: *Creseis chierchiae* has an elongate conical shell, with a circular cross section, which gradually inflates towards the circular aperture. The shell

has no ornamentation and the protoconch is well defined and elongate with a rounded tip.

Remarks: Only the protoconch of this species was found. The protoconch of *C. chierchiae* is similar to that of *C. virgula constricta,* but is shorter and slightly more inflated. Some authors regard *C. chierchiae* to be the same species as *C. virgula constricta* (Janssen, 2012), but it was found in this study to have a distinctly different protoconch.

Distribution: This species has a circum-global tropical to subtropical distribution. Vertical and temperature ranges are not known.

GENUS ***Clio*** Linnaeus, 1767

Type species: *Clio pyramidata* Linnaeus, 1767.

Diagnosis: The genus *Clio* is characterised by an adult shell that is triangular or quasi-triangular in cross section.

***Clio pyramidata* Linnaeus, 1767**

Plate 2, Figure 6a–b.

Clio pyramidata Linnaeus, 1767: p. 1094.
Hyalæa pyramidata (Linnaeus, 1767) – Cantraine, 1841: p. 30, pl. 1, fig. 7, 7a.
Euclio pyramidata (Linnaeus, 1767) – Menzies, 1958: p. 383, fig. 1a–c.
Cleodora lanceolata (Lesueur, 1813) – delle Chiaje, 1830: pl. 83, figs 7–8.
Hyalaea lanceolata (Lesueur, 1813), 1813: p. 284, pl. 5, fig. 3A–B.
Clio pyramidata (Linnaeus, 1767) – Bé & Gilmer, 1977: p. 804, pl. 7, fig. 21a–c.

Diagnosis: *Clio pyramidata* has a large shell, which is triangular in cross section with a wide aperture. Longitudinally, the shell is kite-shaped with a straight posterior end and three longitudinal ridges on the dorsal side. The protoconch is conical with a sharp pointed end.

Remarks: Juveniles of this species can be identified by the conical, pointed protoconch, which is similar but larger than that of *S. subula*. *Clio pyramidata* has a wide range of morphologies, which have been considered subspecies or separate species by different authors (see van der Spoel, 1967; Bé and Gilmer, 1977). Only juvenile forms were found during this study and thus, different forms could not be distinguished.

Distribution: The geographical range of *C. pyramidata* extends to the northern and southern subtropical provinces, between 65°N and 45°S (Bé and Gilmer, 1977). The vertical range of this species is <1500 m in water of 7.0°C–27.7°C in temperature (Chen & Bé, 1964; van der Spoel, 1967).

***Clio convexa* (Boas, 1886)**

Plate 2, Figure 7.

Cleodora pyramidata var. convexa Boas, 1886: pp. 73, 203.
Clio convexa (Boas, 1886): pp. 73, 203.
Clio convexa (Boas, 1886) – Bé & Gilmer, 1977: p. 804, pl. 7, fig. 20a–e.

Diagnosis: *Clio convexa* has a large elongate shell with a triangular cross section and large aperture. The shell is slightly curved dorsally, with visible

transverse growth lines. The protoconch is large, thimble shaped and slightly flattened, with a blunt end.

Remarks: Only the protoconch was found during this study. It is similar in shape to that of *Clio pyramidata* but can be identified by its larger size and blunt end. This is considered a subspecies of *C. pyramidata* by van der Spoel (1967), but here follows the description by Bé and Gilmer (1977), who consider it to be a separate species.

Distribution: Bé and Gilmer (1977) found this species to be restricted to the tropical waters of the southern Indo-Pacific Ocean. It was also found to be present in the Caribbean Sea during this study.

Clio cuspidata **(Bosc, 1802)**

Plate 2, Figure 8.

Hyalœa cuspidata Bosc, 1802: p. 241, pl. 9, figs 5–7.
Cleodora cuspidata (Bosc, 1802) – delle Chiaje, 1830: pl. 83, figs 9–11.
Clio cuspidata (Bosc, 1802) – van der Spoel, 1967, p. 73, figs 64–67.
Cleodora lessonii Rang & Férussac, 1829: p. 261.
Euclio cuspidata (Bosc) – Menzies, 1958: p. 383, fig. 2a–b.
Clio cuspidata (Bosc, 1802) – Bé & Gilmer, 1977: p. 802, pl. 5, fig. 15a–d.

Diagnosis: This species has a large shell that is oval to triangular in cross section with a wide aperture. The adult shell has a distinct dorsal ridge and long lateral ribs ending in protruding spines. The posterior end is curved dorsally, with a bulbous, tear-drop shaped protoconch that has a sharp pointed end.

Remarks: This species is clearly identified by the large, bulbous, sharply pointed protoconch. Only juvenile forms were found during this study.

Distribution: *Clio cuspidata* is a warm water cosmopolitan species with a geographical range between 50°N and 50°S (Bé and Gilmer, 1977). The vertical range of *C. cuspidata* is between 50–1500 m (Bonnevie, 1913). The temperature range of this species is not known.

SUBFAMILY **Cavoliniinae**

GENUS ***Diacria*** Gray, 1842

Type species: *Diacria trispinosa* (Lesueur, 1821).

Diagnosis: Shells of the genus *Diacria* are characterised by an uncoiled, inflated shell with a thickened apertural margin.

Diacria trispinosa (Lesueur, 1821)

Plate 2, Figure 12.

Hyalæa trispinosa Lesueur, 1821 – de Blainville, 1821: p. 82.
Diacria trispinosa Lesueur, 1821 – Menzies, 1958: p. 391, fig. 1d.
Hyalea tricuspidata Lesueur – Deshayes, 1853: p. 61, pl. 103, figs 2–3.
Cavolinia trispinosa (de Blainville, 1821)– Oberwimmer, 1898: p. 590.
Cleodora infundibulum Wood, 1842: p. 459, pl. 5, fig. 13.
Hyalaea aculeata d'Orbigny, 1846: pp. 687, 691, pl. 7, figs 1–5; pl. 20, figs 1–2.
Cleodora compressa Souleyet, 1851: p. 32.
Hyalaea trispinosa var. minor Boas, 1886: pp. 95, 210.
Diacria trispinosa f. atlantica Dupont, 1979: pp. 42–44, figs 4, 6–7, 9.
Diacria rampali (Dupont, 1979) – Rampal, 2002: p. 247, figs 20D–L, 23D.
Diacria trispinosa (de Blainville, 1821) – Bé & Gilmer, 1977: p. 804, pl. 7, fig. 23a–d.

Diagnosis: *Diacria trispinosa* has a large shell that is longitudinally circular (flattened dorso-ventrally), with two lateral spines projecting perpendicular to the aperture and a long tapering flattened posterior, ending in a spherical or flattened circular protoconch. The aperture is wide and flat with a thickened margin and overhanging lip. The dorsal side has three lateral ribs.

Remarks: Often the protoconch and a section of the posterior is all that is found. The juvenile stage is very similar to that of *Diacria quadridentata,* which is also elongate and flattened, but the protoconch of *D. trispinosa* is more circular.

Distribution: This is a warm water cosmopolitan species, with a geographical range of 65°N–45°S (Bé and Gilmer, 1977). The vertical range of *D. trispinosa* is 30 – 190 m in water of 9.1°C–28.0°C in temperature (Williams, 1972).

Diacria quadridentata **(Lesueur, 1821)**

Plate 2, Figure 11a–c.

Hyalaea quadridentata (Lesueur, 1821) – de Blainville, 1821: p. 81.
Diacria quadridentata (Lesueur, 1821) – Herman, 1971: pp. 617, 619.
Hyalaea minuta Sowerby, 1877: pl. 2, fig. 9.
Hyalaea intermedia Sowerby, 1877: pl. 2, fig. 10.
Cleodora pygmaea Boas, 1886: pp. 84, 204–205, pl. 4, figs 50, 57a–c; pl. 5, fig. 90.
Diacria danae Leyen & van der Spoel, 1982: pp. 109–117.
Diacria quadridentata (de Blainville, 1821) – Bé & Gilmer, 1977: p. 804, pl. 7, fig. 24a–e.

Diagnosis: The shell of *D. quadridentata* is inflated and biconvex without lateral spines giving a tulip-shaped side-on profile. The aperture is large and overhanging, with a thickened margin and the posterior is blunt ending. The shell surface is covered in fine transverse ridges. The juvenile shell is elongate and flattened with a small, diamond shaped protoconch, which is discarded in the adult form.

Remarks: *Diacria quadridentata* is a small species within the Cavoliniinae. The shell appears thick and robust, often with a creamy yellow colouration. The majority of specimens found were juvenile stages.

Distribution: This is a warm water cosmopolitan species, with a geographical range of between 45°N to 35°S (Bé and Gilmer, 1977), although higher abundances are found in equatorial waters. The vertical range of *D. quadridentata* is <700 m in water of 19.0°C–25.5°C (Wlliams, 1972).

GENUS ***Diacavolinia*** van der Spoel, 1987

Type species: *Diacavolinia longirostris* (de Blainville, 1821).

Diagnosis: The genus *Diacavolinia* is characterised by inflated shells with a thimble shaped protoconch and a non-thickened apertural margin.

***Diacavolinia longirostris* (de Blainville, 1821)**

Plate 3, Figure 3 a–b.

Hyalæa longirostris Lesueur, 1821 – de Blainville, 1821: p. 81.
Cavolina longirostris (Lesueur, 1821) – Herman, 1971: pp. 614, 618.

Diacavolinia longirostris (de Blainville, 1821) – van der Spoel *et al.,* 1993: p. 132, fig. 3a–b; pl. 1 figs 1–4.
Hyalaea femorata Gould, 1852: pp. 487–488.
Hyalaea obtusa Sowerby, 1877: pl. 2, fig. 8a–b.
Cavolina couthouyi Dall, 1908: p. 501.
Cavolina longirostris (de Blainville, 1821) – Bé & Gilmer, 1977: p. 805, pl. 8, fig. 25a–d.

Diagnosis: *Diacavolinia longirostris* has a large, inflated and biconvex (more convex on ventral side) shell, with an almost spherical tulip-shaped side-on profile. The ventral side is rounded, half-sphere shaped, giving a circular front-on profile. The aperture is large and wide with a furrowed lip protruding, horn-like, on the dorsal side over the aperture. The protoconch is absent, leaving a blunt ending posterior with two projections either side of it. The shell surface is covered in fine transverse ridges.

Remarks: Only adult specimens were found in this study. Adult shells are clearly identified by the large, protruding, horn-like apertural lip.

Distribution: This is a warm water cosmopolitan species, whose geographical range extends from 50°N to 40°S. The vertical range of this species is not well defined, but may be up to 2000 m (Bé and Gilmer, 1977). The temperature range is from 17.4°C–27.8°C (van der Spoel, 1967).

GENUS ***Cavolinia*** Abildgaard, 1791

Type species: *Cavolinia tridentata* (Forskål, 1775).

Diagnosis: The genus *Cavolinia* is characterised by inflated shells with a thimble shaped protoconch and a non-thickened apertural margin.

Cavolinia inflexa (Lesueur, 1813)

Plate 2, Figure 10a–c.

Hyalæa inflexa Lesueur, 1813: p. 285, pl. 5, fig. 4A–D.
Cavolinia inflexa (Lesueur, 1813) – van Straaten, 1966: p. 431.
Pleuropus pellucidus Eschscholtz, 1825: p. 735, pl. 5, fig. 2.
Hyalaea depressa (d'Orbigny, 1834): p.110, pl. 7, figs 11–14.
Hyalea vaginellina Cantraine, 1835: p. 380.
Hyalaea uncinata Philippi, 1836: p. 101, pl. 6, fig. 18.
Cleodora curvata Souleyet, 1851: p. 32.
Cleodora pleuropus Rang, 1852 – Rang & Souleyet, 1852: pp. 48–49, pl. 10, fig. 8.
Hyalea inflexa f. imitans Pfeffer, 1880: p. 90, pl. 7, fig. 9a.
Hyalaea inflexa var. longa Boas, 1886: pp. 123–126, 212–213.
Cavolinia inflexa (Lesueur, 1813) – Bé & Gilmer, 1977: p. 805, pl. 8, fig. 27a–g.

Diagnosis: This species has a slightly inflated shell, biconvex (more convex on ventral side) and drawn out, giving a whale-like profile. The aperture is large with a straight dorsal apertural lip and a straight apertural margin. Two lateral spines protrude perpendicular to the aperture where the shell is at its widest, half way down. The posterior is long and tapering, curving dorsally and ending in a flattened, round ended protoconch. Some transverse striations (possible growth lines) are visible on the shell surface. Transverse striations on the protoconch are visible with the use of SEM.

Remarks: This species is easily identified in both the adult and juvenile form by the broad, elongate profile, which is particular to this species.

Distribution: The geographical range of *C. inflexa* extends to the northern and southern subtropical provinces, between 50°N and 40°S. The vertical range of this species is <250 m (Bonnevie, 1913) and the temperature range is between 16.0°C–28.0°C (Chen and Bé, 1964).

SUBORDER **Pseudothecosomata** Meisenheimer, 1905

FAMILY **Peraclididae** Tesch, 1913

GENUS ***Peracle*** Forbes, 1844

Type species: *Peracle reticulata* (d'Orbigny, 1834).

Diagnosis: Species of the genus *Peracle* have sinistrally coiling shells of various spire height.

***Peracle diversa* (Monterosato, 1875)**

Plate 1, Figure 9a–b.

Peracle diversa Monterosato, 1875: p. 50.
Peracle apicifulva Meisenheimer, 1906: p. 122, pl. 5, fig. 9a–d.
Peraclis brevispira Pelseneer, 1906: p. 146, pl. 12, figs 45–51.
Peraclis apicifulva Meisenheimer, 1906 – van der Spoel, 1976: p. 170, fig. 11a–c.

Diagnosis: This species has a large, high spired shell formed of three whorls in the adult shell with a honey-comb surface ornamentation on the second whorl only. Sutures bear small transverse ridges giving a stitched appearance. The aperture is large and eye-shaped.

Remarks: The shell of *P. diversa* is very similar to *P. reticulata,* with similar ornamentation, but only on the second whorl.

Distribution: This species is found in tropical, subtropical and temperate waters.

***Peracle moluccensis* (Tesch, 1903)**

Plate 1, Figure 8a–c.

Peracle moluccensis Tesch, 1903: p. 112.

Peracle moluccensis (Tesch, 1903) – van der Spoel, 1976: p. 170–171, fig. 12a–d.

Diagnosis: The shell of *P. moluccensis* is highly spired but almost flattened on the apical side. The shell is made up of three whorls that expand rapidly, ending in a broad eye-shaped aperture that has spines on the apical and umbilical aperture margins. Sutures bear small transverse ridges giving a stitched appearance and the apical apertural margin has some surface transverse striation.

Remarks: Juvenile shells of *P. moluccensis* can be distinguished from *L. inflata* by the stitch-like sutures and flattened spire. The apex is also not depressed as in *L. inflata.*

Distribution: This species is found in tropical, subtropical and temperate waters.

FAMILY **Cymbuliidae** Gray, 1840

GENUS ***Gleba*** Forskål, 1776

Type species: *Gleba cordata* Forskål, 1776.

Diagnosis: Shells of the genus *Gleba* are small and fragile with no ornamentation.

Gleba cordata Forskål, 1776

Plate 6, Figure 6a–b.

Gleba cordata Forskål, 1776: p. 14, pl. 43, fig. D.
Gleba chrysosticta – Corselli & Grecchi, 1990: p. 94.
Gleba cordata Forskål, 1776 – Janssen, 2012: p. 91, fig. 52A–G.

Diagnosis: *Gleba cordata* is a shell-less form with a calcified protoconch. The protoconch is small, fragile and thumb shaped, and is followed by a maximum of one whorl. The whorl is circular in cross section and loosely trochospiral to planispiral. There is no surface ornamentation.

Remarks: This larval shell is similar to *Firoloida desmarestia,* but can be distinguished by the extremely loose whorl, which does not touch the protoconch.

Distribution: *Gleba cordata* is a circum-global warm water species and has been identified from all sites in this study, the Caribbean Sea, Mediterranean Sea and Indian Ocean.

ORDER **Gymnosomata** de Blainville, 1824

FAMILY **Clionidae** Rafinesque, 1815

GENUS ***Paedoclione*** Danforth, 1907

Type species: *Paedoclione doliiformis* Danforth, 1907.

Diagnosis: Shells of the genus *Paedoclione* are small, fragile and thimble shaped.

***Paedoclione doliiformis* Danforth, 1907**

Plate 6, Figure 8.

Paedoclione doliiformis Danforth, 1907: pp. 2–18, pls. 1–4, fig. A–B.

Paedoclione doliiformis Danforth, 1907 – Lalli & Conover, 1976: figs 2–3.

Diagnosis: Only the discarded aragonite protoconch of *P. doliiformis* is found in sediments. The protoconch is small, thin, fragile and thimble shaped with an elongated and often transversely striated apertural margin.

Remarks: This is the only easily distinguishable gymnosome protoconch found during this study.

Distribution: This species has been identified in the North Atlantic, but almost certainly has a wider distribution. It was found in sediments at all sites in this study, the Caribbean Sea, Mediterranean Sea and Indian Ocean.

Gymnosome veliger

Plate 6, Figure 7.

Diagnosis: Gymnosome veligers were found in a variety of forms. All are calcified, small and fragile. They are often tear-drop shaped with one turn to the spire, or simply sac-shaped. There is no ornamenation.

Distribution: Global distribution.

5.2 HETEROPOD TAXONOMY

Information on synonymised taxa for heteropods was found in Rosenberg (2009), Janssen (2012) and CLEMAM (2012).

Heteropod species	Caribbean Sea	Mediterranean Sea	Indian Ocean
Atlanta brunnea	**O**	**-**	**O**
Atlanta californiensis	**O**	**-**	**O**
Atlanta frontieri	**-**	**-**	**O**
Atlanta gaudichaudi	**O**	**-**	**O**
Atlanta helicinoidea	**O**	**O**	**O**
Atlanta inclinata	**O**	**-**	**O**
Atlanta peronii	**O**	**O**	**O**
Atlanta rosea	**O**	**O**	**O**
Atlanta selvagensis	**O**	**O**	**O**
Atlanta turriculata	**O**	**-**	**O**
Atlanta sp. D	**O**	**-**	**-**
Carinaria lamarckii	**O**	**O**	**O**
Carinaria pseudorugosa	**O**	**-**	**O**
Firoloida desmarestia	**O**	**O**	**O**
Oxygyrus keraudreni	**O**	**O**	**O**

Table 5.2 Species of shelled heteropod present at each studied location. Present **O**; Absent **–.**

PHYLUM **Mollusca**

CLASS **Gastrapoda**

SUBCLASS **Caenogastropoda**

ORDER **Littorinimorpha** Golikov & Starobogatov, 1975

FAMILY **Atlantidae** Rang, 1829

Diagnosis: All juvenile Atlantidae are characterised by a slit in the middle of the shell aperture.

GENUS ***Atlanta*** Lesueur, 1817

Type species: *Atlanta peronii* Lesueur, 1817.

Diagnosis: Species of the genus *Atlanta* are characterised by dextral coiling.

***Atlanta peronii* Lesueur, 1817**

Plate 4, Figure 8a–b ; Plate 5, Figure 4a–b.

Atlanta peronii Lesueur, 1817: p. 390, pl. 2, figs 1–2.
Steira lamanoni Eschscholtz, 1825: p. 735, fig. 3.
Atlanta costae Mandralisca, 1840: pp. 148–149, fig. 1.
Ladas planorboides Forbes, 1844: p. 186.
Atlanta steindachneri Oberwimmer, 1898: p. 587, figs 1–2.
Schizotrochus palaeomphaloides Nordsieck, 1973: p. 4, fig. 13.
Atlanta peronii Lesueur, 1817 – Seapy, 2011.

Diagnosis: The juvenile shell of *A. peronii* consists of up to three and a half whorls forming a low conical spire with well defined sutures between whorls. The whorls are smooth with no ornamentation. The juvenile shell forms the centre of the adult shell, which may have up to six gradually expanding whorls, with a keel in older specimens..

Remarks: The juvenile shell has deep sutures and is similar to that of *Atlanta gaudichaudi,* but can be identified by the smooth surface of the whorls. *Atlanta gaudichaudi* has longitudinal striations. The juvenile section of large adult specimens of *A. peronii* were found to have a brown colouration. No keeled specimens were found during this study.

Distribution: This species is a cosmopolitan in tropical to subtropical waters. The only known vertical range of 150–300 m is from Hawaiian waters (Seapy, 2011).

***Atlanta brunnea* Gray 1850**

Plate 4, Figure 8.

Atlanta brune – Eydoux & Souleyet, 1841: pl. 21, figs 15–29.
Atlanta brunnea Gray, 1850: p.101, pl. 242, fig 5a.
Atlanta fusca Souleyet, 1852: p. 389.
Atlanta brunnea Gray, 1850 – Seapy, 2011.

Diagnosis: The juvenile shell is small, opaque, creamy brown in colour and highly spired with four whorls. The protoconch is smooth and following whorls are patterned with numerous longitudinal striations. There is a prominent slit in the outer edge of apertural margin.

Remarks: Only the juvenile central part of the *A. brunnea* shell was found (Seapy, 2011). The juvenile form of *A. brunnea* is very similar to *Atlanta echinogyra,* but can be recognised by the much higher spire of the shell.

Distribution: This species is cosmopolitan in tropical and subtropical waters (Seapy, 2011).

Atlanta californiensis Seapy and Richter, 1993

Plate 4, Figure 10.

Atlanta californiensis Seapy and Richter, 1993: pp. 390–391, figs 1–2.
Atlanta californiensis Seapy and Richter, 1993 – Seapy, 2011.

Diagnosis: The juvenile shell is opaque white with no ornamentation. There are three and a quarter whorls to the low domed spire, which is oval shaped in side-on profile. Sutures between whorls are poorly defined, giving a smooth appearance.

Remarks: Only the juvenile central part of this species was found (Seapy, 2011). The juvenile of this species is similar to *Atlanta inclinata,* but can be defined by being generally smaller and lower spired.

Distribution: Seapy (2011) found this species to be limited to the transitional zone of the North Pacific Ocean. During this study it was identified in the Caribbean Sea and the Indian Ocean.

Atlanta frontieri Richter, 1993

Plate 4, Figure 3a–c.

Atlanta frontieri Richter, 1993: p. 192, pl. 1, fig. 3; pl. 2, fig. 7; pl.3, fig. 9; pl. 4, figs 18, 21.
Atlanta frontieri Richter, 1993 – Seapy, 2011.

Diagnosis: This is a larger species, with a very distinct shape. The first two whorls of the juvenile shell form a raised cap, whilst the third and fourth whorls are almost flat in profile. There is a ridge on the outer edge of the second to fourth whorls. The juvenile shell is formed of four and a half whorls. The adult shell has a tall, rounded keel.

Remarks: Some fine longitudinal striations were observed on the surface of juvenile shells. Juvenile shells are similar to juvenile *Atlanta selvagensis,* but can be distinguished by the higher spire in the first two whorls.

Distribution: This species has been recorded from the Indian Ocean and the North Pacific Ocean (Seapy, 2011).

Atlanta gaudichaudi Gray, 1850

Plate 4, Figure 6a–b; Plate 5, Figure 3a–b.

Atlanta gaudichaudi Gray, 1850: p. 101, pl. 241, fig. 4.
Atlanta gaudichaudii Souleyet, 1852: pp. 379–380.
Atlanta gaudichaudi Gray, 1850 – Seapy, 2011.

Diagnosis: The juvenile shell of *A. gaudichaudi* is low, conical and formed of three and a half whorls with well defined whorl sutures. The whorls are largely smooth with some ornamentation in the form of longitudinal ridges. The adult form has rapidly inflating, smooth whorls with no ornamentation and a keel.

Remarks: The shells are similar to *Atlanta peronii,* but juvenile *A. gaudichaudi* have longitudinal striations, whereas juvenile *A. peronii* have smooth whorls.

Distribution: This species has a cosmopolitan distribution (Seapy, 2011).

***Atlanta helicinoidea* Gray, 1850**

Plate 4, Figure 1a–b; Plate 5, Figure 1a–b.

Atlanta helicinoide (Eydoux & Souleyet, 1841): pl. 20, figs 23–30.
Atlanta helicinoidea Gray, 1850: p. 101, pl. 242, fig. 4.
Atlanta depressa Souleyet, 1852: pp. 385–386.
Atlanta helicinoides Souleyet, 1852: p. 384.
Atlanta helicinoidea Gray, 1850 – Seapy, 2011.

Diagnosis: The juvenile shell of this species is often yellow-brown in colour with four and a half whorls to the low conical spire. The surface of the shell from the second whorl onwards is covered in longitudinal striae. In the adult shell, the juvenile form becomes the centre, being surrounded with one flattened, largely inflated, smooth surfaced and partially keeled whorl. There is a slit in the centre of the outer apertural margin.

Remarks: The juvenile shell is distinguished by the well defined and continuous longitudinal striations.

Distribution: This is a cosmopolitan species in tropical to subtropical waters, with a vertical distribution of <100 m (Seapy, 2011).

Atlanta inclinata Gray, 1850

Plate 4, Figure 12a–b; Plate 5, Figure 7a–d.

Atlanta inclinata Gray, 1850: p. 101, pl. 241, fig. 1.
Atlanta inclinata Souleyet, 1852: pp. 375–376.
Atlanta gibbosa Souleyet, 1852: pp. 386–387.
Atlanta affinis Tesch, 1906: p. 53, pl. 7, figs 9–10.
Atlanta macrocarinata Bonnevie, 1920: p. 5, pl. 1, fig. 10a–b.
Atlanta inclinata Gray, 1850 – Seapy, 2011.

Diagnosis: The juvenile shell is formed of a high conical spire made up of five whorls, which has a smooth, rounded appearance due to extremely shallow sutures between whorls. There is some surface ornamentation on the juvenile shell, often in the form of a single longitudinal striation. The juvenile shell also has a large open umbilicus and an angular aperture, with a defined slit in the outer apertural margin. The juvenile shell is set at an angle within the adult shell, which is large with a rounded keel.

Remarks: The juvenile form is similar to *A. californiensis,* but is easily identified by the higher spire, conical shape, smooth surface and large umbilicus. Specimens collected were usually lustrous and opaque white.

Distribution: This is a cosmopolitan species in tropical to subtropical waters (Seapy, 2011).

Atlanta rosea Gray, 1850

Plate 4, Figure 7; Plate 5, Figure 5a–d.

Atlanta rosea Gray, 1850: p. 101, pl. 241, fig. 2.
Atlanta rosea Souleyet, 1852: p. 377.
Atlanta rosea Gray, 1850 – Seapy, 2011.

Diagnosis: The shell of this species is distinguished by the low and domed spire of the juvenile stage, which appears smooth due to shallow sutures between the first two and a half whorls. The outer whorls and aperture are also slightly more angular. This is a moderately large shell.

Remarks: The juvenile shell morphology of *A. rosea* is similar to *A. peronii*, but can be distinguished by the rounded, smooth apical whorls. The shell is lustrous and white.

Distribution: This species has a circum-global distribution and is cosmopolitan in tropical to subtropical waters (Seapy, 2011).

Atlanta selvagensis de Vera and Seapy, 2006

Plate 4, Figure 2a–b; Plate 5, Figure 2a–b.

Atlanta quoyana Soul – Oberwimmer, 1898: p. 587.
Atlanta inflata Souleyet, 1852 – Richter, 1968: p. 351, figs 1–4.
Atlanta selvagensis de Vera and Seapy, 2006: p. 48, figs 2A–D, 3A–D.
Atlanta selvagensis de Vera and Seapy, 2006 – Seapy, 2011.

Diagnosis: This is a small species. The juvenile shell is translucent, white with around three and a half whorls to the low conical spire. Juvenile whorl ornamentation is highly variable and may consist of anything between no ornamentation and several longitudinal striations. In the adult shell, the juvenile spire becomes the centre of the shell and is surrounded by a single, flattened, highly inflated whorl with no surface ornamentation. A tall keel runs along the outer edge of the last whorl and there is a slit in the outer edge of the apertural margin.

Remarks: Juvenile forms of *A. selvagensis* have a similar morphology to *A. helicinoidea,* especially when the *A. selvagensis* specimen has transverse striations. The striations of *A. selvagensis* tend to be discontinuous and fine, where as those on *A. helicinoidea* are very prominent and continuous. *Atlanta helicinoidea* is also a much larger species.

Distribution: This species is found in tropical and subtropical regions of the Atlantic and Indian Oceans (Seapy, 2011).

***Atlanta turriculata* d'Orbigny, 1835**

Plate 4, Figure 5a–b; Plate 5, Figure 6a–b.

Atlanta turriculata d'Orbigny, 1835: pp. 173–174, pl. 20, figs 5–11.
Atlanta turriculata d'Orbigny, 1835 – Seapy, 2011.

Diagnosis: The juvenile shells of *A. turriculata* are turret-like and highly spired with around 4 whorls. A prominent spiral ridge runs around the middle of the

whorls from the second whorl onwards, with further longitudinal striation below this. The juvenile shell forms the central part of the adult shell, being tilted at a slight angle and surrounded by a flattened, highly inflated, smooth surfaced whorl with a keel running around the outer edge. The centre of the outer apertural margin has a small slit. The shell is some times pink to brown in colour but is more often opaque white.

Remarks: This species is very distinct, even in the juvenile form.

Distribution: Seapy (2011) found *A. turriculata* to be limited to the Pacific and Indian Oceans in tropical to subtropical waters. During this study, specimens were also found in the Caribbean Sea. The only known vertical range of *A. turriculata* is in Hawaiian waters at <200 m (Seapy, 2011).

***Atlanta* sp. D**

Plate 4, Figure 11a–b.

Diagnosis: Only what are assumed to be juvenile shells of *Atlanta* sp. D were found. They are large, highly spired, conical shells, with up to four whorls. The whorls are flat topped at the sutures, giving a step shape in side-on profile. The umbilicus is large and open.

Remarks: This species is similar in form to *A. inclinata* but has flat topped whorls. Thirteen specimens were collected from the 150–500 µm fraction and six from the >500 µm fraction of CAR-MON 2. The most recent specimen was found at 40 cm core depth, which equates to around 17 kyr.

Distribution: *Atlanta* sp. D was only found in the Caribbean Sea during this study. This species appears to have a preference for warm climates, all specimens except three (150–500 µm: 570 and 575 cm; >500 µm: 60 cm) were found during interglacial periods.

GENUS ***Oxygyrus*** Benson, 1835

Type species: *Oxygyrus keraudrenii* (Lesueur, 1817).

Diagnosis: Shells of the genus *Oxygyrus* are almost spherical in overall shape with longitudinal striations.

***Oxygyrus keraudrenii* (Lesueur, 1817)**

Plate 4, Figure 4a–c.

Oxygyrus keraudrenii (Lesueur, 1817): p. 391 (= *A. peronii*, Janssen, 2012)
Ladas keraudrenii (Lesueur, 1817) – Cantraine, 1841: p. 38, pl. 1, figs 2a–b.
Oxygyrus inflatus Benson, 1835: p. 176.
Helicophlegma candei d'Orbigny, 1841: p. 100–101, pl. 2, figs 15–17.
Oxygyrus rangii Gray, 1850: p. 101, pl. 240, figs 1, 4.
Oxygyrus keraudrenii (Lesueur, 1817) – Seapy, 2011.

Diagnosis: The juvenile shell of *O. keraudrenii* is trochospiral, gradually becoming planispiral in the adult form. The juvenile shell is covered in longitudinal striae radiating from the spire and has a white or rusty brown colouration. The adult shell has a large notch in the middle of the aperture edge.

Remarks: This species is very distinct and generally spherical in shape.

Distribution: Present in all oceans (Tesch, 1949).

FAMILY **Carinariidae** de Blainville, 1818

GENUS ***Carinaria*** Lamarck, 1801

Type species: *Carinaria cristata* (Linnaeus, 1767).

Diagnosis: Shells of the genus *Carinaria* are characterised by dextrally trochospiral coiling shells that end in a wide conical aperture.

Carinaria lamarckii de Blainville, 1817

Plate 6, Figure 1a–b.

Carinaria lamarck Péron & Lesueur, 1810: p. 69, pl. 2, fig. 15.
Carinaria lamarckii de Blainville, 1817: p. 107.
Pterotrachea lophyra delle Chiaje, 1822: pls 14–15.
Carinaria mediterranea de Blainville, 1824: p. 283.
Carinaria punctata d'Orbigny, 1834: pp. 160–161, pl. 11, figs 6–15.
Carinaria atlantica Adams & Reeve, 1850: p. 63, pl. 13, fig. 12.
Tubiola vatovai Nordsieck, 1973: p. 4, fig. 5.
Carinaria lamarckii de Blainville, 1817 – Seapy, 2011.

Diagnosis: Only the apical part of the *C. lamarckii* larval shell was found during this study. The shell is flattened on the apical side and coils dextrally with around three turns to the spire. The whorls are largely smooth, with two longitudinal ridges on the second whorl. The umbilicus is closed, with some transverse pleats.

Remarks: Specimens are often found to be chalky and are perhaps slightly more susceptible to dissolution.

Distribution: This species is common in the Atlantic and Indian oceans and in the Caribbean and Mediterranean seas, with a vertical range of 50–400 m (Tesch, 1949; Seapy, 2011).

***Carinaria pseudorugosa* Vayssière, 1904**

Plate 6, Figure 4a–b.

Carinaria pseudorugosa Vayssière, 1904
Carinaria challengeri Bonnevie, 1920: pp. 6–7, pl. 2, figs 16–21.
Carinaria challengeri Bonnevie, 1920 – Seapy, 2011.

Diagnosis: This species is regarded as being shell-less, however, a small veliger shell is produced. The shell is extremely fragile, consisting of a small spherical protoconch which develops in half a whorl into a highly expanded aperture. There is fine dimpled shell ornamentation on the protoconch only.

Remarks: The larval shell of this species has a similar morphology to *Firoloida desmarestia,* but can be identified by the largely inflated aperture and very thin fragile shell walls.

Distribution: This species has been recorded from the North Atlantic and is thought to be limited to the upper 200 m (Seapy, 2011).

FAMILY **Pterotracheidae** Rafinesque, 1814

GENUS ***Firoloida*** Lesueur, 1817

Type species: *Firoloida desmarestia* Lesueur, 1817.

Diagnosis: Shells of the genus *Firoloida* are characterised by dextrally trochospiral coiling and no surface ornamentation.

Firoloida desmarestia **Lesueur, 1817**

Plate 6, Figure 5a–c.

Firoloida desmarestia Lesueur, 1817: p. 39, pl. 2, fig. 1a–b.
Firoloida aculeata Lesueur, 1817b: p. 40, pl. 2, fig. 3.
Firoloida blainvilliana (Lesueur, 1817b): pp. 39–40, pl. 2, fig. 2a–b.
Firola gaimardii d'Orbigny, 1834: pp. 153–154, pl. 10, figs 13–14.
Firola lesueurii d'Orbigny, 1834: pp. 151–153, pl. 10, figs 11–12.
Firoloida eydouxii Gray, 1850: p. 100, pl. 238, fig. 3.
Firoloida lesueurii Eydoux & Souleyet – Vérany, 1853: p. 381.
Cyclostrema solutum Di Geronimo, 1974: p. 148, pl. 1, figs 2–6.
Firoloida desmarestia Lesueur, 1817 – Seapy, 2011.

Diagnosis: The juvenile stage of this shell is composed of a small spherical protoconch, with some dimpled ornamentation (only visible with SEM). The shell coils dextrally in a trochospiral shape, with up to two whorls ending in a circular aperture. The diameter of the whorls rapidly expands and the whorls have no ornamentation.

Remarks: The larval stage of this species is similar to both *C. pseudorugosa* and *G. cordata*. It can be distinguished by the circular aperture and high spire.

Distribution: This species has been found in the North Atlantic and the Pacific Oceans. In this study it was found at all locations, in the Caribbean Sea, Mediterranean Sea and Indian Ocean. The only known vertical distribution is from Hawaiian waters in the upper 160 m (Seapy, 2011).

PLATE 1. FAMILY LIMACINIDAE AND PERACLIDIDAE

All scale bars represent 100 µm, except where stated otherwise.

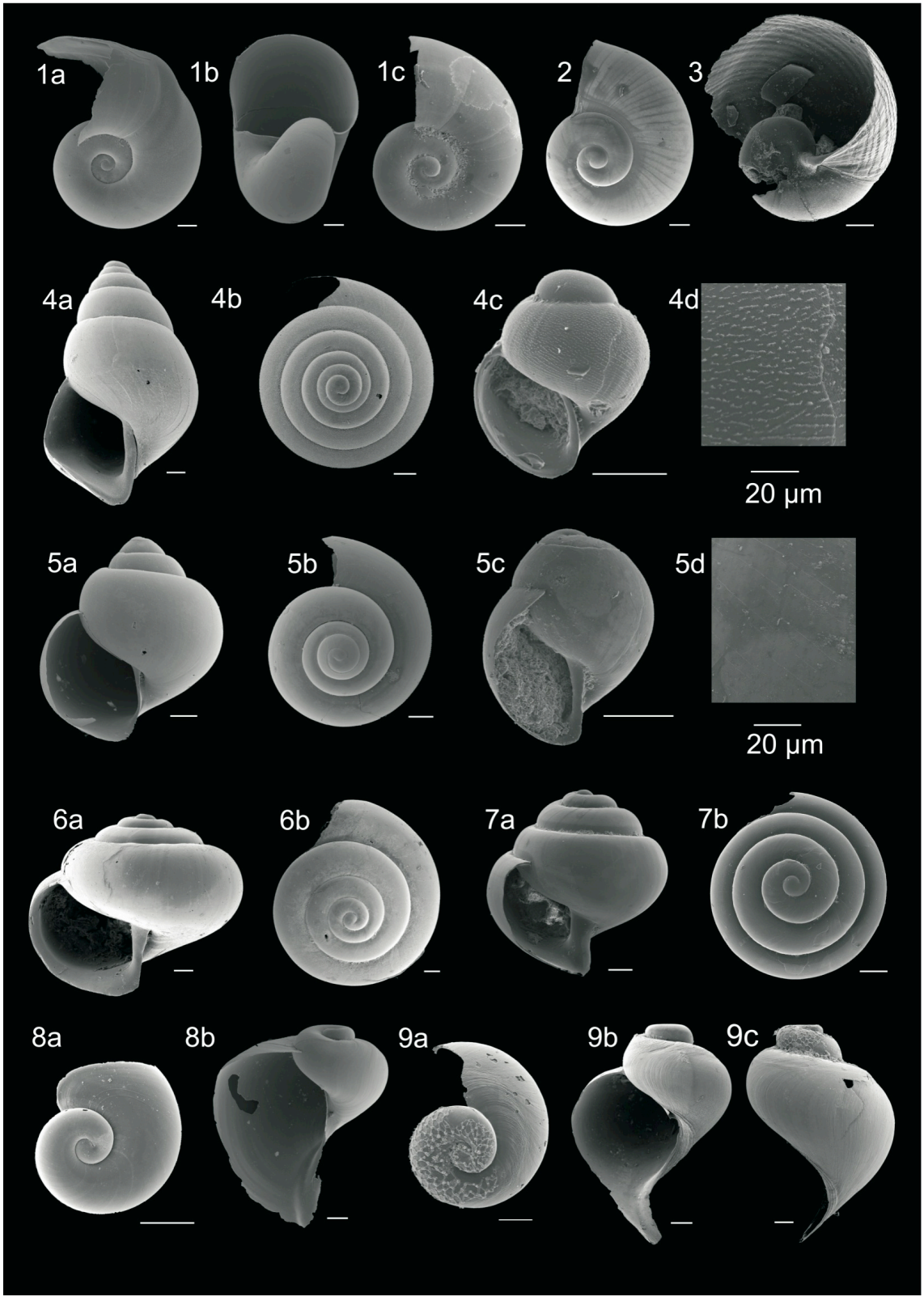

PLATE 1. FAMILY LIMACINIDAE AND PERACLIDIDAE

All scale bars represent 100 µm, except where stated otherwise.

LIMICINIDAE

1. *Limacina inflata* a) apical view (CAR-MON 2, 70 cm); b) aperture (CAR-MON 2, 70 cm); c) apical view (716B, 15 cm).

2. *Limacina* sp. C a) apical view (CAR-MON 2, 45 cm)

3. *Limacina* sp. B a) apical view (B5-1, 100 cm).

4. *Limacina bulimoides* a) apertural view (CAR-MON 2, 80 cm); b) apical view (CAR-MON 2, 70 cm); c) larval shell (B5-1, 20 cm); d) larval shell surface (B5-1, 20 cm).

5. *Limacina trochiformis* a) apertural view (CAR-MON 2, 70 cm); b) apical view (CAR-MON 2, 70 cm); c) larval shell (B5-1, 0 cm); d) larval shell surface (B5-1, 0 cm).

6. *Limacina lesueurii* a) apertural view (CAR-MON 2, 30 cm); b) apical view (CAR-MON 2, 30 cm).

7. *Limacina retroversa* a) apertural view (B5-1, 210 cm); b) apical view (B5-1, 210 cm).

PERACLIDIDAE

8. *Peracle moluccensis* a) larval shell (CAR-MON 2, 365 cm); c) apertural view (CAR-MON 2, 360 cm).

9. *Peracle diversa* a) apical view (CAR-MON 2, 350 cm); b) apertural view (CAR-MON 2, 70 cm); c) side view (CAR-MON 2, 75 cm).

PLATE 2. FAMILY CAVOLINIIDAE

All scale bars represent 100 μm, except where stated otherwise.

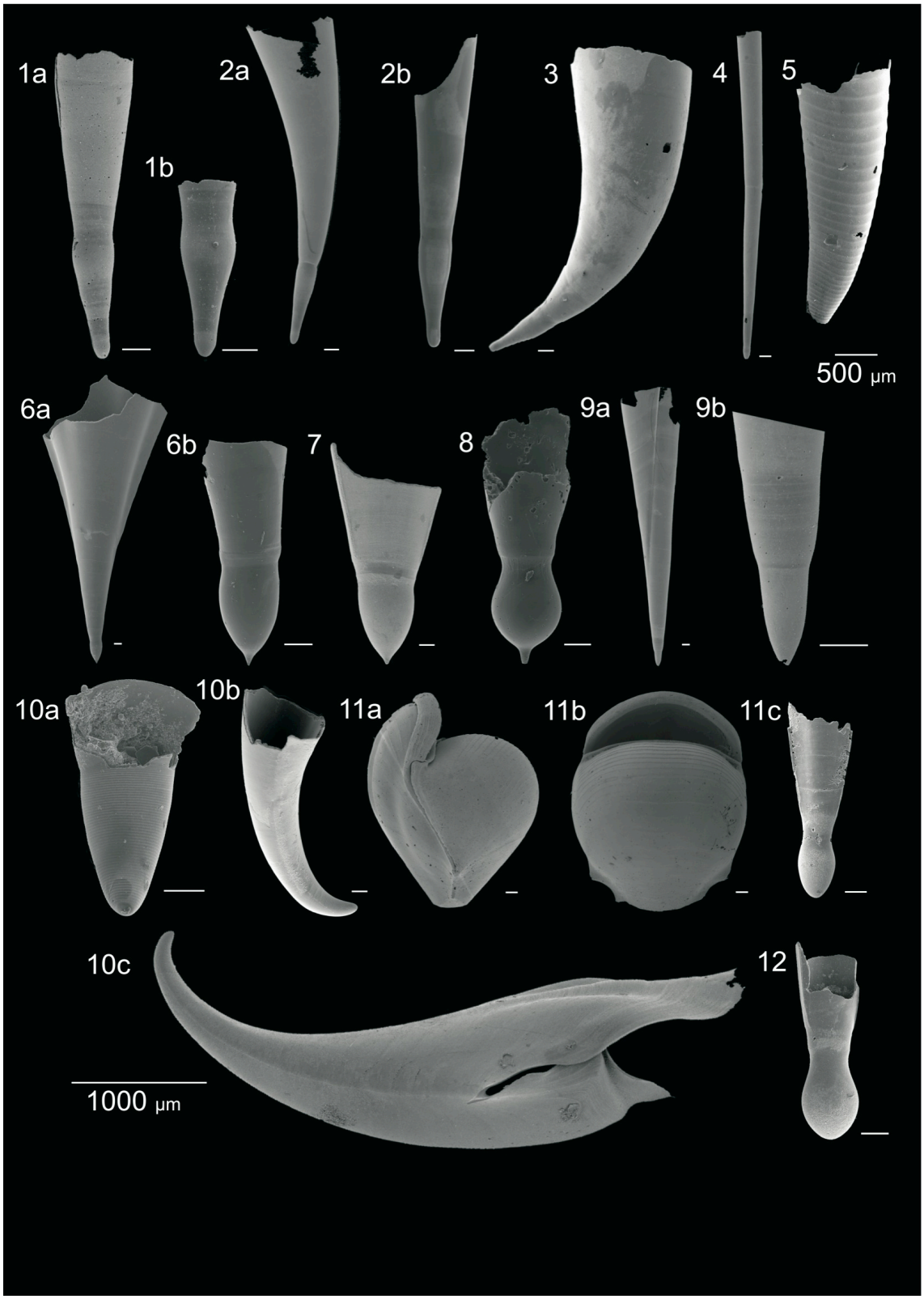

PLATE 2. FAMILY CAVOLINIIDAE

All scale bars represent 100 µm, except where stated otherwise.

1. ***Creseis chierchiae*** a) adult shell (716B, 15 cm); b) protoconch (716B, 15 cm).

2. ***Creseis virgula constricta*** a) adult shell (CAR-MON 2, 70 cm); b) protoconch B5-1, 20 cm).

3. ***Creseis virgula virgula*** adult shell (CAR-MON 2, 30 cm).

4. ***Creseis acicula*** adult shell (CAR-MON 2, 70 cm).

5. ***Hyalocylis striata*** (CAR-MON 2, 80 cm).

6. ***Clio pyramidata*** a) adult shell (CAR-MON 2, 80 cm); b) protoconch (B5-1, 90 cm).

7. ***Clio convexa*** protoconch (716B, 15 cm).

8. ***Clio cuspidata*** protoconch (B5-1, 20 cm).

9. ***Styliola subula*** a) adult shell (CAR-MON 2, 80 cm); protoconch (CAR-MON 2, 80 cm).

10. ***Cavolinia inflexa*** a) protoconch (B5-1, 20 cm); b) protoconch (CAR-MON 2, 80 cm); c) adult shell (CAR-MON 2, 80 cm).

11. ***Diacria quadridentata*** a) adult shell, side view (CAR-MON 2, 70 cm); b) apertural view (CAR-MON 2, 70 cm); c) protoconch (CAR-MON 2, 20 cm).

12. ***Diacria trispinosa*** protoconch (CAR-MON 2, 0 cm).

PLATE 3. FAMILY LIMACINIDAE AND CAVOLINIIDAE

PHOTOMICROSCOPE IMAGES

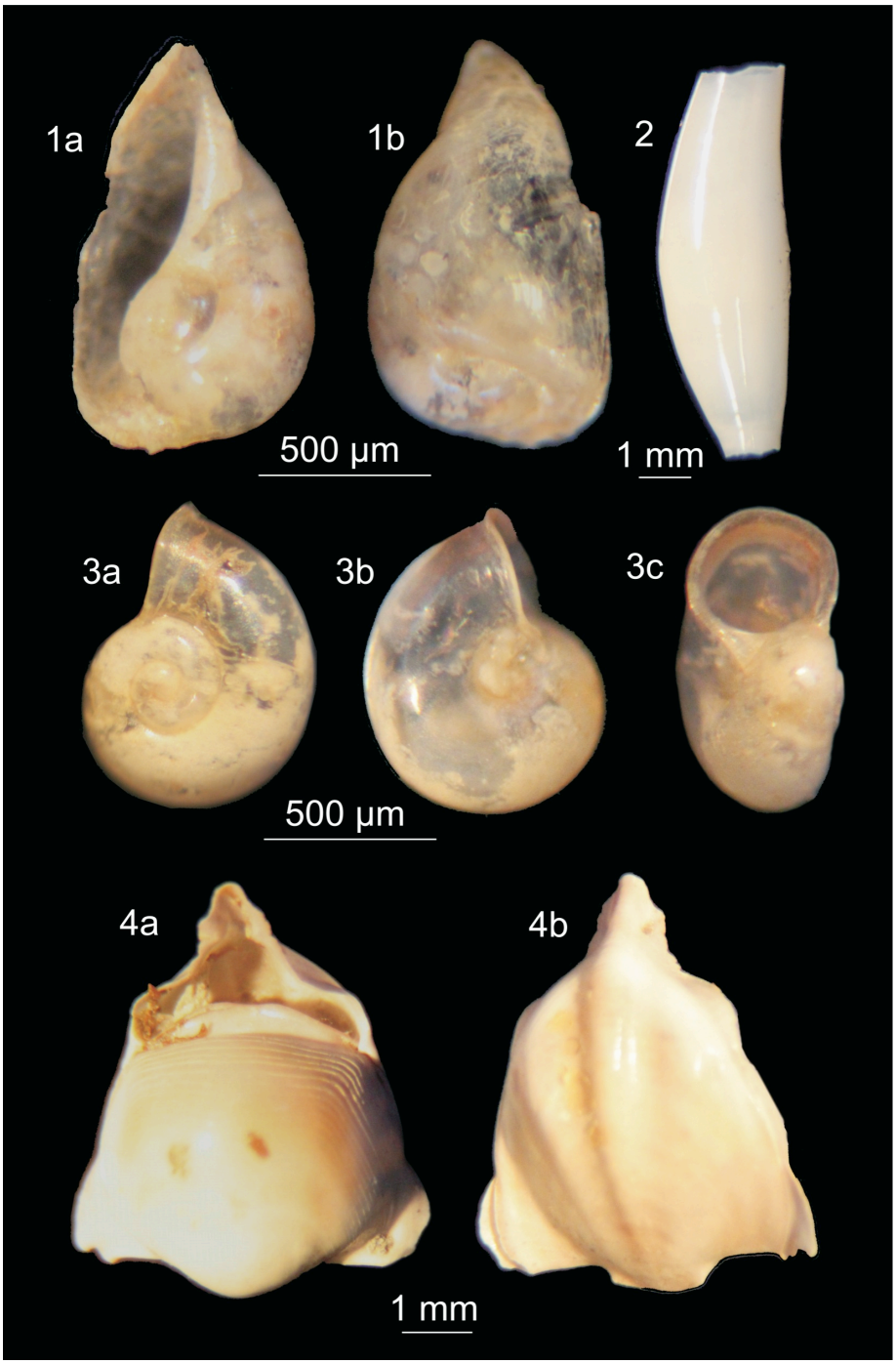

PLATE 3. FAMILY LIMACINIDAE AND CAVOLINIIDAE

PHOTOMICROSCOPE IMAGES

1. *Limacina* sp. D (CAR-MON 2, 45 cm): a) apical and apertural view; b) umbilical view.

2. *Cuvierina columnella* (CAR-MON 2, 310 cm) side view.

3. *Limacina* sp. C (CAR-MON 2, 50 cm): a) apical view; b) umbilical view; c) apertural view.

4. *Diacavolinia longirostris* (CAR-MON 2, 5 cm): a) ventral and apertural view; b) dorsal view.

PLATE 4. FAMILY ATLANTIDAE JUVENILE FORMS

All scale bars represent 100 µm.

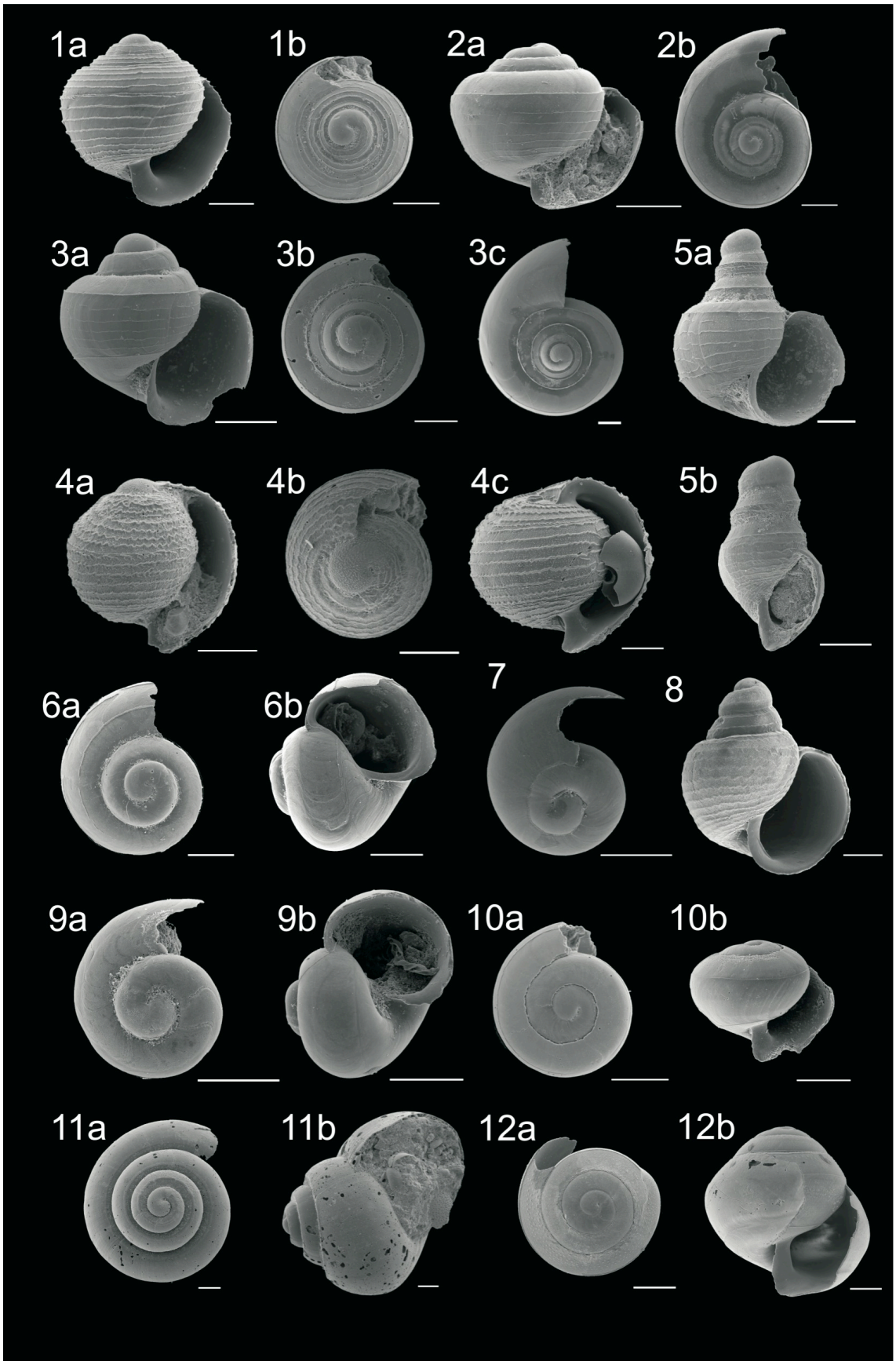

PLATE 4. FAMILY ATLANTIDAE JUVENILE FORMS

All scale bars represent 100 µm.

1. ***Atlanta helicinoidea*** a) apertural view (CAR-MON 2, 520 cm); b) apical view (716B, 855 cm).

2. ***Atlanta selvagensis*** a) apertural view (716B, 75 cm); b) apical view (B5-1, 290 cm).

3. ***Atlanta frontieri*** a) apertural view (716B, 855 cm); b) apical view (716B, 775 cm); c) apical view (716B, 475 cm).

4. ***Oxygyrus keraudreni*** a) apertural view (716B, 75 cm); b) apical view (716B, 75 cm); c) apertural view (CAR-MON 2, 90 cm).

5. ***Atlanta turriculata*** a) apertural view (716B, 75 cm); b) apertural view (716B, 75 cm).

6. ***Atlanta gaudichaudi*** a) apical view (716B, 75 cm); b) apertural view (716B, 75 cm).

7. ***Atlanta rosea*** apical view (B5-1, 150 cm).

8. ***Atlanta brunnea*** apertural view (CAR-MON 2, 350 cm).

9. ***Atlanta peronii*** a) apical view (CAR-MON 2, 90 cm); b) apertural view (B5-1, 20 cm).

10. ***Atlanta californiensis*** a) apical view (716B, 855 cm); b) apertural view (716B, 855 cm).

11. ***Atlanta*** **sp. D** a) apical view (CAR-MON, 2 80 cm); b) apertural view (CAR-MON 2, 40 cm).

12. ***Atlanta inclinata*** a) apical view (CAR-MON 2, 520 cm); b) apertural view (CAR-MON 2, 520 cm).

PLATE 5. FAMILY ATLANTIDAE ADULT FORMS

All scale bars represent 200 µm.

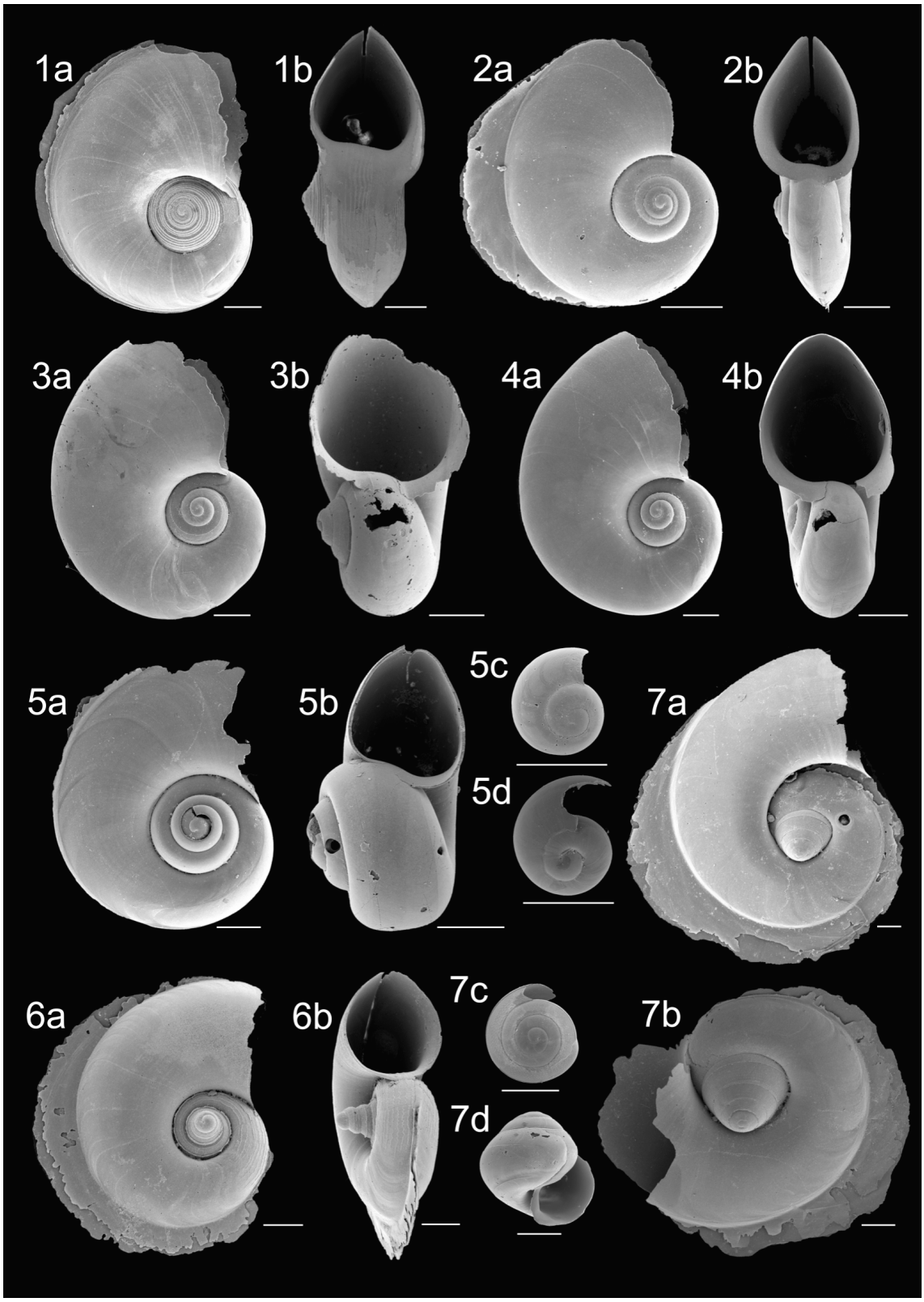

PLATE 5. FAMILY ATLANTIDAE ADULT FORMS

All scale bars represent 200 µm.

1. ***Atlanta helicinoidea*** a) apical view (CAR-MON 2, 75 cm); b) apertural view (CAR-MON 2, 75 cm).

2. ***Atlanta selvagensis*** a) apical view (CAR-MON 2, 75 cm); b) apertural view (CAR-MON 2, 75 cm).

3. ***Atlanta gaudichaudi*** a) apical view (CAR-MON 2, cm); b) apertural view (CAR-MON 2, cm).

4. ***Atlanta peronii*** a) apical view (CAR-MON 2, 75 cm); b) apertural view (CAR-MON 2, 75 cm).

5. ***Atlanta rosea*** a) apical view (CAR-MON 2, 70 cm); b) apertural view (CAR-MON 2, 75 cm); c) juvenile (B5-1, 150 cm); d) juvenile (B5-1, 150 cm).

6. ***Atlanta turriculata*** a) apical view (CAR-MON 2, 80 cm).

7. ***Atlanta inclinata*** a) large specimen apical view (CAR-MON 2, 80 cm); b) apical view (CAR-MON 2, 80 cm); c) juvenile apical view (CAR-MON 2, 520 cm); d) juvenile apertural view (CAR-MON 2, 520 cm).

PLATE 6. FAMILY CARINARIIDAE, CLIONIDAE AND CYMBULIIDAE

All scale bars represent 100 µm.

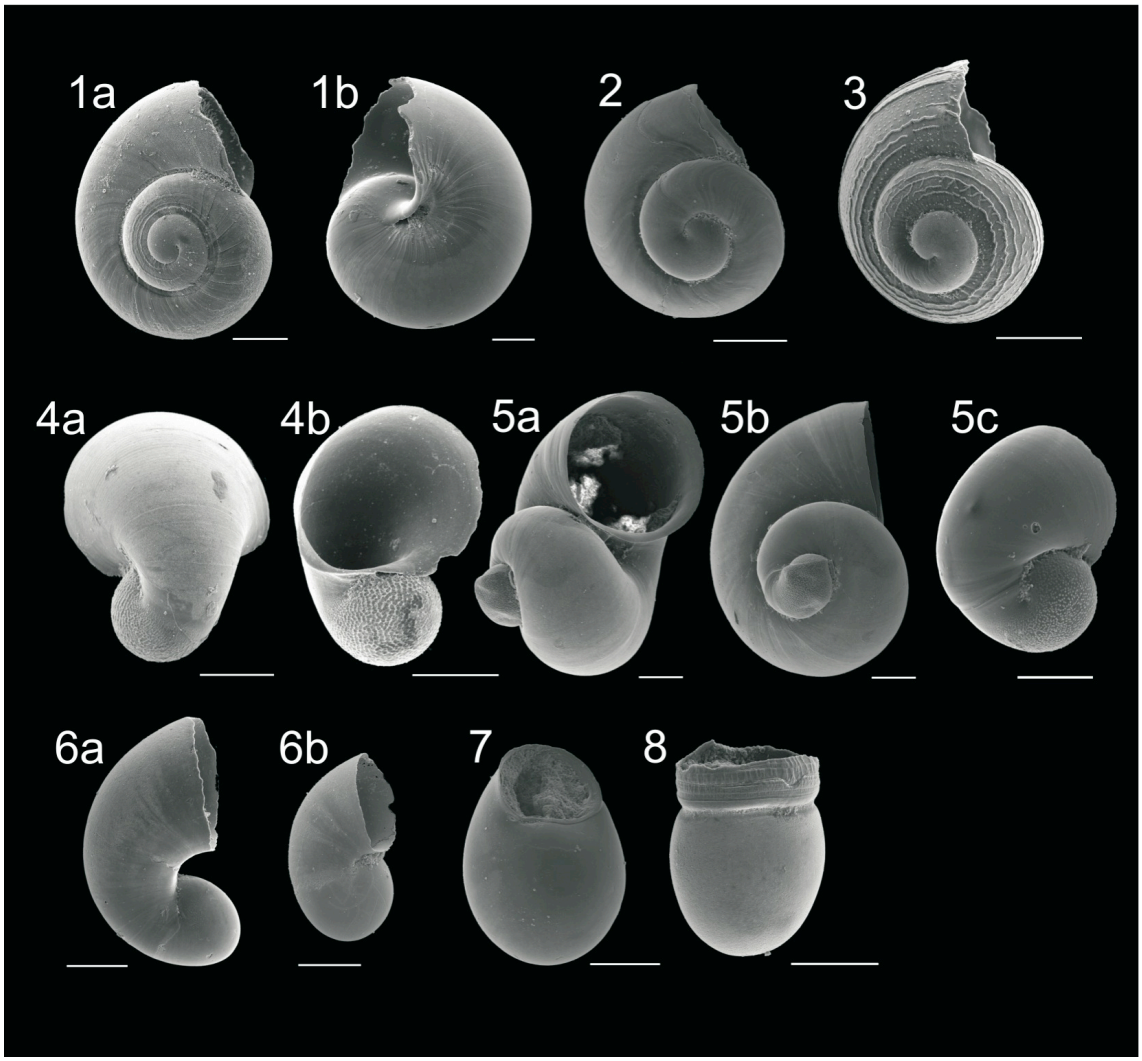

PLATE 6. FAMILY CARINARIIDAE, CLIONIDAE AND CYMBULIIDAE

All scale bars represent 100 µm.

CARINARIIDAE

1. *Carinaria lamarckii* a) larval shell apical view (B5-1, 370 cm); b) umbilical view (B5-1, 370 cm).

2. *Carinaria* sp. larval shell (B5-1, 310 cm).

3. *Carinaria* sp. (*galea?)* larval shell (B5-1, 50 cm).

4. *Carinaria pseudorugosa* a) apical view (B5-1, 20 cm); b) apertural view (B5-1, 20 cm).

5. *Firoloida desmarestia* a) adult shell apertural view (B5-1, 30 cm); b) apical view (B5-1, 30 cm); c) juvenile shell (B5-1, 10 cm).

CLIONIDAE

6. *Gleba cordata* a) and b) larval shell (B5-1, 240 cm).

CYMBULIIDAE

7. Gymnosome veliger (B5-1, 440 cm).

8. *Paedoclione doliiformis* larval shell (B5-1, 90 cm).

6. DISCUSSION

6.1 RELIABILITY OF DATA - POSSIBLE EFFECTS UPON LDX RECORD

It is very difficult to separate the effects of reduced calcification and the effects of increased dissolution, since both influences lead to a similar result. It has been assumed that, where core locations are well above the present day ALy, there has been no dissolution from under-saturated bottom water masses. However, additional factors can be responsible for creating short term changes in water pH, that can cause post-depositional pteropod shell dissolution.

6.1.1 VOLCANIC ASH CONTENT OF CAR-MON 2

CAR-MON 2 contains numerous layers of fine ash produced by volcanic events on the island of Montserrat (South Soufrière Hills and Centre Hills volcanoes, Fisher *et al.,* 2008). One section of the core, between 270–330 cm appears to represent one large volcanic event, although, this is in fact composed of many thin layers, representing several events that spanned 23 kyr (Le Friant *et al.,* 2008). Volcanic events depositing large quantities of volcanic ash into the sea can cause local changes in pH during and just after an eruption (Jones and Gislason, 2008; Wall-Palmer *et al.,* 2011). This dramatic reduction in pH dissolves pteropod shells, both in the water column and on the sea floor (Wall-Palmer *et al.,* 2011). Under laboratory conditions, a recent study has shown that volcanic material from the South Soufrière Hills volcano produces a significant reduction in pH upon entering the sea (Jones and Gislason, 2008). Closer inshore, the effects of recent (2003 and 2006) large scale volcanic events around Montserrat have been found to affect pteropods and produce a distinct pattern of abundant poorly preserved pteropod shells within the upper layers of ash deposits (Jones *et al*., 2009; Wall-Palmer *et al.,* 2011). However,

microfossil analysis of CAR-MON 2 shows no enhanced pteropod dissolution or increased planktic foraminifera fragmentation in relation to ash layers, suggesting that the fine ash layers have had little or no effect upon the LDX profile. This is because the site of CAR-MON 2 is much further from the South Soufrière Hills volcano and only receives small amounts of wind blown ash, relative to sediments located closer to the volcano. The small amounts of ash from individual eruptions would have been so greatly diluted upon entering the ocean, that the acidic impact upon surface water fauna would have been insignificant.

6.1.2 EFFECTS OF ACIDIC PORE WATERS

A pattern of shell dissolution caused by acidic pore waters would show a general trend of gradually increasing dissolution with core depth, until shells disappear. This trend is not found in any of the cores analysed during this study. However, Caribbean core JC18-19 does show some form of pore water dissolution and has been greatly affected by transport of material. During microfossil analysis, it was found that, whilst planktic foraminifera tests were abundant throughout the core, pteropod and heteropod shells were only found in the upper 100 cm of core. Below this, there was no evidence of pteropod shells and no shell fragments. This change coincides with the erosive base of a bioclastic-volcaniclastic (50% bioclastic, 50% volcanic grains) turbidite. If the disappearance of pteropod remains was caused by fragmentation by the transported material, fragments would still be present. Therefore, this pattern is most likely produced by corrosive pore waters in the core section below the turbidite at 100 cm core depth. The pore waters have been acidic enough to dissolve all traces of aragonite, but not to dissolve calcite, since fragmentation

of planktic foraminifera does not increase considerably below 100 cm. The LDX above this (0–100 cm) shows moderate calcification and no obvious dissolution, suggesting that acidic pore waters have not leached upwards.

The microfossil analysis of JC18-19 demonstrates that any slight increase in pore water acidity has an extremely detrimental effect on pteropod remains. Effects of acidic pore waters would therefore be easily identified, had they affected any other core analysed during this study. It can be concluded that cores CAR-MON 2, JR123-35-V, B5-1 and 716B have not been affected by post-depositional dissolution from either volcanic ash or acidic pore waters.

6.1.3 MONSOONAL EFFECTS IN THE INDIAN OCEAN

Climate and oceanography in the Indian Ocean is strongly influenced by the monsoonal wind system, which affects the cycling and upwelling of nutrients in the ocean. Strong monsoonal winds cause an increase of nutrients in surface waters, which ultimately lead to increased surface water productivity. This in turn creates a mid-water oxygen minimum zone by increasing the input and decay of organic matter in sub-surface waters. The increasing concentration of dissolved inorganic carbon then causes a lowering of the pH and shoaling of the ALy (Klöcker *et al.,* 2006).

Klöcker *et al.* (2006) found that pteropod preservation has an inverse relationship to productivity proxies (C_{org}% and Ba/Al) in the Arabian Sea. Poor pteropod preservation was found to coincide with high productivity, in particular, during periods of enhanced south-west monsoon. However, the south-west monsoon is generally enhanced during warm periods; interglacials and interstadials, when poor calcification would also show high LDX values. Therefore, any resulting pattern of preservation and dissolution would be

difficult to separate from the longer term changes in calcification. The study by Klöcker *et al.* (2006) undoubtedly shows a dissolution signal, since the study is based upon a core collected well below (around 800 m below) the ALy. However, the effects of monsoonal sub-surface pH changes upon the LDX record may be applicable to ODP Hole 716B (since it is located close to the ALy) as a dissolution record imprinted over the long term calcification signal.

During LDX analysis and subsequent SEM imaging of pteropod shells from ODP Hole 716B, tiny perforations, approximately 2–3 μm in diameter (Fig. 4.42), were observed in the surface of several shells from most samples. This arrangement of holes is almost certainly not the result of dissolution due to monsoonal movements of the ALy, since the shell surface around the holes is smooth and very well preserved (LDX 1–2). It is most likely that the perforations were created by a type of bioerosion in the form of microboring. Mollusc shells have been found to be amongst the most susceptible sediment grains to bioerosion and often appear to be selectively attacked (Perkins and Halsey, 1971; Perry, 1998). Microboring organisms include bacteria, sponges, fungi and algae (Perkins and Halsey, 1971; Fütterer, 1984; Tudhope and Risk, 1984; Raghukumar and Raghukumar, 1998; Perry, 1998). Fütterer (1984) found similar boring patterns created by sponges in the south eastern Atlantic, however, the holes created by sponges are much larger than those shown in Figure 4.42. It is most likely than fungi are responsible for the arrangement of holes found in shells from ODP Hole 716B. Most studies on microboring have been carried out in shallow water, however, fungi have been shown to tolerate deeper water (Raghukumar and Raghukumar, 1998) and to have increasing abundances with increasing water depth (Perry, 1998). Raghukumar and Raghukumar (1998) found fungi in deep-sea sediments at 965 m in the Indian

Ocean. This bioerosion signal was easily identified and separated from the LDX calcification analysis and has therefore not affected the LDX profile.

6.1.4 EFFECTS OF PAST SEA LEVEL CHANGE

Fluctuations in pteropod abundances in the deep Atlantic have been attributed to post-depositional aragonite dissolution for some time (Damuth *et al.,* 1975), however, a cause for the fluctuation in pteropod abundances with changing climate in shallow water has long been debated (Droxler *et al.,* 1983). During glacial periods, sea level is generally lower, due to the large volume of water trapped as ice (e.g. Fairbanks, 1989). Kier and Pilkey (1971) interpreted variations in the aragonite content of shallow water sediments in the Bahamas as being caused by changes in sea level intermittently exposing and flooding aragonite rich banks. Although favoured by some authors (Droxler *et al.,* 1990; Gerhardt and Henrich, 2001), this theory has been disproved as the major mechanism in aragonite fluctuations (Droxler *et al.,* 1983, 1990). Droxler *et al.* (1983) found that 90% of the fine aragonite present in a core from the Bahamian Trough was from a shallow water source (aragonite from green algae, ooid sand and inorganic precipitates at 26°C), supporting the bank flooding theory. However, it was found that the onset of aragonite increase occurred 8 kyr before bank flooding during the last deglaciation. Droxler *et al.* (1983) also note that the asymmetrical, saw tooth shape of the aragonite content profile would not be the profile shape created by the flooding and exposure of a flat topped bank. This theory can also be disproved by differences in ocean dissolution/calcification patterns. The bank flooding theory assumes increased aragonite content during interglacial periods, when erosion and re-deposition of bank sediments can occur. During glacial periods, the

banks would be exposed, leading to little or no aragonite input. This pattern follows the deep water Atlantic model of aragonite dissolution (see section 6.3.2). At ODP Hole 716B, in the Indian Ocean, the reverse of this pattern is observed, with higher aragonite content during glacial periods, a pattern that would be impossible if the shallow banks of the Chagos-Laccadive ridge were exposed.

Therefore, whilst the presence of shallow water aragonite found by Droxler *et al.* (1983) in the Bahamian Trough suggests some influence of aragonite input from the flooding of banks, the main cause of aragonite fluctuations in this area is most likely due to dissolution due to corrosive bottom waters. This is consistent with sediments of the deep Atlantic Ocean. The bank flooding theory is not applicable to all shallow water peri-platform sediments and at present appears to be particular to the Bahamas. Droxler *et al.* (1990) consider the fluctuations in aragonite content of ODP Hole 716B to also be partially due to bank flooding processes. However, since pteropod shell fluctuations in Hole 716B show an opposing pattern to the Bahama Banks, the influence of bank derived aragonite can be discounted.

Changes in sea level have been found to affect some parts of the Mediterranean Sea, with a lower $CaCO_3$ content found in glacial sediments. This is not due to reduced production, or enhanced dissolution, but to dilution caused by an increase in fluvial inputs when sea level is lower (Hoogaker *et al.,* 2004). However, sedimentation rates were not found to increase during glacial periods of B5-1 (Fig. 4.19) and the abundance of both planktic foraminifera and pteropods was found to be higher during glacial periods. It can therefore be concluded that B5-1 has not been affected by fluvial inputs.

6.1.5 EFFECTS OF SHIFTING INTERMEDIATE WATER MASSES

In the Caribbean Sea, the presence of corrosive intermediate water masses, including Upper Circumpolar Deep Water (UCDW) and Antarctic Intermediate Water (AAIW), creates two aragonite lysoclines, causing dissolution in sediments situated above the known ALy (Gerhardt and Henrich, 2001). Haddad and Droxler (1996) found that sediments at a water depth of <1200 m on the Nicaragua Rise in the Caribbean Sea recorded a dissolution record which at times resembled the deep water Atlantic pattern of enhanced pteropod dissolution during glacial periods, and at times showed the reversed pattern of enhanced dissolution during interglacial periods. This was attributed to different water masses occupying the intermediate water depths at the Nicaragua Rise during the late Quaternary. Gerhardt and Henrich (2001) found the influence of UCDW and AAIW to be minimal at the northern end of the Lesser Antilles Arc, therefore variations in intermediate water masses are unlikely to have affected the sites of CAR-MON 2, JR123-35-V and JC18-19. Trends of calcification around Montserrat show no similarity to sediments affected by corrosive intermediate water masses and it can therefore be concluded that cores CAR-MON 2, JR123-35-V and JC18-19 have not been affected.

6.1.6 DISSOLUTION DUE TO INCREASED PRODUCTIVITY

Dissolution of carbonate foraminifera tests in surface sediments, situated above the calcite lysocline and overlain by supersaturated bottom waters, has been shown to occur in the Atlantic, Indian and Pacific Oceans (Milliman *et al.,* 1999; Schulte and Bard, 2003; Villiers, 2005). Dissolution is attributed to tests passing through a zone of high organic matter and consequent intense organic

matter respiration at the sediment-water interface. When productivity is high, the breakdown of increased amounts of organic matter produces CO_2, reducing the pH at the sediment-water interface and dissolving shells prior to their deep burial (Villiers, 2005). However, in cores analysed during this study, productivity was generally found to be higher during glacial periods (see section 6.5.1). Therefore, if dissolution of shells due to increased breakdown of organic matter had occurred, glacial periods would be characterised by pteropod shells with a poor surface condition and a high LDX. Schulte and Bard (2003) found that sediments affected by this type of dissolution in the Indian Ocean showed high foraminifera fragmentation and low $CaCO_3$ particle size during glacial periods, indicating significant periods of dissolution during glacial stages and substages. This is the reverse of the trends found at site 716B and at all other sites analysed during the present study. It can therefore be concluded that this type of dissolution has not affected sediments at sites CAR-MON 2, JC18-19, JR123-35-V, B5-1 and 716B.

In summary, whilst some minor influences of post-depositional dissolution are certain to have had minimal effects upon the surface condition of pteropod shells in all sediments, the large amount of evidence gathered during this study (see chapter 4) fully supports a trend of varying calcification and in-life corrosion in living pteropods, rather than a trend of post-depositional dissolution. This trend in calcification, which can be detected in sediments situated well above the ALy, in waters super-saturated with respect to aragonite that have not been affected by post-depositional dissolution, has been shown to result from climatic variations in surface water carbonate availability (Figs 4.17, 4.30, 4.43), which in turn results from changes in atmospheric CO_2 concentrations.

6.2 REPRODUCIBILITY OF LDX DATA ACROSS SITES AROUND MONTSERRAT

Trends in the LDX were found to be reproducible in un-interrupted hemipelagic sediments across sites around Montserrat (Fig. 4.15). It was found that core JC18-19, located to the south west of Montserrat and only 11 km to the south east of CAR-MON 2, contained a short record of pteropod and heteropod shells in the upper 100 cm of core only. *Globorotalia menardii* analysis identified an interruption in this short record between 10–50 cm, which showed that parts of MIS 3 and MIS 2 were missing (*G. menardii* zone Y). However, despite this interruption, the LDX record for JC18-19 shows the same trend as that in CAR-MON 2, with high LDX values (poor calcification) coinciding with low $\delta^{18}O$ values (MIS 1 and 3) and low LDX values (enhanced calcification) coinciding with high $\delta^{18}O$ values (MIS 2).

Situated to the north east of Montserrat, 77 km from CAR-MON 2, core JR123-35-V provides a better sedimentary record to compare to CAR-MON 2. Being located upwind of the South Soufrière Hills Volcano, the sediments in this area are un-affected by ash fall and the majority of this core is composed of un-interrupted hemipelagic sediments. One large bioclastic deposit interrupts the core at MIS 2, but does not appear to affect the oxygen isotope record. JR123-35-V also showed high LDX values during interglacial periods (MIS 1, 3 and 5) and low LDX values during glacial periods (MIS 2 and 4).

It can therefore be concluded that the LDX record is reproducible across sites around Montserrat (see section 4.1.4.2, Fig. 4.15) that are situated well above the ALy, in shallow water which is super-saturated with respect to calcium carbonate during both glacial and interglacial periods. The record

shows enhanced calcification during glacial periods and reduced calcification during interglacial periods across all three sites. Calcification has been influenced by carbonate saturation levels in the surface ocean, which are directly influenced by variations in global atmospheric CO_2 concentrations.

6.3 DOES THE CARIBBEAN LDX RECORD REFLECT A GLOBAL TREND?

6.3.1 LDX TRENDS ACROSS SITES IN DIFFERENT LOCALITIES

The trend of high LDX values during interglacial periods and low LDX values during glacial periods was also found to be reproducible across sites in different geographical localities that have the same specific oceanographic constraints. The trend in LDX from the shallow Caribbean Sea sites was identified in the Mediterranean Sea (B5-1) and in the Indian Ocean (716B) at sites located well above the ALy, in water super-saturated with respect to aragonite during both glacial and interglacial periods. It was found that, due to the lower carbonate saturation levels in the Indian Ocean, ODP Hole 716B showed a generally lower LDX, even during glacial periods. Core B5-1 reflects the CAR-MON 2 trend in LDX well, focusing on the last 4 isotope stages. B5-1 shows that variations in atmospheric CO_2 concentration during minor isotope stages MIS 4 and 3 did not have a profound effect on the carbonate levels in the surface ocean. Carbonate saturation in the surface ocean appears to have changed with extremes in climate, from the Last Glacial Minimum (MIS 5.5) to the Last Glacial Maximum (MIS 2.2). This is also reflected in temperature changes, identified by variations in the abundance of key planktic foraminifera, pteropod and heteropod species.

At all sites, the LDX calcification profile was found to be out of phase with

the oxygen isotope record, with the LDX lagging behind changes in global ice volume. When the LDX records of CAR-MON 2, B5-1 and 716B are shifted down by 35 cm, 35 cm and 20 cm respectively, a significant correlation between oxygen isotopes and calcification (LDX) is made. These shifts equate to lags in the LDX of approximately 15.2 kyr, 7–14 kyr and 5.3 kyr respectively, assuming a constant sedimentation rate. Variations in sedimentation rate mean that these values are only approximations, but reflect the best correlation between the two data sets (Appendix 8.2.1.3.C). Reconstructed surface water carbonate concentrations for the Caribbean Sea (Foster, 2008) show a significant correlation to oxygen isotope data for CAR-MON 2 (see section 4.1.4.2) which suggests that the lag in LDX cannot be attributed to a lag in the surface water carbonate concentration. Average shell size data also shows a lag, significantly correlating with the LDX profile for each core. This may indicate a delay in the calcification response of pteropods. The ability of pteropods to calcify in waters under-saturated with respect to aragonite has been shown in laboratory experiments (Comeau *et al.,* 2009, 2010a, 2010b, 2012; Lischka *et al.,* 2011) and may have important implications for the modern oceans. The lag in data in 716B has been previously identified by Droxler *et al.* (1990) and was attributed to short term carbonate preservation cycles (inputs from bank flooding) overlaying long term cycles (dissolution cycle). However, this does not appear to be the case with the pteropod calcification record, which, once shifted, correlates well with the oxygen isotope record, showing there is just one cycle.

This phase relationship has previously been identified in the Pacific Ocean and shows considerable variation in length. Le and Shackleton (1992) found that planktic foraminifera dissolution indices lagged behind ice volume by 6 to 20 kyr in the Equatorial Pacific. Moore *et al.* (1977) also found that the

duration of this lag varied across the Pacific Ocean. It was found that increases in carbonate preservation lagged behind global ice volume by 6 kyr and up to 10 kyr in the tropical Pacific Ocean, but that there was almost no lag in the Northern Pacific. One study in the Pacific Ocean, which used different proxies to detect carbonate in sediments, found the reverse pattern of dissolution indices leading global ice volume by around 5.6 kyr (Pisias *et al.,* 1975). Moore *et al.* (1977) considered this variation in findings, but came to no conclusion.

Despite numerous theories on the reason for leads and lags between environmental variables on land and in the ocean and atmosphere, the cause of ocean carbonate saturation lagging behind ice volume is not understood (Le and Shackleton, 1992; Mudelsee, 2001). Le and Shackleton (1992) attributed a lag in planktic foraminifera dissolution in the western Equatorial Pacific to the response time of the carbonate system. However, the response of the carbonate system encompasses several processes. Firstly, it may indicate that there is a delay in establishing equilibrium between the CO_2 concentration in the atmosphere and in the oceans. However, this is very unlikely, since the effects of increased anthropogenic atmospheric CO_2 in the last 200 years can already be detected within the oceans (Royal Society, 2005). The resulting changes in calcifying plankton are already detectable (Moy *et al.,* 2009), showing that, at most, a lag would be on the scale of hundreds of years, not thousands of years. Although data from the Caribbean Sea suggests that the delayed response in calcification does not reflect a lag in the carbonate saturation of the surface ocean (Fig. 4.17), it may still indicate that CO_2 was not an internal driving force behind glacial changes, with changes in ice volume preceding changes in CO_2 (for example, Shackleton, 1977). This, however, can also be discounted, since, at ODP Site 716B, the Vostok CO_2 record shows a significant correlation to the

oxygen isotope record, showing that they changed at approximately the same time. Mudelsee (2001) and Shackleton (2000) show that changes in ice volume actually lag slightly behind changes in atmospheric CO_2 by around 2.7 kyr and that both ice volume and CO_2 lag behind changes in temperature (Mudelsee, 2001).

A further scenario, which could explain the lag in data found at all sites, would be changes in deep ocean circulation caused by changes in ice volume. Moore *et al.* (1977) explain that during glaciations, the Norwegian Sea did not contribute to the formation of North Atlantic Deep Water (NADW), resulting in changes to the deep waters of the North Atlantic Ocean. This would decrease the age and amount of corrosive of bottom waters flowing into the Pacific Ocean, increasing the carbonate saturation of the entire water column and favouring the calcification of plankton. The lag associated with this scenario would result from the time taken for the polar front to reach the Norwegian Sea, around 10 kyr (Moore *et al.,* 1977). This process would appear to be the most favourable, however, during this study, lags in data were found to the east and west of the Atlantic (Mediterranean and Caribbean Seas), an ocean which is characterised by an increased volume of corrosive bottom waters during glacial periods (Damuth *et al.,* 1975).

It is also possible that the lag in data could be an artefact of post-depositional sedimentary processes. Price *et al.* (1985) found that agitation of sediments by bottom currents at the Rio Grande Rise, delayed the burial of pteropod shells, producing thick deposits of large pteropods termed ‘pteropod pavements’. This produced a pattern of more abundant pteropods towards the end of glacial periods, but also produced synchronous changes in grain size, which is not found at any of the sites analysed in the present study. Factors

such as particle size dependant bioturbation may also be responsible for the offset in LDX and oxygen isotope profiles. It has been shown that different sized particles can be preferentially bioturbated, moving smaller particles downwards (Wheatcroft, 1992). This could account for the lag in CAR-MON 2, where oxygen isotope data is based on <63 μm sediment and LDX data is based on pteropods >300 μm. However, for B5-1 and 716B, both oxygen isotope data and LDX data are based on similar sized organisms (oxygen isotope 250–355 μm, LDX >300 μm). In conclusion, although this study shows that the offset in calcification and climate data is global, no single causal process can be identified conclusively and it is most likely the product of several mechanisms.

6.3.2 COMPARISON TO PREVIOUS STUDIES AND PREVIOUS THEORIES

Numerous studies have been published showing down-core variations in abundances and preservation of Quaternary pteropods (Table 6.1, Fig. 6.1). Fluctuations in the pteropod content of sediments with changes in climate have been identified globally. However, it is evident that, although often producing a similar result, long time scale patterns in pteropod dissolution/calcification are not solely due to one process, but can be attributed to one of three main processes (Table 6.1):

***Deep Water Atlantic*:** Shifting water masses, which cause an increase in corrosive bottom waters during glacial periods, affecting shells on, or close to, the sea floor. This produces a pattern of increased dissolution during glacial periods and enhanced preservation during interglacial periods. This process occurs in sediments below the ALy in the deep Equatorial Atlantic Ocean and in

several parts of the Caribbean Sea (Damuth *et al.,* 1975; Droxler *et al.,* 1983; Haddad and Droxler, 1996; Gerhardt *et al.,* 2000).

Deep Water Indo-Pacific**:** Variations in the carbonate concentration of bottom water masses, which cause a shallowing of the ALy during interglacial periods and a deepening of the ALy during glacial periods, affecting shells on, or close to, the sea floor. This produces a pattern of increased dissolution during interglacial periods and enhanced preservation during glacial periods. This process occurs in the Indian and Pacific Oceans, where the position of the ALy is influenced by monsoonal winds and the OMZ. Sediments affected by this process are generally below, or close to the current ALy (for example, Rottman, 1979; Wang *et al.,* 1997; Klöcker *et al.,* 2006, 2007; Sijinkumar *et al.,* 2010).

Shallow Water**:** Variations in surface water carbonate concentration, which leads to variations in the calcification abilities of living pteropods. This includes the effects of in-life dissolution and the inability to maintain shells, when surface carbonate concentrations are low. This produces a pattern of enhanced pteropod shell calcification during glacial periods and reduced shell calcification or poor maintenance during interglacial periods. This pattern occurs where the sediments are well above the ALy, in waters super-saturated with respect to aragonite during glacial and interglacial periods (Cullen and Droxler, 1990; Messenger *et al.,* 2010; This study).

As an exception to these processes, the Red Sea presents a more complicated mechanism for patterns in pteropod preservation. Several authors have found a pattern of pteropod shell dissolution in the Red Sea, which reflects

the Atlantic sediments, with enhanced preservation and increased abundances during interglacial periods (Ivanova, 1985; Almogi-Labin *et al.,* 1991; Almogi-Labin *et al.,* 1998). Increased abundances of pteropods have been attributed to the lower salinity of waters during interglacial periods (Almogi-Labin, 1982; Ivanova, 1985; Almogi-Labin *et al.,* 1998). However, the processes producing enhanced dissolution during glacial periods are not understood. Almogi-Labin *et al.* (1998) note that the anti-estuarine circulation of the Red Sea prevents a direct connection to the Indian Ocean's corrosive deep water masses during glacial periods. This rules out the possibility of changes in deep water circulation causing carbonate dissolution events.

In contrast to this, Almogi-Labin *et al.* (1982, 1986) found that some Red Sea sediments show reversed or varying patterns of preservation. Almogi-Labin *et al.* (1986) found a pattern linked to anoxic bottom water conditions. In a core situated in the northern Red Sea, at 1050 m water depth, glacial stages were characterised by anoxic bottom waters, with well preserved pteropod shells and interglacial periods were characterised by well ventilated bottom waters, with poorly preserved pteropod shells. Almogi-Labin (1982) found a varying pattern, with dissolution of pteropods shells not relating to changes in oxygen isotope ratio. Cores from the northern Red Sea and the Gulf of Aquaba were found to show dissolution mainly occurring during MIS 5 and 2, both an interglacial and a glacial period.

The pattern of pteropod shell condition observed in both CAR-MON 2 and B5-1 are undoubtedly the result of variations in pteropod calcification. Both cores are situated so far above the present day ALy that are likely to have been situated above the ALy throughout the Late Pleistocene. This discounts the 'Deep Water Indo-Pacific' effects, as shallowing of the ALy would have had no

effect upon the sediments of either site. If the pattern had been due to 'Deep Water Atlantic' dissolution, which does affect sediments in some parts of the Caribbean (Gerhardt and Henrich, 2001), the pattern would be reversed, with enhanced pteropod shell conditions during interglacial periods. This concludes that the circumstances producing the patterns of pteropod shell conditions in both cores, is due to variations in the calcification of living pteropods, reflecting the 'Shallow Water' process.

Due to the shallow position of the current ALy in the Indian Ocean, site 716 may have been positioned on or below the ALy at some time during the Late Pleistocene. Variations in pteropod shell condition may, therefore, indicate the compound effects of the 'Deep Water Indo-Pacific' and 'Shallow Water' processes, as both would create a similar pattern. However, Cullen and Droxler (1990), who analysed ODP Hole 716B for calcite and aragonite content, found that preservation at Site 716 was extremely good, with very low planktic foraminifera fragmentation (average 80 % whole specimens), data which is consistent with the findings of this study. They also noted that the sedimentation rate was unusually high for the Indian Ocean, due to the preservation of most of the calcareous content, which is often dissolved before reaching the seafloor. In addition to this, the trend in average shell size of *L. inflata* (this study) supports a calcification record rather than a dissolution record. During periods of high LDX, shell size is generally smaller, which suggests carbonate availability was limited for the calcification of shells. If the high LDX values represented increased dissolution, smaller shells would be dissolved first, leaving the larger, more robust shells and an opposite trend. In conclusion, the LDX record of 716B, also appears to reflect a calcification record consistent with the 'Shallow Water' process.

Author	Site	Dissolution or calcification process
Gerhardt *et al.* (2000)	Brazilian continental slope (Atlantic)	*DWA*
Damuth *et al.* (1975)	Western Equatorial Atlantic (Atlantic)	*DWA*
Droxler *et al.* (1983)	Bahama Bank (Atlantic)	*DWA*
Haddad and Droxler (1996)	Bahama Bank (Atlantic)	*DWA*
Singh (2007)	Eastern Arabian Sea (Indian Ocean)	*DWI-P*
Klöcker *et al.* (2006)	Arabian Sea (Indian Ocean)	*DWI-P*
den Dulk *et al.* (1998)	Northern Arabian Sea (Indian Ocean)	*DWI-P*
Klöcker and Henrich (2006)	Pakistan shelf (Indian Ocean)	*DWI-P*
Klöcker *et al.* (2007)	Offshore Somalia (Indian Ocean)	*DWI-P*
Sijinkumar *et al.* (2010)	Andaman Sea (Indian Ocean)	*DWI-P*
von Rad *et al.* (1999)	Off shore Pakistan (Indian Ocean)	*DWI-P*
Wang *et al.* (1997)	South China Sea (Pacific Ocean)	*DWI-P*
Rottman (1979)	South China Sea (Pacific Ocean)	*DWI-P*
Gardulski *et al.* (1990)	West Florida ramp slope (Gulf of Mexico)	*DWI-P*
Haddad and Droxler (1996)	Deep water Caribbean Sea	*DWI-P*
Chen (1968)	Deep water Caribbean Sea, Gulf of Mexico	*DWI-P*
Wang *et al.* (1997)	South China Sea (Pacific Ocean)	*SW*
Chen (1968)	Mediterranean Sea	*SW*
This study	Mediterranean Sea	*SW*
Messenger *et al.* (2010) **This study**	Shallow Caribbean Sea (CARMON 2)	*SW*
Cullen and Droxler (1990) **This study**	Shallow Indian Ocean (716B)	*SW*

Table 6.1. Previous studies of pteropod (or aragonite) dissolution/calcification over time and the attributed calcification pattern. ***DWA*** *Deep Water Atlantic*: due to shifting water masses which increase corrosive bottom waters during glacial periods. ***DWI-P*** *Deep Water Indo-Pacific*: due to variations in the carbonate concentration of bottom water masses, which cause a shallowing of the ALy during interglacial periods. ***SW*** *Shallow Water*: Variations in surface water carbonate concentrations, which influence the calcification of living pteropods.

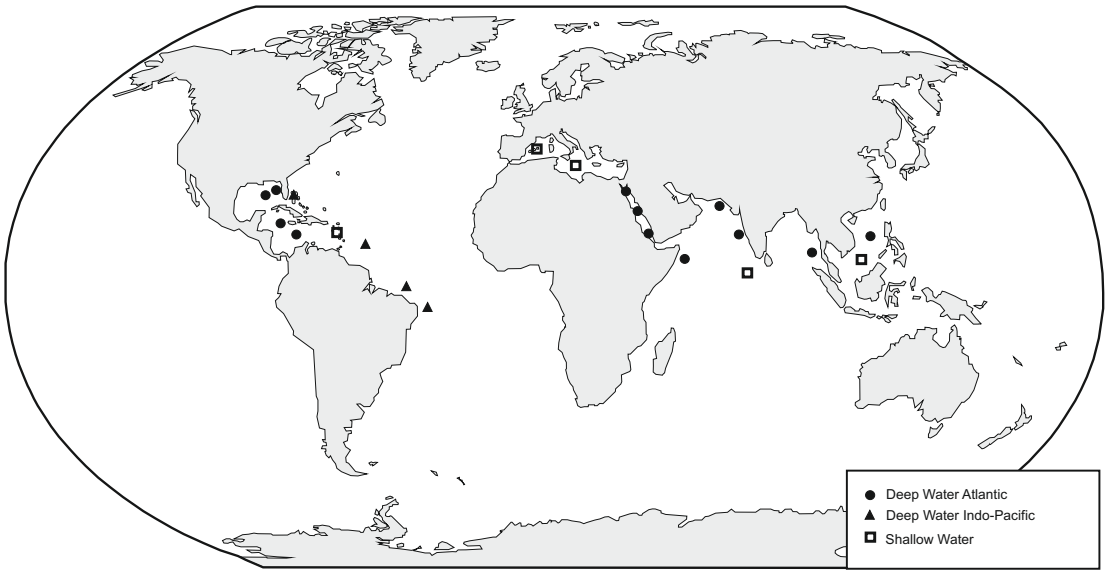

Figure 6.1. World map showing where different processes affect pteropod shells in sediments (Table 6.1).

There are some disparities between the microfossil analysis of this study and the aragonite record of ODP Hole 716B published by Droxler *et al.* (1990). Droxler *et al.* (1990) found a general decrease in pteropod preservation with increasing age. However, this was based on the % whole pteropods, something that is easily biased during sample collection and processing (Gerhardt *et al.,* 2000). Microfossil analysis carried out during the present study shows that, although abundance of pteropods and heteropods generally decreases with increasing time, the LDX does not increase with time.

There are few published records of pteropod shell calcification or dissolution from sites with the specific conditions required to allow direct comparison to CAR-MON 2, B5-1 and 716B. Wang *et al.* (1997) studied the pteropod abundance and fragmentation in four cores from the South China Sea. Three of the cores were collected from below the ALy (ALy at around 800 m water depth) and therefore show a 'Deep Water Indo-Pacific' dissolution record. However, one core was collected from above the ALy (706 m) and was

described by Wang *et al.* (1997) to show little dissolution influence from glacial-interglacial changes. However, Wang *et al.* (1997) only used pteropod abundance and pteropod fragmentation as the dissolution proxy. In shallow water, pteropod and heteropod abundance tends to be higher during glacial periods, due to increased productivity, and does not automatically indicate changes in dissolution (Haddad and Droxler, 1996). Fragmentation has been shown not to necessarily reflect the shell condition and is influenced by sample collection and processing (Gerhardt *et al.,* 2000). Due to the oceanographic setting of this site, well above the ALy, it is likely that revisiting these samples would show an LDX profile and shell size record consistent with that of the 'Shallow Water' calcification record.

Chen (1968) also studied a core from the Mediterranean Sea, collected south of the island of Crete, which is comparable to B5-1. Although other factors, such a sapropel formation (Röhling, 1994), can affect pteropod shells on the sea floor in the eastern Mediterranean Sea, the Mediterranean Sea is entirely super-saturated with respect to calcium carbonate, ruling out dissolution records produced by the 'Deep Water Atlantic' and 'Deep wWater Indo-Pacific' processes. Chen (1968) generally found more abundant pteropods during glacial periods, however, no indication of shell surface condition was made during the study and changes in abundance may reflect changes in productivity. High pteropod and heteropod abundance was found during glacial periods in all cores during this study and reflects high productivity of oceans during these times. The absence of pteropod remains found by Chen (1968) during certain periods suggests some kind of disturbance in this area, as pteropod and heteropod remains were found throughout core B5-1.

6.4 PALAEOCEANOGRAPHIC APPLICATIONS OF PTEROPODS AND HETEROPODS

6.4.1 APPLICATIONS IN SURFACE CARBONATE RECONSTRUCTION

The dissolution patterns of pteropod shells in surface sediments have been widely used in the identification of the ALy (Gerhardt and Henrich, 2001). Klöcker (2005) considers the LDX record, coupled with the abundance of pteropods to be the best proxy of aragonite dissolution. However, down-core studies of pteropod shells have been limited thus far and have exclusively dealt with dissolution records of cores generally below the ALy. This study demonstrates the use of the LDX as an efficient method of determining carbonate saturation levels in the surface ocean by analysing sediments situated well above the ALy. The high resolution record of CAR-MON 2 demonstrates that there are clear associations between the LDX profile and oxygen isotope stratigraphy, atmospheric CO_2 concentrations, surface water pH and surface water carbonate concentrations. In addition to this, the LDX profile shows a correlation with the abundances of certain indicative species of planktic foraminifera and pteropods. Although some environmental episodes appear to create disproportionate excursions in the LDX profile, several events, often only detected in one of the standard palaeoceanographic methodologies (e.g. atmospheric CO_2 concentration, ice volume, pH reconstruction), are highlighted in a single record. Moreover, the analysis of samples using the LDX scale is extremely quick and inexpensive in comparison to the standard methods of reconstructing surface water carbonate levels (for example Foster, 2008). This makes the LDX calcification profile an extremely useful tool in the reconstruction of past surface water conditions.

However, although living pteropods have a global occurrence in the oceans, a pteropod calcification record can only be obtained from sediments where the effects of dissolution are minimal, in shallow, warm waters located well above the ALy. This will limit the wider use of the LDX technique in reconstructing past surface water conditions. Despite this limitation, down-core LDX profiles from sediments below the ALy are also of use in reconstructing bottom water masses. In a study of pteropod preservation in surface sediments, Gerhardt and Henrich (2001) found that the LDX can be used to determine, approximately, the aragonite saturation state of bottom water masses. They found that the transition of a shell to LDX 2 indicated the presence of the ALy, and that the transition of a shell to an LDX of 4–5 indicates the ACD. Therefore, despite reflecting different processes, the LDX profile of all un-interrupted hemipelagic sediments will reflect climate change very accurately and could be a very useful initial assessment of sediment cores. Once the likely process of dissolution/calcification is identified, the LDX is then an extremely useful index in the reconstruction of surface (as in *Process 3*), intermediate (as in *Process 2*) or deep water (as in *Process 1*) conditions.

6.4.2 APPLICATIONS IN PALAEOTEMPERATURE RECONSTRUCTION

This study also demonstrates the use of pteropod and heteropod shells in palaeotemperature reconstruction, something that has previously been given little consideration. Core B5-1 shows that often, when planktic foraminifera species do not react to minor changes in climate, pteropod and heteropod species do, resulting in changes in the dominant species. The temperature preferences of pteropod and heteropod species can then be translated into changes in temperature. The variations in pteropod and heteropod abundances

allowed the constraining of temperature to within, and often with a lower range than, those predicted for the Mediterranean Sea using more sophisticated techniques and computer models (for example Sbaffi *et al.,* 2001). The known temperature range of holoplanktic gastropod species and the distribution of their shells in sediments, therefore, have the potential to be developed into a very useful palaeotemperature reconstruction tool.

6.4.3 APPLICATIONS TO THE MODERN OCEAN

The results of this study suggest that the calcification of shelled pteropods and heteropods through the Late Pleistocene reflects changes caused by variations in atmospheric CO_2 concentrations. This signal appears to be detectable in shallow water sediments worldwide, where post-depositional dissolution has had little or no effect, leaving the original calcification record intact. This trend in calcification is in agreement with recent laboratory work on living pteropods (Fabry *et al*., 2008; Comeau *et al*., 2009, 2010a,b, 2012) and pteropods from sediment traps in the Southern Ocean (Roberts *et al*., 2008). It also compares favourably with shell-weight data of *G. bulloides* and *G. ruber* provided by work in the Southern Ocean (Barker and Elderfield, 2002), in the Arabian Sea (Moel *et al*., 2009) and in the North Atlantic (Moy *et al.,* 2009).

The LDX record of Late Pleistocene sediments may, therefore, be used as a natural laboratory and could help to predict future changes in the aragonitic holoplanktic fauna caused by increases in anthropogenic pCO_2. However, since the level of anthropogenic CO_2 entering the oceans is currently increasing at a rate 100 times faster than any changes seen in the past 650 kyr (Fabry *et al.,* 2008), it might be inappropriate to apply such a model to the modern oceans. The fate of the modern day aragonitic holoplankton is uncertain, although, this

study demonstrates that, at oceanic pH levels relatively higher and changing at a lesser rate than those predicted for the 21st Century, euthecosome pteropods have been noticeably affected.

6.5 COMMENTS ON TAXONOMY

6.5.1 TRENDS IN DIVERSITY AND ABUNDANCE

In general, trends of abundance and diversity are uniform across the Caribbean, Mediterranean and Indian Ocean sites, and species assemblages confirm that sediments have not been affected by post-depositional dissolution (see sections 4.1.3, 4.2.3, 4.3.3). At all sites, abundance of pteropods and heteropods is generally higher during cold periods, which reflects productivity. However planktic foraminifera were more abundant during warm periods in the Caribbean Sea. At all sites, pteropod and heteropod diversity is generally lower during glacial periods, a trend found in the modern ocean. Pteropods in high latitude waters tend to be very specialised and therefore, although occurring in their highest abundances (Royal Society*,* 2005; Fabry *et al.,* 2008), they show very low diversity (Herman, 1971). In the Indian Ocean, it was found that planktic foraminifera were more diverse during glacial periods (but not significantly), possibly a product of monsoonal upwelling increasing the productivity of surface waters.

6.5.2. THE MORPHOLOGY OF INDIAN OCEAN *LIMACINA INFLATA*

During microfossil analysis, it was noticed that some specimens of *L. inflata* from ODP Hole 716B showed a slightly different morphology from specimens from both the Caribbean Sea and the Mediterranean Sea. Although adult forms remain an overall depressed shape, the protoconch and first whorl

of Indian Ocean specimens were found to be slightly raised in comparison to specimens from other locations (Fig. 6.2). Although this is only a slight variation of the morphology, it may indicate a new sub-species of *L. inflata* and requires further investigation.

6.5.3 EXTENDING THE RANGE OF HETEROPOD SPECIES

No previous studies of the assemblages and abundances of living or fossil heteropods have been carried out for the Caribbean Sea. This study, therefore, represents all that is known about the heteropods of this area, extending the range of all heteropod species found within the surface sediments (assumed to represent the living assemblage of the overlying waters) to the Caribbean Sea, with a water depth of 1102 m. The range of *A. rosea,* which is present in tropical and sub-tropical waters of the Atlantic and Indian Oceans, can also be extended to the Mediterranean Sea. Some rare specimens of *Carinaria*, only identifiable to genus level were also found in the Mediterranean Sea. Since *C. pseudorugosa* and *C. lamarckii* (which were also found in the Mediterranean Sea) are the only species of this genus known outside of the Indo-Pacific, the range of *Carinaria* can also be extended. Knowledge of the geographical range of heteropod species is limited, so the results of this study can increase our understanding of the environmental requirements of these gastropods.

6.5.4. PREVIOUSLY UNDESCRIBED SPECIES

Several species of pteropod and heteropod collected during this study appear to be previously undescribed and may, therefore, represent new species. The descriptions of these species can be found in the taxonomic chapter (see

Chapter 5). In particular it is interesting to note three species of the well studied genus *Limacina*: *Limacina* sp. B, *Limacina* sp. C and *Limacina* sp. D, which were found in low numbers in the Caribbean Sea (sp. C and D), in the Mediterranean Sea (sp. B and D) and in the Indian Ocean (sp. C) sediments. *Limacina* sp. B has a similar morphology to the common *L. inflata,* but has an elongated, curled and striated aperture, rather than an apertural tooth. It is possible that *Limacina* sp. B is a juvenile form of the genus *Sinum*, however, a lack of specimens makes detailed identification difficult. Three specimens were found in total, two from the 150–500 µm fraction of B5-1 and one from the >500 µm fraction of B5-1. All specimens were found in sediments relating to cool periods and the oldest specimen was from MIS 6 (B5-1 490 cm).

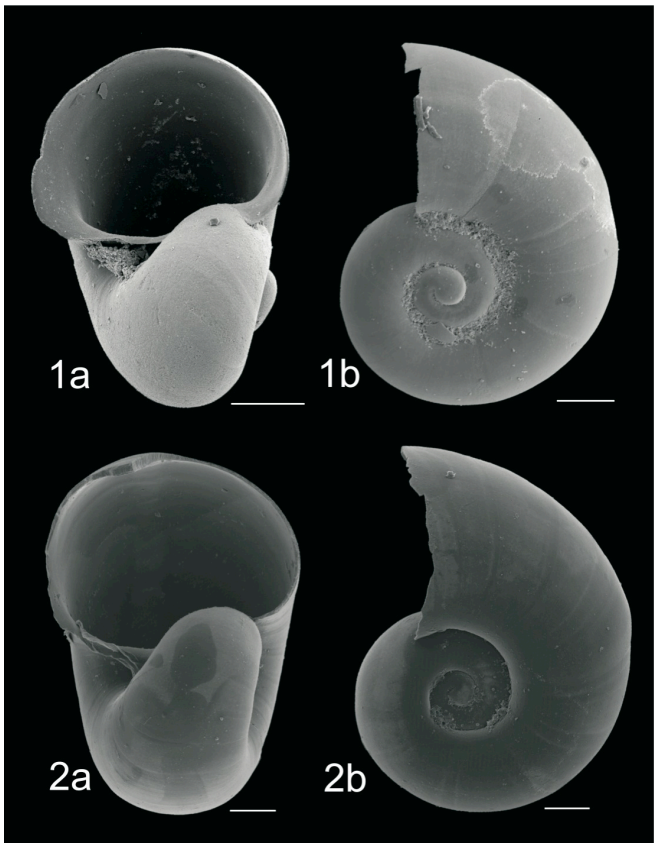

Figure 6.2. Specimens of *Limacina inflata* 1a) and b) from 716B (15–16 cm, 150–500 µm); 2a) and b) from B5-1 (0–1 cm, >500 µm). All scale bars 100 µm.

Limacina sp. C is also similar in morphology to *L. inflata,* but has an apertural lip, rather than an apertural tooth. The protoconch is also less depressed than *L. inflata,* with less defined whorl sutures. It is likely that this species is, or is derived from a previously recorded extinct genus, *Heliconoides* (Cahuzac and Janssen, 2010), known from the Paleocene to the Pliocene. The specimens are all in good condition and are unlikely to be the result of sediment reworking. Fifteen specimens were collected in total from the >500 µm fraction throughout CAR-MON 2 and from the >500 µm and 150–500 µm of 716B. The youngest specimen was collected at 10 cm core depth in CAR-MON 2, which is approximately 4 kyr.

Limacina sp. D shows a similar morphology to *Limacina* sp. C and *L. inflata.* The shell coils sinistrally and consists of two and a half whorls arranged in a similar way to *Limacina* sp. C, with a rounded, slightly protruding apex and no whorl sutures, giving a smooth appearance. The final whorl rapidly inflates to a large aperture. The umbilcal side of the apertural margin curls around the shell, covering the umbilical side and attaching to the spiral side 180° from the spiral side of the apertural margin. The shell is small and transparent. Only two specimens of *Limacina* sp. D were found, one from the >500 µm fraction of CAR-MON 2 and one from the 150–500 µm fraction of B5-1.

Atlanta sp. D was identified from the Caribbean Sea only. Thirteen specimens were collected from the 150–500 µm fraction and six from the >500 µm fraction of CAR-MON 2. This species appears to have a preference for warm climates, all specimens except three (150–500 µm: 570 and 575 cm; >500 µm: 60 cm) were found during interglacial periods. The most recent specimen was found at 40 cm core depth, which equates to around 17 kyr.

7 CONCLUSIONS

The aims of this study have been successfully achieved. Results show that changes in surface ocean carbonate saturation during the Late Pleistocene can be detected by studying pteropod shells in marine sediments. Results also demonstrate the successful application of pteropod and heteropod species counts in the reconstruction of past environments. In addition to this, new taxonomic information on the pteropods and heteropods has been discovered, identifying probable new species, describing and imaging known species and extending the known geographic range of several species. The most significant outcomes of this study are listed below.

- Three main processes which create long time scale variations in pteropod dissolution/calcification with changes in climate have been identified using the current study and by reviewing previous studies. The three processes are:

Deep Water Atlantic) Shifting water masses, which cause an increase in corrosive bottom waters during glacial periods, affecting shells on, or close to, the sea floor. This produces a pattern of increased dissolution during glacial periods and enhanced preservation during interglacial periods. This process occurs in the deep Equatorial Atlantic Ocean and in several parts of the Caribbean Sea.

***Deep Water Indo-Pacific*)** Variations in the carbonate concentration of bottom water masses, which cause a shallowing of the ALy during interglacial periods and a deepening of the ALy during glacial periods, affecting shells on, or close

to, the sea floor. This produces a pattern of increased dissolution during interglacial periods and enhanced preservation during glacial periods. This process occurs in the Indian and Pacific Oceans, where the position of the ALy is influenced by monsoonal winds and the OMZ. Sediments affected by this process are generally below, or close to the current ALy.

Shallow Water) Variations in surface water carbonate concentration, which influences the calcification abilities of living pteropods. This produces a pattern of enhanced pteropod shell calcification during glacial periods and poor shell calcification during interglacial periods. This pattern occurs where the sediments are well above the ALy, in waters super-saturated with respect to aragonite during glacial and interglacial periods.

♦ The sediments of cores CAR-MON 2, JR123-35-V, B5-1 and 716B show a global record of variations in pteropod calcification in sediments located above the ALy, that are bathed in waters super-saturated with respect to aragonite during both glacial and interglacial periods. The variations in calcification have been caused by variations in past atmospheric CO_2 concentrations, which change the carbonate concentration of surface waters. This is shown by significant correlation of the LDX to the global ice volume and to the Vostok atmospheric CO_2 record (once delay in response is accounted for). It is also shown in CAR-MON 2 by the association of the LDX to the reconstructed pH and surface water carbonate concentration of the Caribbean Sea. Variations in the shell size of *L. inflata* and planktic foraminifera fragmentation also support a calcification record.

♦ A delay in the response of pteropod calcification (LDX and shell size) to climate change, shown by a lag in the LDX cycle which varies from 5.3–15.2 kyr, was identified at all sites. This lag has been previously recognised in the Pacific Ocean, however, despite the development of several theories, the cause of this lag could not be determined.

♦ Although the conditions influencing climatic changes throughout the Late Pleistocene are not comparable to the modern oceans, this study demonstrates that, at oceanic pH levels relatively higher and changing at a lesser rate than those predicted for the 21st Century, euthecosome pteropods have been noticeably affected. This does not bode well for the future of aragonitic holoplanktic gastropods.

♦ This study demonstrates the use of pteropods and heteropods in reconstructing past environments. The LDX record is a fast and efficient way of initially assessing climatic changes through a sediment core, whether the LDX is reflecting a calcification or a dissolution record. Pteropods and heteropods are also extremely useful in constraining temperature ranges, showing higher sensitivity to climatic conditions than planktic foraminifera.

♦ This study has identified two possible new species of euthecosomatous pteropod, one possible new species of heteropod and has resurrected a euthecosomatous pteropod genus from extinction. A possible sub-species of *L. inflata* has been identified in the Indian Ocean and the range of several species of heteropod have been extended. This study also represents the only information on heteropods from the Caribbean Sea.

7.1 FUTURE RESEARCH

This study has identified several areas of research that require further investigation:

1) More research upon live pteropods is still required. Current research into the effects of ocean acidification upon shell production do not consider a number of basic factors. For example, why is a shell needed in the first place? Although they provide protection from parasites and infection, they offer little protection from larger marine organisms, such as fish and cetaceans. Do shells aid in migration and stream-lining? Why is the shape of pteropod shells so variable? How do the elongate species differ in their life habits from globular species? It would also be beneficial to quantify how important pteropods are to commercial fisheries. Research into this area is outdated (for example, LeBrasseur, 1966; Takeuchi, 1971) and often overlooks problems associated with predation upon pteropods. For example, the ingestion of large quantities of pteropods can lead to a build up of dimethyl sulphide and dinoflagellate toxins within the fish (Lalli and Gilmer, 1989).

2) Current information available on the taxonomy and geographic distributions of heteropods is extremely poor and requires extensive work. During this study, heteropod shells were found to make up to 70% of holoplanktic gastropod assemblages (150–500 μm) in the Mediterranean Sea. Analysis of core top samples and plankton tow samples worldwide would be necessary to produce a comprehensive guide to these poorly studied gastropods, both living and in the fossil record. As well as documenting the geographic and bathymetric ranges of species, revision of the taxonomy and morphology is required. Taxonomic work

should include genetic studies to conclusively separate species. Other aspects should include investigation of the shell geochemistry, as well as testing the reaction of heteropods to waters under-saturated with $CaCO_3$. It would also be interesting to investigate the commercial importance of this group of organisms as prey of fish and their contribution to the cycling of $CaCO_3$ in the oceans.

3) During this study, it was noticed that species show different reactions to variations in carbonate saturation. This demonstrates the importance of studying the responses of many different species and the response of a community as a whole. An extension of this study, looking in to the variations in response across all calcifying planktic species of one fossil community, by using the material collected throughout CAR-MON 2, would be valuable in assessing the ecosystem effects of ocean acidification.

4) During the recent IODP Expedition 340 (I took part as ship board biostratigrapher, Stroncik *et al.* 2012), a significantly extended hemipelagic record (139.4 metres in length) was collected close to the site of CAR-MON 2. This record extends back to around 4.5 Ma. Analysis of the holoplanktic gastropods present in this core would significantly extend both the LDX record and the biostratigraphic record of the Caribbean Sea.

8 APPENDICES

8.1 METHODOLOGY APPENDIX

8.1.1 COLLECTION OF CORE B5-1.

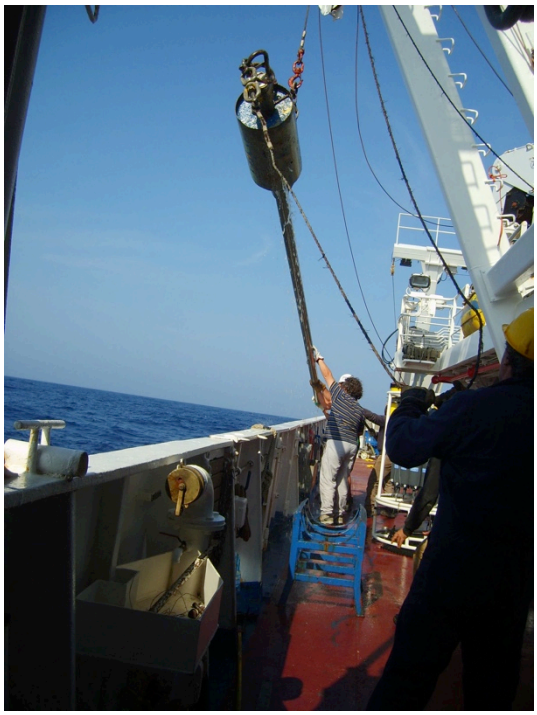

Above: Retrieving and cutting a gravity core on board the R.V. *Urania.*
Below: Preparing samples from gravity core B5-1 for oven drying on board the R.V. *Urania*.

8.1.2 MICROFOSSIL ANALYSIS APPENDIX

8.1.2.A TESTING THE PTEROPOD PICKING METHODOLOGY

Species	Size Fractions	
	125-150 µm	>150 µm
Cavolinia inflexa	1	11
Clio pyramidata	4	4
Clio spp.	0	1
Creseis acicula	15	10
Creseis virgula constricta	0	19
Diacria trispinosa	0	12
Limacina bulimoides	0	21
Limacina inflata	109	94
Limacina lesueuri	0	1
Limacina trochiformis	78	59
Styliola subula	2	14
Gleba cordata	41	10
Paedoclione doliiformis	0	2
Atlanta californiensis	0	1
Atlanta helicinoidea	3	4
Atlanta inclinata	0	1
Atlanta peronii	30	8
Atlanta selvagensis	12	27
Atlanta turriculata	0	1
Atlanta sp. D	0	1
Carinaria lamarckii	2	2
Firoloida desmarestia	0	7
Weight before picking	0.0235	0.4093
Unpicked weight	0.0204	0.339
Picked weight	0.0031	0.0703
Total number specimens	297	310
Pteropods per gram	95806	4410

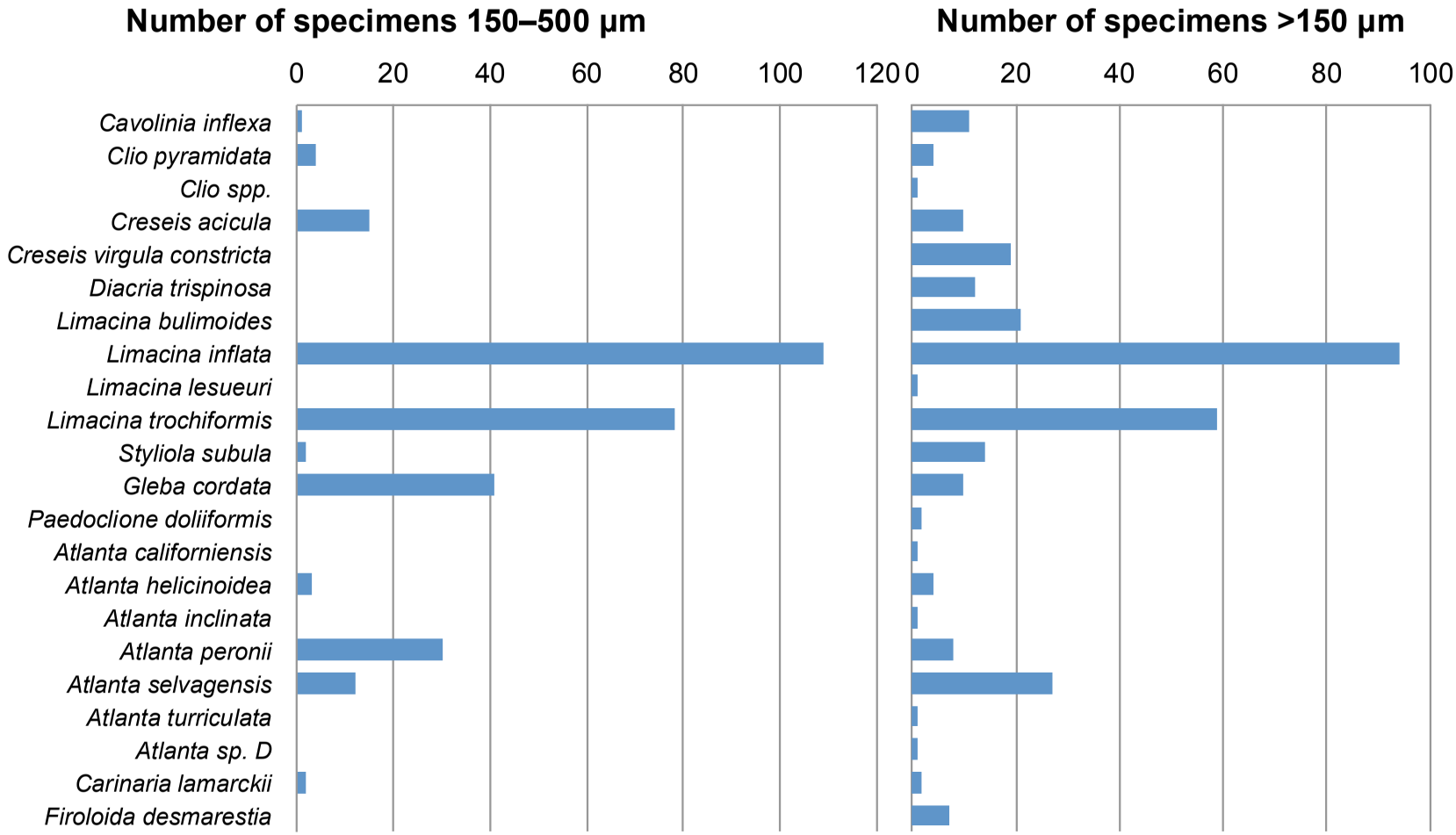
Number of specimens 150–500 µm
0
20
40
60
80
100
120
Number of specimens >150 µm
0
20
40
60
80
100
Cavolinia inflexa
Clio pyramidata
Clio spp.
Creseis acicula
Creseis virgula constricta
Diacria trispinosa
Limacina bulimoides
Limacina inflata
Limacina lesueuri
Limacina trochiformis
Styliola subula
Gleba cordata
Paedoclione doliiformis
Atlanta californiensis
Atlanta helicinoidea
Atlanta inclinata
Atlanta peronii
Atlanta selvagensis
Atlanta turriculata
Atlanta sp. D
Carinaria lamarckii
Firoloida desmarestia

8.1.2.B REPRODUCIBILITY OF LDX DATA

SAMPLE: CAR-MON 2 305−306 cm >500 µm

	LDX										Average	standard deviation of average LDX
Test 1	1	2	1	3	1	2	3	3	1	2	1.9	
Test 2	2	2	2	1	1	2	3	1	2	2	1.8	
Test 3	3	1	1	1	2	1	2	2	2	2	1.7	
Test 4	2	1	2	2	2	2	2	1	2	2	1.8	**0.08**

SAMPLE: CAR-MON 2 305−306 cm 150−500 µm

	LDX										Average	
Test 1	1	1	2	2	1	1	1	2	2	2	1.5	
Test 2	1	2	1	1	1	2	1	2	1	1	1.3	
Test 3	3	1	2	1	2	1	1	1	1	2	1.5	
Test 4	2	1	2	2	3	1	1	1	2	2	1.7	**0.16**

SAMPLE: CAR-MON 2 350−351 cm >500 µm

	LDX										Average	
Test 1	2	2	2	4	3	2	3	2	2	2	2.4	
Test 2	2	3	2	2	2	2	2	2	2	2	2.1	
Test 3	2	2	2	2	2	2	3	2	2	3	2.2	
Test 4	2	3	3	2	3	2	2	2	2	2	2.3	**0.13**

SAMPLE: CAR-MON 2 35−36 cm >500 µm

	LDX										Average	
Test 1	2	2	2	2	2	2	2	2	2	2	2	
Test 2	2	2	2	2	2	2	2	2	2	2	2	
Test 3	2	3	2	2	2	3	2	2	2	2	2.2	
Test 4	3	2	2	2	3	2	2	2	2	2	2.2	
Test 5	2	2	2	2	3	4	3	2	3	2	2.5	
Test 6	2	2	2	2	2	3	2	2	2	2	2.1	
Test 7	2	2	2	2	4	2	2	2	2	2	2.2	
Test 8	2	2	2	2	2	2	3	2	3	3	2.3	
Test 9	3	2	3	3	2	4	2	2	2	2	2.5	
Test 10	2	2	2	2	2	2	2	2	3	2	2.1	
Test 11	4	3	2	2	3	2	2	2	2	2	2.4	
Test 12	2	2	2	3	2	3	2	2	2	2	2.2	**0.17**

SAMPLE: CAR-MON 2 35−36 cm 150−500 µm

	LDX										Average	
Test 1	3	2	2	2	2	2	2	2	2	2	2.1	
Test 2	2	2	2	2	2	2	2	3	2	2	2.1	
Test 3	2	2	2	2	1	2	3	2	1	2	1.9	
Test 4	1	1	2	2	2	2	5	2	2	2	2.1	**0.10**

8.1.3 STATISTICAL METHODOLOGIES APPENDIX

- All correlations were carried out using a bivariate, two-tailed Pearson correlation (Rodgers and Nicewander, 1988). Pearson's correlation coefficient is a measure of linear dependence (known as correlation) between two variables, X and Y. Values lie between +1 and -1, with values close to +1 indicating a strong positive correlation (as X increases, Y also increases and as X decreases, Y also decreases) and values close to -1 indicating a strong negative correlation (as X increases, Y decreases and vice versa). Values close to 0 indicate no correlation. Pearson's correlation coefficient (**r**) can be calculated using the formula:

$$r = \frac{(\sum XY - \frac{\sum X \sum Y}{N})}{\sqrt{(\sum X^2 - \frac{(\sum X)^2}{N})\,(\sum Y^2 - \frac{(\sum Y)^2}{N})}}$$

- Diversity was measured using the Fisher Alpha index (Fisher *et al.,* 1943). Higher values indicate a higher diversity. The Fisher Alpha index can be calculated using the formula:

$$S = a \times \mathrm{Ln}\,(1 + \frac{n}{a})$$

Where **S** is the number of taxa, **n** is the number of individuals and **a** is the Fisher Alpha diversity.

- Assemblage heterogeneity was measured using the Shannon-Wiener index Shannon, 1948). The Shannon-Wiener index takes into account both the number of individuals and the number of taxa. A value of 0 indicates a community with only a single taxon, with values increasing as community heterogeneity increases. The Shannon-Wiener index can be calculated using the formula:

$$H' = -\sum_{i=1}^{R} pi \log pi$$

Where ***pi*** is the proportion of individuals belonging to the ***i***th species and **H** is the heterogeneity.

- Assemblage evenness was measured using Pielou's Evenness index (Mulder *et al*., 2004). Assemblage evenness indicates how close a population is to a perfectly heterogeneous assemblage. Values range between 0 and 1, with values closest to 1 indicating an even population. Pielou's Evenness index can be calculated using the formula:

$$J' = \frac{H'}{H'_{max}}$$

Where **J'** is Pielou's Evenness index, **H'** is the Shannon-Wiener index and the $\mathbf{H'_{max}}$ is the maximum value of **H'** calculated using the formula:

$$H_{max} = -\sum_{i=1}^{S} \frac{1}{S} \ln \frac{1}{S} = \ln S$$

Where **S** is the total number of species.

8.2 RESULTS APPENDIX

8.2.1 THE CARIBBEAN SEA APPENDIX

8.2.1.1 SEDIMENTOLOGY APPENDIX

8.2.1.1.A CAR-MON 2 GRAIN SIZE ANALYSIS

MID-SAMPLE DEPTH (cm)	FRACTION WEIGHT (g)				TOTAL WEIGHT (g)	FRACTION PERCENTAGE				MEAN GRAIN SIZE (µm)
	63-125µm	125-250µm	250-500µm	500µm		63-125µm	125-250µm	250-500µm	>500µm	
0.5	0.3824	0.2766	0.5176	0.2976	1.4742	25.94	18.76	35.11	20.19	342.63
5.5	0.4100	0.2801	0.4817	0.2413	1.4131	29.01	19.82	34.09	17.08	320.34
10.5	0.4292	0.3078	0.4167	0.1744	1.3281	32.32	23.18	31.38	13.13	289.98
15.5	0.4689	0.4053	0.5842	0.2328	1.6912	27.73	23.97	34.54	13.77	303.78
20.5	0.6059	0.3799	0.4761	0.2581	1.7200	35.23	22.09	27.68	15.01	290.87
25.5	0.4284	0.3866	0.4696	0.1661	1.4507	29.53	26.65	32.37	11.45	284.99
30.5	0.5376	0.4927	0.6074	0.2578	1.8955	28.36	25.99	32.04	13.60	297.57
35.5	0.6838	0.6557	0.7989	0.2489	2.3873	28.64	27.47	33.46	10.43	282.11
40.5	0.9786	0.8765	0.9802	0.2363	3.0716	31.86	28.54	31.91	7.69	260.82
45.5	1.0849	0.9211	1.2328	0.3192	3.5580	30.49	25.89	34.65	8.97	274.42
50.5	1.6782	1.5441	2.0195	0.4247	5.6665	29.62	27.25	35.64	7.49	268.79
55.5	0.7709	0.7728	1.3228	0.4617	3.3282	23.16	23.22	39.75	13.87	318.40
60.5	0.8956	0.6719	1.0745	0.3530	2.9950	29.90	22.43	35.88	11.79	293.11
65.5	1.9323	1.0490	1.1434	0.1989	4.3236	44.69	24.26	26.45	4.60	221.18
70.5	0.9864	0.8743	0.7405	0.3699	2.9711	33.20	29.43	24.92	12.45	273.22
75.5	0.2374	0.3342	0.7649	0.5584	1.8949	12.53	17.64	40.37	29.47	417.23
80.5	0.4395	0.5335	0.8734	0.7041	2.5505	17.23	20.92	34.24	27.61	390.88
85.5	0.7491	1.3415	2.5664	0.3653	5.0223	14.92	26.71	51.10	7.27	310.28

MID-SAMPLE DEPTH (cm)	FRACTION WEIGHT (g)				TOTAL WEIGHT (g)	FRACTION PERCENTAGE				MEAN GRAIN SIZE (μm)
	63-125μm	125-250μm	250-500μm	500μm		63-125μm	125-250μm	250-500μm	>500μm	
90.5	0.3820	1.0008	1.5239	0.1314	3.0381	12.57	32.94	50.16	4.33	294.12
95.5	0.9388	0.5891	0.7033	0.1144	2.3456	40.02	25.12	29.98	4.88	233.73
100.5	0.4195	0.1523	0.1280	0.0576	0.7574	55.39	20.11	16.90	7.60	210.18
105.5	0.5166	0.2535	0.2068	0.0787	1.0556	48.94	24.01	19.59	7.46	220.41
110.5	0.4907	0.3562	0.2356	0.0618	1.1443	42.88	31.13	20.59	5.40	216.39
115.5	0.4020	0.2754	0.2400	0.0827	1.0001	40.20	27.54	24.00	8.27	241.43
120.5	0.4295	0.2378	0.3054	0.0964	1.0691	40.17	22.24	28.57	9.02	254.22
125.5	0.3284	0.2233	0.3258	0.1451	1.0226	32.11	21.84	31.86	14.19	297.03
130.5	0.3253	0.2221	0.3292	0.1177	0.9943	32.72	22.34	33.11	11.84	285.57
135.5	0.3428	0.2416	0.2822	0.0946	0.9612	35.66	25.14	29.36	9.84	264.56
140.5	0.2819	0.1813	0.3147	0.1119	0.8898	31.68	20.38	35.37	12.58	294.93
145.5	0.3491	0.1979	0.3295	0.1261	1.0026	34.82	19.74	32.86	12.58	287.31
150.5	0.1449	0.1134	0.1808	0.0856	0.5247	27.62	21.61	34.46	16.31	318.05
155.5	0.1697	0.1038	0.1480	0.0527	0.4742	35.79	21.89	31.21	11.11	275.07
160.5	0.2406	0.1293	0.1779	0.0857	0.6335	37.98	20.41	28.08	13.53	280.74
165.5	0.2224	0.1217	0.1786	0.0848	0.6075	36.61	20.03	29.40	13.96	286.91
170.5	0.2845	0.1344	0.1959	0.0716	0.6864	41.45	19.58	28.54	10.43	260.93
175.5	0.1539	0.0717	0.1084	0.0463	0.3803	40.47	18.85	28.50	12.17	271.59
180.5	0.5547	0.3953	0.5528	0.2023	1.7051	32.53	23.18	32.42	11.86	284.61
185.5	0.7488	0.1705	0.1622	0.0695	1.1510	65.06	14.81	14.09	6.04	187.06
190.5	0.1422	0.0849	0.1341	0.0731	0.4343	32.74	19.55	30.88	16.83	309.46
195.5	0.4705	0.3120	0.4572	0.2473	1.4870	31.64	20.98	30.75	16.63	309.11
200.5	0.5943	0.4311	0.5925	0.3025	1.9204	30.95	22.45	30.85	15.75	305.02
205.5	0.1649	0.1382	0.2671	0.1587	0.7289	22.62	18.96	36.64	21.77	357.53
210.5	0.4113	0.2989	0.4418	0.1871	1.3391	30.71	22.32	32.99	13.97	299.24
215.5	0.2406	0.1474	0.2347	0.1145	0.7372	32.64	19.99	31.84	15.53	304.04
220.5	0.2124	0.1241	0.1527	0.0773	0.5665	37.49	21.91	26.95	13.65	279.74

MID-SAMPLE DEPTH (cm)	FRACTION WEIGHT (g)				TOTAL WEIGHT (g)	FRACTION PERCENTAGE				MEAN GRAIN SIZE (μm)
	63-125μm	125-250μm	250-500μm	500μm		63-125μm	125-250μm	250-500μm	>500μm	
225.5	0.1643	0.0948	0.1147	0.0559	0.4297	38.24	22.06	26.69	13.01	274.97
230.5	0.1824	0.1102	0.1028	0.0434	0.4388	41.57	25.11	23.43	9.89	248.20
235.5	0.1553	0.1038	0.1547	0.0652	0.4790	32.42	21.67	32.30	13.61	294.31
240.5	0.2231	0.1520	0.2454	0.1799	0.8004	27.87	18.99	30.66	22.48	345.35
245.5	0.1562	0.0800	0.1063	0.0495	0.3920	39.85	20.41	27.12	12.63	272.12
250.5	0.1369	0.0748	0.1107	0.0467	0.3691	37.09	20.27	29.99	12.65	280.23
255.5	0.1285	0.0975	0.1390	0.0945	0.4595	27.97	21.22	30.25	20.57	333.75
260.5	0.1037	0.0823	0.1406	0.0668	0.3934	26.36	20.92	35.74	16.98	325.38
265.5	0.1422	0.1124	0.1521	0.0992	0.5059	28.11	22.22	30.07	19.61	327.89
270.5	0.2145	0.1887	0.2283	0.0713	0.7028	30.52	26.85	32.48	10.15	276.94
275.5	0.2309	0.2287	0.2036	0.1069	0.7701	29.98	29.70	26.44	13.88	287.12
280.5	0.2358	0.2083	0.2276	0.0805	0.7522	31.35	27.69	30.26	10.70	275.12
285.5	0.2551	0.2726	0.2618	0.1127	0.9022	28.28	30.22	29.02	12.49	285.74
290.5	0.4093	0.4752	0.2988	0.2845	1.4678	27.89	32.37	20.36	19.38	308.62
295.5	0.4479	0.7064	0.3026	0.0678	1.5247	29.38	46.33	19.85	4.45	222.26
300.5	0.4433	0.5587	0.1961	0.4040	1.6021	27.67	34.87	12.24	25.22	326.42
305.5	0.4440	0.5499	0.2400	0.0524	1.2863	34.52	42.75	18.66	4.07	213.12
310.5	0.4975	0.6533	0.2528	0.0980	1.5016	33.13	43.51	16.84	6.53	224.80
315.5	0.8114	0.9360	0.3259	0.0956	2.1689	37.41	43.16	15.03	4.41	205.49
320.5	1.0114	0.8672	0.1711	0.0560	2.1057	48.03	41.18	8.13	2.66	172.79
325.5	0.6317	0.5366	0.5185	0.0594	1.7462	36.18	30.73	29.69	3.40	228.48
330.5	0.6847	0.5967	0.7261	0.0790	2.0865	32.82	28.60	34.80	3.79	243.36
335.5	0.9966	0.5073	0.2991	0.0558	1.8588	53.62	27.29	16.09	3.00	184.43
340.5	0.6329	0.3450	0.4169	0.0913	1.4861	42.59	23.22	28.05	6.14	234.84
345.5	0.8431	0.3965	0.3759	0.0690	1.6845	50.05	23.54	22.32	4.10	205.58
350.5	0.8946	0.5466	0.4982	0.1221	2.0615	43.40	26.51	24.17	5.92	225.55
355.5	0.7065	0.6661	0.3647	0.2124	1.9497	36.24	34.16	18.71	10.89	249.97

MID-SAMPLE DEPTH (cm)	FRACTION WEIGHT (g)				TOTAL WEIGHT (g)	FRACTION PERCENTAGE				MEAN GRAIN SIZE (μm)
	63-125μm	125-250μm	250-500μm	500μm		63-125μm	125-250μm	250-500μm	>500μm	
360.5	0.7959	0.7718	0.6053	0.3121	2.4851	32.03	31.06	24.36	12.56	273.87
365.5	0.5622	0.5577	0.5496	1.1017	2.7712	20.29	20.12	19.83	39.76	429.34
370.5	0.2786	0.1323	0.0792	0.0261	0.5162	53.97	25.63	15.34	5.06	194.25
375.5	0.2592	0.1895	0.2417	0.0425	0.7329	35.37	25.86	32.98	5.80	248.89
380.5	0.2976	0.2256	0.2752	0.0937	0.8921	33.36	25.29	30.85	10.50	273.23
385.5	0.3645	0.2424	0.2765	0.0596	0.9430	38.65	25.71	29.32	6.32	241.89
390.5	0.6307	0.5267	0.6367	0.0920	1.8861	33.44	27.93	33.76	4.88	246.97
395.5	0.6509	0.5981	0.5085	0.0887	1.8462	35.26	32.40	27.54	4.80	233.20
400.5	0.9742	0.9568	0.4764	0.0412	2.4486	39.79	39.08	19.46	1.68	196.24
405.5	0.4923	1.7714	2.0939	0.1797	4.5373	10.85	39.04	46.15	3.96	286.16
410.5	0.7392	0.5426	1.1057	0.1615	2.5490	29.00	21.29	43.38	6.34	277.36
415.5	0.4639	0.3123	0.7840	0.1345	1.6947	27.37	18.43	46.26	7.94	293.29
420.5	0.7763	0.5011	0.2177	0.0273	1.5224	50.99	32.92	14.30	1.79	176.72
425.5	0.8742	0.3643	0.2973	0.0573	1.5931	54.87	22.87	18.66	3.60	191.42
430.5	0.3482	0.2410	0.1178	0.0163	0.7233	48.14	33.32	16.29	2.25	185.70
435.5	0.2928	0.2650	0.2138	0.0448	0.8164	35.86	32.46	26.19	5.49	233.94
440.5	0.3463	0.2865	0.2386	0.0447	0.9161	37.80	31.27	26.05	4.88	228.44
445.5	0.1695	0.1051	0.2491	0.0302	0.5539	30.60	18.97	44.97	5.45	273.88
450.5	0.1316	0.0982	0.2126	0.0684	0.5108	25.76	19.22	41.62	13.39	316.77
455.5	0.1348	0.1073	0.2213	0.0534	0.5168	26.08	20.76	42.82	10.33	301.52
460.5	0.1345	0.1185	0.3065	0.0569	0.6164	21.82	19.22	49.72	9.23	312.26
465.5	0.1688	0.1242	0.2682	0.0454	0.6066	27.83	20.47	44.21	7.48	286.48
470.5	0.2698	0.1609	0.3117	0.0992	0.8416	32.06	19.12	37.04	11.79	293.27
475.5	0.1897	0.1112	0.2013	0.0789	0.5811	32.64	19.14	34.64	13.58	298.30
480.5	0.1908	0.1119	0.1855	0.0711	0.5593	34.11	20.01	33.17	12.71	289.30
485.5	0.2173	0.1181	0.1866	0.0670	0.5890	36.89	20.05	31.68	11.38	276.39
490.5	0.2268	0.1192	0.1702	0.0769	0.5931	38.24	20.10	28.70	12.97	278.48

MID-SAMPLE DEPTH (cm)	FRACTION WEIGHT (g)				TOTAL WEIGHT (g)	FRACTION PERCENTAGE				MEAN GRAIN SIZE (μm)
	63-125μm	125-250μm	250-500μm	500μm		63-125μm	125-250μm	250-500μm	>500μm	
495.5	0.2875	0.1463	0.1883	0.0697	0.6918	41.56	21.15	27.22	10.08	256.35
500.5	0.3121	0.1519	0.1769	0.0799	0.7208	43.30	21.07	24.54	11.08	255.38
505.5	0.9090	0.3379	0.2452	0.0813	1.5734	57.77	21.48	15.58	5.17	191.77
510.5	0.4791	0.4193	0.2505	0.0635	1.2124	39.52	34.58	20.66	5.24	218.75
515.5	0.4593	0.5415	0.2932	0.0798	1.3738	33.43	39.42	21.34	5.81	228.93
520.5	0.2357	0.1652	0.1124	0.0266	0.5399	43.66	30.60	20.82	4.93	213.43
525.5	0.4325	0.2913	0.3115	0.0930	1.1283	38.33	25.82	27.61	8.24	249.79
530.5	0.3005	0.1552	0.1748	0.0431	0.6736	44.61	23.04	25.95	6.40	230.44
535.5	0.3693	0.1989	0.2098	0.0431	0.8211	44.98	24.22	25.55	5.25	222.88
540.5	0.1962	0.1342	0.1685	0.0337	0.5326	36.84	25.20	31.64	6.33	247.97
545.5	0.1675	0.1947	0.3469	0.0620	0.7711	21.72	25.25	44.99	8.04	296.77
550.5	0.6946	0.5609	0.6951	0.1049	2.0555	33.79	27.29	33.82	5.10	248.02
555.5	0.3025	0.2450	0.3516	0.0689	0.9680	31.25	25.31	36.32	7.12	266.42
560.5	0.4521	0.4128	0.5039	0.0933	1.4621	30.92	28.23	34.46	6.38	259.10
565.5	1.3956	1.3973	1.4686	0.3151	4.5766	30.49	30.53	32.09	6.89	257.88
570.5	0.2990	0.2212	0.1272	0.0268	0.6742	44.35	32.81	18.87	3.98	203.77
575.5	0.2623	0.1676	0.1026	0.0272	0.5597	46.86	29.94	18.33	4.86	205.39

8.2.1.1.B CALCULATION OF CAR-MON 2 AVERAGE GRAIN SIZE

Mid-sample depth (cm)	% <63 µm	Mid-grain size (31.5µm) X proportion <63 µm	% >63 µm (Le Friant *et al.,* 2008)	Average >63 µm grain size (Appendix 8.2.1.1.A)	Average > 63 µm grain size X proportion >63 µm	Average grain size of total sample
0.5	69.13	21.78	30.87	342.63	105.76	127.54
5.5	66.39	20.91	33.61	320.34	107.67	128.58
10.5	72.94	22.97	27.06	289.98	78.48	101.46
15.5	67.91	21.39	32.09	303.78	97.50	118.89
20.5	66.81	21.04	33.19	290.87	96.54	117.59
25.5	73.48	23.15	26.52	284.99	75.59	98.73
30.5	69.71	21.96	30.29	297.57	90.12	112.08
35.5	63.10	19.88	36.90	282.11	104.11	123.99
40.5	50.89	16.03	49.11	260.82	128.09	144.12
45.5	40.46	12.74	59.54	274.42	163.40	176.14
50.5	18.70	5.89	81.30	268.79	218.53	224.42
55.5	34.42	10.84	65.58	318.40	208.81	219.65
60.5	25.63	8.07	74.37	293.11	217.99	226.06
65.5	29.75	9.37	70.25	221.18	155.38	164.75
70.5	23.95	7.54	76.05	273.22	207.79	215.33
75.5	23.33	7.35	76.67	417.23	319.88	327.23
80.5	20.23	6.37	79.77	390.88	311.81	318.18
85.5	20.12	6.34	79.88	310.28	247.85	254.18
90.5	12.99	4.09	87.01	294.12	255.90	260.00
95.5	41.65	13.12	58.35	233.73	136.39	149.51
100.5	74.18	23.37	25.82	210.18	54.26	77.63
105.5	72.31	22.78	27.69	220.41	61.04	83.81
110.5	61.13	19.26	38.87	216.39	84.11	103.37
115.5	64.58	20.34	35.42	241.43	85.51	105.85
120.5	67.91	21.39	32.09	254.22	81.58	102.97
125.5	62.27	19.62	37.73	297.03	112.06	131.68
130.5	68.92	21.71	31.08	285.57	88.75	110.46
135.5	65.37	20.59	34.63	264.56	91.62	112.21
140.5	73.03	23.00	26.97	294.93	79.54	102.55
145.5	68.79	21.67	31.21	287.31	89.68	111.34
150.5	67.38	21.22	32.62	318.05	103.75	124.97
155.5	79.46	25.03	20.54	275.07	56.49	81.52
160.5	72.14	22.73	27.86	280.74	78.21	100.93
165.5	75.66	23.83	24.34	286.91	69.85	93.68
170.5	78.62	24.76	21.38	260.93	55.79	80.56
175.5	81.43	25.65	18.57	271.59	50.44	76.09
180.5	80.37	25.32	19.63	284.61	55.88	81.20
185.5	77.49	24.41	22.51	187.06	42.11	66.52
190.5	83.21	26.21	16.79	309.46	51.97	78.18
195.5	76.04	23.95	23.96	309.11	74.06	98.01
205.5	71.68	22.58	28.32	357.53	101.23	123.82
210.5	74.48	23.46	25.52	299.24	76.36	99.82
215.5	73.33	23.10	26.67	304.04	81.08	104.18
220.5	80.97	25.50	19.03	279.74	53.24	78.75
225.5	84.48	26.61	15.52	274.97	42.69	69.30
230.5	83.94	26.44	16.06	248.20	39.86	66.30
235.5	81.51	25.68	18.49	294.31	54.42	80.09
240.5	76.84	24.20	23.16	345.35	79.99	104.19
245.5	85.40	26.90	14.60	272.12	39.73	66.63
250.5	86.30	27.18	13.70	280.23	38.40	65.58
255.5	82.09	25.86	17.91	333.75	59.78	85.64
260.5	82.85	26.10	17.15	325.38	55.82	81.91
265.5	82.83	26.09	17.17	327.89	56.30	82.40
270.5	81.52	25.68	18.48	276.94	51.18	76.86

275.5	76.29	24.03	23.71	287.12	68.07	92.10
280.5	74.60	23.50	25.40	275.12	69.89	93.38
285.5	72.09	22.71	27.91	285.74	79.76	102.47
290.5	65.75	20.71	34.25	308.62	105.71	126.42
295.5	60.46	19.04	39.54	222.26	87.88	106.93
300.5	60.50	19.06	39.50	326.42	128.93	147.99
305.5	46.12	14.53	53.88	213.12	114.83	129.35
310.5	53.37	16.81	46.63	224.80	104.81	121.63
315.5	58.52	18.43	41.48	205.49	85.23	103.67
320.5	49.45	15.58	50.55	172.79	87.34	102.92
325.5	40.26	12.68	59.74	228.48	136.49	149.17
330.5	35.19	11.08	64.81	243.36	157.74	168.82
335.5	47.08	14.83	52.92	184.43	97.61	112.44
340.5	43.08	13.57	56.92	234.84	133.67	147.24
345.5	57.74	18.19	42.26	205.58	86.88	105.07
350.5	51.50	16.22	48.50	225.55	109.39	125.61
355.5	76.43	24.08	23.57	249.97	58.92	83.00
360.5	84.89	26.74	15.11	273.87	41.39	68.13
365.5	92.81	29.23	7.19	429.34	30.89	60.12
370.5	85.90	27.06	14.10	194.25	27.39	54.45
375.5	75.08	23.65	24.92	248.89	62.02	85.67
380.5	66.05	20.81	33.95	273.23	92.76	113.56
385.5	71.60	22.55	28.40	241.89	68.70	91.26
390.5	43.82	13.80	56.18	246.97	138.74	152.54
395.5	48.62	15.31	51.38	233.20	119.82	135.14
400.5	42.92	13.52	57.08	196.24	112.01	125.53
405.5	28.53	8.99	71.47	286.16	204.53	213.52
410.5	43.63	13.74	56.37	277.36	156.35	170.09
415.5	65.74	20.71	34.26	293.29	100.49	121.20
420.5	47.71	15.03	52.29	176.72	92.40	107.43
425.5	52.12	16.42	47.88	191.42	91.64	108.06
430.5	64.47	20.31	35.53	185.70	65.97	86.28
435.5	75.35	23.74	24.65	233.94	57.66	81.39
440.5	73.97	23.30	26.03	228.44	59.46	82.76
445.5	81.06	25.53	18.94	273.88	51.86	77.40
450.5	75.11	23.66	24.89	316.77	78.84	102.50
455.5	76.82	24.20	23.18	301.52	69.88	94.08
460.5	72.84	22.94	27.16	312.26	84.81	107.75
465.5	73.53	23.16	26.47	286.48	75.83	99.00
475.5	78.01	24.57	21.99	298.30	65.58	90.16
480.5	81.27	25.60	18.73	289.30	54.18	79.78
485.5	80.79	25.45	19.21	276.39	53.09	78.54
490.5	79.39	25.01	20.61	278.48	57.39	82.40
495.5	76.21	24.00	23.79	256.35	61.00	85.00
500.5	78.63	24.77	21.37	255.38	54.57	79.34
505.5	68.06	21.44	31.94	191.77	61.26	82.70
510.5	63.98	20.15	36.02	218.75	78.80	98.95
515.5	64.30	20.26	35.70	228.93	81.72	101.98
520.5	71.00	22.36	29.00	213.43	61.90	84.27
525.5	52.65	16.59	47.35	249.79	118.27	134.85
530.5	74.45	23.45	25.55	230.44	58.87	82.32
535.5	62.27	19.62	37.73	222.88	84.09	103.70
540.5	75.68	23.84	24.32	247.97	60.32	84.15
545.5	63.76	20.08	36.24	296.77	107.54	127.63
555.5	69.28	21.82	30.72	266.42	81.85	103.67
560.5	54.35	17.12	45.65	259.10	118.29	135.41
565.5	47.44	14.94	52.56	257.88	135.54	150.48
570.5	77.53	24.42	22.47	203.77	45.78	70.21
575.5	72.33	22.78	27.67	205.39	56.83	79.61

8.2.1.1.C JC18-19 AND JR123-35-V GRAIN SIZE ANALYSIS

Mid-Sample depth (cm)	Total dry weight (g)	>63 µm dry weight (g)	<63 µm dry weight (g)	% >63 µm
JC18-19				
2.5	1.7027	0.6861	1.0166	40.29
10.5	1.9740	0.6330	1.3410	32.07
50.5	3.2016	0.9210	2.2806	28.77
75.5	2.9027	1.4985	1.4042	51.62
95.5	3.1843	1.3819	1.8024	43.40
130.5	3.2704	1.2022	2.0682	36.76
180.5	2.8043	1.5985	1.2058	57.00
195.5	3.0969	2.2441	0.8528	72.46
210.5	3.1705	1.1467	2.0238	36.17
280.5	3.0184	0.8236	2.1948	27.29
320.5	2.9873	1.2710	1.7163	42.55
350.5	3.3042	1.0594	2.2448	32.06
JR123-35-V				
10.5	2.2928	0.7114	1.5814	31.03
80.5	1.6980	1.1209	0.5771	66.01
150.5	3.8074	1.7981	2.0093	47.23
190.5	4.2904	0.6086	3.6818	14.19
235.5	2.8200	0.4197	2.4003	14.88
305.5	3.8640	0.5434	3.3206	14.06
435.5	4.2327	0.7022	3.5305	16.59
485.5	3.9330	0.7667	3.1663	19.49

MID-SAMPLE DEPTH (cm)	FRACTION WEIGHT (g)					TOTAL WEIGHT (g)	FRACTION PERCENTAGE					MEAN GRAIN SIZE (μm)
	0-63μm	63-150μm	150-250μm	250-500μm	500μm		0-63μm	63-150μm	150-250μm	250-500μm	>500μm	
JC18-19												
2.5	1.0166	0.1947	0.0899	0.2625	0.1390	1.7027	59.71	11.43	5.28	15.42	8.16	160.58
10.5	1.3410	0.2561	0.1205	0.1962	0.0602	1.9740	67.93	12.97	6.10	9.94	3.05	107.57
50.5	2.2806	0.2893	0.1780	0.3274	0.1263	3.2016	71.23	9.04	5.56	10.23	3.94	111.12
75.5	1.4042	0.6015	0.5076	0.3418	0.0476	2.9027	48.38	20.72	17.49	11.78	1.64	128.74
95.5	1.8024	0.4919	0.4043	0.4114	0.0743	3.1843	56.60	15.45	12.70	12.92	2.33	125.62
130.5	2.0682	0.3185	0.2056	0.5811	0.0970	3.2704	63.24	9.74	6.29	17.77	2.97	131.74
180.5	1.2058	0.6875	0.4051	0.4572	0.0487	2.8043	43.00	24.52	14.45	16.30	1.74	142.71
195.5	0.8528	0.9358	0.4802	0.7474	0.0807	3.0969	27.54	30.22	15.51	24.13	2.61	181.91
210.5	2.0238	0.3966	0.1965	0.4471	0.1065	3.1705	63.83	12.51	6.20	14.10	3.36	123.90
280.5	2.1948	0.2891	0.1417	0.3177	0.0751	3.0184	72.71	9.58	4.69	10.53	2.49	100.63
320.5	1.7163	0.2825	0.2399	0.6273	0.1213	2.9873	57.45	9.46	8.03	21.00	4.06	153.43
350.5	2.2448	0.2566	0.1727	0.4977	0.1324	3.3042	67.94	7.77	5.23	15.06	4.01	126.66
JR123-35-V												
10.5	1.5814	0.2918	0.1612	0.1775	0.0809	2.2928	68.97	12.73	7.03	7.74	3.53	104.84
80.5	0.5771	0.4380	0.2249	0.3110	0.1470	1.6980	33.99	25.80	13.24	18.32	8.66	198.28
150.5	2.0093	1.4364	0.2439	0.0839	0.0339	3.8074	52.77	37.73	6.41	2.20	0.89	84.56
190.5	3.6818	0.3871	0.0657	0.1094	0.0464	4.2904	85.81	9.02	1.53	2.55	1.08	57.38
235.5	2.4003	0.2599	0.0625	0.0582	0.0391	2.8200	85.12	9.22	2.22	2.06	1.39	59.20
305.5	3.3206	0.3416	0.0635	0.0897	0.0486	3.8640	85.94	8.84	1.64	2.32	1.26	57.91
435.5	3.5305	0.4753	0.0994	0.0881	0.0394	4.2327	83.41	11.23	2.35	2.08	0.93	57.72
485.5	3.1663	0.3992	0.1305	0.1492	0.0878	3.9330	80.51	10.15	3.32	3.79	2.23	73.77

8.2.1.2 MICROPALAEONTOLOGY APPENDIX

8.2.1.2.A CAR-MON 2 PLANKTIC FORAMINIFERA SPECIES ANALYSIS >500 µm

	0	5	10	15	20	25	30	35	40	45	50	55
Candeina nitida		1				2						
Globigerina bulloides												
Globigerinella aequilateralis	4	6	2	4	1	2	2	2	2	2	2	2
Globigerinella calida												
Globigerinoides conglobatus	26	19	33	31	24	47	50	37	42	54	44	47
Globigerinoides ruber	4	4	8	9	7	10	10	3	3	5	2	6
Globigerinoides sacculifer	45	48	43	56	38	54	40	42	43	41	27	29
Globigerinoides trilobus	13	9	17	8	11	10	7	7	6	6	2	8
Globorotalia crassaformis								1		1	1	1
Globorotalia menardii	71	78	59	111	53	49	13	6				2
Globorotalia flexuosa							15	1	3	3	3	5
Globorotalia tumida	3	8	16		3	6	8	7	5	2	2	7
*Globorotalia truncatulinoides D**	8	3	0	3	4	7	16	9	16	22	18	15
*Globorotalia truncatulinoides S**		4	4	4	1	4	4	4	1	1	1	
Neogloboquadrina dutertrei	32	35	37	40	53	49	97	90	125	94	112	119
Neogloboquadrina incompta												
Orbulina universa	92	82	81	75	111	70	73	75	57	83	85	67
Pulleniatina obliquiloculata	3	3	5	8	3	10	19	15	12	8	2	5
Sphaeroidinella dehiscens	4	4	3	10	4	1	2	5				
Total individuals	305	304	308	359	313	321	356	304	315	322	301	313
Total species	12	13	12	11	12	13	13	14	11	12	12	13
Fisher alpha	2.4920	2.7590	2.4860	2.1460	2.4750	2.7200	2.6490	3.0320	2.2160	2.4570	2.5010	2.7380
evenness	0.5690	0.5454	0.6448	0.6229	0.5321	0.6173	0.6245	0.5039	0.5287	0.5115	0.4245	0.4738
shannon weiner	1.9210	1.9590	2.0460	1.9240	1.8540	2.0830	2.0940	1.9540	1.7610	1.8150	1.6280	1.8180

*D dextral coiling
*S sinistral coiling

60	65	70	75	80	85	90	95	100	105	110	115	120	125	130
	3								1				1	
5	14	36	26	19	14	2	1	5	12	17	13	15	11	12
23	29	24	27	39	43	73	51	9	10	11	36	33	27	19
8	2	6		1	3	13	4	1		3	3	5	10	3
26	18	23	32	25	36	40	32	6	12	18	19	17	17	28
4	4	5	10	3	10	9	7			3	2	4	7	
1	1						1				1	1		4
			1							1	1			
1	2	3		3	5	12	9	2	2	3	7	4	5	5
	2			1	1	2	2			1				1
9	17	9	9	16	24	55	19	3	3	1	12	11	8	9
7		1	3	2	1		2		5	2	3	3	2	8
164	148	88	109	92	131	315	138	25	61	78	97	135	156	165
62	80	119	115	95	55	32	22	30	65	49	62	80	53	62
3		8	23	14	14	29	14		10	6	11	6	10	10
					1		1	1					2	
313	320	322	355	310	338	582	303	82	181	193	267	314	309	326
11	12	10	9	11	12	11	13	9	9	12	12	11	12	11
2.2200	2.4610	1.9570	1.6800	2.2250	2.4270	1.9250	2.7620	2.5780	1.9910	2.8330	2.5810	2.2180	2.4840	2.1970
0.4102	0.4075	0.5649	0.6336	0.5444	0.5369	0.4400	0.4433	0.5806	0.5674	0.4720	0.5194	0.4786	0.4451	0.4495
1.5070	1.5870	1.7310	1.7410	1.7900	1.8630	1.5770	1.7510	1.6540	1.6300	1.7340	1.8300	1.6610	1.6760	1.5980

60	65	70	75	80	85	90	95	100	105	110	115	120	125	130
	3								1				1	
5	14	36	26	19	14	2	1	5	12	17	13	15	11	12
23	29	24	27	39	43	73	51	9	10	11	36	33	27	19
8	2	6		1	3	13	4	1		3	3	5	10	3
26	18	23	32	25	36	40	32	6	12	18	19	17	17	28
4	4	5	10	3	10	9	7			3	2	4	7	
1	1						1				1	1		4
			1							1	1			
1	2	3		3	5	12	9	2	2	3	7	4	5	5
	2			1	1	2	2			1				1
9	17	9	9	16	24	55	19	3	3	1	12	11	8	9
7		1	3	2	1		2		5	2	3	3	2	8
164	148	88	109	92	131	315	138	25	61	78	97	135	156	165
62	80	119	115	95	55	32	22	30	65	49	62	80	53	62
3		8	23	14	14	29	14		10	6	11	6	10	10
					1		1	1					2	
313	320	322	355	310	338	582	303	82	181	193	267	314	309	326
11	12	10	9	11	12	11	13	9	9	12	12	11	12	11
2.2200	2.4610	1.9570	1.6800	2.2250	2.4270	1.9250	2.7620	2.5780	1.9910	2.8330	2.5810	2.2180	2.4840	2.1970
0.4102	0.4075	0.5649	0.6336	0.5444	0.5369	0.4400	0.4433	0.5806	0.5674	0.4720	0.5194	0.4786	0.4451	0.4495
1.5070	1.5870	1.7310	1.7410	1.7900	1.8630	1.5770	1.7510	1.6540	1.6300	1.7340	1.8300	1.6610	1.6760	1.5980

210	215	220	225	230	235	240	245	250	255	260	265	270	275	280
	2	1												
3		4	1	1	1	3	2	6	1	1	2	1	3	9
30	28	43	30	24	38	29	30	28	29	23	30	33	27	24
1	1	1			3			2				2	1	
10	4	12	4	7	3	5	1	12	7	9	7	13	10	5
1	4		1		2	1	1	2			2	1	1	2
	4	2	8	2	15	13	13	5	10	5	10	8	2	3
2	4		3	3	1	3			3	7	28	51	109	114
127	163	144	89	74	101	181	80	84	101	67	53	33	22	4
					6					5				
11	15	4	1	1	3	1			1		1		2	1
			1								1	2	2	1
66	70	50	31	42	70	73	69	81	91	106	93	102	87	74
42	14	36	21	22	10	16	23	32	46	29	60	37	25	41
10	4	9	4	10	4	6	3	5	8	11	6	12	15	11
				2	3	2	1	1	1	1	5	6	10	7
303	313	306	194	188	260	333	223	258	298	264	298	301	316	296
11	12	11	11	11	14	12	10	11	11	11	12	13	13	12
2.2380	2.4750	2.2320	2.5260	2.5500	3.1680	2.4370	2.1500	2.3330	2.2470	2.3190	2.5070	2.7670	2.7310	2.5120
0.4788	0.3752	0.4470	0.4674	0.5040	0.4025	0.3500	0.4824	0.5021	0.4719	0.5006	0.5552	0.5423	0.4892	0.4795
1.6610	1.5040	1.5930	1.6370	1.7130	1.7290	1.4350	1.5740	1.7090	1.6470	1.7060	1.8970	1.9530	1.8500	1.7500

285	290	295	300	305	310	315	320	325	330	335	340	345	350	355
								1			3			
6	3	2	1	2	1			3	3	2		4	6	15
				1										
32	24	30	6	17	9	14	7	60	100	24	45	20	30	16
				1			1	2	2	1	3			4
4	3	7	3	4	3	1	3	9	10	8	15	7	11	21
2	2	1		2				3	12	4	5		3	1
8	3	2		1				1	5			4	5	
165	113	79	14	26	29	22			1		2		4	
3	4	5			1	5	3	12	42	14	13	19	27	15
												2	1	
52	32	34	2	5	5	4	4	22	67	28	31	12	15	3
24	35	31	20	27	13	24	11	31	52	44	136	89	163	37
12	6	7	2	4	2	2	3	14	24				2	
6	3		1	2	5	1								
314	228	198	49	92	68	73	32	158	318	125	253	157	267	112
11	11	10	8	12	9	8	7	11	11	8	9	7	10	8
2.2180	2.4130	2.2220	2.7140	3.6840	2.7800	2.2910	2.7650	2.6890	2.2110	1.9050	1.8220	1.5030	2.0500	1.9720
0.4356	0.4433	0.5442	0.6019	0.5337	0.6062	0.6208	0.8086	0.5529	0.5737	0.6545	0.4685	0.5653	0.4000	0.7225
1.5670	1.5840	1.6940	1.5720	1.8570	1.6970	1.6030	1.7340	1.8050	1.8420	1.6560	1.4390	1.3760	1.3860	1.7540

360	365	370	375	380	385	390	395	400	405	410	415	420	425	430
							1			1			1	
						1								
12	6	1	4	10	5	5	4	3		9	8	12	9	2
											1			
30	6	7	7	26	24	41	35	14	44	88	86	30	49	3
3		1	3	1		4		1	1	8	2		1	
33	5	2	18	9	4	26	7	3	10	19	11	4	3	1
4	1	1		4		1	2			3	3			
1			3	3	4	6	2	5	4	7		1		
4		5	2	1						1	5			
		2	30	42	27	97	49	51	65	183	67	16	17	7
				1										
15	5	4	10	26	9	36	6	7	8	51	20	6	9	
										2				
7	1	1	6	8	6	34	5	4	9	49	16	3	7	1
38	26	8	26	62	32	35	35	8	38	85	89	30	58	26
		1	2	8	1	13	8	12	12	38	18	4	2	
									1		1			1
147	50	33	111	201	112	299	154	108	192	544	327	106	156	41
10	7	11	11	13	9	12	11	10	10	13	13	9	10	7
2.4270	2.2150	5.7780	3.0330	3.1060	2.3060	2.5050	2.7110	2.6900	2.2410	2.3940	2.7070	2.3490	2.3830	2.4270
0.6695	0.6188	0.7304	0.6698	0.5593	0.6785	0.6049	0.5555	0.5698	0.5832	0.5330	0.5076	0.6730	0.5146	0.4748
1.9010	1.4660	2.0840	1.9970	1.9840	1.8090	1.9820	1.8100	1.7400	1.7630	1.9360	1.8870	1.8010	1.6380	1.2010

435	440	445	450	455	460	465	470	475	480	485	490	495	500	505
						1		1						
8	2	2		1	2	1	6	1	2	2		2		2
16	15	19	29	21	27	14	29	23	20	19	22	32	35	39
			2	4	1	4	2	2	3			1	2	6
4	12	2	10	10	19	10	15	4	12	6	13	9	20	21
			1		3	2	3	2	3		3		2	6
1	1				1					1	1			
1	1			1								3	2	
21	16	17	39	41	35	35	147	197	125	100	103	72	114	67
	1	4	2		10	10			3				11	19
4	6	2	5	9	7	9	15	22	24	18	16	17	20	20
			3	15	4	1		1						1
10	8	6	22	17	17	7	10	4	8	3				1
43	43	32	64	32	56	49	53	36	59	53	50	49	56	74
	2	6	10	7	9	14	18	25	35	33	81	63	66	94
2		1	1	4	2	4	3	2	1		2	1	2	
110	107	91	188	162	193	161	301	320	295	235	291	249	330	350
10	11	10	11	11	13	13	11	12	12	9	9	10	11	11
2.6730	3.0740	2.8660	2.5500	2.6680	3.1450	3.3360	2.2420	2.4610	2.5140	1.8560	1.7600	2.0880	2.1910	2.1590
0.5881	0.5536	0.6081	0.5675	0.6756	0.6033	0.6120	0.4805	0.3256	0.4778	0.5440	0.5618	0.5639	0.5527	0.6226
1.7720	1.8070	1.8050	1.8310	2.0060	2.0600	2.0740	1.6650	1.3630	1.7460	1.5880	1.6210	1.7300	1.8050	1.9240

510	515	520	525	530	535	540	545	550	555	560	565	570	575
											2		
3	4	2	7	3	5	1		1		1	1		
16	24	7	33	33	19	15	21	48	56	72	79	16	13
6	2		3	1			2	5		3	3		
18	19	4	8	6	4	2	5	10	6	7	10	2	2
	5		2	4	3		2	2	7	4			
		1		2					1	3			
2			5					4	49	79	116	13	14
84	84	22	100	43	54	61	68	110	38	14		3	
										2			
9	12	8	18	4	7	7	27	37	19	39	18	4	3
			1	1				1					1
	1	1	3	6	5	8	14	31	9	17	23		4
43	69	12	58	36	39	15	19	36	25	36	40	19	20
42	54	10	31	11	10	10	17	23	12	26	29	6	2
6	7		1	2	1	2	2	3		2	2		
229	281	67	270	152	147	121	177	311	222	305	323	63	59
10	11	9	12	12	10	9	10	12	10	14	11	7	7
2.1350	2.2810	2.7980	2.5740	3.0560	2.4270	2.2480	2.2940	2.4800	2.1530	3.0290	2.2020	2.0150	2.0680
0.6020	0.5662	0.7038	0.5145	0.5615	0.5775	0.5441	0.6204	0.5647	0.7085	0.5478	0.5328	0.7732	0.7333
1.7950	1.8290	1.8460	1.8200	1.9080	1.7540	1.5890	1.8250	1.9140	1.9580	2.0370	1.7680	1.6890	1.6360

8.2.1.2.A CAR-MON 2 PLANKTIC FORAMINIFERA SPECIES ANALYSIS 150–500 µm

	0	5	10	15	20	25	30	35	40	45	50	55
Candeina nitida	4	3	4	9	4	7	3	1		1	1	2
Globigerina bulloides		1	2	1			1	1	2	2		
Globigerina digitata	2					1						
Globigerina rubescens					1	1		1			1	
Globigerinella aequilateralis	25	24	14	21	23	21	17	15	10	16	8	10
Globigerinella calida			1	4	8	4	7	2	3	1		1
Globigerinita glutinata	5	1	4	1	3	5	9	3	6	5	4	2
Globigerinoides conglobatus	10	3	3	8	2	1	9	5	7	6	8	7
Globigerinoides elongatus	2	2	4	7	5	3	3	3	2	11	18	5
Globigerinoides pyramidalis						1				1	1	
Globigerinoides ruber	86	103	111	129	102	117	115	109	99	100	91	106
Globigerinoides sacculifer	84	63	79	56	67	61	64	59	46	38	28	38
Globigerinoides trilobus	49	35	30	30	32	32	17	31	14	22	14	24
Globorotalia crassaformis	1	1		1	2	1	2	5	5	10	12	6
Globorotalia flexuosa		7							1			1
Globorotalia inflata		1			1				1	3	6	1
Globorotalia menardii	8		15	9	4	9	3	1				
Globorotalia scitula						1				1		
*Globorotalia truncatulinoides D**	3	4	3	2	2	8	12	14	15	15	22	18
*Globorotalia truncatulinoides S**			5	3	3	3	2	1	1	2	1	
Globorotalia tumida		2	1	2	3			2	2		1	4
Neogloboquadrina dutertrei	45	50	42	18	25	33	50	47	82	87	85	80
Neogloboquadrina incompta												
Orbulina universa	3	10	1	4	8	5	6	3	2	1	3	2
Pulleniatina obliquiloculata	3	2	6	9	6	6	5	7	10	10		8
Sphaeroidinella dehiscens												
unidentifiable	1	3	1						1		1	
Total individuals	331	315	326	314	301	320	325	310	309	332	305	315
Total species	16	18	17	17	19	19	16	18	19	18	17	18
Fisher alpha	3.5110	4.1440	3.8110	3.8520	4.2000	4.4240	3.5290	4.1630	4.1670	4.0810	3.8850	3.8490
Evenness	0.4547	0.3991	0.4104	0.4303	0.4363	0.4041	0.4701	0.4044	0.4008	0.4355	0.4484	0.4195
Shannon weiner	1.9840	1.9720	1.9430	1.9900	2.0610	2.0380	2.0180	1.9850	1.9760	2.0590	2.0310	1.9650

*D dextral coiling
*S sinistral coiling

60	65	70	75	80	85	90	95	100	105	110	115	120	125	130
2		4	3								1			
3	2	6	4	1	1	190	7	26	7	19	13		6	2
				1								1	1	
	1		1											
9	23	22	28	30	8	26	5	3	14	5	17	28	30	30
	1	9	4		3			10	14	2			1	
8	8	29	9	11	3	45	4	25	44	40	23	17	19	25
3	9	3	11	11	4	26	7	10	8	5		7	10	6
15	9	15	6	4	1	127	20	8	3	3	3	1		2
98	95	132	80	95	72	1621	182	192	148	117	133	114	140	129
29	25	21	30	40	45	268	10	25	10	38	31	27	24	17
10	20	8	20	12	20	184	13	15	16	15	10	18	12	19
5	2	5		1	6	97	3	3	3	3	8	12	10	9
1			2		2	3					1	1	1	1
12	5	1	3	7	4	49	5		2	1	1			
												2		
		5	2			8		9	2	6	7	1	2	3
12	5	5	9	16	15	63	8	5	5	2	2	4	1	2
2		1	1	2	1	3	2	3	1	1	1	2		4
1					1	6	1	1		1	1		4	1
113	104	37	78	87	104	488	34	26	34	47	48	66	47	72
			2	4		2	2				1	2	4	2
1	2	1	12	15	15	26	3	1	1	2	2	4	3	1
						1		1						
				2	3	68			1	12				
324	311	304	305	339	308	3301	306	363	313	319	303	307	315	325
16	15	16	18	16	17	20	15	16	16	17	17	16	17	16
3.5320	3.2900	3.5960	4.1830	3.4880	3.8740	2.6680	3.3050	3.4240	3.5670	3.8350	3.8920	3.5860	3.8490	3.5290
0.4094	0.4311	0.4600	0.4956	0.4971	0.4235	0.3258	0.3287	0.3783	0.3999	0.4503	0.3907	0.4365	0.3985	0.4078
1.8790	1.8670	1.9960	2.1880	2.0740	1.9740	1.8230	1.5950	1.8000	1.8560	2.0350	1.8930	1.9440	1.9130	1.8760

135	140	145	150	155	160	165	170	175	180	185	190	195	200	205
					1	1		2	1		1	2	4	1
4	5	11	3	6	3	4	3	5		4	4	7	2	
1			1										1	
23	14	21	28	29	14	24	24	21	22	13	16	18	20	19
		11	2	8		6	9	10	1	22	8	12	5	4
21	12	24	17	24	14	11	14	28	10	30	11	27	11	7
3	9	11	6	11	7	17	15	11	9	5	11	4	26	5
4	2			1	3	1	3	2	4	6	1	10	2	1
				1	2	1	2			2	1			1
93	120	142	132	135	118	84	66	110	43	113	125	113	60	83
34	12	13	16	21	25	20	41	43	31	31	21	38	26	35
15	18	19	14	19	17	26	20	42	26	20	16	27	23	23
17	21	14	14	13	11	11	3	10	10	4	2	8	15	15
1	7	2	2	6	4	13	7	9	22	5	11	6	15	6
				1	1									
													2	
2	1	8	2		3	1	2	5		5	6	1	2	
9	3	7	8	8	11	8	8	7	9	4	5	5	12	10
1	1	2	2			3	2	1	3			1		
2	7	5		28	11	21	12	15	21	14	17	20	29	31
72	68	52	58	71	59	48	68	84	85	51	51	40	64	60
4	2	1	4	1	2		1	1	1			5		
9	4	2	3	8	5	3		3	2	2	3	2	8	3
1														
316	306	345	312	391	311	303	300	409	300	331	310	346	327	304
18	16	16	16	19	19	18	17	18	16	17	18	18	19	16
4.1400	3.5900	3.4710	3.5700	3.8980	4.4620	4.1910	3.9040	3.8500	3.6100	3.7950	4.1630	4.0330	4.3950	3.5960
0.4765	0.4566	0.4951	0.4304	0.4893	0.4395	0.5752	0.5728	0.5304	0.5991	0.5254	0.4503	0.5481	0.6251	0.5510
2.1490	1.9890	2.0700	1.9290	2.1760	2.1220	2.3370	2.2760	2.2560	2.2600	2.1900	1.9200	2.2890	2.4750	2.1770

210	215	220	225	230	235	240	245	250	255	260	265	270	275	280
	2									1	7	5	7	9
	5		1		11		4		7	2				17
	1									1	1			
17	10	14	20	28	14	16	14	20	5	17	27		24	39
4	10	8	7	11	7		20	17	29	18	9	7	17	3
9	9	14	13	2	7	7	18	12	12	5	4	10	18	19
10	14	21	20	22	10	15	19	10	7	18	16	21	23	19
5	1		4	1				13	20	8	17	6	5	1
			2		4	6	9							
88	90	58	55	31	52	52	47	47	64	70	57	77	66	64
32	27	26	24	44	32	45	39	61	53	31	54	50	40	19
28	26	21	26	24	24	20	22	25	32	19	16	33	16	32
8	13	22	25	24	38	29	32	24	17	24	17	10	9	12
21	26	18	2	26	8	22	15	7	3	1	2	1	1	4
									2					
				2			1	2		1	3		6	
3						1				1			1	1
7	11	7	5	2			3	1		1		2	5	2
			2	1										
21	36	40	47	35	40	25	18	24	12	12	15	13	13	31
50	70	49	57	54	67	43	46	61	41	83	67	50	66	61
					1									
4		2		1		1	2				1		2	3
5	3	4	4	3	3	4	1		2	3	1	6	3	6
												1		
312	354	304	314	311	318	286	310	324	306	316	314	292	322	342
16	17	14	16	16	15	14	17	14	15	19	17	15	18	18
3.5700	3.7240	3.0320	3.5640	3.5730	3.2700	3.0830	3.8670	2.9800	3.3050	4.4400	3.8520	3.3480	4.1170	4.0460
0.6251	0.5843	0.7642	0.6551	0.6705	0.6686	0.7134	0.7097	0.7190	0.6674	0.4893	0.5816	0.5740	0.6026	0.6263
2.3030	2.2960	2.3700	2.3500	2.3730	2.3050	2.3010	2.4900	2.3090	2.3040	2.2300	2.2910	2.1530	2.3840	2.4220

285	290	295	300	305	310	315	320	325	330	335	340	345	350	355
2	3	4	1	1	2		3		1	1	2	3	3	2
4	13	15	10	16	14	11	18	3	1	6	10	10	4	5
						1	1				2			
23	11	21	19	22	21	17	16	25	15	16	24	22	61	26
28	12	10	7	11	8		12	1	4	8	6	6	8	1
9	11	13	8	6	14	4	12	8	2	22	20	13	9	9
17	15	23	28	17	25	35	13	30	14	7	21	5	17	15
2	4	8		2	7	13		9	5	3	23	19	21	7
			3											
80	96	77	85	80	105	69	122	76	76	104	99	78	64	87
48	21	38	44	38	33	36	18	35	23	28	41	28	43	40
19	16	33	21	22	18	31	25	21	26	22	31	19	20	15
5	8	2		4	4	1	6	19	9	5	2	1	4	1
														1
						1		11	23		10	2		3
1	3	8	2	7	4	3								
	1	2	1		2	1					4			
3	7	8	9	8	5	10	8	25	34	14	18	20	24	17
		1					1	1						
27	33	17	16	14	14	24			2				1	
45	42	34	40	48	30	39	42	75	81	69	71	82	56	90
	3	7	4	5	3	2	3	2		2	4	3	1	6
1	2	2	6	2	5	3	4	5	2		1	1	1	
4														
		3			3		2							
318	301	326	304	303	317	301	306	346	318	307	389	312	337	325
17	18	19	17	17	20	18	17	15	16	14	18	16	16	16
3.8380	4.2000	4.3990	3.8890	3.8920	4.4360	4.2000	3.5900	3.1960	3.5510	3.0240	3.9030	3.5700	3.4940	3.5290
0.5681	0.5598	0.6465	0.5781	0.6075	0.5527	0.5727	0.5101	0.6406	0.5359	0.5358	0.5723	0.5428	0.5929	0.4876
2.2680	2.3100	2.5080	2.2850	2.3350	2.3510	2.3330	2.0990	2.2630	2.1490	2.0150	2.3320	2.1620	2.2500	2.0540

360	365	370	375	380	385	390	395	400	405	410	415	420	425	430
							1					2	2	1
5	5	7	7	1		6	5	3	2	2	2	2	3	
25	32	8	19	40	24	15	7	3	2	7	6	17	14	21
10		6	12	8	5	3	7	9	2		2	5	3	4
20	21	14	17	6	5	5	5	10	1	3		2	7	5
12	18	12	9	7	8	3	5	8	3	6	15	10	18	8
7	12	24	14	7	9	16	3	12	14	8	16	15	5	12
						1	1							
69	96	93	94	51	71	120	92	90	86	85	42	55	76	83
41	40	29	47	32	38	33	15	47	31	19	22	47	27	32
25	20	25	23	14	18	25	26	15	16	14	32	7	7	10
8	2	4	4	9	6	8	5	4	6	3	8	7	1	7
			1			1				1				
	2			3			2		1					
		3					1							
1					3	1	1	2				2		1
14	16	11	10	9	13	14	14	15	14	24	25	13	17	19
									1			1	1	
		8	24	32	26	16	29	17	31	35	42	13	23	25
81	47	55	82	89	94	93	78	74	114	119	149	98	108	132
									1					
3	6	2	1	3	2	2	2	1	1		1	1	2	4
1	1	2	1			3	3	2	2	5	5	5	1	
											1			
322	318	303	365	311	322	365	302	312	328	331	368	302	315	364
15	14	16	16	15	14	18	20	16	17	14	15	17	16	15
3.2580	2.9950	3.6000	3.4190	3.2900	2.9190	3.9720	4.8140	3.5700	3.8050	2.9630	3.1440	3.8960	3.4290	3.1530
0.5987	0.6121	0.5752	0.5638	0.5898	0.5850	0.4319	0.4162	0.5081	0.3927	0.4699	0.4874	0.4944	0.4625	0.4843
2.1950	2.1480	2.2200	2.2000	2.1800	2.1030	2.0510	2.1190	2.0960	1.8980	1.8840	1.9890	2.1290	2.0020	1.9830

435	440	445	450	455	460	465	470	475	480	485	490	495	500	505
1								2	2			2		2
2	3		1	1						1	1		3	3
					1							1		
15	11	17	5	14	10	18	31	28	39	23	19	11	14	14
2	1		8	1	7	1	2	5	10	3	1	6	10	4
12	2	3	6	2	1	1	2	3	3		5	3	16	14
8	9	6	2	4	7	2	10	4	4	6	7	17	17	19
1	11	6	10	6	10	-	1	2	14	4	3		3	5
78	94	80	80	70	86	74	132	46	58	58	92	79	74	81
28	43	34	62	39	20	34	62	22	37	22	39	31	59	36
18	13	14	22	12	16	25	38	21	22	31	31	26	27	34
3		4	1	2	4	5	5	4	5	2	7	8	1	1
							1							
				1		1					5	2	4	1
	2				1				3		1	1	7	
15	17	15	15	12	13	7	15	20	20	19	41	50	29	40
		1		5	2	1	2				2	1		1
16	26	27	19	22	21	17	38	99	59	74	40	53	22	38
102	67	109	97	115	110	117	105	75	58	45			3	7
		1												
1	1	1	1	5	1	6		2	6			2		3
1		4	2	4	3	5	8	7	7	17	23	26	17	25
								1			1	1		
							1							
303	300	322	331	315	313	314	453	341	347	305	318	320	306	328
16	14	14	15	16	16	14	15	16	16	14	16	18	16	18
3.6000	3.0430	2.9850	3.2340	3.5600	3.5670	3.0050	2.9820	3.4830	3.4660	2.7570	3.5510	3.8310	3.5900	3.8050
0.4472	0.5205	0.4948	0.4673	0.4341	0.4353	0.4591	0.4860	0.4991	0.6411	0.6432	0.5354	0.5317	0.6320	0.5955
1.9680	1.9860	1.9360	1.9470	1.9380	1.9410	1.8610	1.9860	2.0780	2.3280	2.1240	2.1480	2.2010	2.3140	2.3150

510	515	520	525	530	535	540	545	550	555	560	565	570	575
				1			1					1	
4	7	3		22	3				16	3		15	11
												1	
11	15	15	14	22	32	12	22	11	7	14	8	16	11
12	7	14			7	7			5	8	1	12	4
8	11	6	1	6	5	8		4	11	4	7	11	6
6	2	10	8	3	11	4	8	3	16	13	19	9	8
5	6	16	2	15	3	4	5	3	7	6	7	27	4
117	109	83	79	124	75	95	43	66	82	89	92	110	109
29	30	39	39	20	27	31	22	18	20	22	16	36	22
38	28	27	13	10	27	27	13	17	18	13	21	18	13
2	1	4	4	1	2	6	1	2	5	5		1	2
							4	4		5	6	7	7
1		2	5	3		2		1			4		1
1	1			3		4		1	2		1	3	
27	27	17	25	15	6	10	26	40	32	26	32	11	21
1	1								1	1			2
28	32	36	60	29	56	45	67	46	33	31	31	19	42
3	11	16	40	21	54	61	107	83	60	54	48	23	35
1	3	2	1				2	7		2			2
15	13	11	29	7	8	2	8	8	2	10	19	2	6
												1	
309	304	301	320	302	316	318	329	314	317	306	312	323	306
17	16	16	14	16	15	15	14	16	15	16	15	19	17
3.8700	3.5960	3.6070	2.9900	3.6030	3.0000	3.2700	2.9680	3.5640	3.2730	3.5900	3.2870	4.4110	3.8810
0.4812	0.5438	0.6481	0.6066	0.5047	0.6181	0.5464	0.5329	0.5154	0.6353	0.6012	0.6131	0.5291	0.5199
2.1020	2.1630	2.3390	2.1390	2.0890	2.1580	2.1040	2.0100	2.1100	2.2540	2.2640	2.2190	2.3080	2.1790

8.2.1.2.B DISTRIBUTION OF MOST ABUNDANT PLANKTIC FORAMINIFERA SPECIES CAR-MON 2 >500 µm

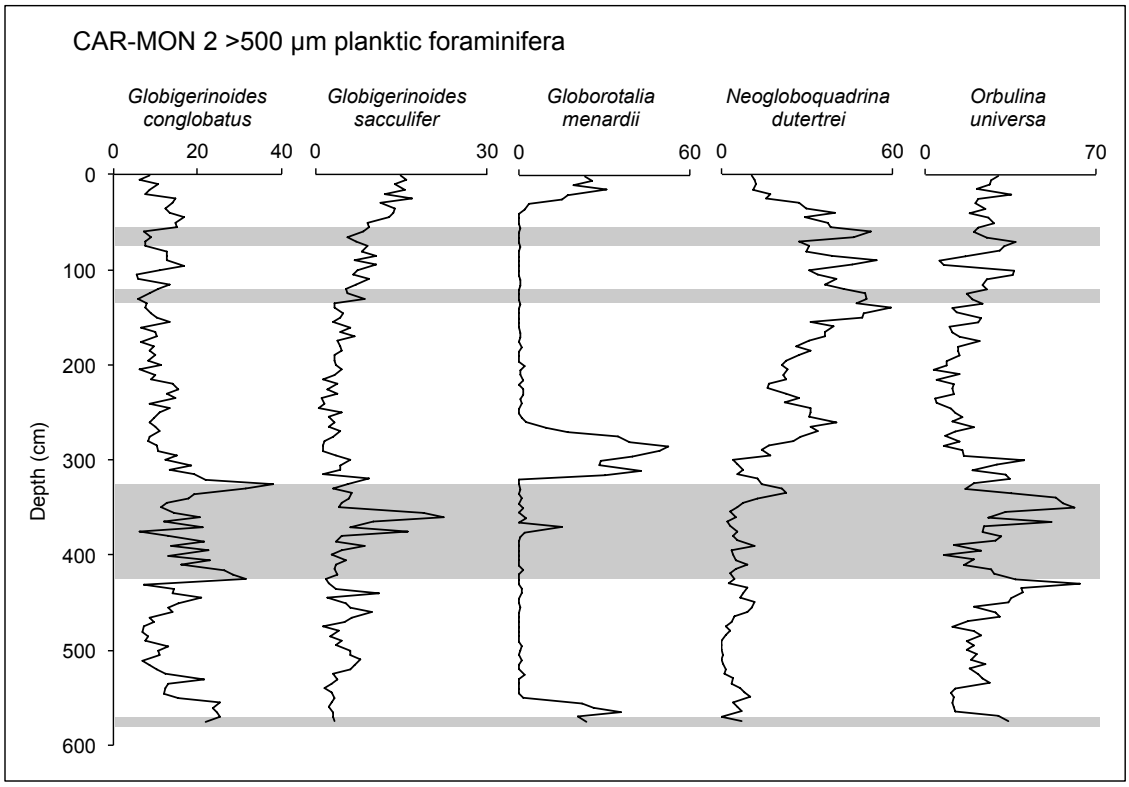

150 – 500 µm

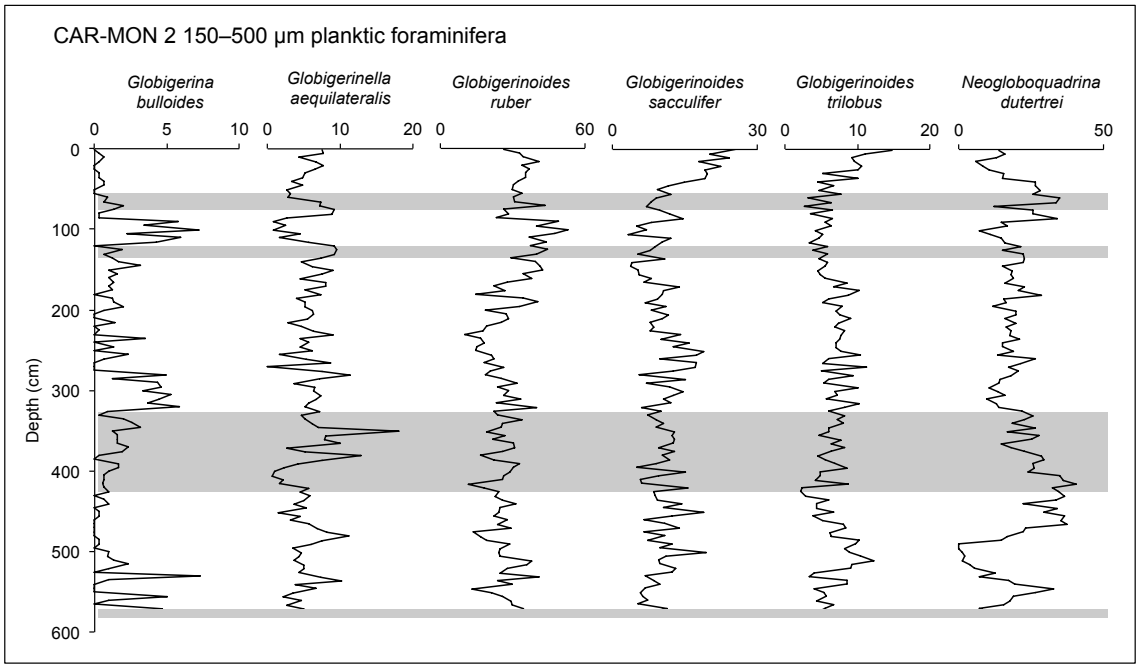

8.2.1.2.C CAR-MON 2 PTEROPOD AND HETEROPOD SPECIES ANALYSIS >500 µm

Species	0	5	10	15	20	25	30	35	40	45	50
PTEROPODA											
Cavolinia inflexa	1		1	1		1	5	2	2	1	
Cavolinia longirostris	1	1		1							
Cavolinia spp.											
Clio convexa											
Clio cuspidata											
Clio pyramidata								1	1		
Creseis acicula						1	2				
Creseis chierchiae											
Creseis virgula				1		1	7	2	2	2	1
Cuvierina columnella											
Diacria quadridentata			1	2	1		2	2	1	1	1
Diacria trispinosa											
Hyalostylus striata							2	1	2		1
Limacina bulimoides		1	1	6		8	14	12	11	2	8
Limacina inflata	4	8	40	66	12	74	195	223	88	127	139
Limacina lesueuri			1	5		6	7	4	3	2	4
Limacina trochiformis											1
Limacina sp. B										1	
Limacina sp. C			1								1
Limacina sp. D										1	
Styliola subula	1	1	3		2	2	3	4	1	1	2
Gleba cordata											
Peraclis diversa											
Peraclis moluccensis				1				1			
Peraclis spp.											
Paedoclione doliiformis											
HETEROPODA											
Atlanta brunnea											
Atlanta gaudichaudi											
Atlanta helicinoidea			1								
Atlanta inclinata				1						1	2
Atlanta peronii	1					1		2		2	4
Atlanta rosea						1			1		3
Atlanta selvagensis			1					2		5	2
Atlanta turriculata											
Atlanta sp. D									2		
Atlanta spp.											
Carinaria lamarckii								2	1	1	1
Carinaria pseudorugosa											
Carinaria spp.											
Firoloida desmaresti											2
Oxygyrus keraudreni										1	
Janthina spp.											
TOTAL	8	11	50	84	15	95	237	258	115	148	172
number of species	5	4	9	9	3	9	9	13	12	14	15

55	60	65	70	75	80	85	90	95	100	105	110	115	120	125	130
	4	1	6	2	6		1	2		1		2		3	1
1			1		2										
			1							1					
												1			
	1	1	7	2	3					1					
2	1		39	6	12		1								
						1									
3	5		24	9	16	1							1	2	2
	5	5	8	10	7		1				1	1		5	2
			1							1					
			7									1		2	
19	6	4	4	17	14	3			2	6	4	12	7	16	12
222	158	121	139	203	177	89	15	11	28	45	29	22	18	7	11
3				1	1	1					1			1	
	4		1	2	3	2			1						
1	1														
1	10	4	31	23	38	5	2	1	3	8	1	4	5	17	3
2			1		3	2									
							1	2	1				2	1	1
1		1		1	1	1	1			1					
5	4	1		2	4										
2	9	3	13	9	10	8		1		2			1		
1	4	1	1		1				1	1					
7	9	1	17	12	10	5			1		1		1		
1			1	1							1		1		
	1				1										
											1			1	1
5	2			4	2								1	3	1
										1					
					2						1			2	
	2	2	1	2									1		
						1									1
276	226	145	303	306	313	118	22	17	37	68	40	43	38	60	34
16	17	12	19	17	20	12	7	5	7	11	9	7	10	12	10

135	140	145	150	155	160	165	170	175	180	185	190	195	200	205	210
1	1	5	1		1									1	
			3		1	1									
				1	4										
		3			2	1									
		1													
1		3	1	2	1	1						4	2	3	
			1		2									1	
		2											1		
5	5	8	5	5	3	2	1		1	1		1	7	2	2
9	7	17	10	1	19	4						2	12	7	11
1	2		2	1	1				1	1		2		2	
2	1	10	6		6	4	2				1	3	1	3	
												1			
2	1	2	1				1							1	
						1							1		
					1										
1	1														
		1	1		1										
															1
	2	2	1		4							1			1
					1									1	
			1											1	
22	20	54	32	10	47	14	4	0	2	2	1	14	24	21	15
8	8	11	12	5	14	7	3	0	2	2	1	7	6	10	4

215	220	225	230	235	240	245	250	255	260	265	270	275	280	285	290
							1								
															1
	1														
		1		1										1	
	1						1							1	
1								1	2	1			1	1	2
	1														
2	3			1					1	1	1	1	2	1	
5	16	1								1			1	1	7
									1						
											1				
	1														
2	4	2				3				1	3	2		2	3
		1													
1														1	

										1					
1	2							1						1	
		1								1					1
						1									
								1		1					
	1		1			1				1					
12	29	6	0	2	0	4	2	3	4	7	5	3	4	9	14
6	9	5	0	2	0	3	2	3	3	8	3	2	3	8	5

295	300	305	310	315	320	325	330	335	340	345	350	355	360	365	370
2	1		1	2					1			1			
			1												
				1							1				
			1	1											
3	2	4	1			1					1				
				1				1	1		2			1	
			1										1	1	
1		1		3	1						1		4		
1				1											
1									1				1	1	1
1	1	2	1	2	2			1	3	2	8	2	7	1	1
27	28	54	53	65	15	20	18	30	66	15	56	17	37	4	2
1										1	2	1	4		
1	1				1								1		
													1		
7	1	3	8	7			1	3	2	1	13	1	19	6	5
1							1								
											1		3		
												1	1	2	
1		1							1						1
1								1	2				1		
1											1				
1							1								
	1		1			1	1								
	1	2								1		1	1	1	
		2					1								
			1	2											
			1												
3	2	1	2			1	2	1	4	1	7		3		1
				1											
	1														1
									1	1			1		
53	39	70	72	86	19	23	25	37	81	21	93	24	84	17	12
16	10	9	12	11	4	4	7	6	10	7	11	7	15	8	7

375	380	385	390	395	400	405	410	415	420	425	430	435	440	445	450
1	2	1													
	3														
	2														
6		4	2	1	1	1		1				3	1		1
3	9	1													1
3	2			1											
	5														
2	10	3		1	1										
									1						
										1					
		1													
	1														
1	1			1	1										
	1							1							
1															
1	1	1										1			
17	36	10	2	4	3	1	0	2	1	1	0	3	1	0	2
8	11	6	1	4	3	1	0	2	1	1	0	2	1	0	2

455	460	465	470	475	480	485	490	495	500	505	510	515	520	525	530
											1				
														1	
									1						
										1			1	1	
1	1		5				1		9	1	1	3		1	1
										1	7	18	16	13	
			1								1	2	2	2	
															1
														1	
			1						1		1	1	2	2	1
													1	1	
													1		
											1	1			
														1	
												1		1	
1	1	0	7	0	0	0	1	0	11	3	12	26	23	24	3
1	1	0	3	0	0	0	1	0	3	3	6	6	6	10	3

535	540	545	550	555	560	565	570	575
						5	1	
						2	1	
1						1		
						1		
2	1		1	1		3	1	2
			1			11	4	4
						11		2
		1						
	1							
3	1	1	2	1	0	34	7	8
2	2	1	2	1	0	7	4	3

8.2.1.2.C CAR-MON 2 PTEROPOD AND HETEROPOD SPECIES ANALYSIS

150–500 µm

Species	0	5	10	15	20	25	30	35
PTEROPODA								
Cavolinia inflexa	12	12	8	7	9	9	4	6
Clio cuspidata				1				
Clio pyramidata	1	2		2	3	1	2	1
Creseis acicula	6	8	14	11	6	25	20	16
Creseis chierchiae	2	1	2		3	1	1	
Creseis virgula	13	24	27	34	26	47	35	21
Creseis spp.								
Cuvierina columnella								
Diacria trispinosa	10	8	8	6	2	7	5	2
Hyalostylis striata								
Limacina bulimoides	12	17	11	11	11	11	12	14
Limacina inflata	86	101	103	103	96	128	118	144
Limacina lesueuri	4	3	5	8	7	5	6	3
Limacina trochiformis	53	54	32	27	50	20	27	25
Styliola subula	32	18	17	25	19	13	19	21
Gleba cordata	11	13	12	11	9	6	8	5
Peraclis diversa								
Peraclis moluccensis	4		2	2	2	1		4
Peraclis spp.								
Paedoclione doliiformis	2			1	2			
Gymnosome veliger	4	2	1	2	1		1	2
Janthia spp.								
HETEROPODA								
Atlanta brunnea				1				2
Atlanta californiensis			1			1		1
Atlanta gaudichaudi	1				2		1	
Atlanta helicinoidea	1		4	3	1	2	1	1
Atlanta inclinata						1		
Atlanta peronii	3	8	3	4	6	8	15	15
Atlanta rosea	2		3	3	6	2	5	3
Atlanta selvagensis	7	12	10	11	9	12	13	4
Atlanta turriculata								
Atlanta sp. D								
Atlanta spp.				1			1	
Carinaria lamarckii	15	13	10	8	10	8	9	4
Carinaria pseudorugosa	1				2		1	
Carinaria spp.								
Firoloida desmaresti	17	15	24	18	20	13	13	8
Oxygyrus keraudreni		1						2
TOTAL	299	312	297	300	302	321	317	304
number of species	23	18	20	23	23	21	22	22
Fisher alpha	5.8070	4.1550	4.8390	5.8010	5.7880	5.0350	5.3730	5.4460
Evenness	0.4838	0.5423	0.5172	0.4681	0.4750	0.4204	0.4490	0.3585
Shannon weiner	2.4090	2.2790	2.3360	2.3760	2.3910	2.1780	2.2900	2.0650

40	45	50	55	60	65	70	75	80	85	90	95
3	3	3	3	5	3	10	8	7	5	2	3
					1						
			2	2	2	5	7	4	4	2	
4	5	2	12	30	23	67	26	40	18	4	2
						1		1			
16	10	8	25	16	16	33	35	41	20	4	4
	1	1	1	6	3	8	3	8	2	6	3
10	10	9	14	8	11	14	16	16	18	27	17
158	162	144	148	88	72	54	81	64	83	74	115
3	2	4	5				2	1	1		
53	60	35	27	63	73	45	44	40	63	63	41
2	9	7	6	9	8	13	26	34	20	15	10
2	5	1	7	7	11	11	9	5	7		7
1	3			1	6	3		7	4		
2	1	2			2						1
	1				1	1		1			
		1									
		2	3				1		1		
						1		1			
2	5	6	7	6	9	1	2	3	6	14	12
8	13	18	14	20	25	14	19	11	24	17	24
5		13	4	6	7	5		2	4		
15	9	18	13	16	17	9	15	10	24	34	27
		1		1		1	1	1	2		2
											1
6	3	6	6	8	3	5	2	3	8	18	14
					1		1	1	2		
									2		3
11	13	23	14	24	17	11	7	15	17	18	10
1	1	3		1							2
302	316	307	311	317	311	312	305	316	335	298	298
18	18	21	18	19	21	21	19	23	22	14	19
4.1960	4.4400	5.1060	4.1590	4.4360	5.0850	5.0800	4.4880	5.7040	5.2810	3.0480	4.5200
0.3178	0.3109	0.3596	0.4235	0.5352	0.5217	0.5461	0.5511	0.5223	0.5321	0.6432	0.4513
1.7440	1.7760	2.0220	2.0310	2.3190	2.3940	2.4400	2.3490	2.4860	2.4600	2.1980	2.1490

100	105	110	115	120	125	130	135	140	145	150	155
4	6	2	9	8	7	12	15	6	11	12	4
				1	1			1	1		
5	8	9	7	3	8	9	5	8	5	3	12
7	3	10	5	5	17	6	7	10	8	7	3
13	9	8	16	11	13	11	7	5	12	10	7
		1									
2	4	4	3	11	12	11	14	9	12	12	11
										1	
20	18	12	18	16	10	31	7	7	15	17	25
119	133	160	135	128	139	146	151	151	139	156	148
					1	2	1	6	2	3	1
37	32	41	20	15	12	15	17	18	18	13	14
35	34	25	44	50	41	36	26	20	12	24	14
18	9	12	13	14	12	15	22	10	22	10	22
2					1		1				
3	3			2	3		1	1		1	1
2	2										
	1			2	2	2		1		1	
				1	2	1		3		2	
1	1	2	4	5	7	3	3	5		1	2
16	9	4	5	8	3	3	8	6	8	10	7
1	2	2	1						2		1
9	4	10	8	6	12	10	5	6	11	13	11
	1	1		2	1	2	4	1	2		
									2	1	
						1					
5	6	4	1	2	10	6	5	6	4	3	3
	2		1								
1											
4	3		2	2	2						
						1					
304	290	307	292	292	316	323	299	280	286	300	286
20	22	17	17	20	22	20	19	20	18	20	17
4.8040	5.5230	3.8780	3.9350	4.5530	5.0700	4.4150	4.5060	4.6240	4.2650	4.5200	3.9590
0.4292	0.3513	0.3534	0.4043	0.3987	0.3985	0.4055	0.3736	0.3469	0.4169	0.3524	0.3783
2.1500	2.0450	1.7930	1.9280	2.0250	2.1240	2.0420	1.9600	1.8860	2.0160	1.9010	1.8610

160	165	170	175	180	185	190	195	200	205	210	215
3	6	3	1	1	3	3	2	6	3	4	3
6	4	7	8	11	10	10	5	5	7	3	7
4	6	8	7	2	8	1	3	8	3	5	9
				2			1	1			
8	8	9	13	4	11	4	6	9	3	7	5
10	11	15	15	16	17	12	9	7	15	13	9
	1										1
3	11	19	9	16	92	19	7	1	20	11	15
175	147	107	94	81	82	100	144	139	125	112	119
		7	4	3	11	9	2	1	2	3	
26	19	28	73	94		42	53	45	18	34	9
19	23	17	26	23	21	21	20	23	17	25	13
20	26	18	4	13	9	13	11	9	36	14	48
		1	1	1			4	5	1	4	3
1		1							1		2
				2				1	1		
3	1	1	3		1		2	1	1	1	
1		1							1		1
						1					
							1				
3	2	1	1	1	1	6	1	2	3	3	4
7	12	8	1	3	1	2	6	7	7	14	11
		1			1		2	2			
10	10	11	9	10	10	11	12	11	17	13	20
2		1	2	1	1	3	4	2	5	3	6
1											1
11	3	5	6	18	11	17	7	5	7	8	3
								1		4	
						2					
							11	21		17	
		1		2		1	1	1		1	
313	290	270	277	304	290	277	314	313	293	299	289
19	17	23	18	20	17	19	23	25	21	22	21
4.1550	3.9390	5.6550	4.3070	5.1220	3.9430	4.6240	6.0410	6.3640	4.8650	5.4630	4.8750
0.3279	0.3902	0.4296	0.4234	0.3949	0.4498	0.4835	0.3249	0.3395	0.4076	0.4719	0.4234
1.7750	1.8920	2.2460	2.0310	2.1150	2.0340	2.2180	2.0540	2.1390	2.0980	2.3400	2.1360

220	225	230	235	240	245	250	255	260	265	270	275
7	3	4	1	5	2	3	5	3	3	1	4
6	4	7	5	2	5	3	1	1	1	2	5
6	4	5	5	8	3	3	1	1	3		3
4	2	4	8	21	6	6	4	2	7	6	5
6	10	9	27	39	28	20	31	28	13	25	21
15	14	16	31	12	23	7	28	26	9	16	16
137	142	137	99	97	125	133	129	144	168	163	157
								4	2		
16	18	26	30	19	21	24	16		9	7	23
20	9	25	16	32	15	19	27	14	18	14	13
31	27	26	9	7	10	11	8	9	11	7	16
6	7	1	5	3	4	1					5
2		2		1	2	1	1		4		
	1	1	2		1	2					
	1	1				2	2	1			
	1					2		1			
1	2	1									1
1	9	3	3	3	5	4	1	1	2		1
13	15	3	6		1	1	1	1	1	1	3
	2										
12	14	15	10	2	12	14	5	2	2	6	4
3	4	4	3	3	1	2	3	5	6		7
									1		
			1								
4	6	7	8	15	19	15	22	20	17	29	15
1			1								
			1								
								1			
291	295	297	271	269	283	273	285	264	277	277	299
19	21	20	21	17	19	21	17	19	19	12	17
4.8540	5.1710	4.8390	5.2830	4.0290	4.5680	4.9760	3.9630	4.3670	4.6180	2.5560	3.9080
0.3938	0.3732	0.3801	0.4625	0.4907	0.4258	0.3565	0.3912	0.3004	0.2788	0.3769	0.3782
2.0640	2.0590	2.0280	2.2740	2.1210	2.0910	1.9640	1.8950	1.6880	1.6670	1.5090	1.8610

280	285	290	295	300	305	310	315	320	325	330	335
2	2	4		4	8	3	3	2	4	1	2
1											
			1	2	5	2		2	1	1	2
1		7	4	2	7	3	5	6		5	
1		2					1				
7	4	5	2	5	5	7	7	7	1	1	
13	8	9	4	2	8	4	3	3	5	3	5
3	12	2	3	4	4	8	1	10	8	12	18
201	164	193	219	198	193	198	170	137	160	175	164
1	2					1		1		2	2
36	29	29	29	12	26	14	34	30	38	37	38
5	13	9	5	8	9	8	13	12	4	10	10
16	9	32	29	28	29	36	42	36	33	51	33
											1
1	5						3	3		3	3
					3						
		1					1		1	1	2
1				1							
								1		1	
									1		2
	3	1		1		1	4	7	4		1
				1							
4	1	6	9	10	21	9	11	22	17	13	20
										1	
3	9	5	3	8	6	5	2	12	18	20	10
1	5	2		1	2	2	1	4	1		
	1										
							1				
10	12	7	3	12	2	4	2	4	4	3	7
				2			1				
						1				4	
307	279	314	311	301	328	306	305	299	300	344	320
19	17	17	12	18	15	17	19	19	16	20	17
4.4570	3.9760	3.8450	2.4800	4.2000	3.2420	3.8810	4.4880	4.5020	3.8960	4.6200	3.8310
0.2247	0.3191	0.2772	0.2647	0.2372	0.3385	0.2504	0.2669	0.3929	0.3189	0.2937	0.3449
1.4520	1.6910	1.5500	1.1560	1.4510	1.6250	1.4480	1.6230	2.0100	1.6900	1.7700	1.7690

340	345	350	355	360	365	370	375	380	385	390	395
7	3	8	2	4		6	2	7	3	2	1
		1		1	1			1			
2	1		1	4	4	5	3	2	3		
5	2	7	1	8	2	1	5		5	1	2
							1				
6	5	7	6	12	8	5		12	2	4	4
1	1	8	5	7	5	3	7	8	10	3	5
									1		
19	9	9	15	17	12	19	10	14	22	21	40
148	146	98	112	106	82	102	150	103	24	126	113
4	4	2	6	4		7	6	6	2	4	3
25	42	44	39	21	38	38	48	31	32	42	51
15	6	23	21	34	31	25	22	34	23	15	8
33	23	32	32	28	27	49	37	33	42	14	12
1		3									
		2	1	10	8		3	4	3		
2	1						1	1		1	
2	1		3	1	3	1	1		1	3	1
			9								
			1		2					1	
									2		
2	2	4	1	1							
2	9	4	1		3	2		5	5	1	2
9	18	12	9	11	17	7	14	12	12	2	4
3	2	6	1	1	3			1			
5	14	6	12	16	9	11	15	10	19	25	37
	1	2		1				1		1	
12	13	9	5	4	3	1	3	4	2	7	8
			2	3	4						
		3		1				2		3	
			24	19	44						
1	1		2		3		1				1
304	304	290	311	314	309	282	329	291	213	276	292
21	21	21	24	23	21	17	19	21	19	20	17
5.4340	5.4400	5.1990	6.1190	5.7150	5.4170	3.9630	4.3760	5.1820	5.0450	4.9020	3.9190
0.3361	0.3190	0.4835	0.3847	0.4744	0.5026	0.4588	0.3625	0.4549	0.5972	0.3636	0.4099
2.0010	1.9490	2.3180	2.2230	2.3900	2.4030	2.0540	1.9300	2.2570	2.4290	1.9840	1.9410

400	405	410	415	420	425	430	435	440	445	450	455
10	1	4		3	1		2	2	3		4
3			1	1	2		5	3	5	5	3
	1	2		12			3	3			4
					1	1	1				1
8	4	5	2		1	1	9	7	6	2	14
5	5	2	10	9	7	9	9	6	15	9	25
55	58	146	15	2	17	3	8	2	39	26	28
90	63	37	50	51	22	27	69	93	79	88	60
1	3	3	2	1	3	5	3	4	9	4	8
26	116	50	151	195	120	208	147	87	38	16	58
13	5	17	12	5	2	7	10	22	11	7	35
14	3	7	4	1	3		14	8	14	36	
1	1						1		3	1	1
										1	
									1	1	
1		1	1		2	1	3		2	1	1
		1									1
			1								
										1	
10	4						5	2	4	1	3
5	2	1	3				1	4	10	22	9
30	22	15	9	2	3	3	2	12	31	23	17
		1			2				2		
									1		
3	13	10	22	3	11	3	3	12	41	16	15
2	1		1	3		1		2	2		
	2		1						1		1
277	304	302	285	288	197	269	295	269	317	260	288
18	18	17	17	14	16	13	19	17	22	18	20
4.2880	4.1710	3.5930	3.9550	3.0710	4.1000	2.8500	4.5200	3.9930	5.3370	4.6500	4.5480
0.4864	0.3576	0.3638	0.3098	0.2338	0.2907	0.2023	0.3018	0.4144	0.5246	0.4957	0.5598
2.1700	1.8620	1.7610	1.6610	1.1860	1.5370	0.9668	1.7470	1.9520	2.4460	2.2430	2.3640

460	465	470	475	480	485	490	495	500	505	510	515
1		4						4	4	1	5
	1						1				
2	1	2		1	1		1		3		1
1				1		2					1
				1					1		
5	2	5	2		1	12	4	15	10	3	5
22	5	13	32	17	16	27	14	3	6	2	4
											1
16	18	36	29	21	33	49	77	37	12	15	11
49	7	54	11	14	20	71	102	86	127	118	120
13	4		4	4	2	3	10	3	10	2	4
21	13	21	5	19	7	35	13	5	10	38	24
12	1	16	4	1		13	9	17	11	4	8
		13	2	2	2	11	11	44	52	47	38
			2				2				
					1			1			1
2		3			1	2	2	1			1
1									1		
									1		
										4	1
1		3		2	1				1	6	4
											1
		6				1	2	3	1	5	14
								26		1	
7	2	20	1		1	8	9		23	39	31
			1					4	1	3	
							1		1		
							2				
12	1	6	5	13	9	21	12	14	7	4	11
6						2					
171	55	202	98	96	95	257	272	263	282	292	286
17	11	15	13	12	14	15	18	16	20	16	20
4.2940	4.1350	3.6970	4.0030	3.6200	4.4900	3.4210	4.2430	3.6990	4.4970	3.8850	5.2050
0.6119	0.6139	0.6677	0.5171	0.6127	0.4887	0.6032	0.4199	0.5401	0.3966	0.4219	0.3794
2.2810	1.9100	2.3040	1.9050	1.9950	1.9230	2.2030	2.0230	2.1570	2.0200	1.9700	2.0750

520	525	530	535	540	545	550	555	560	565	570	575
3	2	2	2	2	2	3	1	6	3		3
		1		1		1					
2		8	2	2	1	4	3	1	2	5	3
		2				2					
								1		1	
1			2	4	2	9	5	1	5	4	6
				1							
8	4	8	11	20	22	18	29	7	3	3	8
1											
4	13	15	26	16	4	16	18	23	25	13	18
121	130	107	94	58	31	105	76	92	121	113	112
3	10	3	4	11	3	9	7	8	11	1	3
51	37	37	51	43	14	32	38	38	28	52	52
19	6	26	21	36	14	29	16	14	19	13	18
28	30	14	16	3	2	9	10	19	7	24	27
	1										2
										1	
1		1		2							2
	1	1	1	2	3	3	1		1	2	3
			2		1	1					
						2			1		
	2										
						2					
2	9	7	5	1		2	3	3	3	3	4
1	1		1								
7	5	8	1	2	1	3	7	5	7	13	7
	1	1								1	3
23	16	10	28	12	3	22	28	39	38	14	23
	2	3	2	1	1	1		1	3	2	3
										1	1
					1						
4	11	11	10	11	4	6	17	8	5	2	3
3				1		1	2				
	2					10			14		
	2	1	1			1					
282	285	266	280	229	109	291	261	266	296	268	301
19	21	21	20	21	18	24	17	17	19	19	21
4.5580	5.1710	5.2650	4.5430	5.5710	5.5990	6.1810	4.0470	3.9930	4.4970	4.6720	5.1220
0.3776	0.3741	0.4388	0.4696	0.4834	0.5394	0.4352	0.5784	0.5157	0.4470	0.3679	0.4219
1.9710	2.0610	2.2210	2.1880	2.3180	2.2160	2.3460	2.2860	2.1710	2.1390	1.9450	2.1820

8.2.1.2.D DISTRIBUTION OF MOST ABUNDANT PTEROPOD AND HETEROPOD SPECIES CAR-MON 2 150–500 µm

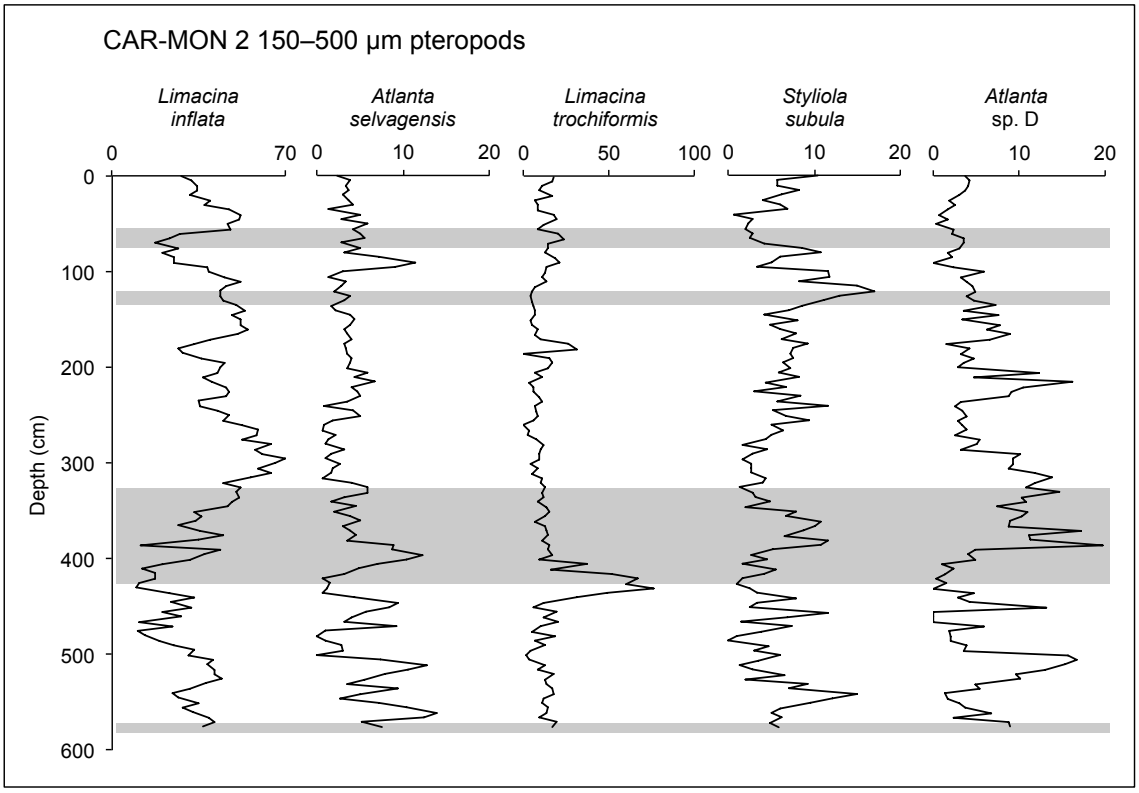

8.2.1.2.E JC18-19 AND JR123-35-V PLANKTIC FORAMINIFERA SPECIES ANALYSIS (**JC18-19)**

JC18-19 >500 µm	2	10	50	75	95	130	180	195	210	280	320	350
Candeina nitida		1			1							
Globigerina bulloides				1								
Globigerinella aequilateralis	1	5	3	17	8	7	1	13	13	14	6	5
Globigerinoides conglobatus	32	35	47	55	73	32	47	40	45	42	43	22
Globigerinoides ruber	2	15		3	1	11	4	1		4	3	
Globigerinoides sacculifer	30	40	6	14	11	23	8	11		12	16	6
Globigerinoides trilobus	8	20	2	1	4	14	6	2	1	5	3	1
Globorotalia crassaformis			12	2	5	2	2		1	2	1	4
Globorotalia menardii	78	55	141	94	47	114	110	121	90	101	172	178
Globorotalia truncatulinoides (sinistral)	1	2			1	1	3	2		1		
Globorotalia truncatulinoides (dextral)	10	1		11	31	11	46	31	34	17	5	5
Globorotalia tumida	11	15	1	1	1		7	4	3			17
Hastigerina pelagica				1								
Neogloboquadrina dutertrei	37	53	77	49	38	38	45	61	65	62	38	28
Orbulina universa	114	78	32	45	71	51	30	32	37	37	36	39
Pulleniatina obliquiloculata	3	6	2	21	12	22	16	7	10	1	7	
Sphaeroidinella dehiscens	3	5	5	4	4	1	2	1	1	4	11	5
Total individuals	330	331	328	319	308	327	327	326	300	302	341	310
Total species	13	14	12	16	16	13	14	13	11	13	12	11

JC18-19 150–500 µm	2	10	50	75	95	130	180	195	210	280	320	350
PTEROPODA												
Cavolinia inflexa	20	6		9	2							
Clio cuspidata		1			1							
Clio pyramidata	4		2	1								
Creseis acicula	5	15	3	5	4							
Creseis virgula	11	18	12	8	11							
Creseis chierchiae	1	1	1	1								
Diacria quadridentata	1	1	85	15	10							
Diacria trispinosa	6	4	10	5								
Limacina bulimoides	16	8	15	4	13							
Limacina inflata	94	98	20	134	147							
Limacina lesueuri	5	7	5		4							
Limacina trochiformis	44	43	104	72	31							
Styliola subula	30	13	2	14	21							
Gleba cordata	11	15	4	12	33							
Peracle diversa	2				1							
Peracle moluccensis	2	4			2							
Gymnosome veliger		1										
HETEROPODA												
Atlanta brunnea			1	1	1							
Atlanta gaudichaudi	1											
Atlanta helicinoides	7	6		6	7							
Atlanta inclinata	1	2										
Atlanta peronii	4	3		1	11							
Atlanta rosea	7	1			2							
Atlanta selvagensis	2	6	1	1	7							
Atlanta turriculata				2								
Atlanta plana				1	1							
Carinaria challengeri	3	1			1							
Carinaria lamarcki	15	14	28	15	12							
Carinaria spp.					1							
Firoloida desmaresti	16	28		1								
Oxygyrus keraudreni			1									
Janthina spp.		3	1	1								
TOTAL	308	299	295	309	323	0	0	0	0	0	0	0
number of species	25	25	18	22	22	0	0	0	0	0	0	0
Fisher alpha	6.0860	5.8270	3.6310	4.7850	5.3420							
Evenness	0.4829	0.4598	0.3976	0.3313	0.3566							
Shannon Weiner	2.4500	2.3590	1.8500	1.8910	2.0600							

8.2.1.2.E JC18-19 AND JR123-35-V PLANKTIC FORAMINIFERA SPECIES ANALYSIS **(JR123-35-V)**

JR123-35-V >500 µm	10	80	151	190	235	305	435	485
Candeina nitida	1					1		
Globigerinella aequilateralis	11	1	5	7		11	8	6
Globigerinoides conglobatus	27	42	12	29	7	42	28	37
Globigerinoides ruber	7	5	1	18		3	1	3
Globigerinoides sacculifer	49	51	9	20		13	8	6
Globigerinoides trilobus	14	24	4	5	8	8	3	1
Globorotalia crassaformis				10			17	
Globorotalia flexuosa	4	17				62	75	2
Globorotalia menardii	37	1					3	79
Globorotalia truncatulinoides (sinistral)		1	2	8				
Globorotalia truncatulinoides (dextral)	11	13	5	6		10	1	6
Neogloboquadrina dutertrei	52	105	44	123	3	112	118	35
Orbulina universa	93	41	32	89	8	43	44	33
Pulleniatina obliquiloculata	2	11	4	5	4		3	11
Sphaeroidinella dehiscens	2		1	1				3
Total individuals	310	312	119	321	30	305	309	222
Total species	13	11	10	11	5	10	12	12

JR123-35-V 150–500 µm	10	80	151	190	235	305	435	485
PTEROPODA								
Cavolinia inflexa	10	2	11	13	3	6	2	2
Clio pyramidata	1	1	4		3	6	1	1
Creseis acicula	11	4	12	3	5	13	4	4
Creseis virgula	13	8	9	9	9	7	5	7
Creseis chierchiae	1			1	7	3	2	
Diacria quadridentata	1	3	5	3	1	7	11	6
Diacria trispinosa	3		3	1	1		1	
Hyalostylus striata				1				
Limacina bulimoides	18	9	12	33	27	5	10	2
Limacina inflata	88	143	110	153	123	131	154	189
Limacina lesueuri		1		2		1		
Limacina trochiformis	31	51	25	20	1	18	19	21
Styliola subula	26	13	51	19	32	24	33	9
Peraclis moluccensis	6		9	8	8	8	6	4
Paedoclione doliiformis		1			1		1	1
Gymnosome veliger	6	2	1	2	2	3		
HETEROPODA								
Atlanta fusca	3							
Atlanta gaudichaudi				2	1	1	1	2
Atlanta helicinoides	8	7	4	2	4	9	3	
Atlanta inclinata					4	1		
Atlanta peronii	12	15	18	14	18	15	9	16
Atlanta rosea	7	6	5	3	4	3		2
Atlanta selvagensis	4	11	4	10	12	11	8	2
Atlanta turriculata				1		3	3	2
Carinaria lamarcki	5	4		2	2	3	9	9
Carinaria pseudorugosa			8	3	2			
Carinaria spp.	1		2	2	2			
Firoloida desmaresti	36	9			3			
Oxygyrus keraudreni			1	1	2			
Janthia spp.	3							
TOTAL	291	290	294	308	277	278	282	279
number of species	23	20	22	26	26	23	21	20
Fisher alpha	5.1930	4.2470	4.5390	6.0860	6.6650	5.2710	4.5980	4.2980
Evenness	0.5282	0.3527	0.4662	0.3046	0.3399	0.3941	0.3151	0.2249
Shannon Weiner	2.4060	1.8480	2.1810	1.9890	2.1400	2.1130	1.7900	1.3980

8.2.1.2.F JC18-19 AND JR123-35-V PTEROPOD AND HETEROPOD SPECIES ANALYSIS **(JC18-19)**

JC18-19 >500 µm	2	10	50	75	95	130	180	195	210	280	320	350
PTEROPODA												
Cavolinia inflexa					1							
Clio pyramidata					1							
Creseis acicula		2										
Diacavolinia longirostris	1	1										
Diacria quadridentata					4							
Diacria trispinosa				1								
Hyalostylus striata					2							
Limacina bulimoides	5	1			6							
Limacina inflata	25	11			6							
Limacina lesueuri	1				2							
Styliola subula	5	2			4							
Peracle moluccensis					3							
Peracle reticulata					1							
HETEROPODA												
Atlanta inclinata		1										
Carinaria lamarcki					1							
Firoloida desmaresti	1											
Janthina spp.	2											
TOTAL	40	18	0	1	31	0	0	0	0	0	0	0
number of species	7	6	0	1	11	0	0	0	0	0	0	0

JC18-19 150–500 µm	2	10	50	75	95	130	180	195	210	280	320	350
PTEROPODA												
Cavolinia inflexa	20	6		9	2							
Clio cuspidata		1			1							
Clio pyramidata	4		2	1								
Creseis acicula	5	15	3	5	4							
Creseis virgula	11	18	12	8	11							
Creseis chierchiae	1	1	1	1								
Diacria quadridentata	1	1	85	15	10							
Diacria trispinosa	6	4	10	5								
Limacina bulimoides	16	8	15	4	13							
Limacina inflata	94	98	20	134	147							
Limacina lesueuri	5	7	5		4							
Limacina trochiformis	44	43	104	72	31							
Styliola subula	30	13	2	14	21							
Gleba cordata	11	15	4	12	33							
Peracle moluccensis	2	4			2							
Peracle reticulata	2				1							
Gymnosome veliger		1										
HETEROPODA												
Atlanta brunnea			1	1	1							
Atlanta gaudichaudi	1											
Atlanta helicinoides	7	6		6	7							
Atlanta inclinata	1	2										
Atlanta peronii	4	3		1	11							
Atlanta rosea	7	1			2							
Atlanta selvagensis	2	6	1	1	7							
Atlanta turriculata				2								
Atlanta plana				1	1							
Carinaria challengeri	3	1			1							
Carinaria lamarcki	15	14	28	15	12							
Carinaria spp.					1							
Firoloida desmaresti	16	28		1								
Oxygyrus keraudreni			1									
Janthina spp.		3	1	1								
TOTAL	308	299	295	309	323	0	0	0	0	0	0	0
number of species	25	25	18	22	22	0	0	0	0	0	0	0
Fisher alpha	6.0860	5.8270	3.6310	4.7850	5.3420							
Evenness	0.4829	0.4598	0.3976	0.3313	0.3566							
Shannon Weiner	2.4500	2.3590	1.8500	1.8910	2.0600							

8.2.1.2.F JC18-19 AND JR123-35-V PTEROPOD AND HETEROPOD SPECIES ANALYSIS **(JR123-35-V)**

JR123-35-V >500 µm	10	80	151	190	235	305	435	485
PTEROPODA								
Cavolinia inflexa	2			3	1	1	1	
Clio pyramidata				1				
Creseis virgula	1	2		3		1		
Diacria quadridentata					1	3	3	5
Diacria trispinosa			1					
Hyalostylus striata				2				1
Limacina bulimoides	3	2	4	3			1	1
Limacina inflata	37	79	61	65	11	24	8	19
Limacina lesueuri		1		1				
Limacina trochiformis		1						
Styliola subula	2	6	8	3	3	3	3	
HETEROPODA								
Atlanta helicinoides			3					
Atlanta inclinata		1			1	1		1
Atlanta peronii		1	3					
Atlanta rosea		2	1					
Atlanta selvagensis				1		1		
Atlanta turriculata				1			1	
Carinaria lamarcki		2				1		
Oxygyrus keraudreni		1						
TOTAL	45	98	81	83	17	35	17	27
number of species	5	11	7	10	5	8	6	5

JR123-35-V 150–500 µm	10	80	151	190	235	305	435	485
PTEROPODA								
Cavolinia inflexa	10	2	11	13	3	6	2	2
Clio pyramidata	1	1	4		3	6	1	1
Creseis acicula	11	4	12	3	5	13	4	4
Creseis virgula	13	8	9	9	9	7	5	7
Creseis chierchiae	1			1	7	3	2	
Diacria quadridentata	1	3	5	3	1	7	11	6
Diacria trispinosa	3		3	1	1		1	
Hyalostylus striata				1				
Limacina bulimoides	18	9	12	33	27	5	10	2
Limacina inflata	88	143	110	153	123	131	154	189
Limacina lesueuri		1		2		1		
Limacina trochiformis	31	51	25	20	1	18	19	21
Styliola subula	26	13	51	19	32	24	33	9
Peraclis moluccensis	6		9	8	8	8	6	4
Paedoclione doliiformis		1			1		1	1
Gymnosome veliger	6	2	1	2	2	3		
HETEROPODA								
Atlanta fusca	3							
Atlanta gaudichaudi				2	1		1	1
Atlanta helicinoides	8	7	4	2	4	9	3	
Atlanta inclinata					4	1		
Atlanta peronii	12	15	18	14	18	15	9	16
Atlanta rosea	7	6	5	3	4	3		2
Atlanta selvagensis	4	11	4	10	12	11	8	2
Atlanta turriculata				1		3	3	2
Atlanta plana						1		1
Carinaria lamarcki	5	4		2	2	3	9	9
Carinaria pseudorugosa			8	3	2			
Carinaria spp.	1		2	2	2			
Firoloida desmaresti	36	9			3			
Oxygyrus keraudreni			1	1	2			
Janthia spp.	3							
TOTAL	291	290	294	308	277	278	282	279
number of species	23	20	22	26	26	23	21	21
Fisher alpha	5.1930	4.2470	4.5390	6.0860	6.6650	5.2710	4.5980	4.2980
Evenness	0.5282	0.3527	0.4662	0.3046	0.3399	0.3941	0.3151	0.2249
Shannon Weiner	2.4060	1.8480	2.1810	1.9890	2.1400	2.1130	1.7900	1.3980

8.2.1.2.G CAR-MON 2 PLANKTIC FORAMINIFERA ABUNDANCE >500 µm

Mid-Sample depth (cm)	Weight before picking (g)	Unpicked weight (g)	Picked weight (g)	Number of planktic foraminifera	Foraminifera per gram	Foraminifera fragments	Broken but counted foraminifera	Fragment to whole ratio	Number of *G. menardii*	% *G. menardii*
0.5	0.149	0.0727	0.076	305	4003	6	25	9.97	74	24.26
5.5	0.111	0.0629	0.049	304	6268	11	26	11.75	85	27.96
10.5	0.082	0.0248	0.057	308	5432	8	24	10.13	75	24.35
15.5	0.109	0.0408	0.068	359	5256	8	35	11.72	111	30.92
20.5	0.112	0.0489	0.063	313	4976	7	16	7.19	56	17.89
25.5	0.08	0.0075	0.072	321	4458	8	28	10.94	55	17.13
30.5	0.124	0.0103	0.114	356	3128	5	28	9.14	36	10.11
35.5	0.116	0.0199	0.096	304	3154	5	31	11.65	14	4.61
40.5	0.109	0.0125	0.097	315	3251	4	19	7.21	8	2.54
45.5	0.126	0.0481	0.078	322	4128	7	25	9.73	5	1.55
50.5	0.179	0.0987	0.08	301	3772	7	29	11.69	5	1.66
55.5	0.174	0.0728	0.101	313	3108	3	19	6.96	14	4.47
60.5	0.169	0.0839	0.085	313	3687	5	23	8.81	1	0.32
65.5	0.097	0.0319	0.065	320	4954	4	23	8.33	4	1.25
70.5	0.158	0.0000	0.158	322	2035	4	22	7.98	3	0.93
75.5	0.243	0.1123	0.131	355	2708	6	30	9.97	1	0.28
80.5	0.273	0.0502	0.223	310	1389	3	22	7.99	4	1.29
85.5	0.132	0.0663	0.0657	338	5145	8	27	10.12	6	1.78
90.5	0.0634	0.0000	0.0634	582	9180	7	15	3.74	14	2.41
95.5	0.5770	0.0225	0.5545	303	546	15	9	7.55	11	3.63
100.5	0.0170	0.0000	0.0170	82	4824	6	2	9.09	2	2.44
105.5	0.0445	0.0000	0.0445	181	4067	12	12	12.44	2	1.10
110.5	0.0298	0.0000	0.0298	193	6477	0	10	5.18	5	2.59
115.5	0.0564	0.0000	0.0564	267	4734	16	17	11.66	8	3.00
120.5	0.0572	0.0109	0.0463	314	6782	11	10	6.46	4	1.27
125.5	0.0863	0.0322	0.0541	309	5712	20	15	10.64	5	1.62
130.5	0.0582	0.0150	0.0432	326	7546	20	14	9.83	6	1.84
135.5	0.0490	0.0075	0.0415	305	7349	10	12	6.98	20	6.56
140.5	0.0607	0.0280	0.0327	304	9297	14	11	7.86	28	9.21
145.5	0.0682	0.0245	0.0437	312	7140	17	17	10.33	19	6.09
150.5	0.0540	0.0050	0.0490	303	6184	14	14	8.83	6	1.98
155.5	0.026	0.0000	0.026	224	8750	19	8	11.11	43	19.20

Mid-Sample depth (cm)	Weight before picking (g)	Unpicked weight (g)	Picked weight (g)	Number of planktic foraminifera	Foraminifera per gram	Foraminifera fragments	Broken but counted foraminifera	Fragment to whole ratio	Number of *G. menardii*	% *G. menardii*
160.5	0.049	0.0125	0.037	309	8420	40	14	15.47	54	17.48
165.5	0.045	0.0061	0.0390	306	7846	19	16	10.77	92	30.07
170.5	0.039	0.0032	0.0354	311	8785	15	14	8.90	78	25.08
175.5	0.026	0.0000	0.0260	179	6885	18	7	12.69	46	25.70
180.5	0.113	0.0447	0.0682	317	4648	3	4	2.19	124	39.12
185.5	0.036	0.0000	0.0358	285	7961	22	18	13.03	96	33.68
190.5	0.0300	0.0000	0.0300	232	7733	9	12	8.71	85	36.64
195.5	0.1274	0.0527	0.0747	303	4056	6	22	9.06	164	54.13
200.5	0.1337	0.0751	0.0586	301	5137	5	17	7.19	130	43.19
205.5	0.0929	0.0471	0.0458	314	6856	6	9	4.69	158	50.32
210.5	0.0910	0.0458	0.0452	303	6704	5	16	6.82	129	42.57
215.5	0.0537	0.0064	0.0473	313	6617	10	23	10.22	167	53.35
220.5	0.0449	0.0000	0.0449	306	6815	10	23	10.44	144	47.06
225.5	0.0265	0.0000	0.0265	194	7321	6	10	8.00	92	47.42
230.5	0.0249	0.0000	0.0249	188	7550	10	2	6.06	77	40.96
235.5	0.0386	0.0000	0.0386	260	6736	10	6	5.93	108	41.54
240.5	0.0840	0.0319	0.0521	333	6392	8	6	4.11	184	55.26
245.5	0.0310	0.0000	0.031	223	7194	4	10	6.17	80	35.87
250.5	0.029	0.0000	0.029	258	8958	23	12	12.46	84	32.56
255.5	0.039	0.0000	0.039	298	7621	3	15	5.98	104	34.90
260.5	0.034	0.0000	0.034	264	7697	14	20	12.23	79	29.92
265.5	0.039	0.0000	0.039	298	7583	7	18	8.20	81	27.18
270.5	0.036	0.0000	0.036	301	8338	6	14	6.51	84	27.91
275.5	0.047	0.0059	0.041	316	7689	10	34	13.50	131	41.46
280.5	0.04	0.0000	0.04	296	7494	4	28	10.67	118	39.86
285.5	0.054	0.0077	0.047	314	6753	9	30	12.07	165	52.55
290.5	0.057	0.0000	0.057	228	3993	1	22	10.04	113	49.56
295.5	0.037	0.0000	0.037	198	5380	6	11	8.33	79	39.90
300.5	0.026	0.0000	0.026	49	1899	0	9	18.37	14	28.57
305.5	0.026	0.0000	0.026	92	3594	2	7	9.57	26	28.26
310.5	0.033	0.0000	0.033	68	2067	5	7	16.44	29	42.65
315.5	0.035	0.0000	0.035	73	2068	2	6	10.67	22	30.14

Mid-Sample depth (cm)	Weight before picking (g)	Unpicked weight (g)	Picked weight (g)	Number of planktic foraminifera	Foraminifera per gram	Foraminifera fragments	Broken but counted foraminifera	Fragment to whole ratio	Number of *G. menardii*	% *G. menardii*
320.5	0.028	0.0000	0.028	32	1164	1	3	12.12	0	0.00
325.5	0.024	0.0000	0.024	158	6583	2	4	3.75	0	0.00
330.5	0.0550	0.0000	0.0550	318	5782	13	15	8.46	1	0.31
335.5	0.0283	0.0000	0.0283	125	4417	8	12	15.04	0	0.00
340.5	0.0508	0.0000	0.0508	253	4980	6	45	19.69	2	0.79
345.5	0.0300	0.0000	0.0300	157	5233	4	21	15.53	0	0.00
350.5	0.0721	0.0000	0.0721	267	3703	2	38	14.87	4	1.50
355.5	0.1052	0.0000	0.1052	112	1065	2	8	8.77	0	0.00
360.5	0.1395	0.0000	0.1395	147	1054	5	12	11.18	4	2.72
365.5	0.0481	0.0000	0.0481	50	1040	1	8	17.65	0	0.00
370.5	0.0094	0.0000	0.0094	33	3511	0	8	24.24	7	21.21
375.5	0.0220	0.0000	0.0220	111	5045	0	13	11.71	32	28.83
380.5	0.0571	0.0000	0.0571	201	3520	11	23	16.04	44	21.89
385.5	0.027	0.0000	0.0274	112	4088	3	19	19.13	27	24.11
390.5	0.045	0.0065	0.0381	299	7848	3	40	14.24	97	32.44
395.5	0.035	0.0000	0.0354	154	4350	2	13	9.62	49	31.82
400.5	0.025	0.0000	0.0246	108	4390	10	11	17.80	51	47.22
405.5	0.084	0.0000	0.0843	192	2278	2	19	10.82	65	33.85
410.5	0.072	0.0000	0.0720	544	7556	15	63	13.95	184	33.82
415.5	0.064	0.0180	0.046	327	7109	2	25	8.21	72	22.02
420.5	0.016	0.0000	0.016	106	6795	4	4	7.27	16	15.09
425.5	0.025	0.0000	0.025	156	6341	4	23	16.88	17	10.90
430.5	0.007	0.0000	0.007	41	6308	0	4	9.76	7	17.07
435.5	0.021	0.0000	0.021	110	5238	6	10	13.79	22	20.00
440.5	0.019	0.0000	0.019	107	5753	1	17	16.67	18	16.82
445.5	0.014	0.0000	0.014	91	6408	1	8	9.78	31	34.07
450.5	0.044	0.0000	0.044	188	4273	6	11	8.76	41	21.81
455.5	0.026	0.0000	0.026	162	6353	4	13	10.24	42	25.93
460.5	0.023	0.0000	0.023	193	8355	5	15	10.10	45	23.32
465.5	0.0200	0.0000	0.02	161	8050	4	15	11.52	45	27.95
470.5	0.051	0.0068	0.044	301	6810	20	40	18.69	147	48.84
475.5	0.048	0.0000	0.048	320	6639	3	23	8.05	197	61.56

Mid-Sample depth (cm)	Weight before picking (g)	Unpicked weight (g)	Picked weight (g)	Number of planktic foraminifera	Foraminifera per gram	Foraminifera fragments	Broken but counted foraminifera	Fragment to whole ratio	Number of *G. menardii*	% *G. menardii*
480.5	0.037	0.0000	0.037	295	7995	6	30	11.96	128	43.39
485.5	0.03	0.0000	0.03	235	7730	10	13	9.39	100	42.55
490.5	0.035	0.0000	0.035	291	8267	2	16	6.14	103	35.40
495.5	0.0312	0.0000	0.0312	249	7981	4	23	10.67	75	30.12
500.5	0.0449	0.0046	0.0403	330	8189	5	27	9.55	127	38.48
505.5	0.0405	0.0000	0.0405	350	8642	6	28	9.55	86	24.57
510.5	0.0303	0.0000	0.0303	229	7558	2	14	6.93	86	37.55
515.5	0.0449	0.0000	0.0449	281	6258	5	18	8.04	84	29.89
520.5	0.0129	0.0000	0.0129	67	5194	2	12	20.29	22	32.84
525.5	0.0492	0.0000	0.0492	270	5488	8	34	15.11	105	38.89
530.5	0.0202	0.0000	0.0202	152	7525	3	15	11.61	43	28.29
535.5	0.0201	0.0000	0.0201	147	7313	3	15	12.00	54	36.73
540.5	0.0192	0.0000	0.0192	121	6302	2	16	14.63	61	50.41
545.5	0.0242	0.0000	0.0242	177	7314	6	25	16.94	68	38.42
550.5	0.0440	0.0000	0.0440	311	7068	6	45	16.09	114	36.66
555.5	0.0276	0.0000	0.0276	222	8043	1	18	8.52	87	39.19
560.5	0.0466	0.0100	0.0366	305	8333	8	30	12.14	95	31.15
565.5	0.1874	0.1111	0.0763	323	4233	8	26	10.27	116	35.91
570.5	0.0115	0.0000	0.0115	63	5478	1	10	17.19	16	25.40
575.5	0.0111	0.0000	0.0111	59	5315	0	7	11.86	14	23.73

8.2.1.2.G CAR-MON 2 PLANKTIC FORAMINIFERA ABUNDANCE 150–500 µm

Mid-Sample depth (cm)	Weight before picking (g)	Unpicked weight (g)	Picked weight (g)	Number of planktic foraminifera	Foraminifera per gram	Foraminifera fragments	Broken but counted foraminifera	Fragment to whole ratio	Number of *G. menardii*	% *G. menardii*
0.5	0.3186	0.3028	0.0158	331	20949	76	13	21.87	8	2.42
5.5	0.3912	0.3787	0.0125	315	25200	64	4	17.94	9	2.86
10.5	0.3144	0.2990	0.0154	326	21169	47	12	15.82	16	4.91
15.5	0.4080	0.3932	0.0148	314	21216	43	6	13.73	11	3.50
20.5	0.3367	0.3233	0.0134	301	22463	57	9	18.44	7	2.33
25.5	0.3438	0.3280	0.0158	320	20253	43	11	14.88	9	2.81
30.5	0.5150	0.4988	0.0162	325	20062	47	10	15.32	3	0.92
35.5	0.6178	0.6024	0.0154	310	20130	31	10	12.02	3	0.97
40.5	0.7130	0.6949	0.0181	309	17072	25	14	11.68	3	0.97
45.5	0.7957	0.7782	0.0175	332	18971	23	7	8.45	0	0.00
50.5	1.3543	1.3379	0.0164	305	18598	24	7	9.42	1	0.33
55.5	0.8257	0.8080	0.0177	315	17797	21	16	11.01	5	1.59
60.5	0.7634	0.7442	0.0192	324	16875	30	9	11.02	2	0.62
65.5	0.8435	0.8283	0.0152	311	20461	32	7	11.37	0	0.00
70.5	0.6429	0.6283	0.0146	304	20822	44	0	12.64	0	0.00
75.5	0.4939	0.4757	0.0182	305	16758	30	8	11.34	2	0.66
80.5	0.5248	0.5021	0.0227	339	14934	27	12	10.66	0	0.00
85.5	1.7230	1.7071	0.0159	308	19371	37	9	13.33	3	0.97
90.5	1.2157	1.1371	0.0786	3301	41997	525	21	14.27	4	0.12
95.5	0.5791	0.5686	0.0105	306	29143	68	4	19.25	1	0.33
100.5	0.0925	0.0850	0.0075	363	48400	52	0	12.53	1	0.28
105.5	0.2030	0.1929	0.0101	313	30990	36	5	11.75	0	0.00
110.5	0.2182	0.2067	0.0115	319	27739	57	6	16.76	1	0.31
115.5	0.2568	0.2449	0.0119	303	25462	63	1	17.49	2	0.66
120.5	0.2552	0.2393	0.0159	307	19308	77	13	23.44	3	0.98
125.5	0.2971	0.2850	0.0121	315	26033	69	8	20.05	5	1.59
130.5	0.2480	0.2331	0.0149	325	21812	46	12	15.63	2	0.62
135.5	0.2596	0.2437	0.0159	316	19874	63	7	18.47	3	0.95
140.5	0.2593	0.2442	0.0151	306	20265	59	8	18.36	14	4.58
145.5	0.2621	0.2508	0.0113	345	30531	36	8	11.55	7	2.03
150.5	0.1620	0.1497	0.0123	312	25366	49	6	15.24	2	0.64

Mid-Sample depth (cm)	Weight before picking (g)	Unpicked weight (g)	Picked weight (g)	Number of planktic foraminifera	Foraminifera per gram	Foraminifera fragments	Broken but counted foraminifera	Fragment to whole ratio	Number of *G. menardii*	% *G. menardii*
155.5	0.9840	0.0849	0.8991	391	435	68	3	15.47	34	8.70
160.5	0.1012	0.0931	0.0081	311	38395	51	2	14.64	15	4.82
165.5	0.1583	0.1456	0.0127	303	23858	55	8	17.60	34	11.22
170.5	0.1650	0.1552	0.0098	300	30612	33	7	12.01	19	6.33
175.5	0.0841	0.0718	0.0123	409	33252	65	5	14.77	24	5.87
180.5	0.4381	0.4156	0.0225	300	13333	24	10	10.49	43	14.33
185.5	0.1150	0.1064	0.0086	331	38488	47	6	14.02	19	5.74
190.5	0.0976	0.0882	0.0094	310	32979	40	6	13.14	28	9.03
195.5	0.3507	0.3401	0.0106	346	32642	36	15	13.35	26	7.51
200.5	0.4276	0.4116	0.0160	327	20438	33	4	10.28	46	14.07
205.5	0.1719	0.1603	0.0116	304	26207	46	9	15.71	37	12.17
210.5	0.3328	0.3180	0.0148	312	21081	27	10	10.91	42	13.46
215.5	0.1589	0.1445	0.0144	354	24583	56	8	15.61	62	17.51
220.5	0.1615	0.1479	0.0136	304	22353	52	15	18.82	58	19.08
225.5	0.0837	0.0607	0.0230	314	13652	47	8	15.24	49	15.61
230.5	0.1061	0.0931	0.0130	311	23923	44	7	14.37	63	20.26
235.5	0.1145	0.0994	0.0151	318	21060	53	7	16.17	48	15.09
240.5	0.2052	0.1941	0.0111	286	25766	37	10	14.55	47	16.43
245.5	0.0970	0.0848	0.0122	310	25410	30	7	10.88	34	10.97
250.5	0.0882	0.0764	0.0118	324	27458	58	11	18.06	33	10.19
255.5	0.1131	0.1064	0.0067	306	45672	40	4	12.72	15	4.90
260.5	0.1147	0.1044	0.0103	316	30680	49	9	15.89	14	4.43
265.5	0.1697	0.1588	0.0109	314	28807	53	7	16.35	20	6.37
270.5	0.2230	0.2139	0.0091	292	32088	40	10	15.06	14	4.79
275.5	0.2413	0.2300	0.0113	322	28496	60	6	17.28	20	6.21
280.5	0.1959	0.1818	0.0141	342	24255	60	10	17.41	35	10.23
285.5	0.2545	0.2440	0.0105	318	30286	34	4	10.80	28	8.81
290.5	0.3520	0.3363	0.0157	301	19172	45	11	16.18	36	11.96
295.5	0.5073	0.4885	0.0188	326	17340	44	16	16.22	25	7.67
300.5	0.3440	0.3231	0.0209	304	14545	45	5	14.33	18	5.92
305.5	0.3643	0.3453	0.0190	303	15947	50	8	16.43	21	6.93

Mid-Sample depth (cm)	Weight before picking (g)	Unpicked weight (g)	Picked weight (g)	Number of planktic foraminifera	Foraminifera per gram	Foraminifera fragments	Broken but counted foraminifera	Fragment to whole ratio	Number of *G. menardii*	% *G. menardii*
310.5	0.3974	0.3753	0.0221	317	14344	59	10	18.35	18	5.68
315.5	0.5567	0.5335	0.0232	301	12974	44	9	15.36	27	8.97
320.5	0.3441	0.3290	0.0151	306	20265	30	1	9.23	0	0.00
325.5	0.4279	0.4111	0.0168	346	20595	34	16	13.16	0	0.00
330.5	0.6410	0.6254	0.0156	318	20385	33	11	12.54	2	0.63
335.5	0.3008	0.2872	0.0136	307	22574	43	7	14.29	0	0.00
340.5	0.3723	0.3584	0.0139	389	27986	68	6	16.19	0	0.00
345.5	0.2764	0.2612	0.0152	312	20526	39	14	15.10	0	0.00
350.5	0.4924	0.4748	0.0176	337	19148	49	12	15.80	1	0.30
355.5	0.5834	0.5317	0.0517	325	6286	11	13	7.14	1	0.31
360.5	0.5423	0.5134	0.0289	322	11142	10	6	4.82	0	0.00
365.5	0.4034	0.3487	0.0547	318	5814	17	12	8.66	0	0.00
370.5	0.0864	0.0744	0.0120	303	25250	11	5	5.10	11	3.63
375.5	0.1868	0.1745	0.0123	365	29675	30	5	8.86	25	6.85
380.5	0.2742	0.2604	0.0138	311	22536	24	8	9.55	32	10.29
385.5	0.2224	0.2086	0.0138	322	23333	28	7	10.00	26	8.07
390.5	0.5158	0.5040	0.0118	365	30932	33	6	9.80	17	4.66
395.5	0.4911	0.4762	0.0149	302	20268	26	10	10.98	30	9.93
400.5	0.6810	0.6608	0.0202	312	15446	34	10	12.72	17	5.45
405.5	1.7349	1.6891	0.0458	328	7162	26	12	10.73	31	9.45
410.5	0.7354	0.7232	0.0122	331	27131	28	11	10.86	36	10.88
415.5	0.5776	0.5633	0.0143	368	25734	27	19	11.65	42	11.41
420.5	0.3056	0.2910	0.0146	302	20685	23	2	7.69	13	4.30
425.5	0.2203	0.2087	0.0116	315	27155	32	14	13.26	23	7.30
430.5	0.1238	0.1067	0.0171	364	21287	30	7	9.39	25	6.87
435.5	0.1798	0.1655	0.0143	303	21189	22	5	8.31	16	5.28
440.5	0.2431	0.2297	0.0134	300	22388	26	4	9.20	26	8.67
445.5	0.1549	0.1435	0.0114	322	28246	47	13	16.26	27	8.39
450.5	0.1686	0.1598	0.0088	331	37614	19	5	6.86	19	5.74
455.5	0.1535	0.1403	0.0132	315	23864	28	11	11.37	23	7.30
460.5	0.2176	0.2085	0.0091	313	34396	40	3	12.18	21	6.71

Mid-Sample depth (cm)	Weight before picking (g)	Unpicked weight (g)	Picked weight (g)	Number of planktic foraminifera	Foraminifera per gram	Foraminifera fragments	Broken but counted foraminifera	Fragment to whole ratio	Number of *G. menardii*	% *G. menardii*
465.5	0.1865	0.1733	0.0132	314	23788	22	8	8.93	18	5.73
470.5	0.2419	0.2270	0.0149	453	30403	55	13	13.39	39	8.61
475.5	0.1622	0.1445	0.0177	341	19266	42	16	15.14	99	29.03
480.5	0.1435	0.1311	0.0124	347	27984	75	13	20.85	59	17.00
485.5	0.1368	0.1224	0.0144	305	21181	45	15	17.14	74	24.26
490.5	0.1380	0.1260	0.0120	318	26500	54	14	18.28	45	14.15
495.5	0.1424	0.1285	0.0139	320	23022	20	9	8.53	55	17.19
500.5	0.1976	0.1882	0.0094	306	32553	64	6	18.92	26	8.50
505.5	0.2226	0.2100	0.0126	328	26032	50	15	17.20	39	11.89
510.5	0.2565	0.2444	0.0121	309	25537	28	6	10.09	29	9.39
515.5	0.4159	0.4031	0.0128	304	23750	23	8	9.48	32	10.53
520.5	0.1346	0.1257	0.0089	301	33820	37	3	11.83	38	12.62
525.5	0.2728	0.2587	0.0141	320	22695	33	21	15.30	65	20.31
530.5	0.1647	0.1504	0.0143	302	21119	48	6	15.43	32	10.60
535.5	0.1796	0.1702	0.0094	316	33617	31	23	15.56	56	17.72
540.5	0.1719	0.1637	0.0082	318	38780	31	9	11.46	47	14.78
545.5	0.2144	0.1992	0.0152	329	21645	45	32	20.59	67	20.36
550.5	0.4982	0.4859	0.0123	314	25528	34	25	16.95	47	14.97
555.5	0.2812	0.2729	0.0083	317	38193	44	15	16.34	33	10.41
560.5	0.4840	0.4742	0.0098	306	31224	22	11	10.06	31	10.13
565.5	1.3125	1.3000	0.0125	312	24960	22	17	11.68	35	11.22
570.5	0.1580	0.1510	0.0070	323	46143	34	7	11.48	19	5.88
575.5	0.0976	0.0857	0.0119	306	25714	33	11	12.98	43	14.05

8.2.1.2.H CAR-MON 2 PTEROPOD AND HETEROPOD ABUNDANCE >500 µm

Mid-Sample depth (cm)	Weight before picking (g)	Unpicked weight (g)	Picked weight (g)	Number of pteropods	Pteropods per gram
0.5	0.1489	0.0000	0.1489	8	54
5.5	0.1114	0.0000	0.1114	11	99
10.5	0.0815	0.0000	0.0815	50	613
15.5	0.1091	0.0000	0.1091	84	770
20.5	0.1118	0.0000	0.1118	15	134
25.5	0.0795	0.0000	0.0795	95	1195
30.5	0.1241	0.0000	0.1241	237	1910
35.5	0.1163	0.0000	0.1163	259	2227
40.5	0.1094	0.0000	0.1094	115	1051
45.5	0.1261	0.0000	0.1261	148	1174
50.5	0.1785	0.0000	0.1785	172	964
55.5	0.1735	0.0000	0.1735	276	1591
60.5	0.1688	0.0000	0.1688	226	1339
65.5	0.0965	0.0000	0.0965	145	1503
70.5	0.1582	0.0593	0.0989	303	3064
75.5	0.2434	0.1123	0.1311	306	2334
80.5	0.2734	0.0863	0.1871	313	1673
85.5	0.132	0.0000	0.1320	118	894
90.5	0.0634	0.0000	0.0634	22	347
95.5	0.0577	0.0000	0.0577	17	295
100.5	0.0170	0.0000	0.0170	37	2176
105.5	0.0445	0.0000	0.0445	68	1528
110.5	0.0298	0.0000	0.0298	40	1342
115.5	0.0564	0.0000	0.0564	43	762
120.5	0.0572	0.0000	0.0572	38	664
125.5	0.0863	0.0000	0.0863	60	695
130.5	0.0582	0.0000	0.0582	34	584
135.5	0.0490	0.0000	0.0490	22	449
140.5	0.0607	0.0000	0.0607	20	329
145.5	0.0682	0.0000	0.0682	54	792
150.5	0.0540	0.0000	0.0540	32	593
155.5	0.0256	0.0000	0.0256	10	391
160.5	0.0492	0.0000	0.0492	47	955
165.5	0.0451	0.0000	0.0451	14	310
170.5	0.0386	0.0000	0.0386	4	104
175.5	0.0260	0.0000	0.0260	0	0
180.5	0.1129	0.0000	0.1129	2	18
185.5	0.0358	0.0000	0.0358	2	56
190.5	0.0300	0.0000	0.0300	1	33
195.5	0.1274	0.0000	0.1274	14	110
200.5	0.1337	0.0000	0.1337	24	180

Mid-Sample depth (cm)	Weight before picking (g)	Unpicked weight (g)	Picked weight (g)	Number of pteropods	Pteropods per gram
205.5	0.0929	0.0000	0.0929	21	226
210.5	0.0910	0.0000	0.0910	15	165
215.5	0.0537	0.0000	0.0537	12	223
220.5	0.0449	0.0000	0.0449	29	646
225.5	0.0265	0.0000	0.0265	6	226
230.5	0.0249	0.0000	0.0249	0	0
235.5	0.0386	0.0000	0.0386	2	52
240.5	0.0840	0.0000	0.0840	0	0
245.5	0.0310	0.0000	0.0310	4	129
250.5	0.0288	0.0000	0.0288	2	69
255.5	0.0391	0.0000	0.0391	3	77
260.5	0.0343	0.0000	0.0343	4	117
265.5	0.0393	0.0000	0.0393	7	178
270.5	0.0361	0.0000	0.0361	5	139
275.5	0.0470	0.0000	0.0470	3	64
280.5	0.0395	0.0000	0.0395	4	101
285.5	0.0542	0.0000	0.0542	9	166
290.5	0.0571	0.0000	0.0571	14	245
295.5	0.0368	0.0000	0.0368	53	1440
300.5	0.0258	0.0000	0.0258	39	1512
305.5	0.0256	0.0000	0.0256	70	2734
310.5	0.0329	0.0000	0.0329	72	2188
315.5	0.0353	0.0000	0.0353	86	2436
320.5	0.0275	0.0000	0.0275	19	691
325.5	0.024	0.0000	0.0240	23	958
330.5	0.0550	0.0000	0.0550	25	455
335.5	0.0283	0.0000	0.0283	37	1307
340.5	0.0508	0.0000	0.0508	81	1594
345.5	0.0300	0.0000	0.0300	21	700
350.5	0.0721	0.0000	0.0721	93	1290
355.5	0.1052	0.0000	0.1052	24	228
360.5	0.1395	0.0000	0.1395	84	602
365.5	0.0481	0.0000	0.0481	17	353
370.5	0.0094	0.0000	0.0094	12	1277
375.5	0.0220	0.0000	0.0220	17	773
380.5	0.0571	0.0000	0.0571	36	630
385.5	0.0274	0.0000	0.0274	10	365
390.5	0.0446	0.0000	0.0446	2	45
395.5	0.0354	0.0000	0.0354	4	113
400.5	0.0246	0.0000	0.0246	3	122
405.5	0.0843	0.0000	0.0843	1	12

Mid-Sample depth (cm)	Weight before picking (g)	Unpicked weight (g)	Picked weight (g)	Number of pteropods	Pteropods per gram
410.5	0.072	0.0000	0.0720	0	0
415.5	0.064	0.0000	0.0640	2	31
420.5	0.0156	0.0000	0.0156	1	64
425.5	0.0246	0.0000	0.0246	1	41
430.5	0.0065	0.0000	0.0065	0	0
435.5	0.021	0.0000	0.0210	3	143
440.5	0.0186	0.0000	0.0186	1	54
445.5	0.0142	0.0000	0.0142	0	0
450.5	0.044	0.0000	0.0440	2	45
455.5	0.0255	0.0000	0.0255	1	39
460.5	0.0231	0.0000	0.0231	1	43
465.5	0.0200	0.0000	0.0200	0	0
470.5	0.0510	0.0000	0.0510	7	137
475.5	0.0482	0.0000	0.0482	0	0
480.5	0.0369	0.0000	0.0369	0	0
485.5	0.0304	0.0000	0.0304	0	0
490.5	0.0352	0.0000	0.0352	1	28
495.5	0.0312	0.0000	0.0312	0	0
500.5	0.0449	0.0000	0.0449	11	245
505.5	0.0405	0.0000	0.0405	3	74
510.5	0.0303	0.0000	0.0303	12	396
515.5	0.0449	0.0000	0.0449	26	579
520.5	0.0129	0.0000	0.0129	23	1783
525.5	0.0492	0.0000	0.0492	24	488
530.5	0.0202	0.0000	0.0202	3	149
535.5	0.0201	0.0000	0.0201	3	149
540.5	0.0192	0.0000	0.0192	1	52
545.5	0.0242	0.0000	0.0242	1	41
550.5	0.0440	0.0000	0.0440	2	45
555.5	0.0276	0.0000	0.0276	1	36
560.5	0.0466	0.0000	0.0466	0	0
565.5	0.1874	0.0000	0.1874	34	181
570.5	0.0115	0.0000	0.0115	7	609
575.5	0.0111	0.0000	0.0111	8	721

8.2.1.2.H CAR-MON 2 PTEROPOD AND HETEROPOD ABUNDANCE

150–500 µm

Mid-Sample depth (cm)	Weight before picking (g)	Unpicked weight (g)	Picked weight (g)	Number of pteropods	Pteropods per gram
0.5	0.3186	0.1571	0.1615	299	1851
5.5	0.3912	0.2505	0.1407	312	2217
10.5	0.3144	0.2324	0.0820	297	3622
15.5	0.4080	0.3617	0.0463	300	6479
20.5	0.3367	0.2632	0.0735	302	4109
25.5	0.3438	0.2770	0.0668	321	4805
30.5	0.5150	0.4830	0.0320	317	9906
35.5	0.6178	0.5775	0.0403	304	7543
40.5	0.7130	0.6637	0.0493	302	6126
45.5	0.7957	0.7441	0.0516	316	6124
50.5	1.3543	1.2554	0.0989	307	3104
55.5	0.8257	0.7700	0.0557	311	5583
60.5	0.7634	0.6901	0.0733	317	4325
65.5	0.8435	0.7658	0.0777	311	4003
70.5	0.6429	0.6240	0.0189	312	16508
75.5	0.4939	0.4568	0.0371	305	8221
80.5	0.5248	0.4923	0.0325	316	9723
85.5	1.7230	1.6499	0.0731	335	4583
90.5	1.2157	1.1371	0.0786	298	3791
95.5	0.5791	0.5143	0.0648	298	4599
100.5	0.0925	0.0800	0.0125	304	24320
105.5	0.2030	0.1891	0.0139	290	20863
110.5	0.2182	0.1983	0.0199	307	15427
115.5	0.2568	0.2344	0.0224	292	13036
120.5	0.2552	0.2118	0.0434	292	6728
125.5	0.2971	0.2646	0.0325	316	9723
130.5	0.2480	0.1947	0.0533	323	6060
135.5	0.2596	0.2036	0.0560	299	5339
140.5	0.2593	0.1845	0.0748	280	3743
145.5	0.2621	0.2251	0.0370	286	7730
150.5	0.1620	0.1343	0.0277	300	10830
155.5	0.9840	0.0559	0.9281	286	308
160.5	0.1012	0.0725	0.0287	313	10906
165.5	0.1583	0.1224	0.0359	290	8078
170.5	0.1650	0.0739	0.0911	270	2964
175.5	0.0841	0.0093	0.0748	277	3703
180.5	0.4381	0.2637	0.1744	304	1743
185.5	0.1150	0.0453	0.0697	290	4161
190.5	0.0976	0.0244	0.0732	277	3784
195.5	0.3507	0.2963	0.0544	314	5772
200.5	0.4276	0.3718	0.0558	313	5609

Mid-Sample depth (cm)	Weight before picking (g)	Unpicked weight (g)	Picked weight (g)	Number of pteropods	Pteropods per gram
205.5	0.1719	0.1111	0.0608	293	4819
210.5	0.3328	0.2613	0.0715	299	4182
215.5	0.1589	0.0968	0.0621	289	4654
220.5	0.1615	0.1228	0.0387	291	7519
225.5	0.0837	0.0436	0.0401	295	7357
230.5	0.1061	0.0559	0.0502	297	5916
235.5	0.1145	0.0214	0.0931	271	2911
240.5	0.2052	0.0700	0.1352	269	1990
245.5	0.0970	0.0041	0.0929	283	3046
250.5	0.0882	0.0187	0.0695	273	3928
255.5	0.1131	0.0229	0.0902	285	3160
260.5	0.1147	0.0300	0.0847	264	3117
265.5	0.1697	0.1118	0.0579	277	4784
270.5	0.2230	0.1647	0.0583	277	4751
275.5	0.2413	0.1963	0.0450	299	6644
280.5	0.1959	0.1552	0.0407	307	7543
285.5	0.2545	0.2183	0.0362	279	7707
290.5	0.3520	0.3190	0.0330	314	9515
295.5	0.5073	0.4741	0.0332	311	9367
300.5	0.3440	0.3000	0.0440	301	6841
305.5	0.3643	0.3338	0.0305	328	10754
310.5	0.3974	0.3685	0.0289	306	10588
315.5	0.5567	0.5109	0.0458	305	6659
320.5	0.3441	0.2981	0.0460	299	6500
325.5	0.4279	0.3530	0.0749	300	4005
330.5	0.6410	0.5603	0.0807	344	4263
335.5	0.3008	0.2560	0.0448	320	7143
340.5	0.3723	0.3338	0.0385	304	7896
345.5	0.2764	0.2418	0.0346	304	8786
350.5	0.4924	0.4546	0.0378	290	7672
355.5	0.5834	0.5083	0.0751	311	4141
360.5	0.5423	0.5023	0.0400	314	7850
365.5	0.4034	0.3065	0.0969	309	3189
370.5	0.0864	0.0454	0.0410	282	6878
375.5	0.1868	0.1578	0.0290	329	11345
380.5	0.2742	0.2240	0.0502	291	5797
385.5	0.2224	0.1648	0.0576	213	3698
390.5	0.5158	0.3884	0.1274	276	2166
395.5	0.4911	0.4038	0.0873	292	3345
400.5	0.6810	0.4289	0.2521	277	1099
405.5	1.7349	0.4697	1.2652	304	240

Mid-Sample depth (cm)	Weight before picking (g)	Unpicked weight (g)	Picked weight (g)	Number of pteropods	Pteropods per gram
410.5	0.7354	0.5761	0.1593	302	1896
415.5	0.5776	0.3726	0.2050	285	1390
420.5	0.3056	0.2075	0.0981	288	2936
425.5	0.2203	0.1088	0.1115	197	1767
430.5	0.1238	0.0226	0.1012	269	2658
435.5	0.1798	0.1029	0.0769	295	3836
440.5	0.2431	0.0850	0.1581	269	1701
445.5	0.1549	0.0000	0.1549	317	2046
450.5	0.1686	0.0887	0.0799	260	3254
455.5	0.1535	0.0099	0.1436	288	2006
460.5	0.2176	0.0000	0.2176	171	786
465.5	0.1865	0.0000	0.1865	55	295
470.5	0.2419	0.1199	0.1220	202	1656
475.5	0.1622	0.0000	0.1622	98	604
480.5	0.1435	0.0000	0.1435	96	669
485.5	0.1368	0.0000	0.1368	95	694
490.5	0.1380	0.0000	0.1380	257	1862
495.5	0.1424	0.0185	0.1239	272	2195
500.5	0.1976	0.1317	0.0659	263	3991
505.5	0.2226	0.1654	0.0572	282	4930
510.5	0.2565	0.2193	0.0372	292	7849
515.5	0.4159	0.3663	0.0496	286	5766
520.5	0.1346	0.1065	0.0281	282	10036
525.5	0.2728	0.2116	0.0612	285	4657
530.5	0.1647	0.0954	0.0693	266	3838
535.5	0.1796	0.0533	0.1263	280	2217
540.5	0.1719	0.0000	0.1719	229	1332
545.5	0.2144	0.0000	0.2144	109	508
550.5	0.4982	0.2728	0.2254	291	1291
555.5	0.2812	0.0221	0.2591	261	1007
560.5	0.4840	0.2827	0.2013	266	1321
565.5	1.3125	1.1636	0.1489	296	1988
570.5	0.1580	0.1349	0.0231	268	11602
575.5	0.0976	0.0551	0.0425	301	7082

8.2.1.2.I JC18-19 AND JR123-35-V PLANKTIC FORAMINIFERA ABUNDANCE

(JC18-19)

JC18-19 >500 µm

Mid-Sample depth (cm)	Weight before picking (g)	Unpicked weight (g)	Picked weight (g)	Number of planktic foraminifera	Foraminifera per gram	Foraminifera fragments	Broken but counted foraminifera	Fragment to whole ratio	Number of *G. menardii*	% *G. menardii*
2.5	0.1390	0.0879	0.0511	330	6458	5	32	11.04	78	23.64
10.5	0.0602	0.0199	0.0403	330	8189	9	31	11.80	55	16.67
50.5	0.1263	0.0782	0.0481	329	6840	6	28	10.15	141	42.86
75.5	0.0476	0.0030	0.0446	320	7175	8	34	12.80	94	29.38
95.5	0.0743	0.0123	0.0620	311	5016	13	41	16.67	47	15.11
130.5	0.0970	0.0590	0.0380	327	8605	10	33	12.76	114	34.86
180.5	0.0487	0.0091	0.0396	327	8258	9	50	17.56	110	33.64
195.5	0.0807	0.0379	0.0428	327	7640	7	44	15.27	121	37.00
210.5	0.1065	0.0714	0.0351	300	8547	6	32	12.42	90	30.00
280.5	0.0751	0.0367	0.0384	302	7865	9	22	9.97	101	33.44
320.5	0.1213	0.0776	0.0437	341	7803	4	42	13.33	172	50.44
350.5	0.1324	0.0850	0.0474	310	6540	4	32	11.46	178	57.42

JC18-19 150−500 µm

Mid-Sample depth (cm)	Weight before picking (g)	Unpicked weight (g)	Picked weight (g)	Number of planktic foraminifera	Foraminifera per gram	Foraminifera fragments	Broken but counted foraminifera	Fragment to whole ratio	Number of *G. menardii*	% *G. menardii*
2.5	0.3524	0.3363	0.0161	313	19441	34	8	12.10	13	4.15
10.5	0.3167	0.3059	0.0108	303	28056	57	13	19.44	15	4.95
50.5	0.5054	0.4897	0.0157	316	20127	54	19	19.73	33	10.44
75.5	0.8494	0.8329	0.0165	302	18303	48	10	16.57	23	7.62
95.5	0.8157	0.7950	0.0207	329	15894	16	11	7.83	8	2.43
130.5	0.7867	0.7755	0.0112	339	30268	40	23	16.62	22	6.49
180.5	0.8623	0.8495	0.0128	344	26875	51	14	16.46	23	6.69
195.5	1.2276	1.2129	0.0147	340	23129	37	18	14.59	35	10.29
210.5	0.6436	0.6287	0.0149	306	20537	46	15	17.33	43	14.05
280.5	0.4594	0.4442	0.0152	314	20658	52	28	21.86	49	15.61
320.5	0.8672	0.8536	0.0136	309	22721	67	26	24.73	42	13.59
350.5	0.6704	0.6549	0.0155	317	20452	40	25	18.21	70	22.08

8.2.1.2.I JC18-19 AND JR123-35-V PLANKTIC FORAMINIFERA ABUNDANCE **(JR123-35-V)**

JR123-35-V >500 µm

Mid-Sample depth (cm)	Weight before picking (g)	Unpicked weight (g)	Picked weight (g)	Number of planktic foraminifera	Foraminifera per gram	Foraminifera fragments	Broken but counted foraminifera	Fragment to whole ratio	Number of *G. menardii*	% *G. menardii*
10.5	0.0809	0.0336	0.0473	312	6596	10	17	8.39	37	11.86
80.5	0.1470	0.0642	0.0828	313	3780	7	25	10.00	1	0.32
150.5	0.0339	0.0000	0.0339	118	3481	11	26	28.68	0	0.00
190.5	0.0464	0.0050	0.0414	323	7802	8	28	10.88	0	0.00
235.5	0.0391	0.0000	0.0391	18	460	2	9	55.00	0	0.00
305.5	0.0486	0.0029	0.0457	309	6761	5	21	8.28	0	0.00
435.5	0.0394	0.0000	0.0394	306	7766	2	10	3.90	3	0.98
485.5	0.0878	0.0000	0.0878	221	2517	5	18	10.18	79	35.75

JR123-35-V 15−500 µm

Mid-Sample depth (cm)	Weight before picking (g)	Unpicked weight (g)	Picked weight (g)	Number of planktic foraminifera	Foraminifera per gram	Foraminifera fragments	Broken but counted foraminifera	Fragment to whole ratio	Number of *G. menardii*	% *G. menardii*
10.5	0.3387	0.3231	0.0156	303	19423	49	8	16.19	8	2.64
80.5	0.5359	0.5125	0.0234	302	12906	36	14	14.79	0	0.00
150.5	0.3278	0.2310	0.0968	306	3161	52	13	18.16	0	0.00
190.5	0.1751	0.1614	0.0137	319	23285	34	7	11.61	0	0.00
235.5	0.1207	0.0708	0.0499	309	6192	40	14	15.47	0	0.00
305.5	0.1532	0.1440	0.0092	329	35761	38	9	12.81	0	0.00
435.5	0.1875	0.1720	0.0155	319	20581	22	7	8.50	0	0.00
485.5	0.2797	0.2669	0.0128	313	24453	35	6	11.78	13	4.15

8.2.1.2.J JC18-19 AND JR123-35-V PTEROPOD AND HETEROPOD ABUNDANCE **(JC18-19)**

JC18-19 >500 µm

Mid-Sample depth (cm)	Weight before picking (g)	Unpicked weight (g)	Picked weight (g)	Number of pteropods	Pteropods per gram
2.5	0.1390	0.0000	0.1390	38	273
10.5	0.0602	0.0000	0.0602	18	299
50.5	0.1263	0.0000	0.1263	0	0
75.5	0.0476	0.0000	0.0476	1	21
95.5	0.0743	0.0000	0.0743	32	431
130.5	0.0970	0.0000	0.0970	0	0
180.5	0.0487	0.0000	0.0487	0	0
195.5	0.0807	0.0000	0.0807	0	0
210.5	0.1065	0.0000	0.1065	0	0
280.5	0.0751	0.0000	0.0751	0	0
320.5	0.1213	0.0000	0.1213	0	0
350.5	0.1324	0.0000	0.1324	0	0

JC18-19 150−500 µm

Mid-Sample depth (cm)	Weight before picking (g)	Unpicked weight (g)	Picked weight (g)	Number of pteropods	Pteropods per gram
2.5	0.3524	0.2454	0.1070	309	2888
10.5	0.3167	0.1975	0.1192	301	2525
50.5	0.5054	0.0317	0.4737	301	635
75.5	0.8494	0.6875	0.1619	317	1958
95.5	0.8157	0.7143	0.1014	322	3176
130.5	0.7867	0.0000	0.7867	0	0
180.5	0.8623	0.0000	0.8623	0	0
195.5	1.2276	0.0000	1.2276	0	0
210.5	0.6436	0.0000	0.6436	0	0
280.5	0.4594	0.0000	0.4594	0	0
320.5	0.8672	0.0000	0.8672	0	0
350.5	0.6704	0.0000	0.6704	0	0

8.2.1.2.J JC18-19 AND JR123-35-V PTEROPOD AND HETEROPOD ABUNDANCE **(JR123-35-V)**

JR123-35-V >500 µm

Mid-Sample depth (cm)	Weight before picking (g)	Unpicked weight (g)	Picked weight (g)	Number of pteropods	Pteropods per gram
10.5	0.0809	0.0000	0.0809	45	556
80.5	0.1470	0.0000	0.1470	97	660
150.5	0.0339	0.0000	0.0339	83	2448
190.5	0.0464	0.0000	0.0464	83	1789
235.5	0.0391	0.0000	0.0391	17	435
305.5	0.0486	0.0000	0.0486	35	720
435.5	0.0394	0.0000	0.0394	17	431
485.5	0.0878	0.0000	0.0878	27	308

JR123-35-V 150−500 µm

Mid-Sample depth (cm)	Weight before picking (g)	Unpicked weight (g)	Picked weight (g)	Number of pteropods	Pteropods per gram
10.5	0.3387	0.2731	0.0656	310	4726
80.5	0.5359	0.4505	0.0854	302	3536
150.5	0.3278	0.2250	0.1028	321	3123
190.5	0.1751	0.1545	0.0206	323	15680
235.5	0.1207	0.0490	0.0717	302	4212
305.5	0.1532	0.1136	0.0396	304	7677
435.5	0.1875	0.1316	0.0559	303	5420
485.5	0.2797	0.2560	0.0237	312	13165

8.2.1.3 CALCIFICATION INDICES APPENDIX

8.2.1.3.A CAR-MON 2 LDX DATA

MID-SAMPLE DEPH (cm)	LDX for *Limacina inflata* >300 µm (n>10)																														No.	MEAN LDX
0.5	4	4	1	2	2	2	4	3	4	2	2	2	4	4	4	4	3	3	2	3	4	3	3	3	3	3	3	3	3	4	30	3.03
5.5	4	3	2	2	3	2	2	2	3	2	0	4	2	3	2	3	3	3	4	5	2	2	2	2	4	4	4	3	4	3	30	2.80
10.5	4	4	2	3	2	4	2	1	3	2	2	2	2	2	2	3	4	2	3	2	2	3	3	2	4	2	2	3	4	3	30	2.63
15.5	3	2	3	4	2	2	2	3	4	4	5	4	3	2	2	2	3	3	2	3	3	2	3	3	3	2	2	2	2	1	30	2.70
20.5	3	1	4	2	2	4	3	3	3	4	2	3	4	4	3	1	3	3	2	4	3	3	3	2	1	2	4	4	2	2	30	2.80
25.5	2	2	3	2	3	1	2	2	2	2	4	2	2	2	2	2	2	3	3	2	2	2	2	2	2	2	2	3	3	3	30	2.27
30.5	2	2	3	2	2	2	2	2	4	3	2	2	2	2	2	2	2	2	2	2	2	2	2	3	1	3	3	2	2	2	30	2.20
35.5	3	2	2	3	1	1	2	3	2	1	2	3	2	2	2	2	1	2	2	2	2	2	2	2	1	2	2	2	2	3	30	2.00
40.5	0	1	1	1	1	1	2	0	1	1	1	2	1	1	2	0	0	1	1	1	0	0	1	1	1	1	1	1	1	1	30	0.90
45.5	1	1	1	1	1	0	2	2	1	0	1	1	0	0	0	1	2	1	1	1	1	1	1	1	1	1	1	0	0	1	30	0.87
50.5	0	1	1	2	1	1	1	1	1	0	1	0	1	1	1	1	1	1	1	0	1	0	0	1	1	0	1	2	1	1	30	0.83
55.5	0	1	1	1	1	0	1	1	1	1	0	0	0	0	0	1	1	1	1	1	1	1	0	1	1	1	1	1	1	1	30	0.73
60.5	1	0	1	1	0	0	0	1	1	1	0	1	0	1	1	1	1	1	0	0	1	0	1	0	1	0	0	1	1	0	30	0.57
65.5	1	1	1	1	0	1	1	1	1	1	1	1	1	0	1	1	1	1	1	1	1	1	2	0	1	1	1	1	1	1	30	0.93
70.5	0	1	1	0	0	1	1	1	1	1	1	1	1	1	1	1	0	1	1	1	2	2	1	1	1	0	1	1	1	1	30	0.90
75.5	1	1	1	1	2	2	2	2	1	1	1	1	1	1	1	1	1	1	1	1	3	1	1	2	1	1	1	1	1	2	30	1.27
80.5	3	1	2	1	1	1	2	2	2	1	2	2	2	2	1	1	1	1	2	2	2	2	2	1	1	2	2	1	2	1	30	1.60
85.5	1	1	3	1	1	1	1	1	1	2	1	2	1	1	2	2	3	2	2	1	3	2	2	2	3	2	2	1	2	1	30	1.67
90.5	2	2	3	4	2	2	2	2	2	2	2	3	2	2	2	1	1	1	2	2	1	2	1	2	1	3	2	2	3	2	30	2.00
95.5	2	2	3	4	2	2	3	3	2	2	4	1	2	1	0	1	2	2	1	2	3	1	2	1	1	1	2	1	2	2	30	1.90
100.5	2	2	2	3	3	3	4	2	2	2	2	2	3	4	3	2	3	3	2	2	2	3	2	3	3	2	4	2	1	2	30	2.50
105.5	5	2	2	3	2	3	2	3	2	3	2	3	2	2	4	2	3	2	3	2	2	3	2	2	3	2	2	2	3	2	30	2.50
110.5	5	4	3	3	2	3	3	2	4	3	3	2	3	2	3	2	2	2	2	2	2	3	3	2	3	3	4	3	3	2	30	2.77
115.5	3	3	5	2	3	5	4	4	3	3	4	2	4	3	3	4	2	2	2	5	5	5	3	3	4	5	3	3	5	3	30	3.50
120.5	3	2	5	3	3	3	4	3	3	5	2	5	5	5	5	5	5	5	3	2	3	3	4	4	4	4	3	3	2	3	30	3.63
125.5	5	5	5	5	2	3	4	3	3	5	3	5	3	4	3	3	4	5	5	3	3	5	5	4	3	4	3	5	5	4	30	3.97

MID-SAMPLE DEPH (cm)	LDX for *Limacina inflata* >300 µm (n>10)																														No.	MEAN LDX
130.5	3	5	3	5	2	2	2	5	2	2	5	3	3	3	3	5	3	4	4	5	4	4	3	3	3	4	5	3	3	4	30	3.50
135.5	3	5	5	5	5	4	3	5	3	4	3	4	4	3	5	4	2	5	5	5	4	3	5	3	3	4	4	3	3	4	30	3.93
140.5	2	2	2	4	3	2	2	2	2	3	3	4	3	4	2	3	2	2	4	3	5	5	3	3	3	3	3	3	4	2	30	2.93
145.5	5	2	5	2	5	5	5	5	5	5	3	3	5	5	3	5	3	3	3	4	5	5	3	2	5	4	3	5	4	5	30	4.07
150.5	3	5	3	5	5	5	4	5	5	5	4	3	2	3	3	4	3	2	5	4	5	5	4	5	3	4	3	2	4	5	30	3.93
155.5	5	3	2	5	3	5	4	5	3	2	3	2	3	3	3	3	3	3	4	5	3	5	2	4	3	4	1	2	4	4	30	3.37
160.5	3	3	5	5	3	5	3	3	5	3	4	3	1	5	2	3	5	4	4	3	3	2	5	3	3	3	3	2	4	5	30	3.50
165.5	5	5	5	3	4	4	3	5	5	3	4	3	4	3	2	4	3	2	2	3	5	5	4	3	5	3	3	2	4	2	30	3.60
170.5	3	3	4	3	5	5	3	2	3	3	3	3	5	4	5	5	4	5	5	3	3	5	3	4	2	5	5	5	3	5	30	3.87
175.5	3	5	5	5	5	5	4	3	3	4	5	5	5	4	4	5	4	5	4												19	4.37
180.5	5	3	3	3	5	3	4	5	5	5	3	3	3	5	3	3	3	5	5	3	3	5	3	5	5	5	3	5	3	5	30	3.97
185.5	5	5	5	4	5	4	3	5	5	5	5	3	5	3	4	3	5	5	5	5	5	5	5	5	5	4					26	4.54
190.5	3	5	5	5	5	3	3	3	5	4	3	4	5	2	5	3	4	5	2	2	5	4	4	4	3	3	3	3	3	4	30	3.73
195.5	2	2	2	3	4	2	2	2	3	2	2	3	2	2	2	3	2	2	2	3	3	3	2	4	2	2	2	3	4	3	30	2.50
200.5	3	3	3	3	3	3	3	3	3	3	3	3	3	3	4	3	3	5	3	3	3	3	3	3	3	4	3	3	3	3	30	3.13
205.5	3	5	5	5	3	5	5	2	3	2	2	3	2	2	2	2	2	4	2	2	3	4	3	3	4	2	2	5	2	5	30	3.13
210.5	2	3	3	3	3	3	3	4	2	3	3	3	3	3	3	3	3	3	3	2	2	2	2	2	2	2	1	2	2	2	30	2.57
215.5	4	4	3	3	5	2	2	2	5	3	2	3	4	3	4	3	5	5	2	5	2	2	3	3	4	2	2	3	5	2	30	3.23
220.5	2	2	3	3	2	5	5	4	4	3	5	3	2	3	5	3	3	2	4	2	4	3	5	2	3	3	2	2	4	4	30	3.23
225.5	3	2	2	2	3	3	2	4	2	2	3	2	3	2	3	2	2	2	2	2	3	3	3	3	3	2	3	2	3	4	30	2.57
230.5	2	5	3	5	2	3	3	3	5	3	3	3	5	3	3	3	5	3	5	3	4	3	3	5	5						25	3.60
235.5	3	3	5	5	5	4	5	5	5	5	3	3	5	5	5	5	3	4	5	3	4	3	4	4	5	4	4	3			28	4.18
240.5	3	5	5	4	5	5	4	5	4	3	4	4	5	2	3	3	3	5	5	5	5	5	4	5	5	4	4	4	4	5	30	4.23
245.5	5	5	4	5	5	5	5	5	3	5	3	5	5	3	5	5	3	5	5												19	4.53
250.5	5	3	5	5	2	3	3	5	4	3	5	5	5	3	3	4	3	4													18	3.89
255.5	3	3	2	3	4	4	3	4	3	5	2	4	4	5	3	4	4	3	3	3	3	3	5	3	3	4	3	4	3	4	30	3.47

MID-SAMPLE DEPH (cm)	LDX for *Limacina inflata* >300 µm (n>10)																														No.	MEAN LDX
260.5	5	5	2	3	3	2	3	3	3	3	3	3	3	3	3	3	3	3	3	3	4	4	3	3	2	3	3	3	4	3	30	3.13
265.5	4	2	2	3	5	5	3	4	4	2	3	3	4	3	5	3	2	3	3	3	4	3	3	2	3	5	3	2	4	2	30	3.23
270.5	3	3	3	3	5	3	4	4	3	2	3	3	4	4	3	4	2	2	3	2	5	3	2	2	3	3	3	2	5	3	30	3.13
275.5	5	4	4	3	1	2	3	2	4	2	3	4	3	3	4	4	3	4	4	2	2										21	3.14
280.5	3	2	3	3	3	3	4	3	5	3	3	3	5	5	3	3	3	3	3	3	3	3	3	3	3	3	3	3	3	3	30	3.20
285.5	4	3	2	3	3	3	4	3	3	4	4	3	2	5	2	3	2	2													18	3.06
290.5	2	2	3	3	3	2	3	3	2	3	3	3	2	2	3	2	3	2	3	2	2	2	2	3	2	2	3	3	3	2	30	2.50
295.5	3	4	2	3	3	2	3	3	3	2	2	3	4	3	3	2	3	3	3	2	5	2	5	2	3						25	2.92
300.5	2	2	2	2	2	2	2	2	2	2	2	2	2	2	2	2	2	2	3	2	3	2	2	2	2	2	2	2	3	2	30	2.10
305.5	1	2	3	1	2	2	3	1	2	2	2	1	1	1	2	2	1	2	2	2	2	1	2	2	1	2	2	1	1	4	30	1.77
310.5	1	1	1	1	1	1	1	1	1	1	1	1	1	1	1	2	1	1	1	1	1	1	1	1	1	1	1	1	1	1	30	1.03
315.5	2	1	1	1	2	1	2	1	1	2	1	1	1	1	1	1	1	1	2	1	1	1	1	2	1	1	4	1	1	1	30	1.30
320.5	1	1	1	1	1	1	1	1	1	1	1	1	1	1	1	0	1	0	1	0	1	1	0	0	0	1	1	2	0	0	30	0.77
325.5	1	1	1	1	1	1	1	1	1	1	1	1	1	2	1	1	1	1	1	1	1	1	0	0	0	0	0	0	0	0	30	0.77
330.5	1	1	1	1	1	2	2	1	1	1	3	2	1	1	1	1	1	1													18	1.28
335.5	2	2	1	2	2	2	2	2	2	2	2	2	2	2	2	2	2	2	2	2	2	2	2	2	2	2	2	1	1	1	30	1.87
340.5	2	1	1	2	1	1	2	1	2	2	1	1	2	2	1	2	2	3	3	2	2	3	2	1	2	1	2	3	2	2	30	1.80
345.5	2	2	2	2	2	2	2	2	2	2	2	2	2	2	2	1	1	1	1	1	1	1	1	1	1	1	1	2	1	1	30	1.53
350.5	2	2	2	2	4	3	3	2	2	2	2	2	4	2	2	2	2	3	2	2	2	2	4	2	2	3	2	3	2	3	30	2.40
355.5	1	1	2	1	1	1	1	1	1	1	1	1	1	1	1	0	1	2	1	1	0	1	1	1	1	1	1	2	1	1	30	1.03
360.5	3	2	4	3	3	3	3	2	2	3	2	3	3	3	2	3	2	3	2	3	3	3	3	3	2	3	2	3	2	2	30	2.67
365.5	3	2	2	3	2	2	2	2	2	2	2	2	2	2	2	2	3	2	2	2	2	2	2	2	2	2	2	2	2	2	30	2.10
370.5	5	3	1	2	2	2	1	2	2	4	2	3	1	2	2	1	2	2	2												19	2.16
375.5	3	3	3	2	2	2	2	2	3	3	3	3	2	2	2	2	2	2	2	2	3	2	2	1	2	2	2	2	1	2	30	2.20
380.5	3	4	4	3	3	3	2	4	5	5	3	2	4	3	2	2	2	1	2	1	3	4	2	2	2	1	4	4	3	2	30	2.83
385.5	4	2	3	2	2	2	2	2	3	2	4	2	2	2	2	3	2	2	2	4	4	2	2	2	2	1	2	2	2	2	30	2.33

MID-SAMPLE DEPH (cm)	LDX for *Limacina inflata* >300 µm (n>10)																													No.	MEAN LDX
390.5	3	5	2	3	3	3	4	2	2	2	2	2	3	0	3	2	3	3	3	3	4	2	2	3	4	4	2	2	1	3	30	2.67
395.5	2	2	2	2	2	3	3	2	2	2	4	2	4	3	2	4	4	4	4	2	4	2	2	2	2	3	4	4	2	2	30	2.73
400.5	3	4	2	3	3	3	3	4	2	3	3	2	3	4	5	4	3														17	3.18
405.5	2	3	3	3	4	3	3	3	1	3	3	3	3	3	4	3	3	3	2	3	4	2	3	3	2	3	3	2	4	3	30	2.90
410.5	3	3	3	3	3	3	3	2	3	3	3	3	3	3	3	3	3	3													18	2.94
415.5	2	3	2	3	2	4	2	2	3	2	3	2	2	2																	14	2.43
420.5	3	4	3	1	3																											-
425.5	3	4	3	3	3	3	3	3	3	4																					10	3.20
430.5	1	3	4	5	4	2	4	3	1	4	5	4	5	1	3	3	0	2													18	3.00
435.5	4	3	4	3	3	3	3	3	3	3	3	3	4	2	3	4	3	3	3	3	3	3	3	2	3	3	3	3	3	2	30	3.03
440.5	4	4	3	3	2	3	2	4	4	5	2	5	5	5	3	2	3	2	2	3	3	3	4	2	2	3	3	2	2	3	30	3.10
445.5	3	3	2	3	3	3	2	3	3	3	3	3	3	3	3	2	3	2	3	3	3										21	2.81
450.5	2	2	3	4	3	3	3	2	2	2	3	1	2	3	3	4	3	2	3	2	2	4	3	3							24	2.67
455.5	2	3	3	2	3	3	2	3	2	3	2	4	3	2	3	2	3	3	3												19	2.68
460.5	3	3	2	3	3	2	2	3	3	3	2	3	3	2																	14	2.64
465.5	2	3	3	2	3	3	3																									-
470.5	3	2	2	4	3	2	3	3	4	3	4	2	3	3	3																15	2.93
475.5	3	3	3	3	2	3	3	4	3	2	3																				11	2.91
480.5	3	4	2	3	5	3	4	4	5	3																					10	3.60
485.5	3	3	4	3	3	3	3	3	3	3	2	2	3	3	3	3	3	3	3	3											20	2.95
490.5	2	4	5	2	2	3	5	2	3	2	3	4	5	2	2	2	5	2	4	2	2	3	2	2	4	3	3	3	3	2	30	2.93
495.5	2	3	3	3	3	1	2	2	2	4	2	3	3	3	3	2	2	3	2	2	3	2	3	3	3	3	4	2	3	3	30	2.63
500.5	5	4	4	4	3	3	3	4	3	4																					10	3.70
505.5	3	2	3	3	3	3	3	2	3	4	2	3	4	3	2	2	3	3	2	2	3	2	3	2	2	4	3	3	2	3	30	2.73
510.5	3	3	2	3	3	2	3	2	3	2	1	2	1	1	1	2	2	2	2	1	2	3	2	1	2	1	1	2	2	1	30	1.93
515.5	3	2	2	3	2	3	3	3	2	3	2	2	4	3	2	2	3	2	3	2	2	2	1	2	1	2	2	2	2	2	30	2.30

MID-SAMPLE DEPH (cm)	LDX for *Limacina inflata* >300 µm (n>10)																														No.	MEAN LDX
520.5	2	3	4	3	4	2	2	2	2	2	2	2	2	2	3	3	2	2	3	3	3	2	2	1	1	3	2	1			28	2.32
525.5	3	3	3	3	3	2	3	2	3	3	4	3	2	1	2	2	2	2	3	2	2	3	2	2	2	2	1	1	2	2	30	2.33
530.5	3	3	2	4	3	2	2	2	4	2	4	2	2	2	5	3	3	2	2	2	2	3	5	2	2	1					26	2.65
535.5	3	2	3	2	3	3	3	3	2	2	2	2	3	2	2	1	3	3	2	3	2	3	2	2	2	2	3	2	2	3	30	2.40
540.5	3	3	3	4	3	4	3	3	4	4	3	5	3	4	4	3	3	2	3	3	2	3	5	2	5	3	3	3	2		29	3.28
545.5	4	3	4	3	4	3	3	3	3	3	2	3	3	4	4	3	3	4	4	3	3										21	3.29
550.5	3	2	3	3	3	2	3	3	2	2	2	3	3	3	3	3	3	3	3	3	3	3	3	3	2	3	3	3	3	3	30	2.80
555.5	3	2	2	3	3	4	2	5	3	3	4	4	2	5	2	2	2														17	3.00
560.5	1	2	1	3	3	4	5	3	3	3	1	4	3	5	2	4	3	2	3	2	2	2	5	1	1	5	2	2	4	2	30	2.77
565.5	2	3	2	1	1	1	2	2	2	1	2	2	2	1	1	1	1	1	3	3	3	3	2	2	2	3	2	2	2	1	30	1.87
570.5	2	2	3	4	1	1	1	1	2	1	1	1	1	2	2	1	1	1	1	1	1	1	1	2	2	1	1	1	2	1	30	1.43
575.5	3	2	2	3	1	1	1	2	2	1	1	3	1	1	1	2	1	1	1	1	1	1	2	1	1	1	2	1	1	1	30	1.43

8.2.1.3.B ALL LDX POINTS FOR CAR-MON 2. RED LINE SHOWS MEAN VALUES, GREY BARS SHOW STANDARD DEVIATION

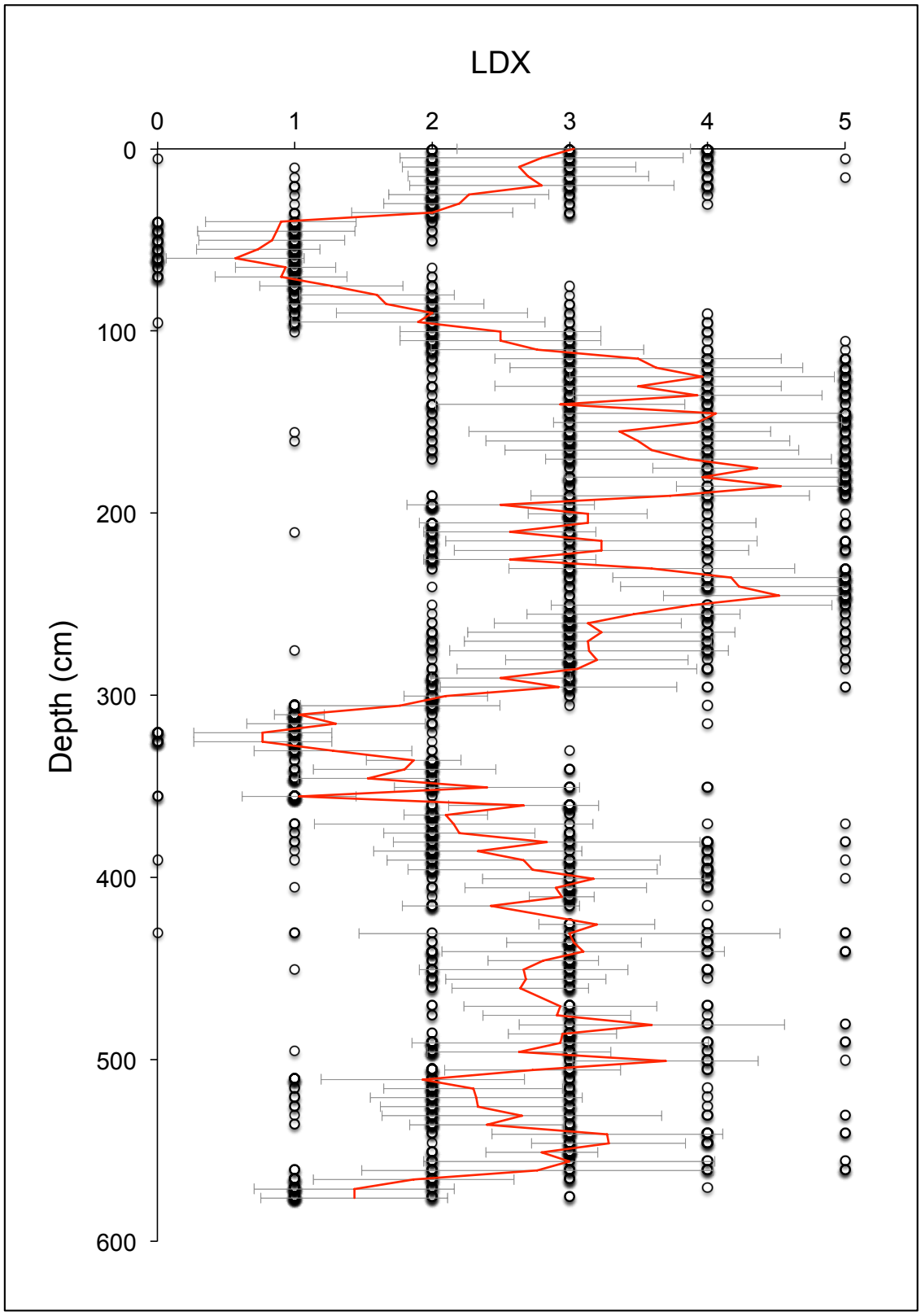

8.2.1.3.C OPTIMUM LDX AND $\delta^{18}O$ CORRELATION CALCULATIONS

CAR-MON 2			
Shift (cm)	r	p	n
0	-0.318	0.001	112
5	-0.406	< 0.0001	112
10	-0.463	< 0.0001	110
15	-0.496	< 0.0001	109
20	-0.534	< 0.0001	108
25	-0.550	< 0.0001	107
30	-0.555	< 0.0001	106
35	-0.572	< 0.0001	105
40	-0.568	< 0.0001	104
45	-0.551	<0.0001	101

B5-1			
Shift (cm)	r	p	n
0	0.137	0.488	28
5	0.034	0.865	28
10	0.092	0.649	27
15	-0.095	0.636	27
20	-0.053	0.795	26
25	-0.281	0.165	26
30	-0.360	0.078	25
35	-0.505	0.010	25
40	-0.459	0.021	25

716B			
Shift (cm)	r	p	n
0	-0.159	0.570	15
5	-0.203	0.378	21
10	-0.563	0.012	19
15	-0.471	0.031	21
20	-0.633	0.002	21
25	-0.551	0.012	20
30	-0.464	0.061	17
35	-0.233	0.352	18

JC18-19

MID-SAMPLE DEPTH (cm)	LDX for *Limacina inflata* >300 µm (n>10)																													No.	MEAN LDX
2.5	5	5	3	3	5	4	5	4	3	3	4	4	4	4	4	4	4	5	4	4	4	3	5	4	3	4	4	5	4	5	30	4.07
10.5	3	4	2	2	2	2	3	3	2	4	2	2	4	3	4	3	2	2	4	2	3	3	2	2	3	3	2	2	3	2	30	2.67
50.5	5	5	4	5	5	4	4	4	5	4																					10	4.50
75.5	3	5	4	5	4	5	4	4	5	5	4	5	5	5	3	2	5	4	4	5	5	5	4	3	5	5	5	4	4	5	30	4.37
95.5	2	3	3	3	3	4	3	2	2	5	3	3	3	3	3	2	5	3	3	2	2	5	5	3	2	2	2	3	3	3	30	3.00
130.5																															0	-
180.5																															0	-
195.5																															0	-
210.5																															0	-
280.5																															0	-
320.5																															0	-
350.5																															0	-

JR123-35-V

MID-SAMPLE DEPTH (cm)	LDX for *Limacina inflata* >300 µm (n>10)																													No.	MEAN LDX
10.5	4	4	4	4	3	4	4	4	5	3	3	4	5	4	4	4	3	3	3	5	4	4	5	4	4	4	4	4	4	5	30	3.97
80.5	1	1	1	1	1	0	0	1	1	1	1	1	1	1	1	1	1	1	1	1	1	1	1	1	1	1	1	2	2	1	30	1.00
150.5	1	1	1	1	1	1	1	1	1	1	1	1	1	1	1	1	1	1	1	1	1	1	1	1	1	1	1	1	1	1	30	1.00
190.5	2	2	2	2	2	2	2	2	2	2	2	2	4	2	2	2	2	2	2	2	2	2	2	2	2	2	2	2	4	2	30	2.13
235.5	1	0	0	0	0	1	1	0	1	0	0	0	0	1	0	1	1	0	1	1	0	1	0	1	1	1	1	1	1	1	30	0.57
305.5	2	2	2	2	2	2	2	3	2	2	3	2	2	2	2	2	2	2	2	2	2	2	2	3	2	2	2	2	2	2	30	2.10
435.5	5	3	2	4	5	3	3	5	5	2	3	4	5	3	4	3	2	4	2	3	2	3	3	3	4	2	3	3	2	3	30	3.27
485.5	3	3	3	3	2	5	5	2	5	4	2	3	3	3	3	2	3	2	3	2	3	2	2	2	2	2	2	2	3	3	30	2.80

8.2.1.3.E CAR-MON 2 SHELL SIZE DATA

0.5 cm	767	686	686	636	328	239	353	193	458	210	210	378	204	199	178	200	223	206	288	215	174	205	478	322	146	201	214	182	212	229	205
	196	210	221	258	205	262	353	268	179	227	200	220	319	225	230	220	210	243	238	188	220	331	200	221	225	294	180	221	198	211	215
	335	259	196	188	209	258	357	183																							
AVERAGE	**266 µm**																														
30.5 cm	786	753	848	761	751	727	723	689	612	748	710	714	826	729	715	584	736	589	758	552	666	800	750	751	565	722	566	700	185	194	209
	525	723	592	739	633	776	825	796	691	804	768	658	622	727	504	792	638	685	662	719	686	622	712	800	523	481	747	740	349	303	195
	743	675	707	682	757	809	723	578	618	611	619	631	692	524	697	723	724	680	738	718	826	669	541	664	779	638	730	769	186	240	196
	720	743	696	732	712	693	693	714	749	702	787	520	770	793	566	784	690	770	382	528	548	759	716	340	234	327	251	223	235	197	225
	797	701	704	742	735	549	768	793	705	739	721	713	741	722	387	251	391	295	322	257	388	372	300	360	278	303	217	236	659	317	577
	691	629	732	585	656	547	817	751	810	762	762	671	705	690	218	335	369	302	204	241	315	260	300	256	510	236	319	203	304	251	368
	747	683	714	718	807	776	788	758	719	815	828	919	738	705	322	379	439	352	368	314	283	219	241	417	231	276	258	306	243	331	207
	682	769	759	690	715	782	785	712	513	727	488	750	739	674	393	181	203	447	268	261	278	201	373	356	187	255	190	225	192	428	399
	745	702	731	765	719	746	593	747	602	440	723	724	768	696	222	218	251	342	243	221	180	203	467	164	253	343	405	255			
AVERAGE	**554 µm**																														
60.5 cm	487	847	671	733	513	863	807	867	845	484	808	720	596	696	797	871	650	754	847	799	712	758	524	736	703	776	765	701	852	830	805
	603	855	760	801	864	839	591	672	888	441	753	580	530	533	448	749	733	750	659	715	740	780	680	740	778	823	611	651	793	611	532
	801	821	751	659	802	558	474	792	543	782	837	835	744	748	738	861	801	832	820	843	842	888	845	853	482	778	873	804	777	648	825
	954	794	792	824	865	458	794	767	765	737	443	527	833	442	535	915	700	558	624	531	590	542	903	785	602	715	497	782	752	566	818
	763	646	822	724	847	883	711	498	552	592	762	783	651	450	779	869	510	718	593	763	780	645	797	824	859	805	935	432	265	196	269
	271	505	263	297	325	421	164	545	455	503	222	278	270	407	341	359	236	376	198	430	345	273	340	331	364	368	335	516	384	389	429
	226	228	311	189	430	197	272	344	288	203	427	425	330	274	204	220	262	198	157	220	209	437	245	262	210	362	335	228	251	228	281
	307	249	203	499	319	267	222	212	313	454	456	460	204	210	570																
AVERAGE	**579 µm**																														
90.5 cm	768	701	715	821	563	783	593	454	564	480	229	170	217	210	225	189	207	170	235	250	251	217	247	177	185	224	181	192	210	209	221
	178	152	207	191	179	225	197	188	212	169	211	232	195	250	254	223	220	230	171	209	180	181	174	351	149	199	193	180	208	182	216
	227	205	216	172	201	178	240	210	234	206	202	217	193	202																	
AVERAGE	**264 µm**																														
CM2 125-126	816	406	754	536	716	232	159	226	249	261	205	244	173	221	197	181	206	175	342	197	200	230	180	213	182	208	234	179	239	238	199
	215	197	285	216	317	204	222	217	228	266	221	223	412	197	213	149	212	180	164	593	185	205	236	231	201	195	166	187	309	314	181
	360	214	223	171	176	380	225	240	227	166	181	227	214	218	232	212	211	206	305	222	210	172	204	227	324	315	425	304	204	282	231
	193	217	187	217	204	195	208	239	296	200	199	209	251	207	235	201	642	206	210	371	165	183	203								
AVERAGE	**251 µm**																														

140.5 cm	923	792	671	836	854	811	787	208	360	283	227	219	215	233	208	182	207	275	260	274	243	324	191	282	260	245	223	208	177	236	216
	414	226	215	341	250	231	221	211	226	197	187	240	262	229	289	234	228	209	212	222	179	266	235	194	206	221	221	191	212	244	190
	226	196	215	191	243	211	207	167	232	241	228	247	230	269	201	190	235	193	283	196	180	342	212	236	217	304	240	442	260	239	198
	240	255	200	212	226	242	191	198	254	214	197																				
AVERAGE	**272 µm**																														
185.5 cm	294	246	406	184	232	159	223	211	186	130	227	216	203	210	199	207	196	218	227	206	211	253	240	261	223	206	208	210	272	173	239
	215	218	209	218	251	166	202	233	232	258	234	219	251	240	233	266	199	234	196	214	295	213	310	297	203	231	220	260	234	221	279
	246	249	192	245	214	205	203																								
AVERAGE	**227 µm**																														
255.5 cm	249	233	272	233	201	208	217	249	212	221	232	204	154	186	182	231	304	258	253	224	237	218	212	294	199	235	201	209	204	201	207
	248	218	293	216	215	230	211	325	259	241	229	262	182	242	148	209	203	248	215	140	218	170	198	206	210	188	223	279	226	167	186
	200	255	214	291	292	254	248	232	184	173	219	250	213	147	323	182	195	230	230	221	166	199	220	208							
AVERAGE	**222 µm**																														
290.5 cm	675	640	731	633	608	500	234	234	261	229	282	220	237	147	248	207	179	734	212	211	207	233	194	263	336	216	201	181	232	260	223
	238	170	240	241	402	240	239	244	252	230	187	255	346	240	274	181	240	224	206	201	218	421	238	193	206	454	182	201	203	218	455
	238	267	222	239	186	173	224	233	249	255	203	215	230	214	241	195	199	221	174	245	233	232	248	249	210	247	219	231	185	215	238
	211	225	234	319	233	212	256	450	215	351	227	224	215	235	216	269	221	230	213	202	198	241	261	206	236	202	213	271	230	183	263
	226	236	170	228	535	278	236	196	269	235	222	197	197	209	180	226	223	230	235												
AVERAGE	**257 µm**																														
320.5 cm	756	680	750	770	763	636	645	843	684	710	715	676	735	704	224	188	194	294	229	196	292	236	187	228	197	266	220	217	208	471	218
	691	215	317	381	271	243	201	376	237	215	206	400	477	235	500	209	215	216	225	590	188	185	224	244	216	209	198	260	183	362	221
	392	312	459	239	353	221	253	179	278	256	453	439	199	289	173	250	232	259	250	407	357	342	232	238	278	332	423	278	250	346	202
	287	380	385	360	335	308	358	187	209	314	251	212	248	283	241	259	227	208	196	191	219	225	246	219	140	320	351	159	239	272	201
	286	272	376	194	250	207	198	205	206	274	177	197	193																		
AVERAGE	**316 µm**																														
350.5 cm	755	817	414	865	755	691	700	765	786	539	667	566	726	744	698	750	735	519	639	754	741	732	696	754	770	809	791	707	707	726	610
	748	698	726	709	556	536	668	668	717	697	782	613	752	689	663	684	685	740	712	754	761	633	227	227	410	298	296	388	197	251	226
	388	218	318	410	269	355	356	353	449	305	345	380	272	235	497	321	337	510	327	403	426	262	608	331	232	444	317	348	252	263	435
	482	234	289	348	248	239	250	270	247	223	213	331	356	248	234	257	343	260	355	242	210	516	452	213	308	303	212	228	235	224	541
	369	372	238	345	334	252	240	381	227	235	324	357	226	242	354	266	260														
AVERAGE	**459 µm**																														

CM2 400-401	299	215	209	224	191	210	248	193	141	218	174	140	176	218	221	242	232	179	235	156	230	222	250	213	142	201	233	188	195	190	180
	192	139	187	205	229	233	194	181	194	213	154	217	187	202	269	192	212	203	195	229	200	200	210	243	167	225	195	181	218	197	206
	190	143	213	219	185	141	220	194	221	226	229	190	264	229																	
AVERAGE	**204 µm**																														
CM2 450-451	220	202	199	223	215	204	255	209	199	214	246	261	228	208	284	214	210	233	247	279	227	203	179	189	197	213	210	255	362	214	191
	182	391	261	242	223	229	219	203	203	225	228	233	199	204	238	200	193	208	228	163	180	244	208	208	214	316	215	182	238	252	407
	196	233	237	217	199	206	228	191	294	214	191	245	248	201	237	223	212														
AVERAGE	**227 µm**																														
500.5 cm	237	205	212	230	208	228	225	246	245	214	250	234	242	232	207	192	207	237	224	218	215	222	203	213	190	284	226	227	234	231	298
	223	232	241	225	255	220	222	217	211	227	263	235	245	244	219	226	189	226	230	229	210	216	206	184	220	228	210	227	212	315	207
	185	200	208	209	237	232	210	210	188	218	223	235	226	211	220	207	210	214	203												
AVERAGE	**223 µm**																														
CM2 550-551	244	219	226	183	211	229	174	190	292	331	168	215	178	206	220	193	208	165	229	270	228	292	239	223	216	311	198	191	194	243	223
	175	158	307	215	191	179	232	221	249	217	228	210	294	207	228	259	203	226	225	192	294	285	186	226	191	190	210	225	240	236	211
	245	290	226	234	248	251	245	195	234	244	200	207	217	217	212	292	201	182	186	195	203	215	166	164	210	174	208	187	250	203	228
	289																														
AVERAGE	**222 µm**																														
575.5 cm	247	235	219	266	224	269	222	225	212	231	221	260	250	205	219	169	201	238	242	223	312	256	203	273	247	204	241	224	237	216	270
	218	222	278	211	197	278	296	487	246	287	264	258	276	316	209	202	251	193	194	209	239	331	238	199	251	209	229	213	203	210	198
	199	232	260	241	215	145	203	232	237	202	213	215	190	219	264	213	250	240	305	480	241	271	231	199	252	307	316	218	224	277	231
	239	567	267	217	310	308	221	290	773	747	768	687																			
AVERAGE	**265 µm**																														

8.2.2 THE MEDITERRANEAN SEA APPENDIX

8.2.2.1 SEDIMENTOLOGY APPENDIX

8.2.2.1.A B5-1 CORE PHOTOGRAPHS

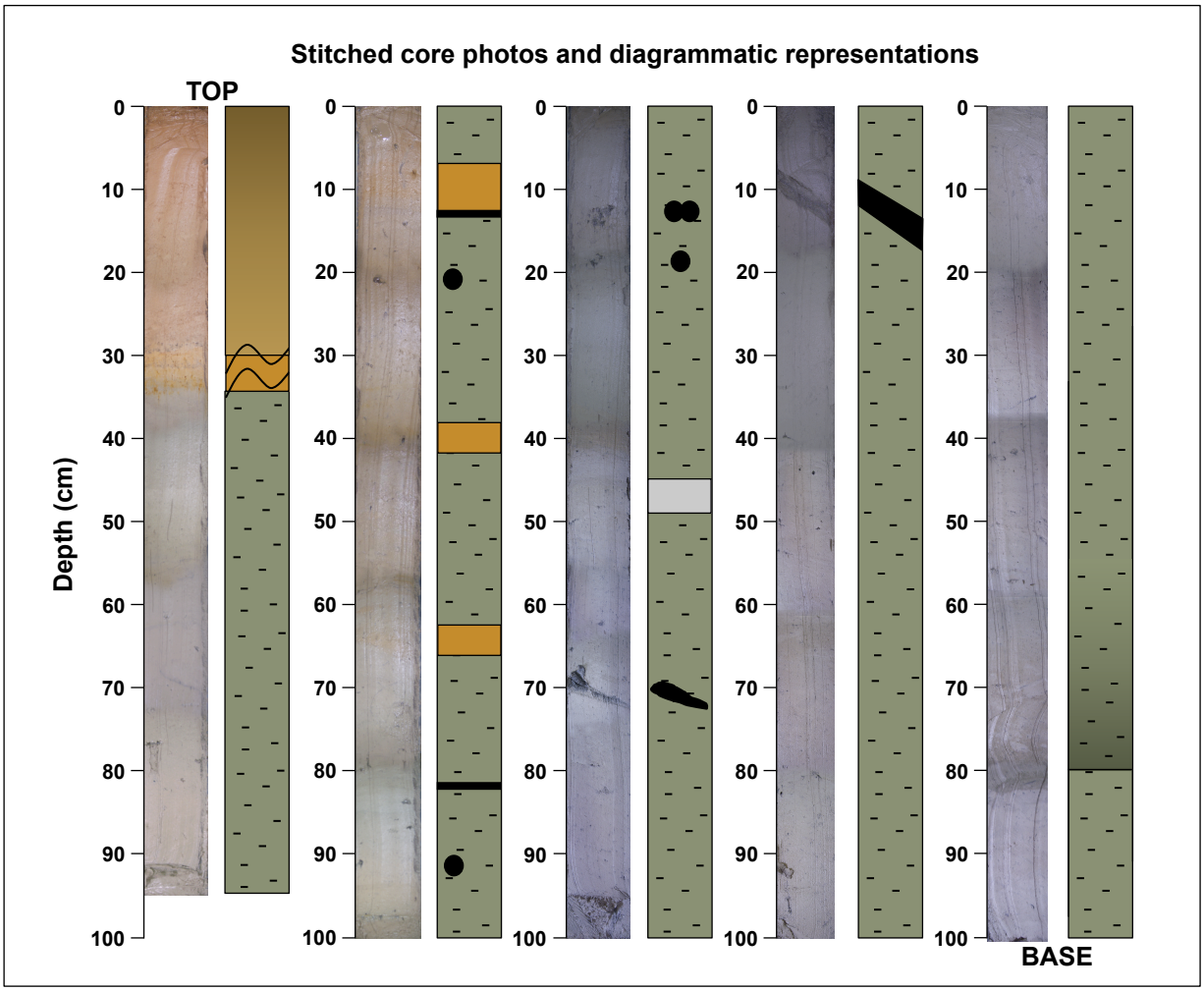

Colours used in diagrammatic representation show the approximate colours of sediment. Black flecks represent flecks in sediment and larger black marks represent dark spots within the sediment.

8.2.2.1.B B5-1 GRAIN SIZE ANALYSIS

Mid-sample depth (cm)	Total dry weight (g)	>63µm dry weight (g)	<63µm dry weight (g)	% >63µm
0.5	11.5973	1.2981	10.2992	11.19
1.5	8.3564	2.2826	6.0738	27.32
2.5	7.2424	2.3067	4.9357	31.85
3.5	7.9679	1.8383	6.1296	23.07
4.5	9.1171	1.3628	7.7543	14.95
5.5	11.7010	0.5531	11.1479	4.73
10.5	10.8338	0.6637	10.1701	6.13
15.5	17.9179	1.7422	16.1757	9.72
20.5	20.8912	2.5059	18.3853	12.00
25.5	20.1360	2.9407	17.1953	14.60
30.5	21.0222	1.6103	19.4119	7.66
35.5	17.8038	1.2853	16.5185	7.22
40.5	18.9938	1.3293	17.6645	7.00
45.5	13.7685	1.1095	12.6590	8.06
50.5	18.7611	1.4081	17.3530	7.51
55.5	19.3426	1.1130	18.2296	5.75
60.5	21.6143	1.4118	20.2025	6.53
65.5	19.2183	0.7172	18.5011	3.73
70.5	22.6022	0.9535	21.6487	4.22
75.5	22.1204	1.5247	20.5957	6.89
80.5	21.9386	1.8202	20.1184	8.30
85.5	23.3830	1.9711	21.4119	8.43
90.5	28.4195	1.8080	26.6115	6.36
95.5	23.1188	1.4939	21.6249	6.46
100.5	25.1123	1.4427	23.6696	5.74
105.5	25.0237	1.3183	23.7054	5.27
110.5	27.4161	1.2053	26.2108	4.40
115.5	30.6902	1.5475	29.1427	5.04
120.5	33.3274	1.4500	31.8774	4.35
125.5	26.2147	2.3645	23.8502	9.02
130.5	29.9874	2.6318	27.3556	8.78
135.5	30.9937	1.2810	29.7127	4.13
140.5	28.5808	1.7934	26.7874	6.27
145.5	25.6430	1.5884	24.0546	6.19
150.5	25.3056	1.6449	23.6607	6.50
155.5	25.6393	1.4807	24.1586	5.78
160.5	24.9462	1.6022	23.3440	6.42
165.5	20.6757	1.9045	18.7712	9.21
170.5	23.4556	2.4734	20.9822	10.55
175.5	26.4947	2.9496	23.5451	11.13
180.5	27.5837	2.6208	24.9629	9.50
185.5	24.8495	2.3567	22.4928	9.48
190.5	26.7637	1.7277	25.0360	6.46
195.5	27.0365	1.1791	25.8574	4.36
200.5	28.3037	2.2506	26.0531	7.95
205.5	17.1095	1.6925	15.4170	9.89
208.5	29.1861	4.5632	24.6229	15.63
210.5	19.6328	1.7652	17.8676	8.99
215.5	30.8004	5.2914	25.5090	17.18
220.5	24.6378	2.2517	22.3861	9.14
225.5	27.5526	2.5597	24.9929	9.29
230.5	27.9857	2.3185	25.6672	8.28

Mid-sample depth (cm)	Total dry weight	>63µm dry weight	<63µm dry weight	% >63µm
235.5	26.6152	1.8743	24.7409	7.04
240.5	28.2876	4.0409	24.2467	14.29
245.5	26.8318	1.9376	24.8942	7.22
250.5	26.6073	3.5155	23.0918	13.21
255.5	26.4449	2.3367	24.1082	8.84
260.5	23.7746	1.9536	21.8210	8.22
265.5	24.6240	2.2439	22.3801	9.11
270.5	32.2833	4.1258	28.1575	12.78
275.5	21.5580	2.0289	19.5291	9.41
280.5	26.3059	3.0127	23.2932	11.45
285.5	25.6783	2.8571	22.8212	11.13
290.5	26.9872	2.7308	24.2564	10.12
295.5	28.7725	2.8281	25.9444	9.83
300.5	18.5006	1.7726	16.7280	9.58
305.5	18.3924	2.3526	16.0398	12.79
310.5	22.9667	1.7982	21.1685	7.83
315.5	15.8562	1.2523	14.6039	7.90
320.5	25.1946	2.0734	23.1212	8.23
325.5	23.1688	1.6900	21.4788	7.29
330.5	23.2013	1.8263	21.3750	7.87
335.5	23.1000	2.3594	20.7406	10.21
340.5	19.4493	1.7893	17.6600	9.20
345.5	17.6322	1.6377	15.9945	9.29
350.5	24.8264	2.5716	22.2548	10.36
355.5	19.2611	2.4754	16.7857	12.85
360.5	30.5816	4.2597	26.3219	13.93
365.5	27.9031	3.8945	24.0086	13.96
370.5	25.8165	3.7868	22.0297	14.67
375.5	25.4341	3.4457	21.9884	13.55
380.5	20.1574	2.8133	17.3441	13.96
385.5	20.7504	2.6884	18.0620	12.96
390.5	26.6215	3.1360	23.4855	11.78
395.5	16.7590	1.6830	15.0760	10.04
400.5	22.2651	2.6740	19.5911	12.01
405.5	25.8440	2.5468	23.2972	9.85
410.5	27.6779	2.1228	25.5551	7.67
415.5	26.9325	2.2616	24.6709	8.40
420.5	29.7618	2.4521	27.3097	8.24
425.5	26.4803	2.0393	24.4410	7.70
430.5	29.4045	2.7483	26.6562	9.35
435.5	37.1771	5.9560	31.2211	16.02
440.5	30.4616	5.5604	24.9012	18.25
445.5	36.9150	7.8953	29.0197	21.39
450.5	29.1314	6.2525	22.8789	21.46
455.5	28.0633	3.7247	24.3386	13.27
460.5	25.2752	3.7407	21.5345	14.80
465.5	27.3159	3.6369	23.6790	13.31
470.5	25.1944	2.8333	22.3611	11.25
475.5	26.4685	2.3866	24.0819	9.02
480.5	30.2573	1.8724	28.3849	6.19
485.5	27.1863	2.5149	24.6714	9.25
490.5	34.5046	3.2613	31.2433	9.45

MID-SAMPLE DEPTH (CM)	FRACTION WEIGHT (g)					TOTAL WEIGHT (g)	FRACTION PERCENTAGE					MEAN GRAIN SIZE (μm)
	0-63μm	63-125μm	125-250μm	250-500μm	500μm		0-63μm	63-125μm	125-250μm	250-500μm	>500μm	
0.5	11.1931	0.3438	0.3836	0.4648	0.1059	12.4912	89.6079	2.7523	3.0710	3.7210	0.8478	56.8840
5.5	4.7269	0.3345	0.1130	0.0848	0.0208	5.2800	89.5247	6.3352	2.1401	1.6060	0.3939	47.1453
10.5	6.1262	0.3602	0.1425	0.1424	0.0186	6.7899	90.2252	5.3049	2.0987	2.0972	0.2739	47.2618
15.5	9.7232	0.7750	0.4971	0.4236	0.0465	11.4654	84.8048	6.7594	4.3356	3.6946	0.4056	58.0931
20.5	11.9950	1.0822	0.6960	0.6205	0.1072	14.5009	82.7190	7.4630	4.7997	4.2790	0.7393	63.6620
25.5	14.6042	1.4992	0.9007	0.4581	0.0827	17.5449	83.2390	8.5449	5.1337	2.6110	0.4714	57.2047
30.5	7.6600	0.6409	0.4670	0.4524	0.0500	9.2703	82.6295	6.9135	5.0376	4.8801	0.5394	64.3180
35.5	7.2192	0.5600	0.3905	0.2845	0.0503	8.5045	84.8869	6.5847	4.5917	3.3453	0.5914	58.5190
40.5	6.9986	0.6988	0.3912	0.2282	0.0111	8.3279	84.0380	8.3911	4.6975	2.7402	0.1333	54.4427
45.5	8.0582	0.5555	0.3242	0.2195	0.0103	9.1677	87.8978	6.0593	3.5363	2.3943	0.1124	49.8352
50.5	7.5054	0.6014	0.3947	0.3765	0.0355	8.9135	84.2027	6.7471	4.4281	4.2239	0.3983	59.9955
55.5	5.7541	0.6558	0.2710	0.1636	0.0226	6.8671	83.7924	9.5498	3.9463	2.3824	0.3291	54.1729
60.5	6.5318	0.8354	0.3371	0.1686	0.0707	7.9436	82.2272	10.5167	4.2437	2.1225	0.8900	58.3786
65.5	3.7319	0.4762	0.1681	0.0633	0.0096	4.4491	83.8797	10.7034	3.7783	1.4228	0.2158	50.5214
70.5	4.2186	0.6120	0.2050	0.0823	0.0542	5.1721	81.5646	11.8327	3.9636	1.5912	1.0479	58.0738
75.5	6.8927	0.8534	0.3542	0.2208	0.0963	8.4174	81.8864	10.1385	4.2079	2.6231	1.1441	61.6314
80.5	8.2968	1.0820	0.4023	0.2952	0.0407	10.1170	82.0085	10.6949	3.9765	2.9179	0.4023	57.3009
85.5	8.4296	1.1517	0.4261	0.3188	0.0745	10.4007	81.0484	11.0733	4.0968	3.0652	0.7163	60.4873
90.5	6.3618	1.1848	0.4132	0.1882	0.0218	8.1698	77.8698	14.5021	5.0576	2.3036	0.2668	58.2838
95.5	6.4618	0.8707	0.3401	0.2261	0.0570	7.9557	81.2224	10.9443	4.2749	2.8420	0.7165	59.9190
100.5	5.7450	0.9865	0.2661	0.1461	0.0440	7.1877	79.9282	13.7248	3.7022	2.0326	0.6122	57.2339
105.5	5.2682	0.9901	0.2112	0.0625	0.0545	6.5865	79.9848	15.0322	3.2066	0.9489	0.8274	55.1021
110.5	4.3963	0.8822	0.0701	0.2173	0.0357	5.6016	78.4830	15.7490	1.2514	3.8792	0.6373	61.1996
115.5	5.0423	1.1472	0.2343	0.0932	0.0728	6.5898	76.5168	17.4087	3.5555	1.4143	1.1047	60.7226

MID-SAMPLE DEPTH (CM)	FRACTION WEIGHT (g)					TOTAL WEIGHT (g)	FRACTION PERCENTAGE					MEAN GRAIN SIZE (μm)
	0-63μm	63-125μm	125-250μm	250-500μm	500μm		0-63μm	63-125μm	125-250μm	250-500μm	>500μm	
120.5	4.3508	1.0435	0.2793	0.0902	0.0370	5.8008	75.0033	17.9890	4.8149	1.5550	0.6378	60.1785
125.5	9.0197	1.6276	0.4474	0.1628	0.1267	11.3842	79.2301	14.2969	3.9300	1.4300	1.1129	59.4751
130.5	8.7764	1.5294	0.6042	0.2932	0.2050	11.4082	76.9305	13.4062	5.2962	2.5701	1.7970	69.8804
135.5	4.1331	0.8456	0.3086	0.0932	0.0336	5.4141	76.3395	15.6185	5.6999	1.7214	0.6206	60.5256
140.5	6.2748	1.0381	0.4858	0.1983	0.0712	8.0682	77.7721	12.8665	6.0211	2.4578	0.8825	63.7176
145.5	6.1943	0.8402	0.4368	0.1756	0.1358	7.7827	79.5906	10.7958	5.6125	2.2563	1.7449	67.2903
150.5	6.5001	0.9157	0.4923	0.1781	0.0588	8.1450	79.8049	11.2424	6.0442	2.1866	0.7219	60.6533
155.5	5.7751	0.8357	0.4178	0.1668	0.0604	7.2558	79.5929	11.5177	5.7581	2.2988	0.8324	61.5588
160.5	6.4226	0.8814	0.4305	0.2002	0.0901	8.0248	80.0344	10.9834	5.3646	2.4948	1.1228	63.3700
165.5	9.2113	0.9877	0.5548	0.3195	0.0425	11.1158	82.8667	8.8856	4.9911	2.8743	0.3823	57.4599
170.5	10.5450	1.1939	0.7514	0.4662	0.0619	13.0184	81.0008	9.1708	5.7718	3.5811	0.4755	61.9531
175.5	11.1328	1.3712	0.6069	0.3088	0.6627	14.0824	79.0547	9.7370	4.3096	2.1928	4.7059	85.6527
180.5	9.5013	1.4292	0.8182	0.3509	0.0225	12.1221	78.3799	11.7901	6.7497	2.8947	0.1856	60.6753
185.5	9.4839	1.0886	0.8394	0.4065	0.0222	11.8406	80.0964	9.1938	7.0892	3.4331	0.1875	61.4451
190.5	6.4554	0.8564	0.5261	0.2710	0.0742	8.1831	78.8869	10.4655	6.4291	3.3117	0.9067	65.9611
195.5	4.3611	0.6625	0.3053	0.1579	0.0534	5.5402	78.7175	11.9580	5.5106	2.8501	0.9639	64.2855
200.5	7.9516	1.1615	0.6493	0.3922	0.0476	10.2022	77.9401	11.3848	6.3643	3.8443	0.4666	65.1011
205.5	9.8922	0.8100	0.4583	0.2996	0.1246	11.5847	85.3902	6.9920	3.9561	2.5862	1.0756	58.6529
210.5	8.9911	0.9618	0.4594	0.2639	0.0801	10.7563	83.5891	8.9418	4.2710	2.4535	0.7447	57.5295
215.5	17.1796	2.1337	1.5074	1.1254	0.5249	22.4710	76.4524	9.4953	6.7082	5.0082	2.3359	81.8860
220.5	9.1392	1.1916	0.6248	0.3474	0.0879	11.3909	80.2325	10.4610	5.4851	3.0498	0.7717	62.6153
225.5	9.2902	1.2301	0.8422	0.4217	0.0657	11.8499	78.3990	10.3807	7.1072	3.5587	0.5544	65.2828
230.5	8.2846	1.1633	0.6300	0.3714	0.1538	10.6031	78.1337	10.9713	5.9417	3.5028	1.4505	70.0800
235.5	7.0422	0.9467	0.4132	0.3078	0.2066	8.9165	78.9795	10.6174	4.6341	3.4520	2.3170	73.8707

MID-SAMPLE DEPTH (CM)	FRACTION WEIGHT (g)					TOTAL WEIGHT (g)	FRACTION PERCENTAGE					MEAN GRAIN SIZE (μm)
	0-63μm	63-125μm	125-250μm	250-500μm	500μm		0-63μm	63-125μm	125-250μm	250-500μm	>500μm	
240.5	14.2851	1.9407	1.2027	0.7405	0.1570	18.3260	77.9499	10.5899	6.5628	4.0407	0.8567	68.3920
245.5	7.2213	1.0690	0.5440	0.2503	0.0743	9.1589	78.8446	11.6717	5.9396	2.7329	0.8112	63.2767
250.5	13.2125	1.8883	1.0515	0.3707	0.2050	16.7280	78.9844	11.2882	6.2859	2.2160	1.2255	64.7783
255.5	8.8361	1.4204	0.6667	0.1818	0.0678	11.1728	79.0858	12.7130	5.9672	1.6272	0.6068	58.7038
260.5	8.2172	0.9513	0.6262	0.3027	0.0734	10.1708	80.7920	9.3533	6.1569	2.9762	0.7217	62.3589
265.5	9.1127	1.0094	0.7109	0.4123	0.1113	11.3566	80.2414	8.8883	6.2598	3.6305	0.9801	66.3329
270.5	12.7800	1.6504	1.2729	0.8988	0.3037	16.9058	75.5953	9.7623	7.5294	5.3165	1.7964	80.5169
275.5	9.4114	0.9940	0.6318	0.3276	0.0755	11.4403	82.2653	8.6886	5.5226	2.8636	0.6600	60.1238
280.5	11.4526	1.4680	0.8802	0.5045	0.1600	14.4653	79.1729	10.1484	6.0849	3.4877	1.1061	67.2627
285.5	11.1265	1.3405	0.8179	0.5653	0.1334	13.9836	79.5682	9.5862	5.8490	4.0426	0.9540	67.3564
290.5	10.1189	1.2517	0.8001	0.5496	0.1294	12.8497	78.7481	9.7411	6.2266	4.2772	1.0070	69.2292
295.5	9.8292	1.2703	0.8192	0.5501	0.1885	12.6573	77.6563	10.0361	6.4722	4.3461	1.4893	73.4984
300.5	9.5813	0.8545	0.5308	0.2996	0.0877	11.3539	84.3878	7.5260	4.6750	2.6387	0.7724	58.1108
305.5	12.7912	0.9575	0.7229	0.5249	0.1473	15.1438	84.4649	6.3227	4.7736	3.4661	0.9727	61.7933
310.5	7.8296	0.9183	0.5559	0.2579	0.0661	9.6278	81.3228	9.5380	5.7739	2.6787	0.6866	60.6028
315.5	7.8979	0.6185	0.3849	0.1954	0.0535	9.1502	86.3139	6.7594	4.2065	2.1355	0.5847	53.8231
320.5	8.2295	0.9869	0.5952	0.3193	0.1720	10.3029	79.8756	9.5788	5.7770	3.0991	1.6694	69.1392
325.5	7.2943	0.8921	0.5256	0.2099	0.0624	8.9843	81.1894	9.9296	5.8502	2.3363	0.6945	59.8478
330.5	7.8715	1.0067	0.5430	0.2165	0.0601	9.6978	81.1680	10.3807	5.5992	2.2325	0.6197	58.8439
335.5	10.2139	1.1982	0.7631	0.3035	0.0946	12.5733	81.2348	9.5298	6.0692	2.4139	0.7524	60.6216
340.5	9.1998	0.9157	0.5449	0.2518	0.0769	10.9891	83.7175	8.3328	4.9585	2.2914	0.6998	57.3421
345.5	9.2881	0.9034	0.5182	0.1962	0.0199	10.9258	85.0107	8.2685	4.7429	1.7957	0.1821	51.5438
350.5	10.3583	1.3748	0.7605	0.3554	0.0809	12.9299	80.1113	10.6327	5.8817	2.7487	0.6257	61.2581
355.5	12.8518	1.2508	0.8003	0.3578	0.0665	15.3272	83.8496	8.1607	5.2214	2.3344	0.4339	55.8819

MID-SAMPLE DEPTH (CM)	FRACTION WEIGHT (g)					TOTAL WEIGHT (g)	FRACTION PERCENTAGE					MEAN GRAIN SIZE (μm)
	0-63μm	63-125μm	125-250μm	250-500μm	500μm		0-63μm	63-125μm	125-250μm	250-500μm	>500μm	
360.5	13.9290	2.1651	1.2732	0.6793	0.1421	18.1887	76.5805	11.9036	7.0000	3.7347	0.7813	68.3018
365.5	13.9572	2.1597	1.2460	0.4275	0.0613	17.8517	78.1842	12.0980	6.9797	2.3947	0.3434	60.6427
370.5	14.6681	2.0779	1.0969	0.4138	0.1982	18.4549	79.4808	11.2593	5.9437	2.2422	1.0740	63.2277
375.5	13.5476	1.8360	1.0784	0.4409	0.0904	16.9933	79.7231	10.8043	6.3460	2.5946	0.5320	60.8871
380.5	13.9567	1.5070	0.8683	0.3619	0.0761	16.7700	83.2242	8.9863	5.1777	2.1580	0.4538	55.8669
385.5	12.9559	1.3756	0.8426	0.3444	0.1258	15.6443	82.8155	8.7930	5.3860	2.2014	0.8041	58.7374
390.5	11.7800	1.6739	1.0202	0.3477	0.0942	14.9160	78.9755	11.2222	6.8397	2.3311	0.6315	61.7285
395.5	10.0424	0.9527	0.5081	0.1705	0.0517	11.7254	85.6465	8.1251	4.3333	1.4541	0.4409	51.5011
400.5	12.0098	1.5131	0.7524	0.3019	0.1066	14.6838	81.7895	10.3045	5.1240	2.0560	0.7260	58.2122
405.5	9.8545	1.2335	0.7511	0.4262	0.1360	12.4013	79.4635	9.9465	6.0566	3.4367	1.0967	66.8496
410.5	7.6697	1.1952	0.5803	0.2811	0.0662	9.7925	78.3221	12.2053	5.9260	2.8706	0.6760	63.0906
415.5	8.3973	1.1914	0.5937	0.3652	0.1113	10.6589	78.7820	11.1775	5.5700	3.4262	1.0442	66.4469
420.5	8.2391	1.2991	0.6612	0.3864	0.1054	10.6912	77.0643	12.1511	6.1845	3.6142	0.9859	68.2405
425.5	7.7012	1.1324	0.5849	0.2599	0.0621	9.7405	79.0637	11.6257	6.0048	2.6682	0.6375	61.8798
430.5	9.3465	1.5371	0.8134	0.3403	0.0575	12.0948	77.2771	12.7087	6.7252	2.8136	0.4754	63.0148
435.5	16.0206	2.7360	1.8091	0.8478	0.5631	21.9766	72.8985	12.4496	8.2319	3.8577	2.5623	83.7840
440.5	18.2538	3.1349	1.8568	0.4269	0.1418	23.8142	76.6509	13.1640	7.7970	1.7926	0.5954	62.3268
445.5	21.3878	4.3124	2.8448	0.5279	0.2102	29.2831	73.0380	14.7266	9.7148	1.8027	0.7178	67.2092
450.5	21.4631	3.7504	2.0439	0.3479	0.1103	27.7156	77.4405	13.5317	7.3745	1.2552	0.3980	58.6328
455.5	13.2725	2.2668	1.1615	0.2033	0.0931	16.9972	78.0864	13.3363	6.8335	1.1961	0.5477	58.5395
460.5	14.7999	2.1761	1.2056	0.3218	0.0372	18.5406	79.8243	11.7370	6.5025	1.7357	0.2006	56.3831
465.5	13.3142	1.9952	1.2166	0.3604	0.0647	16.9511	78.5448	11.7703	7.1771	2.1261	0.3817	60.0983
470.5	11.2458	1.8039	0.8087	0.1977	0.0230	14.0791	79.8758	12.8127	5.7440	1.4042	0.1634	54.4658
475.5	9.0168	1.5426	0.6352	0.1370	0.0718	11.4034	79.0711	13.5276	5.5703	1.2014	0.6296	57.2952

MID-SAMPLE DEPTH (CM)	FRACTION WEIGHT (g)					TOTAL WEIGHT (g)	FRACTION PERCENTAGE					MEAN GRAIN SIZE (μm)
	0-63μm	63-125μm	125-250μm	250-500μm	500μm		0-63μm	63-125μm	125-250μm	250-500μm	>500μm	
480.5	6.1883	1.3288	0.4005	0.1000	0.0431	8.0607	76.7711	16.4850	4.9686	1.2406	0.5347	57.6573
485.5	9.2506	1.5070	0.7389	0.1922	0.0768	11.7655	78.6248	12.8086	6.2802	1.6336	0.6528	59.6039
490.5	9.4518	1.9970	0.9613	0.2588	0.0442	12.7131	74.3469	15.7082	7.5615	2.0357	0.3477	62.6042

8.2.2.2 STABLE ISOTOPE STRATIGRAPHY

8.2.2.2.A B5-1 $\delta^{18}O$ AND $\delta^{13}C$ ISOTOPE DATA

Mid-sample depth (cm)	$\delta^{13}C$	$\delta^{13}O$
0.5	+1.72	+0.72
5.5	+1.79	+0.69
10.5	+1.66	+0.44
15.5	+1.70	+0.28
20.5	+1.66	-0.27
25.5	+1.53	+0.28
30.5	+0.94	+1.00
35.5	+1.30	+0.99
40.5	+1.50	+1.11
45.5	+1.23	+1.69
50.5	+1.34	+1.69
55.5	+1.10	+1.91
60.5	+1.00	+2.40
65.5	+1.28	+2.88
70.5	+1.14	+2.54
75.5	+1.25	+3.07
80.5	+1.39	+2.78
85.5	+1.29	+2.88
90.5	+1.30	+2.72
95.5	+1.38	+2.67
100.5	+1.14	+2.51
105.5	+1.07	+2.61
110.5	+1.08	+2.23
115.5	+0.91	+2.48
120.5	+1.02	+1.15
125.5	+1.24	+2.15
130.5	+1.06	+1.98
135.5	+1.18	+1.52
140.5	+1.18	+2.30
145.5	+1.17	+2.16
150.5	+1.13	+1.83
155.5	+1.09	+2.18
160.5	+1.42	+2.09
165.5	+1.25	+2.16
170.5	+1.28	+1.80
175.5	+1.27	+1.96
180.5	+1.24	+1.78
185.5	+1.40	+1.52
190.5	+1.31	+1.15
195.5	+1.42	+1.33
200.5	+1.30	+1.64
205.5	+1.48	+1.43
210.5	+1.19	+1.54
215.5	+1.01	+1.44
220.5	+1.44	+2.01
225.5	+1.30	+1.66
230.5	+1.52	+1.35
235.5	+1.24	+0.75
240.5	+1.38	+0.37
245.5	+1.38	+0.30
250.5	+1.50	+0.75
255.5	+1.58	+0.83
260.5	+1.58	+1.42
265.5	+1.77	+1.27
270.5	+1.46	+0.91
275.5	+1.04	+1.04
285.5	+1.57	+1.23
290.5	+1.77	+1.19
295.5	+1.56	+1.19
300.5	+1.53	+1.46
305.5	+1.50	+1.44
310.5	+1.54	+1.43
315.5	+1.22	+0.81
320.5	+1.80	+1.00
325.5	+1.26	+0.75
330.5	+1.40	+0.79
335.5	+1.32	+0.90
340.5	+1.58	+0.87
345.5	+1.22	+0.94
350.5	+1.40	+1.40
355.5	+1.31	+0.87
360.5	+1.03	+0.95
365.5	+1.08	+1.05
370.5	+1.07	+1.07
375.5	+1.12	+0.68
380.5	+1.18	+1.00
385.5	+1.01	+0.81
390.5	+1.15	+0.93
395.5	+1.08	+0.84
400.5	+1.11	+0.88
405.5	+1.11	+0.68
410.5	+1.10	+1.77
415.5	+1.02	+1.35
420.5	+0.57	+0.65
425.5	+1.08	+1.40
430.5	+1.33	+1.41
435.5	+1.16	+1.19
440.5	+1.00	+1.44
445.5	+1.06	+0.64
450.5	+0.82	+0.55
455.5	+0.70	+0.01
460.5	+0.76	-0.50
465.5	+0.74	-0.69
470.5	+0.67	-0.31
475.5	+1.12	+1.06
480.5	+1.07	+1.56
485.5	+1.29	+1.22
490.5	+1.34	+1.48

8.2.2.3 MICROPALAEONTOLOGY APPENDIX

8.2.2.3.A B5-1 PLANKTIC FORAMINIFERA SPECIES ANALYSIS >500 µm

	0	10	20	30	40	50	60	70	80	90	100	105	110	120	130	140
Globoquadrina bulloides																
Globigerina cariacoensis																
Globigerinella aequilateralis	1	2	9	2												
Globigerinella calida																
Globigerinoides elongatus				1												
Globigerinoides pyramidalis																
Globigerinoides ruber	1	2	7	3												
Globigerinoides sacculifer	3	6	23													
Globigerinoides trilobus			13													
Globorotalia crassaformis																
Globorotalia inflata	11		18	19	1	35		1								
Globorotalia truncatulinoides S*	139	12	3	20		9										
Globorotalia truncatulinoides D*	4	2		1		2										
Neogloboquadrina dutertrei																
Orbulina universa	167	37	320	50	5	18	2	1		1	1					
Total individuals	326	61	393	96	6	64	2	2	0	1	1	0	0	0	0	0
Total species	6	5	7	6	2	3	1	2	0	1	1	0	0	0	0	0

*D dextral coiling
*S sinistral coiling

150	160	170	180	190	200	210	220	230	240	250	260	270	280	290	300	310	320	330	340	350
			2		1	2			4		1	3								
		1																		
									1			1							1	2
									2											
					6	10	23	45	48			1			1	1				1
											1	17	33	43		1			1	1
							1		7					15	41	7				
1		2	2		1	2	22	63	28	28	9	75	58	189	136	101	256	89	33	83
1	0	3	4	0	8	14	46	108	90	28	11	97	91	247	178	110	256	89	35	87
1	0	2	2	0	3	3	3	2	6	1	3	5	2	2	3	3	0	1	3	4

360	370	380	390	400	410	420	430	440	450	460	470	480	490
			1										
		1				3							
7	16	18	4	1									
2					4								
5	1	3	1	3	7	7		2					
	1				2								
70	36	5	14	9	12	3	1	2	2	4	8	1	12
84	54	27	20	13	25	13	1	4	2	4	8	1	12
4	4	4	4	3	4	3	1	2	1	1	1	1	1

8.2.2.3.A B5-1 PLANKTIC FORAMINIFERA SPECIES ANALYSIS 150–500 µm

	0	10	20	30	40	50	60	70	80	90	100	105	110	120
Beella digitata		1												
Candeina nitida						1								
Globigerina bulloides	26	24	45	43	91	96	259	146	136	104	146	120	234	86
Globigerina cariacoensis	1			1				1			4	4	1	
Globigerinella aequilateralis	8	18	17	4				1						
Globigerinella calida	5	11	2											
Globigerinita glutinata		7	3	13	57		17	46	18	22	33	33	8	34
Globigerinoides elongatus	39	37	46	13		42	4	5				2	12	1
Globigerinoides pyramidalis			1				1	1	1					
Globigerinoides ruber	19	36	62	62	37	18	9	1	89	103	50	7	38	4
Globigerinoides sacculifer	19	16	16	8							1			
Globigerinoides trilobus	11	16	17	8										
Globorotalia crassaformis	4												1	
Globorotalia inflata	71	60	78	108	27	113	8	13	1	2	4		2	12
Globorotalia scitula				2	2	1		25	24	47	34	90	2	110
Globorotalia truncatulinoides S*	81	38		25		4	1						1	1
Globorotalia truncatulinoides D*	2	14				2								
Globorotaloides hexagona			3		18			17	5	4	12	25		20
Hastigerina pelagica														
Neogloboquadrina dutertrei	6	19	28	18	73	20	9	52	30	22	38	25	6	44
Orbulina universa	11	10	20	11	1	4			1	2			1	1
Turborotalia humilis				1										
Unidentifiable	1	2			4	1			3					2
Total individuals	304	309	338	317	310	302	308	308	308	306	322	306	306	315
Total species	14	14	13	14	9	10	8	11	10	8	9	8	11	11
Fisher alpha	3.0320	3.0180	2.6840	2.9970	1.7330	1.9880	1.5010	2.2290	1.9790	1.5040	1.7180	1.5040	2.2320	2.2160
Evenness	0.5775	0.7354	0.6535	0.5320	0.6397	0.4694	0.2518	0.4399	0.4389	0.5727	0.5617	0.5904	0.2245	0.4873
Shannon Weiner	2.0900	2.3320	2.1400	2.0080	1.7500	1.5460	0.7005	1.5770	1.4790	1.5220	1.6200	1.5520	0.9041	1.6790

130	140	150	160	170	180	190	200	210	220	230	240	250	260	270	280	290	300	310
1		2		1	1				1			1						
179	153	157	183	124	120	270	180	143	159	74	121	86	101	93	87	70	83	62
3		9	3	15	12		15	5	1		9	4				1		
											2		1			3	5	7
																1		
36	45	20	28	40	59	31	29	69	48	60	27		6	12	17	1		3
		7	2	4	3	3	6		3	12		5		5			3	1
2	35	11	24	67	19	2	7	23	10	9	24	50	30	33	6	28	22	4
4	7	8	3	2	1	3	19	27	35	40	62	55	26	41	21	26	20	65
24	28	29	28	17	33	18	15	14	20	13	9	5	8				1	3
											1	1	19	47	62	17	1	1
											2		1	1	4	51	54	15
20	7	9	15	5	35	4	6	15	18	76	13	15	34	11	25	15	1	13
												1						
38	39	48	26	38	52	37	27	30	31	22	36	72	66	49	83	55	85	59
1					2	2	1	1	5	6	2	7	16	28	21	46	52	71
																	1	
		5	6								1					1		
308	314	305	318	313	337	370	305	327	331	312	309	302	308	320	326	315	328	304
10	7	11	10	10	11	9	10	9	11	9	12	12	11	9	8	12	11	11
1.9790	1.2690	2.2340	1.9630	1.9710	2.1790	1.6640	1.9830	1.7120	2.1890	1.7310	2.4840	2.4980	1.9790	1.7200	1.4820	2.4710	2.1940	2.2360
0.3945	0.6515	0.4712	0.4413	0.5430	0.5565	0.3016	0.4387	0.5842	0.4811	0.7345	0.5140	0.5009	0.6658	0.7776	0.7577	0.5766	0.5503	0.5814
1.3720	1.5170	1.6450	1.4840	1.6920	1.8120	0.9985	1.4790	1.6600	1.6660	1.8890	1.8190	1.7940	1.8960	1.9460	1.8020	1.9340	1.8010	1.8550

320	330	340	350	360	370	380	390	400	410	420	430	440	450	460	470	480	490
1				1													
									1								
104	78	87	98	79	83	72	111	128	74	117	64	75	93	71	77	87	75
		1	5	4		2	7		4	13	6	12	6	2	1	2	
	11	1			1	2	1	4					2		3	1	
	1	4															
8	1	19	1	18	12	6	44		4	16	10	3		5	8	5	
1			9		4			4			7	8		17	6	9	4
	2																
9	47	70	77	37	84	126	60	34	50	4	12	7	7	22	13	21	6
1	2	2	2			1	17								3		
	4								2								
				2				1	4								
27	66	39	25	62	55	54	32	64	56	90	125	109	85	51	66	85	41
5	1		11	6	5	5	10	10	2	8	4	9	5		2	11	19
													1	1			
		1				1			2		1						1
1		5	11	22	5		16		11		10	8		5	5	27	8
							1								1		
67	31	45	39	84	27	31	73	57	71	57	70	110	101	135	140	94	146
91	59	40	32	8	30	5	2	22	26	2	3	2	2	5	4	5	7
						3						1					
		1			3	1		2	1			1					
315	303	315	310	323	309	309	374	326	308	307	312	345	302	314	329	347	307
11	12	13	11	11	11	13	12	10	14	8	11	12	9	10	13	11	9
2.2160	2.4960	2.7340	2.2250	2.2020	2.2270	2.7480	2.3670	1.9510	3.0210	1.5020	2.2210	2.4150	1.7440	1.9690	2.7030	2.1640	1.7370
0.4494	0.5156	0.5062	0.5872	0.5916	0.5686	0.3874	0.5807	0.5329	0.4864	0.5671	0.4746	0.4257	0.4525	0.4888	0.3757	0.5426	0.4843
1.5980	1.8230	1.8840	1.8660	1.8730	1.8330	1.6170	1.9410	1.6730	1.9180	1.5120	1.6530	1.6310	1.4040	1.5870	1.5860	1.7870	1.4720

8.2.2.3.B B5-1 PTEROPOD AND HETEROPOD SPECIES ANALYSIS >500 µm

Species	0	10	20	30	40	50	60	70	80	90	100	105	110	120	130
PTEROPODS															
Cavolinia inflexa			1												
Cavolinia veliger															
Clio pyramidata			1						1						1
Clio cuspidata															4
Creseis virgula constricta						1									
Creseis virgula virgula			1												
Diacria trispinosa															
Limacina bulimoides															
Limacina inflata	13	8	8	4		5		3							
Limacina retroversa					3	4	33	45	67	11	72	28	28	14	204
Limacina trochiformis															
Limacina sp. B															
Cuvierina columnella															
Peraclis mollucensis															
Peraclis spp.							1								
HETEROPODS															
Atlanta rosea			1												
Atlanta selvagensis			2	1							1				
Firoloida desmaresti			2	1											
Oxygyrus keraudreni															
Carinaria lamarckii						1									
TOTAL	13	8	16	6	3	11	34	48	68	11	73	28	28	14	209
number of species	1	1	7	3	1	4	2	2	2	1	2	1	1	1	3

140	150	160	170	180	190	200	210	220	230	240	250	260	270	280	290	300	310	320	330	340
	1																			
		1							2	1										
					1															
									6											
24	36	65	32	18	40	71	62	111	7	110	18	2	116			2		4	2	
												1								
				1																
								1												
										1										
24	37	66	32	19	41	71	62	112	15	112	18	3	116	0	0	2	0	4	2	0
1	2	2	1	2	2	1	1	2	3	3	1	2	1	0	0	1	0	1	1	0

350	360	370	380	390	400	410	420	430	440	450	460	470	480	490
														1
										1				
										1		6	1	1
	3	2			1	1	32	13	11	7			5	1
														1
1														
1	3	2	0	0	1	1	32	13	11	9	0	6	6	4
1	1	1	0	0	1	1	1	1	1	3	0	1	2	4

8.2.2.3.B B5-1 PTEROPOD AND HETEROPOD SPECIES ANALYSIS 150–500 µm

Species	0	10	20	30	40	50	60	70	80	90	100	105	110	120	130	140
PTEROPODS																
Cavolinia inflexa		5	13													
Cavolinia veliger		1														
Clio pyramidata	2	4	11	9	13	32		2	7	12	9	1			1	20
Clio cuspidata			5	1											5	4
Creseis acicula	1			2												
Creseis virgula	2	2	20	17		2										
Diacria trispinosa				3				1								
Limacina bulimoides	7	8	29	14	2	4		1								
Limacina inflata	145	160	48	132	38	119	1	27				1		1	1	15
Limacina retroversa			5	6	167	4	105	246	262	275	304	285	117	274	296	193
Limacina trochiformis	45	25														
Limacina sp B											1					
Limacina sp. D																
Styliola subula	6															
Gleba cordata																
Peraclis moluccensis	3	1	1	1					1		3				1	2
Peraclis spp.																
Gymnosome veliger														1		
Paedoclione doliiformis						2			1	8	2					
HETEROPODS																
Atlanta helicinoidea				2										1		
Atlanta peronii	4		16			10										
Atlanta rosea	11	12		10	33			5	30	7	3	2		1	2	27
Atlanta selvagensis	50	63	50	50	18	38	1	1								
Atlanta spp.																
Firoloida desmaresti	24	10	55	48	25	63		2	2		1	7		4		21
Oxygyrus keraudreni	1	1														
Carinaria lamarckii			4	1	1	5										
Carinaria spp.	4			2	5	6		1	2	1	2	7		6		6
TOTAL	305	292	257	298	302	285	107	286	305	303	325	303	117	288	306	288
number of species	14	12	12	15	9	11	3	9	7	5	8	6	1	7	6	8
Fisher alpha	3.0290	2.5210	2.6080	3.3290	1.7440	2.2730	0.5730	1.7670	1.2770	0.8506	1.4830	1.0600	0.1502	1.2940	1.0580	1.5250
Evenness	0.3827	0.3507	0.6840	0.3890	0.4785	0.4837	0.3706	0.1968	0.2473	0.3037	0.1768	0.2256	1.0000	0.1864	0.2012	0.4128
Shannon Weiner	1.6790	1.4370	2.1050	1.7640	1.4600	1.6720	0.1059	0.5717	0.5487	0.4177	0.3465	0.3025	0.0000	0.2661	0.1884	1.1950

150	160	170	180	190	200	210	220	230	240	250	260	270	280	290	300	310	320	330
38	10	32	29	3	13	16	5	48	10	1			1	2	4	5	1	
5		5	8	3		1		3	1	1	1		1	2			1	
							2	5		10	12		1	5	2	3	6	1
								1	5	1	2	3	4	6	5	7	4	1
								3	6	6	6		3	1	2			
5	3	6		4	13	22	32	160	47	38	76	53	143	61	15	11	1	
196	258	172	93	281	275	207	250	41	176	110	128	115	6	7	18	30	15	4
															1			
							1											
							1											
									1									
			4	1	3	5	1	1			2							
1		1																
		2		1		1	1	3	2	2		2	8	6	1	5		
						1				3								
37	11	42	28	6	11	17		4	1									1
		3			2	3	6	10	31	118	55	29	100	166	77	63	5	
12	5	26	121	2	1	16	3	4	4	1	1	1	8	25	12	2		
	1	1		1		3			5		1			3			2	2
3	3	2		5		5	3	7	4	2	3	1	7	7	11	11		3
297	291	292	283	307	318	297	305	290	293	293	287	204	282	291	148	137	35	12
8	7	12	6	10	7	12	10	13	13	12	11	7	11	12	11	9	8	6
1.5140	1.2910	2.2590	1.0760	1.9800	1.2660	2.5090	2.2340	2.7950	2.7870	2.5180	2.2690	1.4040	2.2790	2.5230	2.7460	2.1610	3.2420	4.7750
0.3868	0.2427	0.3514	0.6444	0.1585	0.2596	0.2797	0.1911	0.3371	0.3060	0.3334	0.3754	0.4335	0.3194	0.3389	0.4598	0.5693	0.6572	0.8529
1.1300	0.5300	1.3520	1.3520	0.4607	0.5974	1.2110	0.7431	1.4780	1.3810	1.3860	1.4180	1.1100	1.2560	1.4030	1.6210	1.6340	1.6600	1.6330

340	350	360	370	380	390	400	410	420	430	440	450	460	470	480	490
														1	3
	3						1		2		2			3	15
					1	1		2	1				2	1	
1	1	2	12	13	3						1				
1	20	10	14	5	1			1		1	4				1
4	44	3	3	10	22	1	5		1	2			1	1	3
	11	15	52	62	167	143	214	44	55	49	230	250	298	49	112
2	60	233	25	16	8	6	33	274	222	231	18	16	3	201	73
	2			2			3	1	1		1		1		
	1				3	3	1		1		1			3	
			1							1			1	1	
			2		1		7			4	4	2	3		
															1
	2							2		2		3			
	40	27	113	126	86	36	35	3	2		9	16	5	4	37
		1				1									
	8	1	15	17	1	7	6		1	7	8	3		6	20
	28	1	9	8			2				7			4	8
2		6	4	1	3	2	2	2	4	11	6	6	4	4	19
10	220	299	250	260	296	200	309	329	290	308	291	296	318	278	292
5	12	10	11	10	11	9	11	8	10	9	12	7	9	12	11
3.9800	2.7250	1.9930	2.3530	2.0650	2.2510	1.9370	2.2270	1.4790	2.0080	1.7360	2.5230	1.2860	1.7230	2.5540	2.2590
0.8706	0.5741	0.2436	0.4934	0.4758	0.2986	0.2901	0.2776	0.2261	0.2107	0.2658	0.2143	0.2775	0.1585	0.2232	0.5084
1.4710	1.9300	0.8905	1.6910	1.5600	1.1890	0.9596	1.1160	0.5925	0.7453	0.8723	0.9446	0.6640	0.3554	0.9850	1.7210

8.2.2.3.C DISTRIBUTION OF MOST ABUNDANT PLANKTIC FORAMINIFERA, PTEROPOD AND HETEROPOD SPECIES 150–500 µm

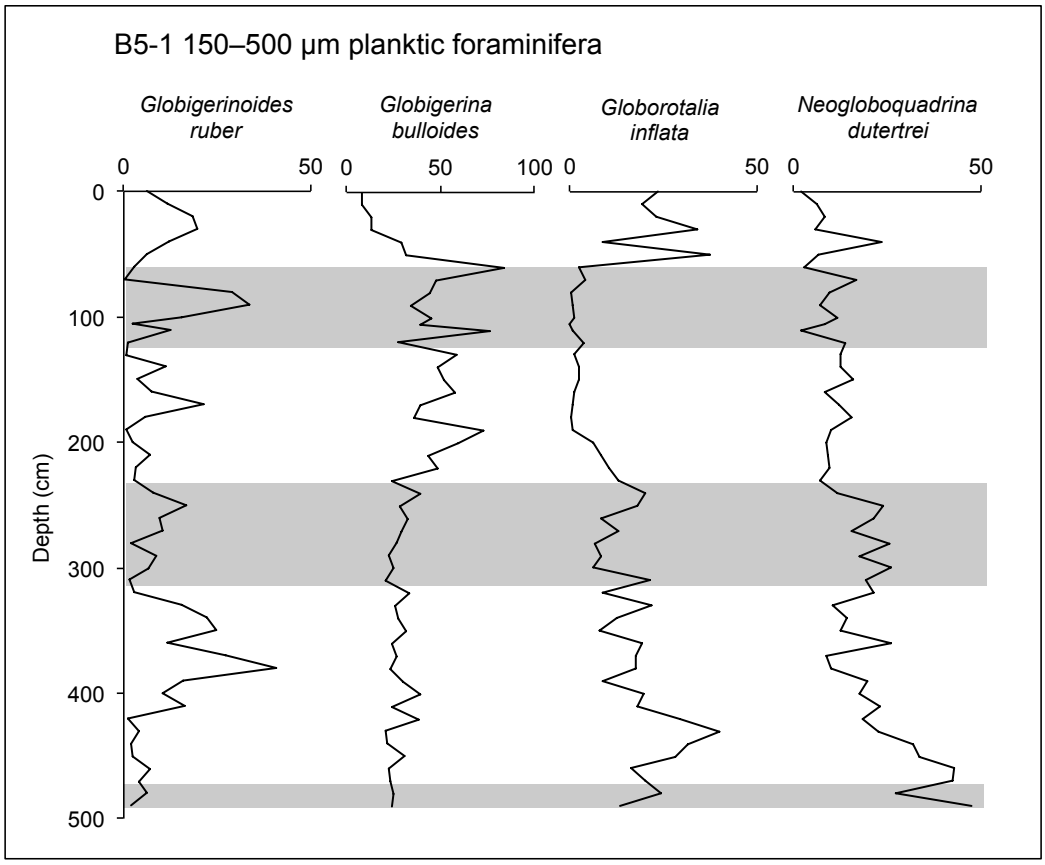

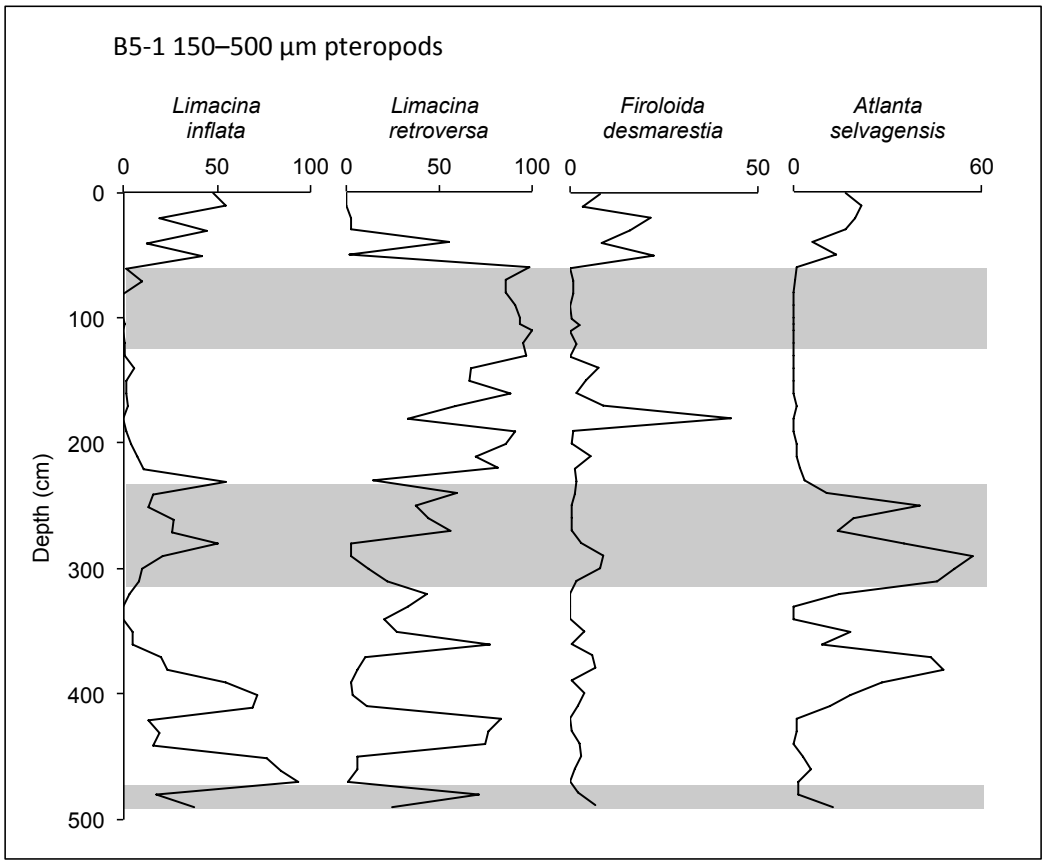

8.2.2.3.D B5-1 PLANKTIC FORAMINIFERA ABUNDANCE >500 µm

Mid-Sample depth (cm)	Weight before picking (g)	Unpicked weight (g)	Picked weight (g)	Number of planktic foraminifera	Foraminifera per gram	Foraminifera fragments	Broken but counted foraminifera	Fragment to whole ratio
0.5	0.0611	0	0.0611	326	5335.52	28	60	24.86
10.5	0.0071	0	0.0071	61	8591.55	3	20	35.94
20.5	0.0426	0	0.0426	393	9225.35	40	136	40.65
30.5	0.0237	0	0.0237	96	4050.63	6	17	22.55
40.5	0.0043	0	0.0043	6	1395.35	2	3	62.50
50.5	0.0206	0	0.0206	64	3106.80	4	17	30.88
60.5	0.0222	0	0.0222	2	90.09	0	1	50.00
70.5	0.0223	0	0.0223	2	89.69	0	1	50.00
80.5	0.0214	0	0.0214	0	0.00	0	0	NA
90.5	0.0065	0	0.0065	1	153.85	0	0	NA
100.5	0.0224	0	0.0224	1	44.64	0	0	NA
105.5	0.0148	0	0.0148	0	0.00	0	0	NA
110.5	0.0160	0	0.0160	0	0.00	0	0	NA
120.5	0.0151	0	0.0151	0	0.00	0	0	NA
130.5	0.1045	0	0.1045	0	0.00	0	0	NA
140.5	0.0380	0	0.0380	0	0.00	0	0	NA
150.5	0.0281	0	0.0281	1	35.59	0	0	0.00
160.5	0.0369	0	0.0369	0	0.00	0	0	NA
170.5	0.0311	0	0.0311	3	96.46	0	1	33.33
180.5	0.0097	0	0.0097	4	412.37	0	1	25.00
190.5	0.0356	0	0.0356	0	0.00	0	0	NA
200.5	0.0229	0	0.0229	8	349.34	1	4	55.56
210.5	0.0249	0	0.0249	14	562.25	0	4	28.57
220.5	0.0416	0	0.0416	46	1105.77	2	16	37.50
230.5	0.0734	0	0.0734	108	1471.39	5	33	33.63
240.5	0.0700	0	0.0700	90	1285.71	0	10	11.11
250.5	0.1006	0	0.1006	28	278.33	3	5	25.81
260.5	0.0386	0	0.0386	11	284.97	1	6	58.33
270.5	0.1619	0	0.1619	97	599.14	4	23	26.73
280.5	0.0686	0	0.0686	91	1326.53	5	33	39.58
290.5	0.0507	0	0.0507	247	4871.79	4	59	25.10
300.5	0.0461	0	0.0461	178	3861.17	3	47	27.62
310.5	0.0261	0	0.0261	110	4214.56	2	33	31.25
320.5	0.0823	0	0.0823	256	3110.57	11	71	30.71
330.5	0.0261	0	0.0261	89	3409.96	5	29	36.17
340.5	0.0188	0	0.0188	35	1861.70	3	11	36.84
350.5	0.0323	0	0.0323	87	2693.50	7	29	38.30
360.5	0.0603	0	0.0603	84	1393.03	1	21	25.88
370.5	0.1169	0	0.1169	54	461.93	1	7	14.55
380.5	0.0345	0	0.0345	27	782.61	0	3	11.11
390.5	0.0508	0	0.0508	20	393.70	0	5	25.00
400.5	0.0494	0	0.0494	13	263.16	1	7	57.14
410.5	0.0286	0	0.0286	25	874.13	0	5	20.00
420.5	0.0464	0	0.0464	13	280.17	0	3	23.08
430.5	0.0266	0	0.0266	1	37.59	0	0	0.00
440.5	0.0609	0	0.0609	4	65.68	0	2	50.00
450.5	0.0515	0	0.0515	2	38.83	0	1	50.00
460.5	0.0205	0	0.0205	4	195.12	0	0	0.00
470.5	0.0085	0	0.0085	8	941.18	0	0	0.00
480.5	0.0147	0	0.0147	1	68.03	0	1	100.00
490.5	0.0221	0	0.0221	12	542.99	0	5	41.67

8.2.2.3.D B5-1 PLANKTIC FORAMINIFERA ABUNDANCE 150–500 µm

Mid-Sample depth (cm)	Weight before picking (g)	Unpicked weight (g)	Picked weight (g)	Number of planktic foraminifera	Foraminifera per gram	Foraminifera fragments	Broken but counted foraminifera	Fragment to whole ratio
0.5	0.4709	0.4543	0.0166	304	18313.25	85	16	25.96
10.5	0.1159	0.0989	0.0170	309	18176.47	80	10	23.14
20.5	0.5676	0.5522	0.0154	338	21948.05	175	17	37.43
30.5	0.4186	0.4024	0.0162	317	19567.90	136	19	34.22
40.5	0.2218	0.2142	0.0076	310	40789.47	72	3	19.63
50.5	0.3355	0.3276	0.0079	302	38227.85	107	14	29.58
60.5	0.0759	0.0605	0.0154	308	20000.00	7	6	4.13
70.5	0.1208	0.1120	0.0088	308	35000.00	17	1	5.54
80.5	0.2838	0.2741	0.0097	308	31752.58	25	1	7.81
90.5	0.1973	0.1867	0.0106	306	28867.92	23	6	8.81
100.5	0.1611	0.1478	0.0133	322	24210.53	44	14	15.85
105.5	0.0873	0.0755	0.0118	306	25932.20	20	3	7.06
110.5	0.0353	0.0151	0.0202	306	15148.51	4	12	5.16
120.5	0.1379	0.1237	0.0142	315	22183.10	8	0	2.48
130.5	0.3613	0.3473	0.0140	308	22000.00	23	10	9.97
140.5	0.2012	0.1880	0.0132	314	23787.88	20	7	8.08
150.5	0.2270	0.2130	0.0140	305	21785.71	35	1	10.59
160.5	0.2616	0.2445	0.0171	318	18596.49	24	10	9.94
170.5	0.5558	0.5350	0.0208	313	15048.08	31	4	10.17
180.5	0.4040	0.3949	0.0091	337	37032.97	41	3	11.64
190.5	0.3042	0.2913	0.0129	370	28682.17	12	10	5.76
200.5	0.4162	0.4041	0.0121	305	25206.61	20	5	7.69
210.5	0.2451	0.2368	0.0083	327	39397.59	26	10	10.20
220.5	0.3894	0.3797	0.0097	331	34123.71	47	5	13.76
230.5	0.3761	0.3685	0.0076	312	41052.63	73	1	19.22
240.5	0.7363	0.7220	0.0143	309	21608.39	33	1	9.94
250.5	0.5888	0.5742	0.0146	302	20684.93	123	4	29.88
260.5	0.3469	0.3325	0.0144	308	21388.89	106	28	32.37
270.5	0.9354	0.9136	0.0218	320	14678.90	99	31	31.03
280.5	0.5288	0.5118	0.0170	326	19176.47	199	45	46.48
290.5	0.5405	0.5240	0.0165	315	19090.91	129	50	40.32
300.5	0.3561	0.3428	0.0133	328	24661.65	212	34	45.56
310.5	0.2748	0.2558	0.0190	304	16000.00	268	23	50.87
320.5	0.3766	0.3586	0.0180	315	17500.00	370	44	60.44
330.5	0.3005	0.2879	0.0126	303	24047.62	243	34	50.73
340.5	0.2519	0.2366	0.0153	315	20588.24	248	26	48.67
350.5	0.3951	0.3837	0.0114	310	27192.98	321	16	53.41
360.5	0.7630	0.7532	0.0098	323	32959.18	148	9	33.33
370.5	0.6395	0.6249	0.0146	309	21164.38	184	17	40.77
380.5	0.4620	0.4506	0.0114	309	27105.26	171	11	37.92
390.5	0.4323	0.4192	0.0131	374	28549.62	202	10	36.81
400.5	0.4092	0.3896	0.0196	326	16632.65	286	10	48.37
410.5	0.3234	0.3093	0.0141	308	21843.97	136	14	33.78
420.5	0.4397	0.4256	0.0141	307	21773.05	73	7	21.05
430.5	0.4494	0.4357	0.0137	312	22773.72	74	10	21.76
440.5	0.6773	0.6570	0.0203	345	16995.07	48	4	13.23
450.5	0.9424	0.9261	0.0163	302	18527.61	81	5	22.45
460.5	0.2275	0.2196	0.0079	314	39746.84	41	4	12.68
470.5	0.3760	0.3613	0.0147	329	22380.95	4	0	1.20
480.5	0.1442	0.1250	0.0192	347	18072.92	134	8	29.52
490.5	0.4670	0.4580	0.0090	307	34111.11	118	7	29.41

8.2.2.3.E B5-1 PTEROPOD AND HETEROPOD ABUNDANCE >500 µm

Mid-Sample depth (cm)	Weight before picking (g)	Unpicked weight (g)	Picked weight (g)	Number of pteropods	Pteropods per gram
0.5	0.0611	0.0000	0.0611	13	212.77
10.5	0.0071	0.0000	0.0071	8	1126.76
20.5	0.0426	0.0000	0.0426	16	375.59
30.5	0.0237	0.0000	0.0237	6	253.16
40.5	0.0043	0.0000	0.0043	3	697.67
50.5	0.0206	0.0000	0.0206	11	533.98
60.5	0.0222	0.0000	0.0222	34	1531.53
70.5	0.0223	0.0000	0.0223	48	2152.47
80.5	0.0214	0.0000	0.0214	68	3177.57
90.5	0.0065	0.0000	0.0065	11	1692.31
100.5	0.0224	0.0000	0.0224	73	3258.93
105.5	0.0148	0.0000	0.0148	28	1891.89
110.5	0.0160	0.0000	0.0160	28	1750.00
120.5	0.0151	0.0000	0.0151	14	927.15
130.5	0.1045	0.0000	0.1045	209	2000.00
140.5	0.0380	0.0000	0.0380	24	631.58
150.5	0.0281	0.0000	0.0281	37	1316.73
160.5	0.0369	0.0000	0.0369	66	1788.62
170.5	0.0311	0.0000	0.0311	32	1028.94
180.5	0.0097	0.0000	0.0097	19	1958.76
190.5	0.0356	0.0000	0.0356	41	1151.69
200.5	0.0229	0.0000	0.0229	71	3100.44
210.5	0.0249	0.0000	0.0249	62	2489.96
220.5	0.0416	0.0000	0.0416	112	2692.31
230.5	0.0734	0.0000	0.0734	15	204.36
240.5	0.0700	0.0000	0.0700	112	1600.00
250.5	0.1006	0.0000	0.1006	18	178.93
260.5	0.0386	0.0000	0.0386	3	77.72
270.5	0.1619	0.0000	0.1619	116	716.49
280.5	0.0686	0.0000	0.0686	0	0.00
290.5	0.0507	0.0000	0.0507	0	0.00
300.5	0.0461	0.0000	0.0461	2	43.38
310.5	0.0261	0.0000	0.0261	0	0.00
320.5	0.0823	0.0000	0.0823	4	48.60
330.5	0.0261	0.0000	0.0261	2	76.63
340.5	0.0188	0.0000	0.0188	0	0.00
350.5	0.0323	0.0000	0.0323	1	30.96
360.5	0.0603	0.0000	0.0603	3	49.75
370.5	0.1169	0.0000	0.1169	2	17.11
380.5	0.0345	0.0000	0.0345	0	0.00
390.5	0.0508	0.0000	0.0508	0	0.00
400.5	0.0494	0.0000	0.0494	1	20.24
410.5	0.0286	0.0000	0.0286	1	34.97
420.5	0.0464	0.0000	0.0464	32	689.66
430.5	0.0266	0.0000	0.0266	13	488.72
440.5	0.0609	0.0000	0.0609	11	180.62
450.5	0.0515	0.0000	0.0515	9	174.76
460.5	0.0205	0.0000	0.0205	0	0.00
470.5	0.0085	0.0000	0.0085	6	705.88
480.5	0.0147	0.0000	0.0147	6	408.16
490.5	0.0221	0.0000	0.0221	4	181.00

8.2.2.3.E B5-1 PTEROPOD AND HETEROPOD ABUNDANCE 150–500 µm

Mid-Sample depth (cm)	Weight before picking (g)	Unpicked weight (g)	Picked weight (g)	Number of pteropods	Pteropods per gram
0.5	0.4709	0.4232	0.0477	305	6394.13
10.5	0.1159	0.0857	0.0302	292	9668.87
20.5	0.5676	0.5313	0.0363	257	7079.89
30.5	0.4186	0.3804	0.0382	298	7801.05
40.5	0.2218	0.1555	0.0663	302	4555.05
50.5	0.3355	0.2963	0.0392	285	7270.41
60.5	0.0759	0.0000	0.0759	107	1409.75
70.5	0.1208	0.0565	0.0643	286	4447.90
80.5	0.2838	0.2460	0.0378	305	8068.78
90.5	0.1973	0.1464	0.0509	303	5952.85
100.5	0.1611	0.1203	0.0408	325	7965.69
105.5	0.0873	0.0331	0.0542	303	5590.41
110.5	0.0353	0.0000	0.0353	117	3314.45
120.5	0.1379	0.0604	0.0775	288	3716.13
130.5	0.3613	0.3311	0.0302	306	10132.45
140.5	0.2012	0.1535	0.0477	288	6037.74
150.5	0.2270	0.1625	0.0645	297	4604.65
160.5	0.2616	0.1989	0.0627	291	4641.15
170.5	0.5558	0.4428	0.1130	292	2584.07
180.5	0.4040	0.3514	0.0526	283	5380.23
190.5	0.3042	0.2232	0.0810	307	3790.12
200.5	0.4162	0.3542	0.0620	318	5129.03
210.5	0.2451	0.1836	0.0615	297	4829.27
220.5	0.3894	0.3399	0.0495	305	6161.62
230.5	0.3761	0.3015	0.0746	290	3887.40
240.5	0.7363	0.6581	0.0782	293	3746.80
250.5	0.5888	0.4797	0.1091	293	2685.61
260.5	0.3469	0.2596	0.0873	287	3287.51
270.5	0.9354	0.8477	0.0877	204	2326.11
280.5	0.5288	0.3325	0.1963	282	1436.58
290.5	0.5405	0.1495	0.3910	291	744.25
300.5	0.3561	0.0000	0.3561	148	415.61
310.5	0.2748	0.0000	0.2748	137	498.54
320.5	0.3766	0.0000	0.3766	35	92.94
330.5	0.3005	0.0000	0.3005	12	39.93
340.5	0.2519	0.0000	0.2519	10	39.70
350.5	0.3951	0.0000	0.3951	220	556.82
360.5	0.7630	0.6310	0.1320	299	2265.15
370.5	0.6395	0.3262	0.3133	250	797.96
380.5	0.4620	0.2268	0.2352	260	1105.44
390.5	0.4323	0.2999	0.1324	296	2235.65
400.5	0.4092	0.3341	0.0751	200	2663.12
410.5	0.3234	0.2646	0.0588	309	5255.10
420.5	0.4397	0.3762	0.0635	329	5181.10
430.5	0.4494	0.3967	0.0527	290	5502.85
440.5	0.6773	0.5879	0.0894	308	3445.19
450.5	0.9424	0.8481	0.0943	291	3085.90
460.5	0.2275	0.0960	0.1315	296	2250.95
470.5	0.3760	0.3334	0.0426	318	7464.79
480.5	0.1442	0.1008	0.0434	278	6405.53
490.5	0.4670	0.4030	0.0640	292	4562.50

8.2.2.4 CALCIFICATION INDICES APPENDIX

8.2.2.4.A B5-1 LDX DATA *L. INFLATA*

MID-SAMPLE DEPTH (cm)	LDX for *Limacina inflata* >300um (n>10)																														No.	MEAN LDX
0.5	1	1	1	1	1	1	1	1	3	2	1	1	1	0	1	1	1	1	0	1	1	1	1	1	1	1	2	1	0	1	30	1.03
10.5	1	1	1	1	1	1	1	1	1	1	1	1	1	1	1	1	1	1	1	1	1	1	1	1	1	2	1	1	1	1	30	1.03
20.5	2	2	2	2	2	2	2	1	2	1	1	0	1	1	3	2	1	1	2	1											20	1.55
30.5	1	1	1	1	1	2	2	2	2	2	1	1	1	1	0	1	1	1	1	1	3	1	1	2	1	3	2	2	2	2	30	1.43
40.5	1	1	3	1	1	1	1	1	2	2	2	1	2	4	1	3	2	3													18	1.78
50.5	1	2	1	1	0	0	1	1	1	1	1	1	0	0	1	1															16	0.81
60.5	1																														1	NA
70.5																															0	NA
80.5																															0	NA
90.5																															0	NA
100.5																															0	NA
105.5																															0	NA
110.5																															0	NA
120.5																															0	NA
130.5																															0	NA
140.5	2																														1	NA
150.5																															0	NA
160.5																															0	NA
170.5																															0	NA
180.5																															0	NA
190.5	2	3																													2	NA
200.5	1	1	1	5	2	2																									6	NA
210.5																															0	NA
220.5	2	2	1	2	2	1	2	1	1	1	1	1	2	2	2	2															16	1.56
230.5	2	2	1	1	1	2	1	2	1	2	1	1	2	1	4	1	2	2	1	1	2	2	1	2	3	3	3	2	1	2	30	1.73
240.5																															0	NA

MID-SAMPLE DEPTH (cm)	LDX for *Limacina inflata* >300um (n>10)																														No.	MEAN LDX
250.5	1	2	4	4	3	4	3	4	2	4	4	2	2	4	3																15	3.07
260.5	4	3	4	3	3	3	2	4	4	2	4	2	3	5	3	2	2	2	4	3											20	3.10
270.5	4	3	4	4	4	4	4	3	4	3	4	4	4	4	3	4	4	4	5	4	4										21	3.86
280.5	5	5	4	4	4	4	4	4	4	4	4	4	4	5	3	3	4	5	3	3	4	4	4	3	4	4	3	4	4	4	30	3.93
290.5	4	4	4	4	4	3	5	4	4	4	3	4	4	5	4	3	4	4	4	3	3	4	4	4	5	4	3	4	5	4	30	3.93
300.5	4	5	4	3	4	4	2	4	4	4	4																				11	3.82
310.5	5	5	5	5	3	5	4	5	3																						9	NA
320.5																															0	NA
330.5																															0	NA
340.5																															1	NA
350.5	1	2	4	5	2	4	4	5	4	4	4	2																			12	3.42
360.5	4	2	4	5	2	2	2	2	3	3	4	4																			12	3.08
370.5	5	4	5	4	3	4	4	2	4	5	4	4	5	3	5	5	4	4													18	4.11
380.5	4	3	5	5	4	2	3	4	4	4	4	4	4	5	4	4	3	3	3	3	4	3	3	4	4	3	3	4	4	3	30	3.67
390.5	5	3	5	4	4	5	4	4	5	3	5	4	5	4	4	5	4	4	4	3	2	4	4	3	3	5	4	3	2	3	30	3.90
400.5	4	4	4	4	4	4	4	4	5	3	5	4	4	4	4	4	3	4	4	2	4	3	2	5	2	4	4	2	2	3	30	3.63
410.5	4	4	4	4	4	4	3	4	3	2	4	4	2	3	3	3	4	4	4	3	4	4	3	4	2	1	2	4	4	4	30	3.40
420.5	4	1	1	4	2	2	4	3	4	2	4	2	3	2	5	3	2	2	2	2	4	4	4	3	4	2	4	2	4		29	2.93
430.5	2	2	4	2	4	2	4	3	4	2	4	2	3	2	2	4	4	2	2	2	3	3	2	3	4	2	2	4			28	2.82
440.5	5	2	4	2	2	5	2	2	2	5	2	2	3	2	3	2	2	3	3	3	5	4	3	3	2	2	3	3	4	3	30	2.93
450.5	3	3	2	4	4	4	4	3	3	2	2	3	2	3	2	2	3	2	2	4	3	3	4	2	3	1	4	1	2	4	30	2.80
460.5	2	2	2	2	2	2	4	3	2	2	2	2	2	2	2	2	3	2	2	2	2	2	2	2	3	2	2	3	2	2	30	2.20
470.5	2	3	2	2	2	2	2	2	3	2	2	4	2	2	2	2	2	2	2	3	2	4	3	2	2	3	4	2	2	2	30	2.37
480.5	2	3	2	1	2	2	4	2	2	2	4	2	2	2	1	2	2	2	2	1	2	2	3	2	2	4	1	2			28	2.14
490.5	2	2	3	3	3	1	1	2	2	4	2	2	2	2	2	4	2	2	4	4	2	4	4	2	2	4	2	4	2	3	30	2.60

MID-SAMPLE DEPTH (cm)	LDX for *Limacina retroversa* >300um (n>10)																														No.	MEAN LDX
0.5																															0	NA
10.5																															0	NA
20.5																															0	NA
30.5																															0	NA
40.5	2	2	3	1	2	2	2	2	2	1	2	1	2	1	2	1	2	1	2	2	1	1	1	2	1	1	1	1	1	2	30	1.57
50.5	0	0	2	2	1	2	2	2	2	1	1	2	2	1	0	1	2	1	1	1	1	1	2	2	0	1	0	1	1	0	30	1.17
60.5	2	2	2	2	4	2	3	2	3	2	4	2	2	2	2	3	2	2	3	2	2	3	3	2	3	2	4	3	3	3	30	2.53
70.5	1	2	2	2	2	1	1	1	1	1	1	1	1	1	1	1	1	1	1	1	1	1	1	1	1	1	1	1	1	1	30	1.13
80.5	1	2	1	1	2	1	1	1	1	2	1	3	1	1	1	1	2	1	1	3	2	1	1	1	3	1	1				27	1.41
90.5	2	2	3	2	2	3	3	3	3	2	2	1	1	2	2	2	1	2	2	2	2	2	2	2	2	3	3	2	3	2	30	2.17
100.5	2	2	2	5	2	2	2	2	5	2	2	2	2	2	2	2	3	2	3	2	2	2	2	3	2	2	2	2	2	2	30	2.30
105.5	2	2	2	2	2	2	2	2	2	2	2	2	2	2	2	2	2	2	2	2	2	2	2	4	2	2	2	2	2	3	30	2.10
110.5	1	1	2	1	1	2	2	2	2	2	2	1	2	2	2	2	2	2	2	2	1	2	2	1	2	1	1	1	2	2	30	1.67
120.5	2	2	2	2	2	2	2	2	2	2	2	2	2	2	2	3	2	2	3	1	1	3	1	2	2	2	2	2	2	2	30	2.00
130.5	2	3	3	2	3	1	1	2	2	1	3	2	2	2	2	1	2	4	2	1	1	1	2	2	1	1	2	3	2	3	30	1.97
140.5	2	1	4	1	2	3	4	1	1	3	2	2	2	2	2	2	2	2	2	1	1	1	1	1	3	1	1	2	2	1	30	1.83
150.5	2	3	2	2	2	2	2	2	4	2	3	3	1	2	2	4	2	2	1	1	1	3	2	2	2	1	1	2	1	1	30	2.00
160.5	1	2	1	2	2	1	3	2	4	3	3	2	2	2	2	2	3	4	2	1	1	3	2	1	2	2	2	2	2	1	30	2.07
170.5	3	3	3	2	4	2	1	2	4	5	2	1	4	1	2	2	2	1	2	1	2	2	2	1	3	2	2	1	3	1	30	2.20
180.5	4	2	1	1	1	1	4	1	5	1	2	1	1	1	1	2	1	4	3	1	1	1	1	1	1	1	1	1	4	2	30	1.73
190.5	2	3	2	2	2	2	2	1	3	3	2	3	3	3	3	3	3	3	3	2	2	2	1	4	3	3	3	3	3	2	30	2.53
200.5	2	2	3	1	2	3	2	2	2	1	2	3	1	2	4	2	2	2	1	4	1	1	1	1	1	1	5	1	1	2	30	1.93
210.5	3	3	2	1	1	3	4	3	2	2	4	1	2	1	1	1	3	1	1	1	1	1	1	1	1	1	1	1	1	2	30	1.70
220.5	1	3	2	2	1	1	1	1	1	1	1	1	2	2	1	3	2	1	2	1	1	2	1	1	1	1	1	3	1	1	30	1.43
230.5	3	3	2	3	3	3	1	2	1	1	4	1	1	3	2	1															16	2.13
240.5	1	2	2	2	2	2	2	2	2	2	2	2	2	2	2	2	2	3	4	2	2	2	2	3	4	1	2	2	2	2	30	2.13
250.5	2	2	2	2	5	2	3	2	2	3	2	4	2	2	3	2	2	2	2	2	2	2	2	2	2	3	2	3	2	3	30	2.37

MID-SAMPLE DEPTH (cm)	LDX for *Limacina retroversa* >300um (n>10)																													No.	MEAN LDX
260.5	5	2	2	2	3	2	2	2	2	4	2	3	2	2	2	3	2	2	2	4	3	2	2	2	2	3	4	2	2	2	30	2.47
270.5	2	2	2	3	2	1	2	2	2	2	2	3	2	2	4	2	2	2	2	4	2	3	2	2	2	2	2	2	4	2	30	2.27
280.5	2	1																													2	NA
290.5	3	5	2																												3	NA
300.5	1	1	1	1	1	1	2	1	2	1																					10	1.20
310.5	2	2	1	2	2	1	2	2	2	2	1	2	1	3	1	2	2														17	1.76
320.5	1	1	1	4	2	1	2	1	1	4	4	4																			12	2.17
330.5	1	1	1	1	2																										5	NA
340	3																														1	NA
350.5	1	5	4	2	1	3	2	1	2	2	2	2	2	3	4	4															16	2.50
360.5	3	2	4	2	2	2	4	2	2	2	2	2	2	2	4	2	2	4	4	2	2	2	2	2	2	2	2	2	2	4	30	2.43
370.5	1	2	2	4	2	2	4	2	4	2																					10	2.50
380.5	1	2	1	2	2	1	2	1	2	2	2	2	2	1	2	2															16	1.69
390.5	2	2	4	2																											4	NA
400.5	2	2	2	1	1	2																									6	NA
410.5	2	3	2	2	2	2	2	1	1	2	2	2	2	2	2	2	2	2	2	2	2	2	2	2	2						14	3.36
420.5	4	2	4	2	2	2	2	3	2	2	3	2	2	3	2	3	3	2	2	4	2	4	2	2	2	2	2	2	2	3	30	2.47
430.5	3	2	3	3	2	4	2	2	2	5	4	2	1	2	2	2	2	2	2	3	2	3	2	2	2	2	2	4	2	4	30	2.50
440.5	1	2	2	2	2	3	2	2	2	3	2	3	3	1	2	2	4	4	2	2	2	2	2	2	3	3	2	3	2	2	30	2.30
450.5	2	4	3	2	2	5	2	2	2	2	2	2	2	2	2	2	2	1	2	2											20	2.25
460.5	2	2	2	2	2	2	2	2	2	2																					10	2.00
470.5																															0	NA
480.5	2	2	2	2	2	1	4	1	1	1	2	1	1	1	1	1	3	2	2	2	1	5	5	1	2	2	1	2	2	2	30	1.90
490.5	2	2	3	2	2	2	3	2	2	2	3	2	1	2	1	2	1	2	2	2	1	1	2	1	2	2	2	1	2	2	30	1.87

8.2.2.4.B ALL LDX POINTS FOR *LIMACINA INFLATA* IN B5-1. RED LINE SHOWS MEAN VALUES, GREY BARS SHOW STANDARD DEVIATION

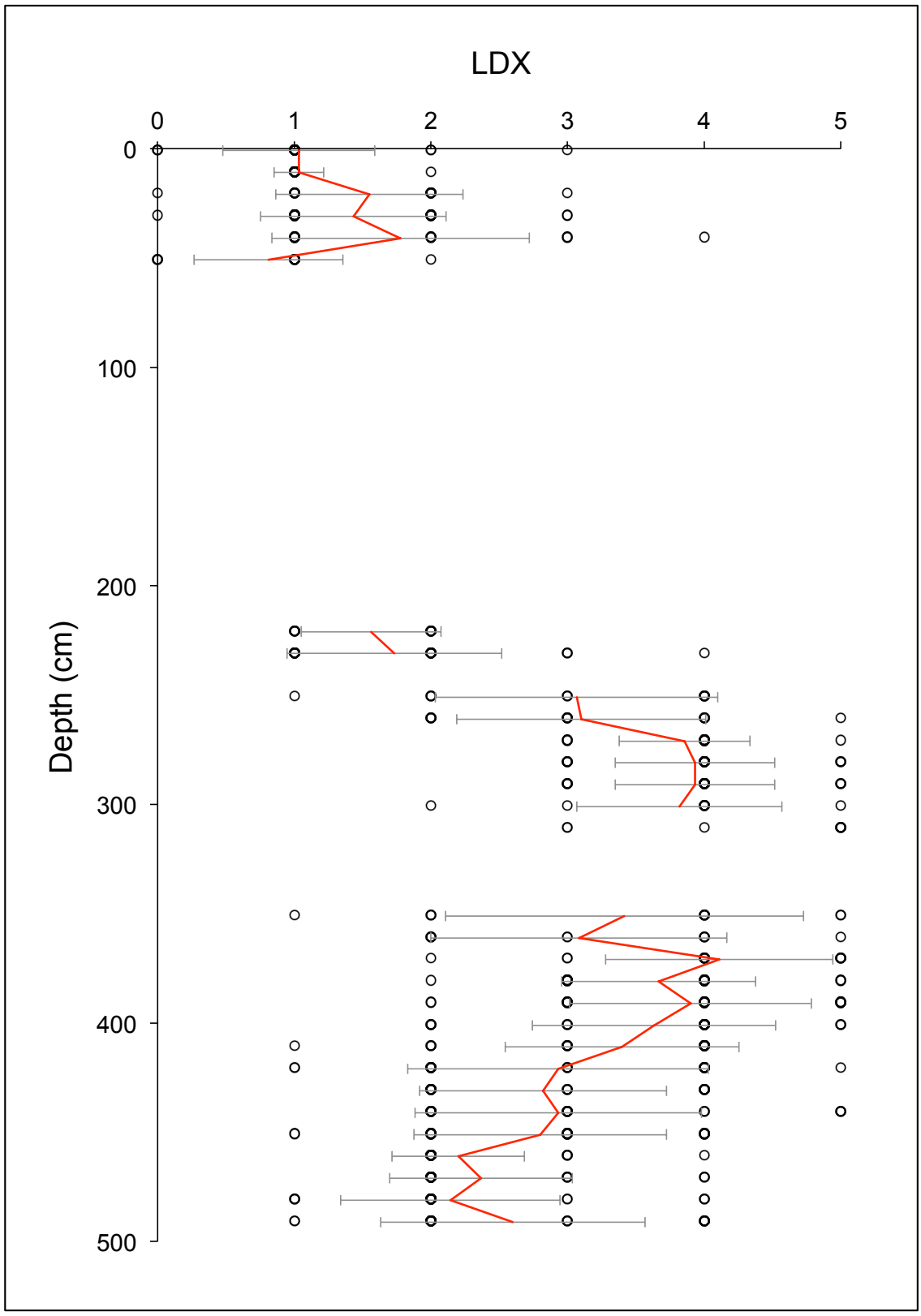

8.2.2.4.C B5-1 SHELL SIZE DATA

0.5 cm	468	542	589	625	675	588	710	503	287	334	220	233	297	203	180	349		
	399	297	279	336	317	269	218	203	239	156	203	347	237	230	231	249		
	333	262	275	283	308	221	231	156	222	209	261	203	333	235	218	266		
	328	242	274	282	277	188	254	234	349	321	230	266	169	228	225	210		
	273	235	246	274	247	229	195	376	199	216	180	296	174	333	216	233		
	260	212	226	212	247	195	299	153	257	215	286	245	233	197	212	201		
	199	187	205	200	232	248	396	254	165	298	357	187	206	293	205	258		
	192	171	178	151	214	166	190	203	289									
Average	**267.12**																	
20.5 cm	664	736	729	769	721	625	672	564	364	434	228	228	245	356	374	304		
	183	181	239	162	184	224	205	155	210	192	189	275	208	214	211	225		
	200	213	196	207	161	230	254	186	175	200	217	192	207	235	338	212		
Average	**306.1**																	
40.5 cm	202	224	198	225	244	216	193	203	185	216	256	236	241	252	221	286		
	174	172	205	245	227	209	194	191	197	141	169	199	183	221				
Average	**210.83**																	
50.5 cm	735	536	549	587	589	423	294	319	261	192	257	224	231	333	316	262		
	252	330	262	195	276	230	267	295	225	251	339	214	204	238	248	292		
	248	232	167	256	204	238	258	282	226	217	267	357	208	301	284	192		
	202	219	322	212	280	357	183	208	428	200	255	193	263	198	388	242		
	242	162	189	222	203	222	256	225	224	252	273	239	227	227	222	359		
	267	219	228	140	292	242	210	280	293	188	240	199						
Average	**270.16**																	
220.5 cm	171	320	265	218	250	194	202	206	242	256	298	214	224	245	193	160		
	211	160	257	287	258	208	223	224	219	258								
	229.35																	
230.5 cm	475	250	665	706	565	504	558	665	154	303	214	295	251	181	157	151		
	231	235	256	182	222	171	239	247	209	248	170	200	226	244	254	284		
	201	228	276	214	290	281	217	265	273	365	240	223	164	248	222	169		
	227	360	387	227	247	222	209	295	244	161	191	274	268	249	207	277		
	262	213	249	327	224	217	254	203	247	236	234	411	183	239	229	386		
	253	229	239	287	285	301	227	222	176	226	227	265	224	287	239	305		
	256	228	295	206	198	237	255	218	244	270	252	234	210	261	214	232		
	196	252	197	275	210	248	237	337	236	299	265	229						
Average	**262.34**																	
250.5 cm	262	192	338	193	225	207	241	222	212	192	203	215	233	212	250	258		
	221	236	214	253	210	232	215	235	265	189	183	171	231	210				
Average	**224**																	

280.5 cm	200	225	147	249	200	249	322	246	190	205	146	274	163	364	324	216
	196	265	219	257	202	205	169	192	187	175	212	227	191	175	192	172
	172	125	176	208	131	128	101	124	143	183	290	208	310	142	243	178
	146	218	123	214	297	205	229	170	167	219	233	248	262	154	189	173
	201	222	234	214	179	274	291	221	187	201	140	194	148	206	269	170
	283	269	223	176	274	172	326	321	190	157	264	157	156	184	209	144
	161	243	136	227	206	323	146	183	167	322	202					
Average	**207.82**															
300.5 cm	255	192	229	220	162	220	186	171	238	230	204	174				
Average	**206.75**															
370.5 cm	211	198	140	243	209	182	214	238	162	185	178	174	235	207	186	171
	194	189	200	183	254	198	153	173	134	201	203	170	168	192	163	186
	275	200	222	184	196	190										
Average	**193.71**															
430.5 cm	357	269	152	177	213	244	200	239	180	267	236	320	214	222	200	197
	192	192	225	192	182	273	244	215	201	175	253	213	228	240	186	259
	233	191	177	521	150	200	275	300	233	232	312					
Average	**232.12**															
480.5 cm	474	246	232	236	184	200	235	292	400	285	234	184	205	366	181	221
	226	212	219	221	239	193	243	261	215	284	212	193	204	178	211	205
	217	210	176	264	204	218	201	206	258	213						
Average	**234.71**															
490.5 cm	657	166	209	250	291	238	260	205	328	196	227	201	244	210	223	268
	173	248	237	201	217	183	433	208	212	254	262	183	252	242	201	236
	185	236	274	243	239	228	208	274	170	247	255	227	206	200	206	245
	201	194	238	173	265	459	227	233	222	265	249	231	216	252	246	244
	268	201	184	186	222	261	230	178	223	174	204	231	180	256	238	205
	224	182	232	207	262	327	234									
Average	**236.57**															

8.2.3 THE INDIAN OCEAN APPENDIX

8.2.3.1 SEDIMENTOLOGY APPENDIX

8.2.3.1.A 716B GRAIN SIZE ANALYSIS

Mid-sample depth (cm)	Total dry weight (g)	>63 µm dry weight (g)	<63 µm dry weight (g)	% <63 µm	% >63 µm
15.5	7.8090	3.0130	4.7960	61.42	38.58
75.5	5.0380	3.3745	1.6635	33.02	66.98
185.5	9.8347	4.3506	5.4841	55.76	44.24
205.5	10.8762	4.7409	6.1353	56.41	43.59
255.5	11.5159	5.9393	5.5766	48.43	51.57
425.5	9.1865	5.5825	3.6040	39.23	60.77
475.5	7.5241	4.6682	2.8559	37.96	62.04
525.5	8.4028	5.1555	3.2473	38.65	61.35
605.5	12.7597	4.7073	8.0524	63.11	36.89
625.5	-	4.0874	-	-	-
705.5	12.9700	4.2607	8.7093	67.15	32.85
725.5	11.1940	4.2568	6.9372	61.97	38.03
775.5	10.5546	6.1289	4.4257	41.93	58.07
855.5	7.7103	4.3564	3.3539	43.50	56.50
915.5	8.9450	2.4424	6.5026	72.70	27.30
955.5	11.6877	4.8014	6.8863	58.92	41.08
1005.5	8.6945	2.3204	6.3741	73.31	26.69
1055.5	-	5.3897	-	-	-
1105.5	7.6146	4.4739	3.1407	41.25	58.75
1205.5	10.5420	5.1050	5.4370	51.57	48.43
1255.5	7.5270	4.3004	3.2266	42.87	57.13
1295.5	8.7750	4.3680	4.4070	50.22	49.78

MID-SAMPLE DEPTH (cm)	FRACTION WEIGHT (g)					TOTAL WEIGHT (g)	FRACTION PERCENTAGE					MEAN GRAIN SIZE (μm)
	0-63μm	63-125μm	125-250μm	250-500μm	500μm		0-63μm	63-125μm	125-250μm	250-500μm	>500μm	
15.5	4.796	1.1074	0.8205	0.6974	0.3877	7.8090	61.4163	14.1811	10.5071	8.9307	4.9648	123.1033
75.5	1.6635	1.0966	0.8971	0.9282	0.4526	5.0380	33.0191	21.7666	17.8067	18.4240	8.9837	200.7169
185.5	5.4841	1.6686	1.0021	1.0745	0.6054	9.8347	55.7628	16.9665	10.1894	10.9256	6.1558	139.7581
205.5	6.1353	2.0530	1.0658	1.1107	0.5114	10.8762	56.4103	18.8761	9.7994	10.2122	4.7020	127.4474
255.5	5.5766	2.1925	1.5011	1.5090	0.7367	11.5159	48.4252	19.0389	13.0350	13.1036	6.3972	154.7091
425.5	3.604	1.8122	1.5186	1.4779	0.7738	9.1865	39.2315	19.7268	16.5308	16.0877	8.4232	185.3995
475.5	2.8559	1.5542	1.2874	1.2501	0.5765	7.5241	37.9567	20.6563	17.1104	16.6146	7.6620	183.2253
525.5	3.2473	2.6015	1.0699	1.0141	0.4700	8.4028	38.6455	30.9599	12.7327	12.0686	5.5934	152.3569
605.5	8.0524	1.8887	1.1414	1.1493	0.5279	12.7597	63.1081	14.8021	8.9454	9.0073	4.1372	115.3721
625.5	-	1.5578	1.0545	1.0547	0.4204	-	-	-	-	-	-	-
705.5	8.7093	1.6906	1.0621	1.0219	0.4861	12.9700	67.1496	13.0347	8.1889	7.8790	3.7479	106.4141
725.5	6.9372	1.6512	0.9791	1.0549	0.5716	11.1940	61.9725	14.7508	8.7466	9.4238	5.1063	123.4236
775.5	4.4257	2.1132	1.6646	1.7379	0.6132	10.5546	41.9315	20.0216	15.7713	16.4658	5.8098	166.9201
855.5	3.3539	1.9462	0.8927	1.0568	0.4607	7.7103	43.4990	25.2416	11.5780	13.7063	5.9751	155.3502
915.5	6.5026	1.0081	0.5224	0.5993	0.3126	8.9450	72.6954	11.2700	5.8401	6.6998	3.4947	95.7776
955.5	6.8863	1.8962	1.2291	1.2892	0.3869	11.6877	58.9192	16.2239	10.5162	11.0304	3.3103	119.7192
1005.5	6.3741	0.9584	0.5417	0.5888	0.2315	8.6945	73.3119	11.0231	6.2304	6.7721	2.6626	90.5018
1055.5	-	1.6840	1.4081	1.6887	0.6089	-	-	-	-	-	-	-
1105.5	3.1407	2.1729	0.8068	1.0156	0.4786	7.6146	41.2458	28.5360	10.5954	13.3375	6.2853	156.8381
1205.5	5.437	1.7226	1.2614	1.5263	0.5947	10.5420	51.5747	16.3404	11.9655	14.4783	5.6412	150.6441
1255.5	3.2266	1.6168	1.0350	1.2507	0.3979	7.5270	42.8670	21.4800	13.7505	16.6162	5.2863	161.4344
1295.5	4.407	1.4489	1.0216	1.3472	0.5503	8.7750	50.2222	16.5117	11.6422	15.3527	6.2712	157.7769

8.2.3.2 MICROPALAEONTOLOGY APPENDIX

8.2.3.2.A 716B PLANKTIC FORAMINIFERA SPECIES ANALYSIS >500 µm

	15	75	185	205	255	425	475	525	605	625	705	725	775	855
Candeina nitida										1				
Globigerinella aequilateralis	19	6	10	9	7	7	5		8	9	7	10	8	14
Globigerinella calida				1			1	1						
Globigerinoides conglobatus	16	13	12	15	28	14	17	22	8	17	6	7	8	10
Globigerinoides ruber				1					1	1		1	1	
Globigerinoides sacculifer	23	10	17	11	5	22	6	11	19	25	36	20	30	45
Globigerinoides trilobus	6	7	2	7	4	1	12	10	8	23	6	4	18	17
Globoquadrina conglomerata	51	52	74	62	52	48	55	51	56	48	43	37	56	48
Globorotalia menardii	148	140	123	120	149	158	147	148	166	155	186	169	141	119
Globorotalia tumida	1	4	10	14	12	6	8	5	2	2	1	6	3	5
Globorotalia flexuosa			2	1					1					2
Neogloboquadrina dutertrei	8	39	17	42	8	18	20	33	9	9	14	18	12	8
Orbulina universa	34	8	28	21	19	26	24	18	35	17	27	18	21	33
Pulleniatina obliquiloculata	8	21	19	13	19	18	9	25	15	20	13	20	13	26
Sphaeroidinella dehiscens	2	3	4	5	5	4	5	2	3	1	1		2	
Total individuals	316	303	318	322	308	322	309	326	331	328	340	310	313	327
Total species	11	11	12	14	11	11	12	11	13	13	11	11	12	11
Fisher alpha diversity	2.214	2.238	2.465	2.985	2.229	2.204	2.484	2.197	2.698	2.705	2.175	2.225	2.475	2.195
Evenness	0.5036	0.5073	0.5365	0.5044	0.5030	0.5018	0.4787	0.5251	0.4066	0.4547	0.4254	0.4575	0.4928	0.6303
Shannon Weiner	1.712	1.719	1.862	1.955	1.711	1.708	1.748	1.754	1.665	1.777	1.543	1.616	1.777	1.936

915	955	1005	1055	1105	1205	1255	1295
1						2	
11	10	10	5	7	9	7	4
		1					
7	13	5	9	8	16	22	13
1	1	3		2			
24	19	19	20	17	17	27	20
3	2	12	16	13	15	3	16
42	46	33	14	46	54	17	18
180	159	172	147	173	146	154	162
4	6	3	12	3	9	6	16
3				4		2	
10	2	8	27	11	5	18	6
12	34	32	34	22	34	35	45
17	18	27	40	27	10	19	12
1	2	2	1		4	2	4
316	312	327	325	333	319	314	316
14	12	13	11	12	11	13	11
3	2.477	2.707	2.199	2.437	2.209	2.736	2.214
0.3450	0.4281	0.4151	0.5600	0.4494	0.5375	0.4580	0.4983
1.575	1.637	1.686	1.818	1.685	1.777	1.784	1.701

8.2.3.2.A 716B PLANKTIC FORAMINIFERA SPECIES ANALYSIS 150–500 µm

	15	75	185	205	255	425	475	525	605	625	705
Candeina nitida		2	2	2							
Globigerina bulloides	4	10		4	3	1	12			6	2
Globigerina digitata											
Globigerina rubescens			5	1			2	1		5	6
Globigerinella adamsi	8			1	1						
Globigerinella aequilateralis	38	24	19	29	25	41	20	43	28	34	19
Globigerinella calida	6	21	9	3	9	3	17	7	1	4	15
Globigerinita glutinata	3	24	24	21	6	6	27	12	9	11	30
Globigerinoides conglobatus	4	2	5	2	4	10	2	5		1	
Globigerinoides elongatus			7	10		8		4	7		10
Globigerinoides ruber	24	39	41	43	33	21	62	38	30	32	76
Globigerinoides sacculifer	32	4	16	18	5	25	5	24	10	11	28
Globigerinoides trilobus	40	35	44	31	43	38	37	33	37	41	25
Globoquadrina conglomerata	7	7	14	13	10	7	4	15	12	7	10
Globorotalia crassaformis		6	1	6	3	9	6	1	8	2	3
Globorotalia hexagonus		3	7	4			7	9			10
Globorotalia menardii	40	54	41	55	46	61	37	72	64	51	62
Globorotalia scitula		2		1			1				2
Globorotalia theyeri	6			1			6			4	2
Globorotalia truncatulinoides											
Globorotalia tumida		2	2	5	3		1	3		1	1
Hastigerina pelagica			1								
Neogloboquadrina dutertrei	57	52	66	81	83	65	51	72	81	86	59
Neogloboquadrina pachyderma										2	
Orbulina universa						2		1	2	3	
Pulleniatina obliquiloculata	29	18	41	20	34	21	21	18	21	25	23
Sphaeroidinella dehiscens	3	1								1	
Total individuals	301	306	345	351	308	318	318	358	310	327	383
Total species	15	19	18	21	15	15	18	17	13	19	18
Fisher alpha	3.32	4.475	4.036	4.9	3.299	3.27	4.132	3.712	2.745	4.395	3.92
Evenness	0.6817	0.5912	0.6283	0.5314	0.5822	0.6474	0.6186	0.5894	0.6448	0.5119	0.6149
Shannon Weiner	2.325	2.419	2.426	2.412	2.167	2.273	2.41	2.305	2.126	2.275	2.404

725	775	855	915	955	1005	1055	1105	1205	1255	1295
		1		3	1		3	1	3	1
	10				12	12	2	4		2
					1		2			
1	3				1	6	6			
16	24	40	35	27	28	31	30	28	17	22
12	12		9	5	9	7	8	4	5	6
15	13	7	5	23	6	6	24	1	7	2
2	3	1	2	3		2	2	6	7	8
2		3	2	4			6		10	
44	50	31	39	35	55	54	43	34	18	29
18	5	19	29	27	6	6	20	17	45	15
28	75	49	25	32	50	60	42	65	35	66
	5	8	12	8	6	9	20	9	9	3
4	6	3	2		1	1	6	1	3	
3	3	5	3	1	1		6			
80	45	67	45	57	67	41	68	73	64	58
				2	1					
1	2		1	1	2	7				
1										
2	1		1		7			1	5	1
3			1							
74	65	65	81	76	56	57	52	51	74	62
	1					4				2
	3	2	1							
21	13	18	25	23	25	15	18	19	28	36
						2				
327	339	319	318	327	335	320	358	314	330	313
18	19	15	18	16	19	18	18	15	15	15
4.099	4.349	3.267	4.132	3.523	4.364	4.124	3.994	3.281	3.237	3.284
0.4983	0.5189	0.5745	0.5247	0.5970	0.4997	0.5608	0.6434	0.5478	0.6413	0.5501
2.194	2.288	2.154	2.246	2.257	2.251	2.312	2.449	2.106	2.264	2.11

8.2.3.2.B DISTRIBUTION OF MOST ABUNDANT PLANKTIC FORAMINIFERA SPECIES 716B >500 µm

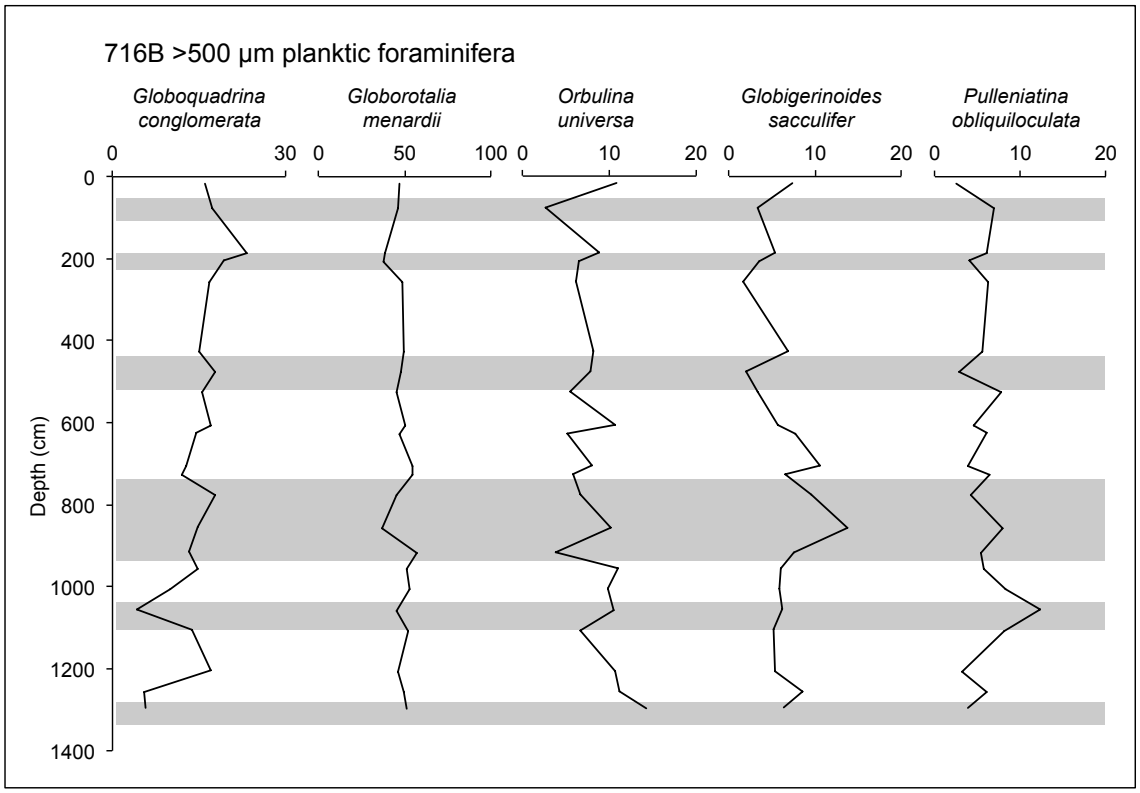

150–500 µm

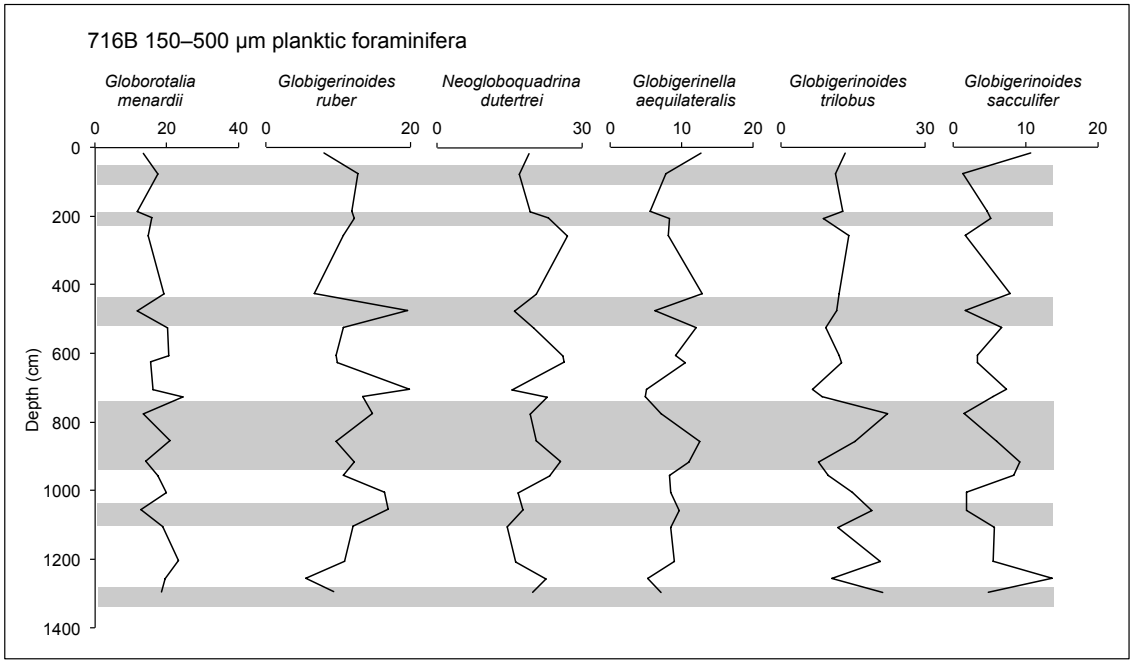

8.2.3.2.C 716B PTEROPOD AND HETEROPOD SPECIES ANALYSIS >500 µm

Species	15	75	185	205	255	425	475	525	605	625	705	725	775	855	915	955	1005	1055	1105	1205	1255	1295
PTEROPODA																						
Cavolinia inflexa	3			1		3		3			2		2	3					1			
Clio cuspidata					1																	
Clio pyramidata					1		1															
Clio convexa	7	5	17	2	10	12	14	5	3	6	4	3	2	6				1				
Creseis acicula	1									1												
Creseis virgula	6	1				5	7															
Creseis virgula constricta					1					2												
Diacavolinia longirostris					2	1	1		2					1								
Diacria quadridentata	1	4	1	1	2	7	2	1	2	3	6	5	1	5	1	1		5			1	1
Diacria trispinosa		1																				
Limacina bulimoides	8	2	2	3	6	9	6	2	3	3	3	2	4					1	1			1
Limacina inflata	62	43	68	3	36	153	185	47	22	66	33	15	35	22	1			23	7		7	3
Limacina lesueuri						3	3	1			1		1		1			5				1
Limacina trochiformis		1	1			7			1	1								1				
Limacina sp. C		1					1															
Hyalostylis striata	1		1	2	1		1		2				1									
Styliola subula	2	1	7	1	9	5	5	2	1			3	1					1	3		1	
Peraclis diversa						2	1		2													
Peraclis molluccensis																						
HETEROPODA																						
Atlanta brunnea						7	5		2	3	1	1	4	2				1	1			
Atlanta frontieri	1		1			6	7	2		4	1											
Atlanta gaudichaudi		2	3																			
Atlanta helicinoidea	1	1				2			1													
Atlanta inclinata	2	4	3	1	1	8	4	2		4			2					1				
Atlanta peronii	1					3	3			2			1					1				
Atlanta rosea			1		2	1	1											1				
Atlanta selvagensis	1						1			1								1				
Atlanta turriculata	1	1	1	1		5	3	1		1	1	1	2	1					1		1	
Carinaria lamarcki	3		4		2	2	3	1	4	2	5	1	2	1				3			2	1
Carinaria spp.			1																			
Firoloida desmarestia								2														
Oxygyrus keraudreni	1		1		2	1	2	2	4	2	1			1				1				
Janthina spp.		2	1	1	2		1		3	2	3	1				3						
TOTAL	102	69	113	16	78	242	257	71	52	103	61	32	58	42	3	4	0	46	14	0	12	7
total species	18	14	16	10	15	20	22	13	14	16	12	9	13	9	3	2	0	14	6	0	5	5

8.2.3.2.C 716B PTEROPOD AND HETEROPOD SPECIES ANALYSIS 150–500 µm

Species	15	75	185	205	255	425	475	525	605	625	705	725	775	855	915	955	1005	1055	1105	1205	1255	1295
PTEROPODA																						
Cavolinia inflexa	9	3	3	4	5	4		3	3	5	2	6	2	3	1	3	4	3	5	2	3	3
Clio convexa	17	2	22	10	17	5	3	4	7	13	5	15	2	4	5	5	8	2	5	4	2	1
Clio pyramidata					1							1					1				1	
Creseis acicula		1	2		2	4	7	4	3	5		5		6	2	2	4		3	1		
Creseis chercheri		1																				
Creseis virgula virgula	11	4	1		1		2			3		1	1							1		2
Creseis virgula constricta	9		3	6		1		1	3	2	2	3		1	6	3		2				
Diacria quadridentata	6	2	3	2	3				1	3		6	1	2	3	5	4	4	8	7	2	1
Diacria trispinosa		1																				
Limacina inflata	130	162	171	159	128	169	182	152	180	138	162	160	168	160	185	188	146	179	150	123	179	153
Limacina lesueuri				1			4	1	2	2				1	2	6	4	2	2		1	4
Limacina bulimoides	7	8	13	9	8	8	9	10	6	8	6	8	1	6	5	18	6	17	7	11	7	5
Limacina trochiformis	36	25	17	30	27	45	21	43	33	25	33	21	32	33	27	18	28	6	26	35	22	21
Limacina sp. C		3															2					
Styliola subula	2	3	7	4	2	3	2	1	2	2		6		1	1		3	1	1	5	1	3
Gleba cordata	6	11	8	8	5	12	5	4	3	6	8	10	7	15	5	9	24	30	37	29	30	42
Peraclis diversa									1													
Peraclis mollucensis	4	3								1		1	1	2					1		1	
Paedoclione doliiformis			1						1		2			1								
Gymnosome veliger		1			2	2		2	1	1	2			3	3	3		1	1	1		
HETEROPODA																						
Atlanta brunnea				1	1	1			1	1		1	1	5		1	1		3	2		2
Atlanta californiensis	1	1					4											1		2		
Atlanta frontieri	7	7	7	14	24	10	21	17	10	13	12	14	23	14	12	5	15	6	5	11	10	9
Atlanta gaudichaudi		1			3	3		1		2	1	1		2					7			1
Atlanta helicinoidea	7	9	14	10	6		16	14	10	16	10	3	11	7	3	7	10	7	8	25	14	19
Atlanta inclinata	4	1	7			4		3	3	3	1	3	9	2		3		1	1		4	1
Atlanta peronii	14	10	9	7	8	14	9	10	6	11	8	5	5	2	3	8	7	14	4	15	8	9
Atlanta rosea	2	4	7	1	2	3	1	4	5	3	12	3	2	5	1	5	4		5		5	52
Atlanta selvagensis	5	15		3	6	12		3		2	2	1	3	4	2		5					
Atlanta turriculata	2	6	5	5	3	4	6	4	5	14	7	5	5	4	7	5	1	6	3	1	1	4
Carinaria lamarckii	17	16	21	20	26	6	6	16	19	19	23	20	25	18	18	31	24	12	19	29	15	12
Carinaria pseudorugosa			1																		1	
Carinaria spp.			1	1									3	4	1		1	1				
Firolida desmarestia	13	12	6	16	25	10	6	11	8	15	6	12	5	5	6	11	7	7		2	16	4
Oxygyrus keraudreni		1			1	3	2		2		2	1		1		2			1	1		
Janthina spp.		1		1							2	4							1	1		
TOTAL	309	314	329	312	306	323	306	308	315	313	308	316	307	311	298	338	309	302	303	308	323	348
total species	21	28	22	21	23	21	18	21	24	25	21	26	20	27	21	21	22	20	23	21	20	20
Fisher Alpha	5.0950	7.0860	5.3110	4.7700	5.7630	5.0260	4.1790	5.1010	6.0410	6.3910	4.7940	6.3980	4.7890	7.1010	5.1540	4.9560	5.4170	4.8140	5.4570	4.7890	4.7160	4.6120
Evenness	0.4465	0.2879	0.3342	0.3500	0.3826	0.3178	0.3040	0.3325	0.2557	0.3787	0.3245	0.3104	0.2895	0.2836	0.2421	0.3070	0.3600	0.2676	0.3198	0.4020	0.2945	0.3540
Shannon Wiener	2.2380	2.0510	1.9950	1.9460	2.1750	1.8980	1.6990	1.9440	1.8140	2.2480	1.8700	2.0490	1.7560	2.0360	1.6260	1.8640	2.0690	1.6770	1.9510	2.0840	1.7730	1.9570

8.2.3.2.D DISTRIBUTION OF MOST ABUNDANT PTEROPOD AND HETEROPOD SPECIES 716B 150–500 µm

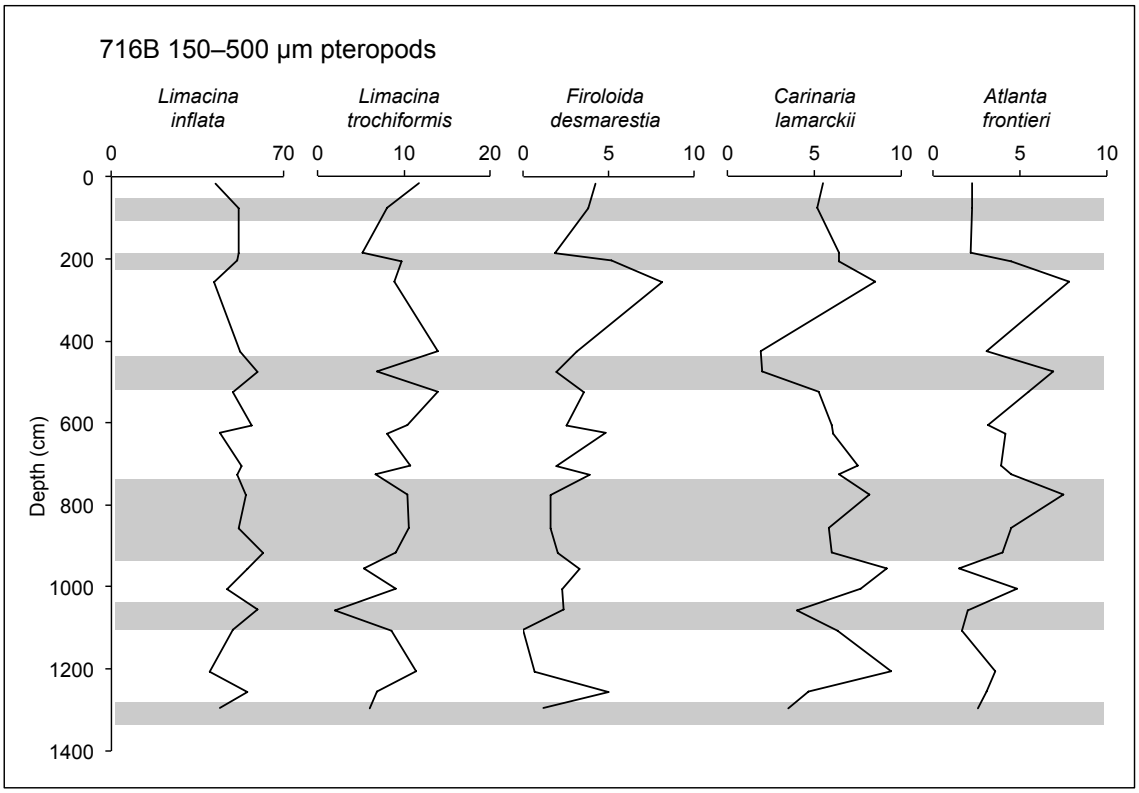

8.2.3.2.E 716B PLANKTIC FORAMINIFERA ABUNDANCE

716B >500 µm

Mid-Sample depth (cm)	Weight before picking (g)	Unpicked weight (g)	Picked weight (g)	Number of planktic foraminifera	Foraminifera per gram	Foraminifera fragments	Broken but counted	Fragment:whole ratio
15.5	0.1626	0.1081	0.0545	316	5798.17	3	47	15.67
75.5	0.2202	0.1374	0.0828	303	3659.42	4	65	22.48
185.5	0.2951	0.2173	0.0778	318	4087.40	2	63	20.31
205.5	0.2104	0.1543	0.0561	322	5739.75	3	41	13.54
255.5	0.3127	0.2362	0.0765	308	4026.14	2	70	23.23
425.5	0.2688	0.1884	0.0804	322	4004.98	1	64	20.12
475.5	0.3057	0.2480	0.0577	309	5355.29	2	50	16.72
525.5	0.1946	0.1503	0.0443	326	7358.92	5	36	12.39
605.5	0.1865	0.1300	0.0565	331	5858.41	7	58	19.23
625.5	0.2102	0.1657	0.0445	328	7370.79	8	74	24.40
705.5	0.1956	0.1522	0.0434	340	7834.10	6	53	17.05
725.5	0.2141	0.1731	0.0410	310	7560.98	1	53	17.36
775.5	0.2485	0.2003	0.0482	313	6493.78	4	64	21.45
855.5	0.2526	0.1887	0.0639	327	5117.37	4	64	20.54
915.5	0.1048	0.0594	0.0454	316	6960.35	6	69	23.29
955.5	0.1543	0.1126	0.0417	312	7482.01	7	54	19.12
1005.5	0.0918	0.0511	0.0407	327	8034.40	5	62	20.18
1055.5	0.2833	0.2371	0.0462	325	7034.63	2	77	24.16
1105.5	0.1984	0.1482	0.0502	333	6633.47	3	46	14.58
1205.5	0.2562	0.1799	0.0763	319	4180.87	4	78	25.39
1255.5	0.1624	0.1206	0.0418	314	7511.96	7	74	25.23
1295.5	0.2099	0.1651	0.0448	316	7053.57	1	84	26.81

716B 150−500 µm

Mid-Sample depth (cm)	Weight before picking (g)	Unpicked weight (g)	Picked weight (g)	Number of planktic foraminifera	Foraminifera per gram	Foraminifera fragments	Broken but counted	Fragment:whole ratio
15.5	0.5782	0.5652	0.0130	301	23153.85	27	29	17.07
75.5	0.6804	0.6709	0.0095	306	32210.53	58	59	32.14
185.5	0.8534	0.8392	0.0142	345	24295.77	43	38	20.88
205.5	0.8098	0.7954	0.0144	351	24375.00	49	39	22.00
255.5	1.1546	1.1415	0.0131	308	23511.45	36	50	25.00
425.5	0.9912	0.9762	0.0150	318	21200.00	24	54	22.81
475.5	1.0985	1.0894	0.0091	318	34945.05	25	38	18.37
525.5	0.8038	0.7887	0.0151	358	23708.61	38	45	20.96
605.5	0.8390	0.8261	0.0129	310	24031.01	26	31	16.96
625.5	0.8476	0.8350	0.0126	327	25952.38	37	40	21.15
705.5	0.7532	0.7434	0.0098	383	39081.63	43	25	15.96
725.5	0.8102	0.7983	0.0119	327	27478.99	48	56	27.73
775.5	1.2339	1.2230	0.0109	339	31100.92	52	36	22.51
855.5	1.0050	0.9917	0.0133	319	23984.96	23	40	18.42
915.5	0.4261	0.4147	0.0114	318	27894.74	33	44	21.94
955.5	0.8928	0.8804	0.0124	327	26370.97	45	43	23.66
1005.5	0.4550	0.4421	0.0129	335	25968.99	63	44	26.88
1055.5	1.1861	1.1750	0.0111	320	28828.83	59	46	27.70
1105.5	0.7766	0.7276	0.0490	358	7306.12	37	48	21.52
1205.5	1.1642	1.1523	0.0119	314	26386.55	51	55	29.04
1255.5	0.8613	0.8457	0.0156	330	21153.85	40	59	26.76
1295.5	1.0304	1.0171	0.0133	313	23533.83	21	60	24.25

8.2.3.2.F 716B PTEROPOD AND HETEROPOD ABUNDANCE

716B >500 µm

Mid-Sample Depth (cm)	Weight before picking (g)	Unpicked weight (g)	Picked weight (g)	Number of pteropods	pteropods per gram
15.5	0.1626	0.0000	0.1626	102	627.31
75.5	0.2202	0.0000	0.2202	67	304.27
185.5	0.2951	0.0000	0.2951	112	379.53
205.5	0.2104	0.0000	0.2104	15	71.29
255.5	0.3127	0.0000	0.3127	76	243.04
425.5	0.2688	0.0000	0.2688	242	900.30
475.5	0.3057	0.0000	0.3057	256	837.42
525.5	0.1946	0.0000	0.1946	71	364.85
605.5	0.1865	0.0000	0.1865	49	262.73
625.5	0.2102	0.0000	0.2102	101	480.49
705.5	0.1956	0.0000	0.1956	58	296.52
725.5	0.2141	0.0000	0.2141	31	144.79
775.5	0.2485	0.0000	0.2485	58	233.40
855.5	0.2526	0.0000	0.2526	42	166.27
915.5	0.1048	0.0000	0.1048	3	28.63
955.5	0.1543	0.0000	0.1543	1	6.48
1005.5	0.0918	0.0000	0.0918	0	0.00
1055.5	0.2833	0.0000	0.2833	46	162.37
1105.5	0.1984	0.0000	0.1984	14	70.56
1205.5	0.2562	0.0000	0.2562	0	0.00
1255.5	0.1624	0.0000	0.1624	12	73.89
1295.5	0.2099	0.0000	0.2099	7	33.35

716B 150−500 µm

Mid-Sample Depth (cm)	Weight before picking (g)	Unpicked weight (g)	Picked weight (g)	Number of pteropods	pteropods per gram
15.5	0.5782	0.5366	0.0416	309	7427.88
75.5	0.6804	0.6361	0.0443	313	7065.46
185.5	0.8534	0.7911	0.0623	329	5280.90
205.5	0.8098	0.7267	0.0831	311	3742.48
255.5	1.1546	1.1069	0.0477	306	6415.09
425.5	0.9912	0.9645	0.0267	323	12097.38
475.5	1.0985	1.0757	0.0228	306	13421.05
525.5	0.8038	0.7705	0.0333	308	9249.25
605.5	0.8390	0.8019	0.0371	315	8490.57
625.5	0.8476	0.7977	0.0499	313	6272.55
705.5	0.7532	0.7267	0.0265	306	11547.17
725.5	0.8102	0.7077	0.1025	312	3043.90
775.5	1.2339	1.1648	0.0691	307	4442.84
855.5	1.0050	0.9585	0.0465	311	6688.17
915.5	0.4261	0.3442	0.0819	298	3638.58
955.5	0.8928	0.7731	0.1197	338	2823.73
1005.5	0.4550	0.2537	0.2013	309	1535.02
1055.5	1.1861	1.1505	0.0356	302	8483.15
1105.5	0.7766	0.6485	0.1281	302	2357.53
1205.5	1.1642	0.5172	0.6470	307	474.50
1255.5	0.8613	0.7944	0.0669	323	4828.10
1295.5	1.0304	0.9208	0.1096	348	3175.18

8.2.3.3 CALCIFICATION INDICES APPENDIX

8.2.3.3.A 716B LDX DATA

Mid-sample Depth (cm)	LDX for *Limacina inflata* >300um (n>10)																														No. Spec	Mean LDX
15.5	4	3	3	3	3	3	3	2	3	4	3	3	3	4	3	3	3	2	3	3	3	4	2	3	3	3	4	3	3	2	30	3.03
75.5	3	3	3	2	1	2	1	1	3	1	2	3	1	1	3	2	2	2	3	2	1	2	3	3	2	2	2	3	2	2	30	2.10
185.5	2	2	2	2	3	3	3	2	3	3	3	3	3	2	3	3	3	2	3	2	3	2	2	2	3	3	2	2	3	2	30	2.53
205.5	2	4	3	3	4	2	3	2	3	2	2	3																			12	2.75
255.5	2	3	2	2	3	3	2	3	4	4	3	3	3	3	2	3	3	3	2	2	2	2	3	3	4	3	3	2	2	3	30	2.73
425.5	3	1	2	3	2	2	2	1	1	2	1	2	3	3	2	2	1	3	3	1	3	2	1	2	1	2	2	3	2	3	30	2.03
475.5	3	3	2	2	2	3	3	2	2	2	4	2	2	2	2	2	3	3	2	3	2	3	2	2	3	2	2	4	2	2	30	2.43
525.5	3	3	2	2	2	3	2	2	2	2	3	3	2	2	2	2	2	2	3	3	2	3	2	2	2	3	2	3	3	2	30	2.37
605.5	3	4	5	3	2	5	4	4	2	2	3	3	3	3	2	5	3	2	4	4	4	4	3	2	2	3	3	3	4	2	30	3.20
625.5	2	2	3	3	3	2	2	3	2	2	2	3	3	2	3	3	2	3	3	2	2	3	3	2	2	3	2	2	2	3	30	2.47
705.5	3	3	2	5	3	3	3	3	2	3	3	4	3	3	3	2	4	3	5	5	4	4	5	4	3	2	3	3	3	4	30	3.33
725.5	3	3	2	5	3	3	3	3	2	3	3	4	3	3	3	2	4	3	5	5	4	4	5	4	3	2	3	3	3	4	30	3.33
775.5	3	2	3	2	3	2	3	2	3	3	3	3	3	3	3	2	3	2	3	3	2	2	2	2	3	3	2	2	3	3	30	2.60
855.5	3	4	3	3	2	2	3	2	5	5	3	2	3	3	4	3	3	3	3	2	3	3	2	2	3	2	5	2	2	2	30	2.90
915.5	2	4	2	3	3	4	4	3	3	4	3	2	2	3	4	3	4	2	3	4	3	4	3	3	3	2	3	2	3	4	30	3.07
955.5	3	3	3	3	3	4	2	3	2	2	3	3	3	2	3	4	3	2	3	3	3	3	3	2	3	3	2				27	2.81
1005.5	3	4	3	3	3	4	3	3	3	3	2	3	3	3	3	3	3	2	2	3	3	4	4	3	4	3	2	4	3	3	30	3.07
1055.5	2	2	3	3	2	3	2	2	3	2	3	2	2	3	2	3	3	3	3	3	3	2	3	3	2	2	3	2	2	3	30	2.53
1105.5	4	4	3	3	3	3	5	2	2	2	2	3	2	2	3	2	3	2	3	3	3	3	2	3	3	3	2	2	2	3	30	2.73
1205.5	3	3	3	3	3	4	3	3	3	3	3	3	2	3	3	3	3														17	3.00
1255.5	3	2	3	2	2	3	3	3	3	2	2	2	2	3	2	2	2	3	2	2	2	2	2	2	2	3	3	3	2	2	30	2.37
1295.5	4	3	3	3	3	3	3	3	2	3	4	2	2	3	3	3	3	3	3	3	3	3	3	3	3	3	3	3	3	3	30	2.97

8.2.3.3.B ALL LDX POINTS FOR 716B. RED LINE SHOWS MEAN VALUES, GREY BARS SHOW STANDARD DEVIATION

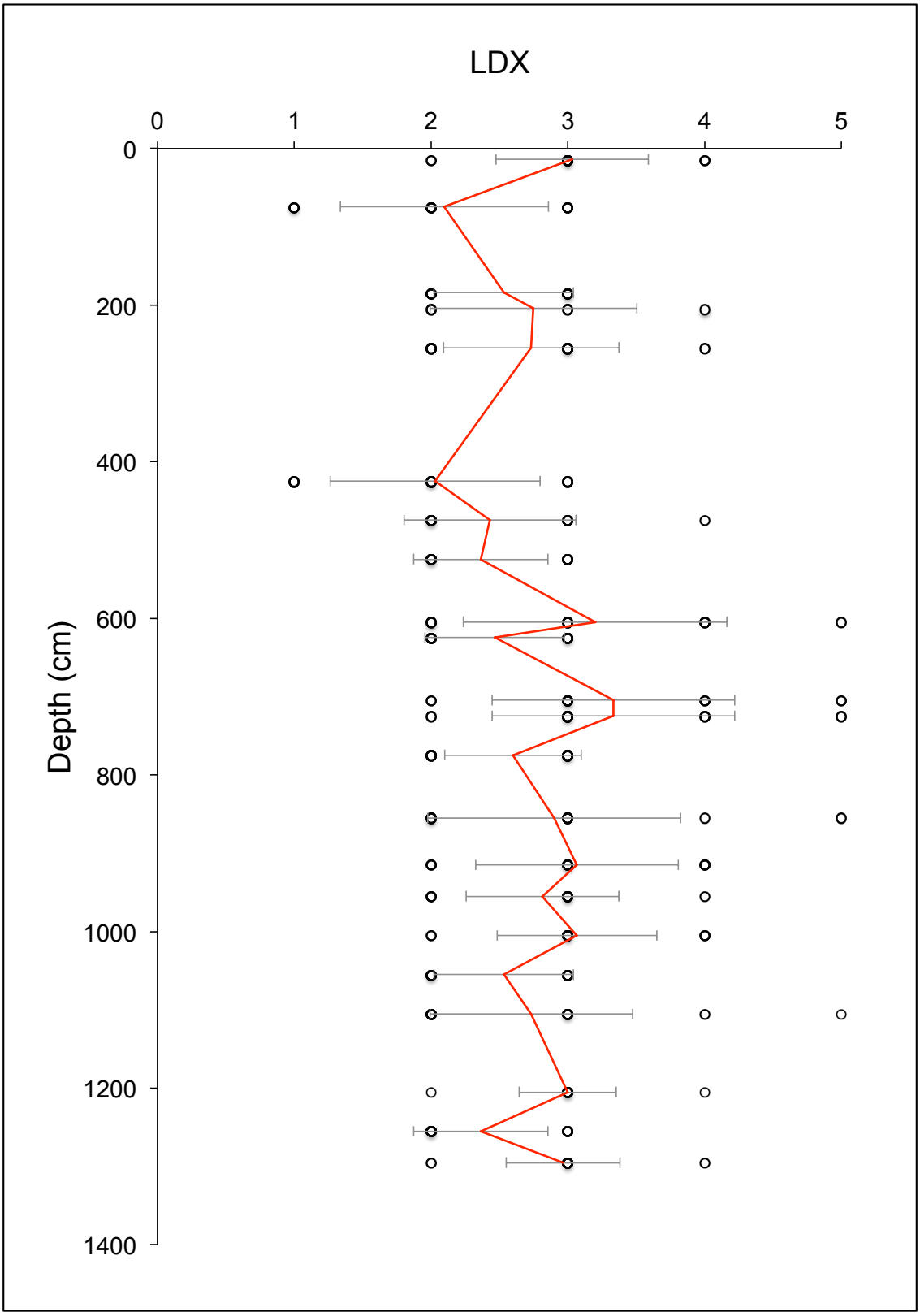

15.5 cm	717	684	727	475	809	592	652	722	576	726	819	873	546	793	744	883	737	829	697	655
	751	715	658	846	785	649	853	902	875	707	832	659	596	643	658	578	831	620	729	845
	750	779	637	836	661	669	708	772	692	696	745	883	624	591	634	514	621	926	642	775
	668	514	306	303	222	304	387	281	214	211	198	397	277	208	467	430	351	431	239	200
	370	272	280	308	252	149	199	351	244	270	183	468	148	196	185	251	158	226	199	249
	193	223	232	207	218	196	219	217	316	245	338	362	214	227	213	217	242	202	181	211
	196	172	186	224	206	221	190	173	185	189	231	262	160	202	249	211	342	267	207	267
	250	312	520	374	235	222	205	185	210	188	239	207	196	262	238	378	343	211	483	503
	296	272	261	293	452	322	315	352	274	194	238	240	509	201						
Average	**424 µm**																			
75.5 cm	723	699	633	822	622	680	581	527	822	657	652	773	783	708	716	614	712	641	655	761
	685	623	766	693	692	844	936	622	660	741	661	676	746	800	714	580	697	597	696	562
	790	497	576	268	297	228	274	410	290	367	306	224	232	219	240	182	423	307	207	269
	263	235	200	204	199	251	303	348	262	474	595	246	407	428	181	217	218	213	287	266
	263	273	294	243	215	248	335	222	277	263	191	216	220	209	318	327	188	182	379	225
	256	290	477	424	219	219	230	294	271	206	167	381	229	233	241	559	270	276	230	253
	218	211	321	226	198	194	213	185	276	212	223	233	312	245	206	212	176	153	233	275
	208	239	280	283	220	355	337	221	236	213	197	250	184	234	237	185	428	220	285	
Average	**379 µm**																			
205.5 cm	632	800	748	215	169	215	210	207	230	201	226	217	208	271	195	239	199	255	225	229
	209	255	226	226	262	254	193	275	239	202	210	211	193	246	264	204	229	182	153	555
	170	247	236	257	285	194	562	209	205	219	183	195	200	175	331	281	291	216	197	231
	240	250	186	206	306	246	288	208	217	255	247	195	236	245	232	250	224	244	218	253
	192	246	254	179	218	227	201	251	237	231	237	230	212	250	233	217	213	244	235	218
	215	237	215	146	239	183	240	201	197	207	187	233	192	203	209	211	259			
Average	**243 µm**																			

425.5 cm	956	665	661	685	607	805	793	698	891	588	783	921	736	936	821	932	993	767	871	957
	726	845	790	542	1033	639	1019	711	640	652	909	672	798	726	645	538	548	781	670	836
	719	1078	574	667	762	609	624	695	646	681	557	750	587	909	698	918	644	883	590	683
	618	469	515	1004	465	628	605	662	710	632	674	609	554	641	999	623	617	723	669	813
	724	619	692	573	608	925	831	888	669	530	819	991	953	688	883	787	707	668	695	778
	538	921	747	748	801	577	850	602	874	803	720	604	797	903	706	646	698	593	561	251
	581	639	642	675	749	719	706	842	738	714	618	997	881	893	793	653	624	621	687	720
	491	869	921	942	909	1059	915	628	721	402	454	449	314	393	288	256	332	476	284	408
	458	330	294	283	396	288	317	333	250	217	197	195	543	354	234	225	187	240	196	235
	212	281	266	359	168	209	211	228	208	327	250	220	271	230	211	249	202	251	187	169
	285	230	231	189	235	200	193	193	234	203	169	224	183	277	247	225	281	231	238	192
	227	254	229	250	212	184	269	219	219	220	270	237	233	209	196	169	233	251	226	170
	169	229	218	222	199	216	197	270	214	247	247	193	232	208	201	220	277	208	234	215
	160	240	230	227	224	282	206	297	340	447	303	221	211	238	278	237	280	250	421	232
	182	195	231	164	316	328	199	229												
Average	**510 µm**																			
475.5 cm	768	914	694	647	690	813	839	867	633	576	687	1074	664	656	242	270	179	386	277	336
	705	807	563	625	626	745	986	962	817	738	806	1081	1003	615	177	242	221	230	268	228
	915	873	1103	525	728	755	879	755	661	647	641	572	829	725	205	248	191	276	226	491
	745	756	753	522	858	748	604	570	636	615	744	932	676	1059	230	285	228	213	238	189
	608	689	1014	947	674	635	927	694	548	708	640	911	734	671	262	227	200	189	193	239
	695	939	745	620	723	961	617	642	767	662	719	602	995	695	317	192	239	202	156	460
	802	648	767	869	773	694	596	798	738	665	537	659	913	592	206	267	273	303	206	372
	691	871	706	1021	793	697	789	947	933	777	741	868	909	1085	196	216	212	292	199	227
	835	679	1079	1019	620	1186	881	1067	671	778	880	967	570	904	188	284	208	191	212	226
	933	770	807	865	689	806	774	814	968	739	663	689	943	866	232	228	225	222	243	214
	576	578	592	696	879	475	970	616	520	594	664	649	761	739	449	269	278	193	245	387
	695	656	566	630	785	919	682	676	538	842	684	704	874	1159	287	205	221	206	323	143
	1053	571	736	447	496	694	580	730	626	991	697	711	594	216	373	220	229	389	180	290
	512	276	280	317	201	327	249	231	185	263	209	190	205	298	246	214	207	209	485	363
	245	255	219	204	270	276	194	342	416	351	228	435	231	201	298	235	178	198	216	234
	440	184	354	242	227	182	167	229	255	219	204	247	255	209	289					
Average	**544 µm**																			

605.5 cm	533	633	816	923	630	620	665	609	949	1132	577	548	568	613	666	637	670	700	956	609
	527	1152	291	228	415	415	409	313	422	207	282	236	225	514	232	263	249	253	294	252
	266	361	224	248	277	218	253	216	275	270	235	238	254	257	212	206	159	207	214	215
	183	272	230	220	175	237	340	229	472	440	196	176	222	253	217	221	199	212	283	237
	179	259	255	332	214	291	243	244	219	192	268	327	249	238	225	251	199	222	232	225
	219	163	192	203	217	273	210	177	217	232	180	184	189	236	194	235	408	275	220	255
	210	221	200	216	217	231	235	191	254	292	533	234	211	276	225	242	291	193	231	212
	219	254	283	150	226	190	264	233	225	226	227	218	203	228	188	249	188	309	235	338
	229	229	196	175	192	201	188													
Average	**308 µm**																			
625.5 cm	857	582	541	758	833	788	667	532	921	689	505	1111	638	274	148	510	370	370	484	417
	674	629	626	862	729	599	570	584	687	562	496	897	418	341	241	292	544	179	199	207
	607	596	648	867	812	870	879	622	562	543	1139	664	566	263	365	342	398	389	209	184
	534	888	562	599	549	869	827	875	791	649	627	751	1027	256	187	209	216	309	378	459
	651	476	815	546	561	800	713	726	827	596	648	721	559	268	191	243	184	275	398	230
	362	506	557	306	490	386	424	583	436	205	369	250	191	356	313	224	278	361	217	274
	400	187	267	165	190	252	180	551	331	358	237	371	200	514	223	274	349	218	413	431
	297	228	369	483	195	251	336	196	373	151	202	273	228	440	378	370	225	297	242	310
	251	267	172	231	257	223	246	230	203	404	327									
Average	**454 µm**																			
725.5 cm	793	568	760	741	584	521	783	615	625	702	828	946	570	513	500	410	316	228	239	245
	226	524	259	207	285	225	362	224	237	238	211	261	186	337	246	229	186	177	227	218
	232	247	516	404	356	192	220	340	279	199	207	208	222	175	452	545	197	217	290	342
	355	232	169	239	230	276	223	215	153	201	233	248	177	182	235	243	248	195	233	327
	268	418	205	229	254	330	353	220	257	191	192	194	250	209	226	214	223	190	278	199
	223	232	205	223	225	207	227	326	240	226	280	214	355	456	346	208	224	295	224	264
	232	202	319	161	345	242	245	238	212	200	230	244	273	277	250	221	233	233	231	233
	204	400	266	219	297	224	355	214	333	165	274	355	255	240	241	404	267	230		
Average	**297 µm**																			

775.5 cm	713	754	663	785	979	593	622	783	793	659	721	612	629	261	327	222	263	181	204	247
	711	734	916	517	671	682	955	1007	893	910	657	696	571	272	284	351	205	251	283	222
	905	939	925	640	873	556	662	900	886	338	354	227	239	231	206	246	269	347	256	212
	375	255	161	374	214	189	219	184	198	181	214	194	299	268	205	286	209	248	239	337
	285	211	209	164	207	187	204	284	241	213	258	224	398	243	169	208	244	190	225	221
	290	198	235	204	199	189	189	216	231	199	212	254	219	228	245	254	241	279	214	203
	205	229	414	183	182	424	240	184	295	237	316	241	257	191	220	225	226	252	232	219
	224	180	245	234	380	487	422	204	483	165	230	248	280	226	175	197	219	198	319	248
	264	253	280	244	253	178	224	238	210	209	203	524	195	258	234	272	278	349	339	180
	364	413	419	366	435	208	192	238	146	214										
Average	**345 µm**																			
915.5 cm	907	187	156	253	229	234	319	217	189	231	168	172	224	262	234	206	270	214	214	189
	221	402	175	243	210	210	225	215	214	230	228	264	193	267	234	255	205	216	200	204
	388	232	229	215	247	184	294	216	235	192	170	182	246	219	203	226	225	285	225	279
	376	280	297	198	221	206	355	261	221	233	209	256	194	224	188	231	209	233	209	269
	229	266	273	211	250	200	243	224	267	214	165	231	254	231	218	179	202	220	253	221
	206	226	199	179	244	191	193	215	224	152	221	192	259	229	170	258	184	160	199	195
	383	177	158	211	203	326	201	211	223	170	215	246	226	226	196	237	210	202	197	161
	207	221	180	224	172	236	235	228	210	203	223	187	214	223	260	210	204	247	190	266
	259	208																		
Average	**229 µm**																			
955.5 cm	496	221	176	237	231	258	267	188	168	245	239	354	259	198	229	217	215	224	236	232
	242	247	260	201	173	220	104	177	217	259	210	195	361	223	193	168	220	279	242	195
	202	321	135	212	179	249	234	223	201	212	221	177	239	206	207	195	191	174	258	250
	218	208	228	266	224	173	234	210	208	248	205	403	176	206	188	211	213	197	229	251
	227	208	205	254	210	214	214	351	212	230	217	237	343	227	216	226	236	224	226	199
	217	211	217	218	220	321	257	249	198	194	238	193	215	217	229	212	265	217	195	256
	204	190	201	270	316	257	219	196	214	306	246	226	224	197	216	177	191	169	184	178
	302	207	217	228	267	261	202	182	201	183	211	219	253	253	210	242	185	272	235	204
	251	270	220	212	203	181	228	166	235	207										
Average	**226 µm**																			

1005.5 cm	622	960	637	711	639	601	739	679	548	597	830	626	650	687	932	611	581	627	615	402
	232	303	226	330	211	284	196	194	174	523	269	206	157	222	217	194	276	216	292	290
	232	258	222	261	251	218	231	191	265	230	226	284	219	227	297	211	235	316	255	239
	216	226	204	227	335	295	202	246	210	297	235	274	225	212	216	214	193	181	244	320
	268	190	219	208	261	224	235	265	262	290	272	372	202	216	193	256	230	204	244	239
	274	179	254	376	397	240	238	199	192	278	193	207	230	251	227	241	217	212	221	195
	233	201	181	414	406	450	226	169	271	262	234	202	201	300	209	197	200	286	227	225
	181	460	187	181	253	195	187	244	242	204	211	481	307	190	251					
Average	**300 µm**																			
1055.5 cm	605	886	645	745	689	628	755	698	628	574	650	818	610	578	235	279	224	184	216	447
	684	876	999	629	571	619	621	600	355	231	201	330	236	300	248	175	206	246	461	267
	218	168	210	223	252	215	339	253	555	211	246	203	212	272	254	201	232	210	230	187
	271	296	188	220	237	333	222	211	199	188	230	277	199	200	183	208	210	239	195	284
	242	213	268	271	268	304	325	218	325	207	306	236	237	338	203	226	219	179	166	197
	221	200	298	203	210	189	193	219	235	296	252	184	256	222	178	479	180	247	261	199
	224	236	254	272	220	238	210	236	252	271	404	237	271	183	205	230	248	318	426	419
	300	227	216	175	284	215	216	216	233	240	183	245	277	373	215	208	271	201	256	218
	272	391	258	229	266	235	193													
Average	**306 µm**																			
1205.5	210	340	205	123	210	272	177	226	239	222	198	243	175	184	246	207	194	208	168	213
	250	125	226	391	265	198	161	203	215	314	214	255	237	245	164	181	212	214	228	205
	213	252	195	208	195	207	214	220	223	231	198	214	217	208	182	194	284	239	215	224
	243	144	287	258	244	172	203	234	187	165	212	233	220	236	214	192	247	286	220	227
	166	158	208	198	196	210	225	191	242	217										
Average	**217 µm**																			
1255.5 cm	667	628	626	591	554	651	382	202	220	213	283	193	195	294	226	199	219	209	206	179
	192	218	221	460	436	199	214	191	214	191	193	271	211	377	203	222	173	202	222	246
	246	246	349	336	251	281	171	202	267	192	207	170	179	260	157	207	193	163	195	155
	213	188	225	222	216	194	223	189	208	219	269	227	167	204	209	226	216	193	202	196
	163	254	204	231	224	228	214	177	280	236	216	311	198	210	196	189	177	359	262	230
	202	178	198	223	275	209	194	202	216	244	221	266	241	192	297	229	218	244	190	237
	199	230	201	216	146	217	168	226	210	225	200	183	227	249	200	228	213	235	153	208
	182	245	175	218	223	244	228	210	192	227	201	209	193	241	251	186	202			
Average	**237 µm**																			

1295.5 cm	814	560	545	185	229	375	401	332	195	211	261	217	275	212	241	219	197	157	149	218
	234	214	340	203	371	210	233	236	277	215	245	251	237	287	246	187	189	234	389	220
	256	256	329	227	280	185	202	236	226	214	213	244	277	209	210	205	263	193	213	187
	299	240	168	289	240	143	199	206	198	212	325	174	200	200	219	219	214	219	202	210
	239	353	178	200	198	200	247	262	216	230	186	272	285	361	178	407	336	241		
Average	**251 µm**																			

9 REFERENCES

Accornero, A., Manno, C., Esposito, F. and Gambi, M. C. 2003. The vertical flux of particulate matter in the polynya of Terra Nova Bay. Part II. Biological components. *Antarctic Science*, **15,** 175–188

Adams A. and Reeve L. 1848–1850. Mollusca. In: Adams A. (ed.) *The zoology of the H. M. S. Samarang under the command of Captain Sir Edward Belcher, C.B., F.R.A.S., F.G.S., during the years 1843-1846 Part 1.* London. 24pp. pls. 1–9.

Alegian, C.R. 1985. The *biogeochemical ecology of Porolithon gardineri (Foslie)*. Unpublished PhD thesis, University of Hawaii.

Almogi-Labin, A. 1982. Stratigraphic and paleoceanographic significance of late Quaternary pteropods from deep-sea cores in the Gulf of Aqaba (Elat) and northernmost Red Sea. *Marine Micropaleontology,* **7,** 53–72.

Almogi-Labin, A., Hemleben, C., Meischner, D. and Erlenkeuser, H. 1991. Paleoenvironmental events during the last 13,000 years in the Central Red Sea as recorded by Pteropoda. *Paleoceanography,* **6,** 83–98.

Almogi-Labin, A., Luz, B. and Duplessy, J.-C., 1986. Quaternary paleooceanography, pteropod preservation and stable-isotope record of the Red Sea. *Palaeogeography, Palaeoclimatology, Palaeoecology*, **57**, 195–211.

Almogi-Labin, A., Schmiedel, G., Hemleben, C., Siman-Tov, R., Segl, M. and Meischner, D. 2000. The influence of the NE winter monsoon on productivity changes in the Gulf of Aden, NW Arabian Sea, during the last 530 kyr as recorded by foraminifera, *Marine Micropaleontology*, **40**, 295–319.

Aravindakshan, P.N. 1977. Pterotracheidae (Heteropoda, Mollusca) of the Indian Ocean from the International Indian Ocean Expedition. In: *Proceedings of the Symposium on Warm Water Zooplankton*. Council of Industrial and Scientific Research, National Institute of Oceanography, Goa. 137–145.

Arnold, A.J. and Parker, W.C. 2002. Biogeography of planktonic foraminifera. In: Sen Gupta, B.K (ed.). *Modern Foraminifera.* Kluwer Academic Publishers, Dordrecht, The Netherlands, 103–122.

Backman, J., Duncan, R.A., Peterson, L.C., Baker, P.A., Baxter, A.N., Boersma, A., Cullen, J.L., Droxler, A.W., Fisk, M.R., Greenough, J.D., Hargraves, R.B., Hempel, P., Hobart, M.A., Hurley, M.T., Johnson, D.A., Macdonald, A.H., Mikkelsen, N., Okada, H., Rio, D., Robinson, S.G., Schneider, D., Swart, P.K., Tatsumi, Y., Vandamme, D., Vilks, G. and Vincent, E. 1988. Site 716. *Proceedings of the Ocean Drilling Program, Initial Reports,* **115**, 1005–1077.

Barker, S. and Elderfield, H. 2002. Foraminiferal calcification response to glacial-interglacial changes in atmospheric CO_2. *Science,* **297,** 833–836.

Barrows, T.T. and Juggins, S. 2005. Sea-surface temperatures around the Australian margin and Indian Ocean during the Last Glacial Maximum. *Quaternary Science Reviews,* **24**, 1017–1047.

Bè, A.W.H. 1977. An ecological, zoogeographical and taxonomic review of recent planktonic foraminifera. In: Ramsay, A.T.S. (ed.). *Oceanic Micropalaeontology*. Academic Press, London, 1–100.

Bè, A.W.H. and Gilmer, R.W. 1977. A zoogeographic and taxonomic review of Euthecosomatous Pteropoda. In: Ramsay, A.T.S. (ed.). *Oceanic Micropalaeontology*. Academic Press, London, 733–808.

Bè, A.W.H. and Tolderlund, D.H. 1971. Distribution and ecology of living planktonic foraminifera in surface waters of the Atlantic and Indian Oceans. In: Funnell, B.M and Riedel, W.R. (eds). *The Micropalaeontology of Oceans,* Cambridge University Press, 105–149.

Beaufort, L., Probert, I., de Garidel-Thoron, T., Bendif, E.M., Ruiz-Pino, D., Metzl, N., Goyet, C., Buchet, N., Coupel, P., Grelaud, M., Rost, B., Rickaby, R.E.M. and de Vargas, C., 2011. Sensitivity of coccolithophores to carbonate chemistry and ocean acidification. *Nature*, **476**, 80–83.

Bednaršek, N., Tarling, G.A., Bakker, D.C.E., Fielding, S., Jones, E.M., Venables, H.J., Ward, P., Kuzirian, A., Lézé, B., Feely, R.A. and Murphy, E.J., 2012b. Extensive dissolution of live pteropods in the Southern Ocean. *Nature Geoscience*, DOI: 10.1038/NGEO1635.

Bednaršek, N., Tarling, G.A., Bakker, D.C.E., Fielding, S., Cohen, A., Kuzirian, A., McCorkles, D., Lézé, B. and Montagna, R. 2012a. Description and quantification of pteropod shell dissolution: a sensitive bioindicator of ocean acidification. *Global Change Biology,* **18**, 2378–2388.

Benson W.H. 1835. Account of Oxygyrus; a new genus of pelagian shells allied to the genus Atlanta of Lesueur, with a note on some other pelagian shells lately taken on board the ship Malcolm. *The Journal of the Asiatic Society of Bengal,* **4**, 173–176.

Berger, W.H. 1977. Deep-sea carbonate and the deglaciation preservation spike in pteropods and foraminifera. *Nature*, **269**, 301–303.

Berner, R.A. and Honjo, S. 1981. Pelagic sedimentation of aragonite: its geochemical significance. *Science,* **211,** 940–942.

Biekhart, J.W., 1989. Euthecosomatous pteropods as paleohydrological and paleoecological indicators in a Tyrrhenian deep-sea core. *Palaeogeography, Palaeoclimatology, Palaeoecology,* **71,** 205-224.

Bigelow, H.B. 1926. Plankton of the offshore waters of the Gulf of Maine. *U.S. Bureau of Fisheries,* **40**, 1–509.

Bijma, J., Honisch, B. and Zeebe, R.E. 2002. The impact of the ocean carbonate chemistry on living foraminiferal shell weight: Comment on

"Carbonate ion concentration in glacial-age deep waters of the Caribbean Sea" by Broecker, W.S. and Clark, E. *Geochemistry Geophysics and Geosystems,* **3,** 1064.

Bijma, J., Spero, H.J. and Lea, D.W. 1999. Reassessing foraminiferal stable isotope geochemistry: Impact of the oceanic carbonate system (experimental results). In: Fischer, G. and Wefer, G. (eds). *Use of Proxies in Paleoceanography: Examples from the South Atlantic*. Springer-Verlag, New York, 489–512.

de Blainville, H.M.D. 1821. Hyale, Hyalæa. (Malacoz.). *Dictionnaire des Sciences Naturelles*, **22**, 1–570.

Blanc-Vernet L., Chamley H. and Froget C. 1969. Analyse paléoclimatique d'une carotte de Méditerranée nord-occidentale. Comparaison entre les résultats de trois études: foraminifères, ptéropodes, fraction sédimentaire issue du continent. *Palaeogeography, Palaeoclimatology, Palaeoecology*, **6**, 215–235.

Boas, J.E.V. 1886. Spolia Atlantica. Bidrag til Pteropodernes, Morfologi og Systematik samt til Kundskaben om deres geografiske Udbredelse. *Kongelige Danske Videnskabernes Selskabs Skrifter, Naturvidenskabelig og Mathematisk Afdeling,* **6**, 1–231, pl. 1–8.

Bonnevie K. 1920. Heteropoda. Report on the scientific results of the "Michael Sars" North Atlantic deep-sea expedition 1910. *Zoology,* **3**, 1–69, pl. 1–9.

Bonnevie, K. 1913. Pteropoda from the Michael Sars North Atlantic Deep-Sea Expedition. *Scientific Results of the Michael Sars North Atlantic Deep-Sea Expedition, 1910,* **III**, 1–69.

Bouchet, P., Rocroi, J.-P. Frýda, J., Hausdorf, B., Ponder, W., Valdés, Á and Warén, A. 2005. Classification and nomenclator of gastropod families. *Malacologia: International Journal of Malacology,* **47**, 1–397.

Buddemeier, R.W., Lane, D.R. and Martinich, J.A. 2011. Modelling regional coral reef responses to global warming and changes in ocean chemistry: Caribbean case study. *Climate Change,* **109**, 375–397, doi: 10.1007/s10584-011-0022-z.

Byrne, R.H., Acker, J.G., Betzer, P.R., Feely, R.A. and Cates, M.H. 1984. Water column dissolution of aragonite in the Pacific Ocean. *Nature,* **312,** 321–326.

Buccheri, G., Capretto, G., Di Donato, V., Esposito, P., Ferruzza, G., Pescatore, T., Russo Ermolli, E., Senatore, M.R., Sprovieri, M., Bertoldo, M., Carella, D. and Madonia, G. 2002. A high resolution record of the last deglaciation in the southern Tyrrhenian Sea: environmental and climatic evolution. *Marine Geology,* **186,** 447–470.

Cahuzac, B. and Janssen, A.W. 2010. Eocene to Miocene holoplanktonic Mollusca (Gastropoda) of the Aquitaine Basin, southwest France. *Scripta Geologica,* **141**, 1–193.

Cantraine F. 1841. Malacologie méditerranéenne et litorale, ou description des mollusques qui vivent dans la Méditerranée ou sur le continent de l'Italie, ainsi que des coquilles qui se trouvent dans les terrains tertiaires italiens, avec des observations sur leur anatomie, leurs moeurs, leur analogie et leur gisement. Ouvrage servant de faune malacologique italienne et de complément à la Conchiologia fossile subap- ennina de Brocchi. *Mémoires de l'Académie royale de Bruxelles,* **13**, 1–173.

Cao, L., Caldeira, K. and Jain, A.K. 2007. Effects of carbon dioxide and climate change on ocean acidification and carbonate mineral saturation. *Geophysical Research Letters,* **34**, L05607, doi:10.1029/2006GL028605.

Capotondi, L., Borsetti, A.M. and Morigi, C. 1999. Foraminiferal ecozones, a high resolution proxy for the late Quaternary biochronology in the central Mediterranean Sea. *Marine Geology,* **153,** 253-274.

Carboni, M.G. and Esu, D. 1987. Paleoclimatology of a late Peistocene – Holocene core from the Tyrrhenian Sea (Western Mediterranean): Foraminifera and Pteropoda. *Geologica Rome,* **26,** 167-185.

Cassidy, M. 2012. *The evolution of volcanism on Montserrat.* Unpublished PhD Thesis, University of Southampton, UK.

Chen, C. 1968. Pleistocene pteropods in pelagic sediments. *Nature,* **219,** 1145–1149.

Chen, C. and Bé, A.W.H. 1964. Seasonal distributions of euthecosomatous pteropods in the surface waters of five stations in the western North Atlantic. *Bulletin of Marine Science of the Gulf and Caribbean,* **14**, 185–220.

delle Chiaje S. 1822–1830. *Memorie sulla storia e notomia degli animali senza vertebre del regno di Napoli*. Figure, Napoli: 109 pls.

Cigliano, M., Gambi, M.C., Rodolfo-Metalpa, R., Patti, F.P. and Hall-Spencer, J.M. 2010. Effects of ocean acidification on invertebrate settlement at volcanic CO_2 vents. *Marine Biology***, 157**, 2489–2502.

CLEMAM. 2012. *Checklist of European Marine Mollusca.* http://www.somali.asso.fr/clemam/index.php

Comeau, S., Alliouane, S. and Gattuso, J.-P. 2012. Effects of ocean acidification on overwintering juvenile Arctic pteropods *Limacina helicina. Marine Ecology Progress Series,* **456**, 279–284.

Comeau, S., Gattuso, J-P., Nisumaa, A-M. and Orr, J. 2011. Impact of aragonite saturation state changes on migratory pteropods. *Proceedings of the Royal Society, B,* doi:10.1098/rspb.2011.0910.

Comeau, S., Gorsky, G., Alliouane, S. and Gattuso, J.-P. 2010b. Larvae of the pteropod Cavolinia inflexa exposed to aragonite undersaturation are viable but shell-less. *Marine Biology, **157,** 2341–2345.*

Comeau, S., Jeffree, R., Teyssié, J.-L. and Gattuso, J.-P. 2010a. Response of the Arctic Pteropod *Limacina helicina* to Projected Future Environmental Conditions. *PLoS ONE,* **5**, e11362.

Comeau, S., Gorsky, G., Jeffree, R., Teyssié, J.-L. and Gattuso, J.-P. 2009. Impact of ocean acidification on a key Arctic pelagic mollusc (*Limacina helicina). Biogeosciences,* **6,** 1877–1882.

Corselli C. and Grecchi G. 1990. Considerazioni sui Thecosomata attuali del Bacino Mediterraneo. *Lavori della Società Italiana di Malacologia*, **24**, 120–130.

Cullen, J.L. and Droxler, A.W. 1990. Late Quaternary variations in planktonic foraminifer faunas and pteropod preservation in the equatorial Indian Ocean. *Proceedings of the Ocean Drilling Program, Scientific Results,* **115**, 579–588.

Cullen, J.L. and Prell, W.L. 1984. Planktonic foraminifera of the Northern Indian Ocean: distributions and preservation in surface sediments. *Marine Micropaleontology,* **9**, 1–52.

Cummings, V., Hewitt, J., van Rooyen, A., Currie, K., Beard, S., Thrush, S., Norkko, J., Barr, N., Heath, P., Halliday, N.J., Sedcole, R., Gomez, A., McGraw, C. and Metcalf, V. 2011. Ocean acidification at high latitudes: potential effect on functioning of the Antarctic bivalve *Laternula elliptica. PLoS ONE,* **6**, e16069.

Dadon, J. R., and de Cidre, L. L. 1992. The reproductive cycle of the Thecosomatous pteropod Limacina retroversa in the western South Atlantic. *Marine Biology*, **114,** 439–442.

Dall, W.H. 1908. A new species of Cavolina, with notes on other pteropods. *Smithsonian Miscellaneous Collections,* **50**, 501–502.

Damuth, J.E. 1975. Quaternary climate change as revealed by calcium carbonate fluctuations in western Equatorial Atlantic sediments. *Deep Sea Research and Oceanographic Abstracts,* **22**, 725–743.

Danforth, C.H. 1907. A new pteropod from New England. *Proceedings of the Boston Society of Natural History,* **32**, 1–19.

Deshayes, G. P. 1853. *Traité élémentaire de conchyliologie avec les applications de cette science a la géologie.* Explication des planches, V. Masson, Paris 1–80, pl. 1–132.

Diaz, B.B., Hart, M.B., Smart, C.W. and Hall-Spencer, J.M. 2010. Modern seawater acidification: the response of foraminifers to high-CO_2 conditions in the Mediterranean Sea. *Journal of the Geological Society, London.* **167**, 1–4.

Doney, S.C., Fabry, V.J., Feely, R.A. and Kleypas, J.A. 2009. Ocean acidification: the othe CO_2 problem. *Annual Review of Marine Science,* **1**, 169–192.

Droxler, A.W., Haddad, G.A., Mucciarone, D.A. and Cullen, J.L. 1990. Pliocene-Pleistocene aragonite cyclic variations in Holes 716A and 716B (The Maldives) compared with Hole 633A (The Bahamas): Records of climate-induced $CaCO_3$ preservation at intermediate water depths. *Proceedings of the Ocean Drilling Program, Scientific Results.* **115**, 539–577.

Droxler, A.W., Schlager, W. and Whallon, C.C. 1983. Quaternary aragonitic cycles and oxygen-isotope record in Bahamian carbonate ooze. *Geology,* **11**, 235–239.

den Dulk, M., Reichart, G.J., Memon, G.M., Roelofs, E.M.P., Zachariasse, W.J. and van der Zwaan, G.J. 1998. Benthic foraminiferal responses to variations in surface water productivity and oxygenation in the northern Arabian Sea. *Marine Micropaleontology,* **35**, 43–66.

Dunker W. 1875. Ueber Conchylien von Desterro, Provinz Sta. Catharina, Brasilien. *Jahrbücher der Deutschen Malakozoologischen Gesellschaft*, **2**, 240–254.

Dupont L. 1979. Note on variation in *Diacria* Gray, 1847, with descriptions of a species new to science, *Diacria rampali* nov. spec., and a forma new to science, *Diacria trispinosa* forma *atlantica* nov. forma. *Malacologia,* **18**, 37–52.

Eberli, G. P., Swart, P. K., Malone, M. J., Anselmetti, F. S., Arai, K., Bernet, K. H., Betzler, C., Christensen, B. A., De Carlo, E. H., De´jardin, P. M., Emmanuel, L., Frank, T. D., Haddad, G. A., Isern, A. R., Katz, M. E., Kenter, J. A. M., Kramer, P. A., Kroon, D., McKenzie, J. A., McNeill, D. F., Montgomery, P., Nagihara, S., Pirmez, C., Reijmer, J. J. G., Sato, T., Schovsbo, N. H., Williams, T. and Wright, J. D.1997. Site 1003, Proceedings of the Ocean Drilling Program, Initial Reports, College Station, Texas (Ocean Drilling Program), **166**, 71–116.

Emery, W.J. 2001. Water types and water masses. In: Steele, H., Thorpe, S.A. and Turekian, K.K. (eds), *Encyclopedia of Ocean Sciences Vol 6,* Academic Press, London, 3179–3187.

Ericson, D.B. and Wollin, G. 1956. Micropaleontological and isotopic determinations of Pleistocene climates. *Micropaleontology*, **2**, 257–270.

Eschscholtz, F. 1829. *Zoologischer Atlas 3*. G. Reimer, Berlin, 18 pp., pls. 11–15.

Eschscholtz F. 1825. Bericht über die zoologische Ausbeute während der Reise von Kronstadt bis St. Peter und Paul. *Isis*, **6**, 733–747.

Eydoux, J.F.T. and Souleyet, L.F.A. 1841. *Voyage autour du monde exécuté pendant les années 1836 et 1837 sur la corvette 'La Bonite', commandée par M. Vaillant, capitaine de vaisseau, publié par ordre du Gouvernement sous les*

auspices du Déparle- ment de la marine. Histoire Naturelle, Zoologie. Atlas. A. Bertrand, Paris, 8 pp., mollusques pls 1-15.

Eydoux J.F.T. and Souleyet L.F.A. 1840. Description sommaire de plusieurs Ptéropodes nouveaux ou imparfaitement connus, destinés à être publiés dans le voyage de la "Bonite". *Revue Zoologique de la Société Cuvierienne, Paris,* 235–239.

Fabry, V.J. 1990. Shell growth rates of pteropod and heteropod molluscs and aragonite production in the open ocean: implications for the marine carbonate system. *Journal of Marine Research,* **48,** 209–222.

Fabry, V.J., Seibel, B.A., Feely, R.A. and Orr, J.C. 2008. Impacts of ocean acidification on fauna and ecosystem processes. *ICES Journal of Marine Science,* **65,** 414–432.

Fairbanks, R.G. 1989. A 17,000-year glacio-eustatic sea level record: influence of glacial melting rates on the Younger Dryas event and deep-ocean circulation. *Nature,* **342**, 637–642.

Feely, R.A., Sabine, C.L., Hernandez-Ayon, J.M., Ianson, D. and Hales, B. 2008. Evidence for upwelling of corrosive 'acidified' water onto the continental shelf. *Science,* **320,** 1490–1492.

Feely, R.A., Sabine, C.L., Lee, K., Berelson, W., Kleypas, J., Fabry, V.J. and Millero, F.J. 2004. Impact of anthropogenic CO2 on the CaCO2 system in the ocean. *Science,* **305**, 362–366.

Fisher, J.K., Hart, M.B., Smart, C.W., Leng, M.J., Sparks, R.S.J., Talling, P.J. and Trofimovs, J. 2008. Tephrochronology of marine sediments around the island of Montserrat, Lesser Antilles volcano arc. *The Sedimentary Record,* **6,** 4–8.

Fisher, R.A., Corbet, A.S. and Williams, C.B. 1943. The relationship between the number of species and the number of individuals in random samples of an animal population. *Journal of Animal Ecology,* **12**, 42–58.

Fleming, J. 1823. On a reversed species of Fusus, (*Fusus retroversus*). *Memoirs of the Wernerian Natural History Society,* **4**, 498–500.

Forbes, E. 1844. Report on the Mollusca and Radiata of the Aegean Sea, and on their distribution, considered as bearing on geology. *Reports of the British Association for the Advancement of Science,* **13**, 130–193.

Forbes E. and Hanley S.C. 1848–1853. *A history of British Mollusca and their shells*. John van Voorst, London, Vol. 1: I-. LXXX (1853) 1-486 (1848). Vol. 2: 1-480 (1 dec. 1849) 481-557 (1850). Vol. 3: 1-320 (1850) 321-616 (1851). Vol. 4: 1-300 (1852). Introduction I-LXXX (1853).

Forskål, P. 1776. *Icones rerum naturalium, quas in itinere orientali depingi curavit Petrus Forskål, Prof. Haun. Post mortem auctoris ad Regis mandatum æri incisas edidit Carsten Niebuhr*. Mölleri, Copenhagen, 15 pp.

Forster, P., Ramaswamy, V., Artaxo, P., Berntsen, T., Betts, R., Fahey, D. W., Haywood, J., Lean, J., Lowe, D.C., Myhre, G., Nganga, J., Prinn, R., Raga, G., Schulz, M. and Van Dorland, R. 2007. Changes in atmospheric constituents and in radiative forcing. In: Solomon, S., Qin, D., Manning, M., Chen, Z., Marquis, M., Averyt, K. B., Tignor, M., et al. (eds). *Climate Change 2007: the Physical Science Basis. Contribution of Working Group I to the Fourth Assessment Report of the Intergovernmental Panel on Climate Change*. Cambridge University Press, Cambridge, 129–234.

Foster, G.L. 2008. Seawater pH, pCO_2 and [CO_3^{2-}] variations in the Caribbean Sea over the last 130 kyr: A boron isotope and B/Ca study of planktic foraminifera. *Earth and Planetary Science Letters,* **271,** 254–266.

Froget C. 1967. Les ptéropodes dans les sédiments sousmarins du Quaternaire: caractérisation du régime 'Nord- Atlantique' au cours des périodes glaciaires en Méditerranée par le ptéropode Spiratella retroversa Fleming. *Comptes rendus hebdomadaires des Séances de l'Académie des Sciences*, **D264**, 2968–2969.

Fujita, K., Hikami, M., Suzuki, A., Kuroyanagi, A. Sakai, K. Kawahata, H. and Nojiri, Y. 2011. Effects of ocean acidification on calcification of symbiont-bearing reef foraminifers. *Biogeosciences,* **8**, 2089–2098.

Fütterer, D.K. 1984. Evidence of *Clionid* sponges in sediments of the Walvis Ridge, southeastern Atlantic Site 526, Deep Sea Drilling Project, Leg 74. *Initial Reports DSDP,* **74**, 557–560.

Gangstø, R., Joos, F. and Gehlen, M. 2011. Sensitivity of pelagic calcification to ocean acidification. *Biogeosciences,* **8**, 433–458.

Gannefors, C., Böer, M., Kattner, G., Graeve, M., Eiane, K., Gulliksen, B., Hop, H. and Falk-Petersen, S. 2005. The Arctic sea butterfly *Limacina helicina*: lipids and life strategy. *Marine Biology*, **147,** 169–177.

Ganssen, G. M., Troelstra, S. R., Van Der Borg, K., and De Jong, A. M. F. 1991. Late Quaternary pteropod preservation in Eastern North Atlantic sediments in relation to climate change. *Radiocarbon*, **33**, 277–282.

Gardulski, A. F., Mullins, H. T., and Weiterman, S. 1990. Carbonate mineral cycles generated by foraminiferal and pteropods response to Pleistocene climate: west Florida ramp slope. *Sedimentology*, **37**, 727–743.

Gattuso, J.-P., Frankignoulle, M., Bourge, I., Romaine, S. and Buddemeier, R.W. 1998. Effect of calcium carbonate saturation of seawater on coral calcification. *Global and Planetary Change,* **18,** 37–46.

Gazeau, F. Quiblier, C., Jansen, J.M., Gattuso, J-P., Middelburg, J.J. and Heip, C.H.R. 2007. Impact of elevated CO_2 on shellfish calcification. *Geophysical Research Letters,* **34**. L07603.

Gerhardt, S., Groth, H., Rühlemann, C. and Henrich, R., 2000. Aragonite preservation in late Quaternary sediment cores on the Brazilian Continental Slope: implications for intermediate water circulation. *International Journal of Earth Sciences*, **88**, 607–618.

Gerhardt, S. and Henrich, R. 2001. Shell preservation of *Limacina inflata* (Pteropoda) in surface sediments from the Central and South Atlantic Ocean: a new proxy to determine the aragonite saturation state of water masses. *Deep-Sea Research I,* **48,** 2051–2071.

di Geronimo, I. 1974. *Hyalocylis obtusa* n. sp. (Pteropoda, Thecosomata) in sedimenti abissali recenti dello Jonio. *Conchiglie* **10**, 113–116.

Gischler, E. 2006. Sedimentation on Rasdhoo and Ari Atolls, Maldives, Indian Ocean. *Facies,* **52**, 341–360.

Gmelin, F.J. 1791. Caroli a Linné systema naturae per regna tria naturae, secundum classes, ordines, genera, species cum characteribus, differentis, synonymus, locis. *Editio XIII aucta reformata*, **1,** 3021–3910.

Gonzalez-Mora, B., Sierro, F.J. and Flores, J.A. 2008. Controls of shell calcification in planktonic foraminifers.*Quaternary Science Reviews,* **27,** 956–961.

Gould, A.A. 1852. *Mollusca & shells. United States exploring expedition. During the years 1838, 1839, 1840, 1841, 1842. Under the command of Charles Wilkes, U.S.N., vol. 12*. Gould & Lincoln, Boston: 510 pp.

Gray, J. E. 1850. *Figures of the molluscous animals vol. 4. Explanations of the plates.* Longman, Brown, Green and Longmans, London, 1–124.

Grecchi G. 1984. Molluschi planctonici e bentonici in sedimenti sapropelitici del Quaternario della dorsale Mediterranea. *Bollettino Malacologico*, **20**, 1–34.

Green, M.A., Jones, M.E., Boudreau, C.L., Moore, R.L. and Westman, B.A. 2004. Dissolution mortality of juvenile bivalves in coastal marine deposits. *Limnology and Oceanography,* **49 (3),** 727–734.

Guinotte, J.M. and Fabry, V.J. 2008. Ocean acidification and its potential effects on marine ecosystems. *New York Academy of Sciences,* **1134,** 320–342.

Haddad, G.A. and Droxler, A.W. 1996. Metastable $CaCO_3$ dissolution at intermediate water depths of the Caribbean and western North Atlantic: implications for intermediate water circulation during the past 200,000 years. *Paleoceanography*, **11**, 701–716.

Herman Y. 1971. Quaternary climate changes in the eastern Mediterranean as recorded by pteropods and planktonic Foraminifera. In: Farinacci A. (ed.) *Second International Plankton Conference Proceedings*. Tecno-Scienza, Roma, 611–622.

Herman, Y. 1971. Vertical and horizontal distribution of pteropods in Quaternary sequences. In: Funnell, B. and Riedel, W. (eds) *Micropaleontology of Oceans,* Cambridge University Press, Cambridge.

Hoogakker, B.A.A., Rothwell, R.G., Röhling, E.J., Paterne, M., Stow, D.A.V., Herrle, J.O. and Clayton, T. 2004. Variations in terrigenous dilution in western Mediterranean Sea pelagic sediments in response to climate change during the last glacial cycle. *Marine Geology,* **211,** 21–43.

Hunt, B.P.V., Pakhomov, E.A., Hosie, G.W., Siegel, V., Ward, P. and Bernard, K. 2008. Pteropods in Southern Ocean ecosystems. *Progress in Oceanography,* **78**, 193–221.

Iglesias-Rodríguez. M.D., Halloran, P.R., Rickaby, R.E.M., Hall, I.R., Colmenero-Hidalgo, E., Gittins, J.R., Green, D.R.H., Tyrrell, T., Gibbs, S.J., von Dassow, P., Rehm, E., Armbrust, E.V. and Boessenkool K.P. 2008. Phytoplankton calcification in a high CO_2 world. *Science,* **320**, 336–339.

Irie, T., Bessho, K., Findlay, H.S. and Calosi, P. 2010. Increasing costs due to ocean acidification drives phytoplankton to be more heavily calcified: optimal growth strategy of coccolithophores. *PLoS ONE,* **5**, e13436.

Ivanova, E.V. 1985. Late Quaternary biostratigraphy and paleotemperatures of the Red Sea and the Gulf of Aden based on planktic foraminifera and pteropods. *Marine Micropaleontology,* **9**, 335–364.

Janssen, A. 2012. Late Quaternary to Recent holoplanktonic Mollusca (Gastropoda) from bottom samples of the eastern Mediterranean Sea: systematics, morphology. *Bollettino Malacologico*, **48**, 1–105.

Janssen, A.W. and King, C. 1988. Planktonic molluscs (Pteropods). In: Vinken, R. *et al.* (eds). *The northwest European Tertiary Basin. Results of the International Geological Correlation Programme Project no. 124, Geologisches Jahrbuch (A),* **100,** 356–368.

Janssen, A.W., Schnetler, K.I. and Heilman-Clausen, C. 2007. Notes on the systematics, morphology and biostratigraphy of fossil holoplanktonic Mollusca, 19. Pteropods (Gastropoda, Euthecosomata) from the Eocene Lillebaelt Clay Formation (Denmark, Jylland). *Basteria,* **71,** 157–168.

Jones, M.T., Fisher, J.K., and Palmer, M.R. 2009. Ocean acidification from explosive volcanism as a cause of mass mortality of pteropods. *Geochimica et Cosmochimica Acta,* **73**, Supplement 1, A604.

Jones, M.T. and Gislason, S.R. 2008. Rapid release of metal salts and nutrients following the deposition of volcanic ash in to aqueous environments. *Geochimica et Cosmochimica Acta,* **72**, 3661–3680.

Jorissen, F.J., Asioli, A., Borsetti, A.M., Capotondi, L., de Visser, J.P., Hilgen, F.J., Röhling, E.J., van der Borg, K., Vergnaud-Grazzini, C. and Zachariasse, W.J. 1993. Late Quaternary central Mediterranean biochronology. *Marine Micropaleontology,* **21,** 169-189.

Kennett, J. P. and Srinivasan, M. S. 1983. *Neogene planktonic foraminifera: a phylogenetic atlas.* Hutchinson Ross, New York. 265 pp.

Kier, J.S. and Pilkey, O.H. 1971. The influence of sea-level changes on sediment carbonate mineralogy, Tongue of he Ocean, Bahamas. *Marine Geology,* **11**, 189–200.

Kirk T.W. 1880. Descriptions of new marine shells. *Transactions and Proceedings of the New Zealand Institute,* **12**, 806–807.

Kleypas, J.A., Buddemeier, R.W., Archer, D., Gattuso, J.P., Langdon, C. and Opdyke, B.N. 1999. Geochemical consequences of increased atmospheric carbon dioxide on coral reefs. *Science,* **284,** 118–120.

Kleypas, J.A. and Langdon, C. 2002. Overview of CO_2- induced changes in seawater chemistry. World Coral Reefs in the New Millennium: Bridging Research and Management for Sustainable Development. In: Moosa, M.K., Soemodihardjo, S., Soegiarto, A. *et al.* (eds). *Proceedings of the 9th International Coral Reef Symposium*, Ministry of Environment, Indonesian Institute of Sciences, International Society for Reef Studies, Bali, Indonesia, **2**, 1085–1089.

Klöcker, R. 2005. *Late Quaternary pelagic aragonite preservation in the Arabian Sea and its paleoceanographic implications*. Unpublished PhD thesis, University of Bremen, Germany.

Klöcker, R., Ganssen, G., Jung, S.J.A., Kroon, D. and Henrich, R., 2006. Late Quaternary Millennial-scale variability in pelagic aragonite preservation off Somalia. *Marine Micropaleontogy* , **59**, 171–183.

Klöcker, R. and Henrich, R. 2006. Recent and Late Quaternary pteropod preservation on the Pakistan shelf and continental slope. *Marine Geology,* **231,** 103–111.

Klöcker, R., Ivanochko, T.S., Brummer, G-J., Jung, S.J.A., Ganssen, G., Kroon, D., Ganeshram, R.S. and Henrich, R. 2007. Variation in production, input and preservation of metastable calcium carbonate off Somalia during the last 90,000 years. *Quaternary Science Reviews,* **26,** 2674–2683.

Kobayashi, H. A. 1974. Growth cycle and related vertical distribution of the thecosomatous pteropod *Spiratella (Limacina) helicina* in the central Arctic Ocean. *Marine Biology*, **26,** 295–301.

Kuffner, I.B., Andersson, A.J., Jokiel, P.L., Rodgers, K. and Mackenzie, F. 2008. Decreased abundance of crustose coralline algae due to ocean acidification. *Nature Geoscience,* **1**, 114–117.

Kurihara, H., Kato, S. and Ishimatsu, A. 2007. Effects of increased pCO_2 on early development of the oyster *Crassostrea gigas*. *Aquatic Biology,* **1**, 91–98.

Kurihara, H and Shirayama, Y. 2004. Effects of increased atmospheric CO_2 on sea urchin early development. *Marine Ecology Progress Series,* **274**, 161–169.

Lalli, C.M. and Conover, R.J. 1976. Microstructure of the veliger shells of gymnosomatous pteropods. *The Veliger,* **18**, 237–240.

Lalli, C.M. and Gilmer, R.W. 1989. *Pelagic snails: The biology of holoplanktonic gastropod molluscs*. Stanford University Press, California. 259 pp.

Langdon, C. and Atkinson, M.J. 2005. Effect of elevated pCO_2 on photosynthesis and calcification of corals and interactions with seasonal change in temperature/ irradiance and nutrient enrichment. *Journal of Geophysical Research,* **110,** 1–54.

Langdon, C., Broecker, W.S., Hammond, D.E., Glenn, E., Fitzsimmons, K., Nelson, S.G., Peng, T.H., Hajdas, I. and Bonani, G. 2003. Effect of elevated CO2 on the community metabolism of an experimental coral reef. *Global Biogeochemical Cycles*, **17**, article number 1011.

Langdon, C., Takahashi, T., Marubini, F., Atkinson, M., Sweeney, C., Aceves, H., Barnett, H., Chipman, D. and Goddard, J. 2000. Effect of calcium carbonate saturation state on the calcification rate of an experimental coral reef. *Global Biogeochemical Cycles,* **14**, 639–654.

Langer, G., Geisen, M., Baumann, K.-H., Kläs, J., Riebesell, U., Thoms, S. and Young, J. 2006. Species-specific responses of calcifying algae to changing seawater carbonate chemistry. *Geochemistry, Geophysics, Geosystems,* **7**, Q09006.

Lawrence, K.T., Herbert, T.D. 2005. Late Quaternary sea-surface temperatures in the western Coral Sea: Implications for the growth of the Australian Great Barrier Reef. *Geology*, **33**, 677–680.

Le, J. and Shackleton, N.J. 1992. Carbonate dissolution fluctuations in the western Equatorial Pacific during the Late Quaternary. *Paleoceanography,* **7**, 21–42.

LeBrasseur, R.J. 1966. Stomach contents of salmon and steelhead trout in the northeastern Pacific ocean. *Journal of the Fisheries Research Board of Canada,* **23**, 85–100.

Le Friant, A., Harford, C.L., Deplus, C., Boudon, G., Sparks, R.S.J., Herd, R.A. and Komorowski, J.C. 2004. Geomorphological evolution of Montserrat (West Indies): importance of flank collapse and erosional processes. *Journal of the Geological Society,* **161,** 147–160.

Le Friant, A., Lock, E.J., Hart, M.B., Boudon, G., Sparks, R.S.J., Leng, M.J., Smart, C.W., Komorowski, J.C., Deplus, C. and Fisher, J.K. 2008. Late Pleistocene tephrochronology of marine sediments adjacent to Montserrat, Lesser Antilles volcanic arc. *Journal of the Geological Society, London,* **165,** 279–290.

Lesueur, C.A. 1813. Mémoire sur quelques espèces d'animaux mollusques et radiaires recueillis dans la Méditerranée, près de Nice. *Nouveau Bulletin des Sciences, par la Société Philomatique,* **3**, 281–285.

van Leyen A. and van der Spoel, S. 1982. A new taxonomic and zoogeographic interpretation of the *Diacria quadridentata* group (Mollusca, Pteropoda). *Bulletin Zoologisch Museum, Universiteit van Amsterdam*, **8**, 101–117.

Linnaeus, C. 1767. *Systema naturae sive regna tria naturae, secundum classes, ordines, genera, species, cum characteribus, differentiis, synonymis, locis*, 12th ed. v. 1 (pt 2). Laurentii Salvii, Holmiae, 533–1327.

Lisiecki, L.E. and Raymo, M.E. 2005. A Pliocene-Pleistocene stack of 57 globally distributed benthic $\delta^{18}O$ records. *Paleoceanography,* **20,** PA1003.

Lischka, S., Büdenbender, J., Boxhammer, T. and Riebesell, U. 2011. Impact of ocean acidification and elevated temperatures on early juveniles of the polar shelled pteropod *Limacina helicina*: mortality, shell degradation, and shell growth. *Biogeosciences,* **8**, 919–932.

Locard, A. 1886. *Catalogue Général des Mollusques Vivants de France--Mollusques Marins.* Henri Georg, Genève et Bale, 779 pp.

Lokho, K. and Kumar, K. 2008. Fossil pteropods (Thecosomata, holoplanktic Mollusca) from the Eocene of Assam-Arakan Basin, northeastern India. *Current Science,* **94,** 647–652.

Maas, A.E., Wishner, K.F. and Seibel, B.A. 2011. The metabolic response of pteropods to ocean acidification reflects natural pCO_2 –exposure in oxygen minimum zones. *Biogeosciences Discussions,* **8**, 10295–10316.

Mandralisca, E.P. 1840. Monografia del genere *Atlante* da servire per la fauna siciliana. *Effemeridi Scientifiche e Letterarie per la Sicilia,* **30**, 147–150**.**

Marubini, F., Barnett, H., Langdon, C. and Atkinson, M.J. 2001. Dependence of calcification on light and carbonate ion concentration for the hermatypic coral *Porites compressa*. *Marine Ecology Progress Series*, **220**, 153–162.

Marubini, F., Thake, B. 1999. Bicarbonate addition promotes coral growth. *Limnology and Oceanography,* **44,** 716–720.

McNeil, B.I. and Matear, R.J. 2007. Climate change feedbacks on future oceanic acidification. *Tellus Series B: Chemical and Physical Meteorology,* **59**, 191–198.

Meisenheimer J. 1906. Die Pteropoden der deutschen Südpo-lar-Expedition 1901-1903. *Deutsche Südpolar-Expedition*, 9 (Zool.) **1**, 92–153.

Menzies R.J. 1958. Shell-bearing pteropod gastropods from Mediterranean plankton (Cavoliniidae). *Pubblicazioni della Stazione Zoologica di Napoli*, **30**, 381–401.

Messenger, R. W., Hart, M. B., Smart, C. W., Leng, M. J., Lock, E. J., and Howard, A. K. 2010. Pteropod faunas as indicators of Late Pleistocene climate change in the Caribbean Sea. In: Whittaker, J. E. and Hart, M. B. (eds). *Micropalaeontology, Sedimentary Environments and Stratigraphy: A tribute to Dennis Curry (1912–2001),* The Micropalaeontological Society, Special Publications, 17–28.

Milliman, J.D., Troy, P.J., Balch, W.M., Adams, A.K., Li, Y.-H. and Mackenzie, F.T. 1999. Biologically mediated dissolution of calcium carbonate above the chemical lysocline? *Deep-Sea Research I,* **46**, 1653–1669.

de Moel, H., Ganssen, G.M., Peeters, F.J.C., Jung, S.J.A., Kroon, D., Brummer, G.J.A. and Zeebe, R.E. 2009. Planktic foraminiferal shell thinning in the Arabian Sea due to anthropogenic ocean acidification? *Biogeosciences,* **6**, 1917–1925.

di Monterosato, T.A. 1875. Nuova rivista delle conchiglie mediterranee. *Atti della Accademia di Scienze, Lettere e Arti di Palermo*, (Cl. Sc. Nat. esatto), **5,** 1–50.

Moore, T.C., Pisias, N.G. and Heath, G.R. 1977. Climate changes and lags in Pacific carbonate preservation, sea surface temperature and global ice volume. In: Andersen, N.R. and Malahoff, A. (eds) *The fate of fossil fuel CO2 in the oceans.* Plenum Press, New York and London, 145–165.

Moy, D., Howard, W.R., Bray, S.G. and Trull, T.W. 2009. Reduced calcification in modern Southern Ocean planktonic foraminifera. *Nature Geoscience*, **2,** 276–280.

Mudelsee, M. 2001. The phase relations among atmospheric CO_2 content, temperature and global ice volume over the past 420 ka. *Quaternary Science Reviews,* **20**, 583–589.

Mulder, C. P. H., Bazeley-White, E., Dimitrakopoulos, P. G., Hector, A., Scherer-Lorenzen, M. and Schmid, B. 2004. Species evenness and productivity in experimental plant communities. *Oikos,* **107**, 50–63.

Nordsieck F. 1973. Molluschi abyssali dello Ionio. Abyssal molluscs from the Ionic-Sea. *La Conchiglia*, **5**, 4–7.

Oberwimmer A. 1898. *Zoologische Ergebnisse, 10. Mollusken, 2 (Heteropoden und Pteropoden, Sinusigera) gesammelt von S.M. Schiff 'Pola' 1889-94. Berichte der Commission für Erforschung des östlichen Mittelmeeres, 21. Denkschriften mathematisch-naturwissenschaftliche Klasse.* Akademie der Wissenschaften, Wien, 24 pp.

d'Orbigny, A. 1834–1847. *Voyage dans l'Amérique méridionale (le Brésil, la République orientale de l'Uruguay, la République Argentine, la Patagonie, la République du Chili, la République de Bolivia, la République du Pérou), exécuté pendant les années 1826, 1827, 1828, 1829, 1830, 1831, 1832 et 1833, vol. 5 (3): Mollusques.* Berger-Levrault, Strasbourg, 758 pp., pl. 1–85.

Orr, J.C., Fabry, V.J., Aumont, O., Bopp, L., Doney, S.C., Feely, R.A., Gnanadesikan, A., Gruber, N., Ishida, A., Joos, F., Key, R.M., Lindsay, K., Maier-Reimer, E., Matear, R., Monfray, P., Mouchet, A., Najjar, R.G., Plattner, G., Rodgers, K.B., Sabine, C.L., Sarmiento, J.L., Schlitzer, R., Slater, R.D., Totterdell, I.J., Weirig, M., Yamanaka, Y. and Yool, A. 2005. Anthropogenic ocean acidification over the twenty-first century and its impact on calcifying organisms. *Nature,* **437,** 681–686.

Parra-Flores, A. and Gasca, R. 2009. Distribution of pteropods (Mollusca: Gastropoda: Thecosomata) in surface waters (0-100m) of the Western Caribbean Sea (winter 2007). *Revista de Biología Marina y Oceanografia,* **44,** 647–662.

Pastouret L. 1970. Étude sédimentologique et paléoclimatique de carottes prélevées en Méditerranée orientale. *Téthys*, **2**, 227–266.

Paul, H.A., Bernasconi, S.M., Schmid, D.W. and McKenzie, J.A. 2001. Oxygen isotopic composition of the Mediteranean Sea since the Last Glacial Maximum: constraints from pore water analyses. *Earth and Planetary Science Letters*, **30**, 1-14.

Pelseneer P. 1906. Biscayan plankton, 7. Mollusca (excluding Cephalopoda). With a note on their distribution by G. Herbert Fowler. *Transactions of the Linnean Society of London,* **10** (Zoology), 137–154.

Pelseneer P. 1888. Report on the Pteropoda collected by H.M.S. Challenger during the years 1873–1876, 2. The Thecosomata. *Reports on the scientific Results of the Voyage of H.M.S. Challenger during the years 1873-1876*, **23**, 1–132.

Pérez-Folgado, M., Sierro, F.J., Flores, J.A., Cacho, I., Grimalt, J.O., Zahn, R. and Shackleton, N. 2003. Western Mediterranean planktonic foraminifera events and millennial climatic variability during the last 70 kyr. *Marine Micropaleontology,* **48**, 49–70.

Perkins, R.D. and Halsey, S.D. 1971. Geologic significance of microboring fungi and algae in Carolina shelf sediments. *Journal of Sedimentary Research,* **41**, 843–853.

Péron, F. and Lesueur, C.A. 1810. Histoire de la famille des mollusques ptéropodes; caractères de dix genres qui doivent la composer. *Annales du Muséum d'Histoire naturelle,* **15**, 57–68.

Perry, C.T. 1998. Grain susceptibility to the effects of microboring: implications for the preservation of skeletal carbonates. *Sedimentology,* **45**, 39–51.

Petit, J.R., Jouzel, J., Raynaud, D., Barkov, N.I., Barnola, J.-M., Basile, I., Benders, M., Chappellaz, J., Davis, M., Delayque, G., Delmotte, M., Kotlyakov, V.M., Legrand, M., Lipenkov, V.Y., Lorius, C., Pépin, L., Ritz, C., Saltzman, E. and Stievenard, M. 1999. Climate and atmospheric history of the past 420,000 years from the Vostok ice core, Antarctica. *Nature*, **399**, 429–436.

Pfeffer, G. 1879. Übersicht der während der Reise um die Erde in den Jahren 1874–1876 auf S. M. Schiff Gazelle und von Hrn. Dr. F. Jagor auf seiner Reise nach den Philippinen in den Jahren 1857–1861 gesammelten Pteropoden. *Monatsberichte der königlich Preussischen Akademie der Wissenschaften zu Berlin,* **24**, 230–247, 1 pl.

Pfeffer G. 1880. Die Pteropoden des Hamburger Museums. *Abhandlungen des Naturwissenschaftlichen Vereins in Hamburg*, **7**, 67–99.

Philippi R.A. 1844. *Enumeratio molluscorum Siciliae cum viventium tum in tellure tertiaria fossilium, quae in itinere suo observavit, 2.* E. Anton, Halis Saxonum, 1–303.

Philippi, R.A. 1836. *Enumeratio Molluscorum Siciliae*. Simonis Schropii et Sociorum, Berolini, 267 pp., 12 pls.

Pierre, C., Belanger, P., Saliège, J.F., Urrutiaguer, M.J. and Murat, A.1999. Paleoceanography of the Western Mediterranean during the Pleistocene: oxygen and carbon isotope records at site 975. *Proceedings of the Ocean Drilling Program, Scientific Results,* **161**, 481–488.

Pisias, N.G., Heath, G.R. and Moore, T.C. 1975. Lag times for oceanic responses to climate change. *Nature,* **256**, 716–717.

Pistevos, J.C.A., Calosi, P., Widdicombe, S. and Bishop, J.D.D. 2011. Will variation among genetic individuals influence species responses to global climate change? *Oikos,* **120**, 675–689.

Portner, H.O., Langenbuch, M. and Reipschläger, A. 2004. Biological impact of elevated ocean CO_2 concentrations: lessons from animal physiology and earth history. *Journal of Oceanography,* **60,** 705–718.

Price, B.A., Killingley, J.S. and Berger, W.H. 1985. On the pteropod pavement of the eastern Rio Grande Rise. *Marine Geology,* **64**, 217–235.

Pujol, C. and Verghaud-Grazzini, C. 1995. Distribution patterns of live planktic foraminifers as related to regional hydrography and productive systems of the Mediterranean Sea. *Marine Micropaleontology,* **25,** 187–217.

Pujol, C. and Verghaud-Grazzini, C. 1989. Paleoceanography of the Last Deglaciation in the Alboran Sea (western Mediterranean). Stable isotopes and planktic foraminiferal records. *Marine Micropaleontology,* **15,** 153–179.

Quoy, J.R.C. and Gaimard, J.P. 1832–1833. *Voyage de découvertes de l'Astrolabe, exécuté par ordre du roy, pendant les années 1826-1827-1828-1829, sous le commendement de M.J. Dumont d'Ur- ville. Zoologie, 2.* J. Tastu, Paris, 1–686 (1832); atlas mollusques pl. 1–93, zoophytes pl. 1–26 (1833).

Quoy, J.R.C. and Gaimard, J. 1827. Observations zoologiques faites á bord de l'Astrolabe, en mai 1826, dans le détroit de Gibraltar (suite et fin). Description

des genres biphore, carinaire, hyale, fläche, cléodore, anatife et briarée. *Annales des Sciences Naturelles,* **10**, 225–239, (atlas) pl. 7–8.

von Rad, U., Schulz, H., Riech, V., den Dulk, M., Berner, U. and Sirocko, F. 1999. Multiple monsoon-controlled breakdown of oxygen-minimum conditions during the past 30,000 years documented in laminated sediments off Pakistan. *Palaeogeography, Palaeoclimatology, Palaeoecology,* **152**, 129–161.

Raghukumar, C. and Raghukumar, S. 1998. Barotolerance of fungi isolated from deep-sea sedimentsa of the Indian Ocean. *Aquatic Microbial Ecology,* **15**, 153–163.

Rampal, J. 2002. Biodiversité et biogéographie chez les Cavoliniidae (Mollusca, Gastropoda, Opisthobranchia, Euthecosomata). Régions faunistiques marines. *Zoosystema,* **24**, 209–258.

Rang, P.C.A.L. 1828. Notice sur quelques Mollusques nouveaux appartenant au genre Cléodore, et établissement et monographie du sous-genre Créseis. *Annales des Sciences Naturelles,* **13**, 302–319, pl. 17–18.

Rang, P.C.A.L. 1827. Description de deux genres nouveaux (Cuvieria et Euribia) appartenant à la classe des ptéropodes. *Annales des Sciences Naturelles,* **12**, 320–329, pl. 45B.

Rang, P.C.A.L. and Souleyet. 1852. *Histoire Naturelle des Mollusques Ptéropodes.* Baillière, Paris, 86 pp., 15 pls.

Reiss, Z., Luz, B., Almogi-Labin, A., Halicz, E., Winter, A., Wolf, M. and Ross, D.A. 1980. Late Quaternary paleoceanography of the Gulf of Aquaba (Elat), Red Sea. *Quaternary Research,* **14**, 294–308.

Renegar, D.A. and Riegl, B.M. 2005. Effect of nutrient enrichment and elevated CO2 partial pressure on growth rate of Atlantic scleractinian coral *Acropora cervicornis*. *Marine Ecology Progress Series,* **293,** 69–76.

Reynaud, S., Leclerqe, N., Romaine-Lioud, S., Ferrier-Pagès, C., Jaubert, J. and Gattuso, J.P. 2003. Interacting effects of CO_2 partial pressure and temperature on photosynthesis and calcification in a scleractinian coral. *Global Change Biology,* **9,** 1660–1668.

Richter, G. 1993. Zur kenntnis der Gattung Atlanta (V), Die Atlanta peroni-Gruppe und Atlanta gaudichaudi (Prosobranchia: Heteropoda). *Archiv für Molluskenkunde,* **122**, 189–205.

Richter, G. 1972. Zur Kenntnis der Gattung Atlanta (Heteropoda: Atlantidae). *Archiv für Molluskenkunde*, **102**, 85–91.

Richter G. 1968. Heteropoden und Heteropodenlarven im Oberflächenplankton des Golfes von Neapel. *Pubblicazioni della Stazione zoologica di Napoli*, **36**, 347–400.

Ridgwell, A. and Schmidt, D.N. 2010. Past constraints on the vulnerability of marine calcifers to massive carbon dioxide release. *Nature Geoscience,* **3**, 196–200.

Riebesell, U., Zondervan, I., Rost, B., Tortell, P.D., Zeebe, R. and Morel, F.M.M. 2000. Reduced calcification of marine plankton in response to increased atmospheric CO_2. *Nature,* **407,** 364–367.

Ries, J.B., Cohen, A.L. and McCorkle, D.C. 2009. Marine calcifers exhibit mixed responses to CO_2-induced ocean acidification. *Geology,* **37**, 1131–1134.

Roberts, D., Howard, W.R., Moy, A.D., Roberts, J.L., Trull, T.W., Bray, S.G. and Hopcroft, R.R. 2008. Interannual variability of pteropod shell weights in the high-CO_2 Southern Ocean. *Biogeosciences Discussions,* **5**, 4453–4480.

Roger, J.L and Nicewander, W.A. 1988. Thirteen ways to look at the correlation coefficient. *The American Statistician,* **42**, 59–66.

Roger, L.M., Richardson, A.J., McKinnon, A.D., Knott, B., Matear, R. and Scadding, C. 2011. Comparison of the shell structure of two tropical Thecosomata (*Creseis acicula* and *Diacavolinia longirostris*) from 1963 to 2009: potential implications of declining aragonite saturation. *ICES Journal of Marine Science,* doi: 10.1093/icesjms/fsr171.

Röhling, E.J. 1994. Review and new aspects concerning the formation of eastern Mediterranean sapropels. *Marine Geology,* **122**, 1–28.

Rosenberg, G. 2009. *Malacolog 4.1.1: A Database of Western Atlantic Marine Mollusca. [WWW database (version 4.1.1)].* http://www.malacolog.org/

Rottman, M.L. 1979. Dissolution of planktonic foraminifera and pteropods in South China Sea sediments. *Journal of Foraminiferal Research,* ***9***, 41–49.

Royal Society. 2005. *Ocean Acidification Due to Increasing Atmospheric Carbon Dioxide. Policy Document 12/05*. The Royal Society. London, UK.

Sabine, C.L., Feely, R.A., Gruber, N., Key, R.M., Lee, K., Bullister, J.L., Wanninkhof, R., Wong, C.S., Wallace, D.W.R., Tilbrook, B., Millero, F.J., Peng, T.H., Kozyr, A., Ono, T. and Rios, A.F. 2004. The oceanic sink for anthropogenic CO_2. *Science,* **305**, 367–371.

Sabine, C.L., Key, R.M., Feely, R.A. and Greeley, D. 2002. Inorganic carbon in the Indian Ocean: Distribution and dissolution processes. *Global Biogeochemical Cycles,* **16**, 1067.

Saito, T., Thompson, P. R. and Breger, D. 1981. *Systematic index of recent and Pleistocene planktonic foraminifera.* University of Tokyo Press, Tokyo. 189 pp.

Sarkar, S. and Gupta, A.K. 2009. Deep-sea Paleoceanography of the Maldives Islands (ODP Hole 716A), equatorial Idian Ocean during MIS 12–6. *Journal of Biosciences,* **34**, 000–000.

Sbaffi, L., Wezel, F.C., Kallel, N., Paterna, M., Cacho, I., Ziveri, P. and Shackleton, N., 2001. Response of the pelagic environment to palaeoclimatic changes in the central Mediterranean Sea during the Late Quaternary. *Marine Geology,* **178,** 39-62.

Schmidt, M. W. Vautravers, M. J. and Spero, H. J. 2006. Western Caribbean sea surface temperatures during the late Quaternary. *Geochemistry, Geophysics, Geosystems,* **7**, Q02P10.

Schneider, A., Wallace, D.W.R. and Körtzinger, A. 2007. Alkalinity of the Mediterranean Sea. *Geophysical Research Letters,* **34**, L15608.

Schulte, S. and Bard, E. 2003. Past changes in biologically mediated dissolution of calcite above the chemical lysocline recorded in Indian Ocean sediments. *Quaternary Science Reviews,* **22**, 1757–1770.

Sciandra, A., Harlay, J., Lefèvre, D., Lemée, R., Rimmelin, P., Denis, M. and Gattuso, J.-P. 2003. Response of coccolithophorid *Emiliania huxleyi* to elevated partial pressure of CO_2 under nitrogen limitation. *Marine Ecology Progress Series,* **261,** 111–122.

Seapy, R. 2011. Tree of life web project. http://tolweb.org/Atlantidae (last accessed January 2012).

Seapy, R.R. and Richter, G. 1993. *Atlanta californiensis,* a new species of atlantid heteropod (Mollusca, Gastropoda) from the California current. *The Veliger,* **36**, 389–398.

Seguenza G. 1875. Studi stratigrafici sulla formazione pliocenica dell'Italia meridionale (continuazione). Elenco dei cirripedi e dei molluschi della zona superiore dell'antico Plioceno. *Bollettino del R. Comitato Geologico d'Italia*, **6**, 145–153.

Shackleton, N.J. 1977. Carbon-13 in Uvigerina: Tropical rainforest history and the Equatorial Pacific carbonate dissolution cycles. In: Andersen, N.R. and Malahoff, A. (eds) *The fate of fossil fuel CO2 in the oceans.* Plenum Press, New York and London, 401–427.

Shackleton, N.J. 2000. The 100,000 year Ice-Age cycle identified and found to lag temperature, carbon dioxide and orbital eccentricity. *Science,* **289**, 1897–1902.

Shannon, C.E. 1948. A mathematical theory of communication. *The Bell System Technical Journal,* **27**, 379–423, 623–656.

Shirayama, Y. and Thorton, H. 2005. Effects of increasing atmospheric CO_2 on shallow water marine benthos. *Journal of Geophysical Research,* **110**, C09S08.

Sijinkumar, A. V., Nagender Nath, B., and Guptha, M. V. S. 2010. Late Quaternary record of pteropod preservation from the Andaman Sea. *Marine Geology*, **275**, 221–229.

Singh, A.D. 2007. Episodic preservation of pteropods in the eastern Arabian Sea: monsoonal change, oxygen minimum zone intensity and aragonite compensation depth. *Indian Journal of Marine Sciences,* **36**, 378–383.

Souleyet. 1852. Voyage autour du Monde exécuté pendant les années 1836 et 1837 sur la Corvette la Bonite. Voyage Autour du Monde exécuté pendant les années 1836 et 1837 sur la Corvette la Bonite. *Zoologie,* **2**, 664 pp.

Souleyet. 1851. Ordre des Ptéropodes. *Journal de Conchyliologie,* **2**, 28–38.

Sowerby G.B. 1878. Monograph of the genus Pteropoda. In: Reeve L.A. and Sowerby G.B. (eds) *Conchologia iconica: or, illustrations of the shells of molluscous animal, 20*. Reeve & Co., London, 14 pp., 6 pls.

Sowerby, G.B. 1877. Monograph of the genus Pteropoda. *ConchologiaIconica,* **20**, pls. 1–6.

Spero, H.J., Bijma, J., Lea, D.W. and Bemis, B.E. 1997. Effect of seawater carbonate concentration on foraminiferal carbon and oxygen isotopes. *Nature,* **390,** 497–500.

van der Spoel, S. 1976. *Pseudothecosomata, Gymnosomata and Heteropoda*. Bohn, Scheltema and Holkema, Utrecht. 484pp.

van der Spoel S. 1967. *Euthecosomata, a group with remarkable developmental stages (Gastropoda, Pteropoda).* Thesis, University of Amsterdam. J. Noorduijn, Gorinchem, 1–375.

van der Spoel, S., Bleeker, J. and Kobayasi, H. 1993. From *Cavolinia longirostris* to twenty-four *Diacavolinia* taxa, with a phylogenetic discussion (Mollusca, Gastropoda). *Bijdragen tot de Dierkunde*, **62**, 127–166.

Steinacher, M., Joos, F., Frölicher, T.L., Plattner, G.-K. and Doney, S.C. 2009. Imminent ocean acidification in the Arctic projected with NCAR global coupled carbon cycle-climate model. *Biogeosciences,* **6,** 515–533.

Steuer A. 1911. Adriatische Pteropoden. Sitzungs-Berichte der Mathematisch-Naturwissenschaftlichen Klasse der Kaiserlichen, *Akademie der Wissenschaften in Wien,* **120**, 709–730.

Stimpson, W. 1851. Descriptions of two new species of shells from Massachusetts Bay. *Proceedings of the Boston Society of Natural History,* **4**, 7–9.

van Straaten L.M.J.U. 1966. Micro-malacological investigation of cores from the southeastern Adriatic Sea. *Proceedings Koninklijke Nederlandse Akademie van Wetenschappen Amsterdam*, (B) **69**, 429–445.

Stroncik, N., Le Friant, A., Ishizuka, O., Expedition 340 Scientists. 2012. Expedition 340: Lesser Antilles Volcanism and Landslides. *IODP Preliminary Report,* **340**, doi: 10.2204/iodp.pr.340.2012

Sykes E.R. 1905. On the Mollusca procured during the 'Porcupine' expeditions, 1869–1870. Supplemental notes, 2. *Proceedings of the Malacological Society London,* **6**, 322–332.

Takeuchi, I. 1972. Food animals collected from the stomachs of three salmonoid fishes Oncorhynchus and their distribution in the natural environments in the northern North Pacific. *Bulletin of the Hokkaido Region Fisheries Research Laboratory*, **38**, 1–119.

Tesch, J.J. 1946. The thecosomatous pteropods. I. The Atlantic. *Dana Report,* **28,** 1–82.

Tesch, J.J. 1948. The thecosomatous pteropods. II. The Indo-Pacific. *Dana Report,* **30,**1–45.

Tesch, J.J. 1949. Heteropoda. *Dana Report,* **34,**1–35.

Tesch J.J. 1906. Die Heteropoden der Siboga expeditie. *Uitkomsten op Zoologisch, Botanisch, Oceanographisch en Geologisch Gebied, verzameld in Nederlandsch Oost-Indië 1899-1900 aan boord H.M. Siboga, onder commando van Luitenant ter zee 1e kl. G.F. Tydeman,* **27**, 1–112.

Tesch J.J. 1904. The Thecosomata and Gymnosomata of the Siboga Expedition. *Uitkomsten op Zoologisch, Botanisch, Oceanographisch en Geologisch Gebied, verzameld in Nederlandsch Oost-Indië 1899-1900 aan boord H.M. Siboga, onder commando van Luitenant ter zee 1e kl. G.F. Tydeman,* **52**, 1–92.

Tesch J.J., 1903. Vorläufige Mitteilung über die Thecosomata und Gymnosomata der Siboga-Expedition. *Tijdschrift der Nederlandse Dierkundige Vereniging,* **8**, 111–117.

Thiriot-Quiévreux, C. 1973. Heteropoda. *Oceanography and Marine Biology, an annual review*, **11,** 237–261.

Trofimovs, J., Fisher, J.K., Macdonald, H.A., Talling, P.J., Sparks, R.S.J., Hart, M.B., Smart, C.W., Boudon, G., Deplus, C., Komorowski, J.-C., Le Friant, A., Moreton, S. and Leng, M.J. 2010. Evidence for carbonate platform failure during rapid sea-level rise; *ca* 14 000 year old bioclastic flow deposits in the Lesser Antilles. *Sedimentology,* **57,** 735–759.

Tughope, A.W. and Risk, M.J. 1984. Rate of dissolution of carbonate sediments by microboring organisms, Davies Reef, Australia. *Journal of Sedimentary Petrology,* **55**, 440–447.

Turley, C.M., Roberts, J.M. and Guinotte, J.M. 2007. Corals in deep-water: will the unseen hand of ocean acidification destroy cold-water ecosystems? *Coral Reefs* **26:** 445–448.

Vatova A., 1974. Sui molluschi di alcuni saggi di fondo prelevati alle soglie del Mar Jonio. *Conchiglie*, **10**, 93–112.

de Vera, A. and Seapy, R.R., 2006. Atlanta selvagensis, a new species of heteropod mollusc from the Northeastern Atlantic Ocean (Gastropoda: Carinarioidea). *Vieraea*, **34**, 45–54.

Vérany, J.-B. 1853. Catalogue des mollusques céphalopodes, ptéropodes, gastéropodes nudibranches etc. des environs de Nice. *Journal de Conchyliologie,* **4**, 375–392.

Verrill, A.E. 1872. Brief contributions to Zoölogy, from the Museum of Yale College. No. XX.--Recent additions to the molluscan fauna of new England and the adjacent waters, with notes on other species. *American Journal of Science and Arts,* **3**, 281–290, pls. 6-8.

de Villiers, S. 2005. Foraminiferal shell-weight evidence for sedimentary calcite dissolution above the lysocline. *Deep-Sea Research I,* **52**, 671–680.

Wall-Palmer, D., Jones, M.T., Hart, M.B., Fisher, J.K., Smart, C.W., Hembury, D.J., Palmer, M.R. and Fones, G.R. 2011. Explosive volcanism as a cause for mass mortality of pteropods. Marine Geology, 282 (3-4), 231-239.

Wang, L., Jian, Z. and Chen, J. 1997. Late Quaternary pteropods in the South China Sea: carbonate preservation and paleoenvironmental variation. *Marine Micropaleontology,* **32,** 115–126.

Weldeab, S., Siebel, W., Wehausen, R., Emeis, K.C., Schmiedl, G. and Hemleben, C. 2003. Late Pleistocene sedimentation in the Western Mediterranean Sea: implications for productivity changes and climatic conditions in the catchment areas. *Paleogeography, Paleoclimatology, Paleoecology,* **190,** 121–137.

Wells, F.E. 1975. Comparison of Euthecosomatous pteropods in the plankton and sediments off Barbados, West Indies. *Proceedings of the Malacological Society London,* **41,** 503–509.

Wells, F.E. 1976. Seasonal patterns of abundance and reproduction of Euthecosomatous pteropods off Barbados, West Indies. *The Veliger,* **18,** 241–248.

Wheatcroft, R.A. 1992. Experimental tests for particle size-dependant bioturbation in the deep ocean. *Limnology and Oceanography,* **37**, 90–104.

Williams, S.W. 1972. *The temporal and spatial variation of selected thecosomatous pteropods from the Florida Middle Ground*. Unpublished M.S. Thesis, Florida State University, 203 pp.

Wood E. 1910. The phylogeny of certain Cerithiidae. *Annals of the New York Academy of Sciences,* **20**, 1–92, pl. 1–9.

10. PUBLICATIONS

10.1 PEER REVIEWED PUBLICATIONS

Wall-Palmer, D., Smart, C.W. and Hart, M.B. Global variations in pteropod calcification as an indicator of past ocean carbonate saturation. **Submitted to Quaternary Science Reviews October 2012, revised manuscript submitted December 2012.**

Global variations in pteropod calcification as an indicator of past ocean carbonate saturation.

Deborah Wall-Palmer[a§], Christopher W. Smart[a] and Malcolm B. Hart[a]

[a]School of Geography, Earth and Environmental Sciences, Plymouth University, Plymouth, PL4 8AA, UK.
[§] Corresponding author

Recent concern over the effects of ocean acidification upon calcifying organisms has highlighted the aragonitic shelled thecosomatous pteropods (planktonic gastropods) as being at a high risk. Laboratory studies have shown that an increased dissolved CO_2 concentration (pCO_2), leading to decreased water pH and low carbonate concentration, has a negative impact on the ability of pteropods to calcify and maintain their shells. Here we present the first evidence of global, climate induced variations in pteropod calcification during the Late Pleistocene by analysing the calcification of pteropod shells in marine sediment cores from the Caribbean Sea, Mediterranean Sea and Indian Ocean. Determination of pteropod calcification was made using the average shell size of *Limacina inflata* specimens and the *Limacina* Dissolution Index (LDX) to detect in-life shell corrosion and the inability to maintain shell structure. By comparison to the Late Pleistocene global ice volume and Vostok atmospheric CO_2 concentrations, we show that pteropod calcification is closely associated to variations in past ocean carbonate saturation. This calcification record was found to be of global significance and confirms the findings of laboratory studies, showing a decrease in calcification when surface ocean carbonate

concentrations were lower. Results demonstrate that Late Pleistocene pteropods were negatively affected by oceanic pH levels relatively higher and changing at a lesser rate than those predicted for the 21st Century.

Key words: *pteropod; ocean acidification; Late Pleistocene; Caribbean Sea; Mediterranean Sea; Indian Ocean.*

1 Introduction

The thecosomatous (fully shelled) pteropods are a common component of the zooplankton in our oceans and the major planktonic producers of aragonite (Orr *et al.,* 2005). Pteropods have a global distribution, but are most abundant in polar and sub-polar waters where they can reach densities of 1,000 to 10,000 individuals per cubic metre, replacing krill as the dominant zooplankton group in some areas (Royal Society*,* 2005; Fabry *et al.,* 2008). In such regions, pteropods are an important food source for large cetaceans and commercially important fish, such as North Pacific salmon, mackerel, herring and cod (LeBrasseur, 1966; Takeuchi, 1972). However, recent concern over the effects of anthropogenic ocean acidification upon calcifying organisms has highlighted the thecosomatous pteropods as being at a high risk (Orr *et al.,* 2005; Fabry *et al.,* 2008; Comeau *et al.,* 2009, 2010a, 2010b, 2012; Lischka *et al.,* 2011; Bednaršek *et al.,* 2012a, 2012b). Their increased susceptibility to ocean acidification is due to a combination of living in the most affected habitat, the surface ocean, and having a shell structure that is prone to dissolution. Pteropods construct their shells of aragonite, a type of calcium carbonate ($CaCO_3$), which is 50% more soluble in seawater than calcite (for example, coccolithophores and planktonic foraminifera produce calcite structures). It has been found that, although pteropods can calcify in waters under-saturated with respect to aragonite, enhanced dissolution corrodes their shells, reducing the ability to maintain the shell structure (Comeau *et al.,* 2012). This results in the production of smaller, weaker shells with damaged outer layers of aragonite (Bednaršek *et al.,* 2012b).

As an important part of the food web, especially in the Arctic and Southern Oceans, understanding the potential demise of thecosomatous pteropods is of

great importance. However, so far, research into the effects of decreased ocean $CaCO_3$ saturation on pteropods is based on the laboratory studies of only three of the 34 species of pteropod: *Cavolinia inflexa, Clio pyramidata* and *Limacina helicina* (Feely *et al.,* 2004; Orr *et al.,* 2005; Fabry *et al.,* 2008; Comeau *et al.,* 2009, 2010a, 2010b, 2012; Lischka *et al.,* 2011; Bednaršek *et al.,* 2012a), The response of *L. helicina antarctica* has also been observed in the natural environment, by analysing the shell structure of live specimens from the Southern Ocean (Bednaršek *et al.,* 2012b). In this study, a different approach has been taken by using a simple methodology to assess the fossil record of the sub-tropical cosmopolitan species, *L. inflata,* for variations in calcification.

2 Methodology

2.1 Site locations

Pteropods from four cores were analysed for calcification indices. Two cores from sites situated close together off-shore Montserrat in the Caribbean Sea (CAR-MON 2 and JR123-35-V, Fig. 1, Table 1) were analysed to test the reproducibility of data at a single location. A single core collected to the south-east of the Balearic Island of Mallorca in the Mediterranean Sea (B5-1, Fig. 2, Table 1) and a single core collected from the Chagos-Laccadive Ridge within the Maldives Islands in the Indian Ocean (ODP Hole 716B, Fig. 3, Table 1) were analysed to test the reproducibility of data across different locations. All core sites are situated well above the Aragonite Lysocline (ALy), the depth at which the ocean becomes under-saturated with respect to aragonite, and are un-affected by post-depositional dissolution. Core collection and sampling techniques and oxygen isotope stratigraphy have been previously published (Backman *et al.,* 1988; Droxler *et al.,* 1990; Le Friant *et al.,* 2008; Trofimovs *et al.,* 2010; Wall-Palmer *et al.,* in review;).

2.2 Calcification Indices

The calcification of pteropod shells was determined using the *Limacina* Dissolution Index (LDX) and the average shell size of *L. inflata* specimens. The LDX is a scale of pteropod shell dissolution, which was originally designed to determine the position of the ALy by studying surface sediments (Gerhardt *et*

al., 2000; Gerhardt and Henrich, 2001). However, the methodology is also of use as a scale of shell calcification. Low surface ocean carbonate concentrations result in the corrosion and poor maintenance of shells, producing dissolution damage of the outer aragonite layer whilst the pteropod is still alive. This in-life corrosion can be used as a measure of pteropod calcification, since the inability to maintain the shell structure demonstrates the inability to calcify. The LDX methodology involves the qualitative analysis of the surface of *L. inflata* shells on a scale of 0 to 5; 0 being a shell that is transparent and lustrous, with a perfect outer aragonite layer and 5 being a shell that is opaque-white, totally lustreless and perforated, showing corrosion and poor maintenance of the outer aragonite layer. Following the original methodology of Gerhardt and Henrich (2001), at least 10 shells (maximum of 30 shells) of adult *L. inflata* of a size of 300 μm or larger were allocated a value from this scale by the use of light microscopy for each sample. The mean for each sample was then calculated to provide the average LDX value. This was carried out for all samples containing the relevant number of adult *L. inflata.*

The average size of *L. inflata* shells was calculated by using a photomicroscope (Nikon DS-Fi1 camera mounted on a Nikon eclipse LV100POL microscope) to measure the diameter of shells perpendicular to the line of the aperture on the spiral side. Measurements were made for all appropriate shells >150 μm that had been picked from a count of 300 pteropod and heteropod specimens for each sample. The average size was then calculated. Shell size data was collected at a lower resolution to supplement the LDX data.

During collection, it was noticed that CAR-MON 2 contained an excellent record of pteropod remains (Le Friant *et al.,* 2008; Messenger *et al.,* 2010). It was therefore chosen to provide a high resolution calcification record. Shells of *L. inflata* in CAR-MON 2 were analysed using the LDX at 5 cm intervals (11.5 kyr) throughout the length of the core. The calcification profile of CAR-MON 2 has been published previously by Wall-Palmer *et al.* (2012). Other cores were analysed at varying intervals. Caribbean core JR123-35-V and Indian Ocean ODP Hole 716B were sampled at lower resolution at points corresponding to major changes in climate. These points were identified with the use of oxygen

isotope stratigraphy (Trofimovs *et al.,* 2010; Backman *et al.,* 1988). Mediterranean core B5-1 was analysed for calcification indices at 10 cm intervals (25–50 kyr) throughout the core. The calcification profile of B5-1 has been previously published by Wall-Palmer *et al.* (in review).

3 Results and Discussion

3.1 Dissolution vs. calcification

Several previous studies have presented the down-core abundances and preservation of pteropod remains (e.g. Chen, 1968). Although of use in detecting past variations in deep ocean chemistry, these studies are based on cores situated close to, or below the ALy, and therefore show variations due to post-depositional dissolution and not variations in calcification. The records presented in this study are all from shallow sites, situated above the ALy, which have not been affected by post-depositional dissolution. Species assemblages and average shell size data collected during this study show that post-depositional dissolution can be ruled out as the main cause of variations in pteropod shell condition. Assemblages of planktonic foraminifera and pteropods throughout all cores are representative of surface ocean conditions at the time of deposition, indicating no bias from post-depositional dissolution. In addition, the average shell size of *L. inflata* demonstrates that variations in calcification are the most likely cause of changes in shell condition (Figs 4–6). A bivariate, two-tailed Pearson correlation of average shell size and LDX shows a significant relationship at all locations studied (CAR-MON 2 r=-0.577, p=0.019, n=16; B5-1 r=-0.760, p=0.003, n=13; 716B r=-0.525, p=0.037, n=16). During glacial periods, the average shell size is generally larger, which reflects the increased availability of carbonate for the production of shells. During interglacial periods, shell sizes are much smaller, which suggests carbonate availability was limited for the calcification of shells. If the high LDX values recorded during interglacial periods represented post-depositional dissolution, smaller shells would be preferentially dissolved, leaving the larger, more robust shells and an opposite trend. Variations in shell size and weight due to carbonate availability have also been found in planktonic foraminifera and coccolithophores in the modern ocean and over glacial-interglacial cycles

(Barker and Elderfield 2002; de Moel *et al.,* 2009; Moy *et al.,* 2009; Beaufort *et al.,* 2011).

It is also important to note that climate induced post-depositional dissolution patterns in the Atlantic ocean show an opposite trend to the calcification record of CAR-MON 2. Deep water, post-depositional dissolution studies in the western Equatorial Atlantic (Damuth *et al.,* 1975), on the Brazilian Slope (Gerhardt *et al.,* 2000) and in the Caribbean Sea (Haddad and Droxler, 1996), show poor preservation of pteropod shells during glacial periods and enhanced preservation during interglacial periods. This trend is attributed to a shallowing of corrosive bottom waters during glacial periods.

3.2 Calcification and climate change

In all cores, calcification indices show a similar trend to global ice volume (oxygen isotope ratio) and Vostok (Petit *et al.,* 1999) atmospheric CO_2 concentration (Figures 4–6). With enhanced calcification (low LDX, larger shell size) during glacial periods and poor calcification during interglacial periods (high LDX, smaller shell size). This suggests that, during the Late Pleistocene, changes in climate, atmospheric CO_2 concentrations and the resulting variations in surface ocean carbonate concentrations, not only affected the size of pteropod shells, but also the ability of pteropods to maintain their shell structure. This is best demonstrated in CAR-MON 2, where reconstructed surface ocean pH and carbonate concentrations (Foster, 2008) are available for comparison (Fig. 4). This trend is reproducible across cores in the same geographical location and across cores in different geographical locations, showing that the response of pteropods to Late Pleistocene climate change is of global significance. It is also in agreement with recent laboratory studies on pteropods, which show reduced calcification and poor shell maintenance at decreasing carbonate concentrations (Orr *et al.,* 2005; Fabry *et al.,* 2008; Comeau *et al.,* 2009, 2010a, 2010b, 2012; Lischka *et al.,* 2011; Bednaršek *et al.,* 2012a). Scanning electron microscopy images of corroded and poorly maintained shells from interglacial periods of CAR-MON 2 are comparable to images of modern pteropods currently living in waters with low carbonate

concentrations (Bednaršek *et al.,* 2012b).

Statistical comparisons, however, show that the relationship between climate and calcification is not straightforward. A bivariate, two-tailed Pearson correlation of LDX and global ice volume for CAR-MON 2 shows that the association is significant, but weak (r=-0.318, p=0.001, n=112). Comparison of the LDX and global ice volume for B5-1 (r=0.137, p=0.49, n=28) and 716B (r=-0.159, p=0.570, n=15) show no correlation. However, if the LDX data for each core is shifted down slightly (CAR-MON 2 35 cm; B5-1 35 cm; 716B 20 cm), all produce a significant negative correlation (CAR-MON 2 r=-0.572, p=0.000, n=105; B5-1 r=-0.505, p=0.001, n=25; 716B r=-0.633, p=0.002, n=21). This not only indicates a clear relationship between climate change and pteropod calcification, but may also suggest a delay in the calcification response of pteropods by 15.2 kyr in the Caribbean Sea, 7–14 kr in the Mediterranean Sea and 5.3 kyr in the Indian Ocean. Several authors have identified similar lags in the Pacific Ocean (Le and Shackleton, 1992; Moore *et al.,* 1977) however, the causes are still not understood. Reconstructed surface water carbonate concentrations for the Caribbean Sea (Foster, 2008) show a significant correlation to the global ice volume record of CAR-MON 2 (r=0.886, p=0.000, n=15). The lag in data therefore does not indicates a delay in the response of surface water carbonate levels. This may therefore suggest a delay in the response of pteropod calcification. The ability of pteropods to calcify in waters under-saturated with respect to aragonite has been shown in laboratory experiments (Comeau *et al.,* 2009, 2010a, 2010b, 2012; Lischka *et al.,* 2011) and may have important implications for the modern oceans. Further work is therefore necessary in detecting the source of this time discrepancy.

4 Conclusions

This study presents the first evidence of global, climate induced variations in pteropod calcification during the Late Pleistocene. Variations in calcification have been found to correlate with past global ice volume, once data has been adjusted for the 5.3–15.2 kyr lag. Periods of high ice volume and low atmospheric CO_2 show enhanced pteropod calcification and larger shells,

whereas periods of low ice volume and high atmospheric CO_2 show poor pteropod calcification, poor shell maintenance and smaller, fragile shells. These results are in agreement with experiments upon modern pteropods and demonstrate that, at oceanic pH levels relatively higher and changing at a lesser rate than those predicted for the 21st Century, the calcification of thecosomatous pteropods has been negatively affected. Despite not being directly comparable to anthropogenic ocean acidification, this causes concern for the future of shelled pteropods in the modern ocean. However, if the lag between climate proxies and calcification indicates a delayed response of pteropods, this suggests that the ability of pteropods to endure prolonged periods of low surface ocean carbonate concentrations may be higher than originally predicted.

Acknowledgements We would like to acknowledge the crew and scientists who took part in the 'Caraval' cruise, the 'BIOFUN'10' cruise and in ODP Leg 115. We would also like to acknowledge the help of Anne Le Friant in the re-sampling of parts of CAR-MON 2, the curators of the Kochi Core Centre, Japan for the sampling of ODP Hole 716B and Michael Cassidy (National Oceanographic Centre, Southampton) for his help with sampling JR123-35-V. Oxygen isotope stratigraphy for B5-1 was funded by a NERC grant and carried out with the help of Melanie Leng (NIGL). This research is part of a PhD funded by Plymouth University.

References

Backman, J., Duncan, R.A., Peterson, L.C., Baker, P.A., Baxter, A.N., Boersma, A., Cullen, J.L., Droxler, A.W., Fisk, M.R., Greenough, J.D., Hargraves, R.B., Hempel, P., Hobart, M.A., Hurley, M.T., Johnson, D.A., Macdonald, A.H., Mikkelsen, N., Okada, H., Rio, D., Robinson, S.G., Schneider, D., Swart, P.K., Tatsumi, Y., Vandamme, D., Vilks, G., Vincent, E., 1988. Site 716. Proceedings of the Ocean Drilling Program, Initial Reports, 115, 1005–1077.

Barker, S., Elderfield, H., 2002. Foraminiferal calcification response to glacial-interglacial changes in atmospheric CO_2. Science, 297**,** 833–836.

Beaufort, L., Probert, I., de Garidel-Thoron, T., Bendif, E.M., Ruiz-Pino, D., Metzl, N., Goyet, C., Buchet, N., Coupel, P., Grelaud, M., Rost, B., Rickaby, R.E.M., de Vargas, C., 2011. Sensitivity of coccolithophores to carbonate chemistry and ocean acidification. Nature, 476, 80–83.

Bednaršek, N., Tarling, G.A., Bakker, D.C.E., Fielding, S., Jones, E.M., Venables, H.J., Ward, P., Kuzirian, A., Lézé, B., Feely, R.A., Murphy, E.J., 2012b. Extensive dissolution of live pteropods in the Southern Ocean. Nature Geoscience, DOI: 10.1038/NGEO1635.

Bednaršek, N., Tarling, G.A., Bakker, D.C.E., Fielding, S., Cohen, A., Kuzirian, A., McCorkles, D., Lézé, B., Montagna, R., 2012a. Description and quantification of pteropod shell dissolution: a sensitive bioindicator of ocean acidification. Global Change Biology, 18, 2378–2388.

Chen, C., 1968. Pleistocene pteropods in pelagic sediments. *Nature,* **219**, 1145–1149.

Comeau, S., Alliouane, S., Gattuso, J.-P., 2012 Effects of ocean acidification on overwintering juvenile Arctic pteropods *Limacina helicina*. Marine Ecology Progress Series 456, 279–284.

Comeau, S., Gorsky, G., Alliouane, S., Gattuso, J.-P., 2010b. Larvae of the pteropod *Cavolinia inflexa* exposed to aragonite undersaturation are viable but shell-less. Marine Biology 157, 2341–2345.

Comeau, S., Jeffree, R., Teyssié, J.-L., Gattuso, J.-P., 2010a. Response of the Arctic Pteropod *Limacina helicina* to Projected Future Environmental Conditions. PLoS ONE 5, e11362.

Comeau, S., Gorsky, G., Jeffree, R., Teyssié, J.-L., Gattuso, J.-P., 2009. Impact of ocean acidification on a key Arctic pelagic mollusc (*Limacina helicina).* Biogeosciences 6, 1877–1882.

Damuth, J.E. 1975. Quaternary climate change as revealed by calcium carbonate fluctuations in western Equatorial Atlantic sediments. Deep-Sea Research, 22, 725–743.

Droxler, A.W., Haddad, G.A., Mucciarone, D.A., Cullen, J.L., 1990. Pliocene-Pleistocene aragonite cyclic variations in Holes 714A and 716B (the Maldives) compared with Hole 633A (the Bahamas): Records of climate-induced CaCO3 preservation at intermediate water depths. Proceedings of the Ocean Drilling Program, Scientifica Results 115, 539–577.

Fabry, V.J., Seibel, B.A., Feely, R.A., Orr, J.C., 2008. Impacts of ocean acidification on fauna and ecosystem processes. ICES Journal of Marine Science 65, 414–432 (2008).

Feely, R.A., Sabine, C.L., Lee, K., Berelson, W., Kleypas, J., Fabry, V.J., Millero, F.J., 2004. Impact of anthropogenic CO_2 on the $CaCO_2$ system in the ocean. Science, 305, 362–366.

Foster, G.L., 2008. Seawater pH, pCO_2 and $[CO^{2-}_3]$ variations in the Caribbean Sea over the last 130 kyr: A boron isotope and B/Ca study of planktic foraminifera. Earth and Planetary Science Letters 271, 254–266.

Gerhardt, S., Groth, H., Rühlemann, C., Henrich, R., 2000. Aragonite preservation in late Quaternary sediment cores on the Brazilian Continental Slope: implications for intermediate water circulation. International Journal of Earth Sciences, 88, 607–618.

Gerhardt, S., Henrich, R., 2001. Shell preservation of *Limacina inflate* (Pteropoda) in surface sediments from the Central and South Atlantic Ocean: a

new proxy to determine the aragonite saturation state of water masses. Deep-Sea Research I 48, 2051–2071.

Haddad, G.A., Droxler, A.W., 1996. Metastable $CaCO_3$ dissolution at intermediate water depths of the Caribbean and western North Atlantic: implications for intermediate water circulation during the past 200,000 years. Paleoceanography, 11, 701–716.

Le, J., Shackleton, N.J., 1992. Carbonate dissolution fluctuations in the western Equatorial Pacific during the Late Quaternary. Paleoceanography 7, 21–42.

LeBrasseur, R.J., 1966. Stomach contents of salmon and steelhead trout in the northeastern Pacific ocean. Journal of the Fisheries Research Board of Canada 23, 85–100.

Le Friant, A., Lock, E.J., Hart, M.B., Boudon, G., Sparks, R.S.J., Leng, M.J., Smart, C.W., Komorowski, J.C., Deplus, C., Fisher, J.K., 2008. Late Pleistocene tephrochronology of marine sediments adjacent to Montserrat, Lesser Antilles volcanic arc. Journal of the Geological Society, London, 165, 279–290.

Lischka, S., Büdenbender, J., Boxhammer, T., Riebesell, U., 2011. Impact of ocean acidification and elevated temperatures on early juveniles of the polar shelled pteropod *Limacina helicina*: mortality, shell degradation, and shell growth. Biogeosciences 8, 919–932.

Messenger, R. W., Hart, M. B., Smart, C. W., Leng, M. J., Lock, E. J., Howard, A. K., 2010. Pteropod faunas as indicators of Late Pleistocene climate change in the Caribbean Sea. In: Whittaker, J. E., Hart, M. B. (eds). Micropalaeontology, Sedimentary Environments and Stratigraphy: A tribute to Dennis Curry (1912–2001), The Micropalaeontological Society Special Publications, 17–28.

de Moel, H., Ganssen, G.M., Peeters, F.J.C., Jung, S.J.A., Kroon, D., Brummer, G.J.A., Zeebe, R.E., 2009. Planktic foraminiferal shell thinning in the Arabian Sea due to anthropogenic ocean acidification? Biogeosciences, 6, 1917–1925.

Moore, T.C., Pisias, N.G., Heath, G.R., 1977. Climate changes and lags in Pacific carbonate preservation, sea surface temperature and global ice volume. In: Andersen, N.R., Malahoff, A. (eds) The fate of fossil fuel CO_2 in the oceans. Plenum Press, New York and London, 145–165.

Moy, D., Howard, W.R., Bray, S.G., Trull, T.W., 2009. Reduced calcification in modern Southern Ocean planktonic foraminifera. Nature Geoscience, 2, 276–280.

Orr, J.C., Fabry, V.J., Aumont, O., Bopp, L., Doney, S.C., Feely, R.A., Gnanadesikan, A., Gruber, N., Ishida, A., Joos, F., Key, R.M., Lindsay, K., Maier-Reimer, E., Matear, R., Monfray, P., Mouchet, A., Najjar, R.G., Plattner, G., Rodgers, K.B., Sabine, C.L., Sarmiento, J.L., Schlitzer, R., Slater, R.D., Totterdell, I.J., Weirig, M., Yamanaka, Y., Yool, A., 2005. Anthropogenic ocean acidification over the twenty-first century and its impact on calcifying organisms. Nature, 437, 681–686.

Petit, J.R., Jouzel, J., Raynaud, D., Barkov, N.I., Barnola, J.-M., Basile, I., Benders, M., Chappellaz, J., Davis, M., Delayque, G., Delmotte, M., Kotlyakov, V.M., Legrand, M., Lipenkov, V.Y., Lorius, C., Pépin, L., Ritz, C., Saltzman, E., Stievenard, M. 1999. Climate and atmospheric history of the past 420,000 years from the Vostok ice core, Antarctica. Nature, 399, 429–436.

Royal Society, 2005. Ocean Acidification Due to Increasing Atmospheric Carbon Dioxide. Policy Document 12/05. The Royal Society. London, UK.

Takeuchi, I., 1972. Food animals collected from the stomachs of three salmonoid fishes Oncorhynchus and their distribution in the natural environments in the northern North Pacific. Bulletin of the Hokkaido Region Fisheries Research Laboratory 38, 1–119.

Trofimovs, J., Fisher, J.K., Macdonald, H.A., Talling, P.J., Sparks, R.S.J., Hart, M.B., Smart, C.W., Boudon, G., Deplus, C., Komorowski, J.-C., Le Friant, A., Moreton, S., Leng, M.J. 2010. Evidence for carbonate platform failure during rapid sea-level rise; *ca* 14 000 year old bioclastic flow deposits in the Lesser Antilles. Sedimentology 57, 735–759.

Wall-Palmer, D., Smart, C.W., Hart, M.B., Leng, M.J., Conversi, A., Borghini, M., Manini, E., Aliani, S., In Review. Quaternary planktonic foraminifera, pteropods and heteropods from the western Mediterranean Sea. Submitted to Marine Geology May 2012.

Wall-Palmer, D., Hart, M.B., Smart, C.W., Sparks, R.S.J., Le Friant, A., Boudon, G., Deplus, C., Komorowski, J.C., 2012. Pteropods from the Caribbean Sea: variations in calcification as an indicator of past ocean carbonate saturation. Biogeosciences, 9, 309-315.

Core	Location	Water depth (m)	Core length (cm)	Sample interval (cm)	Cruise and year	Research Vessel	References
CAR-MON 2	16°27.699'N 62°38.077'W	1102	575	5	'Caraval' 2002	R.V. *L'Atalante*	Le Friant *et al.,* 2008
JR123-35-V	16°53.50'N 62°04.00'W	765	504	varying	'Cruise 123' 2005	RRS *James Clark Ross*	Trofimovs *et al.,* 2010
B5-1	39°14.942'N 03°25.052'E	1519	494	10	'BIOFUN'10' 2010	R.V. *Urania*	Wall-Palmer *et al.,* in review
716B	04°56.0'N 73°17.0'E	533.3	1295*	varying	ODP Leg 115. 1987	*Joides Resolution*	Backman *et al.,* 1988; Droxler *et al.,* 1990

Table 1. Summary of cores analysed for this study (*length of core analysed).

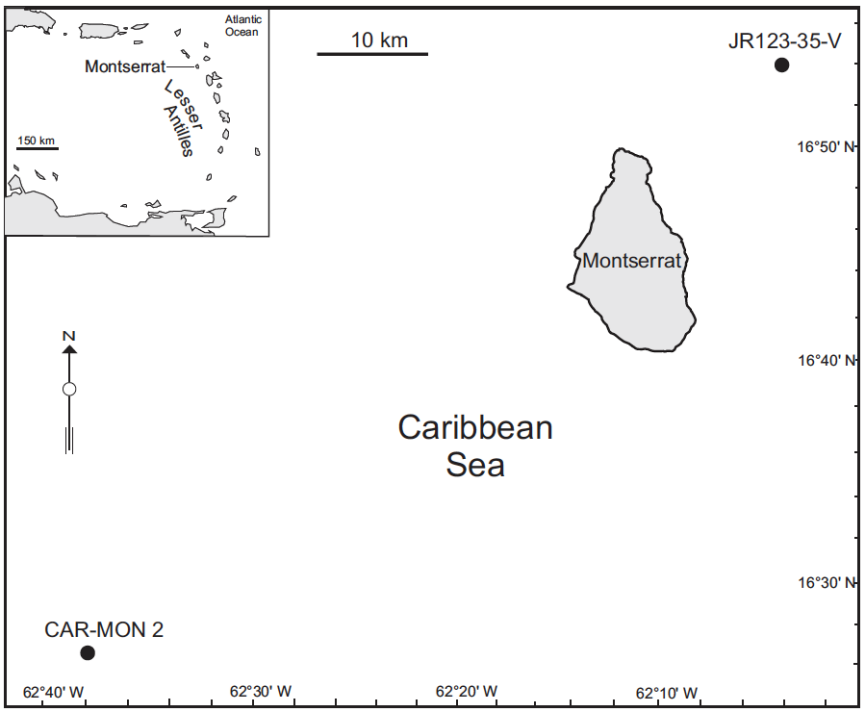

Figure 1. Location of Caribbean sites CAR-MON 2 and JR123-35-V around the island of Montserrat.

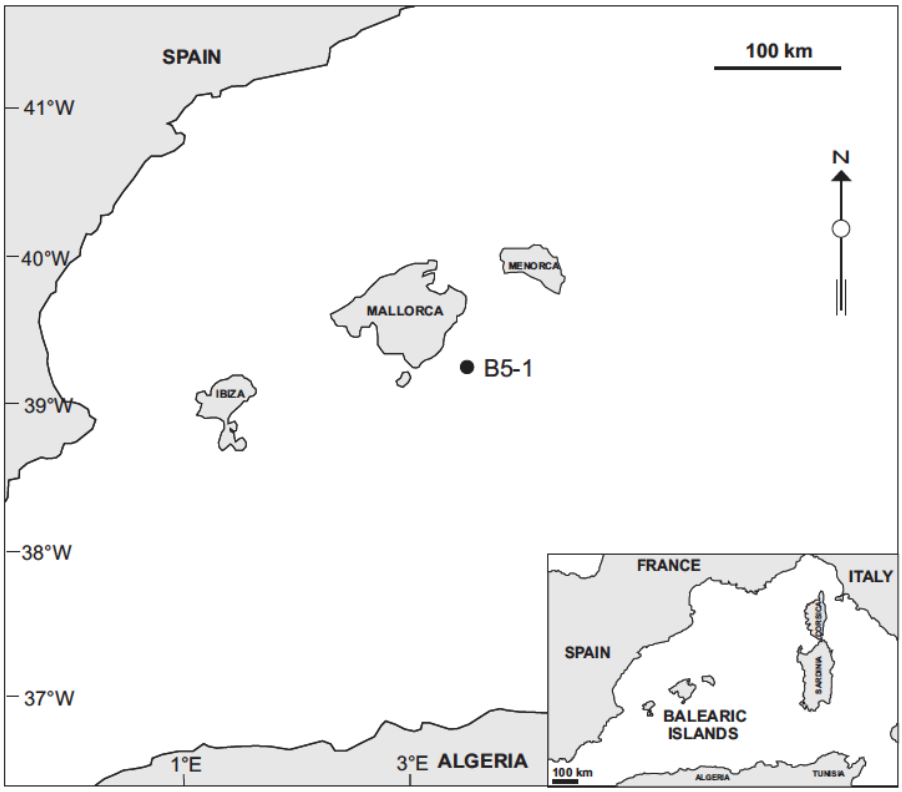

Figure 2. Location of Mediterranean site B5-1 south-east of Mallorca.

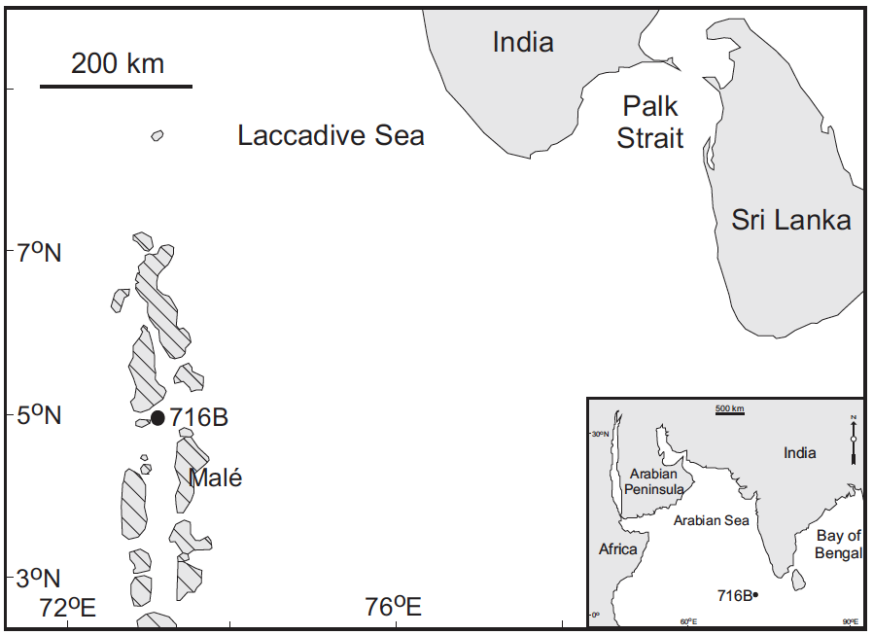

Figure 3. Location of Indian Ocean ODP Site 716, Hole B on the Chagos-Laccadive Ridge, in the Maldives.

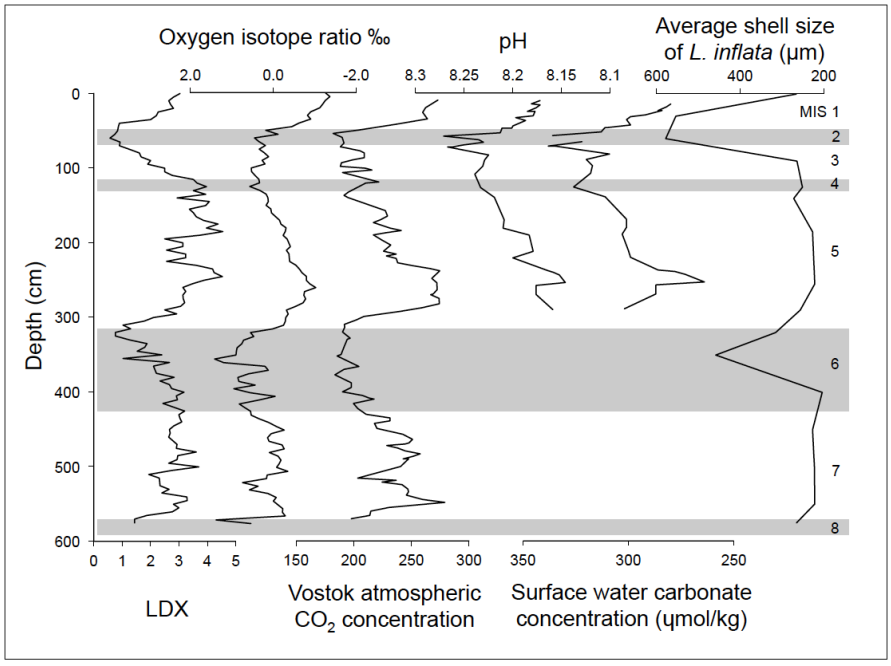

Figure 4. CAR-MON 2 LDX calcification profile (Wall-Palmer *et al.,* 2012), oxygen isotope profile (Le Friant *et al.,* 2008), Vostok atmospheric CO_2 (Petit *et al.,* 1999), pH and surface water carbonate (Foster, 2008) and average *L. inflata* shell size.

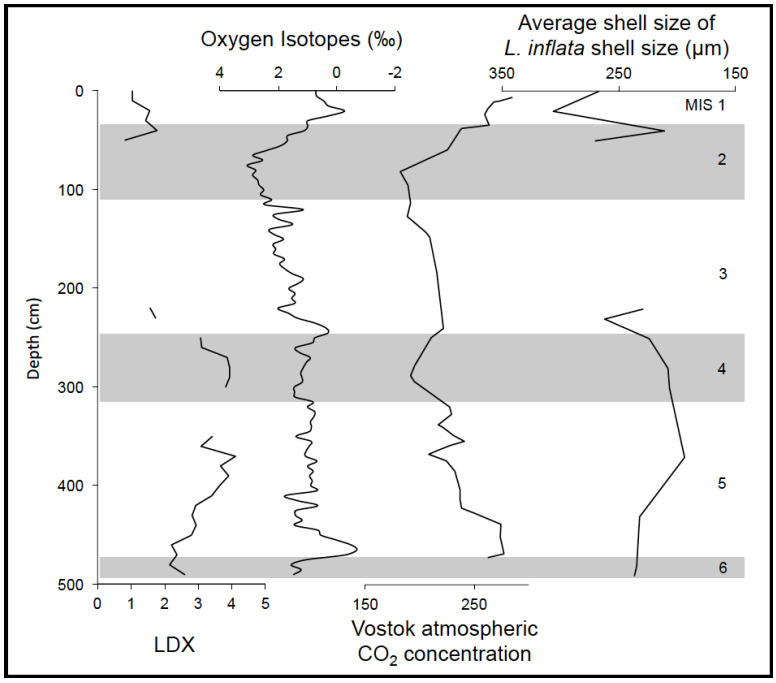

Figure 5. Core B5-1 LDX calcification profile, oxygen isotope profile (Wall-Palmer *et al.,* in review), Vostok atmospheric CO_2 (Petit *et al.,* 1999) and average *L. inflata* shell size.

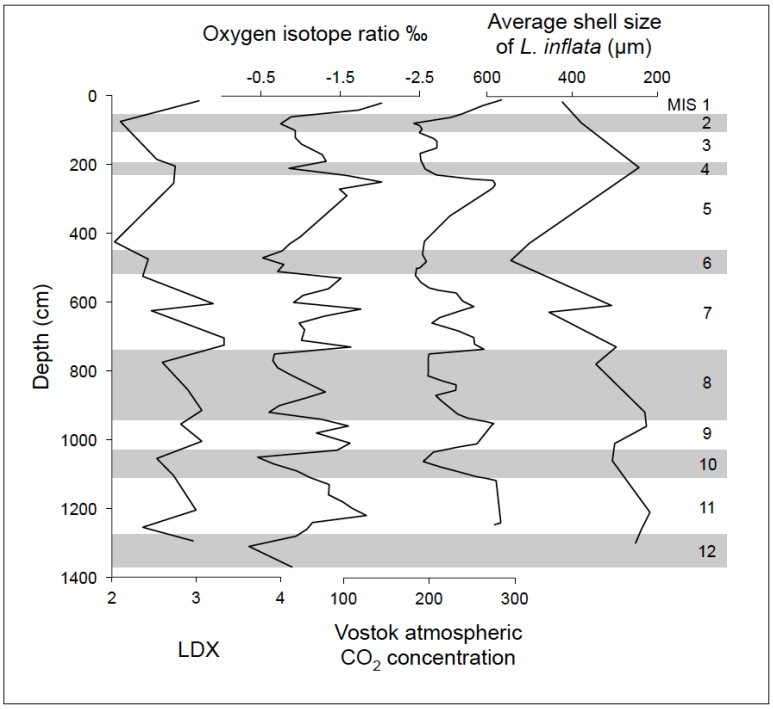

Figure 6. Core 716B LDX calcification profile, oxygen isotope profile (Droxler *et al.,* 1990), Vostok atmospheric CO_2 (Petit *et al.,* 1999) and average *L. inflata* shell size.

Wall-Palmer, D., Smart, C.W., Hart, M.B., Leng, M.J., Conversi, A., Borghini, M., Manini, E. and Aliani, S. Quaternary planktonic foraminifera, pteropods and heteropods from the western Mediterranean Sea. **Submitted to Marine Geology May 2012.**

Quaternary planktonic foraminifera, pteropods and heteropods from the western Mediterranean Sea.

Deborah Wall-Palmer[a,b,*], Christopher W. Smart[a,b], Malcolm B. Hart[a,b], Melanie J. Leng[c], Alessandra Conversi[b,d,e], Mireno Borghini[e], Elena Manini[f] and Stefano Aliani[e].

[a]School of Geography, Earth and Environmental Sciences, Plymouth University, Plymouth, PL4 8AA, UK.
[b]Marine Institute, Plymouth University, Plymouth, PL4 8AA, UK.
[c]Department of Geology, University of Leicester, Leicester, LE1 7RH, UK & NERC Isotope Geosciences Laboratory, British Geological Survey, Keyworth, Nottingham, NG12 5GG, UK.
[d]SAHFOS, Sir Alister Hardy Foundation for Ocean Science, Citadel Hill, Plymouth, PL1 2PB
[e]ISMAR-CNR, Forte Santa Teresa, Pozzuolo di Lerici, 19036 La Spezia. Italy.
[f]ISMAR-CNR, Largo Fiera della Pesca, 60125 Ancona. Italy.

*corresponding author email address: deborah.wall-palmer@plymouth.ac.uk

This study presents microfossil analysis of a marine sediment core collected southeast of Mallorca. The semi-enclosed Mediterranean Sea has been affected by climatic change throughout the Quaternary. Microplanktonic organisms are extremely sensitive to these changes and their fossilised remains can therefore be used to reconstruct the palaeoclimate of the region. Core B5-1 has been analysed for planktonic microfossil content, as well as oxygen and carbon isotope ratios of foraminifera. The isotope data show that the core extends back to Marine Isotope Stage (MIS) 6 (around 130,000 yrs). The microfossil analysis shows two distinct assemblages of calcareous zooplankton. The first is a cold sub-polar assemblage, which appears at the base of the core in MIS 6 and continues to the boundary of MIS 5/6. This assemblage returns during MIS 3, extending through MIS 2 and terminating at

the boundary of MIS 1/2. The second distinct assemblage indicates warm sub-tropical water and appears at the MIS 5/6 boundary and persists through MIS 5, 4 and part of 3. This assemblage returns at the MIS 1/2 boundary and extends to the top of the core. Calcification indices (calcification of pteropods and fragmentation of planktonic foraminifera) also support this trend of a generally warmer climate through MIS 5, 4 and 3, becoming cooler during MIS 3 and 2 and then becoming warmer to the present day. This trend has previously been found in the central and eastern Mediterranean but has not been documented in the western Mediterranean Sea, west of the Tyrrhenian Sea.

Keywords: planktonic foraminifera; pteropod; heteropod; Mediterranean Sea; isotope ratios; palaeoclimate.

1. Introduction

The specific requirements and environmental constraints of many planktonic organisms make them extremely useful indicators of past and present environmental change (Hays *et al.*, 2005). The high abundances of micro-plankton make them particularly useful in reconstructing palaeoclimates. Planktonic foraminifera are present in oceans worldwide and produce a robust test of calcite. Holoplanktonic thecosome pteropods and heteropods (gastropods) produce shells made of aragonite, a polymorph of calcium carbonate, which is 50% more susceptible to dissolution than calcite. Therefore, although such holoplanktonic gastropods are found living in oceans worldwide (Bé and Gilmer, 1977), the occurrence of their shell remains is limited to sediments in relatively shallow water, which is super-saturated with respect to aragonite.

The waters of the Mediterranean Sea are shallow and relatively warm and in consequence are super-saturated with respect to calcium carbonate. Climatic events within the Mediterranean Sea also tend to be amplified due to the semi-enclosed nature of the basin (Pérez-Folgado *et al.,* 2003). In addition to this, the relatively high sedimentation rate produces a high resolution sedimentary record. For these reasons, fossil remains of planktonic foraminifera and

holoplanktonic gastropods are abundant in the sediments of the Mediterranean Sea and have been used by several authors to reconstruct the past climate of the central and eastern Mediterranean (Chen, 1968; Herman, 1971; Jorissen *et al.,* 1993; Capotondi *et al.*, 1999; Sbaffi *et al.,* 2001), the Tyrrhenian Sea (Carboni and Esu, 1987; Biekart, 1989; Buccheri *et al.,* 2002), the Adriatic Sea (Jorissen *et al.,* 1993) and more generally the entire Mediterranean Sea (Hayes *et al.,* 2005).

In this study, the succession of planktonic foraminifera and holoplanktonic gastropods from a sediment core collected in the western Mediterranean Sea are described and compared to similar successions from elsewhere in the Mediterranean Sea. Distinct assemblages of species are identified and related to modern day planktonic assemblages to reconstruct climatic changes through the Quaternary. There is often dissimilarity between a planktonic assemblage living in the water column and that found within the sediments. However, in areas of enhanced preservation, such as the Mediterranean Sea, the assemblage within the sediments accurately reflects both the species composition and the abundance of the living population of the overlying waters (Wells, 1975, 1976; Rottman, 1980; Almogi-Labin, 1982). Distinct assemblages within the sediment can therefore be compared to modern day assemblages and their environmental requirements.

The second aim of this study is to investigate the variations in calcification of the pteropod *Limacina inflata* through the Quaternary, using the *Limacina* Dissolution Index (LDX) (Gerhardt and Henrich, 2001) and relate these changes to atmospheric CO_2 variability. Several recent studies on living marine organisms have found that increasing dissolved CO_2 reduces calcification in a number of, but not all species (for example, Comeau, *et al.,* 2009, 2010a, b; Ries *et al.,* 2009). This relationship can also be found within the fossil record, where periods of low calcification (often seen as periods of low pteropod abundance or enhanced dissolution) are often associated with periods of low global ice volume and high atmospheric CO_2 (Wang *et al.,* 1996). Similarly, periods of high calcification (high pteropod abundance) are generally associated with periods of low atmospheric CO_2, as more carbonate is available

for the production and maintenance of shells. This relationship has recently been shown in a core from the Caribbean Sea (Wall-Palmer *et al.,* 2012). In this study, a comparison of calcification indices and the marine oxygen isotope record (temperature and global ice volume) and Vostok atmospheric CO_2 record are made to establish whether there is a link between past climate change and calcification in the western Mediterranean Sea.

2. Methodology

During May 2010, the BIOFUN'10 cruise of the S.V. *Urania* collected a variety of marine survey data (water and sediment) offshore from the Balearic Islands in the western Mediterranean Sea. Of the cores collected, gravity core B5-1 was chosen for microfossil analysis as it was collected in relatively shallow water of depth 1519 m and appeared to be unaffected by turbidites, which are often recorded from the Balearic Abyssal Plain (for example, Hoogakker *et al.,* 2004). B5-1 was collected by gravity corer from a location approximately 23 km (Fig. 1) to the south east of Mallorca (39°14.942'N, 03°25.052'E). It has a length of 494 cm.

Gravity core B5-1 was sampled in accordance with standard sampling practice on board the ship. Samples of 1 cm width were taken from the working half of the core at 5 cm intervals for the entire 494 cm length. The outer surface of each sample was removed to reduce the risk of contamination caused by smearing during the coring process. Samples were oven dried in foil boats at 30°C for 4 hours and placed in labelled plastic vials. The dried sediment was shipped to Plymouth University for analysis. All cores from the BIOFUN'10 cruise are in cold storage at the Istituto di Scienze Marine, La Spezia, Italy.

All sample processing was carried out at Plymouth University. No chemicals were used during the processing. Dried samples were gently disaggregated into large lumps and a small fraction of the sample was set aside as an archive. The remaining sediment was weighed and then re-hydrated using deionised water. Each sample was then thoroughly washed over a 63 μm sieve, filtered and air dried ready for microfossil analysis.

2.1 Micropalaeontological analysis

Counts of planktonic foraminifera and pteropods were made from two size fractions, 150-500 μm and >500 μm, using a standard methodology. For each sample, just over 300 (or until the sample was exhausted) planktonic foraminifera and fragments of planktonic foraminifera were picked from both size fractions. Planktonic foraminifera were picked from all samples to provide several pieces of palaeoenvironmental data. Whole specimens were picked to provide abundance, diversity and environmental data. Fragments of planktonic foraminifera were picked to provide a fragment to whole specimen ratio. During times of enhanced dissolution or reduced calcification, fragments are more common as the tests of planktonic foraminifera are weakened and easily broken. A high fragment to whole specimen ratio therefore symbolises increased dissolution or reduced calcification (Rottman, 1979; Gonzalez-Mora *et al.,* 2008).

Pteropod and heteropod content was analysed by picking just over 300 (or until the sample was exhausted) pteropod specimens from both size fractions for each sample. Only whole specimens and fragments of pteropod and heteropod retaining their protoconch were counted. Some authors choose to count fragments as specimens (Rottman, 1979; Klöcker and Henrich, 2006), however, Gerhardt *et al.* (2000) noted that pteropod tests are generally very fragile and thus susceptible to mechanical damage, despite careful treatment during washing and sieving of the sediment. Therefore, counting fragments is likely to distort the actual pteropod abundance as one individual may become many fragments. Only counting fragments which retain the protoconch will not distort the results since there is only one protoconch per specimen.

All specimens were picked under a binocular microscope (Olympus SZ11) using a moistened paintbrush and were mounted on slides ready for identification and imaging. The taxonomy of recent planktonic foraminifera is well described and identification was made using the taxonomic reviews by Bé (1977) and Saito *et al.* (1981). Extant euthecosome and pseudothecosome pteropod species are also well described. Consequently, identification of specimens without the soft body parts is possible by using the keys published by Bé and Gilmer (1977) and Van der Spoel (1976), with additional information from Tesch (1946, 1948).

Identification of heteropods was more problematic, as species are not well defined and are often given different names by different authors. However, identification of most species has been made using Tesch (1949), Thiriot-Quiévreux (1973), Van der Spoel (1976) and the online guide compiled by Seapy (last accessed January 2012). In this way, the abundance, diversity, dominant size and form were found for each sample.

Determination of the calcification of pteropod shells was made using the *Limacina* Dissolution Index (LDX), which was devised by Gerhardt *et al.* (2000) and published as a scale by Gerhardt and Henrich in 2001 (Fig. 2). This method was created to analyse post-depositional dissolution of pteropod shells, but will be used in this study as a scale of pteropod calcification (e.g. Wall-Palmer *et al.,* 2012). The method involves the semi-quantitative analysis of the surface of *Limacina inflata* shells on a scale of 0 to 5; 0 being a shell that is transparent, lustrous and perfectly preserved and 5 being a shell that is opaque-white, totally lustreless and perforated. At least 10 shells (up to 30 shells, selected in order of placement on assemblage slide) of adult *L. inflata* of a size of 300 µm or larger were allocated a value from this scale by the use of light microscopy for each sample. The average for each sample was then calculated to provide the LDX value. This was carried out for all samples containing the relevant number of adult *L. inflata.*

The average shell size of pteropod *L. inflata* was calculated by using a photomicroscope (Nikon DS-Fi1 camera mounted on a Nikon eclipse LV100POL microscope) to measure the diameter of shells perpendicular to the line of the aperture on the spiral side. Measurements were made for all appropriate shells >150 µm that had been picked for the species diversity study. The average size was then calculated.

2.2 Stable isotope analysis

Stable isotope analysis ($\delta^{18}O$, $\delta^{13}C$) was carried out at the NERC Isotope Geosciences Laboratory, British Geological Survey, Keyworth. Ten specimens of *Globigerinoides ruber* of size 250 µm to 355 µm were analysed for each data point using a GV IsoPrime mass spectrometer plus Multiprep device. Isotope values ($\delta^{13}C$, $\delta^{18}O$) are reported as *per mille* (‰) deviations of the isotopic ratios

($^{13}C/^{12}C$, $^{18}O/^{16}O$) calculated to the VPDB scale using a within-run laboratory standard calibrated against NBS standards. Analytical reproducibility of the standard calcite (KCM) is < 0.1‰ for $\delta^{13}C$ and $\delta^{18}O$. The isotope profiles produced are comparable to published data for sediments in the area (c.f. Weldeab *et al.,* 2003).

3. Results

3.1 Marine Isotope Stages

The oxygen isotope data suggest that B5-1 contains a relatively uninterrupted marine isotope record extending back to Marine Isotope Stage (MIS) 6 based on visual wiggle matching. The length of the core and estimated age are in agreement with the oxygen isotope record published by Weldeab *et al.* (2003) for site SL87, approximately 60 km south east of B5-1 (Fig. 3). A bivariate, two-tailed Pearson correlation of $\delta^{18}O$ data at minor MIS stages, identified within cores B5-1 and SL87, show a significant relationship between the two records ($r=0.892$, $p=0.001$, $n=10$). The record also compares well to the LR04 stack (Lisiecki and Raymo, 2005) and SPECMAP (NOAA) records of Marine Isotope Stages (Fig. 3).

Changes in the carbon isotope record (Fig. 4), although more variable, generally occur with the oxygen isotope record. Periods of higher $\delta^{13}C$ are generally associated with glacial phases (MIS 6, 4 and 2) and periods of lower $\delta^{13}C$ are associated with interglacial phases (MIS 5, 3 and 1). Since in general increased $\delta^{13}C$ values are associated with increases in productivity, these data suggest higher productivity during glacial periods. This trend has been found in the western Mediterranean by Pierre *et al.* (1999) and Weldeab *et al.* (2003).

3.2 Micropalaeontology

3.2.1 How accurately do the surface sediments represent the overlying waters?

Nineteen species of pteropod, sixteen species of heteropod and twenty one species of planktonic foraminifera were identified from both size fractions (Table 1). Some pteropod and heteropod genera unidentifiable to species level, such as *Pterotrachea* spp. contain more than one species, which are labelled alphabetically.

The pteropod distributions in the modern oceans are described by Bé and Gilmer (1977). The western Mediterranean Sea pteropod assemblage consists of only a few common and abundant species and a number of species that are considered present, which are summarised in Table 2. Due to the patchy, swarming nature of pteropod distributions, it is unlikely that representatives of all the species found in the western Mediterranean will be found within the sediments of one particular area. It is therefore not surprising that not all of the common and abundant species described by Bé and Gilmer (1977) are present in the surface (0-1 cm) sediments of B5-1. The species of the surface sediments and overlying waters are therefore reasonably comparable and there are no species of pteropod in the surface sediments that are not recorded as living in the over-lying waters (Table 1, 2).

Data on the modern Mediterranean heteropod species have been summarised by Thiriot-Quiévreux (1973). All but two of the seven species (or genera) are present throughout B5-1, although, only three species are present in the surface (0-1 cm) sediments (Table 3). There are also some species that were found within the surface sediments of B5-1 that are not recorded from the Mediterranean Sea (Table 1). These include *Atlanta rosea* and *Atlanta selvagensis*, which are found in tropical and sub-tropical waters of the Atlantic and Indian Oceans, and Carinariidae spp., which are found in the Indo-Pacific.

Relatively few substantial studies have been made of the modern living planktonic foraminifera assemblages of the Mediterranean Sea. An extensive study detailing seasonal distribution patterns of live planktonic foraminifera throughout the Mediterranean has been published by Pujol and Verhaud-Grazzini (1995). As well as this, the modern sub-tropical species of planktonic foraminifera have been described by Bé (1977) and Arnold and Parker (2002)

(Table 4). The list of sub-tropical species published by Bé (1977) incorporates the Mediterranean Sea and lists any species, which have a particular distribution (such as Indo-Pacific only). Several of the species (*Globorotalia hirsuta, Globigerina falconensis, Hastigerina pelagica* and *Globigerinita glutinata*), which Bé (1977) found to be dominant, are not found in the surface (0-1 cm) sediments of B5-1. All but one species (*Globigerinella calida*) found within the surface sediments of B5-1 are recorded from the Mediterranean Sea.

3.2.1 Calcification Indices

The LDX calcification index for B5-1 is interrupted because several sections of core either contain too few specimens of *L. inflata* for analysis, or, are devoid of the species all together (Fig. 5). This is largely due to the dominant presence of the pteropod *Limacina retroversa* during cool climatic periods which appears to replace *L. inflata.* However, the overall trend in LDX shows reduced calcification (high LDX values) during extreme interglacial periods (MIS 5) and increased calcification (low LDX values) during glacial periods (MIS 2) (Fig. 5). Between 490 cm and 460 cm (MIS 6 and MIS 6/5 boundary), the LDX values are fairly low, between 2.14 and 2.60. However, following this, the LDX values increase, with high values (2.82 to 4.11) throughout MIS 5. This high LDX signifies reduced calcification and enhanced dissolution. The maximum LDX value (4.11) occurs at 370 cm within MIS 5. Through MIS 4, the LDX values begin to reduce, with a transition to a lower LDX between 250 cm and 220 cm (LDX 3.07 to 1.56), at the MIS 4/3 boundary. Due to the absence of *L. inflata,* no LDX data is available for the section 220 cm to 50 cm. However, when *L. inflata* return to the core at 50 cm, the LDX values are very low, remaining low throughout MIS 2 and 1 (LDX 0.81 to 1.78). These low values indicate enhanced calcification spanning MIS 2 and 1.

The LDX does not correlate well with $\delta^{18}O$ ($r=0.14$, $p=0.49$, $n=28$). This may either be a factor of the poor representation of *L. inflata* but is more likely to be due to changes in either record being disproportionate. In a study of Caribbean pteropods (Wall-Palmer *et al.*, 2012) it was found that, although the LDX values clearly followed the changes in $\delta^{18}O$, the trends were slightly out of phase. The

LDX also shows a similar trend to the atmospheric CO_2 concentration, however, correlation between the two records is not significant (r=-0.46, p=0.073, n=16). This poor value may be due to the low number of corresponding data points.

The low resolution average shell size data for *L. inflata* (Fig. 5) shows a similar trend to the LDX, with larger shells produced during cool periods and smaller shells produced during warmer periods. Average shell size data shows a significant negative correlation to the LDX data (r=-0.871, p=0.024, n=6), this indicates that smaller shells are produced when calcification is poor.

Figure 5 shows four main shifts in planktonic foraminifera fragmentation (150-500 μm fraction). At the base of the core (MIS 6), fragmentation is relatively low with a decrease towards the MIS 6/5 boundary. The fragmentation continues to decrease, with the lowest value of the entire core (1.2%) occurring at MIS 5.5. This is unexpected since the highest fragmentation would be expected to occur at this point in the core. From MIS 5.5, the fragmentation increases steadily to the MIS 4/3 boundary (320 cm), where the maximum fragmentation (60%) occurs. The fragmentation then reduces through MIS 4 until the boundary with MIS 3. Low fragmentation values (down to 2%) persist throughout MIS 3 and 2 and only begin to increase again towards the MIS 2/1 boundary. The fragmentation increases between 30 cm and the surface of the core (up to 37%). Fragmentation of planktonic foraminifera correlates moderately well with LDX values (r=0.52, p=0.004, n=29).

3.2.2 Abundance and diversity

Several samples in the >500 μm size fraction were found to contain an inadequate number of specimens of both planktonic foraminifera and pteropods to be used in statistical analysis. Therefore, for the analysis of abundance and diversity, only the 150-500 μm size fraction was used.

Although the planktic foraminifera species richness (number of species) varies little (between 7 and 13 species) throughout the core, it clearly shows a trend of reduced diversity during glacial periods, with only 7-9 species present in MIS 2,

8-9 species in MIS 4 and 8 species in MIS 6 (Fig. 6). During interglacial periods, the species richness is variable, but generally higher. The heterogeneity (Shannon Weaver) function H(S) provides information about the spread of species in a community and whether there is a dominant species. When compared to the maximum heterogeneity possible for a community, values close to the maximum show an even spread of species. The heterogeneity of planktonic foraminifera varies throughout the core (range H(S) 0.7 to 2.3) with most values around H(S) 1.7. At the top of the core, between 0 cm and 30 cm, the values are higher (H(S) 2 to 2.3), which is close to the maximum heterogeneity (around H(S) 2.3, based on average of 10 species). This shows that the top of the core has a diverse and evenly spread number of species whereas, lower in the core, diversity is reduced and there is often a dominant species in the assemblage.

The diversity of pteropods and heteropods is more variable but shows a similar trend to planktonic foraminifera (Fig. 6). There is a greater range of species richness from 1 to 17 species, with low diversity during glacial periods and generally higher, but variable diversity during interglacial periods. There is a peak in diversity with 17 species following MIS 5.5. The heterogeneity varies throughout the core but shows that the majority of the core has a dominant species and is not heterogeneous. Between 60 cm and 140 cm, the heterogeneity approaches the H(S) max, showing that during MIS 2, the holoplanktonic gastropod community has an even spread of species. The H(S) also approaches H(S) max at MIS 5.5 (470 cm).

The trend in abundance of calcareous micro-zooplankton is more general and does not appear to change closely with isotope stages but with extremes of climate (Fig. 6), being variable, but generally higher during MIS 6, lower during MIS 5 to 4 and higher again during MIS 3 to 1. The abundance of planktonic foraminifera at the base of the core is relatively high, with 39,747 foraminifera per gram of sediment (fg^{-1}) at the MIS 6/5 boundary. Abundance is then variable but generally low throughout MIS 5 and 4 (between 14,679 and 32,959 fg^{-1}), increasing again through MIS 3 with a peak at 230 cm (40,395 pfg^{-1}). Abundance of planktic foraminifera remains high through MIS 3 and 2, with the

highest value occurring at 40 cm (40,789 pfg^{-1}). There are also two periods of low abundance during MIS 3 and 2, at 170 cm and 110 cm (15,048 pfg^{-1} and 15,099 pfg^{-1} respectively).

The abundance of pteropods is generally much lower than the abundance of planktic foraminifera. At the base of the core, abundance is fairly high at the MIS 6/5 boundary and then decreases and remains low throughout MIS 5 and 4, with a low of 44 pteropods per gram (pg^{-1}) at 340 cm. Throughout MIS 3 to 1, abundance is much higher, ranging between 3901 pg^{-1} and the peak in abundance of 10,199 pg^{-1}at 130 cm. There are three excursions to low abundances at 170 cm (2743 pg^{-1}), 110 cm (3371 pg^{-1}) and 60 cm (1423 pg^{-1}), which coincide with similar reductions in planktic foraminifera abundance. These points coincide with climatic events. The two excursions to low abundance at 170 cm and 110 cm coincide with Heinrich events at 39 kyr and 24 kyr respectively. These are brief cool periods in the climate during the interglacial period MIS 3. The reduced abundance at 60 cm coincides with interstadial 1, a slight warming of the climate at 14 kyr during the last glacial period.

3.2.3 Down-core species composition

Core B5-1 contains two distinct assemblages of planktonic fauna, which divide the core up into 4 major zones (*Zone C* is further subdivided into 5 subzones). These zones are not coincident with the 6 MIS, but are characterised by a homogenous set of species preferring either sub-polar water or tropical warm water (Fig. 7).

Zone D (490 cm to 471 cm)

This is a period of cool water, which is associated with MIS 6. The length of this zone is unknown as it is at the base of the core and may extend below the collected record. It is very similar in composition to *Zone B*, with increased numbers of the sub-polar pteropod species *L. retroversa* (25-72% of planktonic gastropods) and low numbers of *L. inflata* (17-38%). Based on the dominant

species of planktonic foraminifera and pteropods present, the temperature during this period was between 12 and 16°C (Fig. 8).

Zone C (470 cm to 221 cm)

This is a zone mainly composed of warm sub-tropical to tropical planktonic species. It spans MIS 5, 4 and 3 and contains alternating warm periods with short term cooler periods. It signifies a gradual warming from the boundary of MIS 6 throughout MIS 5 and then a gradual cooling throughout MIS 4 and 3 towards the glacial maximum (MIS 2.2). The overall species composition of *Zone C* is similar to that of the modern western Mediterranean Sea.

Sub-Zone C (v) (470 cm to 441 cm)

This is a short warm period, occurring during MIS 5.5, characterised by an increase in the number of *L. inflata* (73-93%) and a coinciding decrease in the number of *L. retroversa* (1-6%). It is similar in composition to *Zone C(i)* and *C(iii)*. Cold water species do not disappear, but remain in lower numbers. The temperature during this time had risen to between 16 and 19°C (Fig. 8).

Sub-zone C (iv) (440 cm to 411 cm)

This is a short cooler zone, occurring during MIS 5.4 to 5.2 and is characterised by a sharp peak in *L. retroversa* (from 6% at 450 cm to 83% at 420 cm) and a coinciding reduction in numbers of *L. inflata* (from 73% at 450 cm to 13% at 420 cm). The warm water species such as *Limacina bulimoides* and *A. selvagensis* do not disappear, but remain in lower numbers, suggesting that this period is cooler but not sub-polar. Cold water planktonic foraminifera *Globigerina bulloides* is also present, but in low numbers. The temperature during this period was between 12 and 16°C (Fig. 8)

Sub-zones C (iii) 410 cm to 371 cm; ii) 370 cm to 351 cm; i) 350 cm to 221 cm

This section is characterised by relatively high numbers of the sub-tropical planktonic foraminifera *Orbulina universa* (up to 29% of planktonic foraminifera). In common with *Zone A*, it contains higher numbers of the pteropod *L. inflata* (average 25%), the heteropod *A. selvagensis* (average 30%) and the planktonic foraminifera *Globorotalia inflata* (6-22%) and low numbers of the sub-polar

pteropod *L. retroversa* (variable between 2-57%). The temperature during *Sub-Zone C (iii)* was between 19 and 21°C (Fig. 8). With exception to this, there is a very short cooler period between 370 and 351 cm with higher numbers of *L. retroversa* (*Sub-Zone C(ii)*). During *Sub-Zone C (ii)* the temperature decreased to between 12 and 16°C. The surface water then warmed again during *Sub-Zone C (i)* to between 17 and 19°C (Fig. 8). In general, pteropod species *L. bulimoides* and *Creseis virgula r*eturned to *Zone C* with an increase in the number of *Diacria trispinosa,* a warm water cosmopolitan species of pteropod. *Zone C* also shows a peak in the number of *Globorotalia truncatulinoides,* a species infrequently found within the Mediterranean Sea as it resides in deeper water and is often unable to travel past the shallow sill at the Straits of Gibraltar. Other than a large number of specimens in the surface sediments (*Zone A*), only occasional specimens are present elsewhere in the core. This larger peak (up to 20% of planktonic foraminifera) between 300 cm and 260 cm is consistent with a rise in sea level during this warmer period, allowing more *G. truncatulinoides* to enter.

Zone B (220 cm to 31 cm)

This is a zone of sub-polar species, which spans both the majority of MIS 3 and MIS 2, the last glacial maximum. It is characterised by very high numbers of the sub-polar pteropod *L. retroversa* (up to 100% but generally 85% of planktonic gastropods) and the sub-polar planktonic foraminifera *G. bulloides* (average 50% of planktonic foraminifera). There are also higher numbers of the planktonic foraminifera *Globorotalia scitula* (10%) and *G. glutinata* (10%), which have a range of habitats from sub-polar to equatorial. There are fluctuating numbers of the heteropod *A. rosea* which, surprisingly, is only known from warm waters. It is interesting to note that peaks in *A. rosea* occur when the numbers of *L. retroversa* reduce and may therefore signify temperature fluctuations in this sub-polar zone. There are no species of planktonic fauna exclusively found in *Zone B*. The surface water temperature during this period was between 7 and 10°C (Fig. 8).

Zone A (30 cm to 0 cm depth)

This is a zone of sub-tropical species, which occurs during MIS 1 and is characterised by high numbers of the tropical pteropod *L. inflata* (generally 50% of planktonic gastropods) and very low numbers of the sub-polar pteropod *L. retroversa* (under 2%). There are also large numbers of the transitional planktonic foraminifera *G. inflata* (19-34% of planktonic foraminifera) and the sub-tropical heteropod *A. selvagensis* (16-22%). *Zone A* contains the warm water pteropods *L. bulimoides and C. virgula* and the tropical planktonic foraminifera *Globigerinella aequilateralis* and *Globogerinoides sacculifer* which are not found at all in *Zone B*. This zone also contains large numbers of *G. truncatulinoides*, which suggests the sea level had risen since MIS 2 and is possibly comparable to that found in *Zone C(i).*The temperature during MIS 1 was between 19 and 21°C (Fig. 8).

4. Discussion

Much of the micropalaeontological data derived from core B5-1 points to four distinct climatic periods of varying lengths, which alternate between a warm sub-tropical to tropical climate and cool sub-polar climate. From these data, it can be inferred that the western Mediterranean climate during MIS 6, at the base of the core (*Zone D*) from 490 cm to 471 cm, was cool, with surface water temperatures ranging from 12 to 16°C. Species present in the surface waters were representative of a sub-polar assemblage similar to that of the modern sub-polar North Atlantic (Bé and Gilmer, 1977; Bé, 1977). However, some warm water and transitional species were still found suggesting that this was perhaps the late transition from a colder period present below the 494 cm collected in B5-1. This climate is also confirmed by the $\delta^{18}O$ data, which suggest a relatively high global ice volume, signifying a cool climate.

At 190 kyr (470 cm) the climate began a steady warming which extended through MIS 5 and then began to cool gradually again through MIS 4 and 3 (*Zone C*). The surface water temperature of the western Mediterranean Sea during this time was being elevated to between 16 and 19°C. This period is characterised by higher numbers of warm water species of planktonic gastropod, such as *L. inflata* and *A. selvagensis* and planktonic foraminifera,

such as *Neogloboquadrina dutertrei,* with later peaks in the number of *O. universa* and fluctuations in the number of transitional species *G. inflata.* This gradual swing in temperature is also shown by the fragmentation of planktonic foraminifera, the average shell size of *L. inflata* and the calcification of pteropods. An increase in foraminifera fragmentation and a decrease in pteropod calcification and size occurred throughout MIS 5 and 4 which then reversed towards the last glacial maximum. This suggests an increase in temperature caused by increased atmospheric CO_2, which affected the calcium carbonate saturation level within the ocean. The Vostok atmospheric CO_2 data confirm this by showing high levels of CO_2 through the first part of MIS 5, up to MIS 5.3, where the levels then decreased. This warm period extended to 221 cm and was interrupted several times by short cooling periods (*Zone C (ii) and C (iv)*). The interglacial maximum (MIS 5.5) occurs at 465 cm (130 kyr), shown by the Vostok CO_2 record and the oxygen isotope record as a large increase in the atmospheric CO_2 concentration and a consequent decrease in global ice volume. The species of planktonic fauna at this time were representative of a sub-tropical sea, although some cold water species were still present. Planktonic foraminifera appear to have thrived at this time, with large increases in abundance and diversity. Between 440 cm and 411 cm, the climate recorded a brief cool period signifying MIS 5.4 and 5.2 (115 to 93 kyr). This is confirmed by a sharp increase in cold water species, showing a decrease in temperature to between 12 and 16°C. At 410 cm, the water temperature increased again to between 19 and 21°C, and then cooled at 370 cm with an increase in *L. retroversa.* The temperature at this stage was between 12 and 16°C. At 350 cm, the warm water species returned with a large peak in the number of *O. universa.* The warm climate continued throughout the remainder of MIS 5, the whole of MIS 4 and part of MIS 3, with a temperature of between 17 and 19°C. During MIS 4, between 320 cm and 250 cm there appears to have been a significant rise in sea level, revealed by the appearance of a large number (up to 20% of foraminifera) of *G. truncatulinoides*. Although the rise in sea level suggests an increase in temperature during MIS 4, a slight cooling is detected by the complete disappearance of several warm water species including *G. aequilateralis* and *G. sacculifer.* This may indicate an episode similar to a Heinrich Event (Bard *et al.,* 2000). At 250 cm, the increased abundance of *G.*

ruber (Fig. 9) signifies the Ra bio-event (Fig. 9) (Pujol and Vergnaud-Grazzini, 1989). The climate finally switched to a sub-polar assemblage (*Zone B*) at some time before 60 kyr (MIS 4/3 boundary) at 220 cm.

This cool period (*Zone B*) appears to have been a major turning point in the climate with all evidence suggesting a steady cooling towards the last major glacial event (MIS 2.2). The Vostok atmospheric CO_2 concentration reduces and subsequently, $\delta^{18}O$ suggest an increase in global ice volume. The planktonic foraminiferal fragmentation reduces dramatically and the pteropod calcification increases, suggesting an increase in the calcium carbonate saturation of the western Mediterranean Sea. Planktonic gastropods appear to thrive during this period as abundances increase. However, diversity decreased, signifying that specialised coldwater species became more dominant and warm water species were disappearing. The heterogeneity of the planktonic gastropod assemblage increased towards MIS 2.2, showing a stable community structure at the glacial maximum. Several of the bio-events described by Pujol and Vergnaud-Grazzini (1989) and Pérez-Folgado *et al.* (2003) can be identified within *Zone B* (Fig. 9). Peaks in the abundance of *G. bulloides* indicate bio-events B1, B2, B3, B4 and B5. Events B2, B3 and B4 coincide with cold Heinrich Events and events B1 and B5 coincide with slight increases in temperature known as interstadials (Ist-1 and Ist-14 respectively). The species characterising this period were sub-polar, although some cosmopolitan species were also found. The assemblage is similar to that found in the modern sub-polar North Atlantic (Bé and Gilmer, 1977; Bé, 1977). During this period, *L. retroversa* constitutes up to 100% of the planktonic gastropod assemblage and the foraminifera *G. bulloides* makes up an average of 50% of the planktonic foraminifera population. The peak in *L. retroversa* and *G. bulloides* abundances occurs at 75 cm and signifies MIS 2.2, the last glacial maximum. During the last glacial maximum, reconstructed sea surface temperatures at the site of B5-1 (Fig. 8) agree with data published by Sbaffi *et al.* (2001) and Hayes *et al.* (2005). The seawater temperature at this time was between 7 and 10°C. This period, defined as *Zone B,* has been described by several authors. It is comparable to *Zone 3* described by Biekart (1989) in a deep sea core from the Tyrrhenian Sea. Biekart (1989) found similar

abundances of *L. retroversa*, but much higher abundances of *D. trispinosa,* which are only present in this section of B5-1 in low numbers (Maximum 13%). Chen (1968) also recorded this period of abundant *L. retroversa* in a core collected south of the Island of Crete and Herman (1971) detected it in cores throughout the eastern Mediterranean Sea and in the Balearic Sea. Carboni and Esu (1987), Buccheri *et al.* (2002) and Jorissen *et al.* (1993) all detected this zone in the Tyrrhenian Sea. Jorissen *et al.* (1993) also found it in the Adriatic Sea, being characterised by the common occurrence of *G. scitula.* Capotondi *et al.* (1999) and Sbaffi *et al.* (2001) have expanded on the work of Jorissen *et al.* (1993), splitting the previous '*Zone 3*' into more detailed zones. At either end of *Zone B* (220 cm to 140 cm and 50 cm to 31 cm) are increased numbers of the transitional species *Clio pyramidata* and *G. inflata* signifying the transition between warm and cold periods. Many authors consider the upper transitional period (50 cm to 31 cm) as a distinct zone (Carboni and Esu*,* 1989; Jorissen *et al.,* 1992; Buccheri *et al.,* 2002) characterised by an increase in transitional and warmer water species. Capotondi *et al.* (1999) and Sbaffi *et al.* (2001) also subdivide this period into smaller bio-zones.

Following *Zone B*, the seawater gradually began to warm (*Zone A*). The sea surface temperature at this time, averaged over the entire Mediterranean Sea, ranged from 14 to 25°C (Sbaffi *et al.,* 2001). At the site of B5-1, surface water temperatures ranged from 19 to 21°C (Fig. 8). At the boundary of MIS 2 and 1 (11 kyr), the planktonic assemblage once again became one of warmer water, with increased numbers of the pteropod *L. inflata* and the return of the warm water species of pteropod *L. bulimoides* and *C. virgula.* Planktonic foraminifera show an increase in the transitional species *G. inflata* and the return of *G. aequilateralis* and *G. sacculifer.* This assemblage is similar to that found in Holocene sediments described from the Tyrrhenian Sea (Carboni and Esu,1987; Jorissen *et al.,* 1993; Capotondi *et al.,* 1999; Sbaffi *et al.,* 2001; Buccheri *et al.,* 2002), the Adriatic Sea (Jorissen *et al.,* 1993; Capotondi *et al.,* 1999), south of Sicily (Capotondi *et al.,* 1999), in the western Mediterranean Sea (Pérez-Folgado *et al.,* 2003) and south of the Island of Crete (Chen, 1968). Species present within *Zone A* indicate a sub-tropical to Tropical climate similar

to that of the modern day western Mediterranean Sea (Bé and Gilmer, 1977; Bé, 1977).

The surface assemblage of B5-1 is fairly representative of the modern day overlying waters of the western Mediterranean Sea. Species of pteropod, heteropod and planktonic foraminifera found within the surface (0-1 cm) of the sediments are generally those expected in the overlying waters. A number of species are absent from the sediments, including several species of planktonic gastropod. This is most likely due to the patchy, swarming behaviour of such organisms. Several heteropod species found within the sediments are not recorded from the overlying waters. Two species of heteropod which are not recorded as being present in the modern Mediterranean Sea, *A. rosea* and *A. selvagensis* are present in the sub-tropical Atlantic Ocean. It is therefore highly likely that populations are found within the western Mediterranean Sea. The heteropod genus Carinariidae is, however, only recorded from the Indo-Pacific Ocean. Specimens of *Carinaria lamarcki* and other species of Carinariidae are found throughout the core.

5. Conclusions

The micropalaeontological and stable isotope analysis of core B5-1 provides an extended record of palaeoenvironmental data within the MIS framework in the western Mediterranean Sea over the past 130 kyr. The top section of B5-1 compares very well to earlier studies and bio-zones previously identified from the western, central and eastern Mediterranean Sea and adds new information in the form of calcification indices (pteropod calcification, average shell size and planktonic foraminifera fragmentation), which provide additional data on surface water chemistry.

This study not only expands upon, but also extends the range of previous data, providing a new, high resolution data set that shows four distinct climatic periods, composed of two discrete assemblages of calcareous micro-zooplankton. We also reinforce the effectiveness of using the pteropod record to compliment planktonic foraminifera palaeoenvironmental data. Pteropods

have proved extremely useful in constraining palaeotemperatures, appearing more sensitive to minor changes in temperature which are not recorded by the dominant species of planktonic foraminifera, for example between *Sub-Zones C (iv) and C (v)*. The range of heteropod genus Carinariidae, which was not previously recorded from the Mediterranean Sea, has also been extended. Remains of the genus were identified within the recent surface (0-1 cm) sediments and the species *C. lamarcki* was found in low numbers throughout the core.

Acknowledgements

We would like to thank the organisers and scientists that took part in the BIOFUN'10 cruise, with particular thanks to the crew and captain of the S/V *Urania*. Funding for the cruise was partially funded through the BIOFUN project of the EuroDEEP Eurocores, European Science Foundation. The stable isotope analysis was carried out at the NERC Isotope Geosciences Laboratory, Keyworth, with funding from NERC. We would like to thank Hilary Sloane for her help with the isotope analysis. We would also like to thank Syee Weldeab for providing $\delta^{13}O$ data for core SL87. This research forms part of a PhD (DW-P) funded by Plymouth University.

References

Almogi-Labin, A., 1982.Stratigraphic and paleoceanographic significance of late Quaternary pteropods from deep-sea cores in the Gulf of Aqaba (Elat) and northernmost Red Sea. *Marine Micropaleontology,* **7,** 53-72.

Arnold, A.J., Parker, W.C., 2002. Biogeography of planktonic foraminifera.In: Sen Gupta, B.K (ed.). *Modern Foraminifera.* Kluwer Academic Publishers, Dordrecht, The Netherlands, 103-122.

Bard, E., Rostek, F., Turon, J.-L., Gendreau, S., 2000. Hydrological impact of Heinrich Events in the subtropical northeast Atlantic. *Science,* **289,** 1321-1324.

Bé, A.W.H.,1977. An ecological, zoogeographical and taxanomic review of recent planktonic foraminifera.In: Ramsay, A.T.S. (ed.). *Oceanic Micropalaeontology*. Academic Press, London, 1-100.

Bè, A.W.H., Gilmer, R.W. 1977., A zoogeographic and taxanomic review of Euthecosomatous Pteropoda. In: Ramsay, A.T.S. (ed.). *Oceanic Micropalaeontology*. Academic Press, London, 733-808.

Bè, A.W.H., Tolderlund, D.S., 1971. Distribution and ecology of living planktonic foraminifera in surface waters of the Atlantic and Indian Oceans. In: Funnell, B.M. and Riedel, W.R. (eds). *The Micropalaeontology of Oceans,* Cambridge University Press, London, 105-149.

Biekhart, J.W., 1989. Euthecosomatous pteropods as paleohydrological and paleoecological indicators in a Tyrrhenian deep-sea core. *Palaeogeography, Palaeoclimatology, Palaeoecology,* **71,** 205-224.

Buccheri, G., Capretto, G., Di Donato, V., Esposito, P., Ferruzza, G., Pescatore, T., Russo Ermolli, E., Senatore, M.R., Sprovieri, M., Bertoldo, M., Carella, D., Madonia, G., 2002. A high resolution record of the last deglaciation in the southern Tyrrhenian Sea: environmental and climatic evolution. *Marine Geology,* **186,** 447-470.

Capotondi, L., Borsetti, A.M., Morigi, C., 1999. Foraminiferal ecozones, a high resolution proxy for the late Quaternary biochronology in the central Mediterranean Sea. *Marine Geology,* **153,** 253-274.

Carboni, M.G., Esu, D., 1987. Paleoclimatology of a late Peistocene – Holocene core from the Tyrrhenian Sea (Western Mediterranean): Foraminifera and Pteropoda. *Geologica Rome,* **26,** 167-185.

Chen, C., 1968. Pleistocene pteropods in pelagic sediments. *Nature,* **219,** 1145-1149.

Comeau, S., Gorsky, G., Jeffree, R., Teyssié, J.-L., Gattuso, J.-P., 2009. Impact of ocean acidification on a key Arctic pelagic mollusc (*Limacina helicina). Biogeosciences,* **6,** 1877-1882.

Comeau, S., Jeffree, R., Teyssié, J.-L., Gattuso, J.-P., 2010a. Response of the Arctic Pteropod *Limacina helicina* to projected future environmental conditions. *PLoS ONE,* 5(6), e11362 (2010).

Comeau, S., Gorsky, G., Alliouane, S., Gattuso, J.-P., 2010b. Larvae of the pteropod *Cavoliniainflexa* exposed to aragonite undersaturation are viable but shell-less. *Marine Biology,* 157(10), 2341-2345 (2010).

Gerhardt, S., Groth, H., Rühlemann, C., Henrich, R., 2000. Aragonite preservation in late Quaternary sediment cores on the Brazilian Continental

Slope: implications for intermediate water circulation. *International Journal of Earth Sciences*, **88**, 607–618.

Gerhardt, S., Henrich, R., 2001. Shell preservation of *Limacina inflata* (Pteropoda) in surface sediments from the Central and South Atlantic Ocean: a new proxy to determine the aragonite saturation state of water masses. *Deep-Sea Research I,* **48,** 2051-2071

Gonzalez-Mora, B., Sierro, F.J., Flores, J.A., 2008.Controls of shell calcification in planktonic foraminifers.*Quaternary Science Reviews,* **27,** 956-961.
Hays, G.C., Richardson, A.J., Robinson, C., 2005. Climate change and marine plankton. *Trends in Ecology and Evolution,* **20,** 337-344.

Hayes, A., Kucera, M., Kallel, N., Sbaffi, L., Rohling, E.J., 2005. Glacial Mediterranean Sea surface temperatures based on planktonic foraminiferal assemblages. *Quaternary Science Reviews,* **24,** 999-1016.

Herman, Y., 1971. Vertical and horizontal distribution of pteropods in Quaternary sequences. In: Funnell, B. and Riedel, W. (Eds) *Micropaleontology of Oceans,* Cambridge University Press, Cambridge, 463-486.

Hoogakker, B.A.A., Rothwell, R.G., Rohling, E.J., Paterne, M., Stow, D.A.V., Herrle, J.O., Clayton, T., 2004. Variations in terrigenous dilution in western Mediterranean Sea pelagic sediments in response to climate change during the last glacial cycle. *Marine Geology,* **211,** 21-43.

Jorissen, F.J., Asioli, A., Borsetti, A.M., Capotondi, L., de Visser, J.P., Hilgen, F.J., Rohling, E.J., van der Borg, K., Vergnaud-Grazzini, C., Zachariasse, W.J., 1993. Late Quaternary central Mediterranean biochronology. *Marine Micropaleontology,* **21,** 169-189.

Klöcker, R., Henrich, R., 2006. Recent and Late Quaternary pteropod preservation on the Pakistan shelf and continental slope. *Marine Geology,* **231,** 103-111.

Lisiecki, L.E., Raymo, M.E., 2005. A Pliocene-Pleistocene stack of 57 globally distributed benthic $\delta^{18}O$ records. *Paleoceanography,* **20,** PA1003, doi:10.1029/2004PA001071

NOAA, (last accessed January 2012). National Oceanic and Atmospheric Administration, Vostok atmospheric carbon dioxide data.www.noaa.gov

Pérez-Folgado, M., Sierro, F.J., Flores, J.A., Cacho, I., Grimalt, J.O., Zahn, R., Shackleton, N., 2003. Western Mediterranean planktonic foraminifera events

and millennial climatic variability during the last 70 kyr. *Marine Micropaleontology,* **48,** 49-70.

Pujol, C., Verghaud-Grazzini, C., 1995. Distribution patterns of live planktic foraminifers as related to regional hydrography and productive systems of the Mediterranean Sea. *Marine Micropaleontology,* **25,** 187-217.

Pujol, C., Verghaud-Grazzini, C., 1989. Paleoceanography of the Last Deglaciation in the Alboran Sea (western Mediterranean). Stable isotopes and planktic foraminiferal records. *Marine Micropaleontology,* **15,** 153-179.

Ries, J.B., Cohen, A.L., McCorkle, D.C., 2009. Marine calcifers exhibit mixed responses to CO_2 –induced ocean acidification. *Geology,* **37,** 1131-1134.

Rottman, M.L., 1979. Dissolution of planktonic foraminifera and pteropods in South China Sea sediments. *Journal of Foraminiferal Research,* **9**, 41–49

Rottman, M.L.,1980. Net tow and surface sediment distributions of pteropods in the South China Sea region: Comparison and oceanographic implications. *Marine Micropaleontology,* **5,** 71-110.

Saito, T., Thompson, P.R., Breger, D., 1981. *Systematic index of recent and Pleistocene planktonic foraminifera.* University of Toyko Press, Tokyo, 1-190.

Sbaffi, L., Wezel, F.C., Kallel, N., Paterna, M., Cacho, I., Ziveri, P., Shackleton, N., 2001. Response of the pelagic environment to palaeoclimatic changes in the central Mediterranean Sea during the Late Quaternary. *Marine Geology,* **178,** 39-62.

Tesch, J.J., 1946. The thecosomatous pteropods. I. The Atlantic. *Dana Report,* **28,** 1-82.

Tesch, J.J., 1948. The thecosomatous pteropods. II. The Indo-Pacific. *Dana Report,* **30,**1-45.

Tesch, J.J., 1949. Heteropoda. *Dana Report,* **34,**1-35.

Thiriot-Quiévreux, C., 1973. Heteropoda. *Oceanography and Marine Biology, an annual review*, **11,** 237-261.

Seapy, R., (last accessed January 2012).Tree of life.http://tolweb.org/Atlantidae
Van der Spoel, S., 1976. *Pseudothecosomata, Gymnosomata and Heteropoda*. Bohn, Scheltema and Holkema, Utrecht. 484pp.

Wall-Palmer, D., Hart, M.B., Smart, C.W., Sparks, R.S.J., Le Friant, A., Boudon, G., Deplus, C., Komorowski, J.C., 2012. Pteropods from the Caribbean Sea: variations in calcification as an indicator of past ocean carbonate saturation. *Biogeosciences,* **9,** 309-315

Wang, L., Jian, Z., Chen, J., 1997. Late Quaternary pteropods in the South China Sea: carbonate preservation and paleoenvironmental variation. *Marine Micropaleontology,* **32,** 115-126.

Weldeab, S., Siebel, W., Wehausen, R., Emeis, K.C., Schmiedl, G., Hemleben, C., 2003. Late Pleistocene sedimentation in the Western Mediterranean Sea: implications for productivity changes and climatic conditions in the catchment areas. *Paleogeography, Paleoclimatology, Paleoecology,* **190,** 121-137.

Wells, F.E. 1976. Seasonal patterns of abundance and reproduction of Euthecosomatous pteropods off Barbados, West Indies. *The Veliger*, **18**, 241-248.

Wells, F.E. 1975. Comparison of Euthecosomatous pteropods in the plankton and sediments off Barbados, West Indies. *Proceedings of the Malacological Society London,* **41**, 503-509.

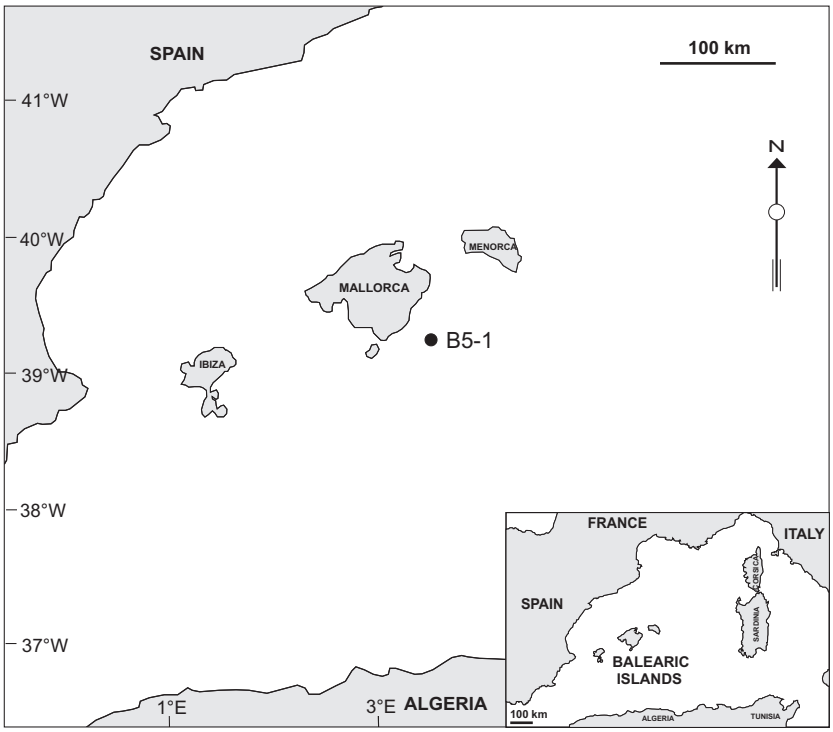

Figure 1. Location map of sampling site for core B5-1, located approximately 23 km to the south east of Mallorca at a water depth of 1519 m.

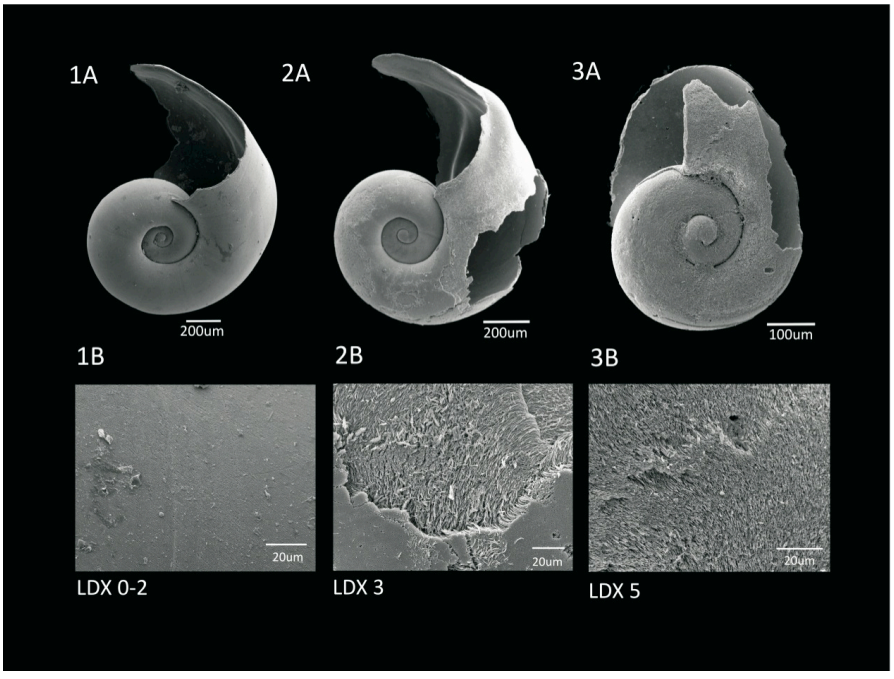

Figure 2. Specimens of the pteropod species *Limacina inflata* at different stages of the *Limacina* Dissolution Index (after Wall-Palmer *et al.,* 2012).

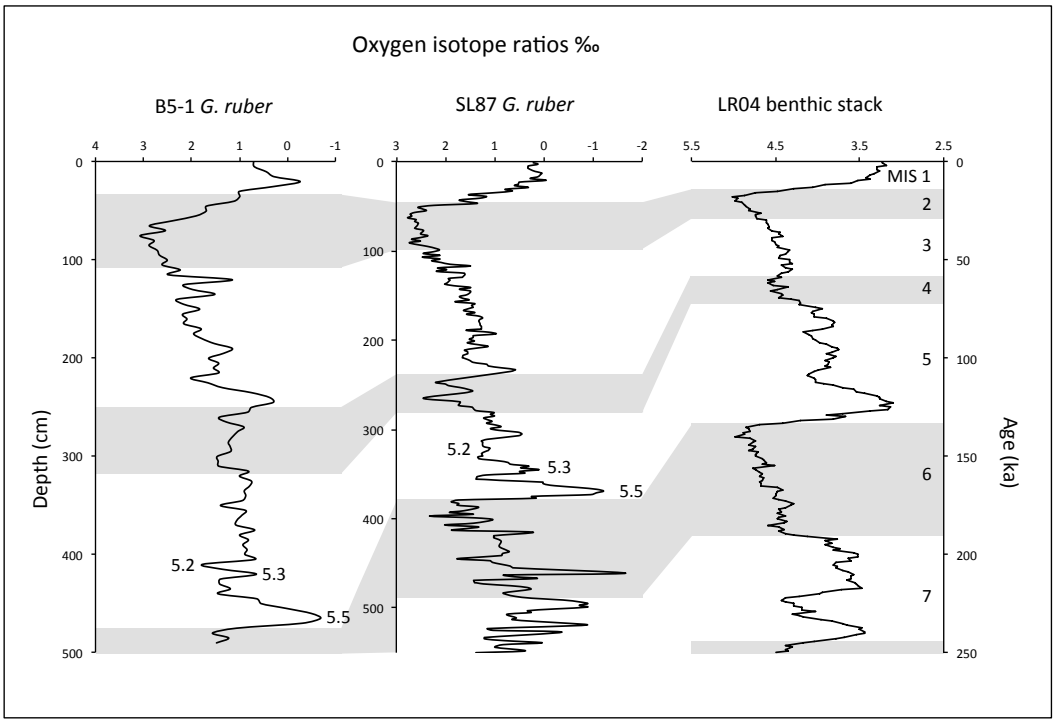

Figure 3. Comparison of the marine oxygen isotope records for B5-1, SL 87 (Weldeab *et al.,* 2003), approximatey 60 km south east of B5-1, and the LR04 benthic stack (Lisiecki and Raymo, 2005) with Marine Isotope Stages (MIS).

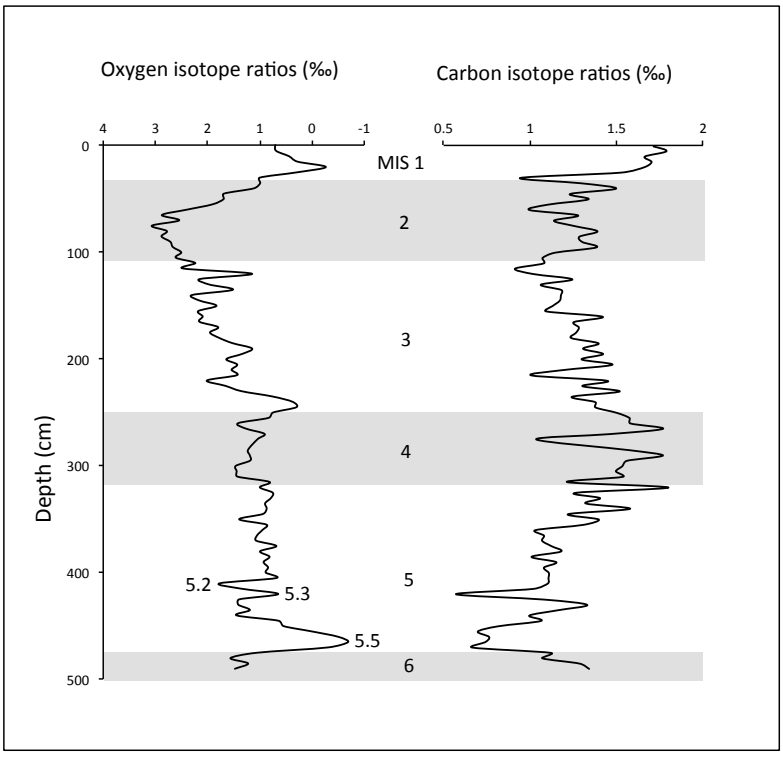

Figure 4. Carbon and oxygen stable isotope data for B5-1, with MIS.

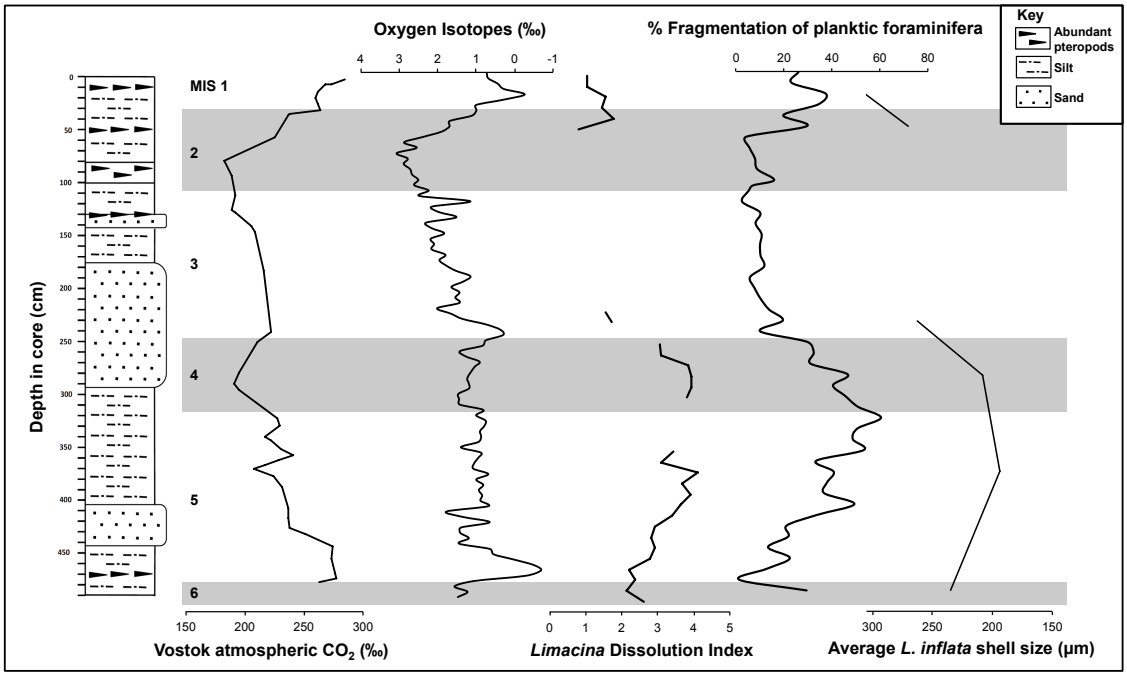

Figure 5. Lithology, Vostok atmospheric CO_2, oxygen isotope profile, *Limacina* Dissolution Index profile and percentage fragmentation of planktonic foraminifera (150-500 µm fraction) for B5-1.

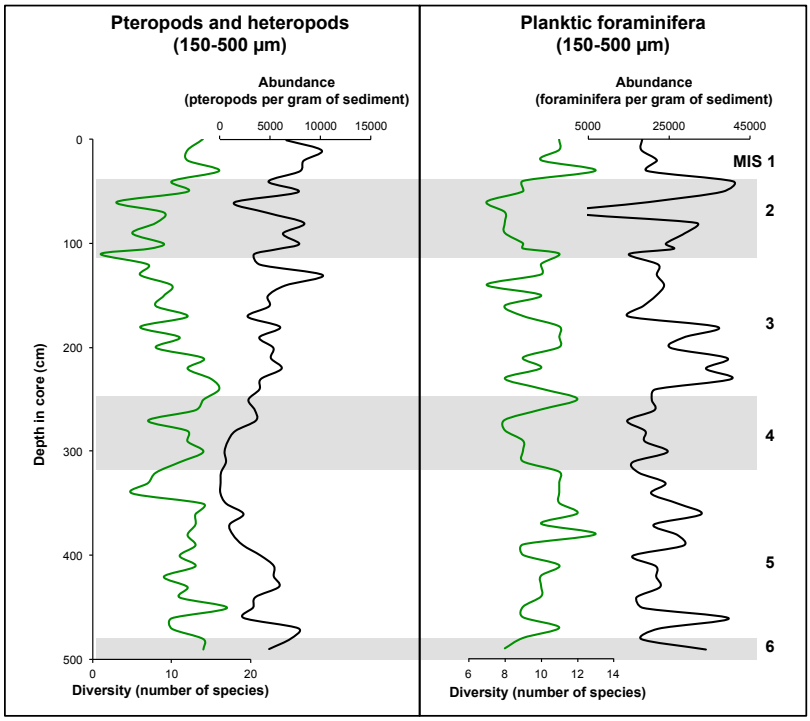

Figure 6. Abundance and diversity of planktonic foraminifera, pteropods and heteropods throughout B5-1 compared to the oxygen isotope record and marine isotope stages.

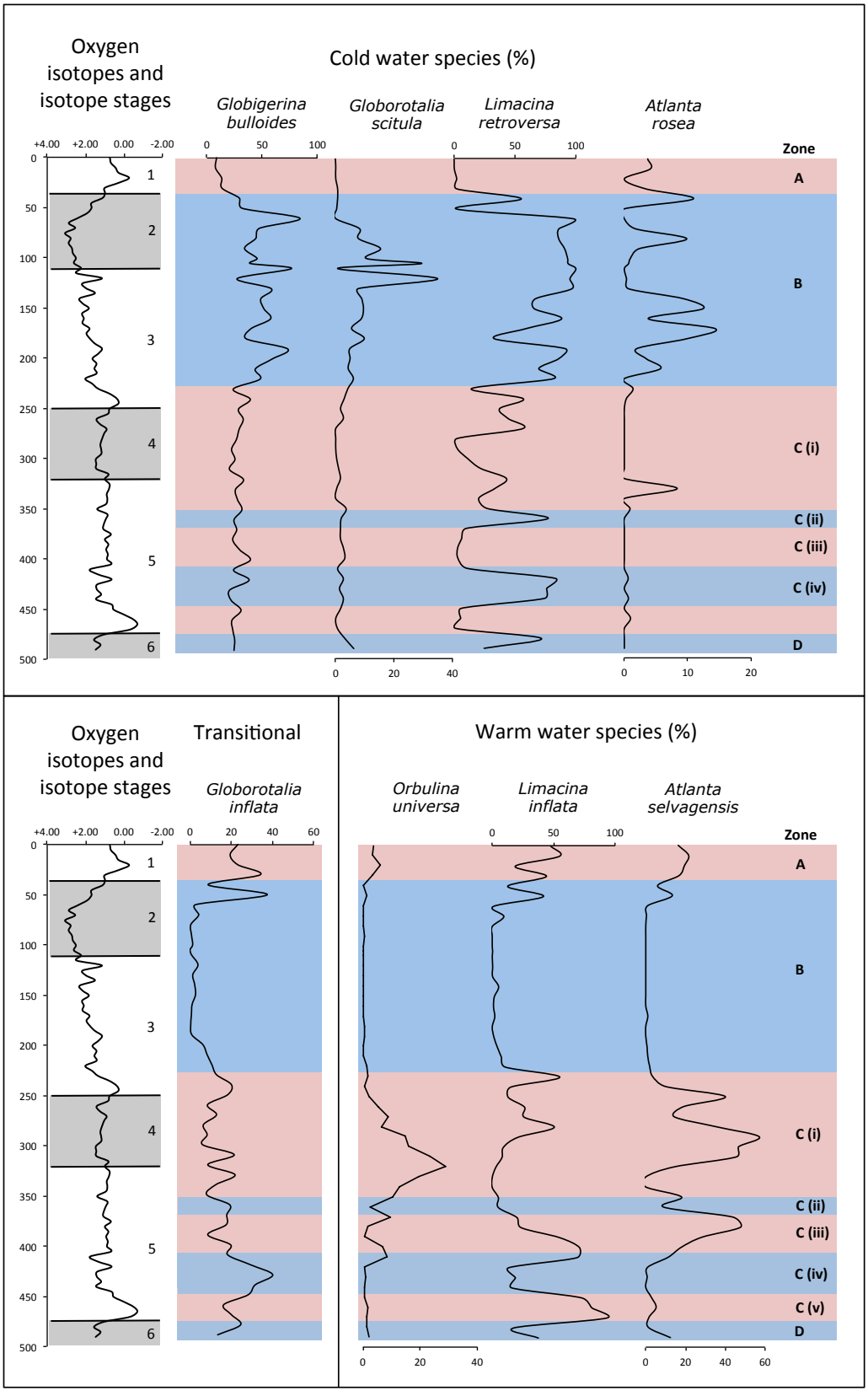

Figure 7. Percentages of indicative warm and cold water species (150-500 µm) throughout B5-1 compared to the oxygen isotope record and Marine Isotope Stages.

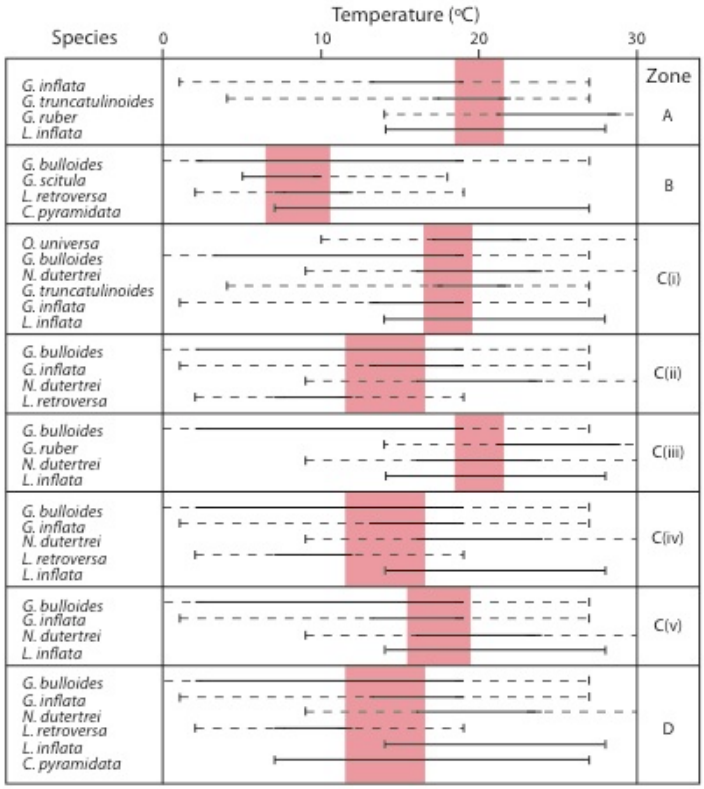

Figure 8. Temperature reconstruction for the zones described in Figure 7 based on dominant indicative species for each zone. Solid lines represent optimal temperatures, dashed line represent total temperature ranges and red boxes represent reconstructed sea surface temperature ranges. Species temperature data from Bé and Gilmer (1977) and Bé and Tolderlund (1971).

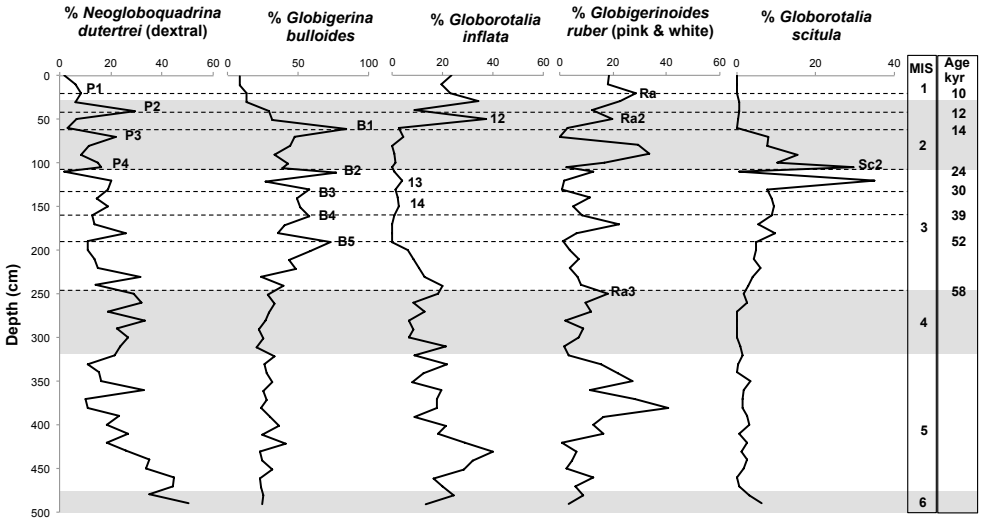

Figure 9. Bio-events of Pujol and Vergnaud-Grazzini (1989) and Pérez-Folgado *et al.* (2003) identified within B5-1 planktonic foraminifera data (150-500 μm).

PTEROPODA	**HETEROPODA**
Cavolinia inflexa (Lesueur, 1813) *Clio pyramidata* Linnaeus, 1767 *Clio cuspidata* (Bosc, 1802) *Clio* sp. C *Creseis acicula* (Rang, 1828) *Creseis virgula* Rang, 1828 *Creseis virgula* (Rang, 1828) *constricta* (Chen and Bé) *Creseis* sp. A *Cuvierina columnella* (Rang, 1827) *Diacria trispinosa* (de Blainville, 1827) *Limacina bulimoides* (d'Orbigny, 1836) *Limacina inflata* (d'Orbigny, 1836) *Limacina retroversa* (Fleming, 1823) *Limacina trochiformis* (d'Orbigny, 1836) *Limacina* sp. A *Limacina* sp. B *Styliola subula* (Quoy and Gaimard, 1827) *Peraclis* spp. *Paedoclione doliiformis* Danforth, 1907	*Atlanta helicinoidea* Gray, 1850 *Atlanta peronii* Lesueur, 1817 *Atlanta rosea* Gray, 1850 *Atlanta selvagensis* de Vera & Seapy, 2006 *Atlanta* sp. A *Atlanta* sp. B *Atlanta* sp. C *Carinaria lamarckii* Blainville, 1817 *Firoloida desmarestia* Lesueur, 1817 *Oxygyrus keraudreni* (Lesueur, 1817) *Pterotrachea* sp. A *Pterotrachea* sp. B *Pterotrachea* sp. C *Pterotrachea* sp. D *Carinariidae* spp. Heteropod sp. A
GLOBIGERINIDA (PLANKTIC FORAMINIFERA)	
Beella digitata (Brady, 1879) *Candeina nitida* d'Orbigny, 1839 *Globigerina bulloides* d'Orbigny, 1826 *Globigerina cariacoensis* Rögl & Bolli, 1973 *Globigerinella aequilateralis* (Brady, 1879) *Globigerinella calida* (Parker, 1962) *Globigerinita glutinata* (Egger, 1893) *Globigerinoides elongatus* (d'Orbigny, 1839) *Globigerinoides pyramidalis* Jones, 1994 *Globigerinoides ruber* (d'Orbigny, 1839) *Globigerinoides sacculifer* (Brady, 1877)	*Globigerinoides trilobus* (Reuss) *Globorotalia crassaformis* (Galloway & Wissler, 1927) *Globorotalia inflata* (d'Orbigny, 1839) *Globorotalia scitula* (Brady, 1882) *Globorotalia truncatulinoides* (d'Orbigny, 1839) *Globorotaloides hexagona* (Natland, 1938) *Hastigerina pelagica* (d'Orbigny, 1839) *Neogloboquadrina dutertrei* (d'Orbigny, 1839) *Orbulina universa* d'Orbigny, 1839 *Turborotalia humilis* (Brady, 1884)

Table 1. Species of thecosome pteropod, heteropod and planktonic foraminifera identified from both size fractions (>500 μm and 150-500 μm) of sediment for the entire core B5-1.

Shelled pteropod species of the Mediterranean Sea	Occurrence in B5-1 surface 1 cm
Cavolinia gibbosa	Absent
Cavolinia inflexa	Absent
Cavolinia longirostris	Absent
Cavolinia tridentata	Absent
Clio cuspidata	Absent
Clio pyramidata	**Present**
Creseis acicula	**Present**
Creseis virgula	**Present**
Cuvierina columnella	Absent
Diacria quadridentata	Absent
Diacria trispinosa	Absent
Hyalocylis striata	Absent
Limacina bulimoides	**Present**
Limacina inflata	**Abundant**
Limacina lesueuri	Absent
Limacina trochiformis	**Common**
Styliola subula	**Present**

Table 2. Summary of pteropod species found in the modern Mediterranean Sea, from Bé and Gilmer (1977) and those found in the surface (0-1 cm) sediments of B5-1 (Present <5%; Common 5-20%; Abundant >20%).

Shelled heteropod species of the Mediterranean Sea	Occurrence in B5-1 surface 1 cm
Atlanta fusca	Absent
Atlanta lesueuri	Absent
Atlanta peronii	**Present**
Carinaria lamarcki	Absent
Firoloida desmaresti	**Common**
Oxygyrus keraudreni	**Present**
Pterotrachea spp.	Absent

Table 3. Summary of calcareous heteropod species found in the modern Mediterranean Sea, from Thiriot-Quiévreux (1973) and those found in the surface (0-1 cm) sediments of B5-1 (Present <5%; Common 5-20%; Abundant >20%).

Planktic Foraminifera species of the Mediterranean Sea	Occurrence in B5-1 surface 1 cm
Globigerina bulloides	**Common**
Globigerina falconensis	Absent
Globigerina rubescens	Absent
Globigerinella aequilateralis	**Present**
Globigerinita glutinata	Absent
Globigerinoides conglobatus	Absent
Globigerinoides ruber	**Abundant**
Globigerinoides sacculifer	**Common**
Globorotalia crassaformis	**Present**
Globorotalia hirsuta	Absent
Globorotalia inflata	**Abundant**
Globorotalia truncatulinoides	**Abundant**
Hastigerina pelagica	Absent
Neogloboquadrina dutertrei	**Present**
Neogloboquadrina pachyderma	Absent
Orbulina universa	**Abundant**
Pulleniatina obliquiloculata	Absent

Table 4. Summary of planktonic foraminifera species found in the modern Mediterranean Sea, from Bé (1977) and those found in the surface (0-1 cm) sediments of B5-1 (Present <5%; Common 5-20%; Abundant >20%).

Wall-Palmer, D., Hart, M.B., Smart, C.W., Sparks, R.S.J., Le Friant, A., Boudon, G., Deplus, C., Komorowski, J.C., 2012. Pteropods from the Caribbean Sea: variations in calcification as an indicator of past ocean carbonate saturation. *Biogeosciences,* **9,** 309-315.

Biogeosciences, 9, 1–7, 2012
www.biogeosciences.net/9/1/2012/
doi:10.5194/bg-9-1-2012

Biogeosciences

Pteropods from the Caribbean Sea: variations in calcification as an indicator of past ocean carbonate saturation

D. Wall-Palmer[1], M. B. Hart[1,*], C. W. Smart[1], R. S. J. Sparks[2], A. Le Friant[3], G. Boudon[3], C. Deplus[3], and J. C. Komorowski[3]

[1]School of Geography, Earth & Environmental Sciences, Plymouth University, Drake Circus, Plymouth PL4 8AA, UK
[2]Department of Earth Sciences, University of Bristol, Wills Memorial Building, Queens Road, Bristol BS8 1RJ, UK
[3]Institute du Physique du Globe de Paris, Case 89, 1 rue Jussieu, 75238 Paris cedex 05, France
[*]*Invited contribution by M. B. Hart, recipient of the EGU Jean Baptiste Lamarck Medal 2011.*

Correspondence to: D. Wall-Palmer (deborah.wall-palmer@plymouth.ac.uk)

Received: 24 June 2011 – Published in Biogeosciences Discuss.: 13 July 2011
Revised: 21 December 2011 – Accepted: 27 December 2011 – Published:

Abstract. The aragonite shell-bearing thecosome pteropods are an important component of the oceanic plankton. However, with increasing pCO_2 and the associated reduction in oceanic pH (ocean acidification), thecosome pteropods are thought to be particularly vulnerable to shell dissolution. The distribution and preservation of pteropods over the last 250 000 years have been investigated in marine sediment cores from the Caribbean Sea close to the island of Montserrat. Using the *Limacina* Dissolution Index (LDX), fluctuations in pteropod calcification through the most recent glacial/interglacial cycles are documented. By comparison to the oxygen isotope record (global ice volume), we show that pteropod calcification is closely linked to global changes in pCO_2 and pH and is, therefore, a global signal. These data are in agreement with the findings of experiments upon living pteropods, which show that variations in pH can greatly affect aragonitic shells. The results of this study provide information which may be useful in the prediction of future changes to the pteropod assemblage caused by ocean acidification.

1 Introduction

The faunal responses to ocean acidification (the reduced availability of carbonate ions) are still largely unknown, although experimental evidence reveals that a reduction in pH typically leads to a decrease in calcification rates of a number of, but not all organisms (Feely et al., 2004; Orr et al., 2005; Guinotte and Fabry, 2008; Turley et al., 2010). To date, little information is available about important planktic producers of calcium carbonate. Several studies have investigated coccolithophore and planktic foraminiferal responses, but only three species of the aragonite-producing thecosome pteropods have been considered (Fabry et al., 2008; Comeau et al., 2009, 2010a, b). Here we demonstrate a relationship between the calcification of pteropod shells and past atmospheric CO_2 concentrations through the last 250 000 years by using low resolution Vostok CO_2 data and the high resolution oxygen isotope record. A diverse and abundant assemblage of pteropods and heteropods is recorded from marine cores collected from the Caribbean Sea offshore Montserrat. A number of these cores contain intervals of well-preserved pteropods which are associated with the glacial periods of the Late Pleistocene (Messenger et al., 2010). These well-preserved levels appear to be of widespread significance and a response to global climate change.

The group of holoplanktic molluscs known as the Pteropoda consists of two orders; the shell-less gymnosomes and the shell-bearing thecosomes (Fig. 1). These two orders are now considered to be less closely related than originally thought, but the term "pteropod" is still widely used (van der Spoel, 1976; Bé and Gilmer, 1977; Lalli and Gilmer, 1989). Thecosome pteropods are a common component of the water column throughout the world's oceans and can reach densities of up to 10 000 individuals per cubic metre (The Royal Society, 2005; Fabry et al., 2008). They are consequently important prey to a number of large cetaceans and commercial fish (The Royal Society, 2005). This study focuses on the species *Limacina inflata*, a common euthecosome (suborder of thecosomata) pteropod.

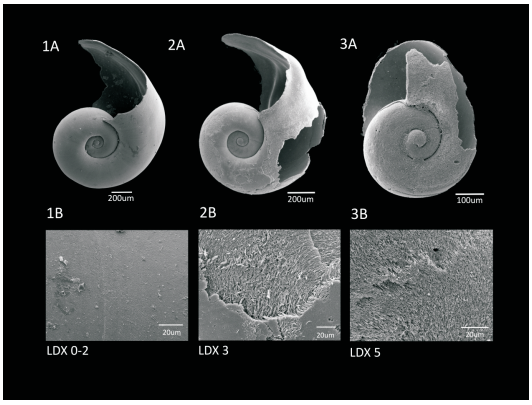

Fig. 1. Thecosome pteropod *Limacina inflata* from the Caribbean Sea near Montserrat at different stages of shell calcification.

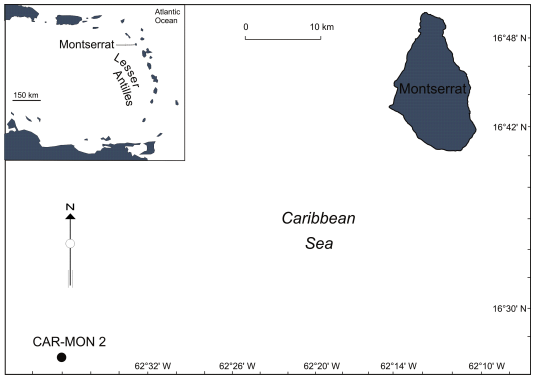

Fig. 2. Map of the Lesser Antilles showing the island of Montserrat and the location of core CAR–MON 2. A full bathymetric map of the area is available in Le Friant et al. (2004).

All euthecosome pteropods produce calcareous shells from aragonite, a polymorph of calcium carbonate, which is particularly susceptible to dissolution (50 % more susceptible than calcite): see Mucci (1983), Millero (1996), Morse and Arvidson (2002) and Klöcker et al. (2006). This makes their shells extremely vulnerable to the effects of ocean acidification, making it more difficult for them to grow and maintain their shells. It also means that, upon death, their shells frequently dissolve as they settle through the water column to the sea floor. This limits their occurrence in sediments to water depths of less than 3000 m and also restricts their presence in the geological record (Curry, 1971; Herman, 1971; Berner, 1977). The distribution of the modern fauna is well known (Bé and Gilmer, 1977) and "pteropod oozes" have been recognised for over one hundred years (Murray and Renard, 1891). With current increasing levels of atmospheric CO_2 and the resulting ocean acidification (Orr et al., 2005; The Royal Society, 2005), pteropods with their aragonitic shells are the subject of renewed interest, since they are likely to be the most vulnerable of the major planktic producers of $CaCO_3$. They are also likely to be the first planktic fauna to experience persistent decreased $CaCO_3$ saturation states. As an important part of the food web, especially in the Arctic and Southern Oceans, their potential demise is of great significance.

2 Marine sediment cores from Montserrat

In March 2002, as part of a multi-disciplinary project on the volcanic activity on the island of Montserrat, the R/V *L'Atalante* recovered a series of piston-cores from the ocean floor surrounding the island (Fig. 2). Of the 12 cores collected on the "Caraval Cruise", CAR-MON 2 provides the longest time record (Le Friant et al., 2008 document in detail the collection techniques and subsequent methodologies employed). The site of CAR-MON 2, in 1102 m of water, is located at 16°27.699′N, 62°38.077′W. The oxygen isotope (δ^{18}O) profile of CAR-MON 2 (Fig. 3) gives an accurate record of the Marine Isotope Stages (MIS) back ∼250 000 years BP and the record compares well with other studies (Imbrie et al., 1984; Prell et al., 1986). This δ^{18}O profile has been verified using a limited number of AMS radiocarbon dates and ^{39}Ar/^{40}Ar radiometric dates (Le Friant et al., 2008). Using the >150 μm size fraction, counts of the planktic foraminifera have allowed the determination of the *Globorotalia menardii* zonation (Ericson and Wollin, 1956; Reid et al., 1996; Le Friant et al., 2008).

Reduced calcification of *Limacina inflata* shells has been quantified throughout CAR-MON 2 using the scale published by Gerhardt and Henrich (2001). As the *Limacina* Dissolution Index (LDX) has only been used by a limited number of workers (e.g., Klöcker et al., 2006) on "fossil" material, its calculation is now described.

Pre-processed and dried sediment (Le Friant et al., 2008) was used to collect just over 300 (or as many as were present) pteropod specimens from two size fractions (>500 μm and 150–500 μm) at varying intervals. Only whole specimens that retained their protoconch and protoconch fragments were counted. Determination of the calcification of the pteropod shells was made using the *Limacina* Dissolution Index (LDX) which was devised by Gerhardt et al. (2000) and published as a scale by Gerhardt and Henrich (2001). This method involves the semi-quantitative analysis of the surface of the pteropod shell on a scale of 0 to 5; 0 being a pristine, transparent, lustrous shell with a smooth surface and 5 being an opaque, white and completely lustreless shell with additional damage. At least 10 shells (max 30 shells) of adult *Limacina inflata* of a size of 300 μm or larger were allocated a value from this scale by the use of light microscopy for each

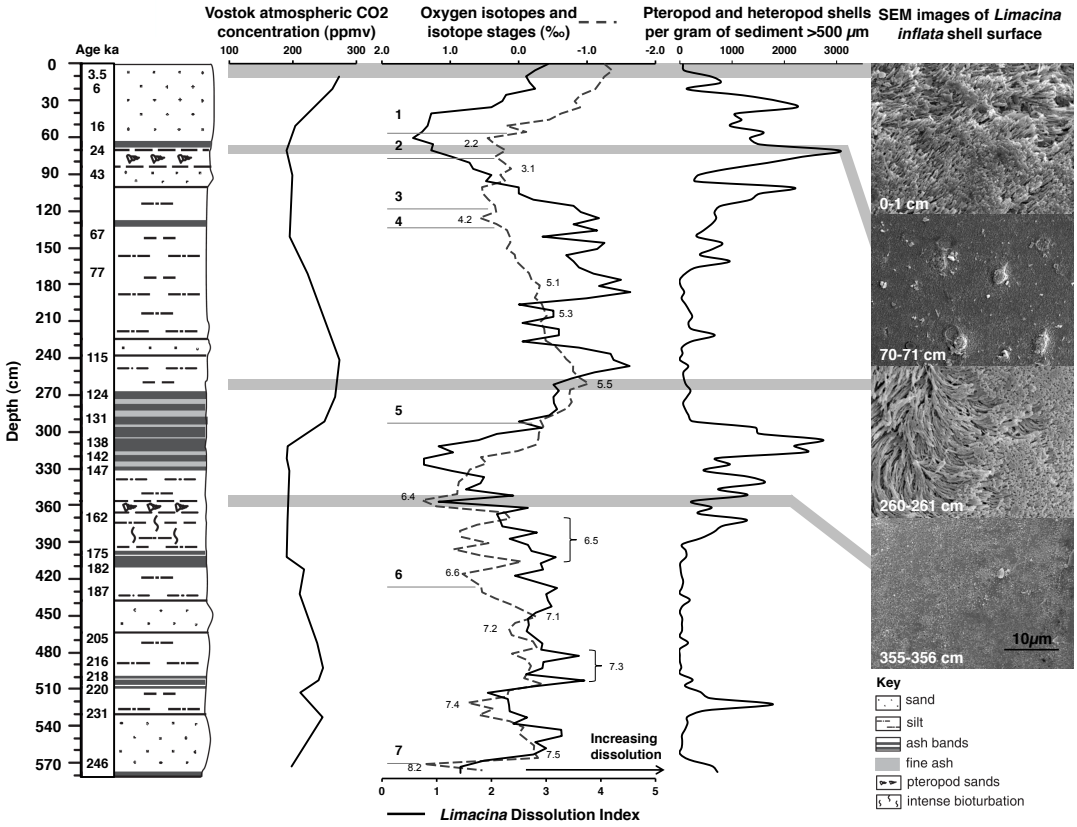

Fig. 3. Sedimentary log for core CAR–MON 2 including age model (from oxygen isotope stratigraphy) from Le Friant et al. (2008), Vostok atmospheric CO_2 concentrations, stable isotope stratigraphy (Marine Isotope Stages), pteropod calcification (LDX) and abundance of $>500\,\mu$m pteropod and heteropod shells: partly modified after Le Friant et al. (2008).

sample. The average for each sample was then calculated to provide the LDX value.

3 Pteropod calcification record

CAR-MON 2 records three levels of particularly well preserved, abundant and diverse pteropods (Fig. 3), two of which have been documented previously (Le Friant et al., 2008; Messenger et al., 2010) but not studied in detail. The upper concentration of pteropods is found in MIS 2 and has been dated at around 25 000 years BP (55–80 cm), with a peak in pteropod preservation at MIS 2.2 (∼20 000 years BP). The middle concentration of pteropods is within MIS 6 (295–425 cm) with a peak in preservation at MIS 6.4, dated at about 150 000 years BP and the lower concentration is found within MIS 8 at the very base of the core (565–575 cm), with a peak in preservation at MIS 8.2. The upper concentration of pteropods corresponds almost exactly with the "pteropod sands" reported by Chen (1968) from the Gulf of Mexico, Venezuela Basin and other occurrences in the Caribbean Sea, Mediterranean Sea and Red Sea. Chen (1968) suggests that their widespread occurrence was controlled by Late Pleistocene climate changes.

This latest Pleistocene occurrence of abundant pteropods has also been recorded in the Andaman Sea (Sijinkumar et al., 2010), in the Red Sea (Almogi-Labin et al., 1991), off-shore Florida (Gardulski et al., 1990), on the western flank of the Great Bahama Bank (Eberli et al., 1997; Messenger et al., 2010), on the Brazilian Slope (Gerhardt et al., 2000), in the Caribbean Sea (Haddad and Droxler, 1996), off-shore Somalia (Klöcker and Henrich, 2006; Klöcker et al., 2006) and in the South China Sea (Wang et al., 1997). In the cores from the South China Sea and the Caribbean Sea, the concentrations at ∼20 000 years BP and 150 000 years BP are both recorded, clearly demonstrating that this enhanced

preservation of aragonitic fossils is of global significance and not the result of local variations in water chemistry (Peterson and Cofer-Shabica, 1987; Peterson, 1990, Broecker and Clark, 2002; Sepulcre et al., 2009). Elsewhere in the CAR-MON 2 core, reduced shell calcification occurs during interglacial periods and is particularly poor during extreme stages, such as at MIS 5.5. In the Gulf of Aden (Core KL15), Almogi-Labin et al. (2000) record the near absence of pteropods during interglacials (MIS 13, 11, 9, 7, 5 and 1). The record from this core shows that pteropod maxima appear to be at the glacial/interglacial terminations (especially the MIS 6 to MIS 5 transition). Such deglaciation "spikes" have also been noted by Frenzel (1975) and Berger (1977, 1990). Berger (1977) describes this world-wide phenomenon as a pteropod-rich layer present at the end of the last glacial, although, the exact timing and cause of this event are in some dispute. Serre-Bachet and Guiot (1987) also linked pteropod preservation to colder periods. This link is particularly striking in the post–MIS 2 records in the N.E. Atlantic Ocean (Ganssen et al., 1991), Equatorial Atlantic Ocean (Kassens and Sarntheim, 1989) and the N.W. Indian Ocean (Klöcker et al., 2006). This preservation relationship to colder periods is, almost certainly, due to fluctuations in pCO_2 causing higher pH and increased availability of carbonate during glaciations (Sanyal et al., 1995; Ruddiman, 2001; Hönisch and Hemming, 2005; Yu et al., 2007) and lower pH and reduced availability of carbonate during interglacials. In the CAR-MON 2 data there are some unexpected excursions from the general trend, which show that variations in calcification are not directly proportional to the $\delta^{18}O$ signal. This can be seen particularly between MIS 5.1 and 5.5, where changes in calcification appear to be accentuated.

Several factors during the sedimentation process, which are summarised in Fig. 4, may have influenced the LDX calcification profile. The pattern produced by the LDX profile could not, however, be an artefact of sea floor dissolution and diagenesis. If pteropods within CAR-MON 2 showed a general trend from LDX 0–2 in the near–surface sediments to LDX 4–5 at depth, this would clearly be a diagenetic signal, however, this is not the case. Klöcker et al. (2006) have also noted that, in their core 905 from the N.W. Indian Ocean, diagenesis has had minimal effect on the LDX record. The correlation of pteropod abundances in MIS 2 and MIS 6 across a range of oceans and environments also implies that the LDX profile is caused by global atmospheric CO_2 fluctuations and not merely by variations in local water chemistry.

Water chemistry around the Lesser Antilles island arc is however, complicated by influences of several water masses flowing between the islands and through a number of deeper passages into the Caribbean Sea (Peterson and Cofer-Shabica, 1987; Peterson, 1990, Broecker and Clark, 2002; Sepulcre et al., 2009). Gerhardt and Henrich (2001) found that the influence of Antarctic Intermediate Water (AAIW), towards the south of the island arc, caused moderate to very poor preservation of *Limacina inflata*. However,

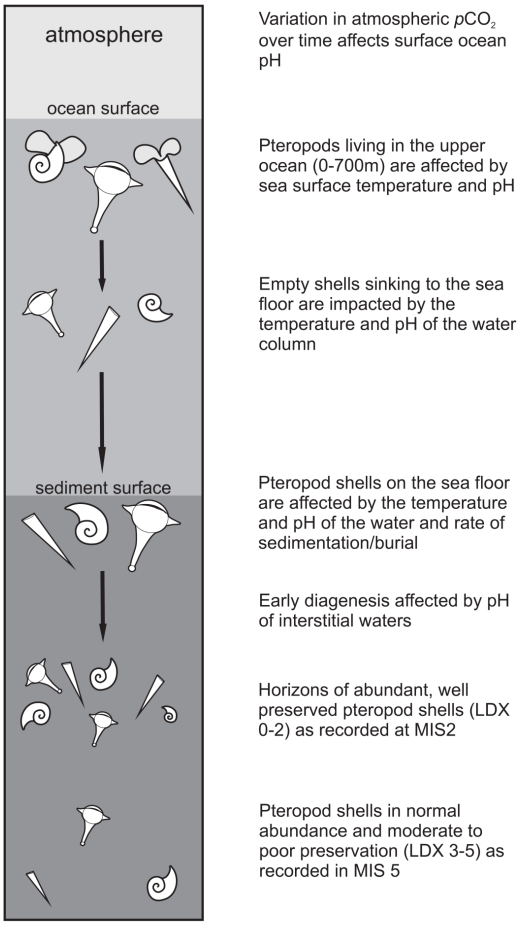

Fig. 4. Conceptualization of pteropod sedimentation, taphonomy and preservation for areas of the sea floor above the aragonite lysocline and aragonite compensation depth. Preservation of pteropod shells is, potentially, impacted by water chemistry during life, passage through the water column (probably minimal as they have quite high settling rates of 1–2.5 cm s^{-1}; see Byrne et al., 1984), on the water/sediment surface and during burial.

towards the north of the island arc, the influence of AAIW is minor due to a large volume of Upper North Atlantic Deep Water (UNADW), which flows through the nearby Anegada Passage. This area consequently shows very good preservation of *Limacina inflata*. Gerhardt and Henrich (2001) place the aragonite saturation depth at 2000 m and the Aragonite Compensation Depth (ACD) at 3800 m water depth in this area. CAR–MON 2 was collected in 1102 m water depth, which is above the aragonite lysocline and ACD, thus discounting any effects that this may cause. It is

Comeau, S., Jeffree, R., Teyssié, J.-L., and Gattuso, J.-P.: Response of the Arctic Pteropod Limacina helicina to Projected Future Environmental Conditions, PLoS ONE, 5, e11362. doi:10.1371/journal.pone.0011362, 2010a.

Comeau, S., Gorsky, G., Alliouane, S., and Gattuso, J.-P.: Larvae of the pteropod *Cavolinia inflexa* exposed to aragonite undersaturation are viable but shell-less, Mar. Biol., 157, 2341–2345, 2010b.

Curry, D.: The occurrence of pre-Quaternary pteropods, in: The Micropalaeontology of Oceans, edited by: Funnell, B. M. and Reidel, W. R., Cambridge University Press, Cambridge, 595, 1971.

de Moel, H., Ganssen, G. M., Peeters, F. J. C., Jung, S. J. A., Kroon, D., Brummer, G. J. A., and Zeebe, R. E.: Planktic foraminiferal shell thinning in the Arabian Sea due to anthropogenic ocean acidification?, Biogeosciences, 6, 1917–1925, doi:10.5194/bg-6-1917-2009, 2009.

Eberli, G. P., Swart, P. K., Malone, M. J., Anselmetti, F. S., Arai, K., Bernet, K. H., Betzler, C., Christensen, B. A., De Carlo, E. H., Déjardin, P. M., Emmanuel, L., Frank, T. D., Haddad, G. A., Isern, A. R., Katz, M. E., Kenter, J. A. M., Kramer, P. A., Kroon, D., McKenzie, J. A., McNeill, D. F., Montgomery, P., Nagihara, S., Pirmez, C., Reijmer, J. J. G., Sato, T., Schovsbo, N. H., Williams, T., and Wright, J. D.: Site 1003, Proceedings of the Ocean Drilling Program, Initial Reports, College Station, Texas (Ocean Drilling Program), 166, 71–116, 1997.

Ericson, D. B. and Wollin, G.: Micropaleontological and isotopic determination of Pleistocene climates, Micropaleontology, 2, 257–270, 1956.

Fabry, V. J., Seibel, B. A., Feely, R. A., and Orr, J. C.: Impacts of ocean acidification on fauna and ecosystem processes, ICES J. Mar. Sci., 65, 414–432, 2008.

Feely, R. A., Sabine, C. L., Lee, K., Berelson, W., Kleypas, J., Fabry, V. J., and Millero, F. J.: Impact of anthropogenic CO_2 on the $CaCO_3$ system in the oceans, Science, 305, 362–366, doi:10.1126/science.1097329, 2004.

Frenzel, B.: The distribution pattern of Holocene climatic change in the Northern Hemisphere, in: Proceedings of the WMO/IAMAP Symposium on Long–Term Climatic Fluctuations, Geneva, convenor: Lamb, H., World Meteorological Organization, 105–118, 1975.

Ganssen, G. M., Troelstra, S. R., Van Der Borg, K., and De Jong, A. M. F.: Late Quaternary pteropod preservation in Eastern North Atlantic sediments in relation to climate change, Radiocarbon, 33, 277–282, 1991.

Gardulski, A. F., Mullins, H. T., and Weiterman, S.: Carbonate mineral cycles generated by foraminiferal and pteropods response to Pleistocene climate: west Florida ramp slope, Sedimentology, 37, 727–743, 1990.

Gerhardt, S. and Henrich, R.: Shell preservation of *Limacina inflata* (Pteropoda) in surface sediments from the Central and South Atlantic Ocean: a new proxy to determine the aragonite saturation state of water masses, Deep-Sea Res. I, 48, 2051–2071, 2001.

Gerhardt, S., Groth, H., Rühlemann, C., and Henrich, R.: Aragonite preservation in late Quaternary sediment cores on the Brazilian Continental Slope: implications for intermediate water circulation, Int. J. Earth Sci., 88, 607–618, 2000.

Guinotte, J. M. and Fabry, V. J.: Ocean acidification and its potential effects on marine ecosystems, New York Academy of Sciences, 1134, 320–342, 2008.

Haddad, G. A. and Droxler, A. W.: Metastable $CaCO_3$ dissolution at intermediate water depths of the Caribbean and western North Atlantic: implications for intermediate water circulation during the past 200,000 years, Paleoceanography, 11, 701–716, 1996.

Herman, Y.: Vertical and horizontal distribution of pteropods in Quaternary sequences, in: The Micropalaeontology of Oceans, edited by: Funnell, B. M. and Reidel, W. R., Cambridge University Press, Cambridge, 463–486, 1971.

Hönish, B. and Hemming, N. G.: Surface ocean pH response to variation in pCO2 through two full glacial cycles, Earth Planet. Sc. Lett., 239, 305–314, doi:10.1016/j.epsl.2005.04.027, 2005.

Imbrie, J., Hays, J. D., Martinson, D. G., McIntyre, A., and Mix, A. C.: The orbital theory of Pleistocene climate: support from a revised chronology of the marine $\delta^{18}O$ record, in: Milankovitch and Climate, edited by: Berger, A. L., Imbrie, J., Hays, J. D., Kukla, G., and Saltzmann, B., Part 1, Reidel, Hingham, MA, 269–305, 1984.

Jones, M. T. and Gislason, S. R.: Rapid releases of metal salts and nutrients following the deposition of volcanic ash into aqueous environments, Geochim. Cosmochim. Ac., 72, 3661–3680, 2008.

Jones, M. T., Fisher, J. K., and Palmer, M. R.: Ocean acidification from explosive volcanism as a cause of mass mortality of pteropods, Geochim. Cosmochim. Ac., 73, Supplement 1, A604, 2009.

Kassens, H. and Sarnthein, M.: A link between paleoceanography, early diagenetic cementation and shear strength maxima in Late Quaternary sediments, Paleoceanography, 4, 253–269, 1989.

Klöcker, R. and Henrich, R.: Recent and Late Quaternary pteropod preservation on the Pakistan shelf and continental slope, Marine Geology, 231, 103–111, 2006.

Klöcker, R., Ganssen, G., Jung, S. J. A., Kroon, D., and Henrich, R.: Late Quaternary millennial-scale variability in pelagic aragonite preservation off Somalia, Mar. Micropaleontol., 59, 171–183, 2006.

Lalli, C. M. and Gilmer, R. W.: Pelagic Snails: The biology of holoplanktonic gastropod molluscs, Stanford University Press, California, 1989.

Le Friant, A., Lock, E. J., Hart, M. B., Boudon, G., Sparks, R. S. J., Leng, M. J., Smart, C. W., Komorowski, J. C., Deplus, C., and Fisher, J. K.: Late Pleistocene tephrochronology of marine sediments adjacent to Montserrat, Lesser Antilles volcanic arc, J. Geol. Soc. London, 165, 279–289, 2008.

Messenger, R. W., Hart, M. B., Smart, C. W., Leng, M. J., Lock, E. J., and Howard, A. K.: Pteropod faunas as indicators of Late Pleistocene climate change in the Caribbean Sea, in: Micropalaeontology, Sedimentary Environments and Stratigraphy: A tribute to Dennis Curry (1912–2001), edited by: Whittaker, J. E. and Hart, M. B., The Micropalaeontological Society Special Publications, 17–28, 2010.

Millero, F. J.: Chemical Oceanography, CRC Press, Boca Raton, Florida, USA, 1996.

Morse, J. W. and Arvidson, R. S.: The dissolution kinetics of major sedimentary carbonate minerals, Earth-Sci. Rev., 58, 51–84, 2002.

Moy, A. D., Howard, W. R., Bray, S. G., and Trull, T. W.: Reduced calcification in modern Southern Ocean planktonic foraminifera, Nat. Geosci., 2, 276–280, doi:10.1038/NGEO460, 2009.

Mucci, A.: The solubility of calcite and aragonite in sea water at various salinities, temperatures and one atmosphere total pressure, Am. J. Sci., 283, 780–799, 1983.

also important to note that firstly, no changes in the benthic foraminiferal community were found during our microfossil analysis. This indicates that water masses are unlikely to have changed during the period covered by CAR-MON 2. Secondly, within CAR-MON 2, interglacial periods coincide with a reduced abundance of large (>500 μm) pteropod and heteropod shells (Fig. 3). If the LDX variations seen throughout CAR-MON 2 were due to post-depositional dissolution, a preferential dissolution of small shells would be expected (Lalli and Gilmer, 1989). However, whilst a reduction in the abundance of small shells during interglacial periods was found, there is also a relatively equal reduction in the number of large shells. This suggests a reduction of calcification, rather than an artefact of dissolution. It can therefore be assumed that the variations in pteropod calcification throughout CAR-MON 2 reflect carbonate availability in the surface ocean. A possible interference in the calcification profile may be caused by inputs of volcanic ash, which can reduce the oceanic pH in the local area dramatically during and just after an eruption. A recent study has shown that, under laboratory conditions, volcanic materials entering sea water produce a significant reduction in pH (Jones and Gislason, 2008), reducing the availability of carbonate. This local impact on the pteropod fauna has been investigated and described elsewhere (Jones et al., 2009; Wall-Palmer et al., 2011). However, our observations suggest that, in this case, the ash from the South Soufrière Hills volcano has had little or no effect upon the overall LDX profile. This is because the ash found within CAR-MON 2 is the result of several relatively short-lived events rather than one large, long–lasting event. Ash from these individual eruptions would have been so greatly diluted upon entering the ocean, that the acidic impact upon surface water fauna would have been insignificant. The assumption that the LDX profile is the result of changing carbonate availability is in agreement with recent laboratory work on living pteropods (Fabry et al., 2008; Comeau et al., 2009, 2010a, b) and pteropods from sediment traps in the Southern Ocean (Roberts et al., 2008). It also compares favourably with shell-weight data of *Globigerina bulloides* and *Globigerinoides ruber* provided by recent work in the Southern Ocean (Barker and Elderfield, 2002), in the Arabian Sea (Moel et al., 2009) and in the North Atlantic (Moy et al., 2009).

Our results suggest that the distribution and abundance of shelled pteropod and heteropod fauna, and the quality of their calcification through the last 250 000 years, reflect changes caused by climate variations. This signal appears to be worldwide and may help to predict future changes in the aragonitic holoplanktic fauna caused by increases in pCO_2 and the resulting changes in oceanic pH. However, since the level of anthropogenic CO_2 entering the oceans is now increasing at a rate 100 times faster than any changes seen in the past 650 000 years (Fabry et al., 2008), it might be inappropriate to apply such a model to the modern oceans. The fate of the modern-day aragonitic holoplankton is uncertain, however, this study shows that, at oceanic pH levels relatively higher than those predicted for the 21st Century, euthecosome pteropods have been noticeably affected.

Acknowledgements. The authors acknowledge receipt of a Research Grant from The Leverhulme Trust (F/00 568/P to Hart, Smart and Sparks), funding from NERC (NER/A/S2002/00963 to Sparks and Talling) for JR123 cruise to Montserrat in 2005 and funding from NERC to cover stable isotope analysis at the National Isotope Geoscience Laboratory (Keyworth). Some data presented here are part of a PhD (Wall-Palmer) funded by the Plymouth University. The authors wish to thank G. M. Ganssen (The Netherlands) and A. Almogi-Labin (Israel) for their advice on the distribution of pteropods in the Late Pleistocene.

Edited by: G. Herndl

References

Almogi-Labin, A., Hemleben, C., Meischner, D., and Erlenkeuser, H.: Paleoenvironmental events during the last 13,000 years in the Central Red Sea as recorded by Pteropoda, Paleoceanography, 6, 83–98, 1991.

Almogi-Labin, A., Schmiedel, G., Hemleben, C., Siman-Tov, R., Segl, M., and Meischner, D.: The influence of the NE winter monsoon on productivity changes in the Gulf of Aden, NW Arabian Sea, during the last 530 kyr as recorded by foraminifera, Mar. Micropaleontol., 40, 295–319, 2000.

Barker, S. and Elderfield, H.: Foraminiferal calcification response to glacial-interglacial changes in atmospheric CO2, Science, 297, 833–836, 2002.

Bé, A. W. H. and Gilmer, R. W.: A zoogeographic and taxonomic review of *Euthecosomatous Pteropoda*, in: Oceanic Micropaleontology, edited by: Ramsay, A. T. S., Academic Press, New York, Vol.1, 733–808, 1977.

Berger, W. H.: Deep-sea carbonate and the deglaciation preservation spike in pteropods and foraminifera, Nature, 269, 301–303, 1977.

Berger, W. H.: The Younger Dryas cold spell - a search for causes, Global Planet. Change, 89, 219–237, 1990.

Berner, R. A.: Sedimentation and dissolution of pteropods in the ocean, in: The fate of fossil fuel CO2 in the oceans, edited by: Anderson, N. R. and Malahoff, A., Plenus Press, New York, 243–260, 1977.

Broecker, W. S. and Clark, E.: Carbonate ion concentration in glacial-age deep waters of the Caribbean Sea, Geochem. Geophy. Geosy., 3, 1–14, doi:2001GC000231, 2002.

Byrne, R. H., Acker, J. G., Betzer, P. R., Feely, R. A., and Cates, M. H.: Water column dissolution of aragonite in the Pacific Ocean, Nature, 312, 321–326, 1984.

Chen, C.: Pleistocene pteropods in pelagic sediments, Nature, 219, 1145–1149, 1968.

Comeau, S., Gorsky, G., Jeffree, R., Teyssié, J.-L., and Gattuso, J.-P.: Impact of ocean acidification on a key Arctic pelagic mollusc (Limacina helicina), Biogeosciences, 6, 1877–1882, doi:10.5194/bg-6-1877-2009, 2009.

Murray, J. and Renard, A. F.: Deep-sea deposits, Scientific Report of the Challenger Expedition, 1873–1876, 1891.

Orr, J. C., Fabry, V. J., Aumont, O., Bopp, L., Feely, R. A., Gnanadesikan, A., Gruber, N., Ishida, A., Joos, F., Key, R. M., Lindsay, K., Maier-Reimer, E., Matear, R., Monfray, P., Mouchet, A., Najjar, R. G., Plattner, G.-K., Rodgers, K. B., Sabine, C. L., Sarmiento, J. L., Schlitzer, R., Slater, R. D., Totterdell, I. J., Weirig, M.-F., Yamanaka, Y., and Yool, A.: Anthropogenic ocean acidification over the twenty-first century and its impact on calcifying organisms, Nature, 437, 681–686, 2005.

Peterson, L. C.: Late Quaternary paleoceanography of the mid-depth Atlantic: Proxy records from the deep Caribbean Sea, Eos Trans. AGU, 71, 1382–1383, 1990.

Peterson, L. C. and Cofer-Shabica, N. B.: Bruhes Cron records of sedimentation and abyssal paleocirculation in the Venezuela Basin, eastern Caribbean sea, GSA, Abstracts with Programs, 19, 804, 1987.

Petit, J. R., Jouzel, J., Raynaud, D., Barkov, N. I., Barnola, J.-M., Basile, I., Benders, M., Chappellaz, J., Davis, M., Delaygue, G., Delmotte, M., Kotlyakov, V. M., Legrand, M., Lipenkov, V. Y., Lorius, C., Pépin, L., Ritz, C., Saltzman, E., and Stievenard, M.: Climate and atmospheric history of the past 420,000 years from the Vostok ice core, Antarctica, Nature, 399, 429–436, 1999.

Prell, W. L., Imbrie, J., Martinson, D. G., Morley, J. J., Pisias, N. G., Shackleton, N. J., and Streeter, H. F.: Graphic correlation of oxygen isotope stratigraphy application to the Late Quaternary, Paleoceanography, 1, 137–162, 1986.

Reid, R. P., Carey, S. N., and Ross, D. R.: Late Quaternary sedimentation in the Lesser Antilles island arc, Geol. Soc. Am. Bull., 108, 78–100, 1996.

Ruddiman, W. F.: Earth's climate past and future, W. H.Freeman & Company, New York, 465 pp., 2001.

Roberts, D., Howard, W. R., Moy, A. D., Roberts, J. L., Trull, T. W., Bray, S. G., and Hopcroft, R. R.: Interannual variability of pteropod shell weights in the high-CO_2 Southern Ocean, Biogeosciences Discuss., 5, 4453–4480, doi:10.5194/bgd-5-4453-2008, 2008.

Sanyal, A., Hemming, N. G., Hanson, G. N., and Broecker, W. S.: Evidence for a higher pH in the glacial ocean from boron isotopes in foraminifera, Nature, 373, 234–236, 1995.

Sepulcre, S., Tachikawa, K., Vidal, L., Thouveny, N., and Bard, E.: Preservation state of metastable magnesian calcite in periplatform sediments from the Caribbean Sea over the last million years, Geochem. Geophy. Geosy., 10, Q11013, doi:10.1029/2009gc002779, 2009.

Serre-Bachet, F., and Guiot, J.: Summer temperature changes from tree-rings in the Mediterranean area during the last 800 years, in: Abrupt Climate Change, edited by: Berger, W. H. and Labeyrie, L. D., D. Reidel, Dordrecht, Netherlands, 89–97, 1987.

Sijinkumar, A. V., Nagender Nath, B., and Guptha, M. V. S.: Late Quaternary record of pteropod preservation from the Andaman Sea, Mar. Geol., 275, 221–229, 2010.

The Royal Society: Ocean Acidification Due to Increasing Atmospheric Carbon Dioxide, Policy Document 12/05, The Royal Society, London, UK, 2005.

Turley, C., Eby, M., Ridgwell, A. J., Schmidt, D. N., Brownlee, C., Findlay, H. S., Fabry, V. J., Feely, R. A., Riebesell, U., and Gattuso, J.-P.: The societal challenge of ocean acidification, Mar. Pollut. Bull., 60, 787–792, 2010.

van der Spoel, S.: Pseudothecosomata, Gymnosomata and Heteropoda, Bohn, Scheltema & Holkema, Utrecht, 1976.

Wall-Palmer, D., Jones, M. T., Hart, M. B., Fisher, J. K., Smart, C. W., Hembury, D. J., Palmer, M. R., and Fones, G. R.: Explosive volcanism as a cause for mass mortality of pteropods, Mar. Geol., 282, 231–239, 2011.

Wang, L.. Jian, Z.. and Chen, J.: Late Quaternary pteropods in the South China Sea: carbonate preservation and palaeoenvironmental variation, Mar. Micropaleontol., 32, 115–126, 1997.

Yu, J., Elderfield, H., and Hönish, B.: B/Ca in planktonic foraminifera as a proxy for surface water pH, Paleoceanography, 22, PA2202, doi:10.1029/2006PA001347, 2007.

Wall-Palmer, D., Jones, M.T., Hart, M.B., Fisher, J.K., Smart, C.W., Hembury, D.J., Palmer, M.R. and Fones, G.R. 2011. Explosive volcanism as a cause for mass mortality of pteropods. Marine Geology, 282 (3-4), 231-239.

Marine Geology 282 (2011) 231–239

Contents lists available at ScienceDirect

Marine Geology

journal homepage: www.elsevier.com/locate/margeo

Explosive volcanism as a cause for mass mortality of pteropods

Deborah Wall-Palmer [a,*], Morgan T. Jones [b,1], Malcolm B. Hart [a], Jodie K. Fisher [a], Christopher W. Smart [a], Deborah J. Hembury [b], Martin R. Palmer [b], Gary R. Fones [c]

[a] School of Geography, Earth & Environmental Sciences, University of Plymouth, Drake Circus, Plymouth PL4 8AA, United Kingdom
[b] School of Ocean & Earth Sciences, National Oceanography Centre, University of Southampton, European Way, Southampton SO14 3ZH, United Kingdom
[c] School of Earth & Environmental Sciences, University of Portsmouth, Burnaby Building, Burnaby Road, Portsmouth PO1 3QL, United Kingdom

ARTICLE INFO

Article history:
Received 23 June 2010
Received in revised form 15 December 2010
Accepted 2 March 2011
Available online 13 March 2011

Communicated by G.J. de Lange

Keywords:
Pteropod
Soufrière Hills Volcano
Montserrat
Ocean acidification
Ash-leachates
Explosive volcanism

ABSTRACT

Recently, it has been proposed that anthropogenic CO_2 emissions may affect marine ecosystems by causing ocean acidification. In particular, it is suggested that within acidified waters, calcifying organisms would be subject to malformation and enhanced dissolution. Here, we present evidence suggesting that this process occurs naturally where explosive volcanism deposits ash directly into ocean surface waters. Sediment cores from around the island of Montserrat, Lesser Antilles volcanic arc, contain distinct horizons of planktic fauna associated with recently deposited volcanic ash layers from the Soufrière Hills volcano. Within these layers are abundant thecosome pteropod shells that display evidence of partial dissolution and etching of their aragonitic shells, and appear to have suffered mass mortality during large eruptions from the volcano. Laboratory studies show that the acids bound to ash surfaces from the 2003 volcanic dome collapse event of the Soufrière Hills volcano could have caused the upper 5 m of the water column to become undersaturated with respect to aragonite. When combined with the large fluxes of acidic aerosols (principally as SO_2) from the volcano during eruptions, it is proposed that volcanogenic ocean acidification by marine ash falls is a significant contributing factor to these observed mass mortality events.

1. Introduction

During explosive volcanic eruptions, a mixture of tephra (airborne volcanic particulate matter) and gases are injected into the atmosphere and deposited at varying distances from a volcano. As the eruption cloud cools, metal salts and condensing volatile phases tend to nucleate on solid or liquid surfaces, leading to preferential adsorption of acids onto tephra surfaces and within local meteoric water (Rose, 1977; Oskarsson, 1980). Both processes lead to the accelerated deposition of acids proximal to a volcano. The acids and metal salts adhered to the particle surfaces, termed ash-leachates, are very soluble; dissolving within minutes of first contact with water (Duggen et al., 2007). Hence, the combined deposition of volcanic ash and acidified meteoric water can rapidly enrich surface waters proximal to a volcano with a wide suite of elements. The subsequent impact on the biological community depends heavily on the concentrations of elements released and the buffering capacity of the affected ecosystem (Frogner-Kockum et al., 2006). In marine surface waters, it has been suggested that increased concentrations of bio-limiting nutrients, such as N, P, Fe, and Mn, may instigate increases in primary productivity (Frogner et al., 2001; Duggen et al., 2007; Jones and Gislason, 2008). If correct, the subsequent amplification of CO_2 uptake through the biological pump may offset, or even exceed, the out-gassing of volcanic CO_2 (Sarmiento, 1993; Watson, 1997).

In addition to the potential nutrient supply from volcanic inputs there is, however, the potential for release of species that may inhibit biological growth, including elements that are fertilizers at lower concentrations (Brand et al., 1986; Sunda, 1988–1989; Bruland et al., 1991). For example, acids released during acid-leachate dissolution or by direct deposition, including H_2SO_4, HCl and HF, lead to a significant decrease in the pH of the water (Frogner et al., 2001; Jones and Gislason, 2008). The extent to which aquatic environments are adversely impacted by tephra deposition varies greatly, with seawater being generally less susceptible due to its high buffering capacity (Frogner-Kockum et al., 2006). This property also limits the bioavailability of toxic ions such as Cu^{2+} and Al^{3+} (Moffett and Brand, 1996; Croot et al., 2000). The most sensitive biogeochemical cycle to surface seawater acidification is the carbonate system. In particular, aragonite, which is 50% more susceptible to dissolution than calcite (Mucci, 1983), is especially sensitive to changes in ocean chemistry. Hence a reduction of surface water pH values below ~7.8 (surface water undersaturated with respect to aragonite) may have deleterious consequences for aragonite precipitating organisms (Comeau et al., 2009).

Laboratory studies (Gattuso et al., 1998, Langdon et al., 2000; Riebesell et al., 2000; Feely et al., 2004; Orr et al., 2005; Comeau et al., 2009; Comeau et al., 2010a,b) and field investigations (Hall-Spencer et al., 2008) have shown that in general, calcification rates are reduced in acidified waters, and that calcareous organisms can show increased malformation and enhanced dissolution of calcareous structures. For

* Corresponding author. Tel.: +44 1752 584760.
E-mail address: deborah.wall-palmer@plymouth.ac.uk (D. Wall-Palmer).
[1] Present Address: Institute of Earth Science, University of Iceland, Sturlugata 7, 101 Reykjavik, Iceland.

0025-3227/$ – see front matter © 2011 Elsevier B.V. All rights reserved.
doi:10.1016/j.margeo.2011.03.001

example, gastropods (which form aragonitic shells) display partial dissolution of their shells around shallow hydrothermal vents that emit CO_2 (Hall-Spencer et al., 2008). In recent controlled pH-temperature (pH_T) experiments, the larvae of the Mediterranean pteropod *Cavolinia inflexa* maintained at pH_T 7.82 exhibited malformations and reduced shell growth when compared to those grown in control conditions at pH_T 8.1. At pH_T 7.51, the larvae failed to make shells, despite otherwise developing normally (Comeau et al., 2010b). However, experiments using *Limacina helicina* (a common high latitude thecosome pteropod) under controlled pH-temperature conditions of 7.78 and 5 °C, show that although calcification rates are reduced, the animal can still precipitate additional aragonitic shell material at an aragonite saturation index close to unity (Comeau et al., 2009). This information shows that even between species of the same taxonomic suborder, the response to acidification is complicated and often species specific, demonstrating a variation in the susceptibility to reduced calcification.

The extent of seawater acidification from volcanic acid deposition will depend on the magnitude of the eruption, the chemistry and volume of the acids adhering to the particles (or incorporated in precipitating fluids), weather conditions, and the rate of mixing in the water column. If conditions are favorable for rapid and voluminous release of acids through tephra deposition and/or rainfall into ocean surface waters, it might be expected that this deposition would result in transient acidification of the uppermost parts of the water column; an effect that would then be buffered by mixing with the underlying water column. Hence, any potential aragonite undersaturation induced in surface waters would be expected to be restricted to periods of heightened and/or sustained volcanic activity.

The aims of this study are to investigate preliminary observations made during a scientific cruise off-shore Montserrat (Lesser Antilles island arc), which have been briefly documented by Jones and Gislason (2008). Marine sediments collected to the west and south-west of the Soufrière Hills volcano contain distinct horizons of abundant planktic microfossils which are closely associated with layers of recent volcanic ash. This study considers factors which may have lead to such events and their position within the sediments.

2. Materials and methods

The scientific cruises of the RRS *James Clark Ross* (JCR123 May, 2005) and RRS *James Cook* (JC18 December, 2007) comprised two multidisciplinary studies of the impact of the ongoing volcanic activity on the island of Montserrat (Lesser Antilles) on the surrounding seas. During the course of these cruises over 80 sediment cores were collected from around the island. Many of these cores contain deposits from the two recent dome collapse events in July 2003 and May 2006. The 2003 event erupted $>210\times10^6$ m^3 of material, most of which entered the ocean east of Montserrat over the course of ~18 h (Trofimovs et al., 2006). The 2006 event erupted slightly less material, but the resulting pyroclastic and marine gravity flows were more energetic as the collapse occurred over only a few hours.

The ash content of all sites from the RRS *James Cook* (JC18) cruise were examined and two of the sites were chosen to illustrate the effects of the most recent eruptions upon the marine fauna of the surrounding area. Site JC18-21 lies in 1270 m of water, well to the southwest of the island (Fig. 1) and did not contain visible ash at the surface. Hence, this area is used as a background site against which to compare the impact of tephra deposition (herein referred to as the control site). A second site, JC18-25 was located in 878 m of water in an area off the west coast of Montserrat, around 10 km from the Soufrière Hills volcano (herein referred to as the affected site). This area has experienced significant disturbance from volcanic deposits and contains two distinct layers of ash. It has also been selected as it has experienced ash fall debris only and has not been affected by pyroclastic flows or lahar deposits, leaving the sequential deposits intact.

Megacore samples were retrieved from both sites (JC18-21M and JC18-25M), providing a 10 cm and 11 cm record respectively. All sample processing was carried out onboard the ship, while the subsequent faunal analysis was carried out at the University of Plymouth. Using a standard foraminifera method, just over 300 (or as many as were present up to 300) specimens of pteropod and heteropod remains were collected from two size fractions (125–500 μm and >500 μm) at various positions within the cores for each site. This provides information about both abundance and diversity. For analysis of the preservation of pteropod shells, a method (the Limacina Dissolution Index) devised by Gerhardt et al. (2000) and published as a scale by Gerhardt and Henrich (2001) was used. This scale extends from 0 (best; pristine, transparent shells) to 5 (worst; opaque-white, totally lusterless and perforated shells). At selected points in both the control and affected cores, two species of pteropod were analysed using this scale; single representative specimens of *Creseis acicula* and between 10 and 30 specimens of *Limacina inflata,* (as in the original designated scale suggested by Gerhardt and Henrich, 2001). Scanning electron microscope (SEM) images were

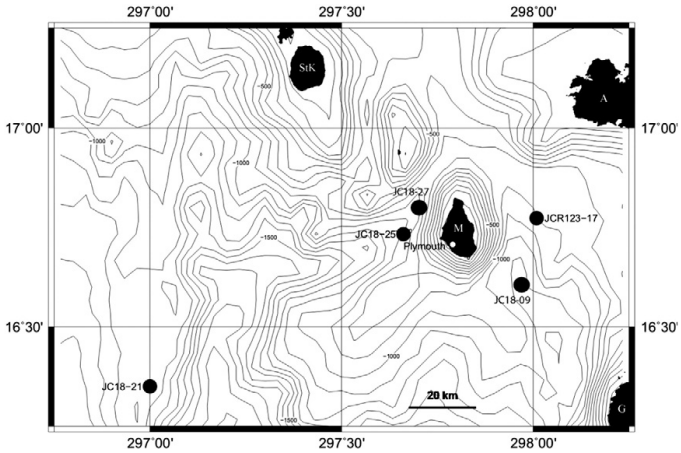

Fig. 1. Map of Montserrat and surrounding islands in the Lesser Antilles, with core sites used in this paper marked on. Key: M = Montserrat, A = Antigua, StK = St Kitts and Nevis, G = Guadeloupe.

also obtained of the surface structures of *C. acicula* specimens to complement the LDX data.

To achieve a first-order estimate of the volume of ash needed to reduce surface water pH below 7.8, a series of mixing experiments were conducted using unhydrated ash from the 2003 and 2005 eruptions from the Soufrière Hills volcano on Montserrat, and the 2008 eruption of Chaitén in Chile. Ash from the 2006 eruption was not suitable for the experiments as the eruption occurred during a thunderstorm, compromising the collection of tephra with associated soluble surface coatings. Ash leachate experiments were carried out at the University of Southampton using the same experimental procedure as Jones and Gislason (2008). Surface water collected from the North Atlantic (pH 8.08 at 21 °C) was pumped at a rate of 60 ± 2 ml h^{-1}, through a Teflon single-pass, plug flow-through reactor containing unhydrated tephra at 19 ± 0.2 °C. The reacted solution passed through a 0.2 μm cellulose acetate membrane filter into a sample bottle. The difference between this and previous experiments was that pH and sample weight were continuously monitored, instead of separating the reacted fluid into aliquots for analysis. This allows a range of ash:water ratios to be considered. Each experiment was repeated three times, with varying amounts of ash in the reactor to test a range of mixing scenarios.

3. Results

Marine deposits from the Soufrière Hills volcano most commonly occur as pyroclastic density current deposits (Trofimovs et al., 2006), but at sites west of the volcano there are deposits of lahar or air-fall origin from the 2003 and 2006 eruptions that are ~4 cm and ~3 cm thick, respectively. At the affected site (Fig. 1), two distinct layers of planktic remains are observed (Fig. 2). The first layer occurs at a depth of 3–5 cm in the core in a matrix of fine ash from the 2003 volcanic event. This layer is dominated by thecosome pteropods and planktic foraminifera. A similar layer lies at the surface of the 2006 ash at the top of the core (0–1 cm). Both these layers are interbedded with fine ash. This suggests that either their deposition was concurrent with the later stage deposition of the volcanic layers (i.e. the finer particles with a slower settling velocity), or that they settled through a turbid benthic boundary of very recently deposited fine ash that had yet to form a cohesive sedimentary layer. Hence, the deposition of pteropod shells and foraminifera tests began during, or very shortly after, the ash deposition.

3.1. Diversity and abundance of pteropods

The typical assemblage of open water pteropods in the vicinity of Montserrat is exemplified by the surface sample (0–1 cm) from the control core. Pelagic sedimentation rates in this area of the Caribbean Sea are of the order of 2–3 cm/kyr (Reid et al., 1996), so the plankton assemblage in this interval is an average for the past ~500 years. Porewater dissolved oxygen levels remain at >10% of bottom water values at a depth of 7 cm in the core, indicating that the sediments in the upper most centimeter have not experienced extensive redox-driven diagenesis. When these observations are coupled with the depth of the core (1270 m), it suggests that the calcitic foraminifera and the aragonitic pteropods would not be expected to exhibit signs of post-depositional carbonate dissolution. Pteropod shells are very abundant in these sediments (Fig. 3); the size ranges 125–500 μm and >500 μm contain ~20,000 and 2000 pteropods per gram of sediment (P/g), respectively. In contrast, the diversity is low, with *L. inflata* and *Creseis virgula constricta* comprising 34% and 20% of the 125–500 μm assemblage, respectively. *Styliola subula* and *Limacina* spp. are also common. Overall, spiral forms comprise 12 out of 19 of the species present and 61% of the total individuals. The >500 μm size fraction is also dominated by *L. inflata*, making up 58% of the total assemblage, although *S. subula* and *C. virgula virgula* are also common. The larger fraction contains a more even spread of morphologies, with 7 spiral species, 6 elongate species, and 5 ornate species, but there are many more spiral individuals (71%).

The plankton-rich layer at 3–5 cm in the affected core is mainly composed of pteropods in the 125–500 μm size fraction (Fig. 3), with larger specimens dominated by *L. inflata*. The diversity is comparable to the control assemblage, with *L. inflata*, *C. acicula*, *C. virgula constricta*, and other *Limacina* spp. being most abundant. The relative proportion of spiral species (15 of 21) and individuals (63%) are also comparable to the control assemblage. The 125–500 μm size fraction has an average abundance of 107 P/g, with a peak of 120 P/g between 4 and 5 cm. The surface layer (0–1 cm) of the affected core is also largely composed of individuals in the smaller size fraction, with

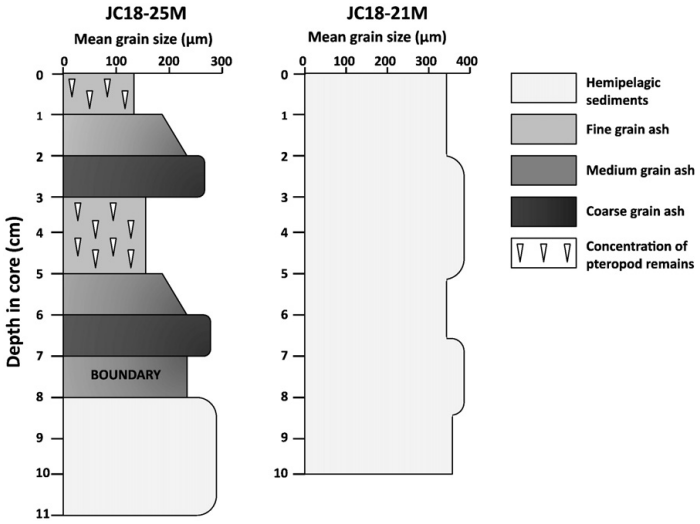

Fig. 2. Sedimentary logs for the cores JC18-25M and JC18-21M. The "M" denotes mode of collection, by multi-core. The logs were calculated by using mean grain size, occurrences of fauna, and laboratory and ship board observations.

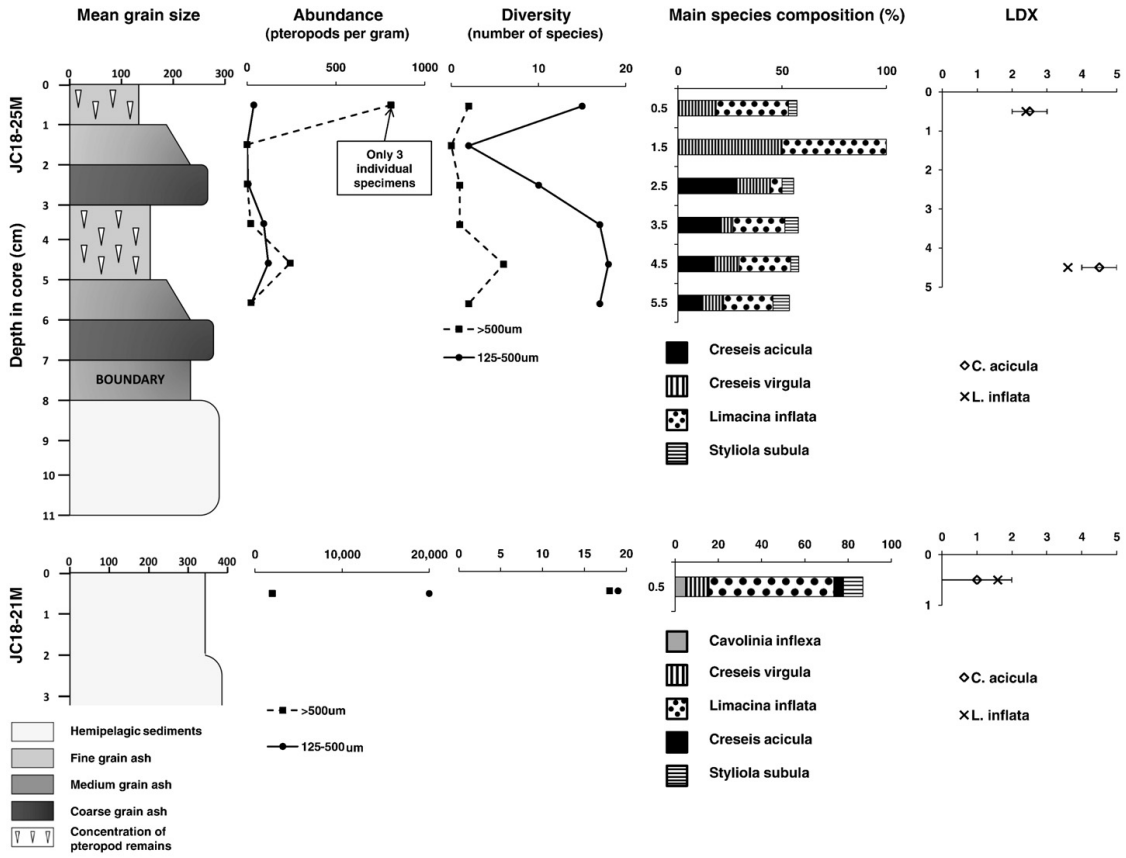

Fig. 3. Pteropod abundance, diversity, percentage of main species and Limacina Dissolution Index (LDX) values for the affected core (JC18-25M) and the control core (JC18-21M).

very few pteropods found >500 μm in size (Fig. 3). Again, the assemblage is made up largely of spiral species and individuals (11 out of 14 and 76%, respectively), and is dominated by *L. inflata* and *C. virgula constricta*. The abundance of pteropods in this layer is much lower, with only 38 P/g in the 125–500 μm fraction, although this is principally due to dilution by the ash matrix, which is denser than the planktic remains.

3.2. Preservation of pteropods

Representative specimens of *C. acicula* from the control site show excellent preservation (LDX scale 0–2); the surface structures are generally not etched or damaged and the wall structures are strong and intact (Fig. 4). Similarly, specimens of *L. inflata* have an average LDX of 1.6. In contrast, specimens of *C. acicula* collected from the 3–5 cm layer of the affected core show poor preservation (LDX scale 4–5). The shell surfaces have been entirely removed by corrosion, exposing the aragonite rods beneath, while the wall structures have been badly damaged and in many instances have separated in two (Fig. 4). During preparation for the SEM study, shells from the 3–5 cm layer also crumbled easily and were far easier to break than specimens from the control site. Again, specimens of *L. inflata* are consistent with this level of preservation, providing an average LDX of 3.6. Pteropods from the upper layer of the affected core also showed poor preservation (LDX scale 2–3), although they were better preserved than in the 3–5 cm layer. The surfaces of the shells are partially dissolved, etched and damaged. Specimens of *L. inflata* provide an average LDX of 2.4.

3.3. Ash leachate experiments

Data from previous ash leachate experiments has been published by Jones and Gislason (2008). Resulting pH changes caused by the addition of Montserrat ash to de-ionized water, Atlantic Ocean water and Southern Ocean water in this previous study can be seen in Table 1. Additionally, Table 1 shows the amount of sulfate (SO_4^{2-}) released per gram of ash for the three water types. These values can be transformed into the amount of sulfur released, giving 0.4, 2.28 and 2.7 mg of sulfur released per gram of ash for de-ionized water, Atlantic Ocean surface water and Southern Ocean surface water, respectively. Using values published by Trofimovs et al. (2006), 210×10^6 m^3 of volcanic material was produced by the 2003 eruption of the Soufrière Hills volcano. If a typical density of 2.5 g cm^{-3} is used, this gives 5.25×10^{14} g of volcanic material erupted. Assuming all of this material had the same coating of sulfur as that measured by Jones and Gislason (2008), then the amount of sulfur on the particle surfaces, as predicted for each water type, would be 0.21, 1.2 and 1.42 million tons. While the larger size fraction particles are likely to have less adsorbed sulfur, these calculations do not include the sulfur deposited by other processes such as precipitation. Trofimovs et al. (2006) also suggest that 90% of all volcanic material directly entered the waters around Montserrat, which would mean that the majority of this

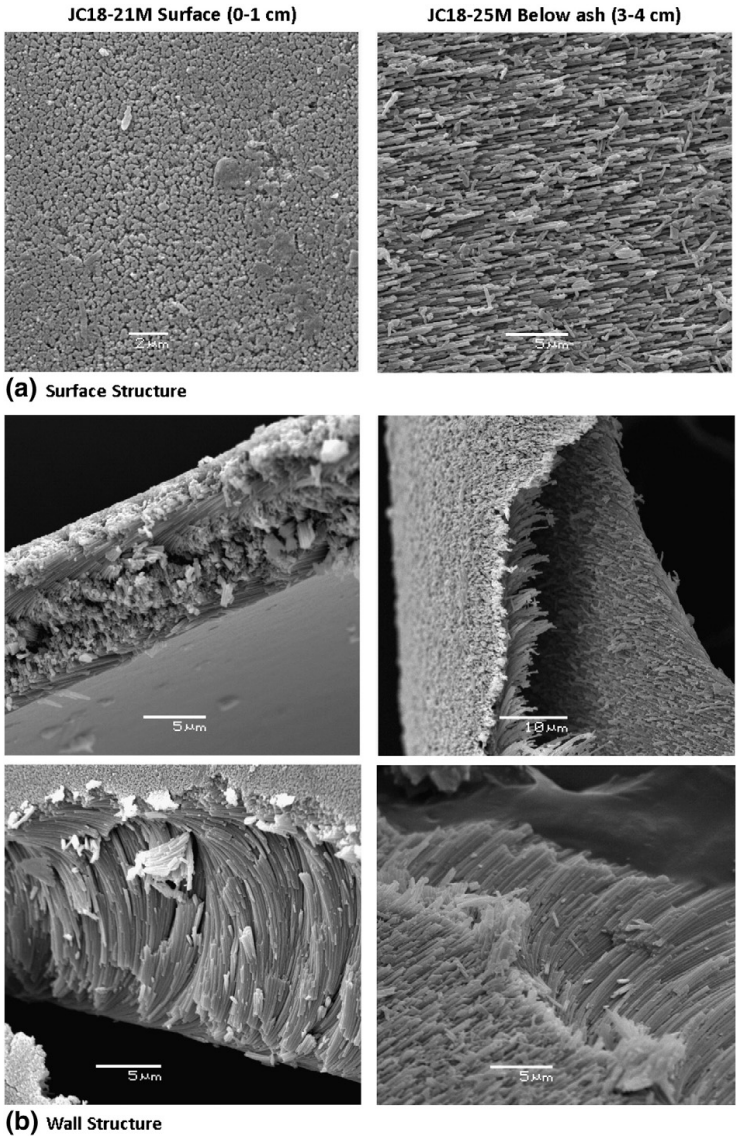

Fig. 4. SEM images of the pteropod *C. acicula*. (a) Surface structures and (b) wall structures of shells from the control assemblage (JC18-21M 0–1 cm) compared to those from below the 2006 ash layer (JC18-25M 3–5 cm).

adsorbed sulfur was transported straight to the sea. Results from the mixing experiments carried out for this study show variations between ash from different events of the Soufrière Hills volcano, which can be seen in Fig. 5. These results show that ash:water mass ratios of 0.025 and 0.014 are required to reduce the pH to below 7.8 and hence achieve aragonite undersaturation by the 2003 and 2005 Montserrat tephras respectively. However, as the reactivity of adsorbed material appears to decrease over time (Jones and Gislason, 2008; Duggen et al., 2009), the observed difference between the samples may not reflect the true coatings at the time of deposition.

4. Discussion

4.1. Abundance and diversity of pteropods

There is often a strong decoupling between the planktic assemblage of the water column and that found within surface sediments. Although there are no plankton data for the oceans around Montserrat, studies have been conducted in the Western Caribbean Sea (Suárez-Morales and Gasca, 1998; Parra-Flores and Gasca, 2009) and offshore Barbados (Wells, 1975, 1976). In the case of the latter studies, the euthecosome

Table 1
Results of ash mixing experiments using Montserrat ash from the 2003 event of the Soufrière Hills volcano (Jones and Gislason, 2008).

	De-ionized water	Atlantic Ocean surface water	Southern Ocean surface water
Time (min)	Resulting water pH		
25	4.66	6.89	7.29
75	5.74	7.4	7.54
125	5.7	7.87	7.62
175	5.9	7.92	7.77
225	5.73	7.9	7.81
275	5.83	7.91	7.91
325	6.04	7.9	7.87
375	6.21	7.91	7.96
425	6.2	7.92	7.94
475	6.16	7.96	7.93
1365	–	7.99	7.88
1415	–	8.01	7.95
SO_4^{2-} released within 8 h (μmol/g of ash)	12.5	71.2	84.2

pteropod assemblage in the upper layers of sediment accurately reflects the species composition and relative abundance of the overlying waters (Wells, 1975). Although the relative abundances of each species vary, most of the species found in the surface sediments of the control core are represented in these studies, and the dominant species are in most cases similar. For example, all of the studies found *L. inflata* to be by far the most abundant species; followed by *Creseis* spp. (including *C. acicula* and various sub-species of *C. virgula*, which is the second most abundant species in the combined size fractions from the control core). It is noteworthy that *S. subula* is abundant in the sediments of the control core, but is not well represented in the plankton studies. This may be due to net avoidance by the pteropods or a large mesh size used in the studies. For example, Parra-Flores and Gasca (2009) used a net mesh of 355 μm, which may have allowed the slender *S. subula* shells to pass through. Conversely, *Limacina trochiformis* is well-represented in the plankton studies, but only contributes 3% of the control assemblage. This discrepancy may be due to patchy distributions of pteropod species caused by local water circulation patterns; for example, Suárez-Morales and Gasca (1998) found that the pteropod community of the Mexican Caribbean Sea contains a mixture of both neritic and oceanic species.

The core collected from the affected site contains two deposits of abundant planktic remains. Although the abundance of pteropods is higher in the control core, the pelagic sedimentation rate of ~2–3 cm/kyr (Reid et al., 1996) means that the number of shells at the control site has built up over many hundreds of years, whereas the planktic remains in the 3–5 cm layer of the affected core must have accumulated within 34 months at most (the time between the 2003 and 2006 eruptions). Similarly, the 0–1 cm pteropod-rich layer in the affected core must have accumulated in less than 19 months — the interval between the dome collapse event that generated the tephra layer and the sampling date. Hence, there can be little doubt that there was a rapid increase in the export of planktic organisms during, or immediately after, the dome collapse events and associated volcanic activity.

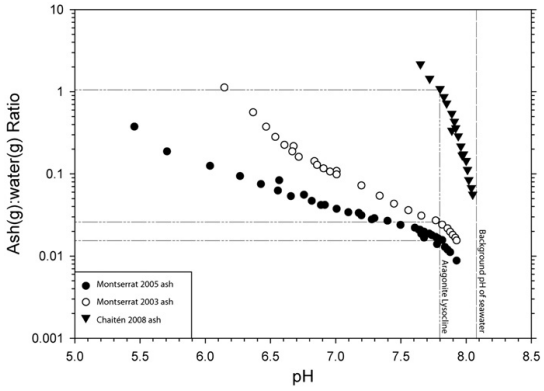

Fig. 5. Results of mechanical mixing experiments using two samples of unhydrated ash from Montserrat (2003 and 2005), and a sample from Chaitén in Chile (2008).

There are several lines of evidence to suggest that the two planktic-rich layers in the affected core resulted from increased mortality of a standing crop of planktic organisms, rather than increased productivity and sedimentation due to nutrient addition. Firstly, if the planktic-rich layers arose from an increase in production, then both layers would be expected to contain a high proportion of phytoplankton remains, whereas they are both dominated by pteropods and planktic foraminifera. High proportions of phytoplankton would be seen as pale carbonate sediment, which was not observed during collection. Secondly, the size distribution of the pteropods observed in the planktic-rich layers favors a sudden increase in mortality. Although the higher concentrations of smaller individuals observed in the affected core compared to the control core may be due to a change in the conditions governing the growth rates and/or life expectancies of individual pteropods, the fact that the larger pteropods are concentrated toward the base of the 3–5 cm layer (Fig. 2) is suggestive of a mortality event, as larger tests have higher settling velocities. If the planktic-rich layers had arisen in response to a phytoplankton bloom, then one would expect to see reverse grading in the pteropod sizes as short-lived immature individuals fell to the sea floor ahead of the longer-lived large specimens. Finally, the over-representation of smaller individuals in the planktic-rich layers relative to the control site is consistent with sudden mortality of a standing crop, in which immature individuals will be more abundant than the assemblage resulting from the deaths and export of tests from a population progressing to their natural life expectancy.

4.2. Preservation of pteropods

Overall, the evidence presented above is strongly supportive of the sudden mortality and sedimentation of a natural population of pteropods in close association with volcanic processes resulting from dome collapse events. The preservation state of pteropod shells from the affected core indicates that they have undergone significant dissolution. Interaction with the aragonite compensation depth (ACD) and/or aragonite lysocline can be discounted as a cause for the poor preservation of these pteropod shells. Although water chemistry around the Lesser Antilles island arc is complicated by water masses from several origins flowing between the islands, Gerhardt and Henrich (2001) found that towards the north of the arc, an area which encompasses Montserrat, the preservation of *L. inflata* is generally very good. This is due to a large influx of Upper North Atlantic Deep Water which flows through the nearby Anegada Passage. Gerhardt and Henrich (2001) place the aragonite saturation depth at 2000 m and the ACD at 3800 m water depth in this area. It is also important to note that the affected core was collected from a shallower depth (878 m) than the control core (1270 m) which contains well-preserved pteropod remains. In addition, none of the 10 CTD casts around the island showed any evidence that the water column was undersaturated with respect to aragonite over the sampled depth range (0–1946 m). GLODAP data (Key et al., 2004) for the Caribbean Sea also shows that both sites are above the aragonite lysocline (Fig. 6).

It is possible that the shells underwent dissolution after arriving at the seafloor. The effect of the breakdown of organic matter can be discounted as total carbon concentrations within 10 ash layers recovered from the JC18 cruise consistently show C<1 wt.%, with organic carbon<0.1 wt.% within the ash layers. This indicates that organic matter is diluted by the deposited ash and hence plays a minor role in diagenesis. However,

porewater pH values at site JCR123-17 (Fig. 1) show pH values falling to <7.4 below depths of ~1 cm within the 2003 ash layer (Fig. 7) in response to diagenesis of the volcanic material. Moreover, pteropods collected beneath ash layers in Andaman Sea sediments show poorer preservation than those collected from sediments from the same water depth, but not containing ash (Bhattacharjee, 2005). The poorer preservation of pteropods from the 3–5 cm layer in the affected core compared to the surface layer in the same core is therefore likely to be the continued dissolution of the shells after burial. However, pteropod shells collected at 1119 m water depth from a further site, JC18-09 (Fig. 1), show that dissolution from volcanically affected pore waters only has a minimal effect on the preservation. The 2006 dome collapse at this site is represented by a pyroclastic density current that scoured the sea bed and incorporated pre-eruption pteropod shells from shallower shelf sediments. Despite the shells being physically fragmented during this transport process, and thus more susceptible to dissolution, pteropod shell fragments from the surface layer of this core display an LDX preservation of 1–2. This observation indicates that the effect of volcanic ash on the pore water was insufficient to degrade pteropod shells.

4.3. Potential impact of acid deposition

As noted above, deposition of volcanic eruption products have the potential to cause acidification of surface waters, although this potential varies considerably between different volcanoes and/or volcanic deposition events (Jones and Gislason, 2008). Calculated ash:water mass ratios of 0.025 and 0.014 are required to achieve aragonite undersaturation by the 2003 and 2005 Montserrat tephras, respectively (Fig. 5). In contrast, ash from the Chaitén eruption has much less adsorbed acids, such that aragonite undersaturation would require a 1:1 ash/seawater ratio. An indication of the potential impact of the 2003 and 2006 eruptions can be made by making simple assumptions — i.e. that the tephra was added to the surface water over a short time period and was well-mixed in the surface layer. Under these conditions, the 3 cm thick ash layer observed in core JC18-25 could have caused the upper 5.1 m of the water column to become undersaturated with respect to aragonite (assuming that the ash had the same adsorbed acid load as the 2005 ash), and the 4 cm thick layer produced by the 2003 eruption could have caused aragonite undersaturation in the upper 3.8 m of the water column.

Clearly, there are important caveats to these calculations. The assumption that the tephra was rapidly added to the surface water is not unreasonable, as both dome collapse events took place over the course of a few hours. The kinetics of adsorbed ash dissolution versus sinking rate of the particles can be constrained from the experimental data (Fig. 5) and Stokes law settling velocities. The average size fraction of the volcanic sediment in the affected core is around Φ 5 (~0.031 mm), and is poorly sorted. Assuming a spherical shape and a density of 2.65 g cm^{-3}, the average terminal (settling) velocity of the tephra is ~0.8 mm s^{-1}. Hence the tephra would take ~2 h to settle through the upper 5 m of the water column, by which time 99% of the ash leachate would have dissolved (Jones and Gislason, 2008). However, the observation that pteropods are still capable of shell calcification at pH 7.8 (Comeau et al., 2009) suggests that the pH would have to be reduced even further to account for both the quantity and preservation state of pteropods at the affected site.

It is likely however, that the experiments have underestimated the extent of acidification induced by ash deposition in seawater as it is very difficult to collect unhydrated ash. Interaction of fresh tephra with atmospheric moisture and/or associated rainfall that accompanies volcanic eruptions means that tephra collected after it has fallen to ground seldom preserves its original adsorbed phase. In addition, simultaneous wet and dry depositions of volcanic acids into the oceans would further increase the acidity of surface waters. For example, the Montserrat Volcano Observatory has measured rainfall in Plymouth (Fig. 1) with a pH as low as 1.8. This would have been particularly important during the 2006 eruption, which occurred during a heavy storm. However, without the fortuitous (and hazardous) collection of ash and rain fallout at the height of the eruption the true scale of acid deposition is difficult to constrain more accurately. Nevertheless, if acidification of surface waters is in part responsible for the quantity and preservation state of pteropods in the affected core, then the coeval contribution of acid from wet and dry deposition of hydrated volcanic gases (principally H_2SO_4 from SO_2) must have been greater than that derived from leaching of tephra particles alone.

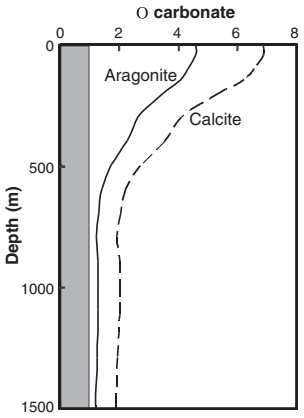

Fig. 6. Carbonate saturation profile of the Caribbean Sea from GLODAP site 17.03°N, 66W (Key et al., 2004).

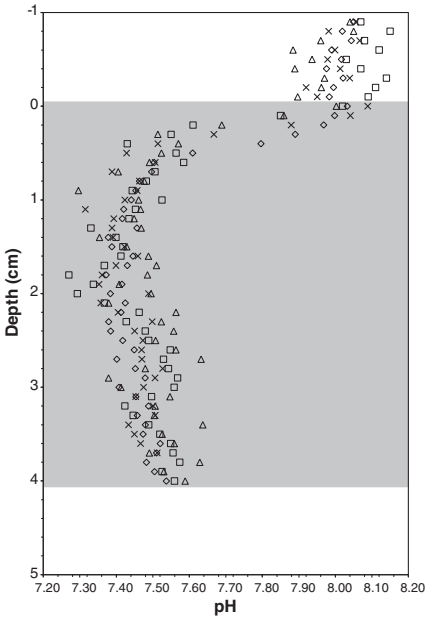

Fig. 7. In situ pH measurements of pore waters from sediment core JCR123-17 to the east of Montserrat in ~850 m water depth. The gray shading denotes ash deposited between 1995 and 2005 at the site, dominantly from the 2003 eruption. Different symbols reflect multiple profiles in the same core.

4.4. Alternative causes for pteropod mortality

Other processes that might cause pteropod mortality related to volcanic events arise from the physical properties of the ash. The species *Diacria quadridentata* is known to respond to any disturbance by withdrawing into its shell and passively sinking (Bé and Gilmer, 1977). A constant fall of ash over several hours would almost certainly have initiated such a response, with the result that the pteropods may have remained in their shells and sunk below the pycnocline and been unable to return to the surface. Some species may have had a similar response to the volcanic induced reduction in pH; the species *Limacina helicina* displayed a marked decrease in active swimmers when subjected to reduced pH conditions (Comeau et al., 2009). Pteropods feed on smaller plankton by producing mucous nets that are much larger than their shell. If they fail to detach from this net during ash deposition, entrainment of relatively dense tephra in the net could cause them to become negatively buoyant. In addition, ash particles could clog the gills of the pteropods and cause suffocation. Although reasonable, these alternative causes of mortality do not explain the dissolution of the pteropod shells. The large abundance of pteropods in the sediments of the affected core may be related to the diurnal vertical migration exhibited by many euthecosome pteropod species which leads to a large abundance of pteropods in surface waters during darkness (Bé and Gilmer, 1977; Parra-Flores and Gasca, 2009). Both the 2003 and 2006 eruptions of the Soufrière Hills volcano occurred at night, affecting the surface waters at a time when the largest density of pteropods would have been present.

Finally, although surface water acidification by dissolution of adsorbed tephra coatings may not be sufficient to be the sole cause of the pteropod mortality, the response of planktonic organisms of all kinds to potentially toxic species released during dissolution of the tephra coatings is much less well-constrained. It may be noteworthy that mussel farming on Chiloé Island, near Chaitén, was particularly bad during 2008/2009 immediately after the 2008 eruption, and appears to be related to a decrease in the phytoplankton population close to the volcano (A. Amigo, pers. comm.). Given that the Montserrat ash is more reactive than that from Chaitén(Fig. 5), this process might be expected to be more important around Montserrat and could account for the presence of both pteropods and foraminifera in the affected sediments.

Montserrat is host to a relatively small volcano (<1 km^3 magma erupted in the past 14 years), other explosive volcanoes have been much larger. For example, the 1815 Tambora (Indonesia) eruption expelled 50 km^3 of pyroclastic material in a single event (Oppenheimer, 2003), and there are examples in the geological record of "super-eruptions" with erupted volumes exceeding 4000 km^3 of dense magma (Mason et al., 2004). A 1000 km^3 super-eruption could blanket an area of 10^7 km^2 with 10 cm of ash (Jones et al., 2007). The potential global significance of explosive volcanism on plankton depends on the mechanism by which the volcanic event causes mortality and whether this process or processes are present in each eruption. If the mechanism of mortality was due to surface water acidification or release of toxic metals, then the impact of a super-eruption would be critically dependent on the magma and volatile phase compositions. The minimal ash-leachate release observed from the Chaitén ash (Fig. 5) is particularly interesting as the eruption was rhyolitic (>70 wt.% SiO_2), comparable in composition to most large volume explosive eruptions. If this ash-leachate release is typical of rhyolitic ashes, then one would expect a relatively low acidification impact from rhyolitic ash deposition into the ocean. However, if the mortality around Montserrat is due to other physical disturbances of pteropods in surface waters, the type of ash would be of lesser significance than the overall scale of the eruption.

5. Conclusions

Affected core JC18-25M contains two distinct layers of pteropod and planktic foraminifera remains produced by the rapid and significant mortality of a standing crop of living organisms. Whereas most previous studies of the impact of volcanism on marine ecosystems have concentrated on their role in supplying limiting nutrients to instigate increases in primary productivity (e.g. Frogner et al., 2001; Duggen et al., 2007), to our knowledge, this study presents the first direct evidence that explosive volcanism can have a detrimental effect on planktic fauna in marine surface water adjacent to a volcano. The mechanism by which this mortality was induced is not clear, but there is some evidence that surface water acidification by dissolution of surface coatings on tephra and/or dry and wet depositions of volcanic gases may have played a role. Other viable causes of the mortality event include release of toxic metals during reaction of the tephra with seawater, and the physical effects of fine-grained ash. Regardless of the precise mortality mechanism, the fact that pteropods and planktic foraminifera are key constituents within the food-web (Hunt et al., 2008), suggests that large explosive eruptions could cause significant disruption of marine ecosystems.

Acknowledgements

The cruises of the RRS *James Clark Ross* JCR123 and the RRS *James Cook* JC18 were supported by NERC grant proposal codes NER/A/S/2002/00963JCR and NE/D004020/1 respectively. The authors would like to thank the valuable assistance of the shipboard scientists and crews of the JCR-123 and JC-18 cruises. Polly Hill is thanked for the donation of North Atlantic seawater, Sue Loughlin and Alvaro Amigo for the collection and donation of ash samples, Sigurður Gislason for the use of Teflon plug reactors, and the staff of the Montserrat Volcanic Observatory for the provision of precipitation data. M.B.H., C.W.S. and J.K.F. acknowledge the support of a research grant (F/00 568/P) from the Leverhulme Trust.

References

Bé, A.W.H., Gilmer, R.W., 1977. A zoogeographic and taxonomic review of *Euthecosomatous pteropoda*. In: Ramsay, A.T.S. (Ed.), Oceanic Micropaleontology, vol. 1. Academic Press, New York, pp. 733–808.
Bhattacharjee, D., 2005. Pteropod preservation profiles in seabed sediments off Middle Andaman Island in Andaman Sea. Indian Journal of Marine Sciences 34, 259–266.
Brand, L.E., Sunda, W.G., Guillard, R.R.L., 1986. Reduction of marine phytoplankton reproductive rates by copper and cadmium. Journal of Experimental Marine Biology and Ecology 96, 225–250.
Bruland, K.W., Donat, J.R., Hutchins, D.A., 1991. Interactive influences of bioactive trace metals on biological production in oceanic waters. Limnology and Oceanography 36, 1555–1577.
Comeau, S., Gorsky, G., Jeffree, R., Teyssié, J.-L., Gattuso, J.-P., 2009. Impact of ocean acidification on a key Arctic pelagic mollusc (*Limacina helicina*). Biogeosciences 6, 1877–1882.
Comeau, S., Jeffree, R., Teyssié, J.-L., Gattuso, J.-P., 2010a. Response of the Arctic Pteropod *Limacina helicina* to projected future environmental conditions. PLoS ONE 5, e11362.
Comeau, S., Gorsky, G., Alliouane, S., Gattuso, J.-P., 2010b. Larvae of the pteropod *Cavolinia inflexa* exposed to aragonite undersaturation are viable but shell-less. Marine Biology 157, 2341–2345.
Croot, P.L., Moffett, J.W., Brand, L., 2000. Production of extracellular Cu complexing ligands by eucaryotic phytoplankton in response to Cu stress. Limnology and Oceanography 45, 619–627.
Duggen, S., Croot, P., Schacht, U., Hoffmann, L., 2007. Subduction zone volcanic ash can fertilize the surface ocean and stimulate phytoplankton growth: evidence from biogeochemical experiments and satellite data. Geophysical Research Letters 34, L01612.
Duggen, S., Olgun, N., Croot, P., Hoffmann, L., Dietze, H., Teschner, C., 2009. The role of airborne volcanic ash for the surface ocean biogeochemical iron-cycle: a review. Biogeosciences 6, 6441–6489.
Feely, R., Sabine, C., Lee, K., Berelson, W., Kleypas, J., Fabry, V., Millero, F., 2004. Impact of anthropogenic CO_2 on the $CaCO_3$ system in the Oceans. Science 305, 362–366.
Frogner, P., Gislason, S.R., Oskarsson, N., 2001. Fertilizing potential of volcanic ash in ocean surface water. Geology 29, 487–490.
Frogner-Kockum, P.C., Herbert, R.B., Gislason, S.R., 2006. A diverse ecosystem response to volcanic aerosols. Chemical Geology 231, 57–66.
Gattuso, J.-P., Frankignoulle, M., Bourge, I., Romaine, S., Buddemeier, R., 1998. Effect of calcium carbonate saturation of seawater on coral calcification. Global and Planetary Change 18, 37–46.
Gerhardt, S., Henrich, R., 2001. Shell preservation of *Limacina inflata* (Pteropoda) in surface sediments from the Central and South Atlantic Ocean: a new proxy to determine the aragonite saturation state of water masses. Deep-Sea Research 48, 2051–2071.

Gerhardt, S., Groth, H., Rühlemann, C., Henrich, R., 2000. Aragonite preservation in late Quaternary sediment cores on the Brazilian Continental Slope: implications for intermediate water circulation. International Journal of Earth Sciences 88, 607–618.
Hall-Spencer, J.M., Rodolfo-Metalpa, R., Martin, S., Ransome, E., Fine, M., Turner, S.M., Rowley, S.J., Tedesco, D., Buia, M.-C., 2008. Volcanic carbon dioxide vents show ecosystem effects of ocean acidification. Nature 454, 96–99.
Hunt, B.P.V., Pakhomov, E.A., Hosie, G.W., Siegel, V., Ward, P., Bernard, K., 2008. Pteropods in Southern Ocean ecosystems. Progress in Oceanography 78, 193–221.
Jones, M.T., Gislason, S.R., 2008. Rapid releases of metal salts and nutrients following the deposition of volcanic ash into aqueous environments. Geochimica et Cosmochimica Acta 72, 3661–3680.
Jones, M.T., Sparks, R.S.J., Valdes, P.J., 2007. The climatic impact of supervolcanic ash blankets. Climate Dynamics 29, 553–564.
Key, R.M., Kozyr, A., Sabine, C.L., Lee, K., Wanninkhof, R., Bullister, J.L., Feely, R.A., Millero, F.J., Mordy, C., Peng, T.-H., 2004. A global carbon climatology: results from Global Data Analysis Project (GLODAP). Global Biogeochemical Cycles 18, GB4031.
Langdon, C., Takahashi, T., Sweeney, C., Chipman, D., Goddard, J., Marubini, F., Aceves, H., Barnett, H., Atkinson, M., 2000. Effect of calcium carbonate saturation state on the calcification rate of an experimental coral reef. Global Biogeochemical Cycles 14, 639–654.
Mason, B.G., Pyle, D.M., Oppenheimer, C., 2004. The size and frequency of the largest explosive eruptions on Earth. Bulletin of Volcanology 66, 735–748.
Moffett, J.W., Brand, L.E., 1996. Production of strong, extracellular Cu chelators by marine cyanobacteria in response to Cu stress. Limnology and Oceanography 41, 388–395.
Mucci, A., 1983. The solubility of calcite and aragonite in seawater at various salinities, temperatures and 1 atmosphere total pressure. American Journal of Science 238, 780–799.
Oppenheimer, C., 2003. Climatic, environmental and human consequences of the largest known historic eruption: Tambora volcano (Indonesia) 1815. Progress in Physical Geography 27, 230–259.
Orr, J., Fabry, V., Aumont, O., Bopp, L., Doney, S., Feely, R., Gnanadesikan, A., Gruber, N., Ishida, A., Joos, F., Key, R., Lindsay, K., Maier-Reimer, E., Matear, R., Monfray, P., Mouchet, A., Najjar, R., Plattner, G.-K., Rodgers, K., Sabine, C., Sarmiento, J., Schlitzer, R., Slater, R., Totterdell, I., Weirig, M.-F., Yamanaka, Y., Yool, A., 2005. Anthropogenic ocean acidification over the twenty-first century and its impact on calcifying organisms. Nature 437, 681–686.
Oskarsson, N., 1980. The interaction between volcanic gases and tephra: fluorine adhering to tephra of the 1970 Hekla eruption. Journal of Volcanology and Geothermal Research 8, 251–266.
Parra-Flores, A., Gasca, R., 2009. Distribution of pteropods (Mollusca: Gastropoda: Thecosomata) in surface waters (0–100 m) of the Western Caribbean Sea (winter 2007). Revista de Biología Marina y Oceanografia 44, 647–662.
Reid, R.P., Carey, S.N., Ross, D.R., 1996. Late Quaternary sedimentation in the Lesser Antilles island arc. Geological Society of America Bulletin 108, 78–100.
Riebesell, U., Zondervan, I., Rost, B., Tortell, P., Zeebe, R., Morel, F., 2000. Reduced calcification of marine phytoplankton in response to increased atmospheric CO_2. Nature 407, 364–367.
Rose, W.I., 1977. Scavenging of volcanic aerosol by ash: atmospheric and volcanologic implications. Geology 5, 621–624.
Sarmiento, J.L., 1993. Atmospheric CO_2 stalled. Nature 365, 697–698.
Suárez-Morales, E., Gasca, R., 1998. Thecosome pteropod (Gastropoda) assemblages of the Mexican Caribbean Sea (1991). The Nautilus 112, 43–51.
Sunda, W., 1988–1989. Trace metal interactions with marine phytoplankton. Biological Oceanography 6, 411–442.
Trofimovs, J., Amy, L., Boudon, G., Deplus, C., Doyle, E., Fournier, N., Hart, M.B., Komorowski, J.C., Le Friant, A., Lock, E.J., Pudsey, C., Ryan, G., Sparks, R.S.J., Talling, P.J., 2006. Submarine pyroclastic deposits formed at the Soufriere Hills volcano, Montserrat (1995–2003): what happens when pyroclastic flows enter the ocean? Geology 34, 549–552.
Watson, A., 1997. Volcanic Fe, CO_2, ocean productivity and climate. Nature 385, 587–588.
Wells, F.E., 1975. Comparison of Euthecosomatous pteropods in the plankton and sediments off Barbados, West Indies. Proceedings of the Malacological Society London 41, 503–509.
Wells, F.E., 1976. Seasonal patterns of abundance and reproduction of Euthecosomatous pteropods off Barbados, West Indies. The Veliger 18, 241–248.

10.2 PUBLISHED ABSTRACTS

Hart, M., Pettit, L., Wall-Palmer, D., Smart, C., Hall-Spencer, J., Medina-Sanchez, A., Prol Ledesma, R.M., Rodolfo-Metalpa, R. and Collins, P. 2012. Investigation of the calcification response of foraminifera and pteropods to high CO_2 environments in the Pleistocene, Paleogene and Cretaceous. *EGU General Assembly Abstracts,* **14**, 9754.

Geophysical Research Abstracts
Vol. 14, EGU2012-9754, 2012
EGU General Assembly 2012

Investigation of the calcification response of foraminifera and pteropods to high CO_2 environments in the Pleistocene, Paleogene and Cretaceous

M. Hart (1), L. Pettit (2), D. Wall-Palmer (3), C. Smart (4), J. Hall-Spencer (5), A. Medina-Sanchez (6), R.M. Prol Ledesma (7), R. Rodolfo-Metalpa (8), and P. Collins (9)

(1) School of Geography, Earth & Environmental Sciences, Plymouth University, Plymouth PL4 8AA, United Kingdom (mhart@plymouth.ac.uk), (2) School of Marine Sciences & Engineering, Plymouth University, Plymouth PL4 8AA, United Kingdom (l.pettit@plymouth.ac.uk), (3) School of Geography, Earth & Environmental Sciences, Plymouth University, Plymouth PL4 8AA, United Kingdom (deborah.wall-palmer@plymouth.ac.uk), (4) School of Geography, Earth & Environmental Sciences, Plymouth University, Plymouth PL4 8AA, United Kingdom (csmart@plymouth.ac.uk), (5) School of Marine Sciences & Engineering, Plymouth University, Plymouth PL4 8AA, United Kingdom (j.hall-spencer@plymouth.ac.uk), (6) Universidad Nacional Autonoma de Mexico, Ciudad Universitaria, Delegacion Coyoacan, 04510 Mexico D.F., Mexico (alba_anms84@yahoo.com.mx, (7) Universidad Nacional Autonoma de Mexico, Ciudad Universitaria, Delegacion Coyoacan, 04510 Mexico D.F., Mexico (prol@geofisica.unam.mx), (8) School of Marine Sciences & Engineering, Plymouth University, Plymouth PL4 8AA, United Kingdom (riccardo@rodolfo-metalpa.com), (9) Benthic Ecology Unit, Zoology, National University of Ireland, Galway, Ireland

Ocean acidification is regarded as a current problem and there is an extensive literature on how various organisms are responding to changes in oceanic pH: the result of increasing atmospheric pCO_2. Acidification is, however, not just a recent phenomenon and there are times in the geological record where pCO_2 has been higher than present day levels (especially in the Cretaceous and Paleogene). Understanding the response of various microfossil groups to the changes in oceanic pH is on-going as part of a major investigation of ocean acidification in both modern and 'fossil' environments.

Extensive carbon dioxide vents have recently been described in the Wagner Basin (northern Gulf of California, Mexico), which cause dramatic changes in carbonate chemistry. The pHT decreased from 7.88 to 7.55 near the most active vents where the lowest saturation states of aragonite (ΩArag) and calcite (ΩCalc) were 0.95 and 1.47 respectively. Foraminifera (unicellular protists) present in the top 2 cm of the sediment (both living and dead individuals) had a range of mainly calcareous taxa (including Bolivina acuminata, B. acutula, Bulimina marginata and Nonionella basispinata). This is a normal composition for these water depths. The lack of dissolution features and the generally good preservation of the tests, even when viewed under a scanning electron microscope, were striking. With no evidence of breakage caused by transportation, it is assumed that this composition is representative in terms of numbers of individuals and taxa represented. Benthic foraminifera from CO_2 vents around the island of Ischia (Italy) have shown dramatic long-term effects of ocean acidification. The foraminifera of the Wagner Basin appear to be surviving in high CO_2 environments comparable to those that occurred during the Cretaceous–Paleogene "greenhouse" world where atmospheric pCO_2 was much higher, but with calcareous foraminifera apparently thriving.

In the Pleistocene, pCO_2 levels are known to have fluctuated in parallel with δ18O during the glacial/interglacial cycles that characterise this interval. Calcification of pteropods through the last 250,000 years shows how this has also fluctuated as a response to the changing oceanic pH. The changes seen in the pteropod assemblages of the Caribbean Sea are mirrored by changes known from the Gulf of Mexico, Mediterranean Sea, Red Sea, Indian Ocean and the South China Sea – all records that confirm the variations in calcification as a global signal.

Wall-Palmer. D., Smart, C.W., Hart, M.B. and Conversi, S. 2011. The dissolution of pteropods from the Caribbean and Mediterreanean Seas. *The Palaeontological Association 55th Annual Meeting Programme and Abstracts,* **55**, 42.

The dissolution of Quaternary pteropods from the Caribbean and Mediterranean Seas

*** Deborah Wall-Palmer[1], C. W. Smart[1], M. B. Hart[1] and A. Conversi[2]**

[1]*School of Geography, Earth and Environmental Sciences, Plymouth University, Plymouth PL4 8AA, UK*

[2]*Marine Institute, Plymouth University, Plymouth, PL4 8AA, UK*

The aragonite producing thecosome pteropods are an important planktic component of the food web in many areas of the world's oceans. In the modern ocean, experimental evidence shows that increasing atmospheric carbon dioxide and the resulting ocean acidification will negatively impact these organisms, since their aragonitic shells are highly susceptible to dissolution. In sediments which are not prone to further dissolution, pteropod shells produce a detailed time series of past aragonite dissolution and environmental conditions. Fluctuations in the preservation and abundance of pteropod shells through glacial and interglacial cycles have been found in several locations; however, these records are largely not comparable due to the use of various methodologies. Here we present and compare pteropod preservation and abundance data for two locations known for their pteropods-rich sediments. It was found that preservation increases during glacial periods and decreases during interglacial periods. Although the magnitude and rate of pH change occurring in the modern ocean is much greater than that shown in the Quaternary record, this study may be useful in predicting future effects on modern pteropod populations.

Wall-Palmer, D., Smart, C., Hart, M. and Conversi, A. 2011. The dissolution of pteropods from the Caribbean and Mediterreanean Seas. *Plankton 2011 Symposium Programme and Abstracts,* Poster 30.

Poster 30

The dissolution of quaternary pteropods from the Caribbean and Mediterranean Seas

Deborah Wall-Palmer, Smart C, Hart M, Conversi A

University of Plymouth, First floor Fitzroy Building, Drake Circus, Plymouth, UK

The aragonite producing thecosome pteropods are an important planktic component of the food web in many areas of the world's oceans. In the modern ocean, experimental evidence shows that increasing atmospheric carbon dioxide and the resulting ocean acidification will negatively impact these organisms, since their aragonitic shells are highly susceptible to dissolution. In sediments which are not prone to further dissolution, pteropod shells produce a detailed time series of past aragonite dissolution and environmental conditions. Fluctuations in the preservation and abundance of pteropod shells through glacial and interglacial cycles have been found in several locations, however, these records are largely not comparable due to the use of various methodologies. In this study we present and compare pteropod preservation, abundance and diversity data for two locations known for their pteropod rich sediments. It was found that preservation increases during glacial periods and decreases during interglacial periods. Although the magnitude and rate of pH change occurring in the modern ocean is much greater than that shown in the Quaternary record, this study may be useful in modelling effects on modern pteropod populations.

Wall-Palmer, D., Smart, C.W. and Hart, M.B. 2010. The preservation of pteropods from the Caribbean Sea as an indicator of past ocean acidification. *Geological Society of America Abstracts with Programs,* **42**, 333.

THE PRESERVATION OF PTEROPODS FROM THE CARIBBEAN SEA AS AN INDICATOR OF PAST OCEAN ACIDIFICATION

WALL-PALMER, Deborah[1], SMART, Christopher W.[2], and **HART, Malcolm Barrie**[2], (1) School of Geography, Earth & Environmental Sciences, University of Plymouth, Drake Circus, Plymouth, PL4 8AA, United Kingdom, deborah.wall-palmer@plymouth.ac.uk, (2) School of Geography, Earth and Environmental Sciences, University of Plymouth, Drake Circus, Plymouth, PL4 8AA, United Kingdom, mhart@plymouth.ac.uk

It is now widely accepted that ocean acidification is an imminent threat to our oceans and although we have a good understanding of the related changes in ocean chemistry, the biological response is still largely understood. It is generally considered that calcifying organisms will be greatly affected by ocean acidification due to under saturation with respect to calcium carbonate. Experimental evidence has already been gathered which demonstrates that a reduction in pH will generally lead to a decrease in calcification rates of a number of, but not all, organisms. Such studies have shown that the response will be complicated and species specific. However, to date, little information is available for important planktonic producers of calcium carbonate; some studies have looked at the effects on coccolithophores and planktic foraminifera, but only three have directly considered the effects on the aragonite producing thecosome pteropods. Due to their highly soluble aragonite shells, thecosome pteropods are likely to be the most vulnerable of the major planktonic producers of $CaCO_3$. They are also likely to be the first to experience persistent decreased $CaCO_3$ saturation states. As an important part of the food web, especially in the Arctic and Southern Oceans, their demise is of significant importance.

In a study of marine cores collected from the Caribbean Sea near the island of Montserrat, it is found there is an exceptional record of thecosome pteropods from the modern sea floor back to Marine Isotope Stage 8. Our research applies a technique, the *Limacina* Dissolution Index (LDX), to an assessment of the dissolution of pteropod shells through the most recent glacial and interglacial stages of the Earth's history (~250 kyrs). It was found that the dissolution of pteropod shells correlates well with climate data (Vostok CO_2, oxygen isotopes and *G. menardii* counts), showing increased dissolution during interglacial periods and enhanced preservation during glacial periods. This method of observing the effects of past ocean acidification on important calcifying plankton can be directly related to the changes occurring in the modern ocean and could be extremely useful in predicting future effects of ocean acidification.

Hart, M.B., Dias, B., Smart, C.W., Wall-Palmer, D., Hayden, J. and Hall-Spencer, J.M. 2010. Modern Seawater acidification: The response of foraminifera to high CO_2 conditions in the Mediterranean Sea and pteropods in the Caribbean Sea. *Geological Society of America Abstracts with Programs,* **42**, 333.

MODERN SEAWATER ACIDIFICATION: THE RESPONSE OF FORAMINIFERA TO HIGH CO2 CONDITIONS IN THE MEDITERRANEAN SEA AND PTEROPODS IN THE CARIBBEAN SEA

HART, Malcolm Barrie[1], DIAS, Bruna[2], SMART, Christopher W.[1], WALL-PALMER, Deborah[3], HAYDEN, Joe[3], and HALL-SPENCER, Jason M.[4], (1) School of Geography, Earth and Environmental Sciences, University of Plymouth, Drake Circus, Plymouth, PL4 8AA, United Kingdom, mhart@plymouth.ac.uk, (2) Laboratorio de Oceanografia Costeira, Universidade Federal de Santa Catarina, Florianopolis, 88040-900, Brazil, (3) School of Geography, Earth & Environmental Sciences, University of Plymouth, Drake Circus, Plymouth, PL4 8AA, United Kingdom, (4) School of Marine Science & Engineering, University of Plymouth, Drake Circus, Plymouth, PL4 8AA, United Kingdom

The seas around the island of Ischia (Italy) have a variable and, on average, lowered pH as a result of volcanic gas vents that emit carbon dioxide from the sea floor at ambient seawater temperatures. These areas of acidified seawater provide natural laboratories in which to study the long-term biological response to rising CO_2 levels. Benthic foraminifera are routinely used to interpret the effects of climate change as they have short life histories, are environmentally sensitive and have an excellent fossil record. Here, we examined changes in foraminiferal assemblages along gradients in pH at CO_2 vents on the coast of Ischia as they may provide a useful model on which to base future predictions of the consequences of ocean acidification. We show that foraminiferal abundance, diversity and ability to calcify decreased markedly in living and dead assemblages as pH decreases, the result of CO_2 percolating through the seawater. These results are in accord with the responses recorded by coralline algae, corals, molluscs, barnacles and echinoderms at the same sites.

Samples from the normal (pH8.17) environments around Ischia contain a diverse fauna dominated by miliolid foraminifera (e.g., *Peneroplis planatus*, *P. pertusus*, *Quinqueloculina* spp.) while those from areas with reduced pH (7.8 to 7.6) have faunas that are progressively less diverse and composed of <100% agglutinated taxa (e.g., *Ammoglobigerina globigeriniformis*, *Miliammina fusca*, *Trochammina inflata*, *Textularia* sp. cf. *T. bocki*). The changes in the benthic foraminifera are quite dramatic for only a slight reduction in pH and confirm the possibility that events, such as the PETM, could quite easily record a widespread loss of diversity or extinction as a result of ocean acidification.

In Cornwall a leak of mine leachate entered Restronguet Creek in 1991 with a pH of 3.0 – 4.0. This decimated the foraminifera, which gradually recovered over 5 years. The high marsh species have not recovered to the same degree, presumably because migration into the head of the estuarine system is almost impossible.

Analysis of ice cores shows that pCO_2 has varied through time, coinciding with glacial/inter-glacial cycles. Using the *Limacina* Dissolution Index (LDX) the preservation of pteropods over time can be used to plot possible pH variations in marine cores in the Caribbean Sea.

Hart. M., Wall-Palmer, D. and Smart, C. 2010. Response of pteropods and foraminifera to changing *p*CO2 and pH in the last 250,000 years. *EGU General Assembly Abstracts,* **12**, 4353.

Geophysical Research Abstracts
Vol. 12, EGU2010-4353, 2010
EGU General Assembly 2010

Response of pteropods and foraminifera to changing pCO2 and pH in last 250,000 years

Malcolm Hart, Deborah Wall-Palmer, and Christopher Smart

University of Plymouth, School of Geography, Earth & Environmental Sciences, Plymouth PL4 8AA, United Kingdom (mhart@plymouth.ac.uk, +44 1752 584776)

Over the last 250,000 years the diversity and quality of preservation of pteropods (holoplanktic gastropods) has fluctuated in response to glacial/interglacial cycles. This is almost certainly related to the change in oceanic pH as the best preservation is recorded in glacial cycles when pCO2 was at a lower level than during interglacials. Detailed studies of the pteropod assemblages from marine cores taken near Montserrat (Caribbean Sea) have provided a high resolution database with which to make comparisons world-wide. There are peaks of diversity (and good preservation) in Marine Isotope Stages 2 and 6 and these can be found elsewhere in the Gulf of Mexico, in the Indian Ocean and the South China Sea. Using a "pteropod preservation index" it can be seen that this parallels the changing pCO2 and pH and is clearly related.

Research on benthic foraminifera living in high CO2, low pH waters near Ischia (Bay of Naples) shows that it is possible to change the foraminifera living in the environment with a change of pH from 8.14 to 7.8 and 7.6. The changes in the diversity and composition of the foraminiferal assemblages parallel changes seen in other benthic faunas (e.g., gastropods, bivalves, echinoderms and calcareous algae). The reductiuon in foraminiferal diversity and the change in the composition of the assemblage is seen to be triggered by a very small change in pH, and something which - if present trends continue - could be seen in the natural world in a few decades.